Joint Meeting

19. Jahrestagung der
Deutschen Gesellschaft für Kristallographie

89. Jahrestagung der
Deutschen Mineralogischen Gesellschaft

Jahrestagung der
Österreichischen Mineralogischen Gesellschaft
(MinPet 2011)

20.-24. September 2011
Salzburg

Referate
Oldenbourg Verlag – München

Inhaltsverzeichnis

Vorträge

Poster

“Small is Strong”: Towards a quantitative understanding of deformation behavior at the micro- and nano-scale

Gerhard Dehm[1]
[1]Erich Schmid Institute of Materials Science, Austrian Academy of Sciences, Leoben, Austria Department Materials Physics, Montanuniversität Leoben, Austria

The mechanical behaviour of materials is well understood for massive samples. When dimensions are reduced to the micro- and nanometer level unexpected effects occur: brittle materials become ductile, metals reveal a stochastic response when exposed to external load, strength increases with reduced dimensions, hardening is caused by a loss of defects, … . At the smallest dimensions, picometer oscillations of interatomic distances at interfaces are predicted to influence hardness in nanocomposites. These length scales must be bridged to understand mechanical properties of miniaturized materials, thin film structures, and superhard coatings. Recent approaches and insights shedding light on the puzzles of micro-/nanomechanics are presented for selected examples. The techniques employed span from micro-Laue diffraction to advanced transmission electron microscopy.

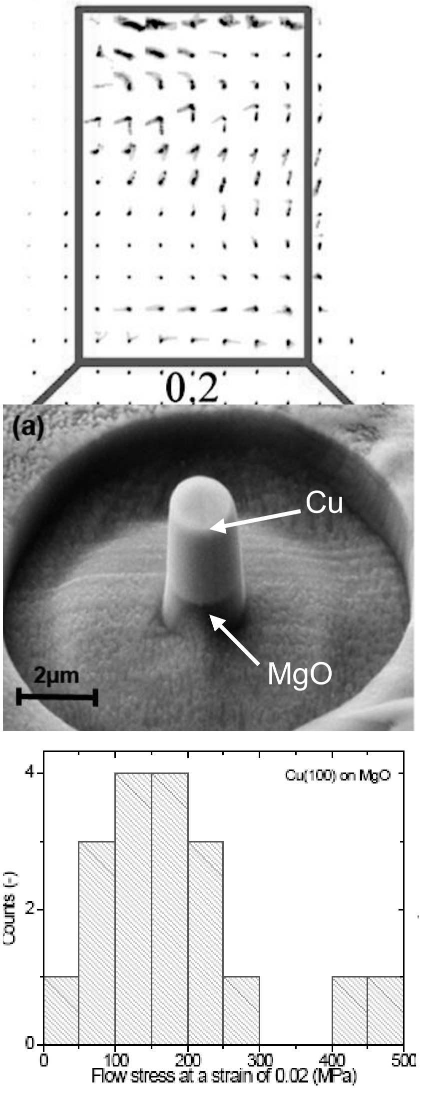

Figures: Micro-Laue composite image of a 20% compressed Cu micropillar, a Cu micropillar on MgO, and distribution of the flow stress for 18 Cu micropillars measured at 2% strain. All micropillars are from the same Cu film.

Chemical variations in ‘calcalkaline’ granitic magmas – neither mixing nor fractionation

J. D. Clemens[1]
[1]Department of Earth Sciences, University of Stellenbosch South Africa

Traditionally, the chemical variations within suites of granitic and silicic volcanic rocks have been attributed to the operation of mechanisms such as restite unmixing, fractionation from more mafic magmas and mixing between felsic and more mafic magmas. An important departure point is that the major magmatic component in most calcalkaline granitoid magmas is derived through fluid-absent partial melting of pre-existing crustal rocks, during high-grade regional metamorphism. Restite unmixing involves the mobilisation of the totality of the partially melted protolith, with progressive separation of the solid (restitic) fraction, to produce the range of compositions observed. An implication is that the most mafic rock of a series would be equivalent in composition to the protolith. Unfortunately, on abundant mineralogical, chemical and physical evidence it is apparent that granitic series are not formed in this way. Restitic material is entrained into most granitic magmas (e.g. inherited zircons) but this process is not responsible for the major variations in the rocks. Thus, the two main ‘surviving’ hypotheses are fractionation and magma mixing. It has become increasingly apparent, from both geochemical and isotope studies, that the more felsic members of granitoid series are not, in general, the results of fractionation of early-formed crystals from more mafic members of the series. This is not to deny that there can be an element of crystal fractionation within granitic magmas. However, it is now clear that what were once considered comagmatic series are better explained as cogenetic series of different magma batches produced from either different source terranes or by partial melting of compositionally contrasting sectors of a single source terrane. I-type granitoid series have sometimes been explained as the products of mixing between mafic, mantle-derived magmas and felsic crustal melts. The isotopic characteristics of these rocks have been used as arguments for this, since they are commonly intermediate between typical mantle and typical sedimentary crust. Additionally, some I-type rocks contain spectacular examples of magma mingling, conclusive evidence that mafic and felsic magma coexisted. The difficulty here is that the isotope evidence is capable of being interpreted in other ways. For example, partial melting of crustal igneous or volcano-sedimentary rocks that were themselves not long separated from the mantle will produce felsic magmas with typical I-type isotope characteristics, without any material contribution from a juvenile mantle melt. Additionally, we have to remember that mingling is not mixing and that both theoretical and geochemical studies have shown that it is the mafic enclave magmas that experienced hybridisation in these systems, leaving the vastly larger volumes of felsic host magmas practically unaffected. If that analysis fails to convince, new ways of viewing the global geochemical dataset for I-type series show clearly that mafic magma is not generally an end-member toward which the chemical variations point. Although magma mixing and mingling are clearly processes that contribute to the diversity seen among granitic series, these processes do not dominate. What process is fully consistent with the major-element, trace-element and isotopic constraints? Partial melting of crustal rocks, coupled with selective entrainment, in varying proportions, of the peritectic minerals formed during melting, together with the accessories hosted in the reactant minerals, can fully account for all the phenomena presented by calcalkaline granitoid series. Up to about 25% peritectic phase entrainment seems to occur. The minerals involved are Cpx, Opx, Pl, Grt and Ilm in I-types (products of melting of Hbl + Bt assemblages) and Opx, Grt, Pl and Ilm in S-types (products of biotite melting reactions). This new view of the origin of chemical variations in granitic magmas opens up the possibility of greatly improving our understanding of the evolution of Earth's crust and the role of the mantle.

High T_c Superconductivity - after a Quarter Century: Ready for Take-off

J. Georg Bednorz[1]
[1]IBM Fellow Emeritus, IBM Research – Zurich
Rüschlikon, Switzerland

When this year the scientific community celebrates the centennial of the discovery of superconductivity and the 25th anniversary of the discovery of high-T_c superconductivity, the field is ready to present a broad spectrum of large-scale applications. Many of these have been envisaged since the early days of superconductivity. However, only with the new cuprate superconductors and as a result of a concentrated, worldwide scientific and engineering effort with efficient international collaborations over the past two decades, does it now become possible – after one century – to finally realize these ideas. Specific segments in applications for power generation, transportation and network reliability are gaining attraction because of the increased importance of using renewable energy. Energy-efficient solutions for industrial processes are being provided by new and surprising concepts that led to the realization of the first commercial high-T_c superconductor products. Large-scale applications, which will need large quantities of superconducting wires, will however have to overcome the usual problems of a new technology – but superconductivity will definitively become a key technology for the 21st century.

Modern Laboratory X-Ray Powder Diffraction - the synchrotron's poor cousin or powerful research tool?

P. Whitfield[1]
[1]National Research Council Canada, Institute for Chemical Process and Environmental Technology, Ottawa

For most researchers, the laboratory diffractometer is their introduction to powder diffraction. Some will graduate rapidly onto synchrotron and neutron diffractometers, but many will barely venture beyond search-match for phase-ID. This is a pity as modern laboratory diffractometers are very powerful instruments and much information may be extracted from even a single, good quality dataset. Software for data analysis has developed rapidly, bringing advanced techniques and new capabilities to an audience outside the usual circle of specialists.
Equipment vendors produce and sell a wide variety of attachments and stages for diffractometers, but researchers should not feel that they are constrained to what appears in the sales brochures. In combination with designers, suppliers and a good machine shop, the researcher may let loose with their imagination. Materials issues, choice of diffractometer geometry, radiation and safety regulations may require considerable attention to detail as well in addition to complex design work - especially so where pressure is involved. The higher energy X-rays produced by molybdenum and silver X-ray tubes are rarely used these days, although the additional penetration and compressed *d*-spacing range makes them very useful for novel *in-situ* cells, as well as highly absorbing transmission samples. The resulting piece of equipment with a suitably optimized diffractometer configuration can produce high-quality results for years with little competition in the field.
Some examples of custom-built sample environments will be given to illustrate the potential of the laboratory diffractometer in modern science. The examples will include *in-situ* high pressure gas cells and high-speed low temperature capillary measurements of both solids and liquids. Some of these experiments require the use of high energy X-rays, but such X-rays may also find application with highly-absorbing transmission samples such as capillaries, and lab-based PDF studies. Material systems described range from existing and potential electrolytes for lithium-ion batteries, polymers, new minerals and samples relating to CO_2 sequestration. The humble laboratory powder diffractometer can never compete head-on with modern synchrotron and neutron beamlines, but can still play an important role in leading edge, diffraction-based science.

Molecular mechanisms of RNA degradation

Elena Conti
Max Planck Institute of Biochemistry, Department of Structural Cell Biology, Martinsried, Germany

All mRNAs in eukaryotic cells are eventually degraded. Studies on mRNA degradation have historically lagged behind those of mRNA synthesis. It is now clear, however, that mRNA turnover is a key step for regulating gene expression not only under different physiological conditions but also during development and differentiation. Regulating mRNA stability at the post-transcriptional level is a widespread and versatile strategy to manipulate the abundance of proteins as well as the timing of their presence in the cell. Not surprisingly in this context, disruption of mRNA decay has been linked to human diseases.
A key player in RNA decay is the RNA exosome, a multiprotein complex that also participates in the processing of structured RNAs and in RNA quality control pathways. The exosome contains one nuclease subunit and nine additional subunits that are catalytically inactive but are nevertheless essential *in vivo*. Using biochemical and structural biology approaches, we have studied the molecular mechanisms with which the ten-subunit exosome recognizes RNA substrates and guides them to the active site for degradation. We found that although the catalytic function of the 9-subunit core of the exosome has been lost during evolution, the substrate recruitment and binding properties have been largely conserved from prokaryotes to eukaryotes. We are now investigating another layer of regulation: how the exosome is activated by protein complexes that are specifically localized in the nucleus or the cytoplasm.

Mineralsimulationen für die Photovoltaik und Thermoelektrik

Klaus Bente[1]
[1]Institut für Mineralogie, Kristallographie und Materialwissenschaft der Universität Leipzig

Aktuelle Forschungen und Entwicklungen von Verbindunghalbleitern auf den Gebieten der Photovoltaik und Thermoelektrik werden nahezu ausnahmslos auf Mineralbasis durchgeführt. Aufgrund entsprechender physikalisch dominierter Studien treten mineralische Namengebungen oft in den Hintergrund, wiewohl Bleiglanz-, Wurtzit und Zinkblendetypen und darauf basierende mineralische Ableitungsstrukturen und chemische Variationen die entscheidende Rolle spielen. Aktuell und perspektivisch sind Randlöslichkeits- und Mischkristallsysteme u. a. mit strukturellen Modifikationen und der Neigung zu Schichtstrukturen besonderer Untersuchungsgegenstand. Diese Verbindungen gehen in ihrer Bedeutung als anwendungsrelevante Multitalente über Volumenmaterialien hinaus und erlauben insbesondere in Form von nanodimensionierten Fäden und Schichten hohe Effizienzen.

Meist werden ausgehend von kubisch bzw. hexagonal dichtest gepackten Strukturen gleich oder niedriger symmetrische Phasen über Substitutionsstrategien in Analogie zu Mineralphasen oder in Erweiterung entsprechender Systematika konzipiert. Mittels geeigneter Synthesemethoden werden mikro- bzw. nanodimensionierte Dünnschichten oder Stäbe freistehend oder in Templaten erzeugt. Die Optimierung der gewünschten physikalischen Eigenschaften und deren Korrelationen werden dabei durch gezielte Orientierungen, Epitaxien, Verwachsungen und Dotierungen sowie durch die Wahl geeigneter Substrate wie z. B. Glas, Mo-Glas, III-V-Hableiter und Imide erzielt.

Rezente Studien, wie sie u. a. in Salzburg und Leipzig durchgeführt werden, fokussieren auf Sulfosalze, die hinsichtlich der auf dem Weltmarkt angebotenen chemischen Grundsubstanzen preisgünstig zu erhalten sind. Ihre Synthese kann durch Modifizierungen bekannter, apparatetechnisch vergleichbar unkomplizierter, jedoch extrem parametersensibler Methoden wie VLS, Hot Wall Deposition etc. im Hochvakuum realisiert werden.

Im Rahmen allgemeinerer Betrachtungen [1] werden Mineral- und Mischkristallbeispiele u. a. aus den Systemen PbX - SnX (X=S, Se, Te) [2] und Ag2S-PbS-(Sb,Bi)2S3 [3] vorgestellt.

[1] H. S. Leipner, H.-R. Höche, Schwerpunktheft Scientia Halensis, 1-40 (2004)
[2] K. Bente, V. Lazenka, D. Unuchak, G. Wagner, and V. Gremenok, Crystal Research & Technology
Vol. 45, № 6, - P. 643 – 646 (2010).
[3] K. Bente, M. Engel and M. Steins, Z. Krist. **205**, 327-328 (1993)

The Economic Mineralogy of high-tech Metals

F.M. Meyer[1]
[1]RWTH Aachen University, Mineralogy and Economic Geology Aachen

Rare and scarce mineral commodities such as Ga, Ge, Se, In, PGE, Te, REE, and others, rank high as raw materials of critical concern. Increasing mineral demand is driven by technological advances as is illustrated by the fabrication of computer chips. Some 30 years ago this required the constituent elements of about twelve minerals, while nowadays high-capacity integrated circuits are made from as many as sixty different elements. The inherent risk of supply shortage of high-tech metals and their impact on emerging technologies has led to the concept of criticality. This is expressed in terms of two essential dimensions: importance in industrial use and availability. Supply shortage as determined by geological availability reflects firstly, considerations of the distribution and abundance of critical minerals and secondly, knowledge of efficient extraction and processing methods.

In most minable ores, the high-tech or critical metals are byproducts that are produced together with their host minerals such as indium from sphalerite-bearing ores or gallium from bauxite. The central problem is that byproducts generally have no own production infrastructure. But mineral production decisions are driven by demand for the principal product, not for byproducts. A salient feature of REE production is that, depending on conditions of ore formation, REE-minerals contain light and heavy REEs at various ratios and concentration levels as well as various levels of deleterious elements such as Th or U. The demand for particular elements among the REEs has seen extreme variations depending on technological advances, and so have their metal prices. Today, the total REE value is largely determined by the abundance of Tb, Eu, and Dy. Many of the known potential REE deposits have a predominance of light REE, so that this could lead to an overproduction of Ce if these deposits would be brought into production. On the other hand, some of the heavy REEs are in high demand, but have limited reserves, whereas Lu presently is rather low in demand and price, and hardly worth recovering.

World resource estimations generally include potential high-tech metal deposits that show good grade and tonnage and consist of a large quantity of valuable elements. Based on current metal prices, this may add up to a considerable in-ground value. However, the elements must be mineable and processable to a saleable concentrate which in many occurrences might not be the case.

Thus, valuating and exploiting high-tech metal deposits requires detailed mineralogical studies about the various mineral species present, their relative abundance, mineral associations, textural features, grain size distribution, and about the chemical make-up of ore and gangue minerals. In conclusion, mineralogy is the key to understanding the variability of scarce and rare metal ores within a deposit, and is essential in determining how to maximize the value of a metal resource.

References:

British Geological Survey, 2010; Angerer, G., et al., 2009; U.S. National Research Council, 2007.

From first-principles to geological processes

Sandro Jahn
Deutsches GeoForschungsZentrum GFZ, Potsdam

Minerals, melts and fluids are the building blocks of our planet. Their abundance in different parts of the Earth depends on the local availability of chemical elements and their isotopes, on pressure and temperature, but also on the history of the actual rocks. Our knowledge about the present state of the Earth and its evolution over geological timescales is based on observations and measurements of the physical and chemical properties of geological materials, which range from individual mineral grains of micrometer size to rock formations on the kilometer scale. Ultimately, material properties are determined by the interaction of atomic nuclei and electrons, which is described by quantum mechanics. It appears attractive to use so-called first-principles simulation methods, which use such basic laws of physics and do not depend on empirical assumptions, to predict the structure, thermodynamic and physical properties of relevant solid and fluid phases. In this talk, I will give a short introduction to atomic scale simulation techniques. Their wide range of applications in geological context will be demonstrated by examples including P-V-T equations of state of single crystals, mechanisms of polymorphic phase transitions, structural models of melts and fluids, and the prediction of equilibrium fractionation factors of stable isotopes between minerals and fluids. I will also highlight the complementary nature of experimental and modeling approaches in geomaterials research.

Vorträge

MS01-T1

Single Crystal X-ray Diffraction at Megabar Pressures and Temperatures of Thousands Degrees: From Geosciences to Materials

L. Dubrovinsky[1], K. Glazyrin[1], T. Boffa-Ballaran[1], E. Bykova[1], N. Dubrovinskaia[2], M. Merlini[2,3], M. Hanfland[3]
[1]Bayreuth University, BGI, Bayreuth, Germany
[2]Bayreuth University, Bayreuth, France
[3]ESRF, Grenoble, France

Modern science and technology rely on the fundamental knowledge of matter that is provided by crystallographic studies. The most reliable information about crystal structures and their response to changes in pressure and temperature is obtained from single crystal diffraction experiments. Advantages in diamond anvil cell techniques (DACs) and modern X-ray sources have increased the accessible pressure range for structural research up to several dozens gigapascals. We have develop a methodology to perform single crystal X-ray diffraction experiments in laser-heated DACs and demonstrate that structural refinements and accurate measurements of the thermal equation of state of metals, oxides, silicates from single crystal intensity data are possible in a megabar pressure range at temperatures of thousands degrees. Particular attention we paid on in situ study of geomaterials at extreme conditions.

A major goal in the geosciences is to understand (and predict) how the Earth works, which requires a detailed knowledge of how the mineral phases, such as silicate perovskite and ferropericalse which make up the Earth, behave under high pressure and high temperature conditions,. Special focus has been on possible phase transformations of the materials due to their significant implications for mantle behavior. The majority of measurements have been made on *pure* $MgSiO_3$ perovskite, however, and almost exclusively using X-ray powder diffraction. Although the importance of Fe and Al as minor components of the silicate perovskite phase has been well documented in the past decade in numerous papers including many published in Science and Nature, the few studies using methods sensitive to these elements (e.g., X-ray emission spectroscopy and nuclear forward scattering) were not sufficiently systematic and/or sensitive to recognize any significant changes in the pressure range below 100 GPa. We studied silicate perovskites (Mg0.88Fe0.12)SiO_3
(Mg0.9Fe0.1)(Si0.975Al0.025)O_3 and
(Mg0.6Fe0.4)(Si0.655Al0.35)O_3 and series of magnesiowustites with different compositions by means of single crystal X-ray diffraction in laser-heated diamond anvil cells, Mossbauer spectroscopy, and nuclear forward scattering at pressure up to 150 GPa and temperature above 2500 K. We will discuss effects of changes in iron electronic state on structure and properties of mantle minerals.

MS01-T2

The Shock-Wave-Synthesis Laboratory at the Freiberg High-Pressure Research Centre

K. Keller[1,2], T. Schlothauer[1,2], M. Schwarz[2,3], G. Heide[1,2]
E. Kroke[2,3]
[1]TU Bergakademie Freiberg, Institute for Mineralogy, Freiberg, Germany
[2]TU Bergakademie Freiberg, Freiberg High-Pressure Research Centre (FHP), Freiberg, Germany
[3]TU Bergakademie Freiberg, Institute for Anorganic Chemistry, Freiberg, Germany

The essential aim of the Freiberg High-Pressure Research Centre (FHP) is the application of high pressures for the material development and synthesis, the optimisation and comprehensive characterisation and understanding of the materials properties as well as to convey the gain of knowledge in saleable products. As one part of this field of research the university of Freiberg operates a subterranean blasting chamber in the Reiche Zeche mine. Therein shock wave synthesis with high explosives to assemble new high-pressure phases (esp. Hard material) were conducted. Actually the flyer plate method with up to 1kg of high explosive-charges is used to obtain pressures as far as 100GPa and temperatures of several thousand degree celsius in the sample powder. The impedance method (mixing sample with high impedance metal) and reflection method (small sample layer) is applied concerning to the sample material and the desired conditions. The sample is encased in a metal capsule or directly in the enclosing steel container. For predictable and reproducible shock conditions a plane-wave-generator to obtain a flat shock front is used.

Comprehensive work in the field of the system Si-Al-O-N with promising high-pressure phases is in progress. For example the γ-Si_3N_4 with spinel structure, the γ-SiAlON and the rocksalt-AlN were succesfully synthesized with the shock wave synthesis at the FHP.

At the moment up to 2g of sample powder in dependency of synthesis conditions can be obtained with one shot. For higher amounts at same pressure or even ultra high pressure (> 300GPa) a new blasting chamber with a capacity of 20kg high explosive per shot is under construction and will be finished in the middle of 2011. The new chamber will be equiped with measurement devices (manganin gauges and shortening pins), active ventilation, water cooling for the samples, installation for sample preheating and internet connection.

Figure 1

MS01-T3
Anomalies and phase transitions of dense ice

R. Caracas[1], R.J. Hemley[2]
[1]CNRS, Ecole Normale Superieure de Lyon, Laboratoire de Geologie, Lyon Cedex 07, France
[2]Carnegie Institution of Washington, Geophysical, Washington, DC, USA, United States

The phase diagram of water ice, H2O is dominated above 3 GPa by several dense structures, which are all based on a body-centered cubic sub-lattice of O. In the ices VII and VIII the molecular integrity is preserved. Ice VII is disordered with the dipole of the water molecules pointing randomly along the three cartesian axis, such as the average structure is cubic. Ice VIII is an ordered low-temperature variant of ice VII with tetragonal symmetry, where the dipoles point along the fourfold symmetry alternatively up and down; the result is an antiferroelectric structure. Both ices VII and VIII exhibit anomalies in the diffraction pattern and Raman spectra inconsistent with their initial symmetry assignment. Beyond about 100 GPa the molecular integrity is lost and the structure, the ice X, becomes ionic. Here the H atoms are midway between their O neighbors, preserving the cubic symmetry.

First-principles calculations based on density-functional and density-function perturbation theories were performed to investigate the stability fields and the transition paths of these different high-dense ices.

We propose that the anomalies in ice VII and ice VIII can be explained by the formation of ferroelectric (FE) and anti-ferroelectric (AFE) domains. In the FE domains the dipoles point along the same direction along the 4-fold axis, while in AFE they point alternatively up and down. The splitting of the X-ray diffraction peaks and the appearance of new Raman modes are the result of different a/c ratios in the two FE and AFE parts of the structure [1,2].

Then, based on lattice dynamical calculations, we show that the transition between ices VII and VIII and ice X goes through a disordered phase X in the 60-115 GPa pressure range. In this regime the H atoms are allowed to freely bounce back and forth between their two O neighbors. Ice X is stable up to about 420 GPa. The first post-ice-X structure occurs due to a phonon softening in ice X. The resulting structure has orthorhombic symmetry [3,4,5]. We show that the softening is also visible in the development of an elastic anomaly after 160 GPa.

[1] M. Somayazulu, J. Shu, C. S. Zha, A. F. Goncharov, O. Tschauner, H. K. Mao, & R. J. Hemley, J. Chem. Phys. 128, 064510 (2008); [2] R. Caracas & R.J. Hemley (2011) submitted; [3] M. Benoit, M. Bernasconi, P. Focher, & M. Parrinello, Phys. Rev. Lett. 76, 2934 (1996); [4] R. Caracas, Phys. Rev. Lett. 101, 085502 (2008); [5] B. Militzer & H. F. Wilson, Phys. Rev. Lett. 105, 195701 (2010).

MS01-T4
New insight into boron phases and their relations under pressure

N. Dubrovinskaia[1], G. Parakhonskiy[2], L. Dubrovinsky[2]
[1]Universität Bayreuth, Lehrstuhl für Kristallographie, Bayreuth, Germany
[2]Universität Bayreuth, Bayerisches Geoinstitut, Bayreuth, Germany

Boron is the fifth element in the Periodic table known for its structural complexity, unusual types of bonding, and for a rich variety of compounds that it forms. Even the number of its existing or hitherto proven elemental modifications is still under discussion. The present study of boron behavior at high pressures and high temperatures comprises various experimental techniques for the high-pressure synthesis and materials characterization. Experimentally established phase relations of the stable boron polymorphs will be discussed.

MS01-T5
High pressure behavior of α-FeOOH studied on powder and single crystal samples

E. Bykova[1], E. Greenberg[2], K. Glazyrin[1], T. Boffa Ballaran[1], N. Dubrovinskaia[3], L. Dubrovinsky[1]
[1]University of Bayreuth, Bayerisches Geoinstitut, Bayreuth, Germany
[2]Tel-Aviv University, School of Physics and Astronomy, Tel-Aviv, Israel
[3]University of Bayreuth, Materials Physics and Technology, Laboratory of Crystallography, Bayreuth, Germany

Goethite, α-FeOOH, is widely present in the Earth surface as a component of soils, sediments and ore deposits. The mineral crystallizes in an orthorhombic structure (Pnma, a = 9.9510(5), b = 3.0178(1), c = 4.5979(2) Å [1]) and is isostructural with diaspore, AlOOH. The figure below shows the α-FeOOH structure at ambient conditions. It consists of distorted FeO3(OH)3 octahedra linked together by sharing edges to form infinite bands. The bands are connected via shared octahedra vertices that results in infinite channels parallel to the b axis. Investigations of the crystal structure of goethite as well as calculations of the equation of state (EoS) based on experimental data at non-ambient conditions (up to 29.4 GPa and 250 °C) have been performed by several authors (see, for example, refs. [2 and, 3]). At higher pressures (up to 57 GPa) the behavior of the material have been studied only theoretically using density-functional theory [4]. A phase boundary between goethite and its high-pressure polymorph, ε-FeOOH, hasn't been established unambiguously. While DFT predicted the transition at 6-7 GPa, Gleason et al. [3] observed a slow conversion above 5 GPa only under heating above 200 °C. Our work presents the first in-situ single crystal X-ray diffraction (XRD) and Raman study of α-FeOOH in a diamond anvil cell under compression up to ~20 GPa. No phase transitions predicted by theoretical calculations [4] were observed. According to our X-ray diffraction data, under compression FeO3(OH)3 octahedra flatten (directions of the distortion are shown by the arrows in the figure below) to decrease the channels size . We have also studied α-FeOOH powder by means of the in-situ synchrotron X-ray diffraction and Raman spectroscopy up to 51 GPa. The powder XRD indicates a reversible first order phase transition at ~44 GPa. The new phase can be described in terms of the Pnma space group with the following unit cell parameters: a = 9.097(2), b = 2.7274(4), c = 3.926(2) Å (at 51.6 GPa). The equation of state parameters of goethite obtained from both single crystal and powder XRD show good agreement.

[1] Yang, H., Lu, R., Downs, R.T. et al. // Acta Crystallogr. E (2006). 62, 250–252.
[2] Nagai, T., Kagi, H., Yamanaka, T. // Am. Mineral. (2003). 88, 1423–1427.
[3] Gleason, A.E., Jeanloz, R, Kunz, M. // Am. Mineral. (2008). 93, 1882–1885.
[4] Otte, K., Pentcheva, R., Schmahl, W.W. et al. // Phys. Rev. B (2009). 80, 205116.

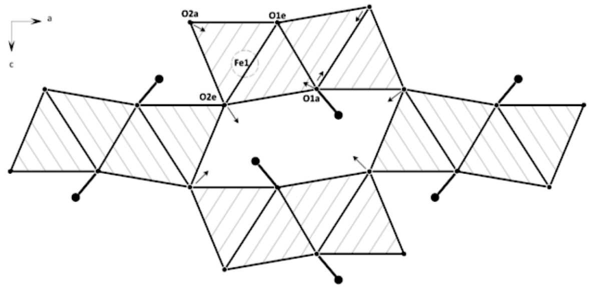

Figure 1

MS01-T6
The fluorescence lifetime of SrB$_4$O$_7$:Sm^{2+} at high pressures and temperatures

J. Bauer[1], L. Bayarjargal[1], B. Winkler[1]
[1]Goethe-Universität Frankfurt am Main, Abteilung Kristallographie, Frankfurt am Main, Germany

The pressure in diamond anvil cell experiments is often determined by the ruby fluorescence method [1]. However, this method has a limited applicability in high-temperature experiments, as the wavelength of the ruby fluorescence is influenced by both pressure and temperature.

SrB$_4$O$_7$:Sm^{2+} is an alternative spectroscopic pressure gauge [2]. It has the advantage, that the fluorescence line normally used for pressure determination has a negligible temperature shift below 500 K and a very small shift between 500 K and 900 K. Here we propose to use this pressure marker in high (p,T) experiments.

Fluorescence lifetime thermometry is an established method at ambient pressure [3], but only a few reports about the pressure dependence of fluorescence lifetime have been published. We have recently demonstrated, that the fluorescence lifetime of ruby can be used as a temperature gauge at high pressures and temperatures. These experiments show that fluorescence lifetime measurements may provide a reliable method for determination of temperature in a DAC at high pressure. A significant advantage will be that fluorescence lifetime measurements will unambiguously give bulk temperatures.

The fluorescence lifetime of the SrB$_4$O$_7$:Sm^{2+} at ambient pressure decreases by about one order of magnitude between 300 K and 550 K. Thus, the use of SrB$_4$O$_7$:Sm^{2+} offers the possibility to determine the pressure in the DAC by measurement of the wavelength shift of the fluorescence and to determine the temperature by measuring the fluorescence lifetime.

Financial support from the DFG (grant WI1232/25-2) is gratefully acknowledged.

[1] K. Mao, J. Xu and P.M. Bell, J. Geophys. Res. B: Solid Earth, 1986, 91(B5), 4673-4676
[2] F. Datchi, R. LeToullec, P. Loubeyre, J. Appl. Phys., 1997, 81(8), 3333-3339
[3] K.T.V. Grattan and Z.Y. Zhang. Fiber Optic Fluorescence Thermometry. Chapman & Hall, 1995.

Keywords: thermometry, fluorescence lifetime spectroscopy, diamond anvil cell

MS01-T7
Synthesis of novel ultra-incompressible rhenium nitrides by reaction of the elements in the laser-heated diamond anvil cell and characterization

A. Friedrich[1], B. Winkler[1], W. Morgenroth[1], L. Bayarjargal[1], E.A. Juarez-Arellano[2], K. Refson[3], V. Milman[4]
[1]Goethe Universität Frankfurt , Institut für Geowissenschaften, Abt. Kristallographie, Frankfurt am Main, Germany
[2]Universidad del Papaloapan, Tuxtepec, Mexico
[3]Rutherford Appleton Laboratory, Didcot, United Kingdom
[4]Accelrys, Cambridge, United Kingdom

Transition-metal carbides, nitrides and borides have a high potential for industrial applications as they generally show higher hardness, lower compressibility and higher melting points than the pure metals. The formation of new materials with high density and hence potential for high hardness is promising at extreme pressures and temperatures. Rhenium has a high density of valence electrons and forms ultra-incompressible, hard Re$_2$C [1] and ReB$_2$ [2]. Up to now no bulk rhenium nitrides were known.

Reaction of rhenium and nitrogen was achieved in the diamond anvil cell at high pressure (<32 GPa) via double-sided laser heating (<3000 K). Samples were analysed in situ using powder synchrotron x-ray diffraction at the ALS (Berkeley, beamline 12.2.2). Recovered samples were characterized using synchrotron x-ray Laue microdiffraction (spot size ~1 x 1 µm²) at the ALS beamline 12.3.2 and micro-Raman spectroscopy.

Re$_3$N is formed at >11 GPa and about 1700-2250 K, while Re$_2$N becomes stable at >20 GPa and about 2000 K [3]. The unit cell parameters and compression data were obtained from the x-ray experiments. Both phases are ultra-incompressible with bulk moduli of ~400 GPa. From the Laue x-ray mapping across the samples the phase distribution was derived and grain sizes were determined to be 3 - 8 µm.

The crystal structures of both phases were obtained from density functional theory (DFT)-based calculations and confirmed by Rietveld refinement of the rhenium positions. Re$_3$N (P-6m2) crystallizes in an ABB stacking sequence of rhenium atoms, Re$_2$N ($P6_3/mmc$) in an AABB stacking sequence, identical to that of Re$_2$C [1]. The nitrogen atoms are located between the AA and BB layers only.

Micro-Raman spectra of recovered Re$_3$N samples show all four Raman-active modes and a perfect agreement with the vibrational properties calculated using DFT [4]. This further confirms the validity of the structural model and the presence of single nitrogen atoms within the crystal structure, which implies that nitrogen dissociates during the synthesis of the rhenium nitrides.

Financial support from the DFG within SPP1236 (Wi1232, Fr2491) and the BMBF (project 05KS7RF1) is gratefully acknowledged. We thank ALS, COMPRES and Vereinigung der Freunde und Förderer der Goethe Uni for beamtime and financial support, and the beamline scientists for their help.

References:
[1] E.A. Juarez-Arellano, B. Winkler, A. Friedrich, L. Bayarjargal, V. Milman, J. Yan, S.M. Clark, *J. Alloys Compd.*, 481, 577, 2009.
[2] H.Y. Chung, M.B. Weinberger, J.B. Levine, A. Kavner, J.M. Yang, S.H. Tolbert, R.B. Kaner, *Science*, 316, 436, 2007.
[3] A. Friedrich, B. Winkler, L. Bayarjargal, W. Morgenroth, E.A. Juarez-Arellano, V. Milman, K. Refson, M. Kunz, K. Chen, *Phys. Rev. Lett.*, 105, 085504, 2010.
[4] A. Friedrich, B. Winkler, K. Refson, V.Milman, *Phys. Rev. B*, 82, 224106, 2010.

MS01-T8
High-pressure crystal structure and Raman spectra of $Bi_{12}TiO_{20}$ sillenite

L. Wiehl[1], A. Friedrich[1], W. Morgenroth[1], E. Haussühl[1], B. Winkler[1]
[1]Goethe-Universität Frankfurt, Institut für Geowissenschaften/Abt. Kristallographie, Frankfurt am Main, Germany

Sillenites, $Bi_{12}MO_{20}$ (M = Si, Ge, Ti), show outstanding electric and optical properties used in many applications, especially the photorefractive effect and a high photoconductivity, which are assumed to be correlated with the stereochemical activity of the $6s^2$ lone electron pair of Bi^{3+}. At ambient conditions the Bi^{3+} lone pair is oriented towards an unoccupied corner in the distorted BiO_5E octahedron. Thus the stereochemical activity is expected to decrease under high external pressure. The crystal structure of $Bi_{12}TiO_{20}$ (BTO) was determined from a single crystal at 9.2(2) GPa in a diamond anvil cell by X-ray diffraction with synchrotron radiation at HASYLAB (beamline D3), Hamburg. Powder diffraction experiments were performed with synchrotron radiation at ESRF (beamline ID09A), Grenoble up to a pressure of 37 GPa. On pressure release of the same sample, Raman spectra were measured in the pressure range from 37 GPa to ambient conditions. The bulk modulus is B_0 = 50(1) GPa. The Bi^{3+} lone pair remains stereochemically active up to the highest pressure reached in this study.

Financial support from the DFG (HA 5137/3-1) and from HASYLAB is gratefully acknowledged. We thank HASYLAB and ESRF for synchrotron beamtime, Martin Tolkiehn for assistance at D3 and Michael Hanfland for assistance at ID09A.

MS02-T1
$Sr_3Gd_2[BO_3]_4$ - Growth, Structure and Analyses of a not so new borate

C. Reuther[1], H. Schmidt[2], M. Hengst[1], G. Heide[1]
[1]Freiberg University of Mining and Technology, Department of Mineralogy, Freiberg, Germany
[2]Freiberg University of Mining and Technology, Department of Chemistry, Freiberg, Germany

1968 Dzhurinskii *et al.* [1] began to synthesize a new borate, $Sr_3Dy_2[BO_3]_4$. They did not know the wide chemical variation of the system, but grew the first single crystal of it. Today borate crystals like the mentioned are of high interest in optics and sensor research because of its wide chemical variation and interesting properties.
The component $Sr_3Gd_2[BO_3]_4$ was sintered in stoichiometric composition. Single crystals were grown in multiple directions after the Czochralski-method (see Fig. 1). X-ray data of the single crystal show two possible solutions because of the systematic extinction. The possible space groups are P*nma* and P*na2₁*. Both structures could be find in literature (e.g. Pan *et al.* [2] or Palkina *et al.* and Bambauer *et al.* [3-4]). The external features of the crystals like ridges and facets point to space group P*nma*. For space group P*nma* the cell parameters are a=0.71450 nm b=1.60547 nm c=0.87555 nm. DTA-measurements offer a congruent melting behavior at 1461 °C ± 5K and crystallization temperature 1388 °C ± 5 K. After several growth experiments some of the crystals show different inclusions like a Gd-rich phase, probable Gd_2O_3 and other. They were characterized by energy dispersive measurements with a SEM.
Literature:

[1] Dzhurinskii, B. F., Tananev, I. V. and Aliev, O. A.: Synthesis of single crystals of double borats in the system Ln_2O_3-SrO-B_2O_3, In: Neorganiceskie Materialy 4 (1968), p. 1972-1974
[2] Pan, S.-K., Wang, G. and Huang, Z.-X.: Synthesis and Structure of $Ba_3La_2(BO_3)_4$ Crystal, In: Chinese Journal of Structural Chemistry 21. 4 (2002), p. 382-384.
[3] Palkina, K. K., Kuznetsov, V. G. und Moruga, L. G.: Crystal structure of $Pr_2Sr_3(BO_3)_4$, In: Journal of Structural Chemistry 14. 6 (1974), p. 988-992
[4] Bambauer, H. U. and Kindermann, B.: Darstellung und kristallographische Daten von Orthoboraten $(SE)_2Ca_3[BO_3]_4$, In: Zeitschrift für Kristallographie 147 (1978), p. 63-74

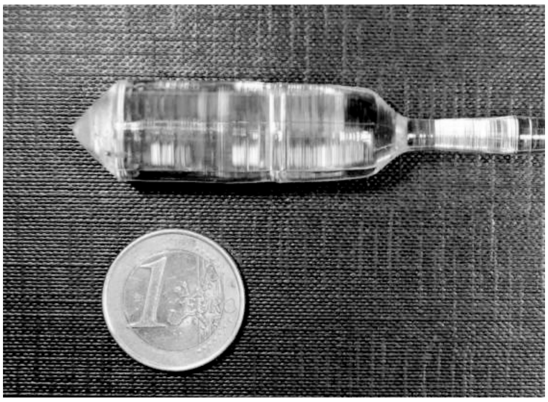

Fig. 1: Single crystal of $Sr_3Gd_2[BO_3]_4$

MS02-T2
Strange high temperature characteristics of $GdCa_4O(BO_3)_3$: singlecrystals for high temperature piezoelectric applications

R. Möckel[1], M. Hengst[1], M. Klinger[2], J. Götze[1], G. Heide[1]
[1]TU Bergakademie Freiberg, Dept. of Mineralogy, Freiberg, Germany
[2]TU Bergakademie Freiberg, Department of Energy Process Engineering and Chemical Engineering, Freiberg, Germany

Introduction It was found that members of the $REECa_4O(BO_3)_3$(REECOB)-family may be very promising candidates for piezoelectric application at elevated temperatures (above 1000°C) as published by Zhang et al. (2008a, 2008b). This opens a new field of application for the group. Recently, we reported thermomechanical data on GdCOB ($GdCa_4O(BO_3)_3$) (Möckel et al., 2011), and showed that the thermal expansion coeffcients are not only anisotropic, but also reveal a sudden increase at around 850°C. By further investigation, we try to clearify this effect.
Materials & methods

Single crystals of $GdCa_4O(BO_3)_3$ (GdCOB) were grown by using the Czochralski technique. Most growth experiments led to single crystals of good quality; free of cracks and inclusions. Investigation on thermal expansion were conducted, using a dilatometer (Netzsch DIL 409 C) in the temperature range of 25-1200°C. For DSC (differential scanning calorimetry) measurements a Netzsch STA 409C/CD was used (25-1200°C, heating rates: 10, 20, and 40 K/min, sample material 30-100 mg). For structural investigation on powder X-ray diffraction (PXRD) at high temperatures Bruker AXS D8 devices with CoK- and MoK-radiation, both equipped with heating chambers, were used.

Results & discussion

Results from thermal expansion measurements of GdCOB led to a characteristic increase of the coefficients at around 850°C (up to 36%). Below and above 850°C the thermal expansion is approximately linear. We found the following thermal expansion coefficients of the main crystallographic directions: below 850°C: α_a=11.1, α_b=8.6, α_c=13.3 x10^{-6}/K, and above 850°C: α_a=14.1, α_b=11.7, α_c=17.8 x10^{-6}/K, see fig.1.

As a result from PXRD, the structure does not change significantly during heating and a phase transition was not detected therefore. Nonetheless, DSC investigation revealed a very small and wide endothermic peak.

Conclusion

It is suggested that ordering processes are the cause for the change in characteristics, also - to be more specific - tilting and rotating of the borate groups (planar BO_3-triangles) may be responsible for changing. However, piezoelectric characteristics do not seem to be affected by the effect, since published investigation do not reveal any changes or anomalies (Zhang et al., 2008b).

References

Möckel, R., Hengst, M., Götze, J. and Heide, G. (2011): $REECa_4O(BO_3)_3$ (REECOB): New material for high-temperature piezoelectric applications. In: Krivovichev, S.V. (ed.), Minerals as advanced materials II. Springer. in press.

Zhang, S., Fei, Y., Chai, B. H. T., Frantz, E., Snyder, D. W., Jiang, X. and Shrout, T. R. (2008a): Characterization of piezoelectric single crystal $YCa_4O(BO_3)_3$ for hightemperature applications. Applied Physics Letters, 92(20).

Zhang, S., Frantz, E., Xia, R., Everson, W., Randi, J., Snyder, D. W. and Shrout, T. R.(2008b): Gadolinium calcium oxyborate piezoelectric single crystals for ultrahightemperature (>1000°C) applications. Journal of Applied Physics, 104(8).

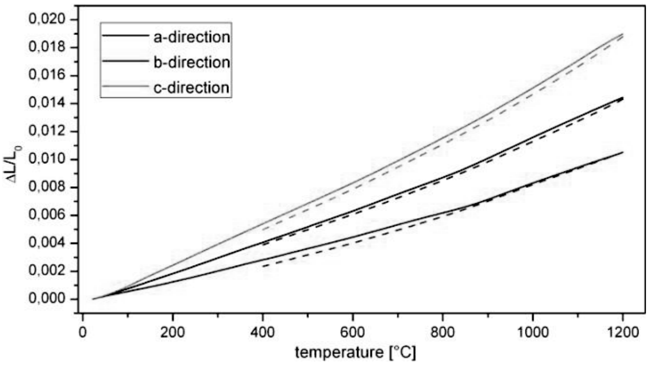

Figure 1
Relationship between thermal expansion and temperature for the crystallographic main directions of GdCOB (dashed lines: cooling)

MS02-T3

Besonderheiten der Mn - Fixierung in Perowskiten $Ca(Al,Fe,Mn,Ti)O_3$-d

S. Stöber[1], G. Redhammer[2], H. Pöllmann[1]
[1]Martin Luther Universität Halle, Institut für Geowissenschaften Mineralogie/Geochemie, Halle (Saale), Germany
[2]Universität Salzburg FB Materialforschung & Physik, Abteilung für Mineralogie , Salzburg, Austria

Bei der Produktion von eisenreichen Mn - Tonerdezementen kristallisieren während des Abkühlungsprozesses aus der Schmelze die Hauptphasen Calciumaluminatferrat Ca(Al,Fe)2O4 und diverse Perovskite AnMnO3n-d. Aufgrund der sehr variablen Sauerstofffugazität während des Abkühlungsprozesses, tritt insbesondere Mangan in unterschiedlichen Oxidationsstufen auf, wodurch bestimmte sauerstoffdefizitäre Perowskite stabilisiert werden.

Der strukturelle Aufbau dieser Verbindungen basiert auf der Wechsellagerung von Tetraeder - Oktaeder (TO), Tetraeder - Oktaeder - Oktaeder (TOO) und Oktaeder-Oktaeder (OO), welche sich von der klassischen Perowskitstruktur z.B. CaTiO3 mit der Raumgruppe Pm-3m ableiten lassen.

Zur Untersuchung der Phasenbreite und Kristallchemie der Perovskitstrukturtypen n = 3 A3B3O8+d: Ca3(Fe,Mn,Ti)3O8+d und n = 1 ABO3-d: Ca(Fe,Mn,Ti)O3-d wurden Mischkristalle im System CaO - MnO_2 - Fe_2O_3 - TiO_2 aus den Oxiden und mittels Sol-Gel - Methode synthetisiert. Die Oxidationsstufen von Mn und Fe wurden mittels iodometrischer Titration bestimmt. Mößbauerspektroskopie wurde an der Universität Salzburg zur Bestimmung der Oxidationsstufe und Koordination von Fe durchgeführt. Neutronenbeugungsexperimente wurden zur Strukturverfeinerung einzelner Mischkristalle am BENSC Gerät E6 des Helmholtz-Zentrum Berlin für Materialien und Energie durchgeführt.

Verbindungen Ca(Fe,Mn,Ti)O3-d mit ABO3-d - Struktur kristallisieren bevorzugt in der Raumgruppe Pnma. Mit zunehmender Fe_2O_3 - Konzentration wechselt die Symmetrie zu Pm-3m. Der Phasenübergang ist ebenso abhängig von der Temperatur, wobei in eisenreichen Mischkristallen Ca(Fe,Mn,Ti)O3-d eine tetragonale Modifikation durch Hochtemperaturpulverdiffraktometrie identifiziert werde konnte [1] [2][3]. Mittels Mößbauerspektroskopie konnte die Entstehung von Sauerstoffleerstellen in Abhängigkeit der Fe - Konzentration indirekt erfaßt werden. Die Phasen Ca3(Fe,Mn,Ti)3O8+d (n = 3 A3B3O8+d) [4] [5] konnten nur in einem engen Bereich nebenphasenfrei synthetisiert werden, solange ausreichend Fe_2O_3 zur Besetzung der Tetraederposition vorlag und ein bestimmtes MnO2/TiO2 Verhältnis berücksichtigt wurde.

[1] Patrick M. Woodward, Acta Cryst.. B53, 32-43 (1997)
[2] Glazer, A. M., Acta Cryst. B28, 3384-3392. (1972).
[3] Glazer, A. M.,Acta Cryst. A31, 756-762. (1975).
[4] Rodriguez-Carvajal, J. Mat. Res. Bull., 24: p. 423-430. (1989)
[5] Nguyen N., et al., J. Solid State Chemistry,. 53: p. 398-405. (1984)

MS02-T4

Deposition of Sulfosalt Thin Films for Photovoltaic Application

J. Stöllinger[1], H. Dittrich[1]
[1]University of Salzburg, Materials Engineering and Physics, Salzburg, Austria

Sulfosalts are semiconductors with a high absorption coefficient due to their bandgap energies around the visible region of the solar spectrum (0,5eV to 2,5eV). This is the reason why these materials are interesting candidates for photovoltaic energy conversion in thin film solar cells. A number of 230 naturally grown and 30 synthetic sulfosalts are described and this large number is the basement of a high potential of possible candidates. As a member of the quaternary sulfosalt system Pb-Sb-Cu-S meneghinite $Pb_{13}CuSb_7S_{24}$ has shown a band gap of 1,44eV [1].

A method to produce meneghinite thin films in a 2 step process was investigated. In a first step the layers were sputtered on an unheated substrate. The thin films were grown with a CLUSTEX 100M cluster sputtering tool of Leybold Optics, by using RF sputtering method with argon as non reactive sputtering gas. As described in [2], an inhomogeneous target consisting of two halve discs of PbS and Sb_2S_3+10wt%CuS, was used to deposit layers. These layers were characterized by a linear concentration gradient.

In a second step post heat treatment was done in evacuated quartz ampoules, applying a defined sulfur vapor pressure. On specific substrate positions thin films of meneghinite were observed. The surface shows planar grown crystallites (see Figure 1). Composition was measured by microprobe. The Rietveld refinement of the XRD patterns show the following lattice constants: a = 11.349; b = 24.026; c = 4.108. These cell parameters fit well to the theoretical lattice parameters described in [3]. Physical properties of the layers will be given. Meneghinite layers grown on glass substrate or on Mo coated glass substrate show the same surface morphologies and diffraction profiles.

References:
1 H. Dittrich, A Stadler, D. Topa, Hermann-Josef Schimper, and Angelika Basch: Progress in sulfosalt research; Phys. Status Solidi A 206, No. 5, 1034-1041 (2009)
2 H. Dittrich, A Stadler, D. Topa, Hermann-Josef Schimper, and Angelika Basch: Thin film deposition of complex chalcogenide gradient layers by sputtering methods ; Phys. Status Solidi C 6, No. 5, 1141-1144(2009)
3 H. Strunz, E. Nickel: Mineralogical Tables 9th Edition, ISBN 3-510-65188-X,Schweizerbart (2001)

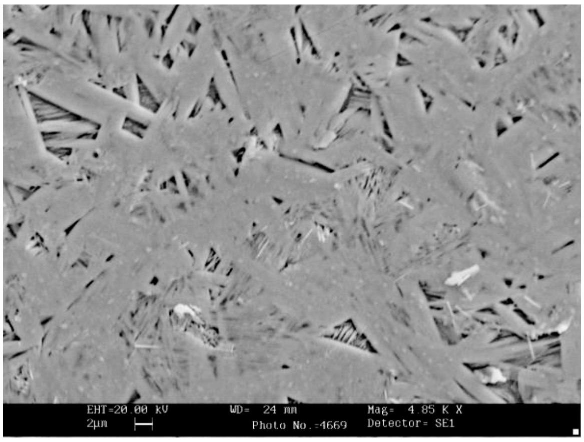

Figure 1: SEM image of the surface of meneghinite thin film layers.

MS02-T5
Thermoelektrisch und photovoltaisch relevante Dünnschichten und Whisker im System SnS-PbS

R. Kaden[1], G. Wagner[1], D. Unuchak[1], K. Bente[1]
[1]University Leipzig, Institut für Mineralogie, Kristallographie und Materialwissenschaft, Leipzig, Germany

Das System SnS - PbS bietet auf Grund der Mischkristallbildung $(Sn_{n-1}Pb_n)S$, mit $n \leq 0{,}55$ für die Randkomponente Teallit, und der hohen Randlöslichkeit von SnS im strukturarchetypen PbS bis 10 mol% vielversprechende Variationsmöglichkeiten photovoltaischer (PV) und thermoelektrischer (TE) Eigenschaften. Der Bandabstand E_g der Randkomponenten variiert von PbS 0.37 eV bis SnS 1.32 eV [1], Teallit 1.47 eV [2], mit optischen Absorptionskoeffizienten $\alpha > 10^4$ cm^{-1}. Maßgebend für TE-Anwendungen ist der Gütewert $ZT = T\sigma S^2/\kappa$ (σ - spez. elektr. Leitfähigkeit, S - Seebeckkoeffizient, κ - therm. Leitfähigkeit, bei Temperatur T). PbS bzw. SnS weisen geeignete Seebeckkoeffizenten von -700 - +370 bzw. bis +430 µV/K auf [3,4]. Die orthorhomb. Schichtstruktur SnS besitzt eine geringere therm. Leitfähigkeit (1.7 W/Km [4]) als das kubische PbS (2.2 - 2.5 W/Km [5]). Im Hinblick auf TE sollen deshalb vor allem Mischkristallzusammensetzungen SnS - Teallit untersucht werden, die auf Grund E_g zudem für PV favorisiert sind. Für Kompaktmaterial ermittelte s von 2.5 Ω^{-1}cm^{-1} für SnS [4] bis 4.4 Ω^{-1}cm^{-1} für PbS [5] sollen durch geeignete Dotierung mit Cu, Ag, Na oder Bi verbessert werden.

Bislang konnten mittels Hot-Wall-CVD dünne $(Sn_{n-1}Pb_n)S$-Schichten homogener Zusammensetzungen auf Glassubstrat hergestellt werden. Abhängig von den Züchtungsparametern zeigen die Schichten ausgeprägte 001-Textur, d.h. die Stapelfolge der Schichtstruktur liegt senkrecht zur Substratoberfläche. Zudem wurde erstmals die Kristallisation von $(Sn_{n-1}Pb_n)S$-Whiskern mit Ø < 300 nm auf dünnen Schichten gleicher Stöchiometrie beobachtet [6]. Das Wachstum dieser Whisker erfolgt über VLS-Mechanismus durch einen Zinntropfen. In gleicher Orientierung wie die darunterliegende Schicht wachsen diese Whisker in [001] und sind nur azimuthal gegeneinander verdreht. Solche Schichtpakete weisen Werte für σ bis 6 Ω^{-1}cm^{-1} und S bis +950 µV/K auf [7].

Unter Ausnutzung der Mischungslücke und der ähnlichen Gittermetrik sollen zukünftig auch chemisch scharf begrenzte, versetzungsarme Heterostrukturen aus den orthorhombischen und kubischen Mischkristallphasen auf Glas und einkristallinen Substraten hergestellt werden. Darüber hinaus sollen gezielt Whisker und Whiskerrasen erzeugt und deren VLS-Wachstumsmechanismus genauer aufgeklärt werden.

Referenzen
[1]S. I. Boldish, W. B. White, Am. Mineral. 83 (1998) 865
[2]B. Thangaraju, P. Kaliannan, Cryst. Res. Technol. 35 (2000) 71
[3]M. Telkes, American Mineralogist 35 (1950) 536
[4]J. D. Wasscher, W. Albers and C. Haas, Sol. Stat. Electron. 6 (1963) 261
[5]N. S. Popovich, Czech. J. Phys. 55 (2005) 739
[6]K. Bente, V. V. Lazenka, D. M. Unuchak, G. Wagner, V. F. Gremenok, Cryst. Res. Technol. 45 (2010) 643
[7]V. F. Gremenok, S. A. Bashkirov, V. A. Ivanov, D. M. Unuchak, V. V. Lazenka, K. Bente, J. Fizika 16 (2010) 3

MS02-T6
Kesterite type semiconductors for thin film solar cells

S. Schorr[1]
[1]Helmholtz-Zentrum Berlin für Materialien und Energie, Kristallographie, Berlin, Germany

The crystal structure of kesterite type compounds A neutron and X-ray diffraction study
Problems concerning enviromental and energy policy belong to the greatest challanges these days. For a long-term solution of the complex energy problem in Europe, the EU set the goal to produce 20% of total energy consumption from renewable energy sources by 2020. Photovoltaics, the direct conversion of sunlight into electrical energy, plays a key role within the renewable energies. Thin film solar cells using compound semiconductors as absorber material are foreseen as one of the most promising and cost-efficient technology.

The multinary chalcogenide Cu_2ZnSnS_4 (kesterite, CZTS) has newly attracted attention as possible photovoltaic material. Since the availability of indium is an object of concern regarding the large scale production of solar cells, its replacement with Zn and Sn is beneficial in this sense. Recently chemical based routes have allowed the synthesis of CZT(S,Se) based devices with a record power conversion efficiency of 9.66% [1].

The electronic properties of a polycrystalline heterojunction thin film solar cell are strongly influenced by the presence of electrical active defects. Especially the native defects in the compound semiconductor acting as absorber, are crucial. Starting with the phase relations in the Cu_2S-SnS-ZnS system discussing the question of stoichiometric CZTS, the atomic structure of the potential photovoltaic materials Cu_2ZnSnS_4 (CZTS) and $Cu_2ZnSnSe_4$ (CZTSe) is discussed on the basis of a structural analysis of neutron powder diffraction data refined by the Rietveld analysis. Both compounds were found to crystallize in the kesterite type structure, but with a disorder within the Cu-Zn layers at z=1/4 and 3/4. The latter causes Cu_{Zn} and Zn_{Cu} anti-site defects, whose concentration depend on the sample growth conditions [2]. Additional a comparative study of polycrystalline CZTS thin films by grazing incidence X-ray diffraction will be presented.

[1] T. Todorov et al., Adv. Mater. 22 (2010) E156-159
[2] S. Schorr, Sol. En. Mat. Sol. Cells 95 (2011) 1482-1488

MS02-T7

Crystal growth and properties of semiconducting sulfosalts in the Ag_2S-PbS-Bi_2S_3 system

S. Lobe[1], K. Bente[1], G. Wagner[1], R. Kaden[1]
[1]Universität Leipzig, Institute of Mineralogy, Crystallography and Materials Science, Leipzig, Germany

Sulfosalts represent a group of complex metal sulfides based on PbS and SnS archetypes. Owing to their semiconducting properties, they are suitable for photovoltaic or thermoelectric applications.

Lillianite, $Pb_3Bi_2S_6$, serves as a model for a large group of inorganic compounds, the lillianite homologues, with the tropochemical cell-twinning as characteristic similarity [1]. Substituting Pb in lillianite by the equation 2 Pb ↔ Ag + Bi leads to another lillianite homologue, gustavite $AgPbBi_3S_6$ [2]. Ikonić *et al.* [3] calculated a bandgap of about 1 eV for lillianite and semimetal properties for gustavite. The difference in the physical properties allows for tuning these properties in dependence to the chemical composition.

To investigate these materials in view of their crystallographic and physical properties powder samples, single crystals and thin films were synthesized.

Powder samples were prepared by solid state synthesis. Vegard's Law was validated for the complete solid solution range with X-ray powder diffraction. All lattice parameters showed a decrease with increasing silver + bismuth content.

Single crystals were synthesized via chemical vapor transport (CVT). The powder samples were used as raw material and I_2 and NH_4Cl as transporting agents. A low transport rate for silver was predicted by transport calculations and approved experimental. The grown single crystals with a characteristic needle-like morphology were investigated by SEM and XRD.

To increase the silver content a hot wall beam deposition construction for thin films was created. With this arrangement it is possible to heat three different binary compounds (PbS, Bi_2S_3 and Ag_2S) independently leading to manageable compositions on the substrate (glass, single crystals).

[1] E. Makovicky, N. Jahrb. Miner. Abh. **160** (3), 269-297 (1989)
[2] K. Bente, M. Engel and M. Steins, Z. Krist. **205**, 327-328 (1993)
[3] Z. Ikonić, G.P. Srivastava and J.C. Inkson, Phys. Rev. B **57**, 4557-4565 (1998)

MS02-T8

Al-doped Zincite (ZnO:Al) Thin Films for Transparent Conductive Oxide Applications

A. Stadler[1], J. Stoellinger[1], H. Dittrich[1]
[1]University of Salzburg, Material Research and Physics, Salzburg, Austria

Conventional materials, as indium-tin-oxide (ITO), used in light emitting diodes (LEDs) and solar cells, can be replaced by the price saving, synthetically produced, mineral zincite, if some few percent aluminum are added (ZnO:Al).

Pulsed direct-current (PDC) and radio-frequency (RF) magnetron sputtered aluminum doped zinc-oxides were prepared under different geometrical and temporary conditions within a Leybold Optics CLUSTEX 100M sputtering cluster tool. Therefore, sputter-depositions have been examined, referring to positions upon the thin-films, r, target-substrate distances, d_{TarSub}, and sputter durations, t_{Sp}. The influence of the equation of state for real gases (gas law) during the sputter process as well as the influence of typical plasma-parameters on the physical values of the sputtered ZnO:Al thin-films have been investigated. ZnO:Al thin-films were sputtered on boron silicate glass (BSG) substrates with different argon pressures, p, and substrate-temperatures, T, within the process-chamber as well as with different frequencies, f, (break times, t_{Br},) and sputtering powers, P. Moreover, ZnO:Al thin-films were produced with respect to reactive oxygen and inert nitrogen additions to the inert argon process-gas.

Advanced ultra-violet/visible/near infra-red (UV/Vis/NIR) spectroscopy measurements, with a Perkin Elmer Lambda 750 spectrometer, allow exact evaluations of refractive indices, n_L, permittivities, e_L, wave numbers, k_L, absorption coefficients, α_L, conductivities, σ_L, band gaps, E_g, effective doping concentrations, n_e, and lifetimes, μ. Conductivities were also measured with a Lucas Labs Pro4 four-tip measurement system (see fig. 1). Additional X-ray diffraction (XRD) measurements (Siemens D500 powder diffractometer) allowed structural analyses, i.e. average crystal diameters, d_{cry}, preferred orientations and lattice parameters, a, b, c. Quantitative chemical analyses were performed with a JEOL JXA-8600 electron microprobe.

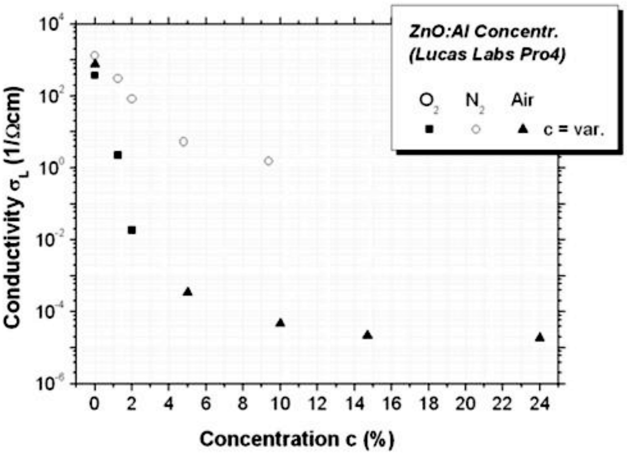

Figure 1: Conductivity measurements as a function of the concentration of O_2, N_2, and air

MS03-T1

Fluids and charnockite formation during high-grade granulite-facies metamorphism in southern India

D.E. Harlov[1]

[1] Deutsches GeoForschungsZentrum, Potsdam, Germany

In a regional high-grade metamorphic terrane representing a cross section of lower Archean crust, (Dharwar craton, Tamil Nadu, S India), the transition going from amphibolite-facies into granulite-facies rocks is characterized by a series of chemical trends, which include whole-rock depletion of Rb, Cs, Th, and U; enrichment in Ti and F and depletion in Fe and Mn in biotite and amphibole; increases in Al and decreases in Mn in orthopyroxene; enrichment of fluorapatite in F; and an increasing oxidation state characterized by coexisting hemo-ilmenite (up to 60% hematite) and magnetite where magnetite is commonly rimmed by pyrite (Harlov and Hansen, 2005, J Met Geol, 23, 241; Hansen and Harlov, 2007, J Petrol, 48, 1641). K-feldspar micro-veins, along quartz-plagioclase grain boundaries, are widespread. In the amphibolite-facies portion of the traverse the principal REE-bearing minerals are allanite and titanite partially replacing ilmenite. The orthopyroxene-in isograd is characterized by a 5 - 10 km wide zone rich in clinopyroxene. Here independent monazite grains are the major REE- and Th-bearing phase. In the granulite-facies rocks fluorapatite, commonly characterized by extensive Th-free monazite inclusions, is the principle REE-bearing phase. During prograde metamorphism, titanite and allanite were replaced by independent monazite, which were replaced by REE- rich fluorapatite in which extensive monazite inclusions later formed. The loss of independent monazite was accompanied by a loss of whole-rock Th. This suggests that mineral hosting of REE follows certain general trends, which are a function of metamorphic grade, whole rock chemistry, and intergranular fluid chemistry. Actinide whole rock chemistry is reflected in the depletion of U and Th in the zircon rims along the traverse, which also give a consistent date of 2520 - 2500 Ma for the metamorphic event. Most mineralogical features along the traverse can be accounted for by progressive dehydration and oxidation reactions. Trace element depletion is best explained by the action of an externally derived low-H2O activity KCl-NaCl brine, with a possible oxidizing component (e.g. CaSO4), migrating from a source at greater depth, possibly preceded or accompanied by partial melting. Similar trends are not limited to southern India are also seen in crustal cross sections from Rogaland-Vest Agder, SW Norway (Bingen et al., 1996, Geochim Cosmochim Acta, 60, 1341) and the Val Strona, Ivrea-Verbano Zone, N Italy (Harlov and Förster, 2002, J Petrol, 43, 769; Harlov and Förster, 2002, J Petrol, 43, 801).

MS03-T2

EMP monazite age dating enhanced with automated mineralogical methods and its application in the polymetamorphic Saualpe basement (Eastern Alps)

B. Schulz[1]

[1] Institut für Mineralogie, Lagerstättenlehre und Petrologie, Freiberg/Sachsen, Germany

Although limitations exist, the *in situ* non-isotopic chemical Th-U-Pb dating of monazite by analysis with an electron microprobe turned out to be an appropriate method to constrain multiple thermal events in polymetamorphic basement terranes. The Austroalpine Saualpe basement in the Eastern Alps is composed of nappes. There are 4 allochthonous units (Phyllite, Micaschist, Eclogite and Preims Unit toward the footwall), which overlie a basement labelled as the Kliening Unit. Cretaceous eclogite-facies metamorphism, but also Permian and older metamorphic events have been reported. On one hand the occurrence of monazite in metapelites is limited to Ca-poor bulk compositions and/or the mineral reactions and phase stabilities of garnet and xenotime along the pressure-temperature paths. On the other hand the EMP monazite dating offers the potential to investigate numerous samples. This requires an efficient procedure of sample selection.

A SEM Quanta 600 FEG (FEI Company) with EDX and mineral liberation analysis software (MLA version 2.9) was used for automated quantification of the mineral mode (150.000 EDX spots per sample) as well as the identification of monazite, xenotime, zircon and Th-minerals in thin sections of garnet micaschists. These phases were located by the rare phase search mode (SPL) which combines BSE graytone and EDX chemical analysis. The SPL mode also delivers a map of phases surrounding the target minerals and thus provides a catalogue of monazite grains and associates in a sample. Monazite grains then were analysed by electron microprobe JEOL JXA 8200 using routines and standards reported in Schulz et al. (2007).

Large monazites mantled by double coronas of apatite and allanite yielded exclusively Permian ages. They appear in the Eclogite Unit, but also in the Preims and the Micaschist units. Satellite structures consist of numerous small Cretaceous-age monazites arranged around apatite and allanite. Distinctly zoned monazite grains with older cores and Cretaceous rims and also grains with both age groups are rare. The Cretaceous (~80-100 Ma), Permian (~250-270 Ma) and Variscan (310-320 Ma) age groups of monazite are variably distributed in individual samples. In the Kliening Unit the Cretaceous ages prevail. In the Preims Unit the Permian ages are abundant. In the Eclogite Unit there are samples with predominant Permian or Cretaceous ages, but also with both age groups. In the Micaschist Unit the Permian ages prevail again. There is a tendency that samples with many grain counts of xenotime have dominantly Cretaceous monazite. The observation of the numerous large Permian monazites with high Y contents implies a pre-Alpine amphibolite-facies metamorphism. Eclogite-facies Cretaceous metamorphism apparently led only to limited new crystallization of monazite with lower Y contents.

Schulz B, Brätz H, Bombach K, Krenn E (2007) Z. Angewandte Geol. 35, 377-392

MS03-T3

Formation and alteration of zircons in Archaean granitoids from Swaziland: Combined insights from CL-imaging, trace element, δ^{18}O, U-Th-Pb and Lu-Hf isotope analyses

A. Zeh[1], A. Gerdes[1], R. Stern[1,2]

[1] Institut für Geowissenschaften, FE Mineralogie, Frankfurt am Main, Canada

[2] Canadian Centre for Isotopic Microanalysis (CCIM), Department of Geosciences, Edmonton, Canada

This study presents results of a detailed investigation of zircon domains from 15 granitoid samples from the Swaziland, which comprises the oldest crust of the Kaapvaal Craton, with magma emplacement ages between 3.66 and 2.70 Ga. The results of this study show that zircon populations in all investigated granitoids show significant internal variations with respect to their U-Pb ages, REE patterns, and δ^{18}O (SMOW) - far beyond analytical uncertainties, but show within error identical initial ^{176}Hf/^{177}Hf isotope compositions. These patterns are most pronounced for the oldest rocks from Swaziland, comprising the 3.65 Ga TTG gneisses from Piggs peak. CL/BSE images of zircons reveal clear core-rim relationships for many zircons, but also zircons with complex zoning patterns perhaps related to several stages of alteration. Pb-Pb ages of the "magmatic" zircon cores scatter between 3.65 to 3.26 Ga, Th/U = 0.32 to 1.12, δ^{18}O = 5.4 to 3.4‰. Furthermore, they show steep to moderate chondrite normalized LREE-patterns with a positive slope (La/Sm$_N$=0.002 to 0.09). In contrast, the "metamorphic" rims commonly show diffuse zoning patterns in CL, and lower Pb-Pb ages (3.28 to 3.20 Ga), Th/U (0.01 to 0.3) and $\delta^{18}O$ (1.3 to 1.7‰), and a negative slopes in LREE patterns (La/Sm$_N$ = 2.8-3.5). Despite these differences, the analyses of all domains yielded identical initial $^{176}Hf/^{177}Hf$ of 0.28040 ± 0.00004 (2 SD). This indicates that all zircon domains (core, rims, alteration zones) were initially formed during magma crystallisation at ca. 3.65 Ga, and that the different domains were differently affected by subsequent alteration processes, causing a reset of the U-Th-Pb system, and dramatic changes of the REE patterns and $\delta^{18}O$, but left the hafnium isotope system unaffected. The low $\delta^{18}O$ of the zircon rims + altered domains (1.5‰) indicate that they probably formed by interaction with hot meteoric water. This interpretation is consistent with the strongly elevated LREE contents. These hydrothermal fluids obviously also altered some of the magmatic cores (5.3-4.1‰), even such which still look pristine in CL images and with concordant U-Pb ages! This observation has clear consequences for the interpretation of the Hadean detrital zircons. Taking the data from the most pristine zircon domains from all investigated Swaziland granitoids, reveal that the oldest exposed rocks of the Kaapvaal Craton rocks (3.65-3.44 Ga) were formed by reworking of an much older mafic crust (with hafnium model ages >3.9 Ga), that new juvenile crust was formed between 3.6 and 3.3 Ga (by direct melting of hydrated mafic crust), and that successive crust reworking (with sediment involvement) took place between 3.3 and 2.72 Ga.

MS03-T4

Fluid-mediated equilibration and self-irradiation in complex euxenite-zircon assemblages of pegmatites from South Norway; implications for U-Pb geochronology

C. Duran[1], A.-M. Seydoux-Guillaume[1], B. Bingen[1,2], P. de Parseval[1], D. Guillaume[1], V. Bosse[3], J.-L. Paquette[3], J. Ingrin[4]
[1]GET-UMR 5563 CNRS-Université de Toulouse, OMP, Toulouse, France
[2]Geological Survey of Norway, Trondheim, Norway
[3]LMV-UMR 6524 CNRS-Université Blaise Pascal, Clermont-Ferrand, France
[4]UMET-UMR 8207 CNRS Université de Lille 1, Lille, France

In most rocks, uranium and thorium are concentrated in few minerals providing favorable crystallographic sites such as zircon, monazite, titanite, and rarely uraninite, thorianite, thorite / huttonite, euxenite, etc ... These minerals are submitted to intense self-irradiation that can lead to amorphization and also modify their environment by irradiating the host minerals. Here, we focus on accessory minerals (zircon, monazite, euxenite, xenotime) in pegmatites from southern Norway (Iveland-Evje); some of these minerals are rich in U (e.g. up to 15wt % for euxenite). A complex paragenesis (zircon + monazite + xenotime + euxenite) was studied in details by multiple methods including optical and electron microscopy and U-Pb geochronology (SIMS and LA-ICP-MS). The aim is to connect textural observations to geochronological signals obtained in these minerals. All observations show that complex relationships exist between the different minerals (especially zircon-euxenite) and the various processes (alteration by fluids and radiation effects) which have repercussions on the U-Pb geochronology response. Irradiation (self and out), destroy the crystal lattice (amorphization) promoting the alteration of more or less amorphous phases (by diffusion-reaction or dissolution-precipitation mechanisms, depending to minerals). Amorphization induces volume increase, leading to the formation of cracks which eventually connected into a network through the rock. This fracturing allows fluid circulation and promotes recrystallization and remobilization of elements (e.g. Ca enrichments, incorporation of OH in the altered zones of zircon and euxenite, Pb loss, Pb precipitating as galena ...). All of these processes have important repercussions on the geochronological signal. Analyses carried out within altered areas give discordant ages reflecting Pb-loss and/or incorporation of common Pb thus leading to disturbed geochronological information.

MS03-T5

Modeling magma differentiation processes in volcanic systems: Key examples from Klyuchevskoy, Bezymianny and Mutnovsky volcanoes, Kamchatka

R. Almeev[1], A. Ariskin[2], R. Botcharnikov[1], F. Holtz[1], T. Shishkina[1], M. Portnyagin[3], J.-I. Kimura[4], A. Ozerov[5]
[1]Leibniz University of Hannover, Institute of Mineralogy, Hannover, Germany
[2]Vernadsky Institute, Moscow, Russian Federation
[3]IFM-GEOMAR, Kiel, Germany
[4]JAMSTEC, Yokosuka, Japan
[5]Institute of Volcanology and Seismology, Petropavlovsk-Kamchatsky, Russian Federation

The key aspect of understanding magma differentiation processes is related to the mechanisms and thermodynamic conditions (P-T-fO_2-aH_2O) at which primary and parental basaltic magmas can generate derivative magmas resulting in the formation of tholeiitic, calc-alkaline, and other magmatic series. Several thermodynamic and empirical models have been developed to predict melting-crystallization relations in basaltic to rhyolitic melts in a wide range of thermodynamic conditions in closed to open magmatic systems (*e.g.* MELTs, COMAGMAT, Petrolog). In practice, however, despite the great efforts in improving models, calculations still yield unsatisfactory results in the prediction of the calculated liquid lines of descent, especially in the presence of H_2O at elevated pressures. On the basis of our new experimental data the COMAGMAT model has been recently refined, allowing one to predict effect of H_2O on phase equilibria more correctly. In this work we demonstrate an application of the refined COMAGMAT model to constrain magma differentiation processes for calc-alkaline series of Klyuchevskoy-Bezymianny volcanoes and low-K tholeiitic series of Mutnovsky volcano.

Mutnovsky volcano. The new version of the COMAGMAT program was initially verified using results of our crystallization experiments on Mutnovsky basalt performed in hydrous conditions at 100 and 300 MPa. The optimal model of Mutnovsky magma evolution was obtained as a result of Ol+Pl+Cpx±Mt polybaric fractionation between 5 and 1 kbar. The existence of magma differentiation at shallow depths and the hydrous (~2 wt% H_2O) character of Mutnovsky magmas are confirmed by the study of melt inclusions, experimental investigations at 100 and 300 MPa as well as by the simulations of Mutnovsky liquid lines of descent.

Klyuchevskoy volcano. The high-magnesian (HMB) to high-alumina (HAB) basaltic suite of Klyuchevskoy volcano has been reproduced by 40% fractionation of Ol-Aug-Sp assemblages during ascent of the parental HMB magma. In contrast to previous estimates, our new calculations demonstrate more shallower depths of initial magma generation (14-15 kbar, 1-2 wt.% H_2O in initial melt). The magma fractionation occurs in the pressure range of 15-2 kbar and typical high-alumina basaltic liquids are formed between 2 and 4 kbar.

Bezymianny volcanoes. Our simulations demonstrate that Bezymianny andesitic and dacitic melts can not be produced by HAB crystallization at isobaric conditions as was suggested in our earlier works. Indeed the Bezymianny petrochemical trend can be only reproduced by polybaric crystallization in the course of magma ascent (5-0.5 kbar) with a slower (in comparison to Klyuchevskoy) pressure release rate of 0.1 kbar/% cryst. The silica enrichment trend of Bezymianny volcanics is explained by the early crystallization of magnetite in hydrous andesitic melt.

MS03-T6

Domain structure in fine-grained orthopyroxene-plagioclase-spinel symplectite in basanite hosted mantle xenoliths from Zinst (Bavaria)

R. Abart[1], G. Habler[1], P. Spacek[2,3]
[1]Universität Wien, Dept. Lithosphärenforschung, Wien, Austria
[2]Insitute of Geophysics ASCR, Prague, Czech Republic
[3]Insitute of Earth Physics, Brno, Czech Republic

Lherzolite xenoliths in the Oligocene basanites from Zinst (Bavaria, western Bohemian Massif) contain several-millimetre sized patches of fine grained orthopyroxene- plagioclase-spinel symplectites, which, based on their integrated composition, are interpreted as pseudomorphs after pyrope-rich garnet. The typical grain size of Opx and Pl in the symplectite is on the order of a few micrometers. Spinel is present as sub-micron sized inclusions in Opx. Symplectite formation supposedly took place during decompression and possibly heating prior or synchronous to the entrainment of the xenoliths into the basanitic magma.

The Opx, Pl and Spl grains show a shape preferred orientation and are loosely arranged in layers so that the symplectite attains a weak lamellar appearance. Lamellae are straight or slightly curved within domains of several tens of micrometer size, whereas their orientation changes abruptly at domain boundaries. EBSD analysis reveals that the crystallographic orientations of Opx, Pl and Spl also change at domain boundaries. Within the individual domains Opx and Pl grains form grain or subgrain aggregates, which display gradual orientation changes up to 30° misorientation within single symplectite domains. Orientation changes are continuous along the lamellae, whereas discontinuous orientation changes are observed across the lamellae. Opx and Pl orientation maxima of different symplectite domains show more than 40° misorientation. Submicron sized Spl inclusions in Opx also show crystallographic orientation maxima within single symplectite domains where Spl (111) seems to coincide with Opx (100) planes. On the other hand no orientation relation between Opx/Spl and Pl has been observed.

Symplectite phases are usually elongated in the direction perpendicular to the reaction front with the precursor phase. The change in shape preferred orientation across domain boundaries indicates a reaction front geometry with lobes of symplectite protruding into the precursor Gt and spikes of remnant Gt pointing into the symplectite. When these spikes retreat they leave behind a suture where symplectite phases with different shape and crystallographic preferred orientation meet. Transformation of garnet into an Opx-Pl-Spl symplectite implies a volume increase of more than10 percent. Due to the complex geometry of the reaction front the transformation strain associated with symplectite formation leads to a heterogeneous stress distribution, which may be responsible for the observed variations in shape and crystallographic preferred orientation of the symplectite phases within a single domain.

MS03-T7

Plagioclase-bearing mantle lherzolites from the Central Dinaridic Ophiolite Zone (CDOB, NE Bosnia and Herzegovina) - evidences of upper mantle metasomatism

B. Segvic[1], R. Altherr[2]
[1]Technische Universität Darmstadt, Institute for Applied Geosciences, Darmstadt, Germany
[2]Ruprecht-Karls-Universität Heidelberg, Institute for Earth Sciences, Heidelberg, Germany

Fertile lherzolites (Krivaja-Konjuh ophiolite complex in CDOB), having modal mineralogy composed of Ol, Opx, Cpx, Sp and occasionally Pl, are subject of this study. Plagioclase is reported as a subhedral matrix phase and depending on its presence, one is able to distinguish two main peridotite masses, *i.e.* Sp and Pl lherzolites, placed opposite to each other (Šegvić 2010). We believe that plagioclase formation in the CDOB peridotites followed the incongruent reaction (Al-rich Sp + $\text{melt}_1 \leftrightarrow$ Cr-rich Sp + Pl + melt_2) resulting in an increased Cr# of spinel. Here, we report on evidences, which tend to be indicative for such subsolidus metasomatic processes.

Olivine shows chemical homogeneity (Fo ~90). The NiO abundances of both rock varieties fit the range from 0.32 to 0.46 wt%, but in Pl bearing rocks we detected a discrete olivine mineralization with a low NiO content ranging from 0.33 to 0.35 wt%. Such a peculiar mineralization is interpreted to be due to low crystallisation degrees of impregnation melts that coexisted with the host peridotite. For Opx and Cpx, the data show similar Mg# (88.9-90.5 and 88.2-94.4), Al_2O_3 (1.40-6.21and 1.45-7.16 wt%), Cr_2O_3 abundances (0.27-0.97 and 0.06 to 1.72 wt%) and CaO (0.32-3.23 and 18.1 to 24.3 wt%) for both lherzolite varieties respectively. The abundances of Al_2O_3 and Cr_2O_3 in Opx and Cpx are positively correlated, displaying a significantly higher correlation for Pl lherzolites (r^2 = 0.56 and 0.76) as compared to Sp lherzolites (r^2 = 0.13 and 0.28). The positive correlation between Cr and Al in pyroxene cannot be interpreted through partial melting and it rather indicates Cr and Al exchange processes related to subsolidus reequilibration. The latter is further indicated by double Ti values in both pyroxenes from Pl lherzolites (~0.005 vs ~0.002 and ~0.012 vs ~0.007 p.f.u., respectively). The Cr# in spinel ranges from 7 to 50, and from 30 to 50 for Sp and Pl lherzolites, respectively. Furthermore, the average TiO_2 content of spinel from Pl lherzolite is around 0.48 wt%. Combined with high Cr#, this suggests subsolidus metasomatism. Plagioclase is mostly bytownite, showing the oscillatory saw-tooth zoning typical for upper mantle impregnation triggered by decompression.

In Pl bearing lherzolite, the LREE abundances are progressively elevated, approaching the shape of "flat" or slightly sigmoid REE patterns (~ 1 x chondrite). In Alpine ophiolites, this feature is reported in those peridotites that underwent metasomatic changes. All the Pl lherzolites containing Ti-rich clinopyroxene (parametre set as a fertilisation indicator) show high $(Ce/Sm)_N \approx 1$.

Peculiarities in mineral chemistry presented here, along with the whole-rock LREE enrichment suggest that subsolidus melt metasomatism of related mantle regions operated during the final stage of peridotite equilibration.

References:

Šegvić, B. (2010), Petrologic and geochemical characteristics of the Krivaja-Konjuh ophiolite complex (NE Bosnia and Herzegovina) — petrogenesis and regional geodynamic implications, Dr. rer. nat. thesis, Heidelberg University, 301 p

MS03-T8

Solubility of Au and Mo in volatile-bearing magmas

R. Botcharnikov[1], R. Linnen[2], F. Holtz[1], M. Wilke[3]
[1]Leibniz Universitaet Hannover, Institut für Mineralogie, Hannover, Germany
[2]University of Western Ontario, Department of Earth Sciences, London, Ontario, N6A 5B7, Canada
[3]Helmholtzzentrum Potsdam Deutsches GeoForschungsZentrum (GFZ), Potsdam, Germany

Magmas are important sources of metals which they mobilize at depths of magma generation and transport to subsurface ore deposits. The behaviour of many ore metals is governed by temperature, redox conditions in magmas and by the activity of volatile components, in particular, H_2O, S, and Cl. Natural observations and experimental data show that the mobility of metals in magmatic environment is strongly controlled by the presence of sulphide phases and complex magmatic fluids due to very high partition coefficients of metals. Here we present new experimental data illustrating that S and Cl have contrasting effects on the solubility of Au and Mo in silicate melts as fO_2 increases from reducing to highly oxidizing conditions. The experiments at 200 MPa and at 1050°C conducted in andesitic systems show that the highest gold solubility (by upto 6 ppmw) in S-bearing magmas is observed at redox conditions characterized by sulfide-sulfate transition (i.e., Au concentration exposes a pronounced maximum). Within this redox range, Au is found to be particularly mobile and is dissolved in silicate melts as a sulphide-bearing component. With further increase in fO_2, the solubility of Au drops dramatically to the level observed in S-free melts (i.e., to 0.5 ppmw). On the contrary, the solubility of gold in S-free but Cl-bearing magmas increases with the concentration of Cl at given fO2, and Cl-enriched magmas can dissolve almost exponentially increasing amounts of gold with increasing fO_2 (upto 15-20 ppmw at highly oxidizing but still geologically relevant conditions). The solubility of Mo is less affected by the presence of S and Cl, resembling no maximum in S-bearing systems in contrast to the solubility behavior of Au. Nevertheless, both S and Cl increase Mo solubility in the silicate melts, and its solubility values strongly depend on the melt composition, increasing from 100-200 ppmw in rhyolitic to 2-3 wt% in andesitic melts. Such a behavior is in contrast to that of Au, which concentrations is almost independent on magma composition from basalt to rhyolite.

The observed contrasting solubility of Au and Mo in S- and Cl-bearing magmas at different redox conditions implies that the presence of S would favour gold transport in a narrow range of sulfide-sulfate transition, whereas Cl is expected to take control over the mobility of gold with progressive magma oxidation. The solubility of Mo increases with fO_2 and decreases with magma differentiation, while the effects of S and Cl are less pronounced in comparison with that for Au. Thus, small variations in the activities of volatiles and redox conditions in natural magmas can lead to mobilization or fixation of Au and Mo as well as to their fractionation during magmatic evolution. Hence, the relative changes in these parameters should be considered for the interpretation of natural magmatic processes leading to the formation of ore deposits.

MS04-T1

Spin transition in Fe-bearing perovskite: implications for the lower mantle

R. Caracas[1]
[1]CNRS, Ecole Normale Superieure de Lyon, Laboratoire de Geologie, Lyon Cedex 07, France

The Earth's lower mantle, which is the largest part by volume of our planet, is mainly formed of Fe- and Al- bearing $MgSiO_3$ perovskite (pv).

The Fe2+ component exhibits a spin transition under pressure whose nature and outcome is still a matter of debate. Here we are using lattice dynamical calculations based on density functional perturbation theory to disentangle a part of its complex phase diagram and the spin behavior. To do this we investigate the dynamic stability of Pbnm FeSiO3 pv and show the existence of unstable phonon modes. We track the eigen-displacements of the phonons modes to find low-spin and intermediate spin states. On solid-state physical basis we explore a set of hypothetical structures with various spin configurations and considerably lower enthalpy than the parent orthorhombic Pbnm structure. We show that the spin evolves along a high-spin to mixed high- and intermediate spin to low-spin transition sequence. We also analyze the thermal behavior of both high-spin and low-spin phases along the entire Mg-Fe solid solution and we discuss a first thermal phase diagram.

We discuss some of the implications of the spin transition on the physical properties of pv. We show that the elastic moduli and the bulk seismic wave velocities are weakly affected by the spin transition. However, the intrinsic differences in seismic anisotropy between the high-spin and low-spin phases of Fe2+-bearing pv coupled with lattice preferred orientation that can develop during mantle flow lead to distinct seismic signatures between the top and the bottom of the lower mantle [1]. These signatures are detectable by seismic observations and they need to be taken into account in tomographic studies of the Earth's lower mantle. We find that the electronic gap widens during crossover to the low-spin phase. This has a direct influence on the electrical conductivity and agrees qualitatively with in situ measurements [2]. We show that the spin transitions in Fe2+-bearing pv can be observed experimentally in X-ray diffraction and Raman measurements.

In the presence of Al, the Fe3+ component exhibits a spin transition, which is associated with an Al/Fe3+ site exchange and with the phase transition to post-pv [3]. However the transition is invisible for seismology [3].

[1] Caracas, Mainprice, and Thomas (2010) Geophys. Res. Lett. 37, L13309. [2] K. Ohta, et al. (2008) Science 320, 89. [3] Caracas (2010) PEPI 182, 10-17. [3] Caracas (2010) GRL 37, L20306.

MS04-T2

Orbital ordering in the ferromagnetic phase of the kagome staircase compound $Co_3V_2O_8$

N. Narayanan[1], N. Qureshi[2], H. Fuess[1], H. Ehrenberg[3]
[1]Materials Science, Structural Research, Darmstadt, Germany
[2]University of Cologne, Institute of Physics II, Cologne, Germany
[3]Karlsruher Institute of Technology, Institute for Applied Materials, Karlsruhe, Germany

The ortho-oxo vanadate $Co_3V_2O_8$ (CVO) crystallizes in the orthorhombic space group Cmca. Its crystal structure is characterized by edge sharing CoO_6 octahedra forming buckled layers of corner-sharing triangles, the kagome staircases, which are separated along the b axis by VO4 tetrahedra [1]. Both CVO and its Ni counterpart NVO exhibit rich magnetic phase diagrams due to competing exchange interactions [2,3]. The ferromagnetic (ground state) structure of CVO consists of two Co sites (cross-tie and spine), which exhibit different magnetic moments of 1.54 and 2.73 μ_B. The reduction of the magnetic moment of the former is attributed to frustration effects although both Co^{2+} are in a high spin state [1]. In the present work the orbital occupation of both Co is investigated with density functional theory. Although the high spin state of both Co could be reproduced, there is a difference between both Co regarding the occupation of the d orbitals. This orbital ordering is interpreted in terms of the oxygen octahedras at both Co sites and the behaviour of it is investigated by applying different corrections to the exchange-correlation potential (LSDA+U). The latter emphasizes the relationship between the orbital ordering and the density of states (DOS) in the vicinity of the Fermi level in CVO. The results are interpreted in terms of DOS, Wannier-functions and spin-density maps. The latter is compared to the experimentally obtained spin-density in [1].

[1] N. Qureshi, M. Zbiri, J. Rodríguez-Carvajal, A. Stunault, E. Ressouche, T. C. Hansen, M. T. Fernández-Díaz, M. R. Johnson, H. Fuess, H. Ehrenberg, Y. Sakurai, M. Itou, B. Gillon, T. Wolf, J. A. Rodríguez-Velamazan, and J. Sánchez-Montero, Phys. Rev. B **79**, 094417 (2009). [
2] N R Wilson, O A Petrenko, and G Balakrishnan, J. Phys.: Condens. Matter **19**, 145257 (2007).
[3] Y. Chen, J. W. Lynn, Q. Huang, F. M. Woodward, T. Yildirim, G. Lawes, A. P. Ramirez, N. Rogado, R. J. Cava, A. Aharony, O. Entin-Wohlman, and A. B. Harris, Phys. Rev. **B 74**, 014430 (2006).

MS04-T3

Surface energy and bond energy calculations of *fcc*- and *bcc*-metals by application of the bond deficiency model

A. Mutter[1], L. Peters[2]
[1]Institute of Geosciences, Mineralogy, Kiel, Germany
[2]RWTH, Institute of Crystallography, Aachen, Germany

The aim of this study is to present a bond-valence application and methodology which is capable to calculate the surface energies and bond energies of *fcc*- and *bcc*-metals. Until now, the bond-valence theory has proven to be a valuable tool to determine the accuracy of experimentally derived crystal structures. But even though all of these applications are based on the interaction between bond-length and bond-valence no model exists to correlate bond-length and bond-valence to bond-energy, and thus to the surface energy of a crystal face. Here we will present two alternative, but as well, combinable methodologies, to derive both the bond-energy as well as the surface energy of *fcc*- and *bcc*-metals.

This approach is closely related to the well established broken-bond-model of Mackenzie et al. (1962) and the bond-valence deficiency model of Mutter (2007). The presented study is based on the assumptions that *i*) the bond strength and the atomic coordination in the crystal structure are constant for a given metal and *ii*) a simple relationship exists between the surface energy, the *d*- spacings and the standard enthalpy of formation ΔH_f.

In the first part we introduce the correlation factors $C_{(fcc)}$ and $C_{(bcc)}$, derived from the bond-deficiency of the crystal surfaces, and we deduce a linear relationship between the lattice spacing and the surface energy of the bulk-termination of *fcc*- and *bcc*-metals. This relationship is than linked to the standard enthalpy of formation ΔH_f.

In a second approach we deduce the bond energy form the exponential relationship between the bond-length and the corresponding bond-valence. Again this relationship is linked to the standard enthalpy of formation ΔH_f and thus the bonding energy of an atom. Having determined the bond energy for different bond length and by summation of the bond deficiency of a crystal surface the corresponding surface energy can be obtained.

Last we will present the surface energies for 10 surfaces of *fcc*-metals Cu, Ni, Ag, Al, Au, Pd, Pt, Rh, Ir and 6 *bcc*-metals Mo, W, V, α-Fe, Nb and Ta having been calculated using our model. The results presented agree well with the results of other established models.

References

(1) J.K. Mackenzie, A.J.W. Moore and J.F. Nicholas (1962) Bonds broken at atomically flat crystal surfaces I: Face-centered and body-centered cubic crystals. J. Phys. Chem. Solids 23 (1962) 185.
(2) Mutter, A. (2007): The bond-valence deficiency model: A new application to describe mineral surface reactions. URN: urn:nbn:de:hbz: 6-98539587759. (Thesis).

MS04-T4

Crystal structure prediction as tool for crystal engineering of co-crystals. The prediction of free lattice energies and its effect on thermodynamic properties, e.g. solubility

L.N. Kuleshova[1], D.W.M. Hofmann[1]
[1]CRS4, Energy and Environment, Pula, Italy

Nowadays crystal structures can be predicted quite successfully, as it has been shown in the last two “Blind Tests” in Cambridge. All current methods of prediction consist of two main steps: a crystal structure generation and a sorting according a scoring function. It was found that within a few KJ hundreds of possible polymorphs can exist, therefore a correct prediction of the experimental polymorph requires a very accurate scoring function. Obviously this scoring function has to be the free energy and comprise intrinsically temperature and pressure.

The challenging application to theoretical crystallography is the crystal engineering, which is aimed to predict and, consequently, to create crystals with desired target properties. The basic characteristics determining nearly all physico-chemical properties of crystalline solids are the symmetry of crystal package and the free energy of lattice formation. Here to estimate the free lattice energy we use the very quick algorithm *FlexCryst.* This algorithm, how we demonstrated previously [1], for the most cases allows to predict correctly the typical synthons for the given crystal structure and, as consequence, allows a proper estimation (within +/- 2KJ) for the free lattice energy.

We will demonstrate that the accurate prediction of the free energy of crystal package opens the excellent opportunity to estimate relative stability of polymorphs, to predict the formation of cocrystals, and to estimate the change in physico-chemical properties (e.g. solubility) of cocrystals in comparison with the crystals of the pure components. [1] D.W.M. Hofmann, L.N. Kuleshova, M.Yu. Antipin. Supramolecular syntons and crystal structure prediction of organic compounds, Crystal Growth & Design 4 (2004) 1395-1402.

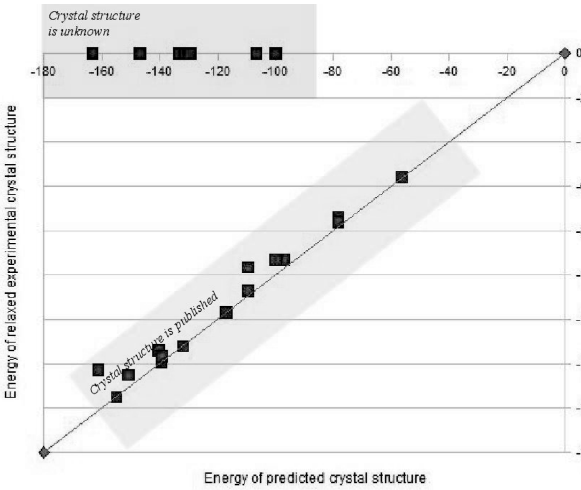

Figure 1: Lattice energy of the experimental crystal structure vs. predicted crystal structure

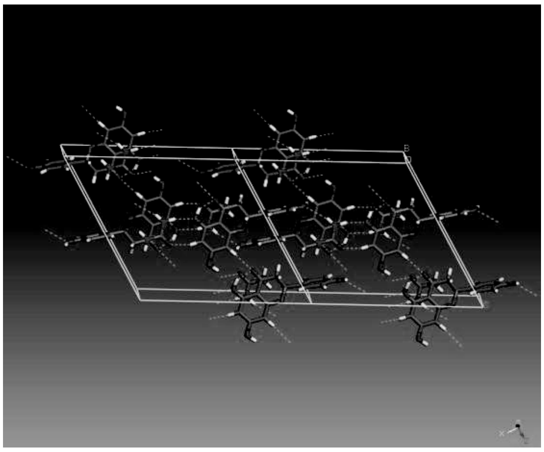

Figure 2: Synthons of a predicted cocrystal (naringenin + urea)

MS04-T5
New Developments on the Bilbao Crystallographic Server

M.I. Aroyo[1], J.M. Perez-Mato[1], D. Orobengoa[1], E.S. Tasci[1], G. de la Flor[1], S.V. Gallego[1]
[1]University of the Basque Country, Condensed-Matter Physics, Bilbao, Spain

The Bilbao Crystallographic Server (http://www.cryst.ehu.es) [1] is a web site offering online crystallographic tools and databases that are collected in different shells aimed at various purposes. The first shell holds referential information including data from the *International Tables for Crystallography*, Vol. A: *Space Group Symmetry*; Vol. A1: *Symmetry Relations between Space Groups* and Vol. E: *Subperiodic Groups*, as well as the wave-vector database with the Brillouin-zones figures for all space groups. There are shells including tools for group-subgroup relations between space groups, their representations and applications in solid state physics and chemistry. The Bilbao Crystallographic Server is freely available in the web since 1997 and since then is being further developed and improved. The purpose of the present contribution is to report on the current state of the server, emphasizing the newly developed tools and the improvements.

Based on the recent compilations of magnetic space groups [2,3], we have started with the development of a Magnetic Space Groups Database. At the moment the database includes basic crystallographic data of the magnetic space groups, such as general positions (symmetry operations in matrix form and their geometrical interpretation), special Wyckoff positions, site-symmetry groups, *etc*. Making use of the database, we have developed an interactive program MAGNEXT for the systematic computation of the extinction rules for magnetic non-polarized diffraction that is useful for the systematic analysis and determination of magnetic symmetry of a given material.

Of particular interest is the set of structure-utility tools available on the server. The programs CELLTRAN and TRANSTRU transform unit cell parameters or atomic coordinates into another space-group setting while SETSTRU converts alternative settings structure description to a standard setting and vice versa. EQUIVSTRU applies the space-group normalizers to derive the equivalent descriptions of the same structure. For a given pair of structures, STRAIN is used to calculate the linear and finite strain tensors as well as the degree of the lattice deformation and COMPSTRU offers a quantitative description of the similarity of two structure models.

One of the latest additions is the program NONCHAR, developed for the determination of the non-characteristic orbits (*i.e.* an orbit whose intrinsic symmetry is higher than that of the generating space group). The interest in the determination of non-characteristic orbits and their eigensymmetry groups is based on their importance in crystal structure determination, crystal physics and structural chemistry.

[1] M. I. Aroyo, J. M. Perez-Mato, C. Capillas, E. Kroumova, S. Ivantchev, G. Madariaga, A. Kirov & H. Wondratschek. Z. Kristallog. (2006), **221**, 15-27.
[2] H. Stokes, Table of Magnetic Space Groups: http://stokes.byu.edu/magneticspacegroupshelp.html
[3] D. Litvin. Acta Crystallogr. (2001) A**57** 729, ibid (2008) A**64** 419 (see also http://www.bk.psu.edu/faculty/litvin/Download.html)

MS04-T6
Data Base driven Crystal Structure Prediction with fine-tuned Force Fields.

D.W.M. Hofmann[1,2], L.N. Kuleshova[1], F. Hofmann[3,2]
[1]CRS4, Pula, Italy
[2]FlexCryst, Uttenreuth, Germany
[3]University, Informatik, Erlangen-Nürnberg, Germany

The successful prediction of crystal structures requires very accurate free energy functions. Already tiny errors in the free energy causes a wrong order in the ranking of polymorphs and predict wrongly the region of stability for the different polymorphs. The complex phase diagrams of most organic crystals, make it obvious that a successful crystal structure simulation has to be sensitive to temperature and pressure.

Nowadays two methods are available for crystal structure prediction, ab-initio calculations and classical mechanics with force fields. The second method is attractive, since the calculations times are much shorter. Till now universal force fields are used for the simulations, i.e. for all atoms of one type (e.g. sp3-C) is always used the same parametrization. It have been proved in several blind tests at Cambridge that the inaccuracy of caused by this approach is the main problem of a successful crystal structure prediction for a specific molecule. Therefore we did investigate the possibility to improve the force fields obtained by data mining on the Cambridge Structure Database by fine tuning. The main idea of the data mining on experimental structures is that the experimental structure has to be a local minimum in the free energy and consequently all others structures must be higher in energy. Therefore a correct force field should be able to separate the experimental and virtual structures in two classes. The method is described in details in the book “Data Mining in Crystallography” [1].

We did investigate, if one single crystal structure is sufficient to fine tune the force field for a specific class of molecules. This approach is reasonable, since very small errors in the force field causes that a specific crystal structure can not be predicted furthermore correctly. The reversal conclusion is that the force field is defined by a single crystal structure. For this purpose we generate with FlexCryst for a given experimental crystal structure virtual polymorphs by a crystal structure prediction and separate in a second step the virtual and the experimental structure by classification. We applied this approach to several molecules and did check the portability of the obtained force field to other molecules of the same class with success.

References

[1] Data Mining in Crystallography, ed. D.W.M. Hofmann and L.N. Kuleshova, Structure & Bonding, Vol. 134, Springer Verlag 2010.

Figure Legends

1.) Seperation of an experimental structure from virtual polymorphs

2.) Prediction of benzene after fine tuning of the force field

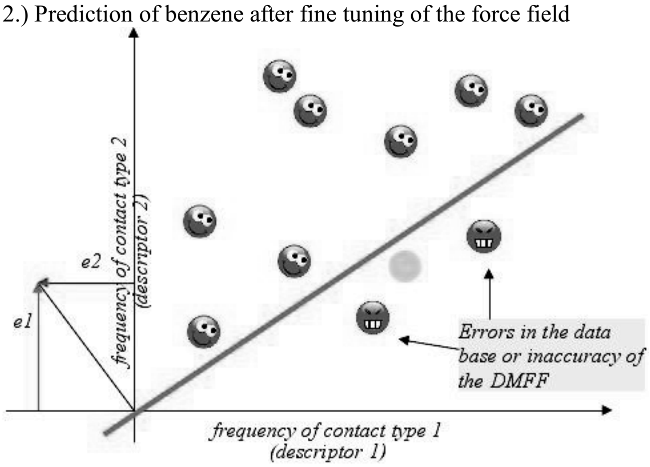

Figure 1: Seperation of an experimental structure from virtual polymorphs

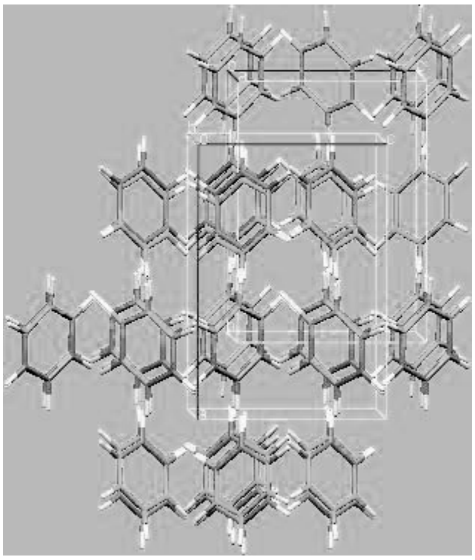

Figure 2: Prediction of benzene after fine tuning of the force field

MS05-T1

The Upgrade Programme of the Structural Biology Beam Lines at the European Synchrotron Radiation Facility (ESRF).

C. Mueller-Dieckmann[1]
[1]ESRF, Structural Biology, Grenoble, France

Structural Biology is faced nowadays to tackle more and more challenging projects, for example larger macromolecular assemblies or more complex membrane proteins. Crystals from such complex systems often show considerable inter- and intra-crystal variability with respect to diffraction quality. Sample evaluation of dozens to thousands of crystals prior to data collection will thus become even more crucial as it is today as will data collection facilities optimised for the collection of diffraction data at longer wavelengths or from crystals that are very small and/or diffract to low resolution (i.e. $d_{min} > 5$ Å).

The Upgrade Programme for the Structural Biology beam lines of the European Synchrotron Radiation Facility (ESRF; http://www.esrf.fr/AboutUs/Upgrade) will develop a unique resource, based on 2nd generation automation, designed to maximise the success rate for Macromolecular Crystallography (MX) experiments. The hub of this resource will be a sample evaluation and sorting facility, *MASSIF* (*M*assively *A*utomated *S*ample *S*election *I*ntegrate *F*acility). Macromolecular crystals that have been tested to be most suitable for diffraction data collection will be distributed from this hub to upgraded MX data collection beam lines that also form an integral part of the ESRF's upgrade plans.

The ESRF's Structural Biology Group's upgrade plans will be presented, with particular emphasis on a refurbished ID29 which will be optimised to enable diffraction data collection from crystals of macromolecules using X-rays of lower energies (E = 5 keV, l = 2.5 Å).

MS05-T2

A sapphire single crystal cell for neutron powder diffraction at high gas pressures

H. Kohlmann[1], N. Kurtzemann[1], C. Reichert[1], P. Wenderoth[1]
[1]Universität des Saarlandes, Anorganische Festkörperchemie, Saarbrücken, Germany

The understanding of many chemical reactions in solid state chemistry is hampered by the fact that reaction pathways are unknown and thus rational synthesis planning of new compounds is hardly possible. *In situ* studies can help by identifying intermediates, but are rarely performed due to technical difficulties, especially if neutron diffraction is required in the case of light atoms such as hydrogen, nitrogen or oxygen. In order to investigate solid-gas reactions, in particular the hydrogenation of intermetallic compounds, we have constructed a gas pressure cell for neutron powder diffraction. It is based on the design of a sample holder for inelastic scattering [1] and consists of a 10 cm long free standing sapphire crystal (Fig. 1) with stainless steel endcaps, such that the neutron pathways is unobstructed. Using a single crystal as container material has got the advantage that Bragg peaks from the cell material can be avoided given a proper orientation of the cell, resulting in a cleaner background than amorphous (e. g. silica) or polycrystalline cell materials (e. g. metals). Sapphire has got additional benefits, such as high yield strength withstanding high gas pressures, chemical inertness, especially no hydrogen embrittlement, and optical transparency. The latter is used to implement a laser heating system (Fig. 2), enabling studies under controlled gas pressure and temperature conditions.

Using the sapphire single crystal gas pressure cell, the hydrogenation properties of several intermetallic compounds could be examined and reaction pathways explored. Reaction conditions up to 100 bar hydrogen pressure and 250°C have been tested successfully. Examples include hydrogen induced gliding mechanisms in palladium rich compounds [2], hydrogen storage in Laves phases and $LaNi_5$, phase transitions in palladium hydride and hydrogen induced decomposition of rare earth compounds.

[1] B. C. Chakoumakos, C. J. Rawn, A. J. Rondinone, L. A. Stern, S. Circone, S. H. Kirby, Y. Ishii, C. Y. Jones, B. H. Toby, *Can. J. Phys.* **2003**, *81*, 183-189

[2] H. Kohlmann, N. Kurtzemann, R. Weihrich, T. Hansen, *Z. Anorg. Allg. Chem.* **2009**, *635*, 2399-2405

Figure 1: Sapphire single crystal gas pressure cell under hydrogen pressure

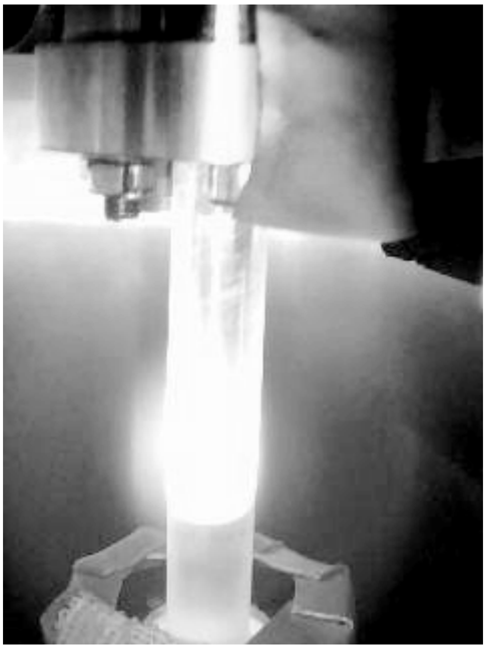

Figure 2: Sapphire single crystal gas pressure cell during in situ measurement on the neutron powder diffractometer D20 (ILL, Grenoble) with laser heating and hydrogen pressure

MS05-T3

Room temperature single-crystal diffuse scattering and ab initio lattice dynamics in titanite, $CaTiSiO_5$

M. Gutmann[1], K. Refson[2], M. von Zimmermann[3], I. Swainson[4], H. Dabkowska[5], A. Dabkowski[5]
[1]Rutherford Appleton Laboratory, ISIS Facility, Chilton Didcot, United Kingdom
[2]Rutherford Appleton Laboratory, CSED, Chilton Didcot, United Kingdom
[3]Deutsches Elektronensynchrotron, DESY, Hamburg, Germany
[4]National Research Council, Canada, Canada
[5]McMaster University, Physics and Astronomy, Hamilton, Canada

Titanite is made of chains of TiO_6 octrahedra which are interconnected by SiO_4 tetrahedra. Ca occupies large cavities in the remainder of the polyhedral framework. At room temperature, the Ti displays and antiferroelectric distortion pattern along the chains with displacements in one direction in one chain and in the opposite direction in neighbouring chains [1]. Minerals can display complicated phonon dispersion relations which are challenging to determine experimentally using inelastic X-ray or neutron scattering. Here, we have recorded diffuse scattering over a large volume in reciprocal space at room temperature in a synthetic single crystal of titanite using high-energy X-rays at BW5 at DESY and neutron Laue single crystal diffraction using SXD at ISIS. Both techniques cover a similar Q-range and display complementary contrast of the diffuse features. In a first step, Monte-Carlo modelling is used to identify the origin of the diffuse scattering as being of thermal nature. Given this result, we calculated in a second step the phonon dispersions from ab-initio lattice dynamics using density functional perturbation theory as implemented in the CASTEP code. The computed diffuse scattering patterns compare very favourably with the measured patterns. Four modes are identified in the phonon dispersions that are linked to the antiferroelectric distortion pattern in the TiO6 chains one of them displaying a large longitudinal - transverse optic splitting.

[1] T. Malcherek, C. Paulmann, M. Chiara Domeneghetti, and U. Bismayer, *J. Appl. Cryst.* **34**, 108 (2001).

MS05-T4

Magnetic and low temperature structural behavior of clinopyroxene-type $FeGeO_3$: a neutron diffraction, magnetic susceptibility and ^{57}Fe Mössbauer study

G. Redhammer[1], A. Senyshyn[2], G. Tippelt[1], W. Treutmann[3], C. Pietzonka[4], G. Roth[5], G. Amthauer[1]
[1]University of Salzburg, FB Materialwissenschaften & Physik, Salzburg, Germany
[2]Forschungsneutronenquelle FRM-II, Garching, Germany
[3]Universität Marburg/ Lahn, Institut für Mineralogie, Marburg/ Lahn, Germany
[4]Universität Marburg/ Lahn, Fachbereich Chemie, Marburg/ Lahn, Germany
[5]RWTH Aachen, Institut für Kristallographie, Aachen, Germany

The clinopyroxene type compounds have gained increasing interest in solid state science due to their magnetic properties at low temperature. As part of our ongoing research we have studied several pyroxenes, among them $LiFeGe_2O_6$, $NaFeGe_2O_6$ and the analogue silicates, $CoGeO_3$ and $MnGeO_3$ [1-4]. As a continuation of this project we here present the results on pyroxene type $FeGeO_3$.

$FeGeO_3$ was synthesized using ceramic sintering techniques at 1273 K in evacuated silica tubes and investigated by powder neutron diffraction between 4 K and 300 K, X-ray diffraction, SQUID magnetometry and ^{57}Fe Mössbauer spectroscopy. The title compound shows $C2/c$ symmetry between 4 K and 900 K, no nuclear phase transition is present at any temperature, while lattice parameters show discontinuities around 50 K and 15 K, which are due to magneto-elastic coupling of the lattice. The magnetic susceptibility data show two maxima in their temperature dependence, one at ~ 47 K, the second around 12 K (depending on the external field), indicative for two magnetic events in the title compound. From the neutron data, it was found that for $T < 45$ K $FeGeO_3$ transforms to a simple magnetic structure, space group $C2/c$, with the spins aligned parallel to the crystallographic ***b***-axis, the coupling within the M1/ M2 band is ferromagnetic while between them it is antiferromagnetic. As the bulk magnetic measurements revealed a dominating ferromagnetic coupling, the intra-chain interactions dominate the inter-chain interaction. At 12 K additional magnetic reflections appear, revealing a second magnetic phase transition. Spins are rotated away from the ***b*** - axis towards the ***a*** - ***c*** plane. The coupling on M1 still is ferromagnetic within and antiferromagnetic between the M1 chains, spins on M1 and M2 however are no longer collinear with the M2 site being more rotated away from ***b*** than on M1.

[1] Redhammer et al. (2009) J. Solid State Chem. 182: 2374 - 2384
[2] Redhammer et al. (2011) Phys. Chem. Mineral. 38, 139 - 157.
[3] Redhammer et al. (2010) Phys. Chem. Mineral. 37(5), 311-332
[4] Redhammer et al (2011)) J. Phys: Cond Matter accepted

MS05-T5
Characterizing the main hardening TaC precipitates by complementary diffraction methods in high melting Co-Re base alloys being developed for applications at temperatures beyond the Ni-base superalloys

R. Gilles[1], D. Mukherji[2], P. Strunz[3], M. Hofmann[1], M. Hoelzel[1], B. Barbier[4], H. Euler[4], J. Rösler[2], U. Gasser[5]
[1]TU Muenchen, FRM II, Muenchen, Germany
[2]TU Braunschweig, Institut für Werkstoffe, Braunschweig, Germany
[3]Nuclear Physics Institute ASCR, Rez near Prague, Czech Republic
[4]Steinmann Institut, Poppelsdorfer Schloß, Bonn, Germany
[5]Laboratory for Neutron Scattering, Paul Scherrer Institut, Villigen, Switzerland

Co-Re based alloys, a new class of high temperature alloy with relatively high melting point was introduced by the Technische Universität Braunschweig, Germany in 2007 [1] to supplement Ni-base superalloys in future gas turbines. The main aim in this material development is to increase the maximum usable metal temperature to 1200°C without additional cooling or coatings. A variation of the Co-Re alloy is hardened by fine TaC precipitates, which are finely dispersed (size ~30 nm) in the microstructure. The fine TaC precipitates effectively interact with dislocations during creep deformation at high temperatures [2]. However, long term stability of the microstructure is an issue, particularly the stability of the fine TaC in the temperatures range of 1000° to 1300°C.

It is known that the C to Ta ratio in the MC carbide phase is generally lean in C and lies between 0.71 to 0.98%. The lattice parameter of TaC is strongly dependent on its C content [3]. Two variation of Ta containing Co-Re alloys: Co-17Re-23Cr-1.2Ta-2.6C (in at. %), one with 200 wt.ppm B addition and one without B were used in this study. The lattice parameters of the TaC in these two alloys were different, suggesting a different C content. Changes of carbon content in TaC after high temperature exposure was also observed along with coarsening of the precipitates. Presence of additional phases like the x Ta_4C_{3-x} could be identified using high resolution XRD after some heat treatments [4].

In this contribution we studied the stability and coarsening of the fine TaC particles (~30 to 50 nm) by ex situ neutron diffraction (ND), in situ small-angle neutron scattering (SANS), room temperature (RT) X-ray diffraction (XRD) and scanning electron microscopy (SEM) measurements.

References:
[1] D. Mukherji, P. Strunz, R. Gilles, M. Hofmann, F. Schmitz, J. Rösler: *Materials Letters* 64 (2010), pp. 2608-2611.
[2] D. Mukherji, P. Strunz, S. Piegert, R. Gilles, M. Hofmann, M. Hoelzel and J. Roesler
Journal of Materials Engineering and Performance (2011) in print.
[3] A.I. Gusev, A.A. Rempel, A.J. Magerl, Disorder and Order in Strongly Nonstoichiometric Compounds, Materials Science, Springer-Verlag Berlin Heidelberg New York, 2001.
[4] R. Gilles, D. Mukherji, P. Strunz, M. Hofmann, M. Hoelzel, B. Barbier, H. Euler, J. Roesler, U. Gasser, Acta. Met., in preparation.

MS05-T6
Crystal structure of $Li_2B_4O_7$

A. Senyshyn[1,2], H. Boysen[3], R. Niewa[4], Y. Burak[5], V. Adamiv[5], I. Chumak[6,7], H. Fuess[2]
[1]Technische Universität München, Forschungsneutronenquelle Heinz Maier-Leibnitz FRM-II, Garching b. München, Germany
[2]Darmstadt University of Technology, Institute for Materials Science, Darmstadt, Germany
[3]Ludwig Maximillians Universität München, Department fur Geo-und Umweltwissenschaften, Sektion Kristallographie, Garching b. München, Germany
[4]Universität Stuttgart, Institut für Anorganische Chemie, Stuttgart, Germany
[5]Institute of Physical Optics, Lviv, Ukraine
[6]Leibniz-Institute IFW Dresden, Institute for Complex Materials, Dresden, Germany
[7]Forschungszentrum Karlsruhe GmbH, Institut für Nanotechnologie, Karlsruhe, Germany

The crystal structure of lithium tetraborate $Li_2B_4O_7$ (mineral name diomignite) at room temperature is tetragonal with space group $I4_1cd$ (point group $4mm$) and with the polar axis situated along the crystallographic c-direction. It consists of a boron-oxygen network with lithium atoms located in interstices. In the basic subunit of the net - the anion $B_4O_7^{2-}$ - two boron atoms are tetrahedrally and two are triangularly coordinated by oxygen atoms.

Lithium tetraborate attracts considerable interest in nonlinear optics as an element of surface acoustic wave devices, a frequency-conversion material for 2nd-5th harmonic generation from a high-power Nd:YAG laser, as a high power ultraviolet light source based on SHG and SFH of the visible laser radiation *etc*. Possible applications for $Li_2B_4O_7$ require deeper understanding of its properties, especially at non-ambient conditions.

Thus, in the literature there is plenty of controversial data on $Li_2B_4O_7$ reporting anomalous behaviour in the different temperature ranges, e.g. thermal scintillations have been observed in $Li_2B_4O_7$ when not excited by hard quanta, incommensurate structure modulation, anomalies in thermal expansion and thermal evolution of bond lengths, numerous phase transitions, anomalies in sound velocities and Raman spectra, strong anisotropy of ionic conductivity *etc*. The existing discrepancies between the experimental results of different authors lead us to perform systematic studies of lithium tetraborate.

Structural studies were performed using coherent elastic neutron scattering on ^{11}B enriched $Li_2B_4O_7$ (99.6% ^{11}B). Powder diffraction examinations unambiguously indicated structural stability of $Li_2B_4O_7$ in the temperature range from 3 K to its melting point at ca. 1170 K. Despite this fact, an evidence for anomalies in thermal dependencies of lattice parameters, bond lengths and displacement parameters has been deduced.

In the current contribution we report on complex studies of lithium tetraborate doped with ^{11}B in the broad temperature range 3-1200 K using neutron powder diffraction, dilatometry, specific heat, calorimetry and impedance spectroscopy. The origin of the $Li_2B_4O_7$ structure type has been analyzed in terms of symmetry-mode analysis of a displacive phase transition (AMPLIMODES) and preferable lithium diffusion pathways have been deduced by a combination of maximum entropy method and anharmonic refinements.

MS05-T7

Native point defects in $CuGaSe_2$ - a structural study based on the complementary use of synchrotron X-rays and neutrons

C. Stephan[1], S. Schorr[1], T. Scherb[2]
[1]Helmholtz-Zentrum Berlin für Materialien und Energie, Kristallographie, Berlin, Germany
[2]Helmholtz Zentrum Berlin für Materialien und Energie, Functional Materials, Berlin, Germany

The crystal structure of kesterite type compounds A neutron and X-ray diffraction study

Problems concerning enviromental and energy policy belong to the greatest challanges these days. For a long-term solution of the complex energy problem in Europe, the EU set the goal to produce 20% of total energy consumption from renewable energy sources by 2020. Photovoltaics, the direct conversion of sunlight into electrical energy, plays a key role within the renewable energies. Thin film solar cells using compound semiconductors as absorber material are foreseen as one of the most promising and cost-efficient technology.

The complementary use of phase sensitive diffraction methods using neutrons and synchrotron radiation allow a non-destructive analysis of the crystal structure of the photovoltaic materials. These investigations are necessary to develop structure-property relations, which are the basis for tailor-made materials.

The chalcopyrite type compound semiconductor $CuGaSe_2$ is a potential absorber material for thin film solar cells. Electronic active defects are strongly influencing the thin film solar cell performance. But the structural origin of point defects in chalcopyrite semiconductors is still under discussion. For the first time a systematic structural study on non-stoichiometric $CuGaSe_2$ was performed applying neutron and anomalous X-ray diffraction. Distinguishing between isoelectronic species like Cu^+ and Ga^{3+} by conventional diffraction techniques, like laboratory X-ray powder diffraction, is almost impossible. Therefore, at first neutron powder diffraction with subsequent Rietveld refinement was applied to evaluate possible cation distribution models for copper - poor $CuGaSe_2$ by the method of average neutron scattering length. To decide if Cu^+ and Ga^{3+} in Cu-poor $CuGaSe_2$ are ordered or partially disordered distributed within the structure, anomalous X-ray diffraction experiments were performed complementary to the neutron diffraction experiments. For the anomalous diffraction experiments synchrotron X-rays with two different wavelengths, close to and far off the Ga-K-absorption edge (10367 eV), were used. This complementary diffraction technique made a differentiation between an ordered and a partially disordered distribution of the cations in copper-poor $CuGaSe_2$ possible.

This complementary approach revealed the influence of stoichiometry on the presence of intrinsic point defects.

MS05-T8

High resolution investigations of cementitious materials by Synchrotron radiation based X-ray diffraction

M.-C. Schlegel[1], U. Mueller[1], U. Panne[2], F. Emmerling[1]
[1]BAM, Structure Analysis, Berlin, Germany
[2]Humboldt Universität zu Berlin, Chemistry, Berlin, Germany

The material properties and durability of cementitious materials depends on both hydration conditions during the construction and resistance against chemical attacks after the construction of buildings. Two different experimental setups working with synchrotron based radiation were developed to investigate both processes during these different time periods of cementitious materials life (Figure 1).

During the construction, cement and water reacts immediately to structurally more complex hydration products, which lead to the setting of cement and subsequently to the hardening of the cement paste. Especially the reaction of C_3A ($Ca_3Al_2O_5$) with calcium sulphate to ettringite ($Ca_6Al_2(SO_4)_3(OH)_{12} \cdot 26\ H_2O$) is a key factor of these kind of processes. Detailed insights into the different stages of the early hydration are needed for a profound understanding in which way these processes can be influenced to optimize applications of cementitious materials. For the investigation of the hydration processes an ultrasonic trap provided the contact free analysis of a sample with no influence of the sample holder and ensures a constant water cement ratio [1]. The experimental setup allows inducing the hydration by an injection device (piezo-syringe). The integration time for a single diffraction pattern was about 500 ms due to the high photon flux of the synchrotron facility and allows a characterization of the hydration processes at early stages.

After construction of buildings consisting of cementitious materials, it is exposed and attacked by solutions of anthropogenic or of natural origin. Solutions containing sulfate or chloride ions penetrating concrete react with components of the cement paste to secondary phases, e.g. ettringite or Kuzel's salt ($Ca_2AlCl_{0.5}(SO_4)_{0.5}(OH)_6 \cdot 10\ H_2O$) and inducing damaging mechanisms. This results in a reduction of mechanical strength and a decrease of the service life of an affected structure. The spatial investigations of the phase compositions were performed on sulphate and chloride attacked cement stone containing different kinds of supplementary cementitious materials. Thick sections ($40 \times 40 \times 0.2$ mm) were investigated in transmission geometry with a spatial resolution 10 µm. Compared to previous X-ray studies these experiments allow for the characterization of phase transformations during the damaging processes in more detail. Furthermore, the experimental setup provides the possibility for analyzing the phase assemblage of a given sample without destroying the micro structure [2].

(1) Wolf, S. E.; Leiterer, J.; Kappl, M.; Emmerling, F.; Tremel, W. *Journal of the American Chemical Society* **2008**, *130*, 12342-12347

(2) Schlegel, M. C.; Mueller, U.; Panne, U.; Emmerling, F.; *Analytical Chemistry* **2011**, dx.doi.org/10.1021/ac200181g

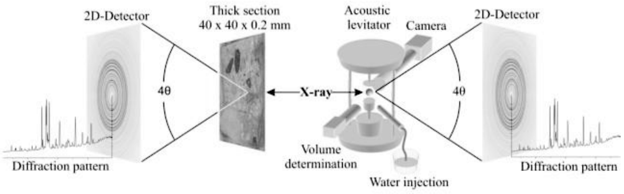

Figure 1

MS06-T1

Crystal Chemistry and Stability of $Li_7La_3Zr_2O_{12}$ garnet: A Fast Lithium-Ion Conductor

C.A. Geiger[1], E. Alekseev[2], B. Lazic[3], M. Fisch[3], T. Armbruster[3], R. Langner[4], M. Fechtelkord[4], N. Kim[5], T. Pettke[6], W. Weppner[7]
[1]Universität Salzburg, Materialforschung & Physik, Salzburg, Austria
[2]Forschungszentrum Jülich, Institute of Energy and Climate Research (IEK-6), Jülich, Germany
[3]Universität Bern, Mineralogische Kristallographie, Institut für Geologie, Bern, Switzerland
[4]Ruhr-Universität Bochum, Institut für Geologie, Mineralogie und Geophysik, Bochum, Germany
[5]Stanford University, Department of Geological and Environmental Science, Stanford, CA, United States
[6]Universität Bern, Institut für Geologie, Bern, Switzerland
[7]Christian-Albrechts-Universität zu Kie, Institut für Anorganische Chemie, Kiel, Germany

Recent research has shown that certain Li-oxide garnets with high mechanical, thermal, chemical and electrochemical stability are excellent fast Li-ion conductors. However, the detailed crystal chemistry of Li-oxide garnets is not well understood, nor is the relationship between crystal-chemistry and conduction behavior. An investigation was undertaken to understand the crystal chemical and structural properties, as well as the stability relations, of $Li_7La_3Zr_2O_{12}$ garnet, which is the best conducting Li-oxide garnet discovered to date.

Single crystals up to roughly 100 micrometers in size were grown. Electron microprobe and laser ablation ICP-MS measurements show small amounts of Al in the garnet, probably originating from the crucibles. The crystal structure was determined using X-ray single-crystal diffraction every 100 K from 100 K up to 500 K. The crystals are cubic with space group Ia3d at all temperatures. The atomic displacement parameters and Li-site occupancies were measured. Li atoms could be located on at least two structural sites that are partially occupied, while other Li atoms in the structure appear to be delocalized. ^{27}Al NMR spectra show two main resonances that are interpreted as indicating that minor Al occurs on the two different Li sites. Li NMR spectra show a single narrow resonance at 1.2-1.3 ppm indicating fast Li-ion diffusion at room temperature. The chemical shift value indicates that the Li atoms spend most of their time at the tetrahedrally coordinated C (24d) site. The second synthesis method, using solely Pt crucibles during sintering, produced fine-grained $Li_7La_3Zr_2O_{12}$ crystals. This material was studied by X-ray powder diffraction at different temperatures between 25 °C and 200 °C. This phase is tetragonal at room temperature and undergoes a phase transition to a cubic phase between 100 and 150 °C.

Cubic "$Li_7La_3Zr_2O_{12}$" may be stabilized at ambient conditions relative to its slightly less conducting tetragonal modification via small amounts of Al^{3+}. Several crystal-chemical properties appear to promote the high Li-ion conductivity in cubic Al-containing $Li_7La_3Zr_2O_{12}$. They are: i) Isotropic three dimensional Li-diffusion pathways, ii) Closely spaced Li sites and Li delocalization that allow for easy and fast Li diffusion, and iii) Low occupancies at the Li sites, which may also be enhanced by the heterovalent substitution $Al^{3+} = 3Li$.

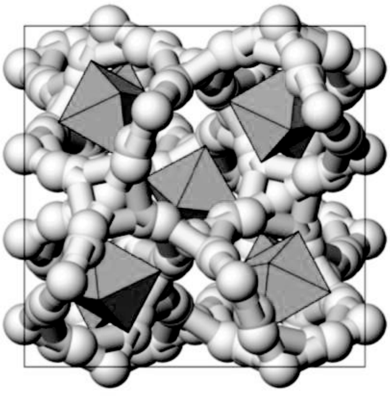

Figure 2. Crystal structure model for cubic Al-containing $Li_7La_3Zr_2O_{12}$ space group $Ia\bar{3}d$ projected on (100). Li sites are shown as white spheres, ZrO_6 octahedra are blue, and La atoms have been omitted for clarity. Adjacent Li positions are connected via white pathways that represent possible routes for Li diffusion.

Figure 1

MS06-T2

Raman-Spektroskopie diamantähnlicher Kohlenstoffbeschichtungen für funktionelle Oberflächen

M. Kahn[1], R. Kaindl[2], W. Waldhauser[2,1]
[1]Infineon Technologies AG, Villach, Austria
[2]JOANNEUM RESEARCH, MATERIALS - Institute of Surface Technologies and Photonics, Niklasdorf, Austria

Dünne Schichten auf Oberflächen, sogenannte funktionelle Oberflächen, ermöglichen die gezielte Anpassung von Materialeigenschaften an bestimmte Anforderungen. Diamantähnliche Kohlenstoffschichten („diamond-like carbon, DLC) lassen sich durch physikalische Dampfphasenabscheidung („physical vapour deposition, PVD) und plasma-unterstützte chemische Dampfphasenabscheidung („plasma-assisted chemical vapour deposition, PA-CVD) in einer großen Bandbreite physikalischer und chemischer Eigenschaften herstellen. Sie haben deshalb vielfältige Anwendungen in der Halbleiter- und Elektronikindustrie, Energiewirtschaft, Biochemie, Biologie, Medizin, analytische Chemie, Lebensmittelindustrie usw.

Ein sehr wichtiger Parameter von DLC-Schichten ist das Verhältnis von Kohlenstoff in unterschiedlichen Bindungsorbitalen. Je nach Herstellungsbedingungen wie Abscheidetemperatur, Beschleunigungsspannung und Gaszusammensetzung entstehen mehr oder weniger Diamant-ähnliche, tetraedrisch koordinierte sp^3- oder planare, Graphit-ähnliche sp^2-Hybridorbitale. Weiters beeinflussen auch Kohlenstoff-Wasserstoff Bindungen die Eigenschaften.

Das Raman-Spektrum von DLC-Schichten zeigt zwei breite Hauptbanden bei 1360 und 1560 cm^{-1}, die als D- und G-Bande bezeichnet werden. Die spektralen Parameter dieser Banden wie Halbwertsbreite und Dispersion der G-Bande (FWHM G, Disp. G) sowie die Intensitätsverhältnisse der D- und G-Banden (I_D/I_G) erlauben die Abschätzung des sp^3-koordinierten Kohlenstoffanteils. Zusätzlich lässt sich auch Größe und Formverteilung von sp^2-Klustern näherungsweise ermitteln. Amorphe, hydrogenierte Kohlenstoffschichten (a-C:H) wurden mittels einer linearen Ionenstrahlquelle und Azetylen bei Entladungsspannungen zwischen 1 und 3 kV auf Silizium-Wafern abgeschieden. Die Raman-Messungen wurden bei zwei Laseranregungswellenlängen von 532 und 325 nm durchgeführt. FWHM G und Disp. G sowie I_D/I_G schwanken zwischen 180 und 195 cm^{-1} bzw. 0.4 und 0.6. Gemessene Nanohärten (H) und reduzierte Elastizitätsmodule (E) zwischen 25 und 36 GPa bzw. 147 und 180 GPa korrelieren linear positiv mit FWHM G und Disp. G bzw. negativ mit I_D/I_G. Dies lässt sich durch eine

Zunahme des gesamten sp^3-Gehaltes durch vermehrte Bildung von Csp^3-Csp^3 Bindungen bei gleich-bleibendem Wasserstoffgehalt erklären.

MS06-T3
Microstructures of coke deposits from high temperature processes

S. Gerhardt[1], K. Bente[1], J. Hofmann[2]
[1]Institut für Mineralogie,Kristallographie und Materialwissenschaft, Universität Leipzig, Leipzig, Germany
[2]Institut für Nichtklassische Chemie, Leipzig, Germany

The transformation of crude oil in industrial useful chemicals is a complex process, in which many partial reactions only take place in presence of catalysts. Some reaction steps require high process temperatures (> 600°C), which can lead to an unwanted side reaction, the so called ‘metal dusting’. This phenomenon causes deposition of carbon on tube walls, which implicates inhibition of catalytic centers and reduces the efficiency of heat transfer. In addition, deposited carbon can diffuse into tube surfaces and cause corrosion of used material. With a high economical importance, there are many studies dealing with cause, mechanisms and possibilities to avoid this phenomenon.
Aim of this work is to resolve open questions by identifying and modelling fundamental correlations between vapour-solid reactions and their consequences for microstructures, morphologies of surfaces and catalytic activities due to the deposited carbon. The high temperature materials are analyzed by using 3D X-ray tomography (volume properties), XRD (phase existences), XPS (chemical bonding), HRTEM (nano-structures), SEM (surface morphologies), electron microprobe analysis and TEM-EDX (chemical composition). After different pre-treatments (surface modification, artificial aging, influence of reaction parameters) material samples are analyzed and correlated with carbon accumulation characteristics.

MS06-T4
Flexible Single-Crystal Media for Dynamic Separation of Gas

S. Takamizawa[1]
[1]Yokohama City University, Nanobioscience, Yokohama, Japan

Gas separation is an important topic not only for industry but also for its scientific aspects. Porosity has been reported as a possible means for the separation of gas. The crystalline porosity has been expected to generate high guest selectivity because of its structural regularity. Single-crystal with ultramicropores would be the most ideal media for the purpose of gas separation. Recent development in synthesized porous materials has generates the novel porosity bearing conflicting properties of regularity and flexibility. It has not been yet clear how the flexibility effects to gas separation ability.
I have studied the gas separation property of the single crystal host $[Cu_2(bza)_4(pyz)]_n$ (**1**) (bza = benzoate; pyz = pyrazine) since single crystal **1** has the flexibility capable of changing its narrow channel structure (2-4 angstrom diameter) even by physisorption of gaseous guests to stabilize the resulting gas inclusion state.[1] (See Fig1a)
The dynamic separating properties were characterized in the three types of gas separation on **1**: 1) the selective for extraction from a gas mixture by selectivity switch depending on the mixing ratio of surrounding gas even under saturated adsorbing state(Fig1b);[2] 2) a large entropic dependence was detected in gas chromatograph with microcrystals packed column;[3] and 3) anisotropic and effective permselectivity for hydrogen and carbon dioxide gases was confirmed in the single-crystal membrane technique(Fig1c).[4]
The flexibility in host **1** expresses dynamic selectivity for a wide range of gases by means of various separation methods.

References
1. S. Takamizawa, E. Nataka, T. Akatsuka, R. Miyake, H. Takeuchi, G. Maruta, S. Takeda, *J. Am. Chem. Soc.* **2010**, 132, 3783.
2. S. Takamizawa, M. Kohbara, R. Miyake, *Chem. Asian J.* **2009**, 4, 530.
3. S. Takamizawa, R. Miyake, *Chem. Commun.* **2009**, 4076.
4. S. Takamizawa, Y. Takasaki, R. Miyake, *J. Am. Chem. Soc.* **2010**, 132, 2862.

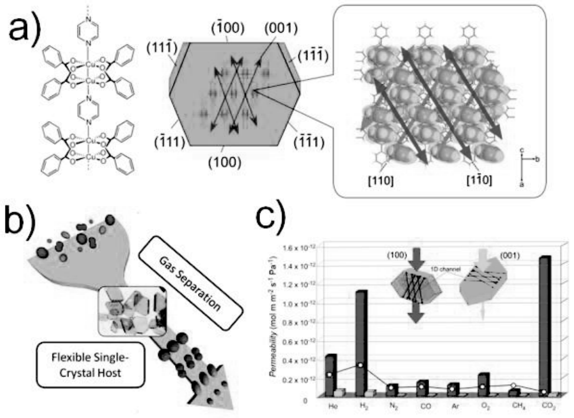

Figure 1: Chain component and crystal morphology with channel direction of **1** (a) and schematic drawing of dynamic gas separation (b) and single crystal permeation (c)

MS06-T5
Fabrication and characterization of piezoceramics from lead based and lead free systems

M. Prakasam[1], A. Largeteau[1], P. Veber[1], M. Maglione[1], E. A.Villora[1], K. Shimamura[1]
[1]ICMCB-CNRS, Crystal growth, high pressure and sintering, Pessac, Bordeaux, Japan

The piezoceramic materials are ubiquitous materials for advanced technology. The device performance greatly depends on the microstructure of piezoceramics. Spark plasma sintering (SPS), which has clear advantages over conventional sintering methods, makes it possible to sinter nanometric powders to near full densification with little grain growth. Ceramic processing of ferroelectrics of lead magnesium niobate (“PMN”) by conventional techniques is difficult and the volatility of Pb resulting in formation of additional phases and preventing the formation of the end product. Therefore in order to obtain uniform, dense ferroelectric based on PMN and PT is undertaken with SPS. Simultaneously, extensive research is being undertaken to replace the lead-based compounds[1]. Saito et al[2] reported on the ternary compound of $(K,Na)NbO_3$-$LiTaO_3$-$LiSbO_3$ with a very high piezoelectric co-efficient, d_{33} of 416 pCN^{-1} in the form of the textured ceramics. The evaporation of one of the constituents of the MPB[3] provokes thus a compositional fluctuation that results in poorer properties, as it was well known for the popular piezoelectric PZT[4] perovskite system. It was established that tetragonal compositions presented higher piezoelectric coefficients (d_{ij}), but same nominal compositions reached different T_c and d_{33} values. Another aspect that remains to be probed is the MPB nature of the system that in some cases was reported to be a polymorphic behavior and shown compositional inhomogeneities. Hence we focus our attention in obtaining uniform composition ceramics by spark plasma sintering process and study the piezoelectric dynamics in this system extensively. The temperature dependence of the dielectric constant of the SPS pellets was examined using a programmable furnace with an impedance analyzer HP4192 in the frequency range 1 kHz- 1.1 MHz and for temperatures between 20°C and 450°C. It was inferred that at 254ºC a clear peak of the relative permittivity that corresponds to the ferroelectric-paraelectric phase transition[5] is observed. The Curie constant was calculated by least-square fitting in the Curie-Weiss law, was found to be 1.13×10^5 K. Such transition temperature is consistent with similar results in ceramics of composition reported by D.A.Ochoa et al[6], which is in agreement with the chemical analysis of our SPS KLN system samples. The initial results show a good indication of ferroelectricity in the material which was confirmed by piezoelectric and pyroelectric experiments. The results will be discussed in detail.

Acknowledgement
The authors acknowledge the funding support from GIS-AMA (Advanced Materials in Aquitaine) for this project. References:

1. M. D. Maeder , D. Damjanovic and N. Setter, J. Electroceramics.
13, 385 (2004).
2.Y. Saito, H. Takao, T. Tani, T. Nonoyama, K. Takatori, T. Homma, T. Nagaya, and M. Nakamura, Nature (London). 432, 84 (2004).
3.Y. Guo, K. Kikuta and S. Hirano, J. Appl. Phys. 97, 114105 (2005).
4.J. F. Fernandez, C. Moure, M. Villegas, P. Durán,. M. Kosec and G. Drazic, J. Eur. Ceram. Soc. 18, 1695 (1998).
5. G. A. Smolenski, J. Phys. Soc. Jpn. 28, 26 (1970).
6. D.A. Ochoa et al. J. Phys. D: Appl. Phys. 42 025402 (2009).

MS06-T6
In search of Li-Na-ionic conductors

S. PARK[1], J. Labbe[1], I.F. Akter[1], C.J. Pietsch[1], L. Garcia B. Lara[1]
[1]Kristallographie/LMU, Geo- & Umweltwissenschaften, München, Germany

Fast Li-ionic conductivity can be obtained in such topologies comprising of LiO_3-, LiO_4- or LiO_6-moieties which are compactly arranged over their common edges or faces to form chains and layers [1, 2]. The Li-ionic conductivity can increase dramatically when defects sites are created right in those compact Li-O-chains and -layers [3]. One of the conventional ways for creation of Li defect sites is to replace multivalent cations for a part of monovalent Li cations. This can be a relatively 'simple' performance if it is possible for Li-O-chains or -layers to build up networks with different structural building units of multivalent cations (denoted as A). Such alternating Li-O-A-networks require charge compensating extra cations (B) occupying relatively porous sites, e.g. between Li-O- and M-O-layers or within their channels. In search of this prototype for anisotropic Li-ionic conductors stable for the use in all-solid-state-Li-batteries, we have recognized several ring-silicates: their Li-O-M-networks take only advantage of the presence of Na^+ as B cations as additional charge carriers [3, 4]. Based on previous studies of naturally occurring sogdianite and sugilite compounds [4-7], we have pursued to synthesize sugilite-sogdianite solid-solutions $(Na, K)_3(Fe, Zr)_2[Li_3Si_{12}O_{30}]$ [8, 9] and Li-Na-bearing willemite-type $(Li, Na)_{2x}[Zn_{2-x}SiO_4]$ compounds [10-12]. These new Li-Na-ionic conductor materials are presented here based on diffraction studies using X-ray and neutron sources with results from impedance spectroscopy, as briefed in **Table**.

Table Various sugilite-type structures with various A cations [8, 9].

Compound	**a [Å]**	**c [Å]**	**Volume [Å³]**	**Ionic radii [Å][13]**	**Occupancy**
Fe-sugilite	10,0708(2)	14,1013(4)	1238.57(7)^N	Fe: 0,645	100% Fe
Ga-sugilite	10.0119(2)	13.9960(4)	1214.97(4) ^{N}	Ga: 0,62	100%Ga
Ti-Fe-sugilite	10,0545(4)	14,0824(8)	1232.9(1) ^{N}	Ti: 0.605	90%Fe;10%Ti
Ge-Fe-sugilite	9,960(2)	14,096(3)	1211.1(4) ^{X}	Ge: 0,53	86%Fe:;14%Ge
Zr-Fe-sugilite	10,088(3)	14,219(5)	1253.1(6)^X	Zr: 0,72	To be analyzed

^{X} X-ray powder diffraction data
^{N} Neutron powder diffraction data

References

- 1. S.-H. Park, et al., *J. Am. Chem. Soc.* **122, No. 44** (2000), 11023-1024.
- 2. S.-H. Park, et al., Micropor. Mesopor. Mater. (2008), 108, 1-12.
- 3. S.-H. Park, A. Senyshyn, C. Paulmann (2007), J. Solid St. Chem., 180, 3366-3380.
- 4. S.-H. Park, M. Hoelzel, H. Boysen, E. Schmidbauer (2007), J.Solid St. Chem., 180, 1306-1317.
- 5. S.-H. Park, Experimetal Report (Proposal # 698,) FRM II, Garching, Germany, 2007.
- 6. S.-H. Park (2008), Acta Cryst., A64, C532.
- 7. S.-H. Park, et al., *Sugilite ($Na_2KFe_2Li_3Si_{12}O_{30}$)-like materials as prototype for combined Li-Na-ionic conductors*, submitted.
- 8. I.F. Akter, MSc. Thesis, LMU, 2010.
- 9. J. Labbe, MSc. Thesis, LMU, 2010.
- 10. C.J. Pietsch, Bachelor Thesis, LMU, 2009.
- 11. L. Garcia B. Lara, MSc. Thesis, LMU, 2010.
- 12. C.J. Pietsch, MSc. Thesis, LMU, 2011.
- 13. R.D. Shannon, Acta Cryst (1976), **A**32, 751-757.

MS06-T7
Synthesis and properties of $NaBH_4$-imbibed aluminosilicate gels and its partial crystalline secondary products

J.-C. Buhl[1]
[1]Institut für Mineralogie, Leibniz Universität Hannover, Hannover, Germany

The hydrides of light elements like boron are interesting substances for hydrogen storage. A problem for wider applications in techniques is the high reactivity of these salts like NaBH4 under atmospheric conditions [1]. Intercalation of the moisture sensitive NaBH4 into the cavities of microporous materials was already shown as a way to protect boranate ions over a long time [2]. Hydrogen can be released from the host matrix "on demand" during heating up the sample. Beside microcrystalline sodalite (SOD) also nanoparticles of boranate sodalite were proved to act as suitable hosts for NaBH4 where hydrogen release already starts significantly above about 373 K. i.e. about 100K lower compared to the microcrystalline material [3]. Regarding to tailor made synthesis of improved hydrogen reservoir compounds with high storage capacities in this study new experiments on enclathration of maximal amounts of NaBH4 salt into aluminosilicate gels are described for the first time. Investigations on the early steps of gel crystallization in the period up to 4 hours after gel preparation were included in this experimental study. The new material was obtained by a two step reaction process. First common sodium-silicate and sodium-aluminate solutions were prepared under addition of high portions of NaBH4 at room temperature, before the gel precipitation was initiated by dropwise mixing of both solutions. A pasty liquid results from this alkaline gel-boranate mixture. Secondly this mixture was exposed a partial stepwise alteration by heating at 383 K for times no longer than 4 h under open conditions in a drying oven. The products were characterized by XRD, FTIR and REM/EDX. The XRD pattern of the new compound shows close resemblance to positional disordered sheet-like structure of slightly different layers. The enclathrated BH4- anions can be clearly detected by FTIR spectroscopy and these tetrahydroborate groups are stable for many weeks under open conditions (see Fig. 1) inside the partial crystalline matrix. Compared with the SOD host of [1-3] the new compound exhibits a much higher hydrogen storage capacity and forms under open conditions. The imbibition of the whole amount of NaBH4 salt, inserted for synthesis, is another advantage over SOD, requiring a high boranate excess for its formation. [1] Buhl, J.-Ch., Rüscher, C.H., Schomborg, L., Stemme, F.,Clean Technology ISBN 978- 1-4398-3419-0 (2010) 236-239. [2] Buhl, J.-Ch., Gesing, Th.M., Rüscher, C.H., Micro. Meso. Mater. 80 (2005), 57-63. [3] Buhl, J.-Ch., Schomborg, L., Rüscher, C.H.; Micro. Meso. Mater. 132 (2010) 210-218. Fig. 1: IR spectra of the as synthesized compound and its aging series: sample as synthesized (a) and after aging for 1 (b), 3 (c) and 4 weeks (d) under open conditions. The spectrum of the pure NaBH4 salt is inserted for comparison.

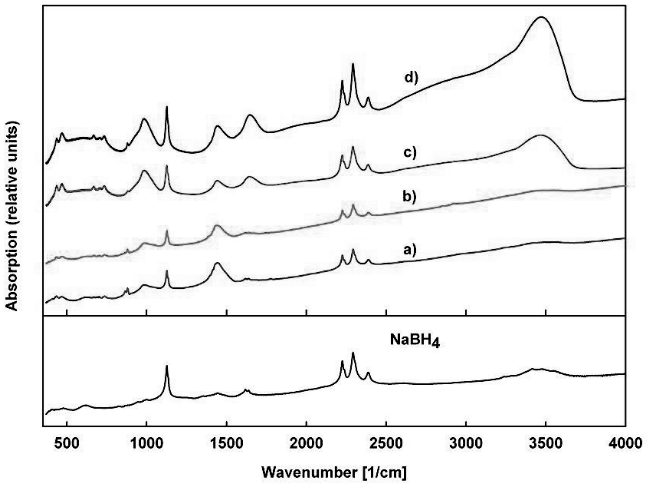

Figure 1

MS06-T8
Hydrogen release and reinsertion reactions in $(BH_x\text{-}(OH)_y\text{-}O_z)$-SOD zoned crystal systems

L. Schomborg[1], C. Rüscher[1], J.-C. Buhl[1]
[1]Leibniz Universität Hannover, Mineralogie, Hannover, Germany

A new material has been developed, namely BH_4-SOD, which encloses and largely protects the BH_4-anion in the sodalite cage. This material enables a controlled release of hydrogen effectively through the reaction of the BH_4-molecule with water molecules in consecutive reaction steps for temperatures between 423 and 773 K finally revealing BO_2-SOD [1, 2]. In this contribution the extraordinary qualities of this material, namely a controlled hydrogen release and as a new aspect the effect of hydrogen reinsertion are further investigated.

Teflon cups for the creation of autogeneous water pressure were filled in a special way with the hydroborate salt, kaolinite and sodium hydroxide solution as described earlier [1]. The autoclaves were typically heated up to temperatures of 393 K using reaction periods up to maximal 24 hours. Samples were also prepared with the addition of special metal powders. The material has been washed and dried at 323 K. Samples were then systematically heated between 473 K and 723 K in air and using hydrogen pressures between 5 and 190 bar in specially designed autoclaves. The samples were mainly characterized by in situ and ex situ infrared absorption spectroscopy (Bruker Vertex 80v), and by TG/DTA (Setaram Setsys Evolution), REM (JEOL JSM-6390A) and XRD (Bruker D4).

A thermally controlled hydrogen release reaction of the BH_4-anion enclathrated in the sodalite cage attached is achieved with water injected through a hydrosodalite type matrix which glues the BH_4-SOD crystals together. A reinsertion of water molecules was repeated in several runs observing a systematic continuation in BH_4-consumption for hydrogen release without any significant destruction of the sodalite structure [2]. The consecutive reaction steps could be followed in temperature dependent infrared (TIR) absorption investigations in heating-cooling runs as well as in ex situ experiments. E.g. as shown in Fig. 1 with increasing heating temperature in air an appearance and systematic increase in intensity of peaks A $((BH_3OH)_{SOD})$; B $((BH_2(OH)_2)_{SOD})$ and C $((BO_2)_{SOD})$ occurs and $(BH_4)_{SOD}$ intensity systematically decreases. This indicates two steps of easily controllable hydrogen generation to species A and B and a sequence of some faster reactions including the formation of $(BH(OH)_3)_{SOD}$, $(B(OH)_4)_{SOD}$ (not seen) and its dehydration to $(BO_2)_{SOD}$. Also shown in Fig. 1 is the result of a reinsertion experiment carried out using 160 bar H_2 at 473K. It can be seen that peak A increases in intensity whereas peak B decreases. Moreover it was observed that $(BH_4)_{SOD}$ does not decrease in intensity. Therefore this implies an effective reinsertion of hydrogen converting back species B to A.

[1] J.-Chr. Buhl, T. M. Gesing, C. H. Rüscher, Microporous Mesoporous Mater. 80 (2005) 57-63

[2] J.-Chr. Buhl, L. Schomborg, C. H. Rüscher, Microporous Mesopourous Mater. 132 (2010) 210-218

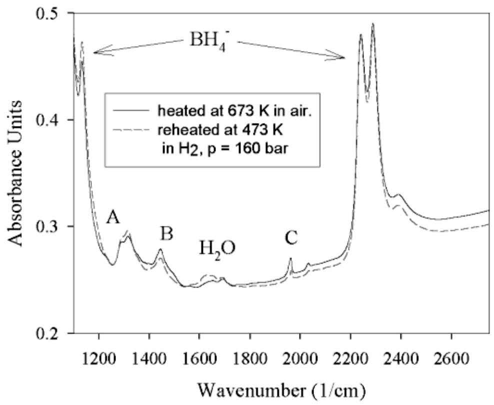

Fig. 1 IR absorption of (BH_4)-sodalite initially heated in air and reheated in hydrogen as denoted.

Figure 1

MS07-T1
Modification of meteoritic tracer element ratios during projectile and target interaction in laser and hypervelocity experiments

L. Hecht[1], M. Ebert[1], A. Deutsch[2], T. Kenkmann[3]
[1]Museum für Naturkunde Berlin, Abt. Forschung, Berlin, Germany
[2]WWU Münster, Institut für Planetologie, Münster, Germany
[3]ALU Freiburg, Geologische Wissenschaften, Freiburg, Germany

Detection and identification of a meteoritic component (i.e., contribution of the projectile) ,in impactites are fundamental for confirming an impact origin and for characterizing the population of the extraterrestrial projectiles that have hit Earth in the past [1]. The processes of mixing projectile matter into target and impactites, however, are poorly understood.

We present results from, (i) melting experiments performed with a 2kW YAG laser welding equipment at the Technical University of Berlin, and (ii) hypervelocity experiments using the two-stage light gas guns at the Fraunhofer Ernst-Mach-Institute (Freiburg). Both experiments aim to simulate the highly energetic and highly dynamic (short term) conditions that characterize natural impact processes.

In our experiments, the projectile was either made of the Campo del Cielo iron meteorite or a Cr-V-Co-Mo-W-rich steel, and the target was the Seeberger Quartz-Sandstone. We have observed partial melting of projectile and target, as well as mixing of these melts in both types of experiments. Partial melting of rocks and minerals and incomplete mixing between locally formed melts result in more or less heterogeneous melt compositions. For example, partial melts of sandstone vary considerably in Al, Fe, Ti and other elements depending on the amount of clay minerals or detrital rutile involved. Mixing between target and projectile can be clearly distinguished from heterogeneity due to partial melting. Silica-rich target melts may be significantly enriched in the elements that are used to trace the projectile, like Fe, Ni, Cr, and V. Inter-element ratios of these tracer elements within the contaminated target melt may be strongly modified from the original ratios in the projectile. This fractionation results most likely from variation in the lithophile or siderophile character and/or from differences in reactivity of the tracer elements with oxygen [2] during interaction of metal melt with silicate melt.

The hypervelocity experiments also produced shocked quartz with planar deformation features (PDF), that are also enriched in Fe and Ni in the case of the Campo del Cielo projectile. After shock compression with formation of PDF's in Qtz and diaplectic glass, and during early unloading, <1 % of projectile matter is added to the glass phases without detectable fractionation between Fe and Ni. In contrast, when waste heat triggers melting of the sandstone, molten projectile is mixed with the sandstone melt and significant element fractionation occurs. In accordance with observations in nature [e.g., 3], Fe is enriched in the silicate melt; whereas, Ni and Co are enriched over Fe in co-existing projectile spherules.

This work is funded by the German Science Foundation DFG, grant FOR-887

[1] Tagle R. and Berlin J. (2008) *Meteoritics and Planetary Sci. 43*, 541-559; [2] Kelly W.R. et al. (1974) *Geochim. et Cosmochim. Acta 38,* 533 - 543; [3] Mittlefehldt D. W. et al. (1992) *Meteoritics 27*, 316-370.

MS07-T2

Li and B equilibrium isotope fractionation between minerals and aqueous solution from first principles calculations

P. Kowalski[1], S. Jahn[1], B. Wunder[1]
[1]GFZ German Research Centre for Geosciences, Chemistry and Physics of Earth Materials, Potsdam, Germany

Isotopes of light elements such as Li or B are excellent geochemical tracers widely used in petrology. They strongly fractionate between minerals and aqueous fluids during fluid-rock interaction processes and have been widely used as tracers of mass transfer processes in the subduction cycle. One of the most important mechanisms leading to the formation of isotopic signatures is the equilibrium isotope fractionation, which nowadays can be modelled on the atomic scale by modern computational methods and hardware. For that purpose we developed an efficient *ab initio* based computational approach for prediction of the equilibrium isotope fractionation factors in high pressure and temperature materials, including fluids. An important aspect of our method is the explicit modelling of solids and fluids as continuous media. This allows for investigation of the expansion and compression effects, which influence the fractionation process in high -T and -P materials. We will show our results for the Li and B isotope fractionation factors between complex Li/B-bearing crystalline solids (staurolite, spodumene, tourmaline and micas) and aqueous solution. The qualitative and quantitative comparison of the results with the existing experimental data [1-3] will be provided. We show that with our atomistic scale simulations we are able to reproduce correctly the experimental isotope fractionation sequences: staurolite-fluid-mica-spodumene for Li and fluid-tourmaline-$B^{[4]}$ micas for B, and reproduce the measured values often within 1 ‰. We will show that by *ab initio* simulations we are also able to model the variation of isotope fractionation with the coordination environment of the fractionating element and with pressure. Our results are in agreement with recent high pressure (P=8GPa) measurements of Li isotopes for spodumene [2] and measurements of B isotopes in differently coordinated states in solids and fluids [3]. Our computational studies give an unique insight into the mechanisms that govern the isotope fractionation on the atomic scale and complement the experimental work.

[1] Wunder B. et al. (2006) *Contrib. Mineral. Petrol.* **151**, 112-120; Wunder B. et al. (2007) *Chem. Geol.* **238**, 277-290.

[2] Wunder, B., Meixner, A., Romer, R. L. and Jahn, S. (2011) *Eur. Mineral.*, in press. DOI: 10.1127/0935-1221/2011/022- 2095

[3] Meyer et al. (2008) *Contrib. Mineral. Petrol.* **156**, 259-267; Wunder et al. (2005) *Lithos* **84**, 206-216

MS07-T3

Understanding peralkaline magmatic systems: an experimental approach

C. Giehl[1], M. Marks[1], M. Nowak[1]
[1]Eberhard-Karls-Universität Tübingen, Faculty of Science - Department of Geosciences, Tübingen, Germany

The formation of peralkaline igneous rocks is commonly accepted to originate from alkali basaltic and nephelinitic mantle-derived sources. Oxygen fugacity (fO_2) and the coexisting fluid phase are crucial factors for the evolution of such magmas. We investigate a dyke rock associated with the plutonic Ilímaussaq magmatic complex (South Greenland), which is believed to represent an early separation of the parental magma, including comparable phase assemblages and parallels with different intrusion phases. We use an iron-rich, extremely evolved composition (#Mg=3; peralkalinity index=1.46) that represents the chilled margin of the dyke rock.

Experiments were carried out in cold seal pressure vessels. According to previous studies on the dyke rock (e.g. Marks&Markl, 2003) P, T and fO_2 were set to 100MPa, 950-750°C (50°C steps), and to $\log fO_2 \sim \Delta$FMQ -1.5 to -3 for the early magmatic phase assemblage. To simulate different fO_2, we used gold capsules (intrinsic $\log fO_2 \sim \Delta$FMQ +1) as well as graphite capsules ($\log fO_2 \sim \Delta$FMQ -1.5) with water contents ranging from nominally anhydrous to fluid saturated.

The variation of fO_2 and water activity cause major differences in the mineral phase assemblage and the compositional evolution of the residual melt. When adjusting H_2O-saturated conditions, the stable phases are mag and cpx coexisting with melt indicating iron depletion with an increase in SiO_2 and slightly increasing peralkalinity. Nominally anhydrous conditions are crucial to synthesize the complete early magmatic mineral assemblage (ulvøspinel-rich mag, fayalite-rich ol, hedenbergite-rich cpx, afs, neph) and iron enrichment with a decrease in SiO_2 and a strongly increasing peralkalinity of the residual melt. Low fO_2 was found to force the evolution of the residual melt towards iron-enrichment. Iron- and sodium enrichment in the residual melt are prerequisites to stabilize late magmatic minerals, e.g. aenigmatite ($Na_2(Fe^{2+})_5Ti^{4+}Si_6O_{20}$) or aegirine ($NaFe^{3+}Si_2O_6$).

With our experimental results, we are able to elucidate the influence of water activity and fO_2 on the liquid line of descent. The experimental conditions to synthesize the early magmatic mineral assemblage are in agreement with observations in natural rocks (Marks&Markl, 2003). To follow up the liquid line of descent, we will simulate fractional crystallization using multi-step experiments to synthesize the late magmatic phase assemblage in upcoming experiments.

Reference: Marks&Markl (2003) MinMag 67, 893-919.

MS07-T4

Water-rock interaction in high pressure MOR hydrothermal systems: an experimental approach for *in situ* sampling of coexisting brine and vapour phases up to 550 bar and 500°C

O. Beermann[1], D. Garbe-Schönberg[1], A. Holzheid[1], C. Kusebauch[1,2]
[1]CAU Kiel, Institut für Geowissenschaften, Kiel, Germany
[2]Westfälische Wilhelms-Universität Münster, Institut für Mineralogie, Münster, Germany

The hydrothermal system discovered at 5°S Mid Atlantic Ridge (MAR) in water depths of ~3000 m (~300 bar) emanates fluids at very high temperatures (~350 to 464 °C, [1]) intersecting the two-phase boundary of seawater at 407°C (at 298 bar).

The rare earth element (REE) patterns of these fluids reacting with MORB source rocks are highly variable: vent fluids at the Red Lion vent field (T~350 °C) show LREE enrichment and a pronounced positive Eu anomaly - a pattern that is typical for many MOR hydrothermal systems. In contrast, high temperature fluids (T~407, transient spikes >460 °C) emanating at two other vents show gradually enforced depletion of LREE accompanied by retreating positive Eu anomalies ('special' pattern) [2].

For a better understanding of fluid-rock interactions under high p-T conditions at slow-spreading MOR it is of fundamental importance to investigate the element partitioning between MORB and fluid within both the single phase seawater field, and, between MORB, vapour and brine at p-T conditions above the two phase seawater boundary. This requires *in situ* sampling of fluid, and coexisting brine and vapour phases, respectively, the latter being stable only at experimental p-T conditions.

We refined the Au reaction cell system by inserting two individual Ti-sampling tubes into an Au reaction cell (Figure 1). This set-up allows *in situ* sampling of both, single phase fluids as well as brine and vapour phases separately above the critical p-T conditions of seawater. The entire reaction cell system is enclosed by a hydrothermal vessel (PARR reactor), which can be externally heated. The pressure inside the vessel can be adjusted by means of a MAXIMATOR pressure pump.

First p-T experiments up to 490°C and 485 bar and distilled water show that no pressure hysteresis occurred between heating and cooling. Within the error of measurement being ± 2°C and, depending on the temperature, ~1-20 bar, the p-T conditions inside the reactor were in good agreement with the equations of state of H_2O given by Wagner & Pruss (2002) [3].

References:
[1] Koschinsky et al. (2008) *Geology* **36**, 615-618; doi:10.1130/G24726A1
[2] Schmidt et al. (2010) *Geochim. Cosmochim. Acta* **74**, 4058-4077.
[3] Wagner & Pruss (2002) *J. Phys. Chem. Ref. Data*, **31**, 387-535.

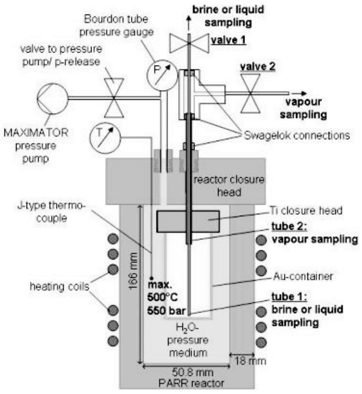

Figure 1: The modified flexible Au reaction cell system equipped with the tube-in-tube technique (inner tube for *in situ* sampling of brine or liquid phases, and outer tube for *in situ* sampling of vapour phases) mounted into a PARR reactor.

MS07-T5

Solubility measurements of $CePO_4$ and YPO_4 in H_2O-NaF at 800°C and 1 GPa: implications for extremely high REE transport during granulite-facies metamorphism

P. Tropper[1], C. Manning[2], D.E. Harlov[2,3]
[1]University of Innsbruck, Institute of Mineralogy and Petrography, Innsbruck, Austria
[2]Department of Earth and Space Sciences, Los Angeles, Germany
[3]Helmholtz Zentrum Potsdam, Deutsches GeoForschungsZentrum, Potsdam, Germany

Monazite ($CePO_4$) and xenotime (YPO_4) are important accessory minerals in metasediments since they host significant REE and are useful for geochronology and geothermometry. It is therefore essential to understand their behavior during metasomatic processes that attend high-grade metamorphism. The occurrence of F-bearing minerals in high-grade metamorphic rocks indicates that F-bearing fluids play an important role in granulite-facies metamorphism. In order to set constraints on the solubility of $CePO_4$ and YPO_4 in the presence of H_2O-NaF bearing fluids at high pressure and temperature, we carried out a preliminary series of weight-loss experiments of synthetic single crystals of each phosphate in a piston-cylinder apparatus at 800°C and 1 GPa. The crystals were placed either in a Pt envelope or an inner Pt capsule (1.6 mm OD), which was added to a 3.5 mm OD Pt capsule with H_2O-NaF. Compared to the very low molal concentration (mol/kg H_2O) of $CePO_4$ and YPO_4 dissolved in pure H_2O ($CePO_4$: 0.00004 molal, YPO_4: 0.0003 molal) our results from the NaF-H_2O system show an enormous increase in the solubility of both phosphates: $CePO_4$ solubility increases to 0.97 *m* in 20 mol% NaF (0.17 *m* in 10 mol.% NaF); YPO_4 shows a stronger solubility enhancement to 0.45 *m* in only 10 mol.% NaF. These data correspond to solubility enhancements by factors of ca. 24000 and 1800 (!) respectively. The results indicate that Y+HREE are much stronger mobilized than LREE and that both, $CePO_4$ and YPO_4 show a similar quadratic solubility behavior and possible dissolution reactions thus could be: $CePO_4 + 2NaF = CeF_2 + Na_2PO_4$ and $YPO_4 + 2NaF = YF_2 + Na_2PO_4$. The results of this study supporting previous indications that REE mobility under granulite-facies conditions is strongly promoted by complexing with F in the aqueous phase.

MS08-T1

Thermodynamic Properties of Grossular Garnet I: Nature of Problem, Analysis of Published Calorimetric Data and Sample Characterization

C.A. Geiger[1], E. Dachs[1]
[1]Universität Salzburg, Materialforschung & Physik, Salzburg, Austria

In spite of the large and varied amount of research that has been done on grossular, $Ca_3Al_2Si_3O_{12}$, there is still uncertainty regarding its exact thermodynamic properties and most prominently its heat capacity, C_p, behavior. Its standard third-law entropy, $S°$, is uncertain with published values ranging between about 255 and 260 J/(mol·K). Because of insufficient sample characterization in the various published studies, it is difficult to interpret and resolve the conflicting calorimetric, i.e. C_p and $S°$, results.

To resolve the discrepancies and to obtain a robust value of $S°$ for grossular, three synthetic grossulars and four natural grossular-rich garnets were investigated by optical microscopy, electron microprobe analysis, IR and MAS NMR spectroscopy and X-ray powder diffraction methods. The compositional and structural properties of the synthetic grossular used in two published C_p studies were (re)investigated as were those of two additional synthetic grossular samples. Two natural grossulars (Jeffrey Mine, Quebec, Canada), which crystallized in relatively low temperature fluid-present geological environments ($T < 400$ °C), were also studied. In addition, two grossular samples (probably from Lualenyi, Kenya) that probably crystallized in the amphibolite facies were characterized.

All synthetic grossular samples contain small amounts of wollastonite estimated at roughly 2 volume percent and the compositions of two samples appear to show slight deviations from grossular stoichiometry. ^{29}Si and ^{27}Al MAS NMR spectra indicate that synthetic grossular crystallized from a glass at high P- and T-conditions is ordered with respect to Al and Si. The natural garnets from the Jeffrey mine are optically anisotropic and the other two are isotropic. These natural garnets have between 94 and 97 mole percent grossular with minor fractions of other garnet components, as well small amounts of structural OH as shown by single-crystal FTIR spectra, in solid solution.

Possible reasons for the observed differences in $S°$ values between synthetic and natural grossulars are discussed. Variations in structural state and composition and assumptions used in correcting for solid-solution components in the natural samples appear to be the most important factors that could account for their slightly smaller $S°$ values around 255-257 J/(mol·K) compared to synthetic grossular. A value of approximately $S° = 260$ J/(mol·K) is considered the best estimate for pure end member grossular based on the existing data.

MS08-T2

Thermodynamic Properties of Grossular Garnet II: Heat Capacity Measurements and Behavior, Standard Entropy and Selected Petrologic Applications

E. Dachs[1], C.A. Geiger[1], A. Benisek[1], K.-D. Grevel[2]
[1]Materialforschung & Physik, Abteilung Mineralogie, Salzburg, Austria
[2]Institut für Geowissenschaften, Jena, Germany

The C_p behavior of seven different grossular samples, three synthetic samples (Gr-Has, Gr-R92, Gr-Kiel) and four natural garnets was investigated in a detailed and systematic manner. Low-temperature heat capacity measurements between 5 and 300 K were made using relaxation calorimetry (PPMS) and between 282 and 764 K using DSC methods. The PPMS C_p data were adjusted slightly using the DSC C_p results to improve the accuracy of the low temperature data set [1]. For the three synthetic grossulars standard entropy values of $S^o = 260.9 \pm 2.0$ J/mol·K for sample Gr-Has, $S^o = 259.1 \pm 2.2$ J/mol·K for Gr-R92 and $S^o = 260.4 \pm 2.0$ J/mol·K for Gr-Kiel were derived. The finally recommended S^o value for end-member grossular is 260.23 ± 2.10 J/mol·K. The S^o values for the four natural grossular-rich garnets vary between 253.7 ± 1.2 J/mol·K and 256.5 ± 1.2 J/mol·K. The standard entropy value for the natural garnets is roughly 5 J/mol·K smaller compared to that of synthetic grossular. The major difference in terms of heat capacity behavior between synthetic and natural samples is that the latter have lower C_p values at temperatures between 20 K and 100 K by up to about 20 %.

The C_p behavior for grossular above 298 K is given by the polynomial:

C_p (J/mol·K) = $556.18\ (\pm 12) - 1289.97\ (\pm 394) \cdot T^{-0.5} - 2.44014\ (\pm 0.24) \cdot 10^{7} \cdot T^{-2} + 3.30386\ (\pm 0.39) \cdot 10^{9} \cdot T^{-3}$,

which is based on our experimental data and the relative enthalpy values measured by Thiéblot et al. (1999) [2].

Finally, using mathematical programming techniques [3], the compatibility of our grossular data with the experimentally determined equilibrium grossular (Grs) + 2 kyanite (Ky) + a-Quartz (Qtz) = 3 anorthite (An) was checked. The data for Ky, Qtz, and An were taken from [4]; the thermal expansion of Grs was described as:

$V/V^0 = (1 + 2.2917 \cdot 10^{-5}\ (T - 298.15) + 0.54603 \cdot 10^{-8}\ (T - 298.15)^2)$ [5].

The refined data for grossular are $\Delta_f H^0_{298} = -6627.0$ kJ/mol and $S^0_{298} = 258.8$ J/mol·K. The enthalpy of formation of grossular is in good agreement with experimental data.

References:
[1] Dachs E., Benisek A. (2011): A sample-saving method for heat capacity measurements on powders using relaxation calorimetry. *Cryogenics*, in press.
[2] Thiéblot L., Téqui C., Richet P. (1999): High-temperature heat capacity of grossular ($Ca_3Al_2Si_3O_{12}$), enstatite ($MgSiO_3$), and titanite ($CaTiSiO_5$). *Am. Mineral.* **84**, 848-855.
[3] Grevel K.-D., Schoenitz M., Skrok V., Navrotsky A., Schreyer W. (2001): Thermodynamic data of lawsonite and zoisite in the system $CaO-Al_2O_3-SiO_2-H_2O$ based on experimental phase equilibria and calorimetric work. *Contrib. Mineral. Petrol.* **142**, 298-308.
[4] Berman R.G. (1988): Internally-consistent thermodynamic data for minerals in the system $Na_2O-K_2O-CaO-MgO-FeO-Fe_2O_3-Al_2O_3-SiO_2-TiO_2-H_2O-CO_2$. *J. Petrol.* **29**, 445-522.
[5] Isaak D.G., Anderson O.L., Oda H. (1992): High-temperature thermal expansion and elasticity of calcium-rich garnets. *Phys. Chem. Minerals* **19**, 106-120.

MS08-T3

Symplectite formation in the $CaO-MgO-SiO_2$ system: experiments and thermodynamic model

R. Abart[1], B. Joachim[1,2], P. Remmert[2], G. Habler[1], R. Wirth[2]
[1]Universität Wien, Dept. Lithosphärenforschung, Wien, Austria
[2]HelmholtzZentrum Potsdam, Deutsches GeoForschungsZentrum GFZ, Sektion 3.3, Potsdam, Germany

Synthetic monticellite with about 8 mole % forsterite content was annealed at 1 GPa and 1000°C in a piston cylinder apparatus using natural CaF_2 as a pressure medium. At the experimental conditions this monticellite (mtc I) is metastable and breaks down into fine grained symplectite at a sharp reaction front

Two types of symplectite are discerned: Type I symplectite is represented by an intimate intergrowth of forsterite rods less than 1 µm wide in a matrix of less magnesian monticellite (mtc II). Type II symplectite consists of a lamellar intergrowth of forsterite and merwinite. The characteristic wavelength of type I symplectite is on the order of 2 µm, whereas the lamellar spacing of type II symplectite is about 600 nm.

Type I symplectite is formed by the segregation of forsterite from the original monticellite (mct I) which eliminates the forsterite oversaturation in mtc I. Following Cahn (1959) this corresponds to a "cellular precipitation" reaction, whereas the process underlying the formation of type II symplectite may be referred to as a "eutectoidal decomposition" reaction. In both cases, the chemical mass transfer that is required at the interface, where the homogeneous precursor phase (mtc I) is replaced by the chemically heterogeneous symplectite assemblage, occurs by diffusion within the moving reaction front. The different wavelength of the two symplectite microstructures is readily explained by the fact that the eutectoidal decomposition implies a larger amount of chemical mass transfer within the reaction front as compared to the cellular segregation reaction. In this case the diffusion distance, and hence, lamellar spacing, is minimized more effectively than with the cellular precipitation reaction. Element analysis using TEM-EELS revealed that in type 2 symplectite both the merwinite and the forsterite lamellae are chemically homogeneous in profiles perpendicular to the lamellae.

Based on this information a simple thermodynamic model was formulated for type 2 symplectite that allows relating the reaction front velocity to phenomenological diffusion coefficients, which describe re- distribution of the forsterite and merwinite components within the migrating reaction front: The necessary component fluxes are derived via kinematic considerations. The rate of free energy dissipation is written for all diffusion fluxes using the formalism of irreversible thermodynamics. Finally the rate of free energy dissipation is equated to the rate of Gibbs energy change. Based on the experimentally observed microstructure evolution this procedure leads to an estimate of the phenomenological coefficients of diffusion on the order of 10^{-16} [m^2/s] for both the forsterite and the merwinite components in the moving reaction front of Type II symplectite.

References: Cahn JW (1959): The kinetics of cellular segregation reactions. Acta Metallurgica, 7, 18-28.

MS08-T4

First-principles thermodynamics of oxides and silicates in the Mg-Si-O system: application to phase equilibria calculation at high pressures and temperatures.

D. Belmonte[1], G. Ottonello[1], M. Vetuschi Zuccolini[1]
[1]University of Genova, DIPTERIS, Genova, Italy

First principles theory plays a key role in the prediction and modelling of thermodynamic properties of Earth's materials at high pressure and temperature conditions [1,2]. *Ab initio* thermodynamics, allowing the computation of the free energy and thermodynamic functions of condensed phases by means of a combined approach of quantum- and statistical mechanics, provide an alternative and self-consistent way to check the confidence of experimental phase boundaries, calorimetric measurements and thermodynamic assessments. In this paper, *ab initio* modelling of the thermodynamic and thermoelastic properties of magnesium oxides and silicates relevant to the physics of the Earth's interior have been carried out with the CRYSTAL code [3] and the hybrid B3LYP density functional method [4]. The mineral phases investigated in this study are periclase (MgO), stishovite (SiO_2), the Mg_2SiO_4 polymorphs (forsterite, Mg-wadsleyite and Mg-ringwoodite), phase anhydrous B ($Mg_{14}Si_5O_{24}$), $MgSiO_3$ ilmenite and tetragonal majorite. The vibrational density of state (vDOS) of these minerals has been reproduced in the framework of quasi-harmonic approximation through a full phonon dispersion calculation or, alternatively, a modified Kieffer's model [5,6] splitting the acoustic and optic modes contribution to thermodynamic functions. The latter approach seems to reproduce well the vDOS, allowing a sufficiently accurate determination of thermodynamic properties [7,8,9]. The calculated properties are in good agreement with the available calorimetric measurements at ambient pressure and, if coupled appropriately with compressibility and thermal expansion data, concur to define an internally-consistent thermodynamic dataset applied to phase equilibria calculation between pure phases at high pressures and temperatures. The results obtained for phase equilibria of geophysical interest are discussed, along with some possible petrological implications concerning phase relations and seismic discontinuities in the Earth's mantle.

[1] Gillan, M.J., Alfè, D., Brodholt, J., Vočadlo, L., and Price G.D. (2006) *Rep. Prog.. Phys.*, **69**, 2365-2441.

[2] Wentzcovitch, R., and Stixrude, L.. (eds.) (2010) *Rev. Mineral. Geochem.*, **71**, Mineralogical Society of America and the Geochemical Society, Washington D.C.

[3] Dovesi, R., Saunders, V.R., Roetti, C., Orlando, R., Zicovich-Wilson, C.M., Pascale, F., Civalleri, B., Doll, K., Harrison, N.M., Bush, I.J., D'Arco, Ph., and Llunell, M. (2010) *CRYSTAL 09. User's Manual*, Università di Torino, Torino.

[4] Becke, A.D. (1993) *J. Chem. Phys.*, **98**, 5648-5652.

[5] Kieffer, S.W. (1979a) *Rev. Geophys. Space Phys.*, **17**, 1-19.

[6] Kieffer, S.W. (1979b) *Rev. Geophys. Space Phys.*, **17**, 35-59.

[7] Ottonello, G., Civalleri, B., Ganguly, J., Vetuschi Zuccolini, M., and Noel, Y. (2009a) *Phys. Chem. Minerals*, **36**, 87-106.

[8] Ottonello, G., Vetuschi Zuccolini, M., and Civalleri, B. (2009b) *CALPHAD*, **33**, 457-468.

[9] Ottonello, G., Civalleri, B., Ganguly, J., Perger, W.F., Belmonte, D., and Vetuschi Zuccolini, M. (2010) *American Mineralogist*, **95**, 563-573.

MS09-T1

Kunstgeschichtlich bedeutsame Ockerpigmente aus Thüringen: Bergbau, Mineralogie und Geochemie

E. Knop[1], A. Karstädt[2], V. Gröschner[3]
[1]Universität Salzburg, Materialforschung & Physik, Salzburg, Austria
[2]Fachhochschule Erfurt, Fakultät Bauingenieurwesen & Konservierung, Erfurt, Germany
[3]Ingenieurbüro für Denkmalpflege, Rudolstadt, Germany

Für die Rekonstruktion historischer Maltechniken und damit für die Restaurierung kunstgeschichtlicher Zeugnisse ist die Kenntnis der verwendeten Farbpigmente von großer Bedeutung. Dabei spielt die Verwendung lokaler Erzeugnisse eine entscheidende Rolle im jeweiligen regionalen Kontext. Ockerpigmente wurden bereits seit der Altsteinzeit zu vielfältigen Malzwecken genutzt und schon im Neolithikum bergmännisch gewonnen. Aus der Antike sind zahlreiche Ockerbergwerke in Ägypten, Griechenland und Südfrankreich bekannt. Im Mittelalter befindet sich der Schwerpunkt des Ockerabbaus im toskanischen Raum. Vermutlich seit dieser Zeit wurde bis ins 19. Jhdt. hinein auch im Thüringer Raum Ocker zur Pigmentgewinnung bergmännisch abgebaut. Da wenig über die Zusammensetzung thüringischer Ockerpigmente bekannt ist, wurde diese Untersuchung durchgeführt, um weitere Kenntnisse über das häufig verwendete Pigment zu erlangen. Diese Informationen sollen mithelfen, den Herstellungs- und Gewinnungsort der in Wand- und Skulpturfassungen verwendeten Ockerpigmente zu bestimmen.

In Zuge der Untersuchungen wurden fünf gelbe Ocker miteinander verglichen: Drei thüringische Ocker, aus Saalfeld, Schmiedefeld und Großneundorf, sowie zwei kommerziell erhältliche Ocker aus Roussillon (Französischer Ocker) und Italien (Terra di Siena). Ein besonderes Augenmerk wurde dabei den drei in Thüringen abgebauten Ockern gewidmet.

Die Ocker wurden zunächst im Streupräparat mit Polarisationsmikroskopie (PLM) untersucht. Weiterhin wurden die fünf Pigmente mittels Röntgendiffraktometrie (XRD) und Röntgenfluoreszenzanalyse (RFA) untersucht. Makroskopisch haben die Ocker von Großneundorf und Terra di Siena dieselbe mittelbraune Farbe, während Saalfeld etwas röter ist. Die braune Farbe ist in allen drei Ockern auf Goethit zurück zu führen, die rötliche Nuance von Saalfeld kann einem geringen Maghemitanteil zugeordnet werden. Demgegenüber hat Schmiedefeld und der Französische Ocker eine helle Färbung, die bei Schmiedefeld ins grünliche und beim Französischen Ocker ins gelbliche tendiert. Dies bei Schmiedefeld auf Eisensulfatphosphat und beim Französischen Ocker auf Verdünnungseffekte durch Quarz zurück zuführen. Die fünf Ocker lassen sich zusammenfassend wie folgt charakterisieren:

- **Großneundorf:** Quarz + Goethit + Hellglimmer + (Lepidokrokit) 44,3 Gew% SiO_2, 15 Gew% Al_2O_3, 22,2 Gew% Fe_2O_3, 3,5 Gew% K_2O, 1800 ppm Ba, 1000 ppm Ni, 2500 ppm Zn
- **Saalfeld**: Goethit (zoniert; dunkle Kerne, heller Saum) + Maghemit + (Kaolinit) + (Kokkolithen) 3,5 Gew% SiO_2, 9,3 Gew% Al_2O_3, 6,8 Gew% P_2O_5, 59,9 Gew% Fe_2O_3, 2,1 Gew% SO_3, 4800 ppm CaO, 240 ppm U, 1830 ppm V, 320 ppm Y
- **Schmiedefeld:** Giniit (Diadochit) + Jarosit + (Hellglimmer) + (Spuren von Kaolinit und Quarz) 1,4 Gew% SiO_2, 0,6 Gew% Al_2O_3, 23,2 Gew% P_2O_5, 48,9 Gew% Fe_2O_3, 4,1 Gew% SO_3, 2600 ppm As, 120 ppm Cl, 340 ppm Cr, 70 ppm Sc, 1580 ppm V
- **Französischer Ocker:** Quarz + Goethit + Kaolinit + (Hämatit) + (Zirkon, akzessorisch) 67 Gew% SiO_2, 19,3 Gew% Al_2O_3, 0,6 Gew% TiO_2, 4,3 Gew% Fe_2O_3, 190 ppm Cr, 95 ppm La, 290 ppm Sr
- **Terra di Siena:** Quarz + Kaolinit + Goethit + (Maghemit) 25,7 Gew% SiO_2, 9,8 Gew% Al_2O_3, 1,2 Gew% MgO, 47,8 Gew% Fe_2O_3, 580 ppm Cr, 220 ppm Ni, 1230 ppm V, 660 ppm Zn

MS09-T2
Provenancing Classical Marbles with Object Based Image Analysis

P. Hofmann[1], R.Mmarschallinger[1], M. Unterwurzacher[1], F. Zobl[1]
[1]öaw, giscience, salzburg, Austria

Knowing material provenance is of utmost importance in archaeology. Results from provenance studies can prove the extraction of material from a specific quarry at a specific time, yielding ideas on economical relations, travel routes, sometimes also on workshops and settlements. As for marbles, in most cases it is impossible to base provenance studies on macroscopical criteria alone. Mineralogical, petrographical and geochemical methods are used to provide additional information to assist with historical interpretations. Especially the data obtained by microscopical studies of the samples, like accessory minerals and grain size, grain shape, twinning types and the texture of grain boundaries of the rock forming mineral calcite (and/or dolomite) have proven successful as a provenance factor (Unterwurzacher et al. 2005). However, for achieving statistically relevant results from microscopy studies, large numbers of calcite grains have to be manually measured under the microscope - a tedious, error-prone and more or less subjective process. As a foundation for consistent and comparable results, we used Object Based Image Analysis ("OBIA") for extracting some key parameters of the calcite crystal population of archeologically relevant marble samples. As compared to classical, pixel based image analysis which mainly considers the (multi)spectral properties of single pixels, OBIA can include additional expert knowledge in the form of flexibly adaptable rule-sets (e.g., Hofmann and Marschallinger, 2009). For the current purpose, we used stepwise rotated marble thin sections under parallel and crossed polarizers. From these redundant input data, we were able to automatically recognize calcite mineral phases in pure and polymineralic marbles with grain recognition rates generally better than 95%. As soon as individual grains are recognized and turned to image objects, key parameters like area, length, width and derived indices like border complexity, compactness or shape index are automatically calculated yielding an unprecedented accuracy of extracted marble parameter. The method is considered a state-of-art approach not only to marble classification, but to petrographic image analysis in general (Marschallinger and Hofmann 2010).

References:

Hofmann, P., Marschallinger, R., Daxner-Höck, G. (2009) 3D volume modelling of fossil small mammal teeth using micro CT and object based image analysis. Computational Vision and Medical Image Processing, CRC Press, 395-399

Marschallinger, R., Hofmann, P. (2010) The application of Object Based Image Analysis to Petrographic Micrographs. In: Microscopy: Science, Technology, Applications and Education, Vol.2 4: Formatex, 1526-1532 .

UNTERWURZACHER, M., POLLERES, J., MIRWALD, P.W. (2005) Provenance Study of Marble Artefacts; Archaeometry, 47, 265-273.

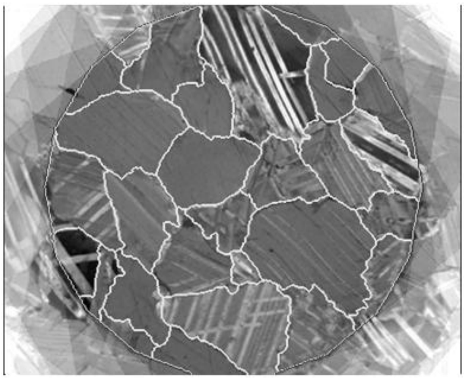

Figure 1: Calcite mineral objects, as derived by OBIA from a stack of co-registered, incrementally rotated micrographs acquired with parallel and crossed polarizers. Here, mineral phase recognition is nearly 100%.

MS09-T3
MS-TG Analysis - a method to detect volatile impurities

K. Galonska[1], G. Heide[1]
[1]Institut für Mineralogie, Fakultät für Geowissenschaften, Geotechnik und Bergbau, Freiberg, Germany

Question

The chemical composition and the source of the raw materials of medieval glasses is an interesting topic of research [1].

Methods

Different mediaeval window glasses from Divi Blasii church (Mühlhausen, Germany) are investigated by MS-TG and EDX Analysis. The used special MS-TG Analysis with strong coupling allows to detect volatile impurities under well-defined high temperature conditions. Heide et. al. [2] verify that gas release profiles from this special method are suitable tools for the identification of glass samples of unknown origin.

Results and Conclusions

In connection with the chemical composition of 27 samples determined by EDX it's possible to reconstruct high temperature processes in the man-made glasses.

The mediaeval windows glasses from Divi Blasii church show significant different gas releases of water, sulphur dioxide, carbon dioxide, chlorine amongst others. The gas release profiles and the chemical composition of the glasses lead to conclusions about the manufacturing process - for instance raw materials, melting temperature and melting quality.

References

[1] Wedepohl, K.H., Simon, K., Glas in Antike und Mittelalter, Geschichte eines Werkstoffs, E.Schweizerbart'sche Verlagsbuchhandlung (Nägele u. Obermiller), Stuttgart, 2003
[2] Heide, K., Hartmann, E., Gert, K., Wiedemann, H.G., MS-TGA of ancient glasses: an attempt to determine the manufacturing conditions (I), thermochimica acta 365 (2000) 147-156

MS10-T1
Sichtbarkeit der Mineralogie in unserer Gesellschaft - ein Spiegelbild unseres Schulsystems

R. Stalder[1]
[1]Universität Innsbruck, Institut für Mineralogie und Petrographie, Innsbruck, Austria

Im Frühjahr 2010 bricht auf Island der Eyafjallajökull aus und beeinträchtigt über Wochen den Flugverkehr über den Nordatlantik. Erst Tage nach dem Beginn des Ausbruchs und nach zahllosen Interviews mit Ökonomen und Reiseveranstaltern über die wirtschaftlichen Konsequenzen wird im Nachrichtenstudio ein Vulkanologe befragt, was da überhaupt geschieht und wann mit einem Abklingen der Aktivität zu rechnen ist.

Die Tatsache, dass Mineralogie (sensu lato) in Deutschland kein Schulfach ist, führt allzu oft dazu, dass in öffentlichen Debatten über Themen mit mineralogischen Inhalten die Fachkompetenz von Mineralogen nicht mit einbezogen wird. Themen mit mineralogischen Kernkompetenzen werden stattdessen in der öffentlichen Wahrnehmung nicht selten zunächst in den (Schul)fächern Geographie oder Chemie angesiedelt. Darüber hinaus lassen Schulbücher aber gerade in Bezug auf mineralogische Themen deutliche Mängel erkennen, von Halbwissen über sachliche Fehler (z.B. Na läge auf der Erde vor allem in Form von Salzen vor) bis hin zu sehr missverständlichen und fehlerhaften, landläufigen Darstellungen (z.B. der Erdmantel sei bis in große Tiefen hochgradig aufgeschmolzen). Ein Problem ist hier das fehlende Mitwirken von Mineralogen, die - mangels eines eigenen Schulfaches - auch bei der Gestaltung von Lehrplänen kaum Einfluss haben.

Dabei sind mineralogische Inhalte bereits vielfältig in allen Abschnitten der gymnasialen Lehrpläne verankert, hierunter gesellschaftlich hochrelevante Themen wie Naturkatastrophen (Vulkanismus), Rohstoffe (Lagerstättenkunde) und Klimarekonstruktion (Geochemie, Biomineralisation). Diese Themen sind in einer breiten Palette von Schulfächern eingebettet, allen voran Geographie, aber auch Chemie, Physik und Natur und Technik.

Die Kommission für Hochschulfragen der Deutschen Mineralogischen Gesellschaft ist bestrebt, (1) Darstellung mineralogischer Inhalte in Schulbüchern bzw. -medien zu verbessern und (2) in Schulbüchern Themen mit mineralogischer Kernkompetenz dem Fach Mineralogie korrekt zuzuordnen. In den vergangenen Monaten ist ein Dialog mit Vertretern von Schulen, Didaktik-Verbänden und Schulbuch-Verlagen in Gang gekommen. Eine engere Zusammenarbeit auf dem Sektor Schulmedien wird angestrebt.

MS10-T2
Vom Lehrplan bis zur Schulbuchgenehmigung - Der Weg naturwissenschaftlicher Inhalte in den Unterricht

W. Schierle[1]
[1]Staatliches Seminar für Didaktik und Lehrerbildung, Heilbronn, Germany

Lehrpläne schreiben fest, welche schulischen Lernanforderungen eine Gesellschaft an die nachwachsende Generation stellt. Ihnen wird eine Reihe von Funktionen zugeschrieben, so signalisieren sie u.a. politische Willensäußerungen über verbindliche Bildungsziele, steuern den Unterricht und gewährleisten einheitliche Lehr- und Lernbedingungen für gleichartige Schulen. Nicht zuletzt stellen sie den Rahmen dar für die Lehrwerksarbeit der Schulbuchverlage.

Nach einer mittleren Gebrauchsdauer von etwa zehn Jahren erfolgt meist eine Überarbeitung oder Neubearbeitung der Lehrpläne durch Expertenkommissionen (Lehrplankommissionen), nach ministeriellen Vorgaben und Rahmenbedingungen. Inhaltlich orientieren sich die Kommissionen u.a. am Stand der wissenschaftlichen und methodisch-didaktischen Entwicklung des Fachgebiets. Darüber hinaus erhalten sie für die inhaltliche Ausgestaltung zahlreiche Anregungen von Verbänden, Institutionen und Einzelpersonen.

In der deutschen Bildungslandschaft (16 Bundesländer!) erfolgt seit einigen Jahren ein Übergang von Lehrplänen (mit exakt angegebenen Zielen und Inhalten) zu Bildungsplänen, mit einer Formulierung von Bildungsstandards, die weniger inhaltliche Festlegungen als bestimmte Kompetenzen der Schüler beschreiben. Damit bieten sich den Lehrplankommissionen, den Lehrern und auch den Verlagen weitaus zahlreichere Variationsmöglichkeiten bei der inhaltlichen Ausgestaltung.

Spätestens nach Veröffentlichung einer ersten Anhörungsfassung der Lehrpläne beginnen in den Redaktionen der Schulbuchverlage die grundlegenden Konzeptionssitzungen mit den Autorenteams sowie die Planung und die Verteilung der inhaltlichen Arbeit. Die Teams bestehen häufig aus Redakteuren, Lehrern mit Aufgaben in der Schulaufsicht, Lehrerausbildern, Lehrern und evtl. Hochschulangehörigen. Anschließend folgt die technische Fertigstellung des Buches in Redaktion und Druckerei.

In 12 von 16 Bundesländern müssen die Bücher als letzte Hürde noch ein (z.T. sehr unterschiedlich ausgeprägtes) Genehmigungsverfahren überwinden. Von der Planung bis zum Einsatz eines Schulbuches vergehen so je nach Ausmaß der Überarbeitung bzw. Neubearbeitung 10 bis 24 Monate. Ob mit einem Werk nach seiner offiziellen Einführung an einer Schule auch tatsächlich gearbeitet wird, hängt jedoch sehr stark von den Lehrkräften ab.

MS10-T3
Schulgeographie 2000 plus... - Mit den Geowissenschaften durchs neue Millennium!?

G. Falk[1]
[1]Pädagogische Hochschule Freiburg, Inst. für Naturwiss. und Technik / Geographie, Freiburg, Germany

Die aktuellen deutschen Lehr- und Bildungspläne offenbaren eine scheinbare Schieflage zwischen Anthropo - und physisch Geographischen Themenfeldern. Besonders die „harten (natur-)geowissenschaftlichen Fakten und aktuelle wissenschaftliche Erkenntnisse aus den benachbarten Disziplinen Geologie, Geochemie, Petrologie, Ozeanographie usw. finden bislang nur rudimentäre Berücksichtigung, während die Themenkreise der

Wirtschafts-, Kultur-, Sozial-, und Siedlungsgeographie vielfach breiten Raum einnehmen und im sozialwissenschaftlichen Gemenge längst auch Fragestellungen anderer Sozial- und Geisteswissenschaften berühren. Die Behandlung anthropogeographischer Aspekte im Unterricht ist grundsätzlich zu begrüßen, doch mangelt es vor dem Hintergrund der fachlichen Breite der Geographie insgesamt an Ausgewogenheit. Parallel zu einem sich zaghaft abzeichnenden Trend nunmehr auch wieder verstärkt Themen der physischen Geographie im Unterricht zu behandeln, vollzieht sich in den benachbarten Geowissenschaften eine Entwicklung, die zunehmend auch den Menschen ins Blickfeld wissenschaftlicher Erkenntnisse rückt. Stand noch vor wenigen Jahren das System Erde in der Diskussion, so ist es heute das System Erde-Mensch. Daraus erwachsen auch für den modernen Geographieunterricht neue inhaltliche Optionen. Viele der aktuellen und oft bahnbrechenden Erkenntnisse tangieren ohnehin auch die physische Geographie und bedürfen somit keiner besonderen didaktischen Legitimierung. Aber auch Themenfelder, die über die unmittelbaren Kernkompetenzen physischer Geographen hinausgreifen (z.B. Lagerstättenexploration, Seismik, Ozeanographie usw.) sollten aufgrund ihrer hohen Zukunftsrelevanz Gegenstand unterrichtlicher Betrachtung sein. Wenn nicht ein neues Schulfach Geowissenschaften die Schulgeographie langfristig substituieren soll ist es quasi unumgänglich, den gesamtgeosystemaren Kontext, also das System Erde-Mensch, wieder als zentralen Gegenstand ins Visier schulgeographischer Bemühungen zu rücken. Bereichert durch spannende, zukunfts- und persönlich relevante Themen, die nicht zuletzt die Lebens- und Überlebensperspektiven auf dem Planeten Erde betreffen und mit der politisch-wirtschaftlichen Lobby aller Geowissenschaften im Rücken dürfte unser Fach in der Schule mittelfristig neuen Aufwind erfahren.

Zunächst gilt es festzustellen was, wie, wo und in welchem Umfang an geowissenschaftlichen Informationen an den Schulen vermittelt wird, um auf dieser Grundlage mögliche Notwendigkeiten oder Probleme zu diskutieren. Überdies gilt es die Themen zu erfassen, die einerseits den benachbarten Geowissenschaften „unter den Nägeln brennen gleichsam aber auch in geeigneter Form in die Schulgeographie integrierbar erscheinen. Dazu müssen auch die Kompetenzen der Lehrerinnen und Lehrer einbezogen werden.

MS10-T4
Unkonventionell und unerlässlich: Mineralogie im Schulalltag

D. Jacob[1], S. Horn[1]
[1]Johannes Gutenberg- Universitaet, Institut fuer Geowissenschaften, Mainz, Germany

Die Mineralogie kommt als eigenständiges Lehrfach an den Schulen nicht vor, obwohl sie doch ein fester - wenn auch oftmals unsichtbarer - Bestandteil der Grundlagenvermittlung in vielen Schulfächern ist. Wichtige Grundlagen der Mineralogie, wie z.B. Symmetrie und Form, sowie Licht und Farben und damit eng verknüpft auch die Mikroskopie, könnten verstärkt unter mineralogischen Aspekten in den klassischen naturwissenschaftlichen Fächern wie Mathematik, Physik, Chemie und Biologie vermittelt werden. Durch den interdisziplinären Charakter der Mineralogie, kommt ihr gerade im Fach Naturwissenschaften der Orientierungsstufe eine bedeutende Rolle zu, die verstärkt eingesetzt werden sollte. Der Alltagsbezug ist in quasi allen Facetten vorhanden.

Darüber hinaus gibt es vielfältige Möglichkeiten die Mineralogie in den Schulalltag zu integrieren, oft auch in Fächern, die nicht offensichtlich eine Verbindung haben, wie z.B. Kunst.

Hier kann man über Projekte zu mineralischen Farbpigmenten die Mineralogie mit der Chemie und der künstlerischen Gestaltung, sowie mit geschichtlichen Hintergründen kombinieren (z.B. Seilnacht 2004). Farben werden dann nicht losgelöst ausschließlich als Zeichenmaterial verwendet, sondern werden lebendig durch die Vielschichtigkeit in denen sie auftreten. Zum Beispiel die Farbe Blau aus Lapislazuli, Zinnoberrot, Ockergelb und viele andere.

Recherchieren, konzipieren, gestalten, experimentieren, produzieren… machen solche Projekte zu Highlights, die durch ihre praktischen Möglichkeiten für die Schüler unvergesslich bleiben.

Grundvoraussetzung für mehr Mineralogie im Schulalltag ist jedoch eine bessere Einpassung der Inhalte in das Lehrplan-Rahmenprogramm gleichberechtigt mit den bisher dort aufgeführten Fächern Physik, Chemie und Biologie. Zu oft wird die Einbringung von mineralogischen Inhalten den individuellen Neigungen der entsprechenden Lehrer überlassen. Um dieser Abhängigkeit von „good will“ zu entgehen, müsste eine allgemein verbreitete/anerkannte und solide Basis geschaffen werden. Dazu sollte die Mineralogie schon in der Ausbildung der Lehramtskandidaten integriert werden.

Es muss das Ziel der mineralogischen Berufsverbände sein sich dort verstärkt einzubringen.

Seilnacht, T. Naturwissenschaftliches Arbeiten mit Schülerinnen und Schülern. Verlag Seilnacht, ISBN 3-9522892-1-3, 2004.

MS11-T1
ICSD Web - Current state and new developments

S. Rühl[1]
[1]FIZ Karlsruhe, Eggenstein-Leopoldshafen, Germany

The new ICSD Web [1] is now available for more than 2 years and it attracts more and more users with its modern graphical user interface combined with the excellent quality of included data entries. ICSD Web is developed by FIZ Karlsruhe in order to meet the increasing requirements of the users.

Features uniquely found in ICSD Web:

The visualization is realized as an interactive web browser applet (Jmol [2]) which offers suitable features for displaying crystal structures and is highly customizable.

A very convenient tool for the comparing similar entries is the so-called synoptic view. It simultaneously shows up to six standardized crystal structures or powder pattern diagrams generated on the fly from the CIF files.

Introduction of quality ranking to allow easier identification of relevant entries. This feature will be developed further by introducing more filter criteria to allow individual selections.

Support for SFX-servers offering direct access to full texts available for your site.

The current version of the ICSD [3] contains 140,116 entries including 123,923 fully determined crystal structures derived from experimental data and 16,193 crystal structures with atom coordinates derived from the corresponding structure types.

[1] ICSD is available online at http://icsd.fiz-karlsruhe.de. More details can be found on http://www.fiz-arlsruhe.de/icsd_web.html
[2] Jmol: an open-source Java viewer for chemical structures in 3D. http://www.jmol.org/
[3] Bergerhoff G., Brown I.D., „*Crystallographic Databases*“, 1987, Allen F.H. (Editor) Chester, International Union of Crystallography.

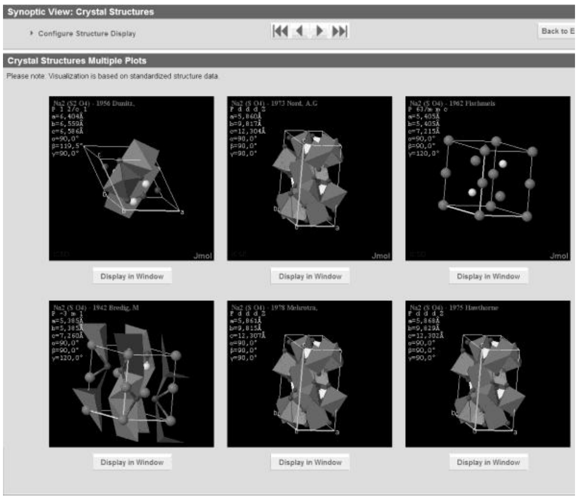

Figure 1

MS11-T2
Fascinating structural and topological complexity of oxocentered units in divalent lead natural and synthetic oxyhalides.

O. Siidra[1], S. Krivovichev[1]
[1]Saint-Petersburg State University, Crystallography, Saint-Petersburg, Russian Federation

Minerals and inorganic compounds with PbO-derivative blocks are important phases that occur under variety of natural and technological conditions. Structural investigations carried out within the past three years revealed that the structures of these phases consist of PbO-like blocks alternating with tetragonal sheets of halide ions, X^-. Since PbO blocks are electroneutral and X sheets are negatively charged, the structure requires a charge-balance mechanism to compensate for the negative charge of the X sheets. This may be achieved through 5 different schemes. In all of the studied structures O atoms have tetrahedral coordination, thus being central for the oxocentered OPb_4 tetrahedra [1].

Recently we have discovered two new lead oxyhalide minerals (IMA 2011-020 and IMA 2011-027) from Kombat mine. Different structural features of new minerals make them the most complex Pb oxyhalides known to date. The crystal structure of IMA 2011-027, $[Pb_{32}(O,\square)_{21}](AsO_4)_2[(Si,As,V,Mo]O_4)_2Cl_{10}$ (*C2/c, a* = 23.139(3)*, b* = 22.683(3)*, c* = 12.389(2) *Å, β* = 102.090(3)°*, V* = 6358.7(4) Å^3*, R_1* = 0.053) consists of alternating PbO double layers and chlorine sheets (1:1 type). The tetrahedral AsO_4 and $(Si,As,V,Mo)O_4$ groups locate in defects within the O-Pb block. The structure of the $[Pb_{32}(O,\square)_{21}]$ layer itself is formed of symesite and kombatite modules which are organized into alternating diagonal stripes of similar structure. Comparing deficient PbO-type layers in the structures of the kombatite-sahlinite series and symesite, one may suggest that dimensions of defects correlate with the dimensions of the incorporated anion; larger $(AsO_4)^{3-}$ and $(VO_4)^{3-}$ anions in the case of kombatite-sahlinite and the smaller $(SO_4)^{2-}$ anion in the case of symesite. This hypothesis is supported by the discovery of IMA 2011-027.

The structure of IMA 2011-020, $[Pb_{32}O_{18}][Pb_4Mn_2O]Cl_{14}(BO_3)_8{\cdot}2H_2O$ (*Pmmn a* = 12.759(1), *b* = 27.169(4), *c* = 11.515(1)Å, *V* = 3992.01(9) Å^3 , *R_1* = 0.048) belongs to the 1:1 type also. The remarkable feature of the structure is the formation of a heterometallic, oxocentred OPb_4Mn_2 octahedron. Jointly, OPb_4Mn_2, MnO_5Cl octahedral and BO_3 groups found in the structure of IMA 2011-020 form unusual oxocentred clusters. The borate groups jointly with the lone pairs on lead cations provide three-dimensional integrity. The formation of heterometallic oxocentred clusters causes the presence of cross-like vacancies in the $[O_{18}Pb_{32}]$ layer.

Comparison and topological analysis with the other PbO-derivative blocks known to date will be given.

This work was financially supported by DFG-RFBR collaboration grant (#11-05-91330) and Russian President grant for young scientists (MK-5074.2011.5).

[1] Siidra, O.I., Krivovichev, S.V. and Filatov, S.K. (2008) Minerals and synthetic Pb(II) compounds with oxocentered tetrahedra: review and classification. *Zeitschrift für Kristallographie*, **223**, 114-125.

MS11-T3
Multi-valence states and multi-coordinations in complex actinide phosphites and phosphates.

E.V. Alekseev[1,2], E.M. Villa[3], W. Depmeier[2], T.E. Albrecht-Schmitt[3]
[1]Forschungszentrum Jülich, IEK-6, Jülich, Germany
[2]Universität zu Kiel, Department of Crystallography, Kiel, Germany
[3]University of Notre Dame, Department of Civil Engineering and Geological Sciences and Department of Chemistry and Biochemistry, Notre Dame, United States

Synthesis and structural chemistry of inorganic actinide compounds is currently a rapidly developing discipline. A variety of valence states and possible coordination environments make the structural chemistry of actinides very rich. Phases containing oxo-anions are of special interest in this field because they are closely related to natural actinide minerals and to problems of safe management of spent nuclear fuel. Here we report on very recent results of our investigations into the formation and structural features of new phases in the actinide-pshosphite system: An+ – An – H3PO3 – H2O (An+ - alkali and alkali-earth elements, An – Th, U or Np).

To date we have obtained 15 new phases in this system. Six of them are pure phosphites (P3+), viz. ThIV(HPO3)2(H2O)2 (1), UIV(HPO3)2(H2O)2 (2), NpIV(HPO3)2(H2O)2 (3), Rb2[(UO2)2(HPO3)3] (4), Cs2[(UO2)2(HPO3)3](H2O) (5), Cs2[(UO2)2(HPO2(OH))2(HPO3)2] (6). Five phases contain both, P3+ and P5+, and are mixed phosphites/phosphates: Rb4[(UO2)4UIV2(HPO4)(PO4)4(HPO3)3(H2O)2] (7), Cs2[UIV3(PO4)2(HPO3)4] (8), Cs2[(UO2)UIV(HPO4)2(HPO3)2] (9), Cs4[(UO2)8(HPO4)5(HPO3)5(H2O)6] (10), (H3O)[(Cax(UO2)1-x)2(UO2)2(PO4)(HPO3)3(H2O)4x] (11). Two further phases are results of full P3+ oxidation to P5+: Cs[UIV(H1.5PO4)(PO4)]2 (12) and Cs[NpIV(H1.5PO4)(PO4)]2 (13). The structure formation can be controlled via pH and the initial ratios of starting compounds.

From the chemical compositions it can be seen that in the new phases the actinides have oxidations states 4+ and/or 6+, in some compounds both states occur simultaneously. The crystal chemistry of these phases is very rich because of the variety of valence states and coordination environments. In total, they crystallize in nine different structure types, and they have different dimensionalities. 1, 2 and 3 are isostructural and crystallize in a 3D framework structure. 7, 8 and 9 are based on 3D frameworks, but crystallize in three different structure types. 12 and 13 are isostructural and have a layered structure based on double layers linked by Cs cations. 11 has a 2D structure based on single layers forming quasi-double layers and linked via protonated H2O molecules. This phase demonstrates the interesting phenomenon of Ca2+/UO22+ isomorphic substitution. All other phases are based on 2D single layers, but crystallize in different structure types. A topological description has been given for the structure of the phases using colored graphs.

MS11-T4

Lanthanido-Ammonium Cations $[\mathrm{NLn_4}]^{9+}$ as Prominent Structural Features in Nitride Derivatives of the 4f-Elements

T. Schleid[1], F. Lissner[1]
[1]Institut für Anorganische Chemie, Universität Stuttgart, Stuttgart, Germany

Almost all lanthanide(III) nitride derivatives contain lanthanido-ammonium cations $[\mathrm{N}Ln_4]^{9+}$ (Ln = 4f-element) as main structural features. They can occur isolated according to 0D-$\{[\mathrm{N}Ln_4]^{9+}\}$ (N:Ln = 1:4) as in compounds of the compositions $Ln_4\mathrm{N}Ch_3X_3$ (Ch = S, Se; X = Cl, Br), $Ln_{10.333}\mathrm{N}Ch_{14}$ and $\mathrm{Na}Ln_{10}\mathrm{NS}_{14}$ or form discrete 0D-$\{[\mathrm{N}_2Ln_6]^{12+}\}$ units (N:Ln = 1:3) as pair of two tetrahedra with a common edge in the crystal structures of some $Ln_3\mathrm{N}X_6$-, $Ln_3\mathrm{NSe}_3$- and $Ln_5\mathrm{NSe}_6$-type representatives. With the same stoichiometry (N:Ln = 1:3), but a one-dimensional infinite topology1D-$\{[\mathrm{N}Ln_3]^{6+}\}$, they share two vertices to build up chains (Fig. 1a) in the formula types $Ln_3\mathrm{N}Ch_3$ and $\mathrm{Cs}Ln_6\mathrm{N}_2\mathrm{Te}_7$. By sharing two edges (*cis*-oriented in $Ln_4\mathrm{N}_2Ch_3$ or *trans*-oriented in $Ln_2\mathrm{N}X_3$, $ALn_4\mathrm{N}_2\mathrm{I}_7$ (A = Li and Na), $Ln_4\mathrm{N}_2\mathrm{Te}_3$ and $Ln_5\mathrm{N}_2\mathrm{Se}_4\mathrm{Br}$), chains of the composition 1D-$\{[\mathrm{N}Ln_2]^{3+}\}$ (N:Ln = 1:2) are generated (Fig. 1b and 1c), but also the condensation via one fused edge and two common corners can lead to chains of the same stoichiometry in $Ln_2\mathrm{N}X_3$ and $Ln_4\mathrm{N}_2\mathrm{S}_3$, when edge-sharing bitetrahedra ($[\mathrm{N}_2Ln_6]^{12+}$) join together with their four free vertices (Fig. 1d). This way of interconnection is also used to construct porous layers 2D-$\{[\mathrm{N}Ln_2]^{3+}\}$ in the nitride chalcogenides $Ln_4\mathrm{N}_2Ch_3$ with four-and-eight- (Ch = S, Fig. 2a) or double-six-ring pores (Ch = Se, Fig. 2b). When two chains of *cis*-edge shared $[\mathrm{N}Ln_4]^{9+}$ tetrahedra are further connected by an extra edge per unit, a complex strand with the composition 1D-$\{[\mathrm{N}_2Ln_3]^{3+}\}$ (N:Ln = 1:1.5, Fig. 1e) emerges in the mixed-anionic compounds $Ln_3\mathrm{N}_2\mathrm{SeBr}$. Crystal structures with double features can either exhibit two kinds of discrete moieties (0D-$\{[\mathrm{N}Ln_4]^{9+}\}$ and 0D-$\{[\mathrm{N}_2Ln_6]^{12+}\}$ units in $Ln_{23}\mathrm{N}_5\mathrm{Se}_{27}$ or 0D-$\{[\mathrm{N}_2Ln_6]^{12+}\}$ and 0D-$\{[\mathrm{N}_3Ln_7]^{12+}\}$ entities in $Ln_{13}\mathrm{N}_5\mathrm{Te}_{12}$) or two kinds of chains (one *cis*-edge and two edge-double-vertex 1D-$\{[\mathrm{N}Ln_2]^{3+}\}$ strands in $Ln_6\mathrm{N}_3\mathrm{S}_4X$ or both an edge-double-vertex 1D-$\{[\mathrm{N}Ln_2]^{3+}\}$ chain and a 1D-$\{[\mathrm{N}_2Ln_3]^{3+}\}$ strand in $Ln_5\mathrm{N}_3\mathrm{S}_2\mathrm{Cl}_2$).

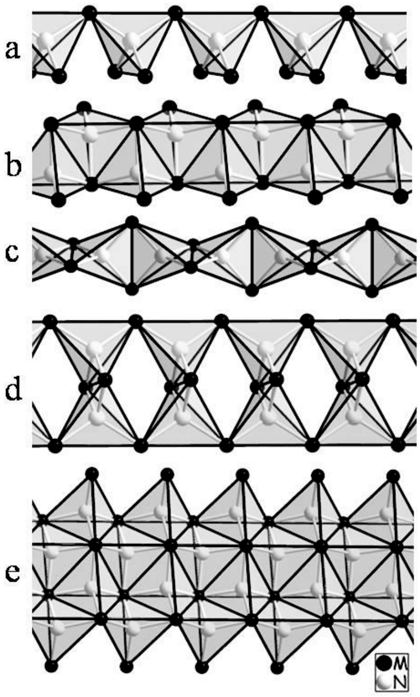

Figure 1

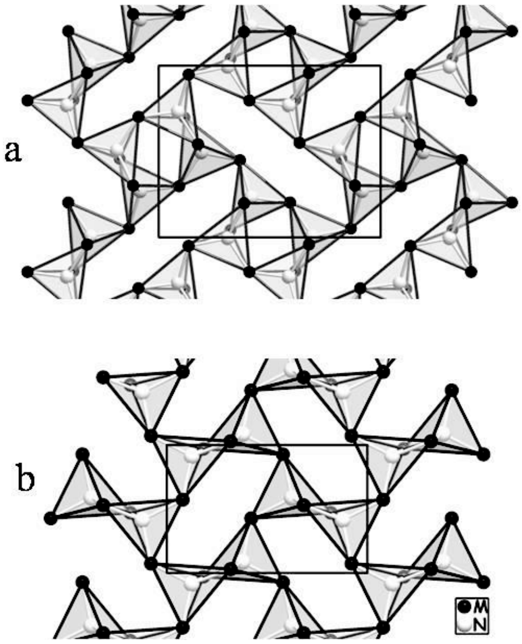

Figure 2

MS11-T5

Das Rätsel der „ungeordneten“ Turmaline

A. Ertl[1], E. Tillmanns[1]
[1]Universität Wien, Institut für Mineralogie und Kristallographie, Wien, Austria

Umfangreiche chemische Untersuchungen an Turmalinen haben gezeigt, dass diese zum Teil sehr komplexe Zusammensetzungen haben können. Die häufigsten Elemente der Erde können wir im Turmalin vorfinden. Aber erst röntgenographische Einkristalluntersuchungen zeigen uns, dass manche Elemente auch an mehreren Positionen auftreten können.

In der Turmalinstruktur gibt es zwei 6-koordinierte Positionen, namentlich die Y- und die Z-Position. Wobei in allen Turmalinen das $\mathrm{YO_6}$-Polyeder größer ist, als das $\mathrm{ZO_6}$-Polyeder. In 6-koordinierter Position können sich die Elemente Al, Mg, Fe, Mn, Li, Ti und seltener auch V, Cr, Cu und Ni befinden. Bindungslängen und Elektronendichten können Hinweise für die Verteilung dieser Elemente in diesen zwei Positionen bringen. Durch Einkristalluntersuchungen konnte in den letzten 30 Jahren nachgewiesen werden, dass Al, Mg und $\mathrm{Fe^{3+}}$ (seltener $\mathrm{Cr^{3+}}$ und $\mathrm{V^{3+}}$) sowohl die Y-, als auch die Z-Position besetzen können. Von verschiedenen Autoren wurden auch $\mathrm{Fe^{2+}}$, $\mathrm{Mn^{2+}}$ und $\mathrm{Ti^{4+}}$ an der Z-Position beschrieben. Allerdings gibt es, aufgrund der Fehlergrenzen von Verfeinerungen und durch induktive Effekte in der Struktur, sowie durch Unklarheiten in der Interpretation von Mößbauer-Spektren, keine eindeutigen Beweise.

Ein „geordneter Turmalin zeichnet sich dadurch aus, dass zum Beispiel die Y-Position komplett mit Mg besetzt ist, während die Z-Position zur Gänze mit Al besetzt ist. Bei einem komplett „ungeordneten Turmalin hingegen, wäre die Z-Position mit $(\mathrm{Al_3Mg_3})$ besetzt, während die Y-Position zur Gänze mit Al besetzt wäre. Aufgrund der ähnlichen Elektronenanzahl von Al und Mg, aber der unterschiedlichen effektiven Ionenradien, lassen sich solche Unordnungen nur durch unterschiedliche mittlere Bindungslängen nachweisen.

In Turmalinen unterschiedlicher Lokalitäten wurden Al-Mg-Unordnungen bestätigt. Aber welche Faktoren begünstigen nun zum Beispiel eine Al-Mg Unordnung zwischen der Y- und der Z-Position? Erklärungsversuche über kristallchemische Zusammenhänge in der Turmalinstruktur waren in der

Vergangenheit nicht sehr erfolgreich. Auffällig ist allerdings, dass in höher metamorphen geologischen Einheiten immer wieder deutliche Al-Mg-Unordnungen in Turmalinen beschrieben wurden. Wobei weniger die Druck- als die Temperaturbedingungen während der Turmalinkristallisation eine wichtige Rolle zu spielen scheinen. Um genauere Gesetzmäßigkeiten zu erhalten, sind noch mehr Einkristalluntersuchungen aus petrologisch gut charakterisierten Einheiten notwendig.

Diese Arbeit wurde vom Fonds zur Förderung der wissenschaftlichen Forschung, FWF, im Rahmen des Projekts P23012-N19, gefördert.

MS11-T6

Straight Si—O—Si bond angles at low temperature

H. Effenberger[1]

[1]Universität Wien, Institut für Mineralogie und Kristallographie, Wien, Austria

In silicates with linked SiO_4 tetrahedra the Si—O_{br}—Si bond angles are usually in the range of 120 to 160°. Occasionally, they are enlarged to (nearly) 180°. For the latter large displacements of the bridging O_{br} atom perpendicular to the O_{br}—Si bond directions were observed. In addition, the Si—O_{br}—Si bond angles and the Si—O_{br} bond distances correlate negatively (Liebau, 1985). (Nearly) straight Si—O_{br}—Si bond angles were discussed extensively on experimental and theoretical considerations and they were compared to pyrophosphates and pyroarsenates. However, the behaviour at low temperatures remained nearly unknown so far. The present investigations focus on the comparison of the crystal chemical behaviour at room temperature (RT) and at 100 K.

The classical example is thortveitite, $Sc_2[Si_2O_7]$ (Kimata *et al.*, 1998). It is isotypic with the high-temperature modification of $Cu_2As_2O_7$ (As—O_{br}—As = 180°) which transforms at ~360°C to a low-temperature modification (As—O_{br}—As = 145.9(2)°) (Weil et al., 2004). Thortveitite shows for the O_{br} atom at RT r.m.s. amplitudes of 0.048-0.031-0.009 Å² which are significantly reduced at 100K (0.034-0.023-0.008 Å²). Si—O_{br} = 1.6061(6) Å (RT) is increased to 1.6088(6) Å (100 K); Si—O_{br}—Si = 180° is maintained. [295 / 100 K, *C*2/*m*: *a* = 6.540(2) / 6.534(2), *b* = 8.509(3) / 8.505(3), *c* = 4.701(1) / 4.699(1) Å, β = 102.89(2)° / 102.84(2)°, *R*1 = 0.022 / 0.021, 823 / 798 reflections, 2δ < 80° (Mo radiation), 35 variable parameters].

Petalite, $LiAlSi_4O_{10}$, is a layer-silicate mineral formed by rugged Si_4O_{10} layers linked by rows of edge-sharing LiO_4 and AlO_4 tetrahedra (Effenberger, 1980; Tagai *et al.*, 1982). Two O_{br} atoms exhibit linear Si—O_{br}—Si bond angles. At RT the r.m.s. amplitudes of the O_{br} atoms are 0.037-0.030-0.009 and 0.029-0.028-0.009 Å², respectively; again a reduction is observed at 100 K (0.032-0.026-0.009 and 0.025-0.024-0.009 Å²). The Si—O_{br} bond lengths of 1.5980(4) and 1.6026(4) Å (RT) are increased to 1.6012(4) and 1.6057 Å (100 K). [295 / 100 K, *P*2/*a*: *a* = 11.758(3) / 11.756(3), *b* = 5.143(1) / 5.134(1), *c* = 7.633(3) / 7.645(3) Å, βbeta = 113.03(2) / 112.99(2)°, *R*1 = 0.030 / 0.037, 2660 / 2656 reflections, 2δ < 80° (Mo radiation), 78 variable parameters].

Pentagonite is the acentric modification of $Ca(VO)[Si_4O_{10}].4H_2O$ (Evans, 1973). It is noteworthy, that even all Si—O_{br}—Si bond angles are not restricted by space-group symmetry, one of them is 176.53(10)°; the r.m.s. amplitudes of this O_{br} atom are 0.026-0.021-0.008 Å²; Si—O_{br} are 1.6016(12) and 1.6042(13) Å. One water molecule p.f.u. is released during cooling to 100 K: Si—O_{br}—Si = 163.3(3)°. In contrast to the other two compounds mentioned above, the r.m.s. amplitudes are slightly increased at 100 K: 0.029-0.023-0.009 Å²; Si—O_{br} = 1.606(4) and 1.614(4) Å. [295 / 100 K, *Ccm*2$_1$: *a* = 10.380(3) / 10.311(5), *b* = 14.082(4) / 14.019(6), *c* = 8.984(3) / 8.910(4) Å, *R*1 = 0.032 / 0.081, 4173 / 4097 reflections; 2δ < 80° (Mo radiation), 105 / 98 variable parameters].

References:

Effenberger, H. (1980): Petalit, $LiAlSi_4O_{10}$: Verfeinerung der Kristallstruktur, Diskussion der Raumgruppe und Infrarot-Messung. - Tscherm. Min. Petr. Mitt. **27**, 129-142.

Evans, H.T.Jr. (1973): The crystal structures of cavansite and pentagonite. - Am. Min. **58**, 412-424.

Kimata, M., Saito, S., Matsui, T., Shimizu, M., Nishida, N. (1998): N. Jb. Min., Mh. **1998**, 361-372.

Liebau F. (1985): Structural chemistry of silicates. - Berlin, Heidelberg, New York, Tokio, Springer-Verlag.

Tagai, T. Ried, H., Joswig, W., Korekawa, M. (1982): Kristallographische Untersuchungen eines Petalits mittels Neutronenbeugung und Transmissionselektronenmikroskopie. - Z. Krist. **160**, 159-170.

Weil, M., Lengauer, C., Füglein, E., Baran, E.J. (2004): The reversible α→β phase transition of $Cu_2As_2O_7$. - Cryst. Growth and Design **4**, 1229-1235.

MS11-T7

$BaPO_3F$ and *β*-Hg_2CrO_4 - Structural Relations Explained by Order-Disorder (OD) Theory

B. Stöger[1], M. Weil[1]

[1]TU Wien, Institut für Chemische Technologien und Analytik, Abt. für Strukturchemie, Vienna, Austria

Order-disorder (OD) theory was conceived in the 1950ies[1] to explain unusual X-ray diffraction effects in minerals like wollastonite[2]. Since then, it has been developed into a versatile theory for the explanation of polytypism, diffuse scattering, non-crystallographic absences, twinning and as a means to classify structures by symmetry principles. It has been applied to all major classes of compounds, *viz.* minerals, synthetic inorganic compounds, organic salts and molecular compounds and recently even proteins and other biological macro-molecules[3,4].

OD theory is based on higher local symmetry (most commonly of layers) than imposed by the space group symmetry of the whole crystal. One way to achieve an OD structure is symmetry reduction of a fully ordered structure pertaining to layers. In this presentation the structures of the seemingly unrelated compounds $BaPO_3F$ and *β*-Hg_2CrO_4 will be derived from a common fully ordered structure (baryte, $BaSO_4$) and described using an OD approach. Thus, they are classified by symmetry principle, emphasizing their common features as well as their differences. The occurrence of systematic twinning by reticular pseudo-merohedry is explained.

Both $BaPO_3F$ and *β*-Hg_2CrO_4 structures belong to orthorhombic category I OD families of layers of one kind. The layers are derived from the corresponding layers in $BaSO_4$ by replacement of the SO_4^{2-}-groups by PO_3F^{2-}-groups and of the Ba^{2+} ions by Hg_2^{2+} dumbbells, respectively. Depending on crystallization conditions, $BaPO_3F$ is obtained as polytype with a maximum degree of order (*P2$_1$/c*, *Z*=8) or as the family structure (*Pmnb*, *Z*=4) isotypic with baryte. The major polytype of *β*-Hg_2CrO_4 (*Pc2$_1$b*, *Z*=16), is not of a maximum degree of order and therefore can be decomposed into simpler stacking sequences.

[1] Dornberger-Schiff K. (1956). On Order-Disorder Structures (OD-Structures). *Acta Crystallogr.* **9**, 593-601.

[2] Jeffery J. W. (1953). Unusual X-ray Diffraction Effects from a Crystal of Wollastonite. *Acta Crystallogr.* **6**, 821-825.

[3] Rye C. A., Isupov M. N., Lebedev A. A. and Littlechild J. A. (2007). An order-disorder twin crystal of L-2-haloacid dehalogenase from Sulfolobus tokodaii. *Acta Crystallogr.* D**63**, 926-930.

[4] Pletnev S., Morozova K. S., Verkhusha V. V. & Dauter Z. (2009). Rotational order-disorder structure of fluorescent protein FP480. *Acta Crystallogr.* D**65**, 906-912.

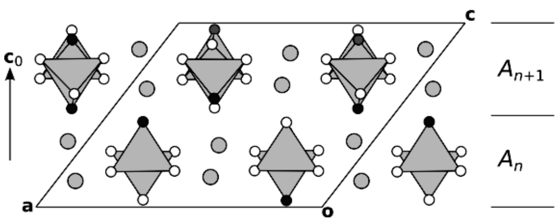

Figure 1: MDO1 polytype of BaPO3F viewed down [010]. PO3F2-groups are represented by grey polyhedra, Ba, O and F atoms by light grey, white and dark grey spheres of arbitrary radius. Layer names are indicated to the right.

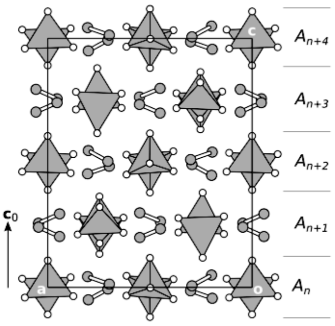

Figure 2: Major polytype of *β*-Hg2CrO4 viewed down [010]. CrO42- groups are represented by grey polyhedra, Hg and O atoms by grey and white spheres of arbitrary radius. Layer names are indicated to the right.

MS11-T8

Disorder in crystalline compounds investigated by a combination of X-ray diffraction, NMR spectroscopy, and DFT calculations

F. Haarmann[1]
[1]RWTH, Institut für Anorganische Chemie, Aachen, Germany

Local ordering of the atoms e.g. disorder is frequently observed in various classes of inorganic materials such as intermetallic compounds [1, 2], ion conductors [3], or Zeolites. Thus, strategies and methods for systematic investigations of this feature are required. Without any doubt diffraction methods are well suited to study long range order of the atoms in crystalline compounds. Local ordering of the atoms may only be indicated by unusual displacement parameters or diffuse scattering by diffraction methods. In contrast, NMR spectroscopy seems to be an ideal tool for the investigation of disorder since this method is related to the local bonding situation of the atoms. The link between short range and long range information is provided by quantum mechanical calculations using super lattice structures to model the local ordering of the atoms. A combined application of NMR spectroscopy, quantum mechanical calculations of NMR coupling parameters based on density functional theory (DFT), and X-ray diffraction can be used for that reason to study the disorder in inorganic materials.

Intermetallic compounds are a fascinating class of materials with respect to structural chemistry and technological applications. The interest of basic research focuses on the chemical bonding and the formation of disorder. The information provided by a combined application of the various techniques were elaborated using the di- and tetragallides $M\mathrm{Ga}_2$ with M = Ca, Sr, Ba and $M\mathrm{Ga}_4$ with M = Na, Ca, Sr, Ba [4, 5] as model systems.

Very good agreement of calculated and experimental NMR coupling parameters is achieved for the electric field gradient (EFG). Useful information about the bonding situation of the atoms can be obtained by deconvolution of the EFG into its contributions according to the calculation scheme used by the program WIEN2k [6]. This analysis reveals the local character of the EFG. It is determined by the population difference of the *p*-like states of the electrons of the Ga atoms. A linear relation of the EFG and the anisotropy ratio $n(p_z)/(\frac{1}{2}[n(p_x)+n(p_y)])$ with $n(p_i)$ corresponding to the population of states by p_i-like electrons is observed.

Due to the reliability of the EFG for the investigation of the bonding situation of the atoms it was chosen to study the influence of cationic substitution on the local bonding situation of the Ga atoms in the solid solutions of $\mathrm{Sr}_{1-x}\mathrm{Ba}_x\mathrm{Ga}_2$ and $\mathrm{Ca}_{1-x}\mathrm{Sr}_x\mathrm{Ga}_4$. Furthermore, local ordering of the atoms was studied in $\mathrm{Cu}_{1-x}\mathrm{Al}_2$ [2]. We emphasize, that all nuclei with nuclear spin $I > \frac{1}{2}$ are subject to this interaction, thus all classes of crystalline compounds having $I > \frac{1}{2}$ can be investigated by this strategy.

Acknowledgement
Funding by the Excellence Initiative of the German federal and state governments is gratefully acknowledged.

[1] U. Burkhardt, V. Gurin, F. Haarmann, H. Borrmann, W. Schnelle, A. Yaresko, Yu. Grin. *J. Solid State Chem.* (2004) **177**, 389-394.
[2] F. Haarmann, M. Armbrüster, Yu. Grin. *Chem. Mater.* (2007) **19**, 1147-1153.
[3] O. Pecher, S.-T. Kong, T. Goebel, V. Nickel, K. Weichert, C. Reiner, H.-J. Deiseroth, J. Maier, F. Haarmann, D. Zahn. *Chem. Eur. J.* (2010) **16(28)**, 8347-8354.
[4] F. Haarmann, K. Koch, D. Grüner, W. Schnelle, O. Pecher, R. Cardoso-Gil, H. Borrmann, H. Rosner, Yu. Grin, *Chem. Eur. J.* (2009), **15**, 1673.
[5] F. Haarmann, K. Koch, P. Jeglič, O. Pecher, H. Rosner, Yu. Grin, *Chem. Eur. J.* (2011) published online DOI: 10.1002/chem.201003486.
[6] P. Blaha, K. Schwarz, G. Madsen, D. Kvasnicka, J. Luitz, WIEN2k: An Augmented Plane Wave Local Orbitals Program for Calculating Crystal Properties, Technische Universität Wien, 2001, ISBN 3-9501031-1-2.

MS12-T1

Reaction kinetics of the 1.13 nm tobermorit formation: new insights on rate constants and activation energies by in-situ-neutron diffraction experiments

S. Bernstein[1]
[1]Rohrdorfer Transportbeton GmbH, Rohrdorf, Germany

1.13nm tobermorite belongs to the mineral group of calcium-silicate-hydrates well known as CSH-phases. Natural CSH-phases are due to the specific areas of formation rare in nature but synthetic members have applications in many different sections of the industry. 1.13nm tobermorite for example is the main binding phase in aerated autoclaved concrete (AAC), a building material which became more and more important over the last decades.

Based on former investigations it is known that 1.13nm tobermorite is formed metastable under the typical production conditions of ~ 180°C and saturated steam pressure. As the formation is controlled by the kinetics the major aim of this work was to obtain a clear picture of the present reaction mechanism and kinetics.

Neutron diffraction is an excellent method to collect data of the reaction process in-situ. A hydrothermal autoclave for neutron diffraction (HAND) was recently designed to record the dynamic process during the hydrothermal reaction with the D20 powder diffractometer of Institute Laue-Langevin (ILL) in Grenoble. Experiments were performed in the temperature range from 170 up to 210°C under saturated steam pressure in the system CaO-SiO_2-D_2O and CaO-SiO_2 -D_2O within a time-range of 8 h. Likewise the influence of quartz-grain size (8 and 16µm) on kinetic and crystallisation was investigated.

The decrease of the intensity of the quartz (101) reflection was taken as a value for the reaction-progress. By applying kinetic models (Chan et al.,1978) the mechanism of the reaction can be determined and displays a non-isokinetic behaviour. Based on this data rate constants were calculated.determining the temperature dependence of the rate constants enables the calculation of activation energies by applying the Arrhenius-equation and the results shall be presented here.

References:

CHAN, C.F., SAKIYAMA, M. and MITSUDA, T. **(1978)**, “Kinetics of CaO-Quartz-H_2O reaction at 120°C in suspension” *Cem. Con. Res*. **8,** 1-6

MS12-T2

A natural CSH-laboratory: CSH-phases and their parageneses from Maroldsweisach, Bavaria

R. Hochleitner[1], K.T. Fehr[2]
[1]Mineralogische Staatssammlung, SNSB, München, Germany
[2]Ludwig-Maximilians University, München, Germany

In the Zeilberg quarry near Maroldsweisach in Lower Franconia, Bavaria, a basalt is quarried, that broke through jurassic sediments, especially limestones containing fossils (belemnites, ammonites, bivalves). As a consequence of this breakthrough the basalt shows many, partly huge, inclusions of calcareous sediments.

These inclusions contain many different CSH-phase-minerals as there are Afwillite, Tobermorite, Plombierite, Scawtite, Hydrocalumite, Ettringite and Jennite. Tobermorite is additionly found in druses within the basalt. There are two different tobermorite phases showing normal and anomalous heating behaviour respectively (1,2).

As a function of the diameter of the calcium-rich inclusions (from few centimeters to meters) different coexistences of CSH-phases have been observed in an intense zoning from outer (hot) zones to (cooler) core.

Unique for Maroldsweisach is the existence of belemnite rostra and other fossils pseudomorphed by CSH-phases (e.g. Tobermorite, Scawtite, Jennite).

Literature:

(1) Hochleitner, R.(2000) : Natural and synthetic tobermorites - a comparison. In Rammelmair, D.; Mederer, J.; Oberthür, Th.; Heimann, R.B. & Pentinghaus, H. (eds.): Applied Mineralogy in Research, Economy, technology, Ecology and Culture. A.A. Balkema, Rotterdam, 799-801

(2) Hochleitner, R. & Fehr, K.T. (2000): Normal and anomalous behaviour of natural tobermorites. Beiheft z. European J. Miner.,12, 82

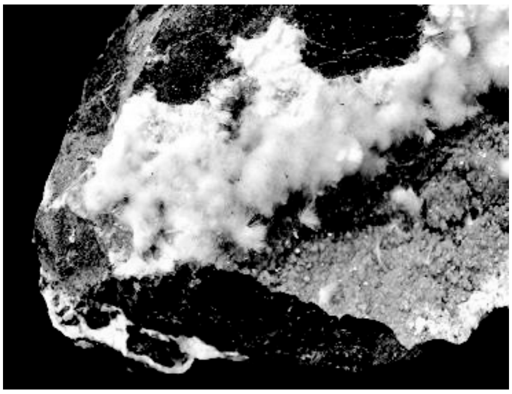

Figure 1: Tobermorite in a druse in the basalt of Maroldsweisach.

MS12-T3

Time resolved in-situ XRD-analysis of the evolution of C-S-H gel during the early hydration of alite with water

S. Bergold[1], D. Jansen[1], F. Goetz-Neunhoeffer[1], J. Neubauer[1]
[1]Mineralogie Erlangen / GeoZentrum Nordbayern - Friedrich-Alexander Universität Erlangen-Nürnberg, Mineralogie Erlangen, Erlangen, Germany

The early hydration of synthetic alite with water was investigated at different temperatures and water to alite ratios by in-situ X-ray diffraction. Magnesium and Aluminium were used to stabilize a monoclinic alite modification that is common in commercial Portland cements. The analysis of the diffractograms was performed by an external standard method after O’Connor & Raven (1988). That G-factor method is very suitable to investigate systems containing unknown or amorphous phases (Jansen et al., 2011) and is therefore requested for quantitative analysis of in-situ paste experiments.

It could be shown, that X-ray diffraction is not limited to the quantitative analysis of the crystalline phases, alite and portlandite. It was also possible to evaluate the evolution of the early, amorphous C-S-H gel in the first few hours.

From the quantitative in-situ XRD analyses, the theoretical heat flow was calculated, assuming equation 1.

Equation 1 $C_3S + 3.9\ H \dashrightarrow C_{1.7}SH_{2.6} + 1.3\ CH\ \Delta H = -561\ J/g$

Because of the good agreement between the theoretical heat flow and the measured heat flow derived from heat flow calorimetric experiments, it could be stated, that the dissolution of alite and the precipitation of Portlandite and C-S-H gel happens synchronously. But evolution of the early C-S-H gel shows, that Portlandite precipitates earlier than the C-S-H gel.

References:

Jansen, D.; Goetz-Neunhoeffer, F.; Stabler, C.; Neubauer, J. (2011): A Remastered External Standard Method Applied to the Quantification of Early OPC Hydration. Cement and Concrete Research, doi:10.1016/j.cemconres.2011.03.004.

O’Connor, B. H., Raven, M. D. (1988): Application of the Rietveld Refinement Procedure in Assaying Powdered Mixtures. Powder Diffraction, Vol. 3, 2-6.

MS12-T4

A model of OPC hydration based on pore solution equilibra - Highly time-resolved monitoring of cement hydration using synchrotron X-radiation

I. Mueller[1]
[1]Wacker Chemie AG, L-B-P-TM Mortar Science, Burghausen, Germany

This work is focused on the hydration kinetics of ordinary Portland cement (OPC) and pore solution equilibra as controling key parameters. In the construction material market it is commonly believed that protective colloid shells of amorphous hydrated phases control the cement hydration within the first hours of cement setting. Such protective layers explain the changes in hydration kinetics over time very well. However, this investigation shows that a protective layer of amorphous phases neither exist in hydrating cement nor that its existence is necessary in order to explain the dormant period of cement hydration. Instead a hydration model is offered in which hydration reactions are rather controlled by the ion saturation level of the pore solution. Phase composition and textural development of hydrating Portland cement and pure phase admixtures have been monitored by ultra sonic, ESEM and highly time-resolved XRD using brilliant synchrotron X-radiation. Results allow conclusions on mutually effects of silicates and aluminates and their phase-specific interactions with retarders respectively accelerators. Within the first 24 hours of cement setting the following phase reactions could be observed:
0 - 10 min: C_3A + bassanite + water → ettringite in Ca^{2+}-undersaturated solution
(1st unretarded ettringite formation) 10 - 30 min: bassanite + water → gypsum in Ca^{2+}-supersaturated solution (slightly, phase-specificly retarded by polysaccharides)
4-24 hours: C_3S + water → CSH + CH in Ca^{2+}-saturated solution (strongly, phase-specificly retarded by polysaccharides) C_3A + anhydrite + gypsum + water → ettringite in slightly Ca^{2+}-undersaturated solution (2^{nd} strongly, unspecificly retarded ettringite formation)
In pure phase admixtures of bassanite, anhydrite C_3A and common tap water in absence of silicates the ettringite formation is an undisturbed, continious process without a dormant period. This process changes tremendously if a $Ca(OH)_2$-saturated aqueous solution is used instead of tap water. The etrringite formation is significantly hindered while gypsum precipitates instead.
Results show that the hydration kinetic is basically controled by the Ca^{2+}-saturation level. ESEM-FEG images demonstrate that a protective layer of amorphous hydrate phases does not exist in hydrating cement.
References

Juilland, P. et al., Dissolution theory applied to the induction period in alite hydration, Cement and Concrete Research (2010), doi:10.1016/j.cemconres.2010.01.012
Möser, B., Ultra high resolution scanning electron microscopy on building materials - Insulators and contaminating samples, ibausil 17. Internationale Baustofftagung, Weimar (2009)
di Murro, H., Mécanismes d'élaboration de la microstructure des bétons, Ph. D. Thesis (2007)
Rothstein, D. et al., Solubility behaviour of Ca-, S-, Al- and Si-bearing solid phases in Portland cement pore solutions as a function of hydration time, Cement and Concrete Research (2002)
Weyer, H. et al., Time-resolved monitoring of cement hydration: Influence of cellulose ethers on hydration kinetics, Nuclear Instruments and Methods (2005)

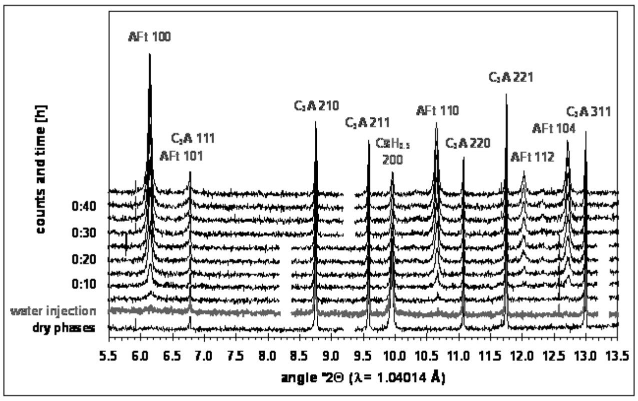

Figure 1: Undisturbed ettringite formation in a pure phase admixture of 70% C_3A, 15% bassanite (C$O.5H) and 15% anhydrite (C$) in water

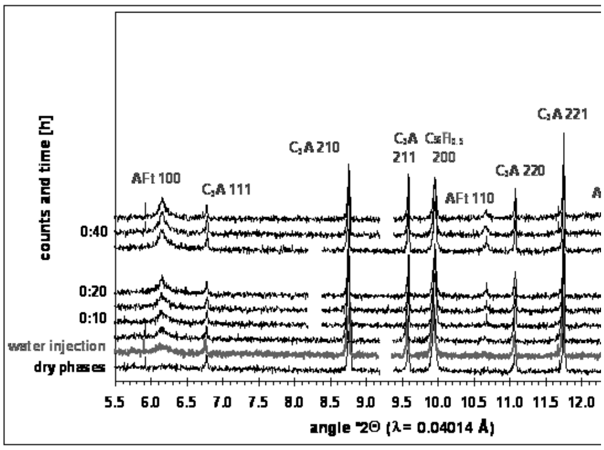

Figure 2: Disturbed ettringite formation in a pure phase admixture of 70% C_3A, 15% bassanite (C$O.5H) and 15% anhydrite (C$) in $Ca(OH)_2$-saturated aqueous solution

MS12-T5

Identification and quantification of phosphate mineral phases generated by CSH-seeded crystallization from sewage

A. Ehbrecht[1], R. Schuhmann[1], T. Fuderer[1], S. Schönauer[1]
[1]Karlsruhe Institute for Technology (KIT), Competence Center for Material Moisture, Eggenstein-Leopoldshafen, Germany

The increasing use of fertilizer and the finite nature and contamination of natural phosphorus (P) resources necessitates a sustainable technology for P-recovery. Because of sewage being an important nutrient sink, the crystallization of phosphate mineral phases e.g. hydroxylapatite or struvite triggered by a reactive substrate represents a promising method of P-Recovery from waste- and processwater.
In P-RoC-technology, P-elimination and -recovery occurs in one singular step without addition of chemicals except for the reactive substrate [Berg et al., 2007]. P-RoC-technology was applied in bench- and semi-technical scale [Ehbrecht et al., 2009a]. The objective of this study was to test the practicability of P-RoC-technology in pilot scale (800 L) with sewage like supernatant liquor and to identify the generated mineral phases.
It had been shown that the semi-technical experiments can be transferred to pilot-scale with a consideration of the boundary conditions of the actual sewage. The most important information that can be obtained from the X-Ray Diffraction pattern is the composition of the product generated with sewage: Different

products were found like less crystalline and very small hydroxylapatite-like phase (HAp) and struvite (MAP), a low soluble and valuable fertilizer.

In summary the efficiency of P-elimination depends on the P-bonding of the influent of a municipal sewage plant [Jenkins et al., 1971]. Due to the generation of the P-containing products in sewage, the conditions differ much from pure solutions. So the organic load of sewage has a remarkable influence on the kinetics [Ehbrecht and Schuhmann, 2009]. All those facts mentioned have an impact on the amount of recovered P. Also the quantification of P is affected by high amounts of organic and other contraries.

References

Berg, U., Knoll, G., Kaschka, E., Kreutzer, V., Weidler, P.G., Nüesch, R. (2007): „P-RoC - Phosphorus recovery from wastewater by crystallisation of calcium phosphate compounds”

Ehbrecht, A., Patzig, D., Schönauer, S., Schwotzer, M., Schuhmann, R. (2009a): „Crystallization of calcium phosphate from sewage: Efficiency of batch mode technology and quality of the generated products“.

Ehbrecht, A., Patzig, D., Schönauer, S., Schuhmann, R. (2008): „Efficiency of CSH substrates with regard to P-elimination from wastewater and the quality of the generated products“.

Jenkins, D., Fergueson, J.F., Menar, A. B. (1971): “Chemical processes for phosphate removal”.

Ehbrecht, A. and Schuhmann, R. (2009): “Crystallisation of Calcium phosphates from waste- and processwater: Influence of the organic load”

MS12-T6
Comparison of phospho-olivines as cathode materials in rechargeable Li-ion batteries

A. Laumann[1], N. Tran[1], G. Nuspl[1], N. Schall[1]
[1]Süd-Chemie AG, Battery Materials, Moosburg, Germany

The system LiFePO$_4$-LiMnPO$_4$ gained high interest due to the usage of olivine-type phosphates as cathode materials in Li-ion rechargeable batteries. In nature, Li-Fe-Mn-phosphates of various Fe/Mn ratios occur with triphylite and lithiophylite as the end-members of the LiFePO$_4$-LiMnPO$_4$ solid-solution. The pure iron end-member triphylite has not yet been found in nature, as part of the iron is throughout substituted with manganese. In contrary, the iron-free end-member LiMnPO$_4$ has been described. For the technical application as cathode in rechargeable Li-ion batteries, phospho-olivines are synthetically produced via various methods like solid state, hydrothermal or sol-gel syntheses.

LiFePO$_4$ is already well established as cathode material for Li-ion rechargeable batteries and currently used e.g. in power tools, and its usage in hybrid- and electric vehicles, as well as its application for energy storage in stationary power plants is discussed. Its advantages compared to commonly used oxides like LiCoO$_2$ are its high theoretical capacity of 170 mAh/g, its environmental compatibility, and especially its intrinsic thermal safety [1]. Besides LiFePO$_4$, other phospho-olivines of the LiMPO$_4$-type with M = Mn, Co or Ni are discussed as active materials for rechargeable Li-ion batteries.

Here we want to show a comparison of LiFePO$_4$ with other phospho-olivines in terms of the energy density and the electrochemical performance. Due to their high potentials, LiCoPO$_4$ (4.8 V vs. Li$^+$/Li) and LiNiPO$_4$ (5.1 V vs. Li$^+$/Li), have the highest theoretical energy density of the olivine phosphates. But the potential of LiNiPO$_4$ is too high for the known electrolytes [2], and also the high potential of LiCoPO$_4$ poses problem when conventional electrolytes are used. LiMnPO$_4$ offers an ideal potential of 4.1 V vs. Li$^+$/Li but is characterized by poor electrochemical performance. Optimized mixed LiFe$_x$Mn$_{1-x}$PO$_4$ materials seem to be a promising concept providing safety, excellent cell performance and durability to large Li-ion batteries.

[1] A.K. Padhi, K.S. Nanjundaswamy, C. Masquelier, S. Okada and J.B. Goodenough, J. Electrochem. Soc., 1997, 144, 1609-1613.

[2] P. Deniard, A.M. Dulac, X. Rocquefelte, V. Grigorova, O. Lebacq, A. Pasturel and S. Jobic, J. Phys. Chem. Sol., 2004, 65, 229-233.

MS12-T7
Behavior of lithium during the topotactic formation of ferrisicklerite from triphylite

P. Schmid-Beurmann[1], T. Geisler[2], F. Hatert[3], L. Ottolini[4], D.M. Többens[5], V. Kahlenberg[5]
[1]Institut für Mineralogie, Universität Münster, Münster, Germany
[2]Steinmann Institut für Geologie, Mineralogie und Paläontologie, Universität Bonn, Bonn, Germany
[3]Laboratoire de Minéralogie, Département de Géologie, Université de Liège, Liège, Belgium
[4]C.N.R.-Istituto di Geoscienze e Georisorse (IGG), Unità di Pavia, Pavia, Italy
[5]Institut für Mineralogie und Petrographie, Universität Innsbruck, Innsbruck, Austria

Triphylite (Li(Fe,Mn)PO4) is a primary phosphate mineral which crystallises in granitic pegmatites at temperatures of ~ 500°C. During later stages of pegmatitic evolution with decreasing temperatures triphylite is transformed to the isotypic minerals ferrisicklerite-sicklerite (Li<1(Fe3+,Mn2+)PO4) and heterosite-purpurite (Fe3+,Mn3+)PO4) by oxidation of Fe2+ and Mn2+ and leaching of Li [1]. In nature [2] as well as in hydrothermal experiments [3] a sharp reaction front between triphylite and the oxidised Li-deficient ferrisicklerite is formed. In our experiments we reacted cuboids (2.5 x 2.5 x 2.5 mm3) and coarse-grained material of a formerly decimeter-sized triphylite single crystal from Palermo Mine, N.H. USA in 0.1N HClaq in presence of KMnO4 or H2O2 as oxidating agent (70<=T<=175°C). Phase characterization identified the product as ferrisicklerite (Li<1(Fe3+,Mn2+)PO4). Chemical electron microprobe and SIMS profiles across the reaction front of the cuboids show no changes in concentration of the main elements P, Fe, Mn and Mg with the exception of lithium. Li shows a sharp concentration gradient starting with FU = 0.94(4) in triphylite, LiFePO4, to 0.32(7) in ferrisicklerite (Li<1(Fe3+,Mn2+)PO4). BSE images showed pores in the product ferrisicklerite which could be taken as evidence for a coupled dissolution-reprecipitation process [4]. As the unit cell volume of the product ferrisicklerite is smaller than that of the educt triphylite by 3 vol.% additional strain would be expected throughout the product phase, which would point to a diffusion-controlled process during which the structural reorganisation is believed to take place in the solid state. Indeed a strain analysis from powder diffraction data revealed an increased apparent maximum strain (13(2) ‰) in the product ferrisicklerite compared to the educt triphylite (5.8(2) ‰). The mechanism of this topotactic reaction which might be diffusion-controlled, as proposed for the delithiation and oxidaton of LiFePO4 [5] in anhydrous rechargeable lithium batteries, or reaction-controlled as in a coupled dissolution-reprecipitation process is still under debate. [1] Fransolet, A.M., Keller, P., Fontan, F. (1986) Contrib. Mineral. Petrol., 92, 502 [2] Keller, P. (1993): Universität Stuttgart, Jahrbuch, 21 pp. [3] Schmid-Beurmann, P., Geisler, Th. (2008) DMG-Meeting, Berlin. [4] Putnis, A. (2002) Mineral. Mag., 66, 689 [5] Wang, Y, He, P. and Zhou, H. (2011): Energy & environmental Science. 4, 805

MS12-T8

Glimpses at *individual reaction steps* accompanying the crystallization of the tridymite form(s) of $AlPO_4$ from an X-ray amorphous precipitate doped with potassium and magnesium

B. Peplinski[1], B. Adamczyk[2], C. Adam[2], F. Emmerling[1]
[1]BAM Federal Institute for Materials Research, Dept. 1 Analytical Chemistry; Reference Materials, Berlin, Germany
[2]BAM Federal Institute for Materials Research, Dept. 4 Materials and Environment, Berlin, Germany

Interest in the crystallography and chemistry of the tridymite form(s) of AlPO4 has recently renewed after it had been discovered to be one of the main components in the ash produced at two large-scale incinerators for sewage sludge operated in Europe, see Peplinski, B. et al. (2010-a), Peplinski, B. et al. (2010-b) and Scholz G. et al. (2010). While attempting to interpret in depth these new data it became soon clear that most investigations into the *chemical* aspects of the crystallization of the different forms and modifications of AlPO4 date back to a time long before it had been recognized that there exit at least three well distinguishable tridymite- modifications that are long-term stable at ambient temperature, their crystal structures were determined, see Graetsch, H.A. (2000) and Graetsch, H.A. (2001), high performance X-ray diffraction instrumentation and data evaluation techniques as well as high resolution solid state NMR had become available.

Consequently, a reinvestigation of the factors specifically influencing the crystallization of the tridymite form(s) of AlPO4 from X-ray amorphous precursors was started with the explicit intention to take full advantage of modern analytical opportunities.

For this, more than 100 model substances were synthesized under well-defined laboratory conditions and the products were analyzed by X-ray diffraction, thermal analysis and other techniques. The present report focuses on the results achieved in one of the sub-projects of these investigations in which the chemical composition of the samples was kept fixed while the temperature of the isothermal treatments ranged from 700 to 1100°C and their duration varied between 1 minute and 3 days.

It was found that - under the given experimental conditions - the crystallization of the tridymite form is a multiple step reaction. It was also found that - in contrast to other synthesis routes - the (primary) crystallization itself is not sluggish. However, the fast primary crystallization is followed by an astonishingly sluggish relaxation of the primary crystalline tridymite structure that can go on for many hours. These findings are in agreement with Ostwald's step rule, see Ostwald W. (1897) and can be interpreted in terms of a new model combining crystallographic and chemical aspects. They are of immediately practical importance for the *unambiguous* identification of tridymite form(s) of AlPO4 in complex multi-component systems as well as for understanding why these *crystalline* AlPO4 components are formed in certain sewage sludge incinerator ashes but not in others.

Peplinski, B. et al. (2010-a), First identification of AlPO4 tridymite in a municipal sewage sludge ash, 12th Euro-pean Powder Diffraction Conference, 27.-30. August 2010, Darmstadt, Germany, Book of Abstracts MS4-P03, accepted for publication in Zeitschrift für Kristallographie, Suppl..

Peplinski B. et al. (2010-b), On the *fast* crystallization of the tridymite form of doped $AlPO_4$ from a mixture of amorphous and crystalline precursor components and the chemical stabilization of its hexagonal high-temperature form at room temperature, 88th Annual Meeting of the German Mineralogical Society, 18.-22. September 2010, Münster, Germany.

Scholz G. et al. (2010), Multinuclear NMR investigation of the tridymite form of AlPO4, 32. Discussion Meeting & Joint Benelux/German Magnetic Resonance Conference, 20.- 23. September 2010, Münster, Germany, organized by the German Chemical Society (GDCh), Book of abstracts, XI-019.

Graetsch, H.A. (2000), Two forms of aluminium phosphate tridymite from X-ray powder data, Acta Cryst. **C56** (2000) pp. 401-403.

Graetsch, H.A. (2001), Hexagonal high-temperature form of aluminium phosphate tridymite from X-ray powder data, Acta Cryst. **C57** (2001), pp. 665-667.

Ostwald W., Studies upon the forming and changing solid bodies, Zeitschrift für Physikalische Chemie **22** (1897) pp. 289-330.

MS12-T9

Crystallochemical investigations in the join Plumbojarosite - Corkite - Kintoreite

R. Hochleitner[1], C. Rewitzer[2], M. Kaliwoda[1], K.T. Fehr[2]
[1]Mineralogische Staatssammlung, SNSB, München, Germany
[2]Ludwig-Maximilians University, Dep. of Geo- and Environmental Sciences, München, Germany

Plumbojarosite, corkite and kintoreite are members of the alunite supergroup (1). Whereas plumbojarosite is a sulphate and kintoreite is a phosphate, corkite is a mixed-anion-member with a supposed ratio of SO_4/PO_4 of 1:1.

Giuseppetti & Tadini (2) suggested the acentric space group *R*3*m* with lower symmetry for corkite, whereas Sato et al. (3), for a SO_4-rich corkite, suggested R-3m as well as Kolitsch (unpubl., cited after (1)) for a corkite from Dernbach, Germany. Accepting this space group, the existence of a discrete mineral corkite would be questionable.

During this study corkites from a new locality in Portugal have been investigated by EMPA together with near-endmember plumbojarosite and a nearly sulphate-free and zinc-free kintoreite for comparison.

The investigated corkites show a heavy zoning with alternating SO_4-rich and PO_4-rich portions. It is interesting that all analyses of these alternating zoning in the corkites plot into the join plumbojarosite-corkite, no higher PO_4-values than PO_4/SO_4 = 1:1 have been found. That could point to the fact that there is a miscibility gap between plumbojarosite and corkite and thus corkite has a defined field of existence and is a valid mineral species regardless of its structure. This demands at least a near-neighbour ordering in corkite and implicates a second miscibility gap between corkite and kintoreite.

Literature

(1) Bayliss, P., Kolitsch, U., Nickel, E.H. and Pring, A.(2010): Alunite supergroup: recommended nomenclature. Min. Mag. 74, pp. 919-927.

(2) Giuseppetti, G. and Tadini C. (1987): Corkite, its structure and ordered arrangement of the tetrahedral cations. N. Jb. Min. Mh. P 71-81.

(3) Sato,E., Nakai, I., Miyawaki, R. and Matsubara, S.(2009): Crystal structures of alunite family minerals. N. Jb. Miner. Abh. 185/3, p 313.-322.

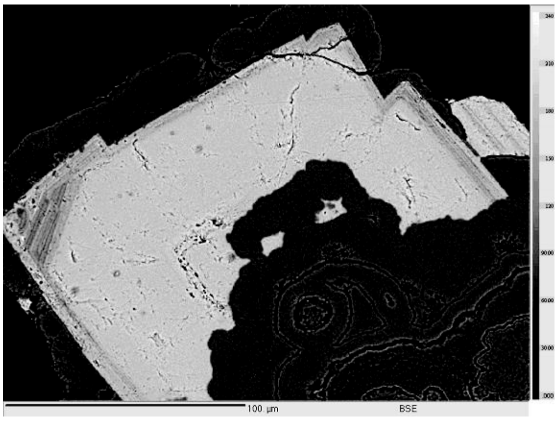

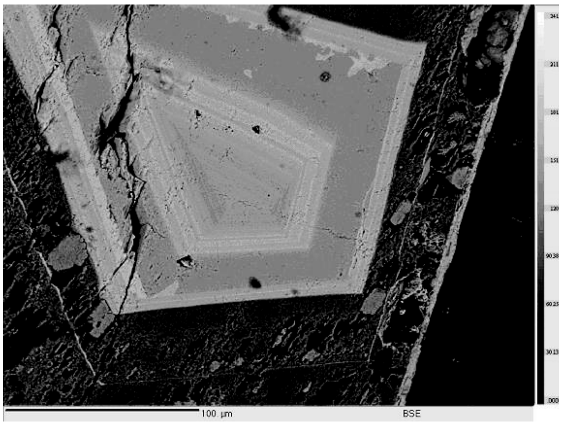

Fig 1+2: Sulfate-rich (darker) and phosphate-rich (lighter) Corkite. The darkest partly spherolithic phase is goethite. BSE picture.

MS13-T1

Metasediment hosted synorogenic cobalt-copper-gold (-nickel) mineralization in the Siegerland-Wied district of the Variscan fold-and thrust belt, Rhenish Massif

A. Hellmann[1], F.M. Meyer[1], A. Cormann[1], M. Peters[1]
[1]RWTH-Aachen University, Institute of Mineralogy and Economic Geology, Aachen, Germany

Metasediment hosted Co-Cu-Au deposits are recently recognized as an outstanding deposit class which requires further definition (Slack et al., 2010). A review of published and unpublished data on quartz-cobalt bearing arsenopyrite mineralization from the Siegerland- Wied district, in combination with new structural and petrological data show, that the cobalt occurrences share characteristics of both Co-Cu-Au-, and orogenic gold deposits (Groves et al., 2003).

The mineralization is mainly structurally controlled and hosted by reverse faults and associated vein systems, of which the NE-SW trending Siegen-Main Thrust is the most prominent. Mineralized structures are quartz, siderite and rarely ankerite-bearing fault fill veins, conjugate shear veins (Wettig, 1974) and minor steeply dipping veins in dilational jogs in the space between reverse faults. Quiring (1930) listed 161 individual occurrences of the mineralization in the district. Host rocks are metasediments of the Lower and Middle Siegen.

A depth extension of the mineralization of > 1000 m is known from the siderite mines (Wettig, 1974) and the siderite veins are reported to host quartz - Fe-Co-sulpharsenides in their extensions. Both disseminated and massif mineralization styles occure, pockets and “fahlband”-like ore accumulations are present.

Field-crosscutting and petrographical relationships show, that the mineralization is younger than siderite, quartz and ankerite (ank-I; Schöne-Warnefeld, 1955) of the main mineralization stage, and older than the lead-zinc mineralization of the sulphide stage. Low angle reverse faults crosscut and brecciate the older siderite mineralization, which is cemented by later quartz and cobalt-mineralization. The observations are contrary to the paragenetic scheme of Hüttenhain (1931), published in a review by Fenchel et al. (1985) who assigned the mineralization to a pre-siderite stage.

Our petrographical studies show, that the major ore minerals are fine grained, gold-bearing alloclasite and cobaltite, with subordinate pyrite and chalcopyrite, whereby the latter is mostly younger.

The gangue is quartz, carbonate is absent. Alteration minerals are illite and chamosite. Siderite and quartz of the main stage shows fractures filled by later sulpharsenides.

Where arsenopyrite is present, it is replaced by later alloclasite. Euhedral pyrite crystals, showing relictic pyrrhotite inclusions, are assigned to the main stage and are replaced and overgrown by sulpharsenides. Where marcasite is present, it replaces older pyrite and both are replaced by Co-Fe sulpharsenides, indicating acidic conditions at the onset of sulpharsenide-crystallization.

References

Fenchel et al. (1985). Geol. Jhb. Reihe D. 77.
Groves et al. (2003). Ec. Geol. 98, pp. 1-29.
Quiring, H. (1930). Glückauf 66, pp. 149 - 155.
Schöne-Warnefeld, G. (1955). Diss. Bergakad. Clausthal, 57 pp.
Slack et al. (2010). U.S. Geological Survey Open File Report 2010-2012.
Wettig, E. (1974). Clausth. Geol. Abh., 19: 363 pp.

MS13-T2

The LREE-, Se- and Au- bearing BiCoNi-U-Ag-association of the Schlema-Alberoda- complex U-deposit

T. Schlothauer[1], A.D. Renno[1], G. Bombach[1], G. Heide[1], W. Klemm[1]
[1]TU Bergakademie Freiberg, Institute for Mineralogy, Freiberg, Germany

The world-class Uranium deposit of Schlema-Alberoda with an output of 88,270 t U-metal (Hiller, Schuppan 2008) of the hydrothermal vein type was mined and explored for a large assemblage of usable elements like U, Bi, Co, Ni, Ag, Se, Pb, Zn, Cu and W in the time from 1946 to 1991.

The application of modern measurement methods like LA-ICP-MS, EMPA and reflected light microscopy with DIC permits the detection of unusual element concentrations.

In the present work the well known BiCoNi-Association from the Schlema-Alberoda complex deposit was reviewed.

The samples (polished sections) were analysed with LA-ICP-MS (linescans), EMPA and RL-microscopy with differential interference contrast.

This association is characterized by an combination of different arsenides, started with for Ni-dominated assemblages with maucherite ($Ni_{11}As_8$), followed by niccolite ($NiAs$), rammelsbergite ($NiAs_2$) chloanthite ($(Ni,Co,Fe)As_{3-x}$) and sometimes native Arsenic (Hiller, Schuppan 2008). The As-contents per formula unit increases here continuously in progression of ore precipitation.

Sometimes in this assemblage pitchblende will be included. In the presented case this mineral is extremely enriched in REE, especially the LREE. Further from this association separated REE-minerals are known. Also the gangue carbonate minerals in the surrounding area show a LREE-enrichment. Further in this assemblage an enrichment of Au, PGE, Se, Bi, Hg, Sb and other elements was observed.

The reason for the accumulation of Au and partially PGE in the youngest parts of the BiCoNi-association is the leaching of the elements Co, Ni, Au (PGE) from the host rocks of the BiCoNi-association like mafic metavulcanites (Lipp 2003) and its concentration in progression of the development of the different stages of the BiCoNi-association.

Literature

Hiller, Schuppan 2008 Hiller, Axel ; Schuppan, Werner: *Geologie und Uranbergbau im Revier Schlema-Alberoda.* Dresden, Freiberg: LfUG, Öffentlichkeitsarbeit; Sächsisches Oberbergamt, 2008
(Bergbau in Sachsen 14). - ISBN 3-9811421-3-6
Lipp 2003 Lipp, Ulrich: *Wismut-, Kobalt-, Nickel und Silbererze im Nordteil des Schneeberger Lagerstättenbezirkes.* mit

Ergänzungen durch Siegfried Flach. Freiberg : Sächsisches Druck- und Verlagshaus, 2003 (Bergbau in Sachsen 10)

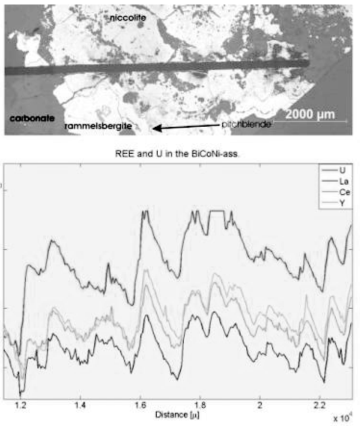

Figure 1: Collomorphous arsenides with pitchblende and the LA-ICP-MS-line with the enrichment in REE-elements (in cps)

MS13-T3
Trace elements in cassiterite and wolframite

S. Goldmann[1,2], F. Melcher[2], H.-E. Gäbler[2]
[1]Leibniz University, Mineralogy, Hannover, Germany
[2]BGR, Mineral Resources, Hannover, Germany

The trace element composition of ore minerals is the principal parameter for the analytical fingerprint to proof the origin of traded ore concentrates, especially in conflict areas such as Central Africa, and increases transparency along the trading chain of mineral resources.

Cassiterite (SnO_2) and wolframite ($(Fe,Mn)WO_4$) constitute the most important ore minerals for the recovery of tin and tungsten, respectively. The major ore deposits of tin and tungsten are generally associated with highly evolved felsic magmatism, such as greisen, hydrothermal quartz veins, pegmatites, skarn, and porphyry deposits. Both metals are geochemically incompatible elements which are enriched in the residual melt during fractional crystallisation and differentiation of the magma. Quantitative in-situ analyses of major and trace elements were performed on polished sections of ore concentrates using LA-ICP-MS which provides high spatial resolution and low detection limits. A Thermo Finnigan ELEMENT-XR High-Resolution sector field inductively coupled plasma mass spectrometer coupled to a New Wave UP193-FX laser ablation system with an ATLEX-300-SI excimer laser was used. A representative number of about 40 grains are measured per ore concentrate in order to determine the variability in the trace element composition of the concentrate.

The chemical compositions of cassiterite show Fe, Ti, Mn, Nb, Ta and W in the weight percent range. Additional significant trace elements are Zr, Hf, Sc, Sb, V, As, In, Ga, Zn Pb, and U with concentrations up to several hundred ppm. However, some elements are predominantly below the detection limits (such as Na, Mg, Ca, Cr, Co, Ni, Ge, Sr, Mo, Cd, Ba, REE, Bi, Th) whereas other elements are characteristic for single deposits only (e.g. antimony and arsenic for Greenbushes, Australia).

The composition of wolframite group minerals is variable because they form a solid solution series between the endmembers ferberite ($FeWO_4$) and hübnerite ($MnWO_4$). The major elements are Mg, Ca, Sc, Ti, Zn, Y, Nb, Sn, and Ta with concentrations of several hundred ppm. Common trace elements are V, Co, Zr, Mo, In, REE, Hf, Pb, Th, U ranging up to 100 ppm. The rare earth element patterns generally show HREE predominating over LREE and a distinct negative Eu anomaly; however, rather different patterns were also observed.

The variability of the trace elements in both cassiterite (Fig. 1) and wolframite can be used to distinguish various ore deposit types as well as different ore provinces or mining sites, and thus may be applied to fingerprint the origin of ore concentrates.

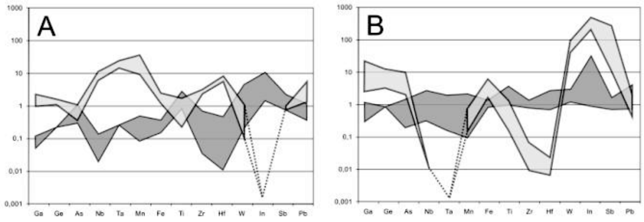

Figure 1: Comparison of trace element composition (25th percentile to 75th percentile) of cassiterite from different ore deposit types normalised to the median of all cassiterite analyses. A: light gray: pegmatite, dark gray: quartz veins; B: light gray: Bolivian polymetallic veins, dark gray: greisen deposits (dotted lines: below detection limit)

MS13-T4
Trace elements in Ta-Nb oxides from granitic and pegmatitic tantalum provinces

F. Melcher[1], H.-E. Gäbler[1], T. Graupner[1], M. Sitnikova[1]
[1]BGR, Mineral Resources, Hannover, Germany

Tantalum is recovered from oxide minerals that are present as minor constituents in rare-metal granites and granitic rare-element pegmatites. Columbite group minerals account for the majority of the current tantalum production; however, a large number of Ta-Nb phases may occur in such rocks, including tapiolite, wodginite, ixiolite, rutile and pyrochlore-group minerals. Little is known about the concentration of trace elements in these oxides. In the course of a project on the establishment of a mineralogical and geochemical fingerprint for Ta-Nb mineral concentrates, a vast dataset has emerged comprising mineralogical, geochemical and textural attributes as well as age determinations using the U-Pb method. Samples from more than 30 rare-element granite and pegmatite districts worldwide were analyzed.

Pegmatites and rare-element granites are among the most variable magmatic rocks in terms of textures, trace element geochemistry and trace element mineralogy. This variation is also reflected by complex zoning patterns producing a wide variety of rare element minerals and, among them, different compositions through processes such as fractional crystallization and contamination. Therefore, the chemical composition of Ta-Nb oxides is highly variable. However, major as well as trace elements show regional characteristics that allow for the distinction of ore provinces.

Columbite-tantalite accommodates various minor and trace elements (median and maximum concentration expressed as the 90th percentile of more than 10,000 trace element determinations by LA-ICP-MS in single grains): TiO_2 (0.43 %, 1.47 %), WO_3 (0.17 %, 0.9 %), SnO_2 (0.12 %, 0.5 %), Mg (28 ppm, 680 ppm), Al (51 ppm, 300 ppm), Sc (7 ppm, 180 ppm), Y (5 ppm, 530 ppm), Zr (950 ppm, 3500 ppm), Hf (130 ppm, 565 ppm), Th (5 ppm, 60 ppm), U (280 ppm, 1630 ppm), Pb (42 ppm, 350 ppm), Li (7 ppm, 71 ppm), Bi (0.2 ppm, 10 ppm), Sb (0.05 ppm, 2.3 ppm), and REE (e.g. Yb: 1 ppm, 88 ppm).

Trace elements are incorporated in Ta-Nb oxides in a systematic fashion, e.g. wodginite and ixiolite carry higher Li, Zr, Hf, Sn, (±Ti, Sb, Bi) concentrations than columbite-tantalite and tapiolite; columbite-tantalite has higher concentrations of all trace elements except Hf (±Zr, Ti, Sn) compared to tapiolite. The composition of Ta-Nb oxides related to rare-element pegmatites is rather different from rare-metal granites: the latter have high REE and Th concentrations, and low Li and Mg. Pegmatite-hosted oxides are highly variable, with types rich in REE and types poor in REE. Regional geochemical peculiarities are demonstrated in normalized trace element spider diagrams. The median values of columbite-tantalite, tapiolite and wodginite/ixiolite from selected rare metal pegmatite provinces indicate common characteristics, suggesting they are cogenetic and reflect specific source characteristics.

MS13-T5
Classification of REE distribution patterns of CGM

T. Graupner[1], F. Melcher[1], H.-E. Gäbler[1], M. Sitnikova[1]
[1]BGR, economic geology, Hannover, Germany

The rare-earth element (REE) geochemistry of tantalum-niobium oxides (columbite-group minerals - CGM, tapiolite, microlite) from Ta-ore provinces worldwide was studied by laser ablation inductively coupled plasma mass spectrometry (LA-ICPMS).
The data allow classification of the chondrite-normalized REE distribution patterns of CGM from lithium-caesium-tantalum (LCT) pegmatites and rare-metal granites into five major types. Features to discriminate between the types include
(1) the generalized shapes of the pattern (e.g. flat or concave),
(2) calculated ratios between groups of the REE (e.g. heavy REE_N/middle REE_N), and
(3) the presence or absence and intensity of anomalies (e.g. Ce, Eu and/or Y anomalies).
Pegmatites in central and southern Africa (e.g. Kibaran province of central Africa, Karas province of southern Namibia) are used as case studies to discuss application of the types of REE patterns in individual deposits.
The REE fractionation during progressive evolution of the melt in a pegmatite body (either Nb - Ta or Fe - Mn fractionation lines, or both) results in smaller heavy REE_N/middle REE_N ratios whereas replacement of primary CGM by secondary CGM produces modifications in the light REE_N patterns and the heavy REE_N/middle REE_N ratios also. Critical features of REE patterns such as highly variable heavy REE_N/middle REE_N ratios or striking differences in the appearance of Eu anomalies are discussed considering structural data of the host minerals and the differentiation behaviour of the pegmatitic melt.
In general, CGM from each individual Ta-ore province are characterized by a predominance of one type of REE distribution pattern. Consequently, these patterns are suitable for tracing the origin of tantalum ore concentrates.

MS13-T6
The Caeiras-Pegmatite - a new occurrence and its potential for high-tech-metals in the Borborema Pegmatite Province, NE-Brazil

S. Sindern[1], C. Piribauer[1], M. Meyer[1], D. Mashev[1], V. Havenith[1], R.F.S. Lima[2], R.A. Petta[2], T.F.C. Campos[2], R.J. Bakker[3]
[1]Institut für Mineralogie und Lagerstättenlehre, RWTH Aachen, Aachen, Germany
[2]Universidade Federal do Rio Grande do Norte, Departamento de Geologia, Natal, RN, Brazil
[3]University of Leoben, Mineralogy and Petrology Group, Leoben, Austria

The Caeiras-Pegmatite is one of the numerous pegmatite occurrences in the Borborema Province. It is exposed in three quarries and exploited by an artisanal operation since 2007. The heterogeneous pegmatite consists of a core of quartz enveloped by meter-sized perthitic feldspars. Within the wall zone texturally different units can be distinguished, generally dominated by quartz and feldspar. In addition to quartz and feldspar from the core zone, other minerals such as tantalite, beryl and tourmaline are extracted in minor amounts from both the intermediate zone and the wall zone. Tantalite mineralization is a salient feature of the general pegmatite zonation pattern known in the province. Ratios of K/Rb vary between 91 and 294 in K-feldspar. Caesium ranges from values < 2 ppm in the presence of ceramic-type feldspar in the central areas, up to 60 ppm in association with rare metal occurrences in the wall zones. An indication of a minimum formation temperature between 600 and 650 °C is provided by fluid inclusions in quartz consisting of an aqueous fluid with salinities up to 21 % equiv. NaCl. Raman spectroscopy identified CO_2 and N_2 as gaseous phases in fluid inclusions and LA-ICP-MS analyses of fluid inclusions in wall zone quartz revealed the presence of Li, in addition to Na and K. This particular fluid composition is a good indication of the rare metal potential of the wall zones. Potassium-rich alkali-feldspar crystals have the composition $Ab_{22.7\text{-}30.7}Or_{69.0\text{-}77.0}An_{0.3}$. Their perthitic exsolution texture is characterised by the occurrence of different Or-rich domains showing either fine or coarse irregular microcline. Ab-rich domains are either fine coherent lamellae or irregular elongated to patchy areas. Compositional data of these domains indicate a first exsolution event at approximately 550 °C followed by a second at 400 to 300 °C. Irregular and partly patchy perthitic exsolutions reveal the presence of a fluid phase at the latter lower temperature stage, as is indicated by secondary low-salinity aqueous inclusions. The post-magmatic hydrothermal fluid overprint resulted in the alteration of primary magmatic phases and in the formation of secondary minerals. The alteration of tantalite and the ubiquitous distribution of secondary U-minerals is attributed to the late fluid overprint. The effect of mineral alteration and redistribution is of concern for the assessment of the economic potential of the rare metal Caeiras-Pegmatite.

MS13-T7
The Potential Of Rare Earth Elements In The co-rich Ferromanganese Crust Deposits Of The Pacific Ocean

A. Jahn[1], P. Halbach[1]
[1]Freie Universitaet Berlin, FB Geowissenschaften, Berlin, Germany

The marine Cobalt-rich ferromanganese crust deposits represent a great raw material reserve for economically relevant metals and promise a potentially valuable addition to the world's metal resources. The crusts are one of the two types of oxidic metallic mineral resources in the deep ocean that incorporate metal compounds supplied and transported from land, atmosphere and sea sources (mainly from the oxygen-minimum zone and the oceanic water column). The crusts are hydrogenetic precipitates from cold seawater, formed under suboxic to oxic conditions as thin layers (2 up to 25 centimetres thick) on hard substrate rocks (e.g. volcanic hyaloclastites, weathered basaltic rocks, phosphatised limestones, consolidated clay sediments and carbonate-fluorapatite; Halbach and Puteanus, 1984).
The crust material consists of a very fine-grained mixture of ferruginous vernadite, X-ray amorphous Fe oxihydroxide, alumosilicate particles, authigenic carbonate-fluorapatite as well as minor admixtures of fine-grained detritus and residual biogenetic phases (mainly calcareous skeletons). The metals mostly associated with the Mn and the Fe-phases are also the elements preferentially representing the economic importance of

the crusts: Mn, Co, Ni, Cu, Mo, Ti, Pt, Te and REEs. All these elements mentioned are highly enriched in the crusts as compared to seawater composition. Several interruptions of growth (hiati) during precipitation caused the formation of several older and one younger generation. The older generations were diagenetically overprinted and are marked by a distinct apatite impregnation.

The REE form a unique group of chemically coherent elements with mostly trivalent oxidation state; exceptions are Ce and Eu which also exist as Ce (IV) and Eu (II), respectively. The average concentration of total REE content in ferromanganese crusts varies approximately between 1400 and 2400 ppm, based on dried matter (Halbach et al., 2008; Halbach et al., 2010; Cui et al., 2009).

In order to estimate the ore potential of this resource type we extrapolated the mineable tonnage according to the known properties of ferromanganese crusts, the frequency of the substrate rocks, and the geometry of the seamount structures. The latter is taken from data of seamounts and guyots published by Wessel et al. (2001). Derived from satellite-based altimetry this database includes the geographic position, age, height and radius of nearly 8.000 objects located in the Pacific Ocean.

The promising structures are selected by their geographic position between 50°N and 50°S, an at least Cretaceous age and a top of the respective mountains in a depth between 1000 m and 2000 m below sea level. With the radius and the height we calculated the overall slope angle and defined two distinct classes of objects, with a slope angle of $\alpha<12°$ representing seamounts and $\alpha>12°$ representing guyots. For both classes we calculated the surface areas; the platform areas of the guyots were only considered by 30%. With a given density, thickness and abundance of manganese crusts on seamounts the potential ore material was calculated and reduced by an empirically derived mineability factor based on rough topography (Halbach and Jahn, 2011).

The amount of mineable manganese crust material depends also on the depth range that is considered. Assuming that the best crust compositions can be found in water depths between 1000 and 3000 m, the total amount of mineable crust material in the Pacific Ocean is in the range of 21.5 * 10^9 t. Based on the estimated amount of dried ore material (15 * 10^9t), and taking into account the average REE concentration for crusts in the Pacific Ocean, the marine REE potential of this marine area can be estimated, and represents a valuable resource.

References:

Cui Y., Liu J., Ren X. and Shi X. (2009) J. of Rare Earth, 27, 169-176.

Halbach P., Jahn A. and Lucka M. (2009) BGR-project no.: 207-4500051248, 61 p.

Halbach P. and Jahn A. (2011) in prep., 50 p.

Halbach P. and Marbler H. (2008) BGR-project no: 211-4500042565, 73 p.

Halbach P. and Puteanus D. (1984) Earth Planet. Sci. Lett., 68, 73-87.Wessel P. (2001) J.of Geophys. Res. 106 , 19.431-19.441.

MS14-T1

Let‘s twist: Unexpected geometry of Schiff-base intermediates and protein dynamics in transaldolase

A. Lehwess-Litzmann[1], P. Neumann[2], C. Parthier[3], S. Lüdtke[1], R. Golbik[3], R. Ficner[2], K. Tittmann[1]

[1]Albrecht-von-Haller-Institute and Göttingen Center for Molecular Biosciences, Georg-August-University Göttingen, Bioanalytics, Goettingen, Germany

[2]Göttingen Center for Molecular Biosciences, Georg-August-University Göttingen, Microbiology and Genetics, Göttingen, Germany

[3]Martin-Luther-University Halle-Wittenberg, Biochemistry and Biotechnology, Halle (Saale), Germany

Transaldolase (TA, EC 2.2.1.2) is one of the key enzymes in the non-oxidative part of the pentose phosphate pathway. The protein with $(\alpha/\beta)_8$ barrel (TIM barrel) fold [1,2] catalyzes the reversible transfer of a three-carbon, dihydroxyacetone moiety between sugar phosphates by a Schiff-base mechanism involving a catalytically active lysine [3]. In the cellular context donor ketose substrates are fructose 6-phosphate (F6P) and sedoheptulose 7-phosphate (S7P) while the aldoses erythrose 4-phosphate (E4P) and glyceraldehyde 3-phosphate (G3P) act as alternative acceptor substrates in an equilibrium reaction (eq 1):

fructose 6-phosphate + erythrose 4-phosphate ↔ sedoheptulose 7-phosphate + glyceraldehyde 3-phosphate (1)

We have examined the catalytic cycle of TA from *Thermoplasma acidophilum* (*Tac*TA) by cryocrystallography, and were able to structurally characterize - for the first time - different genuine TA reaction intermediates including the Schiff-base adducts formed between the catalytic lysine and the donor ketose substrates F6P and S7P, and the Michaelis complex with acceptor aldose erythrose 4-phosphate. These structural snapshots enforce a revision of the accepted reaction mechanism with respect to functional roles of active site residues. Further we observed a nonplanar arrangement of the substituents around the Schiff-base double bond and a high-energy parallel conformation of the 4-OH and 6-OH groups of S7P suggesting a structurally encoded reactant-state destabilization as a driving force of catalysis. As unexpected structural feature the protein assumes alternate “open” and “closed” conformations in the resting state and in complex with acceptor E4P but locks in the closed one after Schiff-base formation. These protein dynamics and the intrinsic hydrogen-bonding pattern appear to be crucial for selective recognition and binding of ketoses as first substrate. The findings reveal fundamental insights into general structural features of enzymic Schiff-base intermediates and the role of conformational dynamics for enzyme catalysis, substrate binding and discrimination.

References:

[1] Jia, J., Huang, W., Schörken, U., Sahm, H., Sprenger, G. A., Lindqvist, Y., Schneider, G., Crystal structure of transaldolase B from Escherichia coli suggests a circular permutation of the alpha/beta barrel within the class I aldolase family (1996). *Structure* **4**, 715-724.

[2] Lehwess-Litzmann, A., Neumann, P., Golbik, R., Parthier, C., & Tittmann, K., Crystallization and preliminary X-ray diffraction analysis of transaldolase from Thermoplasma acidophilum (2011).

Acta Cryst Sect F: Struct Biol Cryst Comm 67, 584-586.

[3] Samland, A. K. & Sprenger, G. A., Transaldolase. From biochemistry to human disease (2009). *Int. J. Biochem. Cell Biol.* **41**, 1482-1494.

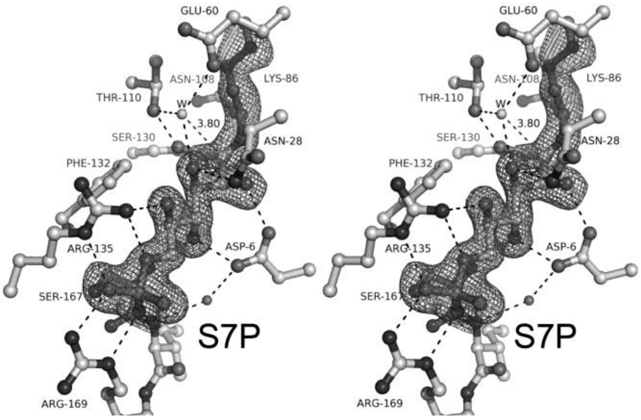

Figure 1: Structure of the S7P Schiff-base intermediate trapped in *Tac*TA in stereo view and ball-and-stick representation. The simulated-annealing mFo-DFc omit map is contoured at 3.3 σ around the intermediate. H-bonding interactions < 3.3 Å are indicated by dashed lines.

MS14-T2

Structure and mechanism of chloromomuconolactone dehalogenase from *Rhodococcus opacus* 1CP

C. Roth[1], S.R. Kaschabek[1,2], J.A.D. Gröning[2], M. Schlömann[2], N. Sträter[3]
[1]Institute for Bioanalytical Chemistry, Center for Biomedicine and Biotechnology, Leipzig, Germany
[2]Environmental Microbiology, Freiberg, Germany
[3]Institute for Structural Analytics of Biopolymers, Center for Biotechnology and Biomedicine, Leipzig, Germany

Chloroaromatic compounds are often very persistent environmental pollutants. Nevertheless numerous bacteria are able to metabolise these compounds and use them as the sole energy and carbon source. *Rhodococcus opacus* 1CP is able to degrade 3-chlorocatechol via a unique variant of the modified *ortho*-pathway. This pathway involves chloromuconolactone dehalogenase which dehalogenates the 5-chloromuconolactone to *cis*-dienelactone. The enzyme shows a high similarity to muconolactone isomerases, but is not able to catalyse the isomerisation reaction. In order to characterize the catalytic mechanism of this unusal dehalogenase, we crystallised the enzyme and subjected it to X-ray structural analysis. Datasets of up to 1.65 Å resolution were collected from two different crystal forms using synchrotron radiation. Based on the available structures and a sequence alignment several mutants were created to explore the functional relevance of the residues. The catalytic residues were identified and an inactive variant could be crystallized with the substrate, yielding to new insight in the binding mode and the catalytic mechanism of the dehalogenase.

MS14-T3

Crystal structure of NirE in complex with its substrate reveals new insights into the catalytic mechanism of SUMT enzymes

S. Saha[1], S. Storbeck[2], J. Krausze[1], B. Klink[1,3], D.W. Heinz[1], G. Layer[2]
[1]Helmholtz Centre for Infection Research, Structural Biology, Braunschweig, Germany
[2]Technische Universität Braunschweig, Braunschweig, Germany
[3]3Duke University Medical Center, Durham, North Carolina, United States

During the biosynthesis of heme *d*1, the essential cofactor of cytochrome *cd*1 nitrite reductase, the NirE protein catalyzes the methylation of uroporphyrinogen III to precorrin-2 using *S*-adenosyl- L-methionine (SAM) as the methyl group donor. We have solved the crystal structure of *Pseudomonas aeruginosa* NirE in complex with its substrate uroporphyrinogen III and the reaction by-product *S*-adenosyl-L-homocysteine (SAH) to 2.0 Å resolution. This represents the first enzyme-substrate complex structure for a SAM dependent uroporphyrinogen III methyltransferase (SUMT). The large substrate binds on top of the SAH in a “puckered” conformation in which the two pyrrole rings facing each other point to the same direction either upward or downward. Three arginine residues, a histidine and a methionine are involved in the coordination of uroporphyrinogen III. Through site-directed mutagenesis and biochemical characterization of the corresponding NirE variants the amino acid residues R111, E114 and R149 were identified to be involved in NirE catalysis. Based on our structural and biochemical findings we propose a potential catalytic mechanism for NirE and other SUMTs in which the methyl transfer reaction is initiated by an arginine catalyzed proton abstraction from the substrate’s C20 position.

Reference : Storbeck S. *, **Saha** S. *, Krausze J., Klink B. U., Heinz D. W., Layer G. (2011) *J. Biol. Chem. (* co first authors) (In press,* doi:10.1074/jbc.M111.239855)

Figure legend: Monomer of NirE (content of the au) in cartoon representation with SAH (light blue) and uro’gen III (light orange) shown as sticks. Domains A and B are shown in lighter and darker shades of green, respectively, and the linker region is shown in gray.

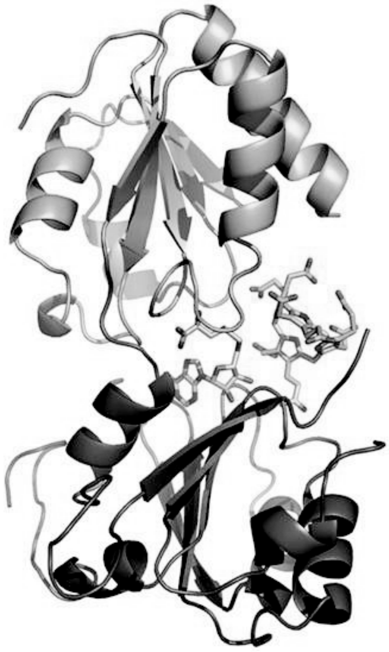

Figure 1

MS14-T4

Structures of P*hyscomitrella patens* AOC1 and AOC2 complexes reveal unexpected conformation of the epoxide ring of the bound substrate analogs

P. Neumann[1], K. Sauer[2], J. Brinkmann[1], F. Brodhun[2], A. Dickmanns[1], I. Feussner[2], R. Ficner[1]

[1]Georg August University, Molecular Structural Biology, Goettingen, Germany
[2]Georg August University, Plant Biochemistry, Goettingen, Germany

Oxylipins comprise a large family of oxidized fatty acids and their derivatives. They are abundant in mammals, fungi as well as in flowering and non-flowering plants like mosses. In plants, these bioactive lipids serve as signal molecules regulating developmental processes and mediating defense reactions. The oxylipin biosynthesis starts with the peroxidation of an unsaturated fatty acid containing an 1Z,4Z-pentadiene system by lipoxygenases (LOXes) followed by further enzymatic reactions in which a set of different oxidized fatty acid derivatives are produced. One specific branch of the LOX pathway starts with the oxidation of 18:3(n-3) by 13-LOX to 13-HPOTE and is followed by the action of 13-AOS that converts the hydroperoxide derivative to the unstable allene oxide 12,13S-epoxy-9Z,11,15Z-octadecatrienonic acid (12,13-EOT). This product can be diverged into pathways different from the Jasmonic acid (JA) biosynthesis, however the reaction catalyzed by allene oxide cyclase (AOC) provides the fist intermediate leading to JA namely the cyclopentenone derivative cis(+)-12-oxo-phytodienoic acid (cis(+)-OPDA). This is the first cyclic and biologically active compound in that pathway. The crystal structure of an AOC from *Arabidopsis thaliana* (AtAOC2) has been already determined [1] and the reaction mechanism as well as the subcellular localization was studied. Recently, we could demonstrate that the moss *Physcomitrella patens*, as an ambassador of low eukaryotes, is able to metabolize both plant like 18:3(n-3) as well as mammalian like 20:4(n-6) fatty acids to form oxylipins [2]. This is achieved by two structurally related AOC enzymes which differ in substrate specificity. In contrast to *Pp*AOC2, *Pp*AOC1 does not accept 12-HEPTE derived C20-allene oxides (mammalian like) and thus shows only substrate specificity against 13-HPOTE derived allene oxides (plant like). In order to analyze the determinants that are responsible for the different specificities we crystallized and structurally characterized both enzymes as well as their complexes with substrate analogs. Our results indicate subtle differences in the binding sites of both structurally related *Pp*AOC2 and *Pp*AOC1 enzymes. The soaking experiments revealed different binding modes of the ligand molecules; ligand induced conformational changes of the residues forming the binding site and an unexpected cis/trans isomerisation of the epoxide ring involving inversion of the absolute configuration of one chiral center. Our findings suggest that the proposed mechanism should be revised in order to explain the unexpected abilities of the studied enzymes.

References:

1. Hofmann, E., Zerbe, P., Schaller, F. The Crystal Structure of Arabidopsis thaliana Allene Oxide Cyclase: Insights into the Oxylipin Cyclization Reaction (2006) Plant Cell 18: 3201-3217.
2. Stumpe M, Göbel C, Faltin B, Beike AK, Hause B, Himmelsbach K, Bode J, Kramell R, Wasternack C, Frank W, Reski R, Feussner I (2010) The moss Physcomitrella patens contains cyclopentenones but no jasmonates: mutations in allene oxide cyclase lead to reduced fertility and altered sporophyte morphology. New Phytol, doi: 10.1111/j.1469-8137.2010.03406.

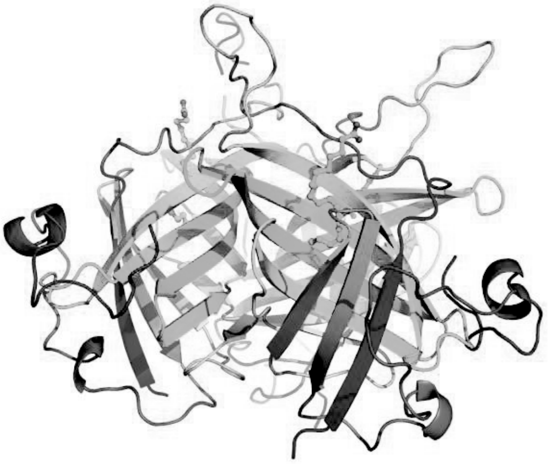

Figure 1

MS14-T5

Structure of human Dipeptidyl peptidase III in complex with an opioid peptide unveils an unusual entropy-driven binding mode

G. Arruda Bezerra[1], M. Abramic[2], P. Macheroux[3], S. Dhe-Paganon[4], K. Gruber[1]
[1]University of Graz, Structural Biology Group, Graz, Austria
[2]Ruđer Bošković Institute, Division of Organic Chemistry and Biochemistry, Zagreb, Croatia
[3]Graz University of Technology, Institute of Biochemistry, Graz, Austria
[4]Structural Genomics Consortium, University of Toronto, Department of Physiology, University of Toronto, Toronto, Canada

The opioid system is involved in a myriad of physiological processes, most notably nociception, and its deregulation is implicated in several pathologies [1]. Dipeptidyl-peptidases III (DPP-III) are zinc-dependent enzymes that specifically cleave the first two amino acids from the N-terminus of its peptide substrates, which includes biologically active neuropeptides like angiotensins and endomorphins. Although the structure of the yeast homolog has been recently elucidated, DPP-III is the only known enkephalin-degrading enzyme with no structural data in complex with substrate/inhibitor [2]. In this context, we solved the X-ray structure of human DPP-III and its complex with the opioid peptide tynorphin at 1.9 and 2.4 Å, respectively. The structures show how the enzyme recognizes the ligand and undergoes a large motion of 60 degrees and 40 Å upon peptide binding. To further characterize the interaction, we performed a series of Isothermal Titration Calorimetry assays at different temperatures, ranging from 5 to 30 Celsius degrees. The binding was always endothermic, revealing an unusual entropy-driven binding mode, which might be implicated in the regulation of the enzyme.Our findings provide a starting point for designing specific DPP-III inhibitors, helping the development of tools to elucidate its function and also to access its potential as a drug target in the pain field, which lacks significant advances for the past decades.

[1] Peptides. 2001 Dec;22(12):2257-328. Review
[2] J Biol Chem. 2008 Aug 8;283(32):22316-24

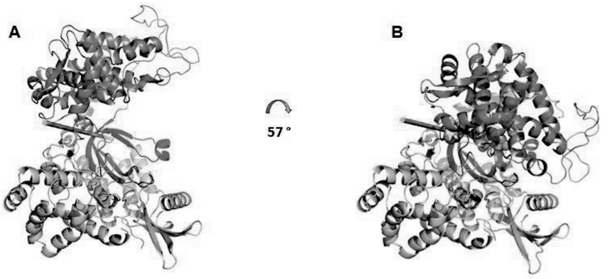

Figure 1: Overview of DPP-III structure depicting a large domain movement upon peptide binding. (A) Cartoon representation of the unbound structure. (B) Cartoon representation of the enzyme in complex with the opioid peptide tynorphin, represented as yellow spheres in the active site.

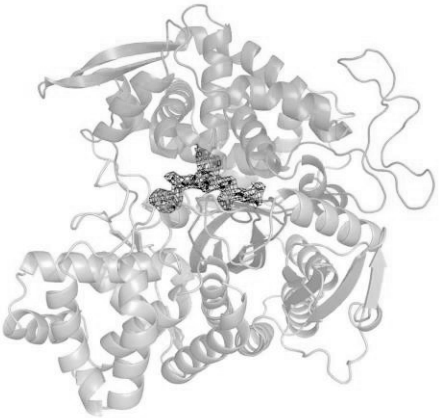

Figure 2: 2.4 Å 2Fobs - Fcal electron density map of the opioid peptide tynorphin in the acitve site of hDPP-III, contoured at 1σ.

MS14-T6

Unusual Carbon Fixation Giving Rise to Diverse PolyketideExtender Units

N. Quade[1], L. Huo[2], D.W. Heinz[1], R. Müller[2]
[1]Helmholtz Centre for Infection Research, Molecular Structural Biology, Braunschweig, Germany
[2]Helmholtz-Institute for Pharmaceutical Research Saarland, Saarbrücken, Germany

In recent years, several strains of bacterial pathogens have arisen that are resistant against many of the antibiotics used today. Most of these drugs are derived from natural products. Especially polyketides, often produced by soil bacteria, have found many medical applications, such as erythromycin as an antibiotic or epothilone as an anticancer drug. The polyketides are produced by large multienzyme complexes called polyketide synthases. These assemble the complex molecules piece by piece by adding small fragments called extender units to the growing chain to form large, structurally complex molecules. We will present structural and biophysical data on a protein involved in the generation of these extender units derived from precursors from primary metabolism. Our data provide the first detailed insights into the production of these extender units by a novel reaction mechanism as well as into the residues necessary for substrate selectivity.

This work will allow for a rational approach in protein engineering to change the substrate specificity of these proteins to be able to produce new compounds incorporating novel extender units. These compounds could lead to new drugs, which are urgently needed in times of emerging antibiotic resistance.

Weissman, K.J. & Muller, R. Protein-protein interactions in multienzyme megasynthetases. *Chembiochem* **9**, 826-48 (2008).

MS15-T1

High-pressure phase transformation of SiO_2 polymorphs to Seifertite

U. Bläß[1], F. Langenhorst[1]
[1]Friedrich-Schiller-Universität Jena, Institut für Geowissenschaften, Jena, Germany

Silica phases are well known for their rich polymorphism, which occurs over wide temperature and pressure conditions. In low-pressure polymorphs, silicon is generally in fourfold coordination showing a three dimensional network of silicon-tetrahedra. All these structure types show a highly symmetric high-temperature form and one or more distorted low-temperature polymorphs, formed by a rapid displacive phase transition during cooling, whereas the transition between the various high-temperature forms are reconstructive and extremely sluggish due to the necessity of breaking strong covalent Si-O-Si bonds. In addition to these low-pressure silica polymorphs, a couple of high-pressure polymorphs are known, of which only coesite occurs naturally in highly metamorphic rocks and consists of a network of fourfold coordinated silica. For all the other polymorphs, silicon is in six-fold coordination and the phases are known only from highly shock-metamorphic meteorites, but may also occur deep inside planetary interiors, if free silica could occur there. With increasing pressure these polymorphs are stishovite with rutile-structure, a polymorph with CaCl2-structure (distorted rutile-structure), a polymorph with alpha-PbO2 structure, recently called seifertite, and a further polymorph of ZrO2-structure (e.g. El Goresy et al., 2004). In order to investigate the formation conditions of seifertite occurring e.g. in the Martian meteorites Shergotty and Zagami, our results have shown that seifertite appears in mesostasis areas of a highly differentiated magmatic eutectic melt as a shock metamorphic product of a tridymite or cristobalite precursor phase. 1-5 µm large crystals show the characteristic amorphous sets of lamellae as initially described by Sharp et al., 1999. In contrast, stishovite crystallises exclusively from shock melt veins or pockets in these meteorites. The defect microstructure of accessories like tranquillityite indicate that seifertite-bearing areas are not re-molten during the shock event and therefore seifertite must have been formed by a rapid solid state transformation process at pressures of about 30 GPa, which is far below the equilibrium crystallisation pressure of seifertite. However, significantly higher pressures, as necessary for an equilibrium formation of seifertite, would have caused severe melting of these areas and a comparison with appropriate Shergottites revealed that resulting high post-shock temperatures would even prohibit the recovery of potentially formed seifertite. In contrast to the low-pressure regime, fast and metastable transformation processes must occur to high-pressure silica polymorphs, which do not involve a breaking of several bonds like a reconstructive transition. Potential crystallographic models will be discussed as well as their implications to the formation of seifertite in natural samples. References: El Goresy A., Dubrovinsky L., Sharp T.G. and Chen M. (2004), J. Phys. Chem. Sol., 65:1597-1608. Sharp T.G., El Goresy A., Wopenka B. and Chen M. (1999), Science 284:1511-1513.

MS15-T2

High pressure synthesis of single crystals of a-boron

G. Parakhonskiy[1], N. Dubrovinskaia[2], L. Dubrovinskiy[1],
S. Mondal[2], S. van Smaalen[2]
[1]Universität Bayreut, Bayerisches Geoinstitut, Bayreuth, Germany
[2]Universitat Bayreuth, Lehrstuhl fur Kristallographie, Physikalisches Institut, Bayreuth, Germany

A method of synthesis of single crystals of alfa-boron (a-B) is presented. α-boron has been crystallized from a boron–platinum melt at high pressures (6–11 GPa) and high temperatures (1200–1600 C). The method is based on the high-pressure large volume (multi-anvil) press technique. For the first time single crystals of α-boron were synthesised from β-boron as a starting material. An average size of the as-grown isometric crystals is 60–80 mm in maximum dimension. The colour of crystals varied from light red to deep red and yellowish depending on the size of the crystals and experimental conditions A refinement of an accurate crystal structure of a-B against single crystal X-ray diffraction data demonstrates the excellent quality of the single crystals. The morphology and chemical composition of the synthesized samples of single crystals were studied by means of the scanning electron microscopy. Chemical purity of the samples was confirmed using WDX microprobe analysis. The crystal structure is in good agreement with the literature. Purity of the crystals was confirmed with Microprobe analysis.

MS15-T3

Symmetry Mode based parametric Rietveld refinement applied to structural phase transitions

M. Müller[1,2], R. Dinnebier[1], S. Schorr[3]
[1]Max Planck Institute for Solid State Research, Stuttgart, Germany
[2]University of Trento, Trento, Italy, Germany
[3]Free University Berlin, Berlin, Germany

In this work parametric Rietveld refinement [1] is combined with a symmetry mode based description of the parameters in a phase transition in order to investigate that transition in detail.

Parametric Rietveld refinement offers the possibility to refine non-crystallographic parameters directly from *in-situ* diffraction data by implementing functional dependencies of refineable parameters instead of performing analysis of those parameters after refinement.

For refinement the low symmetry crystal structure is described as a distorted modification of the high symmetry crystal structure (parent phase) using the atomic coordinates of the parent phase and a structural distortion composed of a set of so called symmetry modes [2]. According to Landau theory, symmetry modes of one given type (e.g. lattice strain, displacement or occupancy) comprise an order parameter.

In this work a case study of the temperature dependent phase transition of $CuInSe_2$ [3] is presented. This phase transition combines an order-disorder transition in the cation lattice and a displacive transition of the anions. The ISODISTORT software [4], a web based software package, is used for symmetry mode decomposition and the creation of a parameter set for parametric Rietveld refinement using the Topas software [5] (Fig. 1).

References

[1] G.W Stinton, J.S.O. Evans, J. Appl. Cryst. (2007) 40(1), 87-95.

[2] J.M. Perez-Mato, D. Orobengoa, M.I. Aroyo, Acta. Cryst. A (2010), 66(5), 558-590.

[3] M. Müller, R.E. Dinnebier, S. Schorr (submitted to Zeitschrift für Kristallographie)

[4] B.J. Campbell, H.T. Stokes, D.E. Tanner, D.M. Hatch, J. Appl. Cryst. (2006) 39, 607-614.

[5] Topas v.4.1 (Bruker AXS, 2007)

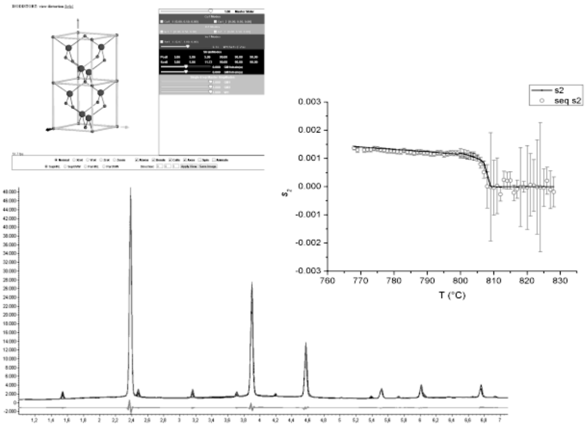

Figure 1: Parametrically refined powder pattern, ISODISTORT template and a comparison of the results of traditional sequential refinement (dots) and parametric refinement (line) for the s2 symmetry mode describing the tetragonal distortion of the unit cell during the phase transition.

MS15-T4

Crystal orientation investigation of Japanese twins in quartz using EBSD

A. Lenart[1], Z. Samardžija[1,2], M. Gec[1], B. Mirtič[3], S. Šturm[1]
[1]Jožef Stefan Institute, Department for Nanostructured Materials, Ljubljana, Slovenia
[2]Center of Excellence NAMASTE, Ljubljana, Slovenia
[3]University of Ljubljana, Faculty for Natural Sciences and Engineering, Department of Geology, Ljubljana, Slovenia

Quartz is one of the most extensively studied minerals due to its numerous applications. While its composition is simple, its structure displays considerable complexities [1]. Macroscopic quartz crystals in nature are known to frequently form twins, which can be of mechanical, growth or transformation origin. Dauphiné twins are classified as penetration twins and are determined by twofold rotation about the vertical *c* axis. On the contrary, the rarely found Japanese twins are a form of contact twins. These growth twins are characterized by the composition plane as or . In the literature there are limited investigations of the structure of the composition plane; this study combines electron backscatter diffraction (EBSD) with the optical microscopy.

The composition plane of natural Japanese twinned quartz crystals was located on double-side polished specimens using polarized light in an optical microscope. To determine the crystallographic orientation relations using the EBSD technique, the surface of the crystal was finally polished with colloidal silica in [ ].

Optical observations showed that by changing the focus throughout the crystal sample the composition plane changes its morphology. In its interior crystal exhibits ~100 µm flat composition plane, whereas closer to the surface it becomes irregular and shows no distinct crystallographic relations. EBSD confirmed that the crystal orientation of one twin individual in comparison to the other, irrespective of depth of acquired sample, differs by an angle of ~84° (Fig. 1). This angle corresponds to the enclosing angle of both *c* axes, which match with the known theoretical angle for Japanese twins [2]. Within the crystal matrix, Dauphiné twins were also detected, which are characterized by the 180° (or 60°) rotation about the *c* axis.

From these studies it can be concluded that the formation of Japanese twins can be divided into nucleation and growth stage. The twin formation is believed to be initiated in the nucleation stage, which also determines the morphology of the crystal. This is followed by the growth of the already-nucleated twin, which continues in the same direction, but with a less crystallographically defined interface, which results in the formation of the general interface between both sides of the twinned quartz.

[1] Wenk, H.-R., Rybacki, E., Dresen, G., Lonardelli, I., Barton, N., Franz, H., Gonzales, G. (2006): Dauphiné twinning and texture memory in polycrystalline quartz. Part 1: Experimental deformation of novaculite. *Phys. Chem. Minerals*, **33**, 667-676.

[2] Hahn, T. & Klapper, H. (2006): Twinning of crystals. Chapter 3.3 *in* "International tables for crystallography, Vol. D", A. Authier, ed. Kluwer Academic Publishers, Dordrecth, 393-448.

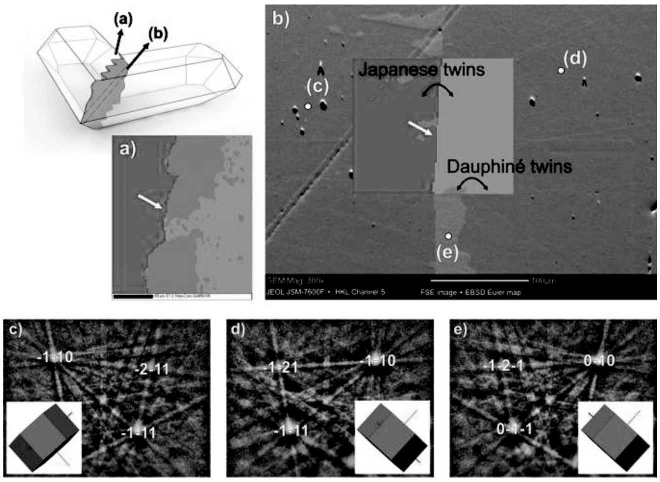

Figure 1: a) SEM/EBSD analyses of Japanese twinned crystal in direction. EBSD crystal orientation map (COM) of composition plane (marked with arrow) closer to the surface exhibit irregular growth layers. b) FSE image with superimposed COM window shows regular twin boundary, when the sample is acquired from interior part of a crystal. EBSD patterns from c) and d) confirm the rotation of the unit cell by ~84° which is adequate to the composition plane of Japanese twins. Dauphiné twins penetrates

mostly from the composition plane into the matrix and can be detected via corresponding EBSD patterns shown in d-e).

MS15-T5

A^{57}Fe Mössbauer Study of Local Structure and Cation Distribution in Mullite-type $Bi_2(Fe_xMn_{1-x})_4O_{10}$ and in $Bi_2(Fe_xM_{1-x})_4O_9$, M=Al, Ga, Mn

S.-U. Weber[1], T.M. Gesing[2], M. Lufaso[3], H. Schneider[4], K.-D. Becker[1]
[1]TU Braunschweig, Institut für Physikalische & Theoretische Chemie, Braunschweig, Germany
[2]Universität Bremen, Institut für Kristallographie, Bremen, Germany
[3]University of North Florida, Institute of Chemistry, Jacksonville, United States
[4]Universität Köln, Institut für Kristallographie, Köln, Germany

In the present work, the local structure of solid solutions of $Bi_2(Fe_xMn_{1-x})_4O_9$ (designated as O9-phases) with M=Al, Ga, and Mn and of $Bi_2(Fe_xM_{1-x})_4O_{10}$ (designated as O10-phases) is studied by ^{57}Fe Mössbauer spectroscopy. Spectra are composed by superposition of two quadrupole doublets due to iron located on octahedrally and tetrahedally coordinated sites, see Fig. 1, where the smaller of the two splittings is always due to octahedrally coordinated species. The spectra yield quantitative information on the iron occupancy of the two structural sites in the mullite-type lattices. In the Fe-Al system, the distribution of cations is found to be almost random, whereas in the Fe-Ga system, gallium ions are found to develop a strong preference for the occupation of tetrahedral sites, thus displacing Fe cations to the octahedral sites. In the Fe-Mn system, manganese ions reveal a strong preference for the octahedral position: in the O9-solid solution phase Mn ions are found to exclusively occupy this site, whereas the tetrahedrally coordinated sites are completely filled by Fe. In the O10-phase, the Fe occupancy of the pyramidal site is twice as large as that of the octahedral sites.

Hyperfine parameters, isomer shifts, and quadrupole splittings derived from the spectra as a function of composition, e.g., provide evidence for a strong distortion of the iron sites at low iron concentrations in the Fe-Al system. In addition to measurements at room temperature, high-temperature in-situ Mössbauer spectroscopy provides information on the temperature dependence of the cation distribution of Fe, Al, and Ga on the two inequivalent lattice sites of the O9-structure. In both solid solutions, cation distributions show almost no temperature dependency, yielding site exchange energies close to zero. Temperature-dependent studies of the Fe-Mn system are under way.

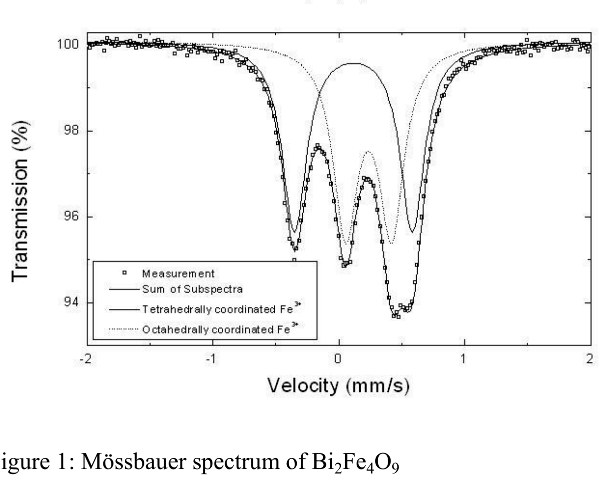

Figure 1: Mössbauer spectrum of $Bi_2Fe_4O_9$

MS15-T6

Dehydration studies of cation-exchanged natrolites

K. Hoffmann[1], R.X. Fischer[1]
[1]Universität Bremen, FB05 Geowissenschaften, Bremen, Germany

Natrolite ($Na_{16}Al_{16}Si_{24}O_{80} \cdot 16H_2O$) belongs to the group of fibrous zeolites with a NAT topology. Because of the high rotation ability of the tetrahedral chains, the NAT framework structure shows an extreme flexibility upon cation-exchange [1]. Fully K-exchanged natrolite (K-NAT) was synthesized from the original Na-natrolite (Na-NAT) under mild aqueous conditions and used to synthesize Cs-natrolite (Cs-NAT) [2]. Successive volume expansions of 10.17% (K-NAT) and 18.22% (Cs-NAT) compared with Na-NAT were observed. The thermal stability of the crystalline samples was studied by means of high-temperature powder X-ray diffraction between room temperature and 1200°C, using a HTK1200N heating chamber, in combination with thermal analyses.

Heating of cation-exchanged natrolite results in a collapsed framework, caused by the loss of water molecules. The symmetry is reduced from space group *Fdd*2 (hydrous cation-exchanged natrolite) to space group *F*112 for the anhydrous phases. For the fully dehydrated phases, unit-cell volume contractions of 18.98% at 160°C and 15.75% at 100°C were observed for K-NAT and Cs-NAT, respectively. Therefore, it is proposed, that the decrease of the dehydration temperature and the degree of framework collapsibility depend on the size of non-framework cations. Further heating shows a unit-cell volume expansion, decreasing with the increasing size of non-framework cations. An increase of the decomposition temperature is observed, being 1060°C for K-exchanged and >1200°C for Cs-exchanged natrolite. Rehydration takes place as long as the anhydrous phases exist, getting decelerated by the exchange of bigger non-framework cations. It was shown, that the channel water content of cation-exchanged natrolite is very sensitive and mechanical exposure leads to a transformation into the anhydrous phases.

[1] Stuckenschmidt, E., D. Kassner, W. Joswig and W. Baur (1992): Flexibility and distortion of the collapsible framework of NAT topology: The crystal structure of NH_4-exchanged natrolite. European Journal of Mineralogy **4**: 1229-1240.

[2] Lee, Y., Y. Lee and D. Seoung (2010): Natrolite may not be a soda-stone anymore: Structural study of fully K-, Rb-, and Cs-exchanged natrolite. American Mineralogist **95**: 1636-1641.

MS15-T7

Zum Dehydratationsverhalten von Zeolithen: Tieftemperatur-Untersuchungenan Paulingit

A. Bieniok[1], P. Göttig[2], U. Brendel[2]
[1]Universität Salzburg, Materialforschung & Physik, Salzburg, Austria
[2]Universität Salzburg, Molekulare Biologie, Salzburg, Austria

Paulingit ist einer der ungewöhnlichsten natürlichen Zeolithe. Die farblosen, transparenten Rhombendodekaeder kristallisieren in der kubischen Raumgruppe Im3m mit Gitterkonstanten um 35.1 Å. Die aluminosilikatische Gerüststruktur bildet ein 3-dimensionales Kanalsystem mit Achterringen als größte Porenöffnungen aus (**8** 3.6x3.6***). Die komplexe Struktur weist 7 verschiedene polyedrische Baueinheiten auf, die von Wassermolekülen und den Kationen gefüllt sind (1). K- und Ca-Varianten von Paulingit sind am häufigsten(2). Das Dehydratationsverhalten von Paulingit zeigt bei 373 K eine Phasenumwandlung zu einer Zwischenphase in der Raumgruppe I-43m. Hier deformieren 8er-Ringe (S8R) zu elliptisch verzerrten

Formen, die den verbliebenen Kationen und Wassermoleküle günstige Koordinationsmöglichkeiten bieten. Unter Wasserabgabe reduziert sich das Zellvolumen um 11.2% und die Gitterkonstante verkleinert sich auf 33.88 Å (5). Bei weiterer Temperaturzufuhr kollabiert die Gerüststruktur irreversible.
Jetzt wurde das Verhalten der Paulingit-Struktur unter tiefen Temperaturen kristallographisch untersucht. Einkristalle von Paulingit-Ca,K (Ritter, Oregon, USA) wurden auf einem Diffraktometer (CuKα, 2.3 kW, MAR345) im N_2-Strom bis auf 100K gekühlt und Beugungsbilder in ϕ-Scans aufgenommen. Die Gitterkonstante reduziert sich dabei bis auf 34.245(5) Å, was einer Abnahme des Volumens um 7.4% entspricht. Die Deformation der Gerüststruktur durch Kippen und Drehen der Tetraeder ist in der reduzierten Zelle in der Raumgruppe Im3m unter Beibehaltung plausibler T-O-T Winkel nicht mehr möglich, so dass auch hier schon die Umwandlung in die Untergruppe I-43m erfolgt ist. Dabei deformieren vorher annähernd kreisförmige S8R zu in Richtung gestreckten, elliptischen Ringen. Die Verfeinerung des Strukturmodells ergibt mit isotropen Auslenkungskoeffizienten eine Übereinstimmung von R=0.0895 und S=1.2. Die Reduktion des Zellvolumens wird aber in erster Linie durch die trockene Umgebungsluft bei den Messungen hervorgerufen, auf die der Zeolith sofort mit Wasserabgabe reagiert. Bei Raumtemperatur (293 K) kann man durch den trockenen N_2-Strom reversible bereits eine Reduzierung der Gitterkonstante auf 34.345(6) Å hervorrufen, also eine Anpassung der Struktur um 6.6 Vol.-% auf die Wasserabgabe. Die Untersuchungen zeigen also nicht nur das Tieftemperaturverhalten des Paulingits, sondern auch, wie empfindlich kollapsible Zeolithstrukturen auf Änderungen der Luftfeuchtigkeit reagieren.

(1) Bieniok A., Joswig W., Baur W.H. (1996) N.Jb.Miner.Abh. ***171(2)***, 119. (2) Passaglia E., Gualtieri A.F., Marchi E. (2001) Eur.J.Mineral. ***13***, 113. (3) Lengauer C.L., Giester G., Tillmanns E. (1997) Min. Mag. ***61***, 591. (4) Bieniok A. (1997) N.Jb.Miner.Mh. ***11***, 498. (5) Bieniok A. (2000) in Colella C. & Mumpton F.A.: Natural Zeolites for the Third Millennium, 53.

MS15-T8
Highly symmetric complex intermetallics

J. Dshemuchadse[1], D.Y. Jung[1], W. Steurer[1]
[1]ETH Zurich, Laboratory of Crystallography, Zurich, Switzerland

A growing number of structurally highly complex intermetallic phases is being discovered and described with the emergence of new crystallographic methods. We are still not able to understand, why unit cells containing hundreds or even thousands of atoms are being formed by simple, binary and ternary metallic compounds. To approach this important question, we are working on a systematization of complex intermetallics, starting with the highest-symmetric lattice, i.e. the cubic face-centered structures.
There is a bigger group of phases with approximately 400 atoms per unit cell - 43 reported structures -, which crystallizes in only two different space groups and can be roughly assigned to a common aristotype structure. The few structures with even bigger unit cells - 11 phases with around 1000 atoms per unit cell, not mentioning the even bigger Al-Cu-Ta compounds [1,2] - show a slightly broader structural variety but can also largely be traced back to some common geometrical characteristics. We try to understand all of these structures in terms of the cluster approach, describing them as packings or coverings of highly symmetric building blocks. In addition, features of the average structure and findings from first-principle studies are discussed with respect to complexity and phase formation.

[1] T. Weber, J. Dshemuchadse, M. Kobas, M. Conrad, B. Harbrecht, W. Steurer (2009). Acta Cryst. B, 65(3), 308-317. [2] M. Conrad, B. Harbrecht, T. Weber, D. Y. Jung, W. Steurer (2009). Acta Cryst. B, 65(3), 318-325.

MS16-T1
U-Pb dating of scheelite by LA-SF-ICP-MS constrains the Variscan age of the Felbertal tungsten deposit

J. Raith[1], A. Gerdes[2], D. Cornell[3]
[1]Montanuniversitaet Leoben, Chair of Resource Mineralogy, Leoben, Austria
[2]Goethe Universität Frankfurt, Institut für Geowissenschaften, Frankfurt, Germany
[3]Geovetarcentrum, Gothenburg, Sweden

The Felbertal scheelite deposit is one of the biggest tungsten mines in the world (annual capacity about 0.4 Mt/yr; total production until 2009: 12.9 Mt at 0.5% WO_3). It has long been regarded as the type locality of stratiform-stratabound scheelite deposits. Syngenetic exhalative hydrothermal as well as granite-related epigenetic models were proposed to explain ore formation. In this contribution we present a new *in-situ* U-Pb age for scheelite obtained by LA-SF-ICP-MS allowing us to decipher the timing of the oldest stage of scheelite ore; this new age is crucial for unravelling the ore genesis. The Felbertal deposit is situated in the lower parts of the Habach Complex, an Early Cambrian to Ordovician sequence of metavolcano-sedimentary rocks with ophiolitic to arc sequence characteristics. A chemically unusual fractionated W-bearing granite, the K1 orthogneiss, was emplaced in the Early Carboniferous (336 ± 19 Ma) into the western ore zone of the deposit. Several economic ore bodies are spatially associated with this orthogneiss, that is not exposed at the surface. Economic scheelite mineralisation is associated with SiO_2-rich lithologies. It includes well foliated fine-grained scheelite-quartz ores ("Quarzitisches Scheelitreicherz") that were the main target of former mining in the eastern ore zone, as well as deformed quartz veins (Quartz 1) and stockwork like mineralisation. The ore deposit was affected by metamorphism (up to the lower amphibolite facies) and tectonics during the Variscan (~330 Ma) and Alpine (~30 Ma) orogenies. Trace element analyses using LA-QP-ICP-MS techniques, controlled by cathodoluminescence (CL) images, confirmed the previously established classification of scheelite stages. Scheelite 1 is preserved as relict cores in fine-grained scheelite in the foliated scheelite-quartz ores. It preserves delicate oscillatory growth zoning, is characterised by flat wing-shaped REE patterns, and contains between 50 to 1120 ppm U. In-situ U-Pb dating by LA-SF-ICP-MS of Scheelite 1 yielded a concordia age of 335.5 ± 4.6 (2 sigma). This new age constrains the timing of scheelite formation of the "Scheelitreicherz" for which an Early Cambrian age was previously assumed. These foliated fine-grained scheelite-quartz ores are therefore not exhalites but are re-interpreted as mylonitic ores formed during the Variscan orogenic cycle. Within the uncertainty this new age is indistinguishable from the 336 ± 19 Ma emplacement age of the K1 orthogneiss (Eichorn et al., 1999). The new scheelite age is inconsistent with previous genetic models, which proposed either syngenetic ore formation in the Cambrian or two stages of epigenetic ore formation, the first in the Cambrian and the second in the Early Carboniferous (Eichorn et al., 1999). The Felbertal scheelite deposit is best interpreted as a metamorphosed, syntectonic granite-related magmatic-hydrothermal ore deposit of exclusively Early Carboniferous age.

References

Eichhorn R. et al. (1999). Int. J. Earth Sci., 88, 496-512

MS16-T2

Proof of origin of coltan ores by in-situ microanalytical methods - MLA and SF-LA-ICP MS

M. Sitnikova[1], E. Gäbler[1], T. Graupner[1], F. Melcher[1]
[1]BGR, Resource Geology, Polar Geology, Hannover, Germany

In order to improve transparency along the tantalum trade chain, a “certificate of origin” for so-called “conflict minerals” has been recommended by the United Nations. Analytical fingerprint of the ores should exclude illegally traded material from the world market.

The analytical fingerprint for coltan (trade name for concentrates of Ta-Nb oxides, mainly columbite-tantalite) consists of 3 steps. The 1st one is the characterisation of the mineralogical composition of the concentrate. Mineralogical parameters such as modal mineralogy, grain size distribution and mineral relationships are determined on polished sections that are investigated by scanning electron microscopy (ESEM Quanta 600 FEG, FEI Company, equipped with an EDAX 32 module) using the Mineral Liberation Analysis (MLA) software. The MLA software combines backscattered electron (BSE) images with EDX spectra. A series of BSE images including an X-ray spectrum for each mineral particle was collected. The offline processing routine compares the measured mineral spectra with known mineral standards to determine the mineral identity for each grain. To identify intermediate members of complex solid solution series such as columbite-tantalite, calibration was done using wave-length dispersive EPMA for comparison with EDX spectra. More than 20000 particles are detected in concentrates at typical measurement times of two to three hours. Therefore, even rare phases are identified with high probability. The presence of rare phases in the coltan concentrates may already serve as a fingerprint for single deposits.

In a 2nd step data on the chemical composition of major as well as 34 trace elements of columbite-tantalite minerals grains are collected. On the basis of the results obtained by MLA, about 50 representative grains are localised in each section and analysed by sector field LA-ICP MS. An Element XR (Thermo-Fisher Scientific) with a detector system covering an extended linear range, and coupled to a 193 nm excimer laser ablation system (UP193-FX) is used. The 3d step - estimation of mineral formation ages using the U-Pb isotope system, on the basis of the sector field LA-ICP-MS data, traces the origin of a coltan concentrate to one out of five “age provinces” known from African tantalum-bearing pegmatites. An internal standard-independent calibration strategy allows data for major and trace element determination and mineral formation age estimates to be obtained simultaneously.

The application of a streamlined workflow combining SEM / MLA and LA-ICP-MS methods allows determining those critical parameters necessary to discriminate the origin of coltan concentrates from Africa: mineralogy, chemistry of the major Ta oxide phase(s), and mineral formation age. Using a large coltan concentrate dataset of known origin, the source of material sampled along the trade chain may be assessed.

MS16-T3

Fractionation of the Lu-Hf Isotope System during Formation of Nb-Ta Mineralisations

A. Gerdes[1], L. Marko[1], F. Melcher[2]
[1]Goethe University Frankfurt, Institute of Geosciences, Frankfurt am Main, Germany
[2]Bundesanstalt für Geowissenschaften und Rohstoffe, Geozentrum , Hannover, Germany

As a reconnaissance study we analysed the Lu-Hf isoptope compostion of columbite-tantalite minerals from different rare element pegmatite provinces. The aim was to see if each mineralisation has its distinct isotopic signature, which can be used as fingerprint to characterise a certain locality or even an entire pegmatite province. This mineralisation are commonly associated with the crystallisation of larger felsic magma systems. The Nd and Hf isotope compostion of such system is assumed to be rather homogeneous and normally used to characterize the origin and source of the parent magma. As the intial ^{176}Hf/^{177}Hf of the earth 4.56 Ga ago was about 0.2797, melting of the oldest continental crust during Cenozoic time would yield magmas with a ^{176}Hf/^{177}Hf as low as 0.28084 while present day MOR basalts have a ^{176}Hf/^{177}Hf of about 0.28325. Thus the total variation of earth crustal rocks expressed in the epislon notation is about 86 eHf-units.

Samples and Method

We selected samples from 32 different pegmatite province worldwide, including 16 pegmatites of late Kibaran age from Central Africa. The U-Pb age of the minerals were obtained independently by LA-SF-ICP-MS. Lu-Hf isotopes were analysed by isotope dilution technique using a Neptune MC-ICP-MS after dissolution in acid and subsequent separation of the Lu and the Hf fraction by ion exchange chromatography. For this 0.5 to 15 mg of each sample were drilled out of thick sections. To test the homogeneity within one location we analysed multiple samples from a drill core.

Results

The Hf concentration in the different samples varied from 19 to 3100 ppm with Lu/Hf ratios of 0.04 to 0.00001. The low Lu/Hf makes the correction for Hf ingrowth since crystallisation moderate to small. Preliminary results show variation of the intial ^{176}Hf/^{177}Hf of more than 1000 eHf-units, thus more than 12times the variation known from crustal rocks. The majority of the minerals analysed show a Hf isotope composition that is more radiogenic than the bulk earth and even the depleted mantle at that time.

MS17-T1

Structure and Biochemical Analysis of Alzheimer’s Disease Amyloid Precursor Protein (APP)

M.E. Than[1], S.O. Dahms[1], S. Hoefgen[1], I. Könnig[1], D. Roeser[1]
[1]Leibniz Institute for Age Research - Fritz Lipmann Institute (FLI), Protein Crystallography Group, Jena, Germany

The amyloid precursor protein (APP) is the key player in Alzheimer’s disease (AD) pathology. In addition, APP and its analogues are essential for neuronal development and cell homeostasis in mammals. Its proteolytic processing by the α- β- and γ-secretases is well established and results in the release of the neurotoxic Aβ-peptide, the generally believed causative agent of AD. In contrast, both, the physiologic function of APP and its true three-dimensional structure are widely unclear. We have been able to establish the heterologous expression and large-scale purification of several subdomain-constructs of the multidomain protein APP. Employing biochemical and biophysical studies of different constructs we analyze the exact domain architecture of APP and prove for the first time that it consists of two rigidly folded entities (E1 & E2) that are connected by the acidic domain (AcD), a highly flexible linker. The protein crystallographic analyses of the rigidly folded E1- and E2-domains show that APP is dimerized in a heparin dependent manner by its E1-domain and that a novel metal binding site within its E2-domain acts as a conformational switch of its physiologic function.

MS17-T2

The Structure of Collagenase G at 2.55 angström resolution reveals a Chew & Digest Mechanism of Bacterial Collagenolysis.

U. Eckhard[1], E. Schönauer[1], D. Nüss[1], H. Brandstetter[1]
[1]University of Salzburg, Division of Structural Biology, Salzburg,
Austria

Collagen constitutes one third of the body protein in man, reflecting its extraordinary role in human health and disease. Of similar importance are the specific proteases that nature evolved for collagen remodeling. Interestingly, the most efficient collagenases are found in bacteria, namley clostridia, which enable them to colonize their host tissues. Despite intense studies, the structural and mechanistic basis of these enzymes remained elusive up to now. Here we present the crystal structure of collagenase G from *C. histolyticum* at 2.55 angström resolution. Fully consistent with our complementary enzymatic and mutagenesis studies, we derived a conformational two-state model of bacterial collagenolysis, in which the recognition and unraveling of collagen microfibrils into triple helices as well as the unwinding of the latter go hand in hand with collagenase opening and closing.

MS17-T3

The structural basis of proteolysis and host-pathogen interaction by pestivirus protein Npro

T. Zögg[1], M. Sponring[2], M. Koll[2], R. Schneider[2],
H. Brandstetter[1], B. Auer[2]
[1]University of Salzburg, Molecular Biology, Salzburg, Austria
[2]University of Innsbruck, Institute of Biochemistry, Innsbruck, Austria

The bi-functional protein Npro is a key effector of pestiviruses such as classical swine fever virus (CSFV) to abolish host cell anti-viral defense mechanisms. Synthesized as the N-terminal part of the single viral polyprotein, Npro releases itself via an auto-proteolytic cleavage event. The proposed atypical arrangement of catalytic residues is the basis to assign Npro to a new subfamily of cysteine proteases, C53.

Processed, proteolytically inactive Npro exerts an additional function as it interferes with transcription factor IRF3 and targets it to the proteasome. Three conserved cysteine residues coordinating a zinc ion were proposed to be essential for this interaction. As a result, Npro suppresses the production of IFN-α/β, both typical mediators for anti-viral immune responses, thus enabling the virus to evade this host cell defense mechanism.

Here we present the crystal structure of Npro to 1.5 A resolution. The structure reveals a modular architecture comprising an all-β fold together with random coil elements. The geometric arrangement of the catalytic residues explains the enigmatic latency of the protease, ensuring a single cleavage in cis. Additionally, the conserved cysteine residues rationalise the zinc binding properties that relate to its transcription factor targeting.

MS17-T4

Cap architecture conservation in monoglyceride lipases from bacteria to humans

S. Rengachari[1], G. Arruda Bezerra[1], C. Sturm[1], L. Riegler[1],
C.C. Gruber[1,2], U. Taschler[1], A. Boeszoermenyi[1],
R. Zimmermann[1], K. Gruber[1], M. Oberer[1]
[1]University of Graz, Graz, Austria
[2]ACIB GmBH, Graz, Austria

Monoglyceride lipases (MGL) catalyze the hydrolysis of monoglycerides into free fatty acid and glycerol. MGL have been identified in all kingdoms of life and have adopted different substrate specificities with respect to chain lengths, depending on their different roles in the host organisms. In humans, MGL play an integral part in lipid metabolism affecting energy homeostasis and signaling processes and in cancer progression. It also hydrolyzes the endocannabinoid 2-arachidonoylglycerol, which regulates a range of physiological processes (e.g. pain sensation). In bacteria, especially short chain monoglycerides are highly toxic. Thus, MGL is crucial for the survival of the bacteria. Despite the biological, pharmacological and biotechnological interest in MGL, the 3D structure of human MGL was the first member of this enzyme family to be solved in 2010. We report the first crystal structures of MGL from a bacterial species (Bacillus sp. H257) in its free form at 1.2Å and covalently complexed to phenylmethanesulfonyl fluoride at 1.8Å resolution, molecular dynamics simulation of bacterial MGL (bMGL, 250 aa) and a comprehensive comparison of the resulting structural insights with the human homolog (303 aa): The core structure is composed of an α/β hydrolase fold. A cap region, which is often observed in α/β hydrolase, is inserted between $\alpha4$ and $\beta5$ elements of the core structure. An ~22Å long tunnel leads from the surface of bMGL to the catalytic triad and thus keeps the active center unexposed to the polar environment. The rim at the entrance to the tunnel has a diameter that is ~12Å wide and is lined with hydrophobic side chains mostly from the cap domain. A hole is located in the cap region of the protein and corresponds to the proposed exit hole for glycerol to leave the active site in human MGL. Molecular dynamics simulation shows open and closed states of the entrance tunnel and the glycerol exit hole.

No electron density was observed for a stretch of 3 aa in the cap region. In human MGL, a corresponding region was also found to be highly flexible and was not visible in one chain of the dimeric structure. Comparison of the cap regions of hMGL and bMGL shows intriguing similarities, despite a sequence identity of only 10%. The 62-amino acid cap of hMGL has been described as U-shaped and comprises of three helices connected by loop regions. The 45-amino acid cap of bMGL harbors a short helical turn and a short two-stranded antiparallel β-sheet connected by linkers. It is very interesting that despite these differences in length and secondary structure composition, the overall shape and arrangement of the cap region of both the proteins superimposes almost precisely in the observed open conformation. It can be speculated that this specific lid architecture is conserved throughout evolution of MGLs.

References:

[1] Bertrand, T., Auge, F., Houtmann, J., Rak, A., Vallee, F., Mikol, V., Berne, P. F., Michot, N., Cheuret, D., Hoornaert, C. and Mathieu, M. *J Mol Biol.* **2010**,*396*, 663-673 [2] Labar, G., Bauvois, C., Borel, F., Ferrer, J. L., Wouters, J. and Lambert, D. M. *Chembiochem*. **2010** *11*, 218-227.

Figure legend: Comparison of the cap region of bacterial MGL and human MGL by structural superposition.

Figure 1

MS17-T5

Crystal structures of Velvet transcription factors reveal an unexpected fold

Y.L. Ahmed[1], P. Neumann[1], Ö. Bayram[2], J. Gerke[2], G. Braus[2], R. Ficner[1]
[1]Georg-August-Universität Göttingen, Molekulare Strukturbiologie, Göttingen, Germany
[2]Georg-August-Universität Göttingen, Department of Molecular Microbiology & Genetics, Göttingen, Germany

Important processes in the morphogenesis and development of fungi are regulated by light. Hence, photoreceptors and other proteins are involved in the translation of light signals into cellular responses. In order to understand the molecular mechanisms of light-driven switches and processes on an atomic level, we are pursuing the determination of the three-dimensional structures of photoreceptors and other regulatory proteins involved in the light-response of *A. nidulans*.

The proteins VeA (velvet) and VelB (velvet-like protein B) play a key role in the light-dependent developmental regulation of *A. nidulans*. Together they form a hetero-trimeric complex with LaeA, a master regulator of secondary metabolism in *Aspergilli* (Bayram et al., 2008). VeA is thought to act as transcription factor, however, it lacks any known DNA-binding domain (Shaaban et al., 2010). Interestingly, the nuclear import of VeA is inhibited by light in a yet unknown way (Bayram et al., 2008a). The 3D-structures of VeA and VelB are unknown and these proteins have no sequence similarity to any other protein of known 3D-structure. Importantly, VeA and VelB share a homologous domain (denoted as velvet domain) that is also found in other fungal proteins like VosA. VosA appears to be a transcription factor as it is localized in the nucleus and is involved in the control of sporogenesis and trehalose biogenesis (Ni & Yu, 2007). Furthermore, VosA was shown to form a stable complex with VelB (Bayram et al., 2008a). This complex seems to be required for the transcription of several genes essential for spore viability.Recently the spore viability of ΔVelB-strain was extensively studied, with the conclusion that VosA's interaction with VelB is required for proper upregulation of the trehalose biosynthesis genes (Bayram et al., 2010). Similar to the ΔVosA-strain the ΔVelB-strain produces spores that contain virtually no trehalose rendering them much more susceptible to extreme conditions.

We report the crystal structures of the VosA-homo-dimer and VosA-VelB-hetero-dimer that represent the first structures for this family and also reveal an unexpected fold among the fungi kingdom.

References

Bayram O, Krappmann S, Ni M, Bok JW, Helmstaedt K, Valerius O, Braus-Stromeyer S, Kwon NJ, Keller NP, Yu JH & Braus GH. (2008a). VelB/VeA/LaeA complex coordinates light signal with fungal development and secondary metabolism. Science 320, 1504-1506.

Bayram O, Biesemann C, Krappmann S, Galland P & Braus GH (2008b). More than a repair enzyme: Aspergillus nidulans photolyase-like CryA is a regulator of sexual development. Mol. Biol. Cell. 19, 3254-62.

Ni M & Yu JH (2007). A novel regulator couples sporogenesis and trehalose biogenesis in Aspergillus nidulans. PLoS One 2, e970.

Shaaban MI, Bok JW, Lauer C & Keller NP (2010). Suppressor mutagenesis identifies a Velvet complex remediator of Aspergillus nidulans secondary metabolism. Eukaryot Cell., in press.

Sarikaya Bayram O, Bayram O, Valerius O, Park HS, Irniger S, Gerke J, Ni M, Han KH, Yu JH & Braus GH (2010). LaeA control of velvet family regulatory proteins for light-dependent development and fungal cell-type specificity. PLoS Genet. 2010 Dec 2;6(12):e1001226.

MS17-T6

X-ray structure refinement with canonical distributions of electrons

S. Ginzinger[1], M. Gruber[1], H. Brandstetter[1], M. Sippl[1]
[1]University of Salzburg, Molecular Biology, Salzburg, Austria

X-ray crystallography reveals the three-dimensional structures of biological macromolecules with atomic details of functional sites and disease relevantaberrations. As the reliability of molecular structures obtained from experiment is always limited by experimental conditions, the construction of a realistic atomic model heavily relys on the available refinement and validation techniques. We use the observation that recurring groups of atoms, like aromatic rings or carbonyl groups, are surrounded by characteristic distributions of electrons which are largely independent of their particular molecular environment [1]. It follows immediately that accurate atomic models of molecular structures have to satisfy these canonical distributions. Therefore, canonical distributions of electrons can be applied in the detection as well as in the refinement of unrealistic molecular environments.

For the detection of unrealistic molecular environments we calculate the electron difference of the density implied by the molecular model and the corresponding canonical density, ρ_{canon}-ρ_{calc}. The result, expressed in electron deficit/excess per cubic Angstrom (Å^3), is easy to comprehend and does not require an understanding of sophisticated error recognition strategies because all unrealistic environments result in regions of deficit or excess electron density.

For the refinement of X-ray structures we expand the crystallographically observed electron density ρ_{obs} with the canonical density ρ_{canon} and subtract the model density ρ_{calc} to obtain the hybrid electron density distribution ρ_{hybrid}. Hybrid maps are compatible with the major crystallographic programs and can be used immediately in model refinement. The resulting molecular models have significantly reduced electron excess and correlate better with the experimental diffraction pattern as measured by the crystallographic free R-value.

References: 1. Ginzinger, S.W., Weichenberger C.X., Sippl, M.J., J Biomol NMR **47(1)**, 33-40 (2010).

MS17-T7
Structural aspects of CRM1 cooperativity: a hybrid methods approach

N. Doelker[1], C. Blanchett[2], T. Monecke[3], D. Svergun[2], R. Ficner[3], H. Grubmüller[1], A. Dickmanns[3]
[1]Theoretical and computational Biophysics, MPI f. biophysikalische Chemie, Goettingen, Germany
[2]EMBL Hamburg, SAXS, Hamburg, Germany
[3]Universitaet Goettingen, Molekulare Strukturbiologie, Goettingen, Germany

Interaction of the small GTPase Ran with the transport receptors of the Importin-b transport receptor superfamily is required for regulation of nucleocytoplasmic trafficking in eukaryotic cells. The majority of members of the importn ß superfamily require a direct interaction of the cargo with Ran in the bound GTP conformation. An exception is the exportin CRM1 with no direct interaction between the cargo and Ran. Moreover and in contrast to the other members, structural information suggests no significant conformational change of CRM1 between the empty and cargo/Ran bound state. The structural transition required for the observed cooperative binding of Ran and the cargo is poorly understood. By employing a combination of SAXS-experiments and MD simulations based on the known crystal structures we wanted to increase the understanding of the structural flexibility of CRM1 in solution. Moreover, we wanted to gain insight into the motions underlying the cooperative binding of Ran and the cargo Snurportin1. CRM1 in the free form exhibits a high degree of conformational flexibility within the ring like structure. The binding of RanGTP decreases this flexibility shifting the possible conformations towards a more rigid form of CRM1 preferentially with the binding cleft in an open conformation prone for NES binding, thus increasing the affinity for the cargo.

MS17-T8
Optimal fine φ slicing for single photon counting pixel detectors

M. Mueller[1], M. Wang[2], C. Schulze-Briese[1]
[1]Dectris Ltd., Baden, Switzerland
[2]Swiss Light Source at PSI, Villigen-PSI, Switzerland

The data collection parameters used in a diffraction experiment have a strong impact on the quality of the acquired data. A careful choice of parameters leads to better data and can make the difference between success and failure in phasing attempts and better data will also result in a more accurate atomic model. The selection of data acquisition parameters has to account for the application of the data in various phasing methods or high-resolution refinement [1]. Furthermore, experimental factors like crystal characteristics, available experiment time, and the properties of X-ray source and detector have to be considered.

CCD detectors are for many years the prevalent type of detectors used in macromolecular crystallography. Most recommendations for data collection strategies as well as the experience of the experimenters are based on the characteristics of this detector type. Recently, hybrid pixel X-ray detectors that operate in single-photon-counting mode became available for macromolecular crystallography [2,3]. The commercially available PILATUS hybrid pixel detector is now in standard user operation at an increasing number of macromolecular crystallography synchrotron beamlines. Hybrid pixel detectors have fundamentally different characteristics and offer various advantages over CCD detectors [3,4]: (i) No readout noise and dark current. (ii) A sharp point spread function of one pixel. (iii) A short readout time in the millisecond range. (iv) A high dynamic range of 20 bits.

To fully exploit the advantages of hybrid pixel detectors different data collection strategies than those established for CCD detectors have to be applied because of the different characteristics of the two types of detectors. Fine φ slicing is a strategy particularly well suited for hybrid pixel detectors because of the fast readout time and the absence of readout noise. We systematically collected a large number of data sets from crystals of four different proteins to investigate the benefit of fine φ slicing on data quality with a noise-free detector in practice. Our results show that fine φ-slicing can substantially improve scaling statistics and anomalous signal providing that the oscillation angle is comparable to half the crystal mosaicity.

[1] Dauter Z, *Acta Crystallographica Section D* 2010, **66**:389-392.
[2] Broennimann C, Eikenberry EF, Henrich B, Horisberger R, Huelsen G, Pohl E, Schmitt B, Schulze-Briese C, Suzuki M, Tomizaki T, et al., *Journal of Synchrotron Radiation* 2006, **13**:120-130.
[3] Hülsen G, Broennimann C, Eikenberry EF, Wagner A, *Journal of Applied Crystallography* 2006, **39**:550-557.
[4] Tate MW, Eikenberry EF, Gruner SM, In *International Tables for Crystallography, Vol. F.* Edited by Rossmann MG, Arnold E. 2006:148-153.

MS18-T1
Interaction of Silicic Acid with Mineral Surfaces in the Aspects of Silicate Weathering and Adsorption

M. Dietzel[1]
[1]Graz University of Technology, Institute of Applied Geosciences, Graz, Austria

The silica cycle in natural aqueous environments is strongly related to complex reaction mechanisms and kinetics at the solid-liquid boundary layer. Silicic acid is primarily liberated into aqueous solutions by weathering of silica containing minerals and rocks. Subsequently, the concentrations of primarily released silicic acid can be reduced by adsorption and precipitation of silica induced by inorganic reactions or biogenic activity.

The amount and also the type of mobilized and transported silicic acids in natural aqueous environments depend significantly - besides temperature and solution chemistry - on the individual mineral solubility and the dissolution kinetics of the siliceous solids as well as on the adsorption behaviour of silicic acids at distinct solid surfaces and on the mechanisms for neo-formation of siliceous solids. Decisive parameters for such kind of processes are respective solid surface characteristics, dissociation behaviour of silicic acids, and individual (de)polymerization behaviour of silicic acids in the solution and at the surfaces of solids. Reaction mechanisms and kinetics between silicic acids and surfaces of selected minerals are discussed concerning studies on weathering of silicates, formation of surface complexes, and decomposition of polysilicic acid.

MS18-T2
Pyrrhotite oxidative dissolution: Crystallographic and microstructural controls observed by FIB-TEM and 3D topometry.

D. Harries[1], K. Pollok[2], F. Langenhorst[2]
[1]Bayerisches Geoinstitut, Universität Bayreuth, Bayreuth, Germany
[2]Institut für Geowissenschaften, Friedrich-Schiller-Universität, Jena, Germany

Pyrrhotite is an abundant, non-stoichiometric iron sulfide ($Fe_{1-x}S$) in the Earth's crust. Due to variable Fe deficiency many structural variants arise from the ordering of Fe vacancies within the NiAs-based structure [1]. The resulting superstructures show different physicochemical properties, bearing on many issues in environmental geochemistry, petrology, and technical mineral processing (e.g., [2]).

In order to study differences in reactivity of pyrrhotite varieties, we conducted oxidative dissolution experiments on carefully polished pyrrhotite surfaces containing crystallographically coherent intergrowths of 4C- and NC-pyrrhotite (N = 4.81-4.87). These samples offer the possibility to eliminate the effect of crystal anisotropy and study intrinsic differences of 4C and NC superstructures. Experiments were done at 30-50 °C using Fe^{3+} and H_2O_2 as oxidants. Surface cross sections were prepared using the FIB technique and were studied using analytical TEM. The surface topography after reaction was recorded by vertical scanning confocal microscopy and used to deduce individual reaction rates of the intergrown pyrrhotite varieties.

Our results show, that reaction rates on a $\{100\}_{NiAs}$ surface strongly and abruptly decrease as pH becomes larger than 2.65 (close to the isoelectric point [3]). At pH < 2.65, NC-pyrrhotite oxidizes and dissolves faster than 4C-pyrrhotite and abundant elemental sulfur precipitates among ferric oxyhydroxides. At pH > 2.65, 4C-pyrrhotite reacts faster and sulfur is always absent. High resolution TEM and TEM-EDX do not show evidence for the formation of S-enriched sulfides (e.g., FeS_2) below the reaction interface at any pH studied.

Comparison of different orientations reveals that the reactions at pH < 2.65 proceed much slower on the $(001)_{NiAs}$ surface than on $\{100\}_{NiAs}$ surfaces. At pH > 2.65 the contrary is observed. On corroding $\{100\}_{NiAs}$ surfaces at pH < 2.65 the reaction proceeds along basal cleavage planes and leads to the formation of pyrrhotite flakes dominated by $(001)_{NiAs}$ faces, which are more resistant against dissolution. The result is strongly enhanced roughness of the reaction interface. On the same $\{100\}_{NiAs}$ surfaces above the transition at pH 2.65, the change in direction dependence of dissolution speed causes smooth reaction interfaces as flakes no longer form due to preferred dissolution on the $(001)_{NiAs}$ faces. These observations exemplify complex physicochemical and microstructural (or rather micromechanical) processes at the reaction interface. Preliminary results suggest that the reduced symmetry of ordered 4C- and NC-pyrrhotites (relative to the hexagonal NiAs subcell) leads to different behaviors of nominally symmetry-equivalent, hexagonal $\{hk0\}_{NiAs}$ surfaces.

References:

[1] Harries D. et al. (2011) American Mineralogist, 96, 716-731.
[2] Becker M. et al. (2010) Minerals Engineering, 23, 1045-1052.
[3] Dekkers M.J. and Schoonen M.A.A. (1994) Geochimica et Cosmochimica Acta, 58, 4147-4153.

MS18-T3
Citrate induced effects on magnesite growth kinetics

U.-N. Berninger[1], Q. Gautier[2], J. Schott[2], G. Jordan[1]
[1]Ludwig-Maximilians-Universität München, Department für Geo- und Umweltwissenschaften, München, Germany
[2]Université de Toulouse-CNRS, Géosciences et Environnement Toulouse, Toulouse, France

Carbonate mineral growth is a fundamental fluid-solid interaction in the upper crust and decisively influences natural mass transfer of many metals as well as carbon dioxide. The accurate description of involved kinetics holds the promise to quantify consequences of industrial applications ranging from geothermal drillings to long-term CO_2 sequestration in natural environments. However, organic ligands occur ubiquitously in natural fluids and interfere to various degrees with mineral growth. The influence of ligands on steady state crystal growth of Mg-containing carbonate minerals still needs further clarification.

In this study, magnesite was chosen because of its high stability in natural environments, and citrate was chosen as a proxy ligand to cover the effects of molecules with three carboxyl groups. In order to determine the effect of citrate on magnesite growth, we performed macroscopic and microscopic crystal growth experiments using Mixed-Flow Reactors (MFR) and Hydrothermal Atomic Force Microscopy (HAFM). Experiments were conducted at pressures of 2-12 bars, temperatures of 100 °C and 120 °C, alkaline conditions (pH 7.5-8.5) and with varying citrate concentrations.

MFR experiments showed that citrate concentrations above 0.01 mM inhibited magnesite growth. Growth rate was reduced with increasing complexation of Mg^{2+} by the ligand in the liquid phase. Furthermore, by correcting saturation states from the complexation effect, it became evident that citrate caused a reduction of the kinetic rate constant of magnesite growth: citrate concentrations as low as 0.2 mM induced a 4-fold decrease of the rate constant. This result points towards a prominent surface effect of citrate.

HAFM observations showed that citrate interacted with steps on the magnesite surface and modified the shape of growth islands. Measurements of step advancement rates suggested that citrate strongly reduced acute step advancement, which have been suggested to control magnesite growth at similar conditions [1].

In summary, inhibition of magnesite growth under the investigated conditions appears to be a consequence of both saturation reduction due to complexation and growth inhibition due to specific interactions of the ligand on the magnesite surface. Both effects contribute to an overall growth rate, which, applied within geochemical modelling, may help to assess effects of ligands on the fluid-solid interactions in the carbonate system.

[1] Saldi et al. (2009) Geochim. Cosmochim. Acta 73, 5646-5657.

MS18-T4
Strontium Titanate Surface Modifications due to Nitrogen Implantation investigated by Grazing Incidence XANES

H. Stöcker[1], F. Hanzig[1], J. Seibt[1], C. Richter[1], M. Zschornak[1], D.C. Meyer[1]
[1]TU Bergakademie Freiberg, Institut für Experimentelle Physik, Freiberg, Germany

Strontium titanate $SrTiO_3$ is an oxidic semiconductor and crystallizes in the perovskite-type of structure; however, several methods have been shown to induce distortions of this perfect cubic lattice. One of the key parameters is the oxygen stoichiometry that on the one hand acts as doping and has great influence on the electric conductivity but on the other hand also couples to the crystal structure. A common way to tune the real structure of surfaces is the implantation of ions. Therefore, we tested several species and found a strong impact of nitrogen implantation on the Ti-*K* absorption edge fine structure of $SrTiO_3$.

X-ray absorption near-edge spectroscopy (XANES) in grazing incidence geometry was used to characterize the nitrogen implanted samples and revealed a slight shift of the Ti-*K* edge position and a strong increase of the second pre-edge peak compared to pure $SrTiO_3$. As both of these observations showed a dependence on the angle of incidence, clear evidence of a distorted surface layer is given. This layer is characterized by a shift of the Ti-*K* edge from the Ti^{4+} state of $SrTiO_3$ towards Ti^{3+} in the layer phase, which may be related to an increased concentration of oxygen vacancies or the formation of Ti-N bonds. The strong increase of the second pre-edge feature in the distorted phase can be explained by a static displacement of the Ti atom relative to the surrounding oxygen octahedron. Finally, the replacement of oxygen by implanted nitrogen may be the reason for both observations.

MS18-T5

Molecular Dynamics Simulations of Olivine-Melt Interfaces

S. Gurmani[1], S. Jahn[1], H. Brasse[2], F.R. Schilling[3]
[1]GeoForschunsZentrum, 3.3, Potsdam, Germany
[2]Freie Universität Berlin, Germany, Germany
[3]Institut für Angewandte Geowissenschaften, Karlsruhe, Germany, Germany

The major part of the Earth's upper mantle is thought to be solid, with some regions in the mantle where the rocks contain a small melt fraction. Melt fractions in partially molten rocks have large effects on their physical and transport properties. For a better understanding of the physical and transport properties of these rocks on the atomic level, molecular dynamics simulations of crystal-melt interfaces are performed (Gurmani *et al.*, 2011). The particle interactions are represented by an advanced ionic model (Jahn and Madden, 2007). Our model system consists of 0.8 to 7.0 nm thick $MgSiO_3$ silicate melt confined between Mg_2SiO_4 olivine crystals. This system is studied at a temperature of 2000K and ambient pressure, which ensures thermodynamic coexistence of crystal and melt. From the particle trajectories, we derive various properties, like charge density, cation coordination, chemical compositions and self-diffusion coefficients. The simulation results indicate that for crystal orientations with higher surface energy, the self-diffusion coefficients of all ionic species in the melt decrease at constant melt layer thickness. By increasing the melt layer thickness between the crystals, the average mobility of ions in the melt is increased. On the interfacial part the charge mobility of all species decreases due to solid-like ordering between atoms. For modeling the petrophysical behavior of partially molten rocks, the effective diameter for the conducting channels is reduced by up to two nanometers, which may effect the rheological and transport properties of the partially molten rocks, especially in the presence of ultrathin melt films in well wetted systems.

References: S. Jahn and P.A. Madden (2007) Modeling Earth materials from crustal to lower mantle conditions: A transferable set of interaction potentials for the CMAS system. Phys. Earth Planet. Int. 162, 129-139.

S. F. Gurmani, S. Jahn, H. Brasse and F. R. Schilling (2011) Atomic Scale View on Partially Molten Rocks: Molecular Dynamics Simulations of Melt-Wetted Olivine Grain Boundaries. Submitted.

MS18-T6

Grain boundary diffusion in Mg_2SiO_4 forsterite: Insights from Molecular dynamics simulations

O. Adjaoud[1], S. Jahn[1]
[1]Deutsches GeoForschungsZentrum GFZ Potsdam, Section 3.3, Potsdam, Germany

Grain boundary diffusion is of considerable importance in controlling geomaterial properties. It is generally established that the grain boundaries are short circuits for diffusion and thus they can play an important role in the properties of materials such as electrical conductivity, or in the rates at which the minerals grow, creep, or phase transform.

Although grain boundary diffusion has been studied experimentally in minerals, atomistic simulations are not only useful to determine diffusion coefficients but they are also an unique tool to supply a detailed description of the diffusion mechanisms at microscopic level. In the present study, we use large-scale molecular dynamics simulations to investigate grain boundary diffusion in forsterite. With this method there is no assumption on diffusion paths and the system can be studied as a function of the temperature. The interactions between the atoms are modeled by an advanced ionic interaction potential (Jahn and Madden, 2007). The parameters of the potential are fitted to *ab initio* results. The model was optimized for the Ca-Mg-Al-Si-O system and shows good transferability in a wide range of pressures, temperatures, and compositions. Here, we report results on self-diffusion for a series of tilt grain boundaries with different misorientations in forsterite from molecular dynamics simulations at temperatures of 1250, 1500, 1750, and 2000 K. We have found that the self-diffusion coefficients of Mg and O depend significantly on the tilt angle of the grain boundaries and that they are well fitted with Arrhenius laws. We compare our results to MgO grain boundary diffusion in forsterite derived from reaction rim growth experiments (Gardés and Heinrich, 2010).

References:

S. Jahn and P.A. Madden (2007), Modeling Earth materials from crustal to lower mantle conditions: A transferable set of interaction potentials for the CMAS system. Phys. Earth Planet. Int. 162, 129-139.

E. Gardés and W. Heinrich (2010), Growth of multilayered polycrystalline reaction rims in the $MgO-SiO_2$ system, part II: modelling. Contrib Mineral Petrol, doi: 10.1007/s00410-010-0581-4.

MS19-T1

Secondary phases and surface topography: How can reliable mineral weathering rates be obtained?

K. Pollok[1,2]
[1]Bayerisches Geoinstitut, Universität Bayreuth, Bayreuth, Germany
[2]Friedrich-Schiller-Universität Jena, Institut für Geowissenschaften, Jena, Germany

Weathering processes are strongly associated with the hydrosphere, atmosphere, and biosphere and are controlled by reactions at mineral surfaces. The kinetics of mineral dissolution (dissolution rates) controls for example soil formation, the release of toxic elements to ground and surface waters, as well as the fate of CO_2 after sequestration. It plays thus a fundamental role for the local and global biogeochemical cycles. However, a conundrum still exists how to transfer laboratory rates to natural systems (e.g. [1]). Two sparsely considered factors are gaining increasing attention: the role of secondary phase formation and the evolution of the reactive surface area.

Most laboratory dissolution experiments are performed under far from equilibrium conditions in order to determine rates simply by the analysis of the dissolved species. Although natural system may also approach far from equilibrium conditions (e.g., weathering of sulfides on mine tailings), secondary phase formation is abundant due to limited or variable fluid flow or low solubility of the secondary phases (e.g., iron oxyhydroxides). Mineral replacements are frequent and striking records of a spatial coupling of dissolution and precipitation reactions and have been demonstrated to control the reactions kinetics because an interconnected porosity is needed to prevent passivation and thus to facilitate the mineral-fluid exchange [2].

The determination of surface area in dissolution experiments is needed to normalize the measured element release. However, what part of the surface is reacting and how surface area and thus surface topography change with time is not yet well established. Topographic methods have been introduced to directly measure dissolution rates and surface roughness [3]. Such measurements offer new insides into the reaction mechanisms and surface reactivity. Furthermore, they allow a systematic assessment on the evolution of surface roughness parameters with time [4].

In this contribution, such new approaches towards effective dissolution rates are presented and discussed. They include a full assessment of secondary mineral formation during dissolution in batch experiments with low solubility secondary phase as a "buffer" to obtain quasi-constant conditions. Furthermore, surface topography measurements is utilized to identify reactive parts of the surface and to constrain the relation between surface roughness and reactive surface area.

References:

[1] Maher, K. et al. (2006) Geochimica et Cosmochimica Acta, 70, 337-363.

[2] Pollok, K. et al. (2010) American Journal of Science, 311, 211-236.

[3] Luttge, A. et al. (1999) American Journal of Science, 299, 652-678

[4] Pollok, K. et al. (2010) GEOTECHNOLOGIEN Science Report, 16, 182-197.

MS19-T2

Experimentally determined standard properties for synthetic $MgSO_4{\cdot}4H_2O$ (starkeyite) and $MgSO_4{\cdot}3H_2O$; a revised internally consistent thermodynamic dataset for magnesium sulfate hydrates

K.-D. Grevel[1,2], J. Majzlan[1], A. Benisek[3], E. Dachs[3], M. Steiger[4], A.D. Fortes[5], B. Marler[2]
[1]Friedrich-Schiller-University, Inst. of Geosciences, Jena, Germany
[2]Ruhr-University, Inst. for Geology, Mineralogy and Geophysics, Bochum, Germany
[3]Salzburg University, Dept. of Materialscience & Physics, Mineralogy Division, Salzburg, Austria
[4]University of Hamburg, Dept. of Chemistry, Hamburg, Germany
[5]University College London, Dept. of Earth Science, London, United Kingdom

A number of different hydrated forms of $MgSO_4{\cdot}nH_2O$ ($1 \leq n \leq 11$) are known to exist on Earth and also on Mars. Recently, the enthalpies of formation from the elements ($\Delta_f H^0_{298}$) of kieserite ($n = 1$), sanderite ($n = 2$), hexahydrite ($n = 6$), and epsomite ($n = 7$) were measured by solution calorimetry in water at $T = 298.15$ K [1]. Now, using the same technique, we have obtained $\Delta_f H^0_{298}$ of synthetic $MgSO_4{\cdot}3H_2O$, -2210.3 ± 1.3 $kJmol^{-1}$, and $MgSO_4{\cdot}4H_2O$ (starkeyite), -2498.7 ± 1.1 $kJmol^{-1}$.

The standard entropy of starkeyite was derived from low-temperature heat capacity measurements using a PPMS® system [2] in the temperature range $5\ K < T < 300\ K$ resulting in S^0_{298} (starkeyite) = $254.5 \pm 2.0\ J{\cdot}K^{-1}mol^{-1}$.

Additionally, DSC measurements with a Perkin Elmer Diamond DSC in the temperature range $280\ K < T < 295\ K$ were performed to check the reproducibility of the PPMS® measurements around ambient temperature.

All Mg sulfate hydrates change their hydration state in response to the local temperature and humidity conditions. Based on recently reported equilibrium relative humidities [3] and the new standard properties described above, the internally consistent thermodynamic database for the $MgSO_4{\cdot}nH_2O$ system [1] was refined.

References

[1] Grevel, K.-D., Majzlan, J., 2009: Internally consistent thermodynamic data for magnesium sulfate hydrates. *Geochim. Cosmochim. Acta* 73, 6805-6815.

[2] Dachs, E., Bertoldi, C., 2005: Precision and accuracy of the heat-pulse calorimetric technique: low-temperature heat capacities of milligram-sized synthetic mineral samples. *Eur. J. Mineral*. 17, 251-261.

[3] Steiger, M., Linnow, K., Ehrhardt, D., Rohde, M., 2011: Decomposition reactions of magnesium sulfate hydrates and phase equilibria in the $MgSO_4$-H_2O and Na^+-Mg^{2+}-Cl^--SO_4^{2-}-H_2O systems with implications for Mars. *Geochim. Cosmochim. Acta* 75, 3600-3626.

MS19-T3

Thermodynamics of mixing in barite-celestite solid solution from quantum-mechanical calculations

V. Vinograd[1], B. Winkler[2], D. Bosbach[1]
[1]Forschungszentrum Juelich, Institute of Energy and Climate, Jülich, Germany
[2]University of Frankfurt, Institute of Geosciences, Frankfurt a.M., Germany

$BaSO_4$-$SrSO_4$-sulfates are often discussed as scavengers for various contaminants in aqueous solutions. The calculation of the uptake capacity of a solid solution requires the knowledge of its total solubility product, which is a function of the Gibbs free energy of mixing. However, due to experimental difficulties in the synthesis of samples of intermediate composition, the thermodynamic mixing properties of the barite-celestite solid solution remain poorly constrained. In this study the mixing properties are modeled with the aid of atomistic simulations. Similarly to a previous simulation study [1], our approach involves the construction of a generalized Ising Hamiltonian, which is used to predict ordering states at intermediate compositions via a Monte Carlo algorithm. However, at variance with [1], our approach does not rely on the use of empirical interatomic potentials. The pairwise interactions are evaluated with the double defect method [2], while the energies of the relevant supercell structures are calculated with a density functional theory-based model. Consistently with the previous study [1], we observe a tendency to form an ordered compound with the 50:50 composition. However, the predicted ordering scheme differs from that reported earlier [1]. In our study, Ba and Sr atoms tend to align themselves in rods parallel to *a* direction (Fig. 1). The enthalpy of the ordered compound (space group $P2_1/c$) is nearly equal to that of the mechanical mixture of barite and celestite. Due to the ordering, the Gibbs free energy isotherms and the total solubility product functions are greatly perturbed at intermediate compositions. We infer that a similar ordering tendency could be present in other binary systems of the barite family such as $(Ba,Ra)SO_4$ and $(Ba,Pb)SO_4$.

[1] U. Becker, A. Fernández-González, M. Prieto, R. Harrison, A. Putnis (2000) Direct calculation of thermodynamic properties

of the barite/celestite solid solution from molecular principles. Phys. Chem. Minerals, 27: 291

[2] V.L. Vinograd, M.H.F. Sluiter, B. Winkler. (2009) Subsolidus phase relations in the $CaCO_3$-$MgCO_3$ system predicted from the excess enthalpies of supercell structures with single and double defects. Physical Review B, 79:104201

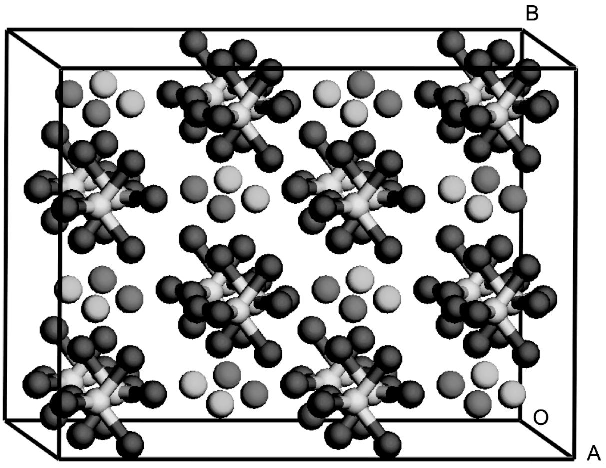

Figure 1: A 2x2x2 supercell with the composition of $Ba_{0.5}Sr_{0.5}SO_4$ with ordered distribution of Ba/Sr. The space group symmetry of the ordered structure is $P2_1/c$. Ba and Sr cations are shown as pink and green balls, respectively.

MS19-T4

The Structure of Schwertmannite and its Relevance to Ion Exchange Capabilities for Environmental Applications

P.M. Kadletz[1], A.J. Götz[1], K. Otte[1], R. Pentcheva[1], S.-H. Park[1], W.W. Schmahl[1], A. Ziegler[2], F.E. Wagner[3], S. Pfeiffer[4], S. Paikaray[4], J. Kipry[5], C. Wiacek[5], M. Schlömann[5], E. Janneck[6]
[1]LMU, Dept. for Geosciences, Crystallography, Munich, Germany
[2]Universität Ulm, Zentrale Einrichtung Elektronenmikroskopie, Ulm, Germany
[3]TUM, Physik-Department E15, Garching, Germany
[4]Universität Bayreuth, BayCEER, Bayreuth, Germany
[5]Bergakademie TU Freiberg, Institut für Biowissenschaften, Freiberg, Germany
[6]G.E.O.S. Ingenieurgesellschaft mbH, Wasseraufbereitung/Verfahrensentwicklung, Halsbrücke, Germany

Schwertmannite is a poorly crystalline iron-oxyhydroxy-sulfate. It has a non-stoichiometric composition that is close to $Fe_8O_8(OH)_6SO_4$. It is occurring in contaminated environments [1] but is also produced with the aid of Fe-oxidizing bacteria to remove Fe(II) and sulfate from open pit mining waste water [2]. This schwertmannite product can later be used as an absorbent for toxic metals in water, since there is ion exchange between the sulphate and e.g. arsenate, chromate or vanadate.

We synthesised schwertmannite by different biotic and abiotic pathways. The products show different particle morphologies and slightly varying XRD Profiles. Most importantly the “hedgehog” morphology previously attributed to bacterial cells encrusted with fibrous schwertmannite has also been obtained with purely abiotic synthesis.

The quasi amorphous structure is commonly assumed to consist of a porous structure close to that of akaganeite (Fig. 1, right). Our Mössbauer spectra show that Fe is entirely octahedrally coordinated Fe^{3+}. We performed Rietveld refinements on the basis of the Fernandez-Martinez et al. 2010 [3] structure model and obtained a good fit to observed diffraction profiles when anisotropic crystallite size broadening was applied (Fig. 1, left). We successfully explain the minor differences in the diffraction profiles of schwertmannites synthesized by different biotic and abiotic pathways by varying the shape anisotropy of the nano-crystals composing the schwertmannite particles. The schwertmannites are typically in the order of 2 nm perpendicular to the channels and 5 nm along the channels. Bigham et al. 1994 assumed, that sulfate is both adsorbed to the surface and incorporated into the tunnels of schwertmannite with changing proportions of both species [4]. We studied schwertmannite-like compounds in which the sulfate is substituted against chromate, arsenate and vanadate. The XANES spectra showed isosbestic points (Fig. 2) for samples with varying toxic metal concentration indicating that a mixture of different configurations is present.

Figures:

Fig. 1: Rietveld refinement of schwertmannite (left) based on the Fernandez-Martinez et al. 2010 [3] structure model (right). The lattice constants and anisotropic grain size broadening parameters were refined.

Fig. 2: As- and Cr-K-edge XANES spectra of heavy metal substituted schwertmannite samples and references that adsorbed the corresponding heavy metal (SHM=schwertmannite, Goe=goethite, Lep=lepidocrocite). Isosbestic points of the K-edge-XANES spectra of the As-substituted schwertmannite samples are shown in the small graph on the left hand side.

References:

[1] Regenspurg S., Brand A., Pfeiffer S. (2003): Formation and stability of schwertmannite in acidic mining lakes, Geochimica et Cosmochimica Acta 68 (6), 1185-1197.

[2] Pfeiffer S., Burghardt D., Janneck E., Pinka J., Schlömann M., Wiacek C., Seifert J., Schmahl W., Pentcheva R., Meyer J., Rolland W. (2008): Development and Optimisation of a Process to Biosynthesize reactive Iron Mineral Surfaces for Water Treatment Purposes (SURFTRAP). Mineral Surfaces - From anionic Processes to industrial Application Kick-Off-Meeting, Geotechnology Science Report, 12, 641-648.

[3] Fernandez-Martinez A., Timon V., Roman-Ross G., Cuello G. J., Daniels J. E., Ayora C. (2010): The structure of schwertmannite, a nanocrystalline iron oxyhydroxysulfate. American Mineralogist, 95,1312-1322.

[4] Bigham J. M., Carlson L., Murad E. (1994): Schwertmannite, a new iron oxyhadroxy-sulphate from Pyhäsalmi, Finnland, and other localities. Mineralogical Magazine, 58, 641-648.

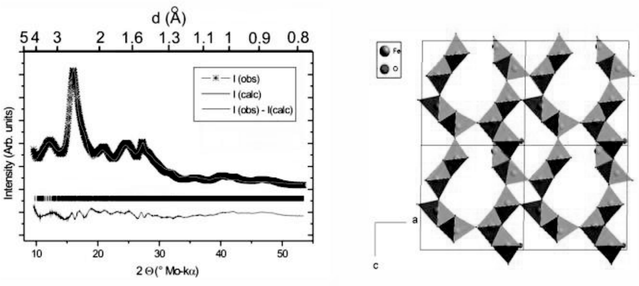

Figure 1: Rietveld refinement of schwertmannite (left) based on the Fernandez-Martinez et al. 2010 [3] structure model (right). The lattice constants and anisotropic grain size broadening parameters were refined.

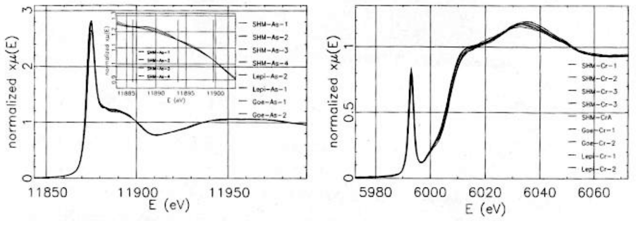

Figure 2: As- and Cr-K-edge XANES spectra of heavy metal substituted schwertmannite samples and references that adsorbed the corresponding heavy metal (SHM=schwertmannite, Goe=goethite, Lep=lepidocrocite). Isosbestic points of the K-edge-XANES spectra of the As-substituted schwertmannite samples are shown in the small graph on the left hand side.

MS19-T5

Raman microprobe analysis and thermodynamic equilibrium modelling of corrosion products formed on depleted uranium ammunition in soil

M. Kersten[1], M. Quadir[1], T. Häger[1]
[1]Gutenberg University, Geosciences Institute, Mainz, Germany

Depleted uranium (DU) ammunition has been used in several major recent military conflicts because of their armour-piercing and pyrophoric behaviour, and thus high capability not only to destroy armoured vehicles but also to burn oil rigs and gasoline trucks. The soils were contaminated due to projectiles missed the targets. The pyrophoric effect has led also to a widespread contamination by DU aerosol particles. DU is not only radio- and chemotoxic, but may also become highly mobile if to be weathered in form of hexavalent uranyl species which can impact groundwater resources. The aim of this study is to identify the alteration products of the DU weathering reaction. Corrosion and leaching of DU was traced using munition fragments, each buried in a soil column and irrigated weekly with 16 mm of synthetic rainwater (pH 6, 0.09 mM NH4NO3, 0.08 mM NH4SO4, 0.05 mM CaSO4) over a period of 3 years (Schimmack et al. 2007). On average, 8 % of the initial DU mass was corroded. The U(VI) concentrations in the leachates reached an apparent steady state in the third year of observation, but still by two orders of magnitude higher than the WHO threshold for groundwater use (15 ppb). Individual corrosion rims derived from the long-term soil column experiments were characterized by various spectroscopic and microprobe techniques including a Raman microprobe. These analysis have revealed that the DU surfaces are corroded first to schoepite, UO2(OH)2•2H2O. However, depth profiles of the corrosion rims revealed that this phase appears to be metastable and transforms into becquerelite, Ca(UO2)6O4(OH)6•8H2O. No uranyl silicate, phosphate, or carbonate phases have been found. This phase transformation sequence has not been reported from previous short-term corrosion tests, and is promoted by direct but slow reaction of the schoepite with Ca2+ ions. Becquerelite is by more than one order of magnitude less soluble than schoepite at a circumneutral pH. Batch titration experiments in combination with voltammetric measurements have been additionally performed to determine the pH-dependent U(VI) dissolution curves of the corrosion products and to validate that the more stable becquerelite in fact controls the uranium mobility in the soil samples.

Reference:
Schimmak W., Gerstmann U., Schultz W., Geipel W. (2007): Long-term corrosion and leaching of depleted uranium (DU) in soil. Radiat. Environ. Biophys. 46, 221–227.

MS20-T1

Characterization of Copper minerals recovered from process water

D. Klapper[1], S. Heuss-Aßbichler[1], G. Kochetov[2], D. Zorya[2]
[1]Ludwig-Maximilians University, Earth and Environmental Sciences, Munich, Germany
[2]National University of Construction and Architecture, Kiev, Ukraine

Various production processes in the metalworking (e.g. electroplating) or chemical industry generate copper-containing wastewater. On one hand, copper at high contents is toxic and, therefore, it is necessary to purify the water before it is released into the environment or reused within the production process. On the other hand, copper is a valuable heavy metal resource and it is desirable to recover it economically.

In general, after reagent-based treatment of heavy metals in wastewater the contents are by an order of magnitude higher than the standard requirements. Ferritisation is a well known method to extract copper from minor concentrated solutions up to 1 g/L. A new method was developed to treat higher concentrated solutions. First, the wastewater is purified by means of ion-exchange procedure and a high concentrated solution with copper values up to 10g/L is produced. Afterwards it is treated by ferritisation process in order to precipitate copper ferrite, a mineral phase with ferrimagnetic properties (Kochetov et al., 2010).

Various experimental designs in laboratory-scale were performed to derive optimal reaction conditions for precipitation of Cu mineral phases. Following parameters were varied: Cu concentration in the solution, Cu: Fe-ion ratio, temperature, pH, amount of aeration of the solution. In addition alteration at water saturated conditions was studied. The samples were characterized by XRD, FT-IR, SEM and magnetic methods like Curie temperature and hysteresis measurement. The degree of water purification and leachability of the solid samples were determined too.

The best conditions for copper ferrite precipitation were worked out. In addition mineral phases like cuprite and iron hydroxides were determined. At higher Cu content the aeration rate may be insufficient and oxygen deficit may occur. In this case the production of copper ferrites can be promoted by alteration processes at room temperature over 20 days. The reaction time can be reduced to 5 days at hydrothermal conditions and 70 °C. SEM studies and hysteresis measurements of the precipitate verify that the crystals are in the nanoscale range. The course of the Curie temperature measurement indicates a heterogeneous distribution of the Cu ions in the copper ferrites. This distribution is homogenized by heating the samples up to 600 C°.

This process is a low cost method for wastewater treatment. The obtained copper ferrites can be used either in a variety of technological applications or at least deposited safely in a landfill due to its low solubility.

Kochetov, J.G., Zorya, D, Grinenko, J. (2010) Integrated treatment of rinsing copper-containing wastewater. Civil and Environmental Engineering

MS20-T2

Energetics of well and poorly crystalline arsenates of ferric iron

J. Majzlan[1]
[1]Friedrich-Schiller University, Institute of Geosciences, Jena, Germany

Arsenates of ferric iron are candidates for arsenic storage at sites contaminated by this metalloid. The remediation technologies today usually involve precipitation of poorly crystalline hydrous ferric oxide which is capable of adsorbing As(V) or crystalline scorodite ($FeAsO_4 \cdot 2H_2O$). We seek alternatives which could be used for such processes, if found to be advantageous. To this end, we study the mineralogy and geochemistry of various sites polluted with arsenic and measure the solubility of the arsenate minerals by calorimetric techniques.

In this work, we present the formation enthalpies (D_fH^o) of As-rich hydrous ferric oxide (As-HFO) ($0.2090Fe_2O_3 \cdot 0.04536As_2O_5 \cdot 0.7456H_2O$), scorodite, kaňkite ($FeAsO_4 \cdot 3.5H_2O$), and bukovskýite

($Fe_2(AsO_4)(SO_4)(OH)\cdot9H_2O$). The D_fH^o values were determined by acid-solution calorimetry at T = 298 K in 5 N HCl as the solvent, using $HCl\cdot9.96H_2O$, g-FeOOH, a-$MgSO_4$, MgO, KCl, and KH_2AsO_4 as the reference compounds. The resulting values for As-HFO, scorodite, kaňkite, and bukovskýite are -429.6±1.2, -1508.9±2.9, -1940.2±2.8, and -4742.2±3.8 kJ/mol, respectively. We have also determined the D_fH^o value for anhydrous $FeAsO_4$ (not known as a mineral) as -899.0 ±3.0 kJ/mol.

Scorodite served as a test of our approach as many studies have been conducted on this phase (e.g., [1]). Using our D_fH^o value and a Kopp rule estimate of entropy of 180.3 J/mol·K, we arrive at a solubility product of -25.4, in good agreement with -25.8 in [1] or -25.4 in [2].

The results presented here will be soon complemented by heat capacity measurements and entropy calculations. Once these data are secured, calculations of phase diagrams for the title and related phases will be done and presented (Fig. 1).

Fig. 1. References: [1] Langmuir, D., Mahoney, J., Rowson, J., 2006: *Geochim. Cosmochim. Acta* 70, 2942-2956. [2] Bluteau, M.-C., Demopoulos, G.P., 2007: *Hydrometallurgy* 87, 163-177.

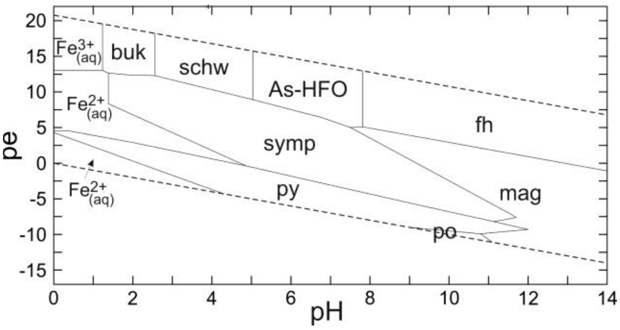

Figure 1: A preliminary pe-pH diagram for the system Fe-As-S-O-H. Calculated for 25 ºC, 1 bar, activities of 10^{-3} for dissolved iron, 10^{-4} for dissolved arsenic, 10^{-4} for dissolved sulfur. Hematite and goethite were not considered in the calculations. Minerals: buk = bukovskýite; schw = schwertmannite; As-HFO = arsenic-rich hydrous ferric oxide; fh = ferrihydrite; symp = symplesite; mag = magnetite; py = pyrite; po = pyrrhotite.

MS20-T3

Sekundär-Mineralisationen aus Karstgebieten im Land Salzburg am Beispiel des Gamslöcher-Kolowrat-Höhlensystems im Untersberg

A. Bieniok[1], U. Brendel[2], G. Zagler[2], F. Neubauer[3]
[1]Universität Salzburg, Materialforschung & Physik, Salzburg, Austria
[2]LVHK Salzburg, Salzburg, Austria
[3]Universität Salzburg, Geographie & Geologie, Salzburg, Austria

Karstgebirge sind typisch für den Nordrand der Alpen im Land Salzburg. Für die Stadt Salzburg sind die Karstwasserquellen des Untersbergs in Verbindung mit vorgelagerten Porengrundwasser-Vorkommen das wichtigste Wasserreservoir. Das gesamte Hochplateau des Untersbergs, eines ~70 km^2 großen Massivs aus Ramsau-Dolomit und Dachsteinkalk, entwässert in einer am nordöstlichen Rand des Massivs gelegenen Quelle. Die dahinter liegenden Höhlensysteme sind in den letzten Jahren intensiv erforscht worden, wobei zahlreiche wasserführende aber auch auffallend trockene Bereiche mit seltenen Ausbildungen von Höhlenmineralen entdeckt wurden (1).

Im Gamslöcher-Kolowrat-System, das den Untersberg in über 35 km langen Gängen durchzieht, findet man in 1100m Seehöhe Bereiche, die durch einen extrem lockeren, weißen Calcit-Schnee charakterisiert werden. Die Dichte liegt bei 0.075 g/cm^3 und ist mit dem Wert für Neuschnee vergleichbar. Die Bildung hängt vermutlich mit dem starken Luftzug in diesem Bereich zusammen. Ebenfalls häufig findet man hier lumineszierende Krusten von Hydromagnesit, die mit Aragonit vergesellschaftet sind. Der typische, lamellenartige Aufbau dieser Krusten lässt sich in REM-Aufnahmen gut zeigen. Ein eher seltener Fund in den Karsthöhlen des Untersbergs ist das Natriumsulfat-Hydrat Mirabilit. Mirabilit ist nur unter den klimatischen Bedingungen innerhalb der Höhle stabil und wandelt sich unter reduzierter Luftfeuchtigkeit schnell zu Thenardit um. Die Thenardit-Kristalle zeigen aber in den elektronenmikroskopischen Aufnahmen deutlich die Spuren der Dehydratisierung. Gips kommt in der Gamslöcher-Kolowrat-Höhle in zwei verschiedenen Ausbildungen vor. Einmal als Gipsnadeln und zum anderen in Form von Quallen-ähnlichen Halbkugeln, die an vertikalen Höhlenwänden ausblühen (gypsum-balls). Die Untersuchung der Schwefel-Isotopie der drei Sulfatvorkommen zeigt, dass der $\delta^{34}S$-Wert der Gips-Bälle(+2.9‰) deutlich von dem der Gipsnadeln(-18.4‰) und des Mirabilits (-16.9‰) abweicht. Es existieren also unterschiedliche Sulfat-Quellen für die Bildung dieser Höhlenminerale. Analysen von Sulfaten aus den Schichten des Haselgebirges, die die Kalke des Unterbergs unterlagern, zeigen Werte im Bereich von +10.8‰ bis +12.7‰ und damit einen deutlichen Hinweis auf marine Sedimente (2). Die Schwefelisotop-Signatur der Gips(Nadeln) und des Mirabilits aus dem Unterberg weist dagegen auf einen Zusammenhang mit bakteriogenetischem Schwefel aus Sulfiden hin. Als Schwefelquelle kommen hier nur Sulfide aus den Raibler Schichten in Frage, einer Zwischenschicht, die den Unteren und Oberen Ramsau-Dolomit trennt.

Für die Untersuchung von Karstgebieten - sei es im Hinblick auf Karsthydrologie, Geologie oder den Trinkwasserschutz - ist die Charakterisierung der sekundären Mineralbildungen der Karsthöhlen ein wichtiger Bestandteil.

MS20-T4

Results of an experimetal study on geochemical behaviors of potential reservoir materials during the CO_2-sequestration process: determination of kintetic data and reasons for their variations

K. Beier[1], A. Holzheid[1]
[1]Christian-Albrechts Universität zu Kiel, Institut für Geowissenschaften, Kiel, Germany

Due to the increasing global energy consumption the CO_2 emission of fossil fuel burning power plants is a worldwide problem and contributes significantly to the climate change. As one of the joint research projects within the German GEOTECHNOLOGIEN program the CO_2-MoPa* project represents the aim of dimension and risk analyses for subterrestrial CO_2 sequestration by virtual scenario investigations. In addition to numerical and process oriented modeling as well as the compilation & validation of known data, laboratory experiments were accomplished in respect of three main objectives: (I) determination of geochemical reaction behaviors in virtual CO_2 reservoirs, (II) derivation of kinetic data from laboratory experiments and (III) comparison of collected experimental and existing literature data.

Generally the experiments were accomplished in static teflon autoclaves under p-T conditions (p_{total}: 87 bar / T: 100°C & 150°C) similar to CO_2 reservoir rocks far from the injection site. To simulate geochemical interactions between CO_2-bearing brines & potential reservoir materials, a synthetic model brine (TDS: ~ 156 g/l) based on a natural formation water of a Lower Cretaceous sandstone reacted with calcite, dolomite, orthoclase or anorthite minerals of different grain size fractions. Dry ice was used as CO_2-source.

To get an adjusted knowledge of dissolution and/or precipitation processes during the reaction progress the chemical changes of the fluid composition during the experiments were monitored by ICP-OES measurements (D. Garbe-Schönberg, IfG, CAU Kiel) of initial and post-run fluids. Based on these data various kinetic data (dissolution/precipitation rates, activation energy) were derived. Within the considered run duration (up to 30 days) a significant dissolution/precipitation process on the used feldspar samples were not observed. In contrast the carbonate samples show significant dependencies of the grain size and the temperature with advanced run duration. For example the largest grain size fraction (250-500 µm) of calcite compared to the smallest grain size fraction (< 63µm) exhibits higher dissolution rates by a factor of 23. All experiments with carbonates show an increasing dissolution process with increasing run duration and achieve an equilibrium state after 20 days. Determined kinetic data are comparable with existing literature data.

The presentation will describe the main results of the accomplished laboratory experiments. Furthermore the results will be compared with already existing literature data.

(*) This study is funded by the German Federal Ministry of Education and Research (BMBF), EnBW Energie Baden-Württemberg AG, E.ON Energie AG, E.ON Ruhrgas AG, RWE Dea AG, Vattenfall Europe Technology Research GmbH, Wintershall Holding AG and Stadtwerke Kiel AG as part of the CO_2-MoPa joint project in the framework of the Special Programme GEOTECHNOLOGIEN.

MS20-T5

Geochemical and geomechanical effects on sandstones during the exposure to impure CO_2: an experimental approach

H. Marbler[1], M. Schmidt[1], K.P. Erickson[1], C. Lempp[1],
H. Pöllmann[1]
[1]Martin-Luther-University Halle-Wittenberg, Geosciences, Halle (Saale), Germany

Within the German national project COORAL* the behavior of reservoir rocks from deep saline aquifers during the injection and geological storage of CO_2 with inherent impurities such as SO_X and NO_X is studied in laboratory experiments. Samples are taken from sandstone outcrops of possible reservoir formations of Rotliegend and Bunter Sandstones from the North German Basin. A combination of geochemical and geomechanical studies was carried out on these rocks. Alterated rock samples after long-term treatment in an autoclave system were loaded in a triaxial cell under in situ pressure and temperature conditions in order to study the geomechanical changes of the rock properties. After the exposure to supercritical (sc)CO_2 + SO_X, NO_X and brine for two to three weeks, geochemical alterations were observed, mainly in the carbonatic, but also in the silicatic cements as well as in single minerals within the sandstones. Besides the partial solution effects during the geochemical experiments also secondary carbonate mineral precipitations are observed within the pore space of the treated sandstones. These alterations may weaken the rock structure. Results of geomechanical experiments with unaltered samples show that the rock strength is influenced by the degree of rock saturation and the type of pore fluid media ($scCO_2$ + SO_X + NO_X). After long-term treatment with impure $scCO_2$, sandstone samples exhibit reduced strength parameters and modified deformation behaviour as well as changes in porosity compared to untreated samples.

* The project COORAL (CO2 Purity for Capture and Storage; acronym derived from German project title) is supported by the German Federal Ministry of Economics and Technology on the basis of a decision by the German Bundestag (grant ID: 032779D). Third-party funding: EnBW, EON, Vattenfall Europe, VNG, Alstom.

MS21-T1

Irradiation effects on the luminescence of monazite

L. Nasdala[1], D. Grambole[2], K. Ruschel[1], J.M. Hanchar[3]
[1]Univ. Wien, Inst. f. Mineralogie & Kristallographie, Wien, Austria
[2]Helmholtz-Zentrum Dresden-Rossendorf, Institute of Ion Beam Physics and Materials Research, Dresden, Germany
[3]Memorial University of Newfoundland, Department of Earth Sciences, St. John's, Canada

We have investigated effects of the structural irradiation damage in monazite-(Ce) caused by alpha particles on the luminescence behaviour of this mineral. Crystals of synthetic $CePO_4$ grown in a Li-Mo flux [1] were irradiated with 8.8 MeV He ions, which are the analogues of alpha particles generated in the ^{212}Po decay in the ^{232}Th chain. The He ions were found to penetrate ca. 34 micrometres into the monazite target. They lose most of their energy through structure ionisation (i.e., electronic interaction) along their flight paths, whereas damage due to atomic knock-ons and the creation of scattered point defects (i.e., nuclear interaction) is mainly generated after significant slow-down of the ions, near the ends of their trajectories. Here, irradiation with 10^{16} ions per cm^2 has resulted in significant damage but not yet amorphisation, which is concluded from the detection of notably broadened but still present Raman bands of crystalline $CePO_4$. This observation is consistent with similar findings for significantly damaged but still unamorphised zircon produced by irradiation with 10^{16} 8.8 MeV He ions per cm^2 [2].

The unirradiated host shows weak but detectable photoluminescence (PL) emissions of rare-earth elements (REE) including Nd^{3+} [3], which are due to some minor contamination of the commercial CeO_2 used for the synthesis (Fig. 1a). Correlating with the amount of irradiation damage, the single emission lines of the REE electronic transitions (which are split due to crystal-field effects) are broadened (Fig. 1b). This agrees well with the general observation of luminescence suppression with increasing radiation damage [4,5]. Alternatively, an orange defect-related luminescence is generated. This broad band is centred near 600 nm wavelength; only its low-energy tail is seen in Figure 1a. The intensity of the defect luminescence correlates also with the degree of lattice damage (Fig. 1c). This is again consistent with the behaviour of the analogous, orange (centered near 615 nm wavelength) defect luminescence in irradiated zircon [2]. Further investigations are planned to quantify the irradiation effects on the emission of REE-related centres.

References:

[1] Hanchar, J.M., et al., Am. Mineral., 86, 667-680 (2001)
[2] Nasdala, L., et al., Contrib. Mineral. Petrol., 161, 777-789 (2011)
[3] Gaft, M., et al., Phys. Chem. Mineral., 28, 347-363 (2001)
[4] Nasdala, L., et al., Chem. Geol., 191, 121-140 (2002)
[5] Panczer, G., et al., Geophys. Res. Abstr., 7, 04851 (2005)

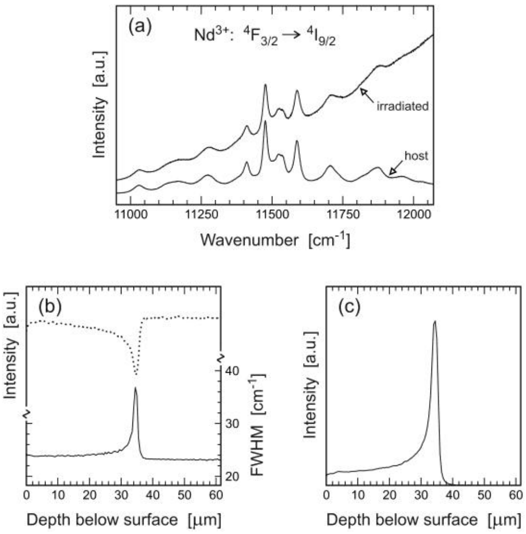

Figure 1: Photoluminescence of synthetic $CePO_4$ irradiated with 8.8 MeV He ions. (a) PL spectra of an irradiated volume-area and the un-irradiated host in the near-infrared range. (b) Plot of intensity (dotted) and full width at band half-maximum (FWHM, solid) of the 11588 cm^{-1} line assigned to a Nd^{3+} emission, against penetration depth. (c) Plot of the intensity of the orange, broad defect emission against penetration depth.

MS21-T2

Recrystallisation behaviour and structural phenomena of metamict titanite

T. Beirau[1], C. Paulmann[1], U. Kolb[2], G. Matveeva[2],
I. Andrusenko[2], U. Bismayer[1]
[1]Universität Hamburg, Mineralogisch-Petrographisches Institut, Hamburg, Germany
[2]Johannes Gutenberg-Universität Mainz, Institut für Physikalische Chemie, Mainz, Germany

The permanent disposal of nuclear waste is of increasing importance. Therefore, it is crucial to obtain a better understanding of the long-term influence of nuclear radiation on condensed matter. On this account we will present new results of detailed investigations of the natural metamict mineral titanite exposed to alpha-radiation over geological timescales. [1]

In nature the mineral titanite occurs in igneous rocks and often incorporates various impurities like radiogenic elements U and Th. Because of the resulting alpha-decay the mineral becomes metamict. Hence, the periodic ordered crystal structure of the mineral is partially destroyed by recoil processes due to alpha radiation and becomes locally disordered with persisting short-range order but destroyed long-range order. Our study was focused on the recrystallisation behaviour on thermal annealing of highly metamict titanite from the Cardiff uranium mine in Canada. [2,3,4]

The crystal structure of pure titanite with the general formula $CaTiSiO_5$ consists of corner linked TiO_6-octahedra, SiO_4-tetrahedra and sevenfold coordinated Ca^{2+} ions. Near 500 K pure titanite undergoes a phase transition from the monoclinic paraelectric high-temperature phase A2/a via an intermediate phase with average symmetry A2/a to the monoclinic antiferroelectric low-temperature phase $P2_1/a$. In impure natural titanite this transition can be suppressed and the RT phase adopts macroscopically A2/a symmetry. [5]

The structural recovery of metamict titanite upon annealing was followed in detail by single-crystal synchrotron diffraction, Raman and infrared spectroscopy; also we present TEM images of the metamict titanite crystal. The Raman and IR modes are strongly broadened in the metamict material and reduce their FWHM on annealing. The synchrotron diffraction data confirm an increasing correlation length of the crystal structure during annealing. Crystalline and amorphous parts of the metamict material are observable in the TEM images simultaneously. [3,4]

Reference:

[1] Ewing, R.C.; Chakoumakos, B.C. et al. (1988) Metamict minerals: Natural analogues for radiation damage effects in ceramic nuclear waste forms, Nuclear Instruments and Methods in Physics Research Section B: Beam Interactions with Materials and Atoms, **32**, 487-497.
[2] Hawthorne, F.C.; Groat, L.A. et al. (1991) Alpha-decay damage in titanite, American Mineralogist, **76**, 370-396.
[3] Bismayer, U.; Paulmann, C. et al. (2010) Local Phenomena in metamict Titanite, Acta Phys. Pol. A, **117**, 74-77.
[4] Beirau, T.; Bismayer, U. et al. (2010) Structural phenomena of metamict titanite: a synchrotron, X-ray diffraction and vibrational spectroscopic study, Phase Transitions, **83**, 694-702.
[5] Meyer, H.W.; Zhang, M. et al. (1996) Phase transformation of natural titanite: An infrared, Raman spectroscopic, optical birefringence and X-ray diffraction study, **59**, 39-60.

MS21-T3

Combination of Raman Spectroscopy and Electron Microprobe within the Almahata Sitta Meteorite

M. Kaliwoda[1], R. Hochleitner[1], V. Hoffmann[2], T. Mikouchi[3],
A.M. Gigler[4], K.-T. Fehr[4], W.W. Schmahl[4]
[1]Mineralogical State Collection, SNSB, Munich, Germany
[2]University Tuebingen, Department of Geosciences, Tuebingen, Germany
[3]University of Tokyo, Tokyo, Japan
[4]Ludwig Maximilians University, Dep. of Geo and Environmental Science, Munich, Germany

Introduction: $2008TC_3$ was the first meteorite previously observed as asteroid in space and found afterwards. $2008TC_3$ fall took place on 7 October 2008 in the Nubian Desert (Northern Sudan). Its mass was around 3.95 kg.

All specimen, belonging to this fall, were called Almahata Sitta (AS), and could be classified as multi-component breccia composing of different meteoritic lithologies, like anomalous polymict ureilites, different chondrites and iron meteoritic material [1,2,3]. Therefore the meteorite revealed to be a rather seldom type of extraterrestrial material. Furthermore large amounts of carbonaceous grains could be found.

Raman research: The investigation of minerals by Raman spectroscopy is a suitable method to typify minerals within planetary material. Raman measurements could be used to classify the structure and composition of quartz, pyroxenes, olivines and other materials within meteorites. In combination with electron microprobe, Raman spectroscopy is an excellent tool to characterize different polytypes and polymorphs. Therefore it is possible to distinguish between graphite, graphene and diamond within the investigated AS samples. In addition we could also map areas of 90 µm to 90 µm to determine mineral phases in rather inhomogenous clusters within the AS meteorite. Later on we measured the same positions with electron microprobe and combined the achievements.

The following **minerals** could be classified within our AS samples due to Raman measurements: Graphite (Figure 1), Diamond (Figure 2), Graphene, Suessite, Schreibersite Cohenite, Kamacites

Troilite/Cr troilite, Pyroxene, Plagioklas

Results: By means of our Raman measurements it was possible to characterize graphite, graphene and also diamond. To some extend, these three minerals occur in clusters within one sample. Especially graphene and graphite change within diminutive areas.

Moreover it was possible to acquire the first good suessite and schreibersite Raman spectra.

In addition we mapped areas, i.e. clusters and mineral inclusions within AS, to investigate mineral change and furthermore to classify chemical change of minerals within small zones.

Conclusion: Micro-Raman spectroscopy proved to be a quick and valuable tool for investigation of extraterrestrial material. No special sample treatment is needed, with the exception of polished surface. Therefore it is a good method to characterize different minerals and polytypes within one sample and to make preliminary work for later microprobe measurements.

References:

[1] Jenniskens P. et al. (2009), *Nature , 458:* 485-488.

[2] Bischoff A. et al. (2010), *MAPS, in press.*

[3] Hochleitner R. et al. (2004), *Journal of Raman spectroscopy, 35,* 515-518

Additional Information: This study was performed partly under the cooperative research program of the Center for Advanced Marine Core Research (CMCR), Kochi University, Japan (10B033).

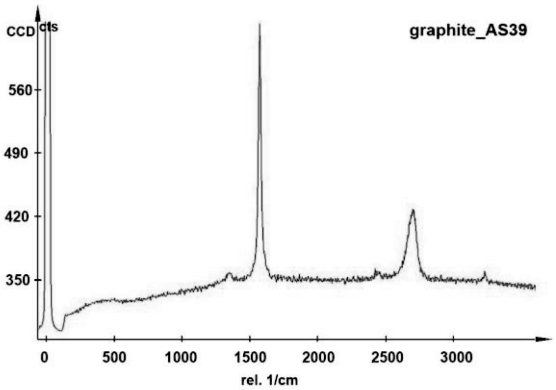

Figure 1: Raman Spectra of Graphite measured in sample AS39

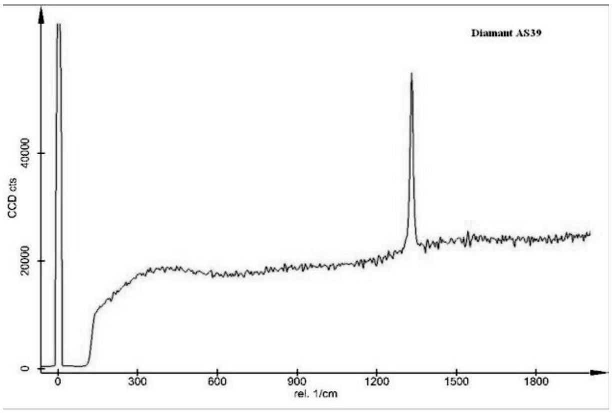

Figure 2: Raman Spectra of Diamond maesured in sample AS39

MS21-T4

Aluminum ordering and clustering in Al-rich synthetic phlogopite: $\{^1H\} \rightarrow {}^{29}Si$ CPMAS HETCOR spectroscopy and atomistic calculations

M. Fechtelkord[1], R. Langner[1], A. Garcia[2], E.J. Palin[3], J. Lopez-Solano[4]
[1]Ruhr-Universität Bochum, Institut für Geologie, Mineralogie und Geophysik, Bochum, Germany
[2]Universitat Autonoma de Barcelona, Institut de Ciència de Materials de Barcelona, Bellaterra, Spain
[3]University of Cambridge, Department of Earth Sciences, Cambridge, United Kingdom
[4]Universidad del País Vasco, Departmento Fisica de la Materia Condensada, Bilbao, Spain

Cationic ordering in octahedral and tetrahedral sheets of Al-rich synthetic phlogopites with nominal composition $K(Mg_{3-x}Al_x)[Al_{1+x}Si_{3-x}O_{10}](OH)_2$ ($0.0 \leq x \leq 1.2$) has been investigated using a combined approach of Monte Carlo simulations based on the 'J formalism' (Bosenick et al. 2001, Warren et al. 2001) and ^1H, ^{29}Si MAS and $\{^1H\} \rightarrow {}^{29}Si$ CPMAS/HETCOR solid-state NMR spectroscopic experiments. Si/^{IV}Al and Mg/^{VI}Al ordering has been found to be controlled mainly by three mechanisms: ^{IV}Al-O-^{IV}Al linkages in tetrahedral sheets are avoided according to Loewenstein's rule (Loewenstein 1954). This leads to long-range ordering in the tetrahedral sheets at very high Al-contents with Al and Si occupying sites alternately. Secondly, ^{VI}Al neighbor pairs in the octahedral sheets are prevented in a similar manner, with Al atoms in the octahedral sheets always surrounded by six Mg atoms on adjacent sites. Finally, we observe a preference for ^{VI}Al and ^{IV}Al to occupy directly neighbored octahedral and tetrahedral sites. As a result the structure is separated into clusters of original phlogopite composition ($KMg_3[AlSi_3O_{10}](OH)_2$) and clusters of 'eastonite' composition ($K(Mg_2Al)[Al_2Si_2O_{10}](OH)_2$) that encompass a whole T-O-T layer package, although Al is solved in the phlogopite structure homogeneously on a macroscopic level.

Reference:

Bosenick, A., Dove, M.T., Myers, E.R., Palin, E.J., Sainz-Diaz, C.I., Guiton, B., Warren, M.C., Craig, M.S., Redfern, S.A.T. (2001) Computational methods for the study of energies of cation distributions: applications to cation-ordering phase transitions and solid solutions. Mineralogical Magazine, 65, 193-219.

Loewenstein, W. (1954) The distribution of aluminum in the tetrahedra of silicates and aluminates. American Mineralogist, 39, 92-96.

Warren, M.C., Dove, M.T., Myers, E.R., Bosenick, A., Palin, E.J., Sainz-Diaz, C.I., Guiton, B.S., Redfern, S.A.T. (2001) Monte Carlo methods for the study of cation ordering in minerals. Mineralogical Magazine, 65, 221-248.

MS21-T5

Electron channelling spectroscopy of Cr-spinels

N. Miyajima[1], W. Sun[1]
[1]Universität Bayreuth, Bayerisches Geoinstitut, Bayreuth, Germany

Electron channeling spectroscopy is a powerful technique to determine site occupancy of elements in complex mineral solid solutions (e.g., garnet, spinel and perovskite). We can localize an inelastic scattering along specific atom planes or columns by setting excitation error (s) around a Bragg condition. This phenomenon is known as an electron channeling effect. The effect has been used in ALCHEMI (Atom Location by CHanneling Enhanced Microanalysis) for energy dispersive X-ray spectroscopy (EDXS) and electron energy loss spectroscopy

(EELS) in transmission electron microscope (TEM). However, the latter is more difficult to perform even qualitatively, because the signal-to-noise ratio is usually very low under the planner channeling conditions due to the off-axis measurement by EELS-aperture under the two-beam excitation condition (e.g., Tafto and Krivaneck, 1982). In this paper, we report the atomic site-specific analyses of electron energy loss near edge structure (ELNES) under electron channeling conditions.

Cr-spinels in the harzburgite assemblages synthesized using a piston-cylinder apparatus at 1200 °C and 2 GPa under different redox conditions (fO_2) were studied by EDXS and EELS in a TEM. The ALCHEMI-ELNES method for the Cr-spinel indicates a preferential distribution that ferric iron into the octahedral sites and ferrous irons into the tetrahedral sites respectively (see Figure 1 & 2). However, Cr-spinel synthesized in the magnetite-hematite buffer sample has more magnetite component than in the other samples, which may represent a change from normal spinel to inverse spinel. In the recovered mineral assemblages from different fO_2 experiments, the $Fe^{3+}/\Sigma Fe$ ratios and total Fe contents in Cr-spinel increase with increasing fO_2, which indicates the potential as oxygen barometer in the Earth's upper mantle (e.g., Ballhaus et al. 1991).

Reference

Ballhaus, C., Berry, R. F., and Green, D. H. (1991) Contrib. Mineral. Petrol., 107, 27-40.

Tafto, J., and Krivaneck, O. L. (1982) Phys. Rev. Lett., 48, 560-563.

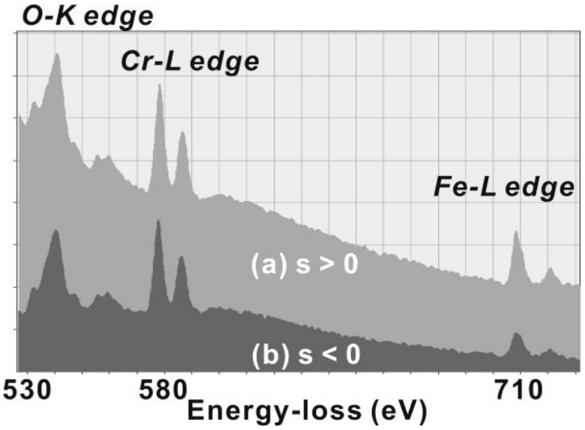

Figure 1: Electron electron-loss spectra of Cr-spinel (starting material of the experiments) taken under two conditions. (a) Tetrahedral sites selected and (b) octahedral sites selected.

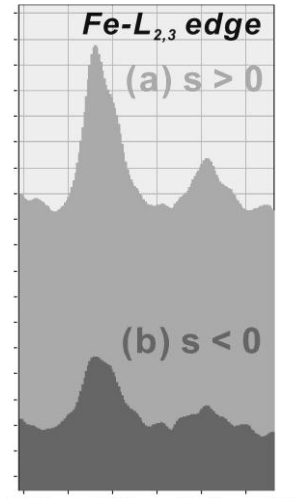

Figure 2: Detail of the iron L2,3 edge in the same spectra as Figure 1.

MS21-T6

The WURM project - a web-based freely available database of computed physical properties for minerals

R. Caracas[1], E. Bobocioiu[1]
[1]CNRS, Ecole Normale Superieure de Lyon, Laboratoire de Geologie, Lyon Cedex 07, France

We present an update of the WURM database.

The WURM project aims to build a freely accessible web-based database of computed physical properties for minerals. The database provides for each mineral various physical properties: the crystal structure used in the calculation, the dynamical charges and the dielectric tensors, the refractive index, the Raman spectra with both peak position and intensity and the infrared spectra with peak position. Additional information comprises the parameters of the calculation, to ensure reproducibility of the results.

The vibrational information makes the bulk of the database and constitutes the major computational effort. For each vibrational mode in the zone-center we determine the frequency, the symmetry assignment, the atomic displacement patterns, and the Raman tensors. The Raman spectra are represented in both single crystal and powder with different possible laser polarizations. For the infrared modes we give both the TO and the LO components. The effect of isotopes of the position of he vibrational peaks is also illustrated.

The database is freely available on the web at http://www.wurm.info and is highly interactive. Jmol-powered applets incorporated in the website allow the quick visualization of the crystal structure and of the atomic displacement patters of all vibrational modes.

All the results are exclusively obtained from first-principles calculations performed using the local density approximation of density functional theory and density functional perturbation theory in the ABINIT implementation [http://www.abinit.org], based on planewaves and pseudopotentials.

MS21 –T7

25 Years Mössbauer Spectroscopy in Salzburg

Georg Amthauer[1], M.Grodzicki[1], W. Lottermoser[1],
G. Redhammer[1], G. Tippelt[1]
[1]Fachbereich Materialforschung und Physik, Universität Salzburg, Austria

Mössbauer spectroscopy provides information on nuclear and crystallographic properties mainly by the so called hyperfine interactions: isomer shift, quadrupole splitting, and magnetic hyperfine interaction. In 1985, Mössbauer spectroscopy of ^{57}Fe in minerals and related inorganic compounds has been established at the University of Salzburg with one constant acceleration spectrometer and a liquid nitrogen bath cryostat. Nowadays, 3 spectrometers can take spectra at temperatures between 4.2 K and 700 K using either a bath cryostat or a gas flow cryostat or a furnace, which allows to measure spectra at defined oxygen fugacities. Spectra can also be taken with the sample in external magnetic fields up to 5 Tesla using a superconducting magnet. In addition to ^{57}Fe, also ^{119}Sn has been measured. Very informative are studies on both Mössbauer isotopes in the same crystal, e.g. in stannite, Cu_2FeSnS_4.

One of the main fields still being studied is the determination of the oxidation and spin state of iron and its distribution over several lattice sites in natural and synthetic minerals and related inorganic compounds, such as oxides (garnets), silicates (garnets, pyroxenes, micas), sulfides, phosphates, etc. in dependence on the temperature and on the oxygen fugacity of their formation or synthesis, respectively. In addition to these spectroscopic measurements, crystal structure refinements of the investigated crystals based on X-ray or neutron diffraction provided supplementary information.

Other subjects of our investigations are minerals and compounds with mixed valence of iron due to thermally activated electron delocalization. In most of these compounds, the occurrence of extended fast electron hopping is combined with crystallographic phase transitions, which complementarily have been studied by X-ray diffraction and crystal structures refinements. The occurrence of mixed valence states in inorganic compounds has a strong influence on their physical properties, such as color, electrical conductivity, magnetic susceptibility, etc.

Mössbauer spectroscopy has also been applied in order to study magnetic properties of oxides, silicates, and sulfides, such as magnetic ordering temperatures and sizes of local magnetic fields. From the Mössbauer spectra, in particular from those of oriented single crystals, the orientation of the electric field gradient as well as the orientation of local magnetic fields relative to the crystallographic axes can be evaluated and supplement magnetic susceptibility measurements as well as magnetic structure determinations by neutron diffraction. All these data have been explained and related to crystallographic properties, such as cation anion distances, bonding angles, etc., as well as to chemical bonding. In some cases, e.g. fayalite, Fe_2SiO_4, it was possible to calculate the electric field gradient as evaluated from Mössbauer spectra on the basis of electron densities as evaluated from XRD.

For a more sophisticated interpretation of the spectra a calculation of the electronic structure and the hyperfine parameters on the basis of density functional theory (DFT) has been performed for many crystals on the basis of their structures and compared to the experimentally evaluated data.

References

1. R. A. Vargas, A. Garciá, M. A. Vargas, Electrochim. Acta 43 (1988) 1271.
2. J. Newman, Electrochemical Systems, 2nd ed., Prentice-Hall, Englewood Cliffs, NJ,1991.
3. A. R. Hillman, in: R.G. Linford (Ed.), Electrochemical Science and Technology of Polymers, vol. 1, Elsevier, Amsterdam, 1987, Ch. 5.
4. B. Miller, Proc. 6th Australian Electrochem. Conf., Geelong, Vic., 19-24 Feb., 1984.

MS22-T1
Intercluster Compounds for Nanosized Materials

F. Gschwind[1], M. Jansen[1]
[1]Max Planck Institute for Solid State Research, Max Planck Institute for Solid State Research, Stuttgart, Germany

The term “intercluster compound” refers to assemblies that are constituted of at least two different, large, inorganic building blocks [1, 2]. A few intercluster compounds already exist and it has been possible to determine their crystal structures by single crystal X-ray diffraction.

These results deliver insights into the arrangement of large building units in the solid state material and the underlying intermolecular forces [3, 4].

These first results show that intercluster compounds are very promising for the study of structural and physical properties of nanosized particles.

They also open a wide range for new applications (lithography techniques, electronic or optical devices, study of quantum effects and also of orbital bands). Since only a few compounds have been studied, there is a huge potential for new discovery in this field.

We would like to present new building blocks [5] and their corresponding intercluster compounds.

[1] M. Schulz-Dobrick, M. Jansen, *Eur. J. Inorg. Chem*. **2006**, 4498.

[2] G. Schmid, *Angew. Chem*. **2008**, 120, 3548.

[3] M. Schulz-Dobrick, M. Jansen, Z. Anorg. Allg. Chem. **2007**, 633, 2326.

[4] F. Gruber, M. Jansen, *Angew.Chem. Int. Ed*., **2010**, 49, 4924.

[5] F. Gschwind, M. Jansen, *Z. Naturforsch.* 2011, *66b,* 1 - 4.

MS22-T2
Solid-state versus gas-phase structures of inorganic molecular compounds exhibiting weak correlation driven interactions

R.J.F. Berger[1]
[1]Paris-Lodron Universität Salzburg, Materialchemie, Salzburg, Austria

While single crystal X-ray diffraction is a wide-spread standard method of structure determination in molecular inorganic chemistry, gas-phase electron diffaction is rarely used nowerdays. The method is shortly introduced on a theoretical and practical basis exemplified on the Bielefed gas-phase electron diffractometer[1]. Some exemplary structure determinations of molecular compounds are discussed in detail: N,N-Dimethylaminopropyl silane[2] showing a weak van-der-Waals enhanced N-donor, Si-acceptor interaction, dimeric copper(I)-dimetyhl-methylene-phosphino-methylid showing weak metallophilic Cu-Cu contacts and a homoleptic iridium(III) phenyl-pyridino complex[3]. Comparisons with ab-initio calculations are made.

[1] R. J. F. Berger, M. Hoffmann, S. A. Hayes, N. W. Mitzel*
Z. Naturforsch. **2009**, *64b*, 1259 - 1268.

[2] M. Hagemann, R. J. F. Berger, S. Hayes, H.-G. Stammler, N. W. Mitzel*
Chem. Eur. J. **2008**, *14*, 11027 - 11038.

[3] R. J. F. Berger, B. Neumann, H.-G. Stammler, N. W. Mitzel*
Eur. J. Inorg. Chem. **2010**, 1613-1617.

MS22-T3
Solvate der Cholsäure - nützliche Co-Kristalle

U. Englert[1], R. Wang[1]
[1]RWTH Aachen University, Institute of Inorganic Chemistry, Aachen, Germany

Das Steroid Cholsäure kristallisiert als Ansolvat, als Hemihydrat und als Monohydrat. Ausserdem sind zahlreiche Einschluss-verbindungen mit organischen Lösungsmitteln bekannt. Qualitativ hochwertige, für eine experimentelle Elektronen-dichtebestimmung geeignete Kristalle der lösungsmittelfreien Cholsäure konnten wir bisher nicht erhalten; es gelang aber, Einkristalle hervorragender Qualität aus wenig gebräuchlichen organischen Lösungsmitteln zu erhalten.

a) Bei tiefen Temperaturen erlauben diese Solvate die Strukturbestimmung an organischen Molekülen, deren tiefe Schmelzpunkte ansonsten aufwendige in-situ-Kristallisationen erfordern [1,2].

b) Bei 100 K und hinreichend hoher Auflösung der Beugungsexperimente gestatten diese Solvate auch eine Ladungsdichtebestimmung am Wirtsmolekül Cholsäure [2].

[1] I. Kalf, U. Englert: The molecular conformation of pentan-3-one studied in cholic acid pentan-3-one solvate. Acta Crystallogr. C67, o206-o208 (2011).
[2] H. Mouhib, D. Jelisavac, W. Stahl, R. Wang, I. Kalf, U. Englert, The Conformation of Odorants in Different States of Aggregation : A Joint Venture in Microwave Spectroscopy and X-ray Diffraction. ChemPhysChem 12, 761-764 (2011).

Diese Arbeit wurde von der Deutschen Forschungsgemeinschaft im SPP 1178, Experimentelle Elektronendichte als Schlüssel zum Verständnis chemischer Wechselwirkungen, unterstützt.

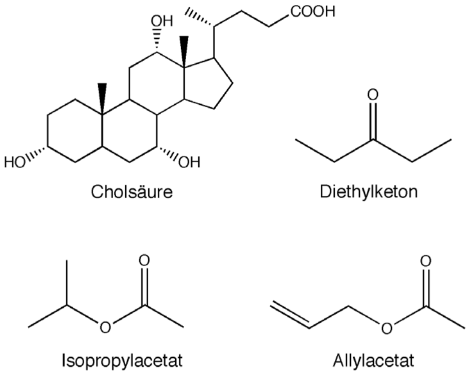

Figure 1

MS22-T4
Small changes - big influence: Deuterium and Fluorine affect crystal packing

K. Merz[1]
[1]Ruhr-University Bochum, Inorganic Chemistry I, Bochum, Germany

The nature of self-organization in the solid state is complicated and depends on different parameters such as symmetry, secondary interactions and supramolecular synthons, so a general prediction of crystal packing has not been possible. A number of weaker and softer interactions, have been shown to play a role in structure stabilization of organic compounds in solid state. Our strategy for analyzing weak dipole-dipole-interactions is to reduce the complexity of parameters and investigate small molecules, such as halogen substituted arenes and pyridines.
The behaviour of organic fluorine in crystal packing is therefore quite different from the heavier halogens. In comparison to iodoaromates, the C-F group, the so-called organic fluorine, does not form hydrogen bonds or significant F$\cdots$F interactions. A comparison of fluorine-substituted benzonitriles shows, in opposite to Cl-, Br- and I-substituted benzenes, no supramolecular synthons with weak intermolecular interactions on participation of fluorine or nitrogen. In contrast, several F-substituted pyridines show different intermolecular interactions depending on the substitution pattern of the fluor atoms at the pyridine backbone.
Continuing our investigations on aggregation of substituted aromatic molecules in the solid state, we studied the influence of H/D Substitution on the aggregation of molecules. H/D-exchange, the smallest possible modification of a molecule, is generally seen as a non-dominating parameter of crystal structures or physical properties of chemical compounds.

(1) Merz. K. Acta Cryst. C 59 **2003** o65.
(2) Merz. K. Crystal Growth & Design 6 **2006**, 1615.
(3) Merz, K.; Vaslyeva, V. Crystal Growth & Design 10 **2010**, 4250.
(4) Vasylyeva, V; Kedziorski, T.; Metzler-Nolte, N.; Schauerte C.; Merz, K.; Crystal Growth & Design 10 **2010**, 4224.
(5) Merz, K.; Vaslyeva, V. Journal of Fluorine Chemistry 131(3) **2010**, 446.
(6) Merz, K.; Vaslyeva, V. CrystEngCom. 12 **2010**, 3989.

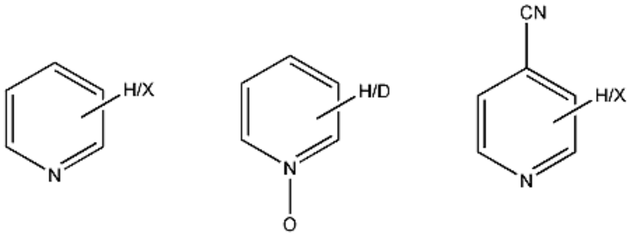

Figure 1

MS22-T5
H-bonding and changes in anion bond lengths

B.-C. Nourredine[1]
[1]Laboratoire des Structures, Propriétés et Interactions Inter Atomiques (LASPI2A), Centre Universitaire Abbes Laghrour, Khenchela, Algeria

Systematic studies on hybrid compounds incorporating organic cations (amines or amino acids) and mineral anions have been recently realized. The structural, optical, thermal properties and structural phase transitions have been investigated [1-3]
During the past ten years, we are interested to hydrogen bonding, hydrogen atoms and their localization by X-ray diffraction. We have synthesized many original compounds and published their structures [4-7]. Our prepared hybrids compounds are generally combination of organic matrix and mineral anions, we obtain new structures with strong, medium and weak hydrogen bonds, with two, three and four centers: OH ... O, NH ... O, NH ... N, OH ... N
and CH ... O.
Interactions between different residues in the asymmetric unit, through hydrogen bonds significantly affect some lengths of covalent bonds. Indeed, any molecule subjected to fields of this type of interaction is deformed and exhibits different geometrical parameters (bond lengths and bond angles).
In this work, part of the research potential of new hybrid compounds obtained by the addition of amines or amino acids with nitric acid, phosphoric acid, sulfuric or perchloric, we discuss some recent examples of crystal structures with geometrical variations, in direct relation with the three-dimensional networks of hydrogen bonds.

[1] Z. Boutobba, A. Direm and N. Benali-Cherif, Acta Cryst. (2010). E66, o595. **[2]** K. Bouchouit , E.E. Bendeif , H. EL Ouazzani , S. Dahaoui , C. Lecomte , N. Benali-cherif & B. Sahraoui, Chemical Physics 375 (2010) 1-7. **[3]** Benali-Cherif, N., Allouche, F., Direm, A., and Soudani, K., Acta Cryst. 2009. E65, O664-O665. **[4]** Benali-Cherif, N., [1] Messai, A., Direm, A., Benali-Cherif, N., Luneau, D and Jeanneau, E. Acta Cryst. 2009. E65, O460**.** **[5]** N. Benali-Cherif, H. Boussekine, Z. Boutobba and N. Dadda, Acta Cryst. (2009). E65, o2744. **[6]** N. Benali-Cherif, W. Falek and A. Direm, Acta Cryst. (2009). E65, o3058-o305. **[7]** N. Benali-Cherif, Acta Cryst. (2009). A65, s98

Keywords: Interactions, Structure determination, X-ray, hybrid compounds, hydrogen bonding, Amino-acids

MS22-T6

Electron Densities of Balls and Bowls

P. Luger[1], D. Lentz[1], S. Mebs[2], S. Grabowsky[3], B. Schmidt[1], M. Weber[1], H. Sakurai[4], S. Onogi[4]
[1]Chemistry, Bio-Che-Pha FU Berlin, Berlin, Germany
[2]Chemistry, Math.-Nat. Faculty HU Berlin, Berlin, Germany
[3]Chemistry, School of Biomed., Biomol., Chem. Sciences, Perth, Australia
[4]Molecular Science, Research Center for Mol. Scale Nanoscience, Myodaiji, Japan

Since the appearance of the more or less spherically shaped bucky balls C_{60}, C_{70}, … in the last decades of the previous century carbon cage structures came into the focus of interest. The geometric and electronic structure of fullerenes can change considerably if structures with addends like halogens are considered or if close intermolecular interactions take place. In addition bowl shaped fragments of fullerenes were examined raising the question whether properties of the entire cage are conserved in the considered fragments. Prominent representatives of bowl shaped fullerene subfragments are corannulene, $C_{20}H_{10}$ with a central five-membered ring and the corresponding hydrocarbon sumanene, $C_{21}H_{12}$ (central six-membered ring). We will report on the experimental electron densities and derived topological properties of corannulene [1] and sumanene and compare the results with corresponding findings of some C_{60} and C_{70} derivatives examined earlier [2,3].

We thank the Deutsche Forschungsgemeinschaft (DFG) for the support of this study within the special priority program 1178.

[1] Grabowsky, S., Weber, M., Chen, Y-S. , Lentz, D., Schmidt, B. M. , Hesse, M. & Luger, P. (2010) *Zeit. Naturf.* **65b**, 452-460.
[2] Kalinowski, R., Weber, M., Troyanov, S. I., Paulmann, C. & Luger, P. (2010) *Zeit. Naturf.* **65b**, 1-7.
[3] Checinska, L., Troyanov, S. I., Mebs, S., Hübschle, C. B. & Luger, P. (2007) *Chem. Commun.*, 4003-4005.

Fig. 1. Superposition of corannulene and sumanene with appropriate parts of the C_{70} and C_{60} cages (left and right).

Fig. 2. Deformation density in a selected plane of sumanene parallel to the central six-membered ring.

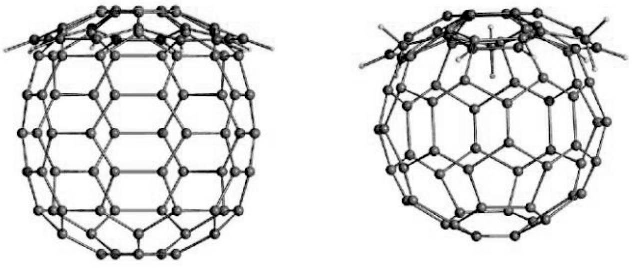

Figure 1: Superposition of corannulene and sumanene with appropriate parts of the C70 and C60 cages (left and right).

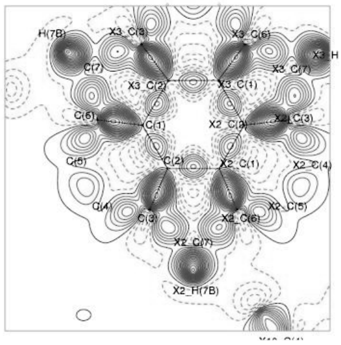

Figure 2: Deformation density in a selected plane of sumanene parallel to the central six-membered ring.

MS22-T7

Stacking disorder in Pigment Red 170 explained by lattice-energy minimizations

J.L. Teteruk[1], M.U. Schmidt[1], T. Gorelik[2], A. Linden[3]
[1]Goethe-University, Inorganic and Analytical Chemistry, Frankfurt am Main, Germany
[2]Johannes Gutenberg University, Institute of Physical Chemistry, Mainz, Germany
[3]University of Zurich, Institute of Organic Chemistry, Zurich, Switzerland

Lattice-energy minimizations were used to explain the stacking disorder in Pigment Red 170. In X-ray and electron diffraction experiments the compound shows strong diffuse scattering in parallel rods perpendicular to the monoclinic axis, pointing to a layer structure with a stacking disorder. Within each layer the molecules form a hydrogen-bridged network. Neighbouring layers are held together by van der Waals interactions. Subsequent layers may be shifted laterally in different directions.

[Figure 1: Molecule of Pigment Red 170 with hydrogen-bridge bonds]

Extensive lattice-energy minimizations were performed on ordered models (including models with much larger supercells) with various stacking sequences derived from a combinatorial approach. Small-cell models were optimized by dispersion-corrected density-functional theory calculations using the program GRACE [1], which uses VASP [2-4] for single-point DFT calculations. Large supercell models were optimized using customized force-field methods [5] with the Materials Studio software [6].

The lattice-energy minimizations revealed local structures, structural correlations and lattice energies. Boltzmann statistics were used to obtain preferred arrangements and neighbourhood probabilities for all neighbouring and next-nearest layers, which provide a much more detailed picture of the structure than the averaged results from the X-ray structure determination. Results were used to model diffuse scattering with the program DISCUS [7].

[1] http://www.avmatsim.eu. [2] G. Kresse, J. Hafner, Phys. Rev. B, 1993, 47, 558-561. [3] G. Kresse, J. Furthmüller, Phys. Rev. B, 1996, 54, 11169-11186. [4] G. Kresse, D. Joubert, Phys. Rev. B, 1999, 59, 1758-1775. [5] S.L. Mayo, B.D. Olafson, W.A. Goddard III, J. Phys. Chem., 1990, 94, 8897-8909. [6] Accelrys Software Inc., San Diego, 2008. [7] T. Proffen, R.B. Neder, J. Appl. Cryst., 1999, 32, 838-839.

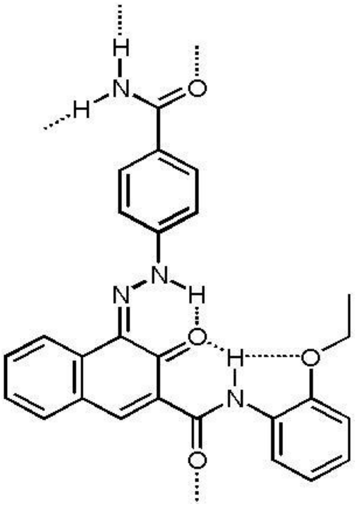

Figure 1: Molecule of Pigment Red 170 with hydrogen-bridge bonds

Poster

P01-P01

Experimental phasing using a hexa-sodium α-metatungstate cluster

S.O. Dahms[1], M. Kuester[1], M.E. Than[1]
[1]FLI-Jena, Than-Laboratory, Jena, Germany

As heavy atom clusters contain a large number of specifically arranged electron-dense scatterers, they proved especially useful for experimental phase determination of large complex structures. Usually exact orientation of the cluster and hence of the individual heavy atom positions proved as critical point for successful phasing.

A hexa-sodium alpha-metatungstate cluster was applied for phasing of the structure of the death receptor 6 (DR6). Even though the cluster is bound in a multiple occupied state and is located at a special position, we were able to localize and orient the cluster at resolutions as low as 4.4 Å in an automated approach. The phasing procedure succeeded with isomorphous as well as with anomalous differences. Our work implicates a special usefulness of W12 tungstate cluster compounds for phasing of medium and low diffracting crystals or crystals composed of large unit cells.

P01-P02

Facilities for Macromolecular Crystallography at BESSY II - HZB Berlin

S. Pühringer[1], M. Bommer[1], R. Förster[1], M. Hellmig[1], M. Krug[1], K.S. Paithankar[1], M. Steffien[1], M. Ühlein[1], M.S. Weiss[1], U. Müller[1]
[1]Helmholtz-Zentrum Berlin für Materialien und Energie, , Institute F-I2, Macromolecular Crystallography, Berlin, Germany

The Macromolecular Crystallography (MX) group at the Helmholtz-Zentrum Berlin (HZB) has been in operation since 2003. Since then, three state-of-the-art synchrotron beam lines (BL14.1-3) for MX have been built up on a 7T-wavelength shifter source [1,2]. Currently, the three beam lines represent the most productive MX-stations in Germany, with more than 500 PDB depositions. BLs14.1 and 14.2 are energy tunable in the range 5.5-15.5 keV, while BL14.3 is a fixed-energy side station (13.8 keV). All three beam lines are equipped with CCD-detectors. Beam lines BL14.1 and BL14.2 are in regular user operation providing about 200 beam days per year and about 600 user shifts to approximately 50 research groups across Europe. BL14.3 has been equipped with a HC1 crystal dehydration device and has been set back to user operation as a screening and test beam line in 2010. BL14.1 has recently been upgraded with an MD2-microdiffractometer including a kappa-geometry option and an automated sample changer. Additional user facilities include office space adjacent to the beam lines, a sample preparation laboratory, a biology laboratory (safety level 1) and high-end computing resources. On the poster, a summary on the experimental possibilities of the beam lines and the provided ancillary equipment for the user community will be given.

[1] U. Heinemann, K. Büssow, U. Mueller & P. Umbach, Acc. Chem. Res. **2003**, *36*, 157-163. [2] U. Mueller *et al.*, in preparation

Keywords: synchrotron, beam line, macromolecular crystallography

P02-P01

Mineralogisch-petrologisch-geochemische Untersuchungen von bronzezeitlichen Kupferschlacken aus dem Revier Mitterberg

H.-P. Viertler[1], P. Tropper[1]
[1]University of Innsbruck, Institute of Mineralogy and Petrography, Innsbruck, Austria

Ziel dieser Untersuchungen ist, die petrologisch-mineralogisch-geochemische Charakterisierung von Schlacken, die von zwei bronzezeitlichen Verhüttungsplätzen (SP20 u. SP52) am Mitterberg stammen. Aus diesen Daten sollen eventuelle Unterschiede mineralogisch chemischer Art herausgearbeitet werden, um daraus folgend Rückschlüsse auf Prozessbedingungen (T-$f\mathrm{O}_2$), Verhüttungstechniken, Rohstoffbasis etc. machen zu können. Bei den untersuchten Schlackenkuchen der Lokalitäten SP20 und SP52 handelt es sich um Eisen-Silikatschlacken, die aus den Hauptbestandteilen FeO und SiO_2 zusammengesetzt sind. In beiden Schlacken findet man die Paragenese: Fayalitischer Olivin + Wüstit + Magnetit + Glas. Untergeordnet treten Pyroxene (Pigeonit/Augit/Hedenbergit) und Sulfideinschlüsse (Neubildungen) auf. Der Phasenbestand der Sulfideinschlüsse erstreckt sich über eine große Bandbreite. Von fast reinem Kupfer und die Mitglieder der Bornit-Digenit Familie über Chalkopyritentmischungen hin zu Pyrrhotin. Erstmals konnte in bronzezeitlichen Schlackenkuchen aus dem Alpenraum Pentlanditbildungen, $\mathrm{(Fe,Ni)_9S_8}$, nachgewiesen werden. Dies scheint ein Spezifikum für die bronzezeitliche Verhüttung am Mitterberg darzustellen und ist ein Hinweis dass neben Chalkopyrit auch Nickelminerale (Gersdorfit) verhüttet wurden. Pauschalchemische Analysen zeigen, dass Schlackenkuchen der Lokalität Wilder See (SP52) tendenziell höhere Spurenelementgehalte an Arsen, Barium, Nickel und Zinn gegenüber jenen vom Verhüttungsplatz Windrauchegg (SP20) haben. Dies steht im Einklang mit der mikroskopischen Beobachtung des vermehrten Auftretens von Pentlanditbildungen in den Sulfideinschlüssen der Schlacken von SP52.

Die Schmelztemperaturen der Schlacken konnten durch experimentelle Untersuchungen und deduktive Ableitungen aus Phasendiagrammen auf eine Mindesttemperatur von ~1200°C festgesetzt werden. Durch das Auftreten von Wüstit und eisenreichem Olivin kann von einem reduzierenden Verhüttungsprozess mit Sauerstoffpartialdrucken kleiner 10^{-10} atm ausgegangen werden. Die Bildung des Magnetits erfolgt nach Abkühlung und durch Änderung der Sauerstoffpartialdrücke. Dass es sich um einen effektiven Verhüttungsvorgang gehandelt hat, beweisen die moderaten Kupfergehalte der Schlackenkuchen, die keinen Vergleich zu neuzeitlichen industriellen Kupferschlacken scheuen müssen.

Bemerkenswert ist die Tatsache, dass nach industriellen neuzeitlichen Verhüttungsverfahren von Kupfererzen die Schlacken Kupfergehalte von 0.5 - 7.0 Gew.% aufweisen. So liegen die Kupfergehalte der Schlackenkuchen beider Lokalitäten im Mittel bei 2.9 Gew.% und zeigen, dass durch den bronzezeitlichen Verhüttungsprozess der Wertträger (Kupfer) zum Großteil von der Gesamtcharge extrahiert werden konnte.

P02-P02
Mineralogisch-petrologische Untersuchungen spätbronzezitlichen Kupferverhüttung aus dem Revier Mauken (Brixlegg, Tirol)

M. Krismer[1], P. Schneider[1], G. Goldenberg[2], P. Tropper[1]
[1]University of Innsbruck, Institute of Mineralogy and Petrography, Innsbruck, Austria
[2]University of Innsbruck, Institut für Archäologien, Innsbruck, Austria

Das Bergbaurevier Mauken ist Teil des Fahlerzlagerstättenkomplexes Schwaz und Brixlegg im Tiroler Unterinntal. Bei archäologischen Ausgrabungen im Rahmen des Bergbauforschung-sschwerpunktes HiMAT konnte die komplette Abbau-, Aufbereitungs-, und Kupferproduktionskette im Befund nachgewiesen werden. Im Bereich des Verhüttungsplatzes wurden eine Batterie von zwei großen Schmelzöfen sowie ein Röstbett dokumentiert welche von einer ausgeprägten Schlackenhalde begleitet sind.

Bei den Proben aus dem Röstbett handelt es sich um Matten, massive Cu-Sulfidagglomerate, welche durch thermische Zersetzung aus sulfidischem Primärerz entstanden sind und als ein Zwischenprodukt des metallurgischen Prozesses gesehen werden dürfen, sowie teilweise geröstete Erzbruchstücke, welche noch reliktisches Ausgangserz enthalten. Die teilweise gerösteten Erzbruchstücke sind durch eine selektive Anreicherung von Kupfer und Abreicherung von Eisen in den primären Sulfiden (Chalcopyrit, Bornit und Fahlerz) hin zu Digenit und Covellin charakterisiert. Das freiwerdende Eisen bildet dabei randlich und innerhalb der Cu-Fe Sulfidaggregate Fe-Spinelphasen.

Die Schlacken zeigen durchwegs Mineralparagenesen welche auf relativ oxidierende Schmelzbedingungen zurückzuführen sind. In der Silikatmatrix der Schlacken sind zahlreiche tropfenförmige mehrere 100 µm große Chalkosin (Cu_2S) Tropfen mit feinsten metallischen Kupfereinschlüssen zu finden. Teilweise koexistieren die Sulfidtropfen mit großen, segregierten metallischen Kupfertropfen. Diese Texturen zeigen die fortlaufende Umsetzung von Kupfersulfid in metallisches Kupfer durch Entschwefelung während des Schmelzprozesses.

Die chemische und mineralogische Zusammensetzung der metallurgischen Kupferschlacken als auch die Röstprodukte weisen auf die Verhüttung von sulfidischen Cu-Sb-As-Fe-Zn Erze in Form von massiven Fahlerzen aus den unmittelbar benachbarten Lagerstätten hin. Die Anwesenheit von Fahlerz, Chalkopyrit, Bornit sowie Kobalt- und Nickel Phasen in der Primärerzparagenese in nur teilweise gerösteten Proben, können als Hinweise auf die Verwendung von Erzen aus den triassischen Gesteinen der Region gedeutet werden.

Der metallurgische Prozess begann mit einem ersten Röstprozess der, lokal in der Region Mauken abgebauten, sulfidischen Erze (Eisen-Zink Tetraedrit-Tennantit ± Chalcopyrit ± Bornit ± Kobalt- und Nickel Phasen). Grund für diese Annahme ist die Anwesenheit von primärem Fahlerz in den teilweise gerösteten Erzen. Ein vorangegangener reduzierender Schmelzprozess >1000°C würde das primäre Erz vollständig umsetzen. Auffallend ist, dass der Reduktionsprozess (Schmelzen) relativ oxidierend gefahren worden ist. Dies hatte zur Folge dass sich die Elemente Antimon sowie Arsen vom metalischem Cu physikalisch trennten. Dies führt zur Bildung eines relativ reinen Kupfers aus fahlerzdominierten Erzen.

P02-P03
Mineralogische Charakterisierung der Kupfervererzungen aus der Region Mauken (Lagerstätte Schwaz-Brixlegg, Tirol)

M. Krismer[1], P. Schneider[1], G. Goldenberg[2], P. Tropper[1]
[1]University of Innsbruck, Institute of Mineralogy and Petrography, Innsbruck, Austria
[2]University of Innsbruck, Institut für Archäologien, Innsbruck, Austria

In den östlichen Revieren des Lagerstättenkomplexes Schwaz-Brixlegg, speziell in der Region Brixlegg-Mauken) treten die Kupfervererzungen sowohl im devonischen Schwazer Dolomit als auch in den darüberliegenden triassischen Kalken der Nördlichen Kalkalpen auf. Während der vererzte, devonische Schwazer Dolomit Teil der Grauwackenzone ist, markieren die permoskythischen Schichten die Basis der permomesozoischen Abfolgen der Nördlichen Kalkalpen. Die Vererzungen in den hangenden triassischen Kalken zeigen mineralogisch eine Verwandtschaft mit den devonischen Vererzungen. Nichtsdestotrotz ist die Erzparagenese der Vererzungen in der Trias deutlich komplexer, neben massivem Fe-Zn Tetraedrit-Tennantit treten vor allem Vaesit (NiS_2) - Cattierit (CoS_2) - Pyrit - Cobaltit (CoAsS) - Gersdorffit (NiAsS) - Arsenopyrit (FeAsS) - Chalcopyrit und Bleiglanz auf. Eine weitere Spezialität der Vererzungen der Trias sind Bi-hältige Fahlerze. Die Erze aus der devonischen Dolomitscholle im Maukengraben sind durch das Auftreten von monomineralischem Fe-Zn Tetraedrit-Tennantit mit submikroskopischen Zerfallstexturen hin zu Enargit-Famatinit + Pyrit + Sphalerit + Chalcostibit gekennzeichnet. Diese Paragenese ist typisch für die Vererzungen des Schwazer Dolomites im gesamten Bergbaugebiet Schwaz-Brixlegg.

Sowohl die Vererzungen in den devonischen Dolomiten als auch in den triassischen Kalken aus der Region Mauken sind für archäometallurgische Untersuchungen von großer Bedeutung. In der Region Mauken gibt es zahlreiche Lokalitäten mit prähistorischen, feuergesetzten Abbauen (Mauk E, Moosschrofen, Geyer/Silberberg), welche auf eine intensive Nutzung hinweisen. Es tritt in bronzezeitlichen Befunden eine Kupfersorte mit Fahlerzsignatur (Sb- und As-reich) auf, welche auch durch erhöhte Co- und Ni-Gehalte gekennzeichnet ist. In Röstprodukten aus dem spätbronzezeitlichen Schmelzplatz treten Kobalt- und Nickelphasen sowie Chalkopyrit und Bornit auf. In der frühbronzezeitlichen Siedlung am Kiechlberg bei Thaur/Innsbruck konnte eine Verhüttungstätigkeit festgestellt werden. Das dort produzierte Rohkupfer zeigt eine klare Fahlerzsignatur, wobei einige Gußkuchen auch beträchtliche Mengen an Bi enthalten. Roherzbruchstücke vom Kiechlberg zeigen massive Tetraedrit-Tennantit Vererzungen mit den charakteristischen Zerfallstexturen aus dem devonischen Dolomit.

Daher ist die mineralogische und geochemische Charakterisierung der Erzvorkommen in den triassischen- als auch in den devonischen Gesteinen aus der Region Mauken essentiell um bronzezeitliche metallurgische Produkte aus dem Unterinntal sowie Mitteleuropäische Kupfersorten, speziell Fahlerzkupfer, zu interpretieren.

P02-P04
Water proofing method for alabaster archaeological building elementsby using nano-quartz-particle coatings

M. Doukakis[1]
[1]Technical University of Crete, Mineral Resources Engineering, Hania, Greece

The alabaster structural elements found in outdoor archaeological monuments in Greece have suffered irreparable deteriorations, because of their dissolution by rainwater. The widely used synthetic water proof resins has problematic behaviour, due to the small reversibility, workability and the high toxicity, as well as their small humidity and U.V radiation resistance.

The aim of this study is to investigate the efficacy of water proofing coatings on alabaster, by increasing the surface roughness with nano quartz particle solutions.

The water proofing capacity of coatings in different water suspensions (5-20% m/V) of nano-quartz particles (20-30nm) modified with polymeric resin (Sulphapore T of Nanophos) is examined, in relation to the widely used (poly)methyl-siloxan (Rhodorsil of Rhone Poulenc) for stone maintenance in Greece.

For the experimental investigation of the influence of roughness on the hydrophobic degree, there were determined the constitution by XRD analysis, the kinetic potential, the waterproof alabaster surface morphology by SEM scanning, and by precise weighing for the mass of coatings. The research includes measurement of the effect of inter surface tensions between water droplets and the waterproof surface, measurements of water vapour permeability, capillary absorption and determination of the protection degree from the dissolving action of water. The investigation of the resistance to erosion, includes ageing of waterproofed alabaster samples under the natural erosive conditions of Faistos archaeological site in Crete, their artificial ageing under U.V radiation and their reversibility after ageing.

From the experimental results, it was realised that the hydrophobicity properties were best at a 10% m/v nano particles concentration, and that they were better compared to the (poly)methyl-siloxan. Both tested materials, presented before aging similar degree of protection in capillary absorption, while the water suspension halves the permeability, in relation to the commercial resin. Synthetic resin provides better protection to the dissolving action of water, but deteriorates after aging and in addition degrades the colour of stone and the reversibility.

The smaller concentration of 10% (m/v) modified nano particles with polymeric resin, was found to be insufficient to retain the original relief shaping in nano dimensions. In the higher contents, the resin membrane overfills the nano-relief and annuls the hydrophobic ability.

In conclusion, the waterproofing of stone by using nano particles coatings, can become more systematic for different types of rocks through the quantification of surface roughness, using the Atomic Force Microscopy method. Additionally the measurement of electric force effects by kinetic potential measurements, between layer and different nano particles shape and size could avoid or reduce the need for their modification by polymeric resins.

P02-P05
Plaster mortars synthesis for the consolidation of archaeological alabaster building elements

T. Markopoulos[1], M. Ntoukakis[1]
[1]Technical University Crete, Mineral Resources Engineering, Hania, Greece

The alabaster decorative building materials in outdoor archaeological areas, mainly in the Cretan architecture of the Minoan period, have suffered irreparable deteriorations or total destruction, because of their dissolution by rainwater and the inappropriate repair by using conventional mortars on the walls. The aim of this study is the synthesis of suitable and compatible plaster mortars, for the consolidation of outdoor alabaster structures. All the mortar synthesis mixtures from hemi anhydride natural anhydride and calcium hydroxide (portlandite) have been investigated via XRD analysis. Specimens of alabaster stones and plaster mortars have been investigated in order to determine their mechanical strength, their capillary water absorption and permeability, the degree of solubility and the amount of the produced solvent salts. For the investigation of resistance to erosion, cubic samples from plaster mortars and alabaster were exposed under the natural erosion conditions of the archaeological site of Faistos palace in Crete. The results of pore size analysis are in agreement with those for the capillary water absorption and permeability analysis. It was found that porosity increases with increasing calcite content and particularly anhydride. The volume expansion of the hemi anhydride after hydration in gypsum, reduces the voids between plaster crystals, while the voids between the remaining anhydride crystals, partially fill with calcite crystals, following the portlandite reaction with atmospheric . From the measurements of solubility and the production of soluble salts it was found that solubility increases with increasing anhydrite content and decreases with increasing calcite content. The measurements have shown that the compressive strength increases with increasing content of gypsum. Ageing under natural erosion conditions, showed an increase of material loss by either increasing the anhydrite content or decreasing the calcite content. Gypsum has compressive strength and permeability in water vapours similar to the alabaster. However plaster presents a fivefold increase of capillary absorption compared to alabaster and is unsuitable for exterior use, because solvent salts accumulate in sub layer in combination with the secondary crystallization of plaster by water adsorption that gradually decreases the affinity between sub layer and mortar. The results suggest that the solubility of the mortar in water decreases by increasing the calcite content in the cured mortars, approaching alabaster solubility. All mortar applications can be reversed, because they can be removed by wet brushing without deterioration of the alabaster material. It is concluded that most suitable mortars for outdoor uses on alabaster stones should contain at least 60% portlandite and hemi anhydride, to achieve an effective resistance to the rainwater.

P02-P06
Computertomographische Untersuchungen des Fettsäureangriffs auf altägyptische Calcitalabaster-Salbgefäße

A. Franz[1], I. Haferkorn[1], K. Scholz[2], D. Raue[2], G. Kloess[1], K. Bente[1]
[1]Universität Leipzig, Inst. f. Min., Krist. u. Mat.wiss., Leipzig, Germany
[2]Universität Leipzig, Ägyptologisches Institut und Ägyptisches Museum –Georg Steindorff– , Leipzig, Germany

Die in Nubien, dem heutigen Sudan gelegene Stadt Aniba (altägyptisch Miam) lag am Westufer des Nil und ist heute durch den Assuan-Staudamm überflutet. Während einer Grabungskampagne Georg Steindorffs wurde im Winter 1912 das Grab S91 entdeckt.

Untersuchungsgegenstand sind zwei Salbgefäße aus diesem Grab. Sie datieren in das Neue Reich, in die 2. Hälfte der 18. Dynastie. Beide Gefäße bestehen fast ausschließlich aus reinem Calcit, dem sogenannten Calcitalabaster. Die Zusammensetzung der Salbfüllung wurde mittels IR, NMR und GC-MS spektroskopisch bestimmt. Wesentliche Bestandteile sind

Stearin-, Palmitin- und Ölsäure. Das deutet auf die Verwendung von Rindertalg hin.

Der Angriff der organischen Säuren auf die Innenwände der Calcitgefäße findet seit ca. 3400 Jahren statt. Dieser „Langzeitätzversuch” kann mittels Röntgencomputertomographie zerstörungsfrei quantifiziert werden. Dazu stand ein 3D µ-CT-Gerät zur Verfügung (Hersteller: IZFP Dresden der Fraunhofer Gesellschaft).

Neben der bildlichen Darstellung wird versucht, den Säureangriff durch Grauwertprofile zu quantifizieren. Die Dichte des Calcitalabasters zeigt am Außenrand höhere Werte als am Innenrand. Besonders in den 2D-Schnittbildern sind ausgefranste Innenränder deutlich zu erkennen, was auf die chemische Wechselwirkung des Gefäßinhalts mit dem Alabaster zurückzuführen ist. Im Inneren sind zudem Rekristallisationseffekte zu beobachten. Der Gefäßboden ist signifikant stärker in Mitleidenschaft gezogen als die oberen Gefäßwände. Die erreichbare Auflösung wird durch die Gefäßhöhe von 14 cm bestimmt und betrug hier ~180 µm.

Figure 1: Salbgefäß 6043 aus der Sammlung des Ägyptischen Museums der Universität Leipzig: 3D-Abbildung

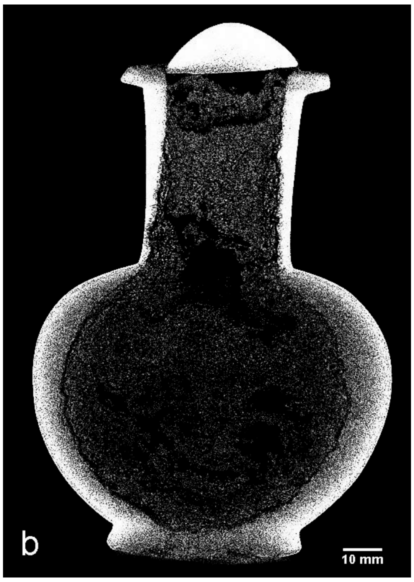

Figure 2: 2D-Längsschnittbild mit deutlich sichtbaren Grauwertgradienten in der Wandung und Salbfüllung

P02-P07

Geochemical Characteristics of Prehistoric Styrian Chert (Silex) Artefacts and their Source Material

C. Hauzenberger[1], W. Postl[2], M. Brandl[3], C. Kurta[4]
[1]University of Graz, Department of Earth Sciences, Graz, Austria
[2]c/o Universalmuseum Joanneum, Graz, Austria
[3]Austrian Academy of Sciences, Vienna, Austria
[4]University of Graz, Institute of Chemistry – Analytical Chemistry, Graz, Austria

Chert tools are commonly found in prehistoric sites within Styria (e.g. Repolust cave). The geographic source region of most of these chert tools was originally thought to be the well known prehistoric deposit in Baiersdorf, 25 km west of Regensburg (Fränkische Alb, Germany) due to its substantial similarity in appearance. However, the discovery of abundant chert tools in a Copper Age village close to Rein (near Graz, Austria) as well as a chert (Silex) deposit nearby led to the conclusion that it is more likely that the chert raw material comes from the local deposit. In order to solve this question, fresh chert samples from Rein and Baiersdorf as well as prehistoric chert artefacts were investigated, mineralogically and geochemically (Postl et al., 2008).

Optically both occurrences look very similar and a clear differentiation based on mineralogical arguments is not possible. Although fossils are different in both localities, the scarce fossil content hampers a classification of the archeological artefacts. Textural differences in the chert material could not be seen by SEM investigation.

Geochemical parameters like lithium, boron and to a lesser extent Al, Ti, V, Sr, Rb, Cu, Zn were found to be useful in distinguishing samples from Rein and Baiersdorf. The low lithium and boron contents in Silex samples from Rein can be explained by the lacustrine origin of the cherts compared to the marine origins (e.g. radiolarites) of most of the chert deposits (e.g. Baiersdorf, Vižula, ...). Sea water contains about 0.17 mg/kg Li and 4.5 mg/kg B while fresh water has 0.003 mg/kg Li und 0.01 mg/kg B (Taylor & McLennan, 1985). Thus the deposited cherts inherited these significant differences in Li and B concentrations. The measured Li and B contents differ between the samples from Rein and Baiersdorf by one order of magnitude. In contrast, the elements Fe, Mn, Cr, Ni could not be used for discrimination. The content of these elements vary with the color of the chert. Brownish areas are enriched in these elements, independent of the origin of the chert samples.

Based on these elements we are now able to assign prehistoric chert artefacts from Styria to their source region. It is likely that most artefacts originated from the chert deposit in Rein and not, as has been assumed earlier, from Baiersdorf, Fränkische Alb. Further chert deposits and artefacts from Central Europe will be investigated and compared to each other. First results show that most of the “classical prehistoric” deposits can be distinguished by a combination of geochemical fingerprinting and mineralogical-petrographical observations.

References

Taylor, S.R. & McLennan S.M. (1985): The Continental Crust: Its Composition and Evolution. Blackwell Scientific Publications, Oxford, England, 312 pp.

Postl, W., Hauzenberger, Ch. & Goessler, W. (2008): Vergleichende geochemische und mineralogische Untersuchungen an Hornstein aus Rein bei Graz (Steiermark, Österreich) und Baiersdorf bei Riedenburg, W Regensburg (Bayern, Deutschland). - Joannea Mineralogie, 4, 99-114.

P03-P01

Molecular structure of 4,4 Di-Methyl Amino Cyano Biphenyl by X-ray diffraction and DFT calculations

A. CHOUAIH[1], N. BENHALIMA[1], N. BOUBEGRA[1],
F. HAMZAOUI[1]
[1]University of Mostaganem, Department of Engeneering, Mostaganem, Algeria

The molecular structure of 4, 4 dimethylamino - cyanobiphenyl (DMACB) were determined by both X-ray diffraction and ab initio calculations. The study of the electron density and the determination of the dipolar moment of the title compound in the crystalline state have been ca1culated from a high-resolution X-ray diffraction study. The data were collected at 123 K. DMACB crystallize in the monoclinic form with the space group Cc which has a non centrosymmetric structure. The crystal structure was refined using the experimental model of Hansen and Coppens (1978). The ca1culated net charges, the dipole moment and the electrostatic potential around the molecule deduced from this study reveal the nature of the intra-molecular charge transfer due to the electron-accepting nitro and N-oxide groups.

P03-P02

Molecular mechanical simulations ofnitramines: a comparison of force fields

P.B. Kempa[1], M. Herrmann[1]
[1]Fraunhofer-ICT, Energetic Materials, Pfinztal, Germany

The fundamental computation of a force field-based simulation is the calculation of the potential energy for a given configuration of atoms or cells. The calculation of this energy, along with its first and second derivatives with respect to the atomic coordinates or cell coordinates, yields the information necessary for minimization, vibration analysis, and dynamics simulations.
The molecule structures of Methylnitramine (MNA), Methylenedinitramine (MEDINA), Hexogen (RDX), Octogen (HMX) and Hexanitrohexaazaisowurzitane (HNIW) were optimized using molecular mechanical force field and quantum mechanical DFT methods. These optimized molecules were taken for the geometric simulation with five the standard force fields Universal, Dreiding, cvff, pcff, COMPASS. Bond lengths and angles were simulated and compared with those of the quantum mechanical DFT-calculation. These serve as benchmark for the question, which force fields is useful for the simulation of energetic nitramines?

P03-P03

Structure from low resolution (x-ray) powder diffraction data: Slices through the rocky mountains of a target function

J.M. Simons[1], G. Roth[1]
[1]RWTH Aachen, Inst. f. Kristallographie, Aachen, Germany

The determination of crystal structures from powder diffraction data is quite a difficult task. For organic structures there are some commonly used strategies to reduce complexity and dimensionality of the parameter space. For inorganic structures with low symmetry the situation is different, as there is no widely accepted method to deduce the crystallographic structure only from the atomic content of the unit cell and low resolution x-ray powder diffraction data. Our research focusses on finding and evaluating new algorithms of global optimisation for this particular case. For non-trivial inorganic systems the main problem in finding good (or even better the optimal) structural models is the very large size (=total number of grid points) of the parameter space: As each atom in general position has (at least) 3 degrees of freedom (x,y,z), the number of parameters is at least $3*N_{atom}$, leading to a 3N-dimensional parameter space. The size of this parameter space grows exponentially with the dimensionality $n_{dim}=3*N_{atom}$. Even for a moderate gridding of only 10 steps in each parameter direction the number of possible parameter vectors for interesting structures with 10 to 15 or even more atoms is bigger than 10^{30}. Even if one could calculate and check a million of those vectors per second, traversal of the whole parameter space would take far longer than the age of the universe (= 4.32×10^{17} s). Due to the time argument given above other ways to find local and global optima in this parameter space are highly needed. Finding and analysing general features of the target function for this parameter space looks like a promising way to exclude large portions of parameter space and to quickly converge into regions of good or even optimal parameter vectors leading to good or optimal structure models. We present some preliminary results of our ongoing research in locating the global optimum of those high dimensional ($n_{dim}>20$) crystallographic target functions. Additionally we will present some first (general) findings on different structures and the corresponding parameter space of the target function accompanied with some 2-dimensional cuts (slices) through the parameter space of some (simple) model structures.

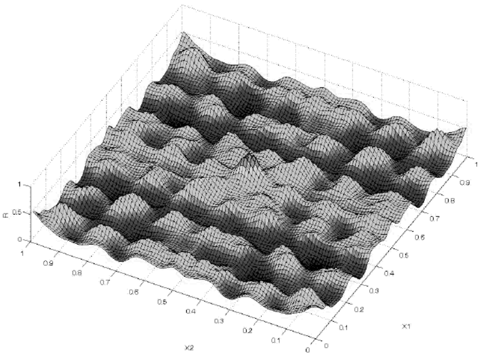

Figure 1

P03-P04

Quantumcrysca: A new approach for the prediction of molecular crystal structures by a crystallographic QM-MM-shell-model

P. Mörschel[1], M.U. Schmidt[1]
[1]Goethe Universität Frankfurt, Anorganische Chemie, Frankfurt, Germany

The *ab initio* treatment of molecular crystals in due consideration of space group symmetry is still an underdeveloped field.
Quantumcrysca is an innovative attempt to calculate the energy in periodical systems by quantum-mechanical means including full treatment of space group symmetry using a QM-MM-approach. Dividing the crystal in disjunct spherical regions gives rise to a shell-model. All interactions between atoms in the inner sphere are treated on a quantum mechanical level, whereas the interactions in the outer sphere are calculated by classical force-fields.
The correct prediction of weak long-range interactions (London dispersion, van der Waals-interaction) in periodical systems turns out to be especially challenging. Correlation methods include this kind of interaction but are computationally demanding. Pure density-functional theory neglects long-range interactions. A good compromise can be found in dispersion-corrected density-functional theory (DFT-D). [1],[2]
First efforts have been made by Neumann et. al. using plain wave DFT-D in periodical systems. [3] In Quantumcrysca, the

quantum-mechanical sphere is efficiently described using localised orbitals (Gaussian type orbital, GTO), leading to a massive saving of computing time and a more intuitive view of the electronic state using molecular orbitals.

Various local optimization algorithms using analytical derivatives, including steepest-descent, conjugate-gradient and quasi-Newton-methods, are implemented.[4] Faster convergence is achieved by additional linesearch in each optimization step.[5] The combination of these local optimization techniques with a structure-generation algorithm can be used to perform a complete crystal structure prediction in the absence of experimental data. Quantumcrysca is designed for the validation of crystal structures as well as for the performance of a full crystal structure prediction.

[1] Grimme S., *J. Comp. Chem*. **2004** *25*, 1463.
[2] S. Grimme, J. Anthony, S. Ehrlich, H. Krieg, *J.Chem. Phys.*, **2010**, *132*, 154104.
[3] Neumann M.A., *J. Phys. Chem. B* **2008**, *112*, 9810.
[4] J. H. Lii, N. L. Allinger, *J. Am. Chem. Soc.*, **1989**, *111*, 8566.
[5] F.A. Potral, Y. Shi, *J. Opt. Appl.,* **1995**, *85*, 1389.

P03-P05

First principles phase diagram calculations for oxides and nitrides

O. Adjaoud[1,2], G. Steinle-Neumann[2], B.P. Burton[3], A. van de Walle[4]
[1]Deutsches GeoForschungsZentrum GFZ Potsdam, Section 3.3, Potsdam, Germany
[2]Bayerisches Geoinstitut, University of Bayreuth, Bayreuth, Germany
[3]National Institute of Standards and Technology, Ceramics Division, Materials Science and Engineering Laboratory, Gaithersburg, United States
[4]California Institute of Technology, Engineering and Applied Science Division, Pasadena, United States

First-principles (FP) computations, in which properties of materials are derived from quantum mechanics, are particularly interesting because they allow for the exploration of new materials even before a procedure to synthesize them has been devised. The cluster expansion (CE) formalism [1] is increasingly used as a valuable tool for predicting and interpreting thermodynamic effects in a wide class of materials, including solubility limits and chemical ordering.

Here we investigate the phase diagrams of quasibinary oxide systems MO-M'O (with M, M' = Mg, Ca, Sr, Ba, or Cd) and nitride systems MN-M'N (with M, M' = Hf, Ti, or Zr) from FP calculations, including vibrational contribution to the free energy. We have used the ATAT code [2] which provides a procedure to compute phase diagrams from first principles using the CE formalism [1] combined with Monte-Carlo (MC) simulations. The CE is fit to ab-initio results (electronic structure calculations by the VASP package [3]) on selected compositions and structures along the binary sections. The CE is then used to calculate phase diagrams via MC simulations. Our calculations predict asymmetric miscibility gaps in all the systems studied here, except for the system HfN-ZrN which exhibits stable ordered crystalline phases. The inclusion of vibrational contribution to the free energy improves considerably agreement with available experimental data.

References:

[1] J. M. Sanchez et al., Physica A 128, 334, 1984.
[2] A. van de Walle and G. Ceder, J. Phase Equilib. 23, 348 (2002); A. van de Walle, M. Asta, and G. Ceder, CALPHAD: Comput. Coupling Phase Diagrams Thermochem. 26, 539 (2002); A. van de Walle and M. Asta, Modell. Simul. Mater. Sci. Eng. 10, 521 (2002).
[3] G. Kresse and J. Hafner, Phys. Rev. B 47, 558 (1993); 49, 14251 (1994); G. Kresse and J. Furthmüller, Comput. Mater. Sci. 6, 15 (1996); Phys. Rev. B 54, 11169 (1996); cf. http://tph.tuwien.ac.at/vasp/guide/vasp.html.

P03-P06

Multifunctional oxides - Influence of defects on the ferroic properties

S. Gemming[1], T. Weissbach[2], M. Zschornak[1,2], H. Stöcker[2], D.C. Meyer[2], T. Leisegang[1], I. Ronneberger[1], K. Potzger[1]
[1]HZ Dresden-Rossendorf, FWI, Dresden, Germany
[2]TU Bergakademie Freiberg, Freiberg, Germany

Transition metal oxides exhibit a wealth of physical phenomena, among them ferroic properties such as ferroelasticity, ferroelectricity and ferromagnetism, or their combination in multiferroics. In addition, transition metal oxides are sensitive to the chemical environment via the external partial pressure of oxygen; changes induce stoichiometry deviations, which cause conductivity changes and modify the ferroic characteristics. Ternary and quaternary compounds from the perovskite family will be discussed as examples, which correlate local changes due to point and planar defects with changes of the elastic, polarization and magnetic properties. The microscopic interactions are determined by density functional calculations, which yield the basis for more large-scale simulations with effective Hamiltonian approaches.

Under oxygen-poor conditions, oxygen vacancies in $SrTiO_3$ accumulate in an external electric field and reduce the hardness. In an Sr/O-rich environment the phases $SrO(SrTiO_3)_n$ are formed, which yield a distinct change of the X-Ray reflectivity due to the regular arrangement of extrinsic SrO(001) stacking faults. YMn_2O_5 has a series of complex antiferromagnetic phases in coexistence with ferroelectricity. In $YFeMnO_5$, only one commensurable ferrimagnetic phase was found and ferroelectricity is absent. Based on spin-polarized DFT calculations a Heisenberg model yields the coupling constants of the Fe-substituted and the mangenese-only compounds and relates them to crystal-field interactions. $BiFeO_3$ is a rhombohedral multiferroic with several domain wall configurations. Among them, the 109° and 180º degrees walls have a significant change in the component of their polarization perpendicular to the wall; the corresponding step in the electrostatic potential is consistent with a recent report of electrical conductivity at the domain walls. Changes in the Fe-O-Fe bond angles at the walls change the canting of the Fe magnetic moments which can enhance the local magnetization.

P04-P01

Measurement and analysis of high-pressure pair distribution functions in diamond anvil cells at PETRA III

N. Rademacher[1], W. Morgenroth[1], L. Bayarjargal[1], B. Winkler[1]
[1]University of Frankfurt, Institute of Geosciences, Frankfurt am Main, Germany

The analysis of the pair distribution function (PDF) is a powerful method for the determination of accurate structural parameters of crystalline as well as disordered, amorphous and nanocrystalline materials.[1] *In situ* PDF studies under high pressure in diamond anvil cells (DAC) are challenging, because the set-up of DAC experiments in principle does not fulfill the requirements for high-quality PDF data, such as access to large scattering angles and high sample-to-background ratios.[2]

This study presents the first high-pressure PDF experiments at the Extreme Conditions Beamline P02.2 at PETRA III. X-ray powder diffraction patterns of silicon were collected at room temperature to pressures of 20 GPa. PDFs of good quality were obtained ($Q_{\max} = 10$ Å^{-1}). As a result, the local structural changes during compression and due to the two phase transformations could be studied. The figure presents the PDF fit (PDFgui[3]) of Si at 6 GPa. Here, the experimental PDF is shown as filled circles and the calculated PDF from a structural model and the difference curve (bottom of figure) are shown as solid lines.

[1] T. Proffen and H. J. Kim; *J. Mater. Chem.*, 2009, 19, 5078-5088.

[2] K. W. Chapman, P. J. Chupas, G. J. Halder, J. A. Hriljac, C. Kurtz, B. K. Greve, C. J. Ruschman and A. P. Wilkinson; *J. Appl. Cryst., 2010*, 43, 297-307.

[3] C. L. Farrow, P. Juhas, J. W. Liu, D. Bryndin, E. S. Bozin, J. Bloch, Th. Proffen and S. J. L. Billinge; *J. Phys.: Condens. Matter*, 2007, 19, 335219.

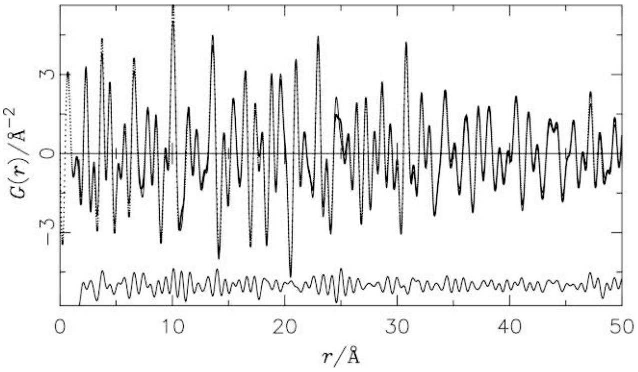

Figure 1

P04-P02

First experiences with a modified 4-circle diffractometer for HP-HT single-crystal X-ray diffraction by means of laser-heating

T. Pippinger[1], R. Miletich[1], L. Dubrovinsky[2]
[1]Institut für Mineralogie und Kristallographie, Universität Wien, Wien, Austria
[2]Bayerisches Geoinstitut, Universität Bayreuth, Bayreuth, Germany

Laser-heating in diamond-anvil cells (DACs) has become a common technique to achieve simultaneously high-pressure (HP) and high-temperature (HT) conditions on a sample suitable for in-situ investigations at extreme conditions (i.e. exceeding 3000 K even at multimegabar pressures). The technical development of laser-heating systems nowadays leads to compact mobile devices which resemble properties (e.g. spot size, beam circularity and beam intensity profile) similar to stationary systems.

Within this study we report the technical solutions and first experiences to integrate a portable laser-heating system [1,2] onto a four-circle diffractometer, which is capable for mechanical loads up to 15 kg (Fig.1). The laser focusing optic, mainly a stationary unit inside the UniHead laser-head, is attached by means of an adjustable adapter on the Chi-circle of a Huber 5042 Eulerian cradle. With an optical working distance of 80mm the 1064nm laser beam of a SPI fiber laser (operated up to 100W power in continuous or modulated operation mode) is focused via an Ag-coated X-ray transparent graphite mirror onto the sample inside the DAC. Alignment of the laser relative to the DAC is realized by means of three linear stages in x-y-z directions, whereas two additional adjusting devices on the mirror control laser focusing on the sample. The alignment of the DAC is independent from the mounted laser-head and can be accomplished by the standard procedure.

We performed first test measurements on hematite single-crystals using a DAC equipped with diamond backing plates [3]. We could accomplish centering routines using a point detector of unique reflections at ambient temperatures with roughly 20% decreased in intensity. At HT operation the reached temperature exceeded the melting point of hematite [4]. The mechanical influence of the mounted laser-head on the diffractometer is displayed in an appearing offset of about 50µm at Chi-rotations due to the additional load. Using a conventional point detector, the most serious problem is the movement of the single crystal accompanied by steady changes of orientation matrix.

Referenzen
[1] L.Dubrovinsky et al. J. Synchr. Rad. 16 (2009)
[2] L.Dubrovinsky et al. High Press. Res. 30, 4 (2010)
[3] T.Pippinger et al. High Press Res (2011) submitted
[4] T.Pippinger et al. (2011) Fisica della Tierra, in press

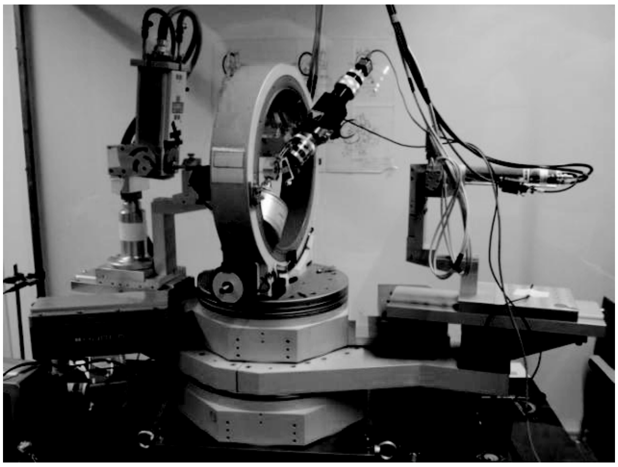

Figure 1: Modified Huber diffractometer (Mo-source, unmonochromated beam, point-detector) for HP-HT single crystal X-ray diffraction experiments.

P04-P03

Microfocus X-ray Sources for High-Pressure Crystallography

J. Graf[1], B. Hasse[1], F. Fabbiani[2], M. Probert[3], C. Michaelsen[1]
[1]Incoatec GmbH, Geesthacht, Germany
[2]GZG, Crystallography, Göttingen, Germany
[3]Durham University, Chemistry, Durham, United Kingdom

Diamond anvil cells (DAC's) are widely used for examining the crystal structure of materials under high pressure. The area of reciprocal space accessible in a high-pressure X-ray diffraction experiment is primarily restricted by the geometry of the DAC. For a typical high-pressure experiment using Mo radiation, only a small fraction of all reflections can be collected. This can be as low as 30% for triclinic crystal structures. Using radiation with a shorter wavelength, such as Ag-K$_{\alpha}$, a larger portion of the reciprocal space is accessible, thus increasing the number of observations and the resolution of the data. However, because of the low intensity of conventional Ag sealed tubes, Ag sources are rarely used for high-pressure studies in the home lab.

Microfocus sealed tube sources have proven to deliver flux densities beyond that of traditional X-ray sources when combined with 2D focusing multilayer mirrors. The sharp beam profile of these sources produces a high flux density at the sample position, thus leading to strong diffracted intensities. Furthermore, the small beam cross-section significantly reduces the background that usually results from scattering at the gasket of the DAC.

Therefore, this type of source presents a promising alternative to classical sealed tube sources currently being used in high-pressure crystallography.

We will be reporting on the latest developments on microfocus X-ray sources which enable a clear increase in intensity compared to other sealed tube sources. Selected results on the use of these sources in high-pressure crystallography will be presented.

P04-P04

High-pressure phase transition of Benitoite $BaTiSi_3O_9$

C. Hejny[1], R. Miletich[2], A. Jasser[3], L. Leydet[3]
[1]Universität Innsbruck, Mineralogie und Petrographie, Innsbruck, Austria
[2]Universität Wien, Mineralogie und Kristallographie, Wien, Austria
[3]Universität Heidelberg, Institut für Geowissenschaften, Heidelberg, Germany

The mineral benitoite, $BaTiSi_3O_9$, is remarkable in many respects: Not only is it a well-priced gemstone with strong pleochroism, but it is also used in electron microprobe laboratories as standard material and for alignment of the electron beam due to its fluorescence. The basis of the structure is a mixed framework of $\{Ti[Si_3O_9]\}^{2-}{}_{\infty\infty\infty}$, composed of discrete Ti octahedra and $[Si_3O_9]$ triple rings. Ba atoms lie in columns between the triple rings giving the overall symmetry of the very rare space group P-6c2 [1,2]. The ring like structural units of cyclosilicate structures are in the focus of a systematic study to investigate the elastic behaviour and potential nonlinear anomalies originating from this remarkable structural feature. For this aim in-situ investigations of $BaTiSi_3O_9$ by means of single-crystal diffraction and Raman spectroscopy have been carried out using diamond-anvil cell techniques with various pressure media under hydrostatic and non-hydrostatic conditions.

Additional Bragg peaks in the single crystal diffraction experiments occurring at $P > P_c$ (=3.70 GPa) indicate the non-isomorphous transition from P-6c2 (no.188) to P31c (no.159) space group symmetry with $a'=a\sqrt{3}$. High-precision single-crystal diffraction yields a second-order phase transition with no detectable volume discontinuity but a significant discontinuity for the bulk modulus. The equation-of-state parameters are K_0= 114.6(1.8) GPa and K'= 6.2(9) for the hexagonal low-P phase, and K_0 = 88.2(1.4) GPa and K'= 4 for the high-P form. It is remarkable that the changes in compression is highly anisotropic and only affects the c-axis direction.

The crystal structure investigations reveal the off-centre displacement of the Ba atoms on release of symmetry constraint to be responsible for the high compressibility of the high-pressure form. The triple ring in the Benitoite structure loses the mirror symmetry resulting in an increasing deviation from 90° of the angle spanning between the connecting line between the terminal oxygen atoms of the silicon tetrahedra and the central ring plane from 0° at the phase transition to a maximum of 15° at 8,88 GPa. Similar behaviour with pressure has also been observed in closely related $K_2ZrSi_3O_9$, wadeite, as well as other cyclosilicates with triple rings of silicate tetrahedra[3].

References:

1) Zachariasen, W. (1930) The crystal structure of Benitoite, BaTiSi3O9. *Zeitschrift für Kristallographie*, 139-146.

2) Fischer, K. (1969) Refinement of the crystal structure of benitoite BaTi[Si3O9]. *Zeitschrift für Kristallographie Kristallgeometrie Kristallphysik Kristallchemie*, 222-&.

3) Kahlenberg, V., J. Konzett & R. Kaindl (2007) Structural studies on a high-pressure polymorph of NaYSi2O6. *Journal of Solid State Chemistry*, 1934-1942.

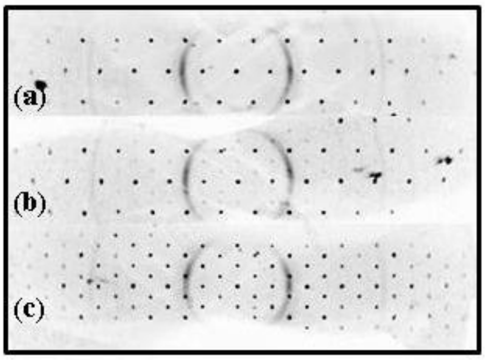

Figure 1: Reconstructed *hk4* reciprocal layer in Benitoite, $BaTiSi_3O_9$, at (a) at 2.56 GPa, (b) 4.53 GPa and (c) 8.88 GPa.

P05-P01

Stokes and anti-Stokes lasing emission in celestine, $SrSO_4$, barite, $BaSO_4$, and anglesite, $PbSO_4$

L. Bohatý[1], P. Becker[1], H. Rhee[2], H.-J. Eichler[2], A.A. Kaminskii[3]
[1]Universität zu Köln, Institut für Kristallographie, Köln, Germany
[2]Technische Universität Berlin, Institut für Optik und Atomare Physik, Berlin, Germany
[3]Russian Academy of Sciences Moscow, Institute of Crystallography, Moscow, Russian Federation

The continuing demand for efficient sources of high-quality laser radiation with specific wavelength in the visible, near- and mid-IR ranges has intensified the interest in laser converters based on nonlinear optical processes in crystalline materials, including stimulated Raman scattering (SRS). In this $\chi^{(3)}$ nonlinear inelastic process laser radiation of a fundamental wavelength is converted into laser emission at Stokes and anti-Stokes wavelengths, accompanied by the excitation, respectively deexcitation, of an internal SRS-promoting vibration mode of the material. In contrast to well-known $\chi^{(2)}$ nonlinear optical processes such as second harmonic generation (SHG), Raman induced $\chi^{(3)}$-lasing is possible in media of any symmetry. As showed in numerous investigations SRS exhibits high efficiency and has a great potential for wide application in modern laser physics and technologies [1]. In the present contribution we report on the results of SRS and Raman induced four wave mixing (RFWM) experiments in crystals of centrosymmetric $SrSO_4$ (celestine), $BaSO_4$ (barite) and $PbSO_4$ (anglesite), all with orthorhombic barite-type structure (space group *Pnma;* see e.g. [2, 3]). The natural crystals of high optical quality used for the investigations are from the localities Sakoany Mine, Mahajanga, Madagascar for celestine, Clarashall near Baumholder, Germany for barite and Toussite, Morocco for anglesite. Crystals of all three compounds possess a broad transparency range from ~0.22 µm to ~4.20 µm (celestine, barite), resp. ~0.32 µm to ~4.38 µm (anglesite). SRS experiments were performed with single-wavelength picosecond laser excitation in the near IR (λ_{f1} = 1.06415 µm, 110 ps) and in the visible spectral range (λ_{f2} = 0.53207 µm, 80 ps) as well as with collinear dual-wavelength excitation using both wavelengths simultaneously. Stimulated Raman scattering in all three compounds $SrSO_4$, $BaSO_4$ and $PbSO_4$ arises each from a single SRS-promoting vibration mode with $\omega_{SRS} \approx 999\ cm^{-1}$, $\approx 985\ cm^{-1}$ and $\approx 977\ cm^{-1}$, respectively, that is related to the fully symmetric $A_g(\nu_1)$ vibration of the $[SO_4]$ structural units. With single-wavelength pumping the generation of broadband lasing frequency combs of more than two octaves bandwidth is observed for all three crystals, while with dual-wavelength pumping additional cascaded up-conversion $\chi^{(3)} \leftrightarrow \chi^{(3)}$ nonlinear lasing effects were observed [4].

[1] Kaminskii, A.A. *Laser Photon. Rev.*, **1** (2007) 93.
[2] James, R.W., Wood, W.A., Proc. Royal Soc. London, Ser. A **109** (1925) 598.
[3] Jacobsen, S.D., Smyth, J.R., Swope, R.J., Downs, R.T., Can. Mineral. **36** (1998) 1953.
[4] Kaminskii, A.A., Bohatý, L., Becker, P., Rhee, H., Eichler, H.J., Lux, O., Koltashev, V.V., Appl. Phys. B (2011), online first, DOI 10.1007/s00340-011-4388-4.

Keywords: $SrSO_4$, celestine, $BaSO_4$, barite, $PbSO_4$, anglesite, stimulated Raman scattering

P05-P02

Phase transition in stimulated Raman scattering (SRS)-active crystals of hardystonite, $Ca_2ZnSi_2O_7$

P. Becker[1], L. Bohatý[1], J. Liebertz[1], E. Libowitzky[2], H. Rhee[3], H.-J. Eichler[3], A.A. Kaminskii[4]
[1]Universität zu Köln, Institut für Kristallographie, Köln, Germany
[2]Universität Wien, Institut für Mineralogie und Kristallographie, Wien, Austria
[3]Technische Universität Berlin, Institut für Optik und Atomare Physik, Berlin, Germany
[4]Russian Academy of Sciences Moscow, Institute of Crystallography, Moscow, Russian Federation

In our recent studies of nonlinear optical properties (including both, $\chi^{(2)}$ and $\chi^{(3)}$ effects) of germanates $A_2M\mathrm{Ge}_2\mathrm{O}_7$ (A = Sr, Ba, M = Mg, Zn) with tetragonal ($P\bar{4}2_1m$) melilite-type crystal structure it turned out that these melilites are promising crystals for efficient frequency conversion of laser light [1-3]. The substitution of the cations A (Sr, Ba) and M (Mg, Zn) affects markedly the optical $\chi^{(1)}$ and $\chi^{(2)}$ properties. In contrast, it has only small effect on $\chi^{(3)}$ -based stimulated Raman scattering (SRS) processes, that arise from the SRS-promoting vibration mode $\nu_s(GeO_3)$ of the digermanate groups $[Ge_2O_7]$ of the structure. This motivated the present investigation of SRS properties of a silicate melilite, here $Ca_2ZnSi_2O_7$ (hardystonite), one of the few examples of a silicate melilite that can be grown to large single crystals of optical quality. In addition, hardystonite offers the possibility to study SRS lasing generation in both, the normal (*N*) melilite-type structure (high-temperature phase of $Ca_2ZnSi_2O_7$) and, at room temperature, in its two-dimensionally incommensurately modulated (*IC*) low-temperature modification [4, 5]. Our crystals of hardystonite were grown from a melt of composition $Ca_2ZnSi_2O_7$ with slight excess of ZnO by the Czochralski technique. The *IC* - *N* phase transition was found at 402.9(2) K by means of differential scanning calorimetry, in good agreement with literature data (e.g. [6, 7]), and shows a marked effect on thermal expansion of the crystals. A detailed investigation of temperature-dependent spontaneous Raman scattering in the range 298 - 483 K reveals that the low-wavenumber bands $<600\ cm^{-1}$ and bands $>900\ cm^{-1}$ are most affected by the structural phase transition. Stimulated Raman scattering in $Ca_2ZnSi_2O_7$ arises from three SRS-promoting vibration modes with $\omega_{SRS1} \approx 906\ cm^{-1}$, $\omega_{SRS2} \approx 663\ cm^{-1}$ and $\omega_{SRS3} \approx 614\ cm^{-1}$, which are bands that show only minor changes due to the *IC* - *N* phase transition. So, while in spontaneous Raman scattering distinct changes between the *IC*-phase and *N*-phase of hardystonite are observed, no significant differences in $\chi^{(3)}$ nonlinear lasing generation characteristics were detected for SRS measurements in the *IC*-phase and *N*-phase.

[1] Kaminskii, A.A., Bohatý, L., Becker, P., Liebertz, J., Held, P., Eichler, H.J., Rhee, H., Hanuza, J., Laser Phys. Lett. **5** (2008) 845.
[2] Kaminskii, A.A., Bohatý, L., Becker, P., Liebertz, J., Eichler, H.J., Rhee, H., Hanuza, J., Laser Phys. Lett. **7** (2010) 528.
[3] Becker, P., Bohatý, L., Liebertz, J., Kleebe, H.J., Müller, M., Eichler, H.J., Rhee, H., Hanuza, J., Kaminskii, A.A., Laser Phys. Lett. **7** (2010) 367.
[4] Röthlisberger, F., Seifert, F., Czank, M., Eur. J. Mineral. **2** (1990) 585.
[5] Iishi, K., Fujimoto, K, Fujino, K., N. Jahrb. Mineral. Mh. **1989**, 219.
[6] Iishi, K., Mizota, T., Fujino, K., Furukawa, Y., Phys. Chem. Minerals **17** (1991) 720.
[7] Webb, S.L., Ross, C.R., Liebertz, J., Phys. Chem. Minerals **18** (1992) 522.

Keywords: $Ca_2ZnSi_2O_7$, hardystonite, stimulated Raman scattering, phase transition

P06-P01

Clay Minerals Deposit of Halakabad (Sabzevar- Iran)

S.M. Hashemi[1]
[1]Islamic Azad University,Mashhad Branch, Geology, Mashhad, Iran, Islamic Republic of

Clay minerals are expanded in south of Sabzevar. They are identified with light color in the filed. The XRD and XRF chemical and mineralogical studies on the Clay minerals indicated that their main clay minerals are Kaolinite, Illite and Dickite. Pyrophyllite is minor clay mineral. Quartz and Sanidine non clay minerals are present with clay minerals .Ratio of Al2O3 is about 40 per cent, it is very good for industrial minerals .Volcanic rocks are origin clay minerals .Their composition are basic to acidic. In south of Sabzevar town there is a small part of these rocks available which include volcanic and volcaniclastic rocks .Geochemical and petrographic studies showed that their compositions are generally acidic and intermediates and are of Dacite and Rhyolite and Andesite rocks type that have changed into clay minerals.

Key words: Kaolinite -Industrial clay minerals -Volcanic rocks -Sabzevar -Iran

References:

[1] Hashemi, S.M, Genesis of Clay Minerals in Volcaniclastic rocks of Tabas (East of Iran)-14 international clay conference -Barry- Italy- June 2009
[2] Gorbani, M .,Arzani, K. Kaolin and fireproof clays, G.S. of Iran,(1994),No.16
[3] Davis, F.,(1985),*SME Mineral processing Hand book*, V.2.PP.22-29
[4] Baccour, H. , Medhioub, M., Jamoussi, F., Mhiri, T., Daoud,A., Mineralogical evaluation and industrial applications of the Triassic clay deposits, Southern Tunisia ,*Materials Characterization*, Volume 59, Issue 11, November 2008, Pages 1613-1622
[5] Ian J. Ferguson, Johannes P. Ristau, Virginia G. Maris, Ifti Hosain, *Geophysical imaging of a kaolinite deposit at Sylvan, Manitoba, Canada*, Journal of Applied Geophysics, Volume 41, Issue 1, February 1999, Pages 105-129
[6] Javier Huertas, José Linares María Bentabol, María Dolores Ruiz Cruz, Francisco ,Chemical and structural variability of illitic phases formed from kaolinite in hydrothermal conditions *Applied Clay Science*, Volume 32, Issues 1-2, April 2006, Pages 111-124
[7] Jorge C. Miranda-Trevino, Cynthia A. Coles, Kaolinite properties, structure and influence of metal retention on pH , *Applied Clay Science*, Volume 23, Issues 1-4, August 2003, Pages 133-139
[8] J. Kroos, J. Kasbohm, Lethi lai, Pyrophyllite deposit in Tan

Tanmai, Vietnam*, 'Institute of Geological Sciences, VAST, Hà Nội,*1999
[9] P. Chiozzi, V. Pasquale, M. Verdoya, Radiometric survey for exploration of hydrothermal alteration in a volcanic area *,Journal of Geochemical Exploration*, Volume 93, Issue 1, April 2007, Pages 13-20
[10] Hashemi,S.M., Clay Minerals Reserve in Volcanic Rocks of South East Gonabad (East of Iran), International Conference of Cities on Volcanoes 6th,31 May - 4 June 2010,Tenerife,Spain

Fig.1: Geological setting of Halakabad Deposit

A.da: Altered dacite (Kaolinitized)

Kt.v : Green t uff and andesite and dacite

ag,v: Agglomerate tuff and andesite

Mineralization stage	Characteristic mineral assemblage	Forming temperature (^{o}C)
Kaolin	Kaolinite, dickite and quartz	~260
Pyrophyllite	Pyrophyllite, kaolinite and quartz	~260-290
Alunite	Alunite, pyrophyllite and diaspore	~290-320

Table 1. Different mineralization stages in Halakabad deposit

P06-P02

Mineralogical Study of Evaporite Minerals in the Sahl-Abad playa (East of Iran)

H.A. Torshizian[1], H. Mollaie[1]
[1]Mashhad Branch, Islamic Azad University, Geology, Mashhad, Iran, Islamic Republic of

The Iranian playas are one of the important playa zones in the world. The study area is located in the North of Birjand in the East of Iran. Sahl-Abad playa is located about 125 km southeastern of Birjand in Birjand-Nehbandan road. The climate in study area is dry and desertic. Based on structural geology study, forming of this basin related to function of strike-slip faults that themselves branch of Nehbandan strike-slip fault.Quaternary sediments include of alluviall trace, alluvial fan, recent alluvium, piedmont plain sand dune and salty pan sediments. Based on aerial photo, landsat image and sampling, 3 major units distinguished including of highland (mountain), flat area(alluvial fan, piedmount plain, sand dune) and playa(mud flat, wet zone and salt crust). Sahl-abad playa based on geomorphlogical view is a Structural playa, Recharge playa and Wet, Clay flat and Salt zone playa. Sahl-Abad basin based on tectonic, faulted, weathered and folded that formated in one pan convergent.

Based on texture of sediments, lithofacies and them sediment structural study, then of fulting in east and west of area, first coarse grain sediments deposited in margin mountain and gravel facies formated in alluvial fans that gradual change to finer sediments of piedmount unit. Meteoric water in rainy years format saline lake and evaporite sediments resulted of drying this lake, to be seen playa form. From hydrogeochemical point of view, the brines of this playa is of the Na- Ca- Mg- K-Cl- SO4 series, with the PH ranging from neutral to slightly alkaline. The concentration of some the above ions are very high in these brines, which is due to the composition of parent rocks in the surrounded area. The evaporate minerals within the brines are NaCl and CaSO4. On the basis of chemical composition of the brines especially their trace element(concentration of Br less than 27ml and ratio of Cl to Br which is more than 290) and concentration of Gypsum and Halite in sediments, a meteoric origin(meteoric water of first order of neutral group) is suggested for these brines.

Key words: Iran, Playa, Evaporate minerals, Hydrogeochemistry

Refrences:

- Gani, M.R., and Alam, M., 2004, Fluvial facies architecture small- scale river system in the upper pupitilia formation Northeast Bengal Basin, Bangoladesh, Journal of Asian earth science, 24, Pp.225-360.
- Goodal, T.M., North, C.P., and Galennie, K.W., 2000, Surface and subsurface sedimentary structures produced by salt crusts, Sedimentology 47, Pp.99-118.
- Jones, B.F. and Deocampo, D.M. (2003), Geochemistry of Saline Lakes, In: Drever, J.I. (Ed) Treatise on Geochemistry vol. 5: Surface and ground water weathering, and soils. – Elsevier, 393-424.
- Mideltone. G.V., 2005, Encyclopedia Of Sediments And Sedimentary Rocks. Springer Verlog, 821p. .
- Mees, F. and Richardson, N. (1994) Holocene sediments of the Carter Lake at Malha, northwestern Sudan, Sedimentology and Geochemistry of modern and saline Lakes, SEPM, Special Publication No. 50.

P06-P03

Use of an autoclave system for the study of geochemical/ mineralogical rock behaviour under reservoir conditions during the geological storage of CO_2: results of the COORAL[1] project

M. Schmidt[1], H. Marbler[1], K. Erickson[1], C. Lempp[1],
H. Poellmann[1]
[1]Martin-Luther-Universität Halle, Institut für Geowissenschaften und Geografie, AG Technische Mineralogie, Halle (Saale), Germany

Within the German national project COORAL* the behavior of reservoir rocks during the injection and storage of CO_2 with inherent impurities such as SO_X and NO_X is studied. Core asset of this project is the combination of geochemical/mineralogical experiments and geomechanical tests on possible reservoir rocks. Injection and storage of CO_2 affect fluid-fluid and fluid-rock interactions. Mineral alterations as well as changes in porosity and permeability may be the results of these interactions. A special coupled autoclave system (i.e. two BERGHOF BR-2000 autoclaves) was designed and used in order to gain knowledge about rock alteration processes. Sample material for the experiments was taken from sandstone quarries of possible reservoir formations in the North German Basin (Rotliegend Sandstone and Bunter Sandstone). Experiments were carried out in the before mentioned coupled autoclave system with supercritical (sc) CO_2 as well as (sc) CO_2 + ($SO_{x,}$ NO_x). For the experiments temperatures of 100°C and pressures of 100 bars were used. A 2mol/l NaCl brine was used as formation fluid. Duration of the experiments ranged from two to four weeks. During the experiments fluid samples of 5ml each were taken and analysed with ICP-OES and IC. Also values for pH, conductivity and redox potential were measured in an "*in-situ*" measuring stage at the same time. This set up proved very reliable over the course of the experiments. Retrieved rock samples from the autoclaves were investigated by SEM as well as XRD. Results of the investigations will be presented. Also modifications to the autoclave setup will be discussed.

* The project “COORAL“ (“CO_2 Purity for Capture and Storage”; acronym derived from German project title) is supported by the German Federal Ministry of Economics and Technology on the basis of a decision by the German Bundestag (grant ID: 032779D). Third-party funding: EnBW, EON, Vattenfall Europe, VNG, Alstom.

P06-P04

Zeoltihe aus Porenbeton: Synthese und Eigenschaften von Wairakit und intermediärer Phase zwischen Sodalith und Cancrinit

A. Hartmann[1], J.-C. Buhl[1], W. Lutz[2]
[1]Institut für Mineralogie, Leibniz Universität Hannover, Hannover, Germany
[2]Lehrstuhl für Luftchemie und Luftreinhaltung, Brandenburgische Technische Universität Cottbus, Berlin, Germany

Modellreaktionen zum Recycling von Porenbetonabfällen werden zunehmend an Bedeutung gewinnen, da mit einem Anstieg an Altmaterial zu rechnen ist, dessen Deponierung zur Bodenkontamination durch Alkalien führen kann und daher ökologisch bedenklich ist. In [1-2] wurden bereits experimentelle Untersuchungen zur Synthese von Zeolithen aus Porenbetonresten vorgestellt. Im Rahmen dieser Arbeiten werden weiterführende Untersuchungen zum hydrothermalen Verhalten der Syntheseprodukte durchgeführt.

Zur Zeolithsynthese wurden 2 g Porenbetonaltmaterial zunächst in 8 M NaOH bei 180°C für 20 h behandelt und die Lösungsphase anschließend abdekantiert. Sie stellt eine wertvolle Natriumsilikatlösung dar, die für weitere Verarbeitungsschritte genutzt werden kann, hier aber nicht weiter untersucht wurde. Der Feststoff wurde anschließend in 1 M Zitronensäure (1h bei 60°C) behandelt und dabei der Elementbestand des Tobermoritanteils in Lösung gebracht. Im Anschluss daran erfolgte unter Zusatz von $NaAlO_2$ und 8 M NaOH die Kristallisation (4h bei 100°C). Dieses Produkt (Produkt 1) wurde anschließend zur Untersuchung seiner hydrothermalen Stabilität in H_2O bei 200°C für 72 h behandelt. Die Analyse beider Produkte erfolgte mittels XRD, REM, FTIR und H_2O Sorptionsmessungen.

Produkt 1 erwies sich als intermediäre Phase zwischen Sodalith und Cancrinit (INT) mit geringen Anteilen an Calcit und Hydrogrossular. INT stellt eine Verbindung mit Stapelfehlordnung zwischen A-B Sequenz (Cancrinit) und A-B-C Sequenz (Sodalith) dar [3]. Die Sorptionskapazität dieser Verbindung mit einer typischen Zusammensetzung von $Na_{7,2}[AlSiO_4]_6(CO_3)_{0,6} \cdot 6,5\ H_2O$ beträgt 137 mg/g. Dieser Wert belegt, dass neben Sodalith-käfigen hier zusätzlich größere Käfige, ähnlich denen des Zeoliths Losod [4], vorliegen, die mit Wassermolekülen gefüllt sind.

Die Analyse von Produkt 2 zeigte, daß die Hydrothermalbehandlung in H_2O zur Bildung einer neuen Phase führte. Es entstand ausschließlich Wairakit $Ca[AlSi_2O_6]_2 \cdot 2H_2O$ mit mini-malem Anteil an Calcit. Wie schon bei der Umsetzung von Zeolith KA und SrA [5] wurde anstelle einer üblicherweise beobachteten Amorphisierung der direkte Phasenübergang kristallin - kristallin festgestellt. Die Wassersorptionskapazität beträgt 105 mg/g. Die Kristallitgröße dieser pseudokubischen Zeolithe beträgt 20 µm und mehr (Abb. 1).

References
[1] Hartmann, A., Buhl, J.-Ch.: Z. Krist. Supple No. 28 (2008), XII.
[2] Hartmann, A., Buhl, J.-Ch.: 23. Deutsche Zeolith Tagung, Erlangen 2011, Book of Abstracts, S. 104.
[3] Hermeler, G., Buhl, J.-Ch., Hoffmann, W.: Catalysis Today, 8 (1991) 415-426.
[4] Sieber, W., Meier, W.M.: Helvetica Chimica Acta, 57 (1974 1533-1549.
[5] Fichner-Schmittler, H., Lutz, W., Amin, S., Dyer, A., Wark, M.: Zeolites 12 (1992) 749-755

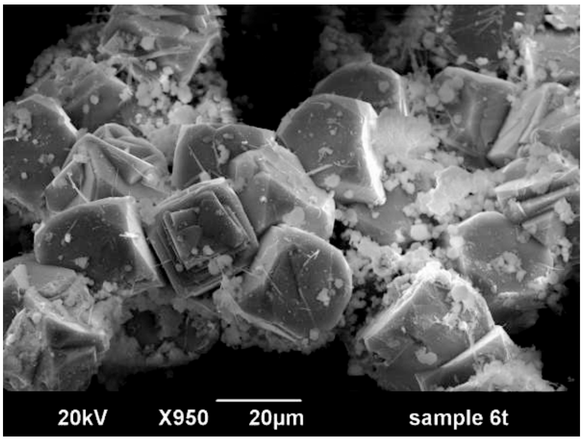

Figure 1: REM Aufnahme Syntheseprodukt 2: Wairakit

P06-P05

Heavy metal extraction from electroplating sludge using *Bacillus subtilis* and *Saccharomyces cerevisiae*

J. Wazeck[1]
[1]Senckenberg Naturhistorische Sammlungen Dresden, Museum für Mineralogie und Geologie, Dresden, Germany

Every year, a large amount of heavy metal bearing sludge is produced by the electroplating industry and has to be categorized and deposited as hazardous waste. However, beside its environmental toxicity, electroplating sludge can also be considered as a resource due to its high concentration of valuable metals like Cu, Cr, Zn and Ni. Microorganisms are capable of mobilising and binding heavy metals by a number of different mechanisms and may be used for a cost-effectiv and non-polluting treatment.

In the present study, the extraction of Cu, Cr, Ni, Fe and Zn from electroplating sludge via living cells of *Bacillus subtilis* (hay bacillus) and *Saccharomyces cerevisiae* (bakers yeast) was investigated. Both organisms are characterized by their harmlessness and uncomplicated cultivation conditions. The results show that *Bacillus subtilis* is capable to leach all heavy metals contained in the sludge, while *Saccharomyces cerevisiae* was only able to leach Cu, Ni and Zn. Furthermore, leaching the sludge with *Bacillus subtilis* was much more effective than the yeast-leaching. *Saccharomyces cerevisiae* extracted only 0,4 % of Ni and Zn and 4 % of Cu, while the leaching rates with *Bacillus subtilis* are 3 % Cr, 25 % Cu, 37 % Ni, 26 % Zn and 10 % Fe.

The leaching rate depends on parameters such as contact time, culture conditions and pH. The most effective contact time for leaching via *Bacillus subtilis* is 19 days for all metals. The largest extraction rates achieved with *Saccharomyces cerevisi*ae were carried out after 5 days (Ni and Zn) and 26 days (Cu).

P06-P06

Development and Assessment of Water and Sediment Status of mining influenced Watercourses: A case study at Mulde River/Germany

A. Greif[1], W. Klemm[1]
[1]TU Bergakademie Freiberg, Institut für Mineralogie, Freiberg, Germany

Question

A large proportion of the running waters of Eastern Germany have their source in the geological basement areas of mountains like Erzgebirge (e.g. Zwickauer and Freiberger Mulde rivers), Thüringisch-Vogtländisches Schiefergebirge, Thüringer Wald, Harz, and Upper Lusatia. The catchment areas of these rivers consist a variety of rocks of different genesis which differ in the lithogenic content due to processes of geochemical specialization. Additionally, chalkogenic components of numerous mineralizations and ore deposits influence the chemical composition of the catchments.

Methods and Results

Investigations of the catchment area of Mulde river show an initial arsenic and heavy metal contamination of running waters and sediments from the upper reaches of Freiberger and Zwickauer Mulde rivers originating from the Erzgebirge mountains. The contamination persists downstream via Elbe river to the astuary at Hamburg harbour. Within the part catchment areas main contamination areas can be designated from which due to superposition of geogenic and anthropogenic portions a permanent subsequent delivery of contaminants occurs.

With the coming into force of the European Water Framework Directive partial restoration measures can be necessary at river basin districts not reaching the good ecological and chemical status. Actual to be planned measures in the catchment area of Mulde river aim on the one hand at the reduction of point contaminant inputs coming from old mining areas and the diminution of diffuse input of substances from contaminated sites.

Conclusions

It is foreseeable that some sections of rivers will not attain the stringent environmental quality objectives because the geogenic background contamination of the running waters can not be eliminated even by intense remediation measures. Definition of realistic remediation targets and the evaluation of remediation success require in addition to a solid knowledge of the actual ecological and chemical state extensive information on the natural background and the temporal evolution of the contamination. Definition of less stringent environmental objectives, e.g. in the form of application of geogenic background values, is until now infrequent discussed. Derivation of regional geogenic background values is more complex for areas with increased geogenic background contamination and additional impact of emissions from mining areas. At the one hand small scale variations of the contaminations are to be expected, on the other appropriate sampling points are rare in the catchment areas.

On the basis of the case study of the part catchment areas of the upper Zwickauer and Freiberger Mulde river, respectively, the problem of contamination and their evaluation are illustrated.

P06-P07

On the use of an empirical model equation to predict the hydraulic conductivity of sand - kaolin mixtures

E. Steiakakis[1], G. Alevizos[1], C. Gamvroudis[1]
[1]Technical University of Crete, Mineral Resources Engineering, Chania, Greece

Several empirical formulae are available for the estimation of hydraulic conductivity of soils, from their physical characteristics.

Kozeny-Carman equation is approximately valid for sands, but is not valid for clays. The problem arises mainly with clayey particles because solid-fluid interactions are not considered in the equation [1].

Furthermore, in the geotechnical literature, there is a large consensus that the hydraulic conductivity of compacted clays (clay liners and covers) cannot be well predicted by the Kozeny-Carman equation.

This report evaluates the validity of the Kozeny-Carman equation in compacted soil.

Kaolin in powdered form (with particle size less than 0.075mm), was mixed with different amounts of fine graded sand to obtain various mixtures.

After the optimum moisture content determination, samples were compacted in the compaction mould with a dry density about 95% of the maximum dry density and water content 2% wet of optimum, in order to obtain a fairly homogeneous distribution of voids within the material and the lower hydraulic conductivity [2].

Next, the specific surface of the soil samples, (which is necessary for the hydraulic conductivity estimation using the KC equation), was measured with the method of nitrogen adsorption (BET).

In addition, the correlation between the values of the specific surface and the liquid limits of the samples was investigated.

Finally, comparisons have been made between the measured hydraulic conductivities using the falling head permeameter and those predicted using the Kozeny-Carman equation.

Based on the aforementioned analysis and results, the following conclusions are drawn:

a) Kozeny-Carman's formula provides good estimations of the vertical hydraulic conductivity of the homogenized sand kaolin mixtures compacted under given (2% wet of optimum) moisture content and a standard compactive effort.

b) A formula based on Chapuis equation, is proposed for the prediction of the specific surface of the soil mixtures, taking into consideration their liquid limit.

The use of this relationship appears to be suitable for the hydraulic conductivity achievement of any medium to low plasticity non active soil that has not developed a secondary porosity.

It is worth noting that further research and experience are needed to expand the conclusions into specific guidelines, which could reduce the need for time-consuming permeability tests.

References

[1] Chapuis R.P. and Aubertin M. (2003). On the use of the Kozeny-Carman equation to predict the hydraulic conductivity of soils. Canadian Geotechnical Journal V40, No 3.

[2] Elsbury, B.R., Daniel, D.E., Sraders G.A. and Anderson D.C. (1990). Lessons learned from compacted clay liners. The Journal of Geotechnical Engineering, 116 (11).

P06-P08
Radiation tolerance of potential wasteforms for plutonium disposition

G. Deissmann[1]
[1]Brenk Systemplanung GmbH, Nuclear Waste Management, Aachen, Germany

Plutonium is generated in nuclear reactors as a result of irradiating the uranium in nuclear fuels through capture of neutrons. It is contained within the spent nuclear fuel matrix but is recovered during fuel reprocessing. The amount of plutonium produced in nuclear reactors as well as its isotopic composition depend on a number of factors including the type of reactor and its neutron spectrum, the method of reactor operation, the initial level of uranium enrichment in the fuel, and the burn-up of the fuel at the time of discharge. Separated plutonium is stored in purpose built facilities within high integrity containers mainly as plutonium oxide powder. Similar to other countries utilising nuclear energy, separated stocks of UK civil plutonium are currently held as zero value asset in storage, since there is no consensus on whether it should be treated as resource for future use as nuclear fuel (e.g. as mixed-oxide fuel (MOX) in light water reactors, or potentially in future fast reactors) or as waste. Irrespective of future UK governmental strategies regarding plutonium, at least a portion of the UK plutonium inventory will be designated for geological disposal.

Throughout the last decades, a variety of wasteforms and disposal concepts for separated plutonium from civil or military stockpiles have been investigated, including various nuclear waste glasses, single- and polyphase ceramic matrices, as well as cementitious wasteforms, polymer encapsulation, or the concept of storage MOX. Single phase ceramics, which are often seen as the most promising immobilisation matrices for plutonium exhibiting low radionuclide release rates, comprise a wide variety of oxide (e.g. zirconia, pyrochlore, zirconolite), silicate (e.g. zircon, garnet, titanite) and phosphate (e.g. monazite, apatite) phases. One major concern for crystalline ceramic wasteforms for plutonium is that they will experience self-irradiation damage from alpha-decay and may undergo a crystalline to amorphous transformation (‘metamictisation’) as function of the alpha dose over time. Alpha self-irradiation may lead to volume expansion, changes in physical properties, cracking, and reduced chemical durability of the wasteform, due to atomic displacements, formation of point effects, accumulation of stored energy, and formation and accumulation of He bubbles.

Within the context of the evaluation of the performance of various candidate wasteforms for the disposition of the UK stocks of separated civil plutonium, we used Monte-Carlo simulations to assess the extent of amorphisation in various single-phase ceramics due to alpha-decay as function of waste loading, plutonium isotopic composition, and disposal time. The simulation results were compared to experimental results from studies using samples doped with short-lived alpha-decaying isotopes and studies using ion irradiation techniques.

P06-P09
Experimental diffusion studies on water-related species through quartz

G. Doppler[1], M. Baumgartner[1], R.J. Bakker[1]
[1]Chair of Resource Mineralogy, Department Applied Geological Sciences and Geophysics, Leoben, Austria

Fluid inclusion studies are used to determine diffusion rates of water-related species such as D_2O, H_2O, $H_2{}^{18}O$, H_2 and O_2 through the quartz crystal. Primary fluid inclusions of well known composition and density are synthesised in cold seal pressure vessels under hydrothermal conditions. In addition, natural fluid inclusions from well selected quartz samples, containing a $NaCl$-CO_2-H_2O mixture, are used for experimental diffusion studies. Synthesised as well as natural inclusions are exposed to different water-related species by varying re-equilibration time, pressure and temperature. Re-equilibration experiments are carried out at high experimental temperatures and pressures up to 700 °C and 1 GPa. Due to the induced pressure and concentration gradient fluid exchange between the pore fluid and the fluid inclusions is expected. Inclusions are analysed before and after re-equilibration by petrographical investigations (morphological properties), microthermometry (homogenisation and melting temperatures of the entrapped fluid phases) and Raman spectroscopy (compositional changes of the fluid phases). Concentration profiles in quartz can be indirectly obtained from the analysis of the re-equilibrated fluid inclusions. First results of the study show, that there are significant changes in fluid properties. Correlations with inclusion size, shape and location (3-dimensional distance from the surface) in dependence of re-equilibration time, pressure and temperature gradient are found. Due to the possibility of post-entrapment compositional and density changes of fluid inclusions, interpretations of fluid properties have to be done with particular attention. Re-equilibration processes are not yet fully understood, therefore further investigations in crystal microstrucutes are required to characterise all aspects of post-entrapment changes in fluid inclusions. The experimental studies allow to estimate the main factors of diffusion through nominally anhydrous minerals and furthermore to determine diffusion rates. In addition, the type of diffusion, i.e. bulk diffusion and diffusion along crystal defects such as dislocation and nano cracks can be characterised. The new experimental data will be used for comparsion of already established diffusion models as well as to determine new models.

P06-P10
As-bearing pyrite-marcasite intergrowths from the Pb-Zn Erma Reka deposit, South Bulgaria

R. Vassileva[1], R. Atanassova[1], K. Kouzmanov[2], E. Stefanova[1]
[1]Geological Institute, BAS, Mineralogy, Sofia, Bulgaria
[2]University of Geneva, Mineralogy, Geneva, Switzerland

Peculiar pyrite crystal formations with marcasite relics have been studied from the Erma Reka Pb-Zn hydrothermal deposit, Madan ore district. Formed in the later phases of the main quartz-galena-sphalerite mineralization, such aggregations are known with their specific porous textures and environmental significance. Large barite crystals and late chalcedony are in association with complex FeS_2 formations.

Marcasite relics are revealed from optical characteristics under reflected light and in the powder diffraction patterns. Morphological features of polymorphs and their intergrowths are described. A systematic study on their chemical composition and zonal pattern of the aggregates is achieved applying EPMA, BSE and LA-ICP-MS. The alternation of different in chemical composition (from As-free up to 5.4 wt.% As) fine zones along [001] and [111] are observed. In the zones with increased As-content, the values measured by EPMA for Sb, Se, Te also show enhancement, as well as Tl (up to 1700 ppm), correlated with the As content and zonal distribution determined by LA-ICP-MS (Vassileva et al., 2010). Some of the studied pyrites show an intensive incorporation of Ge (averages 300 ppm).

The fine oscillatory zoninig of pyrite crystals observed in BSE (Fig. 1) indicating complex growth history is primarily and is commonly attributed to episodic variation in fluid composition during pyrite crystallization (Vaughan, 2006). Pyrite-marcasite transformation could be used as an indicator of ore fluid evolution in the Erma Reka deposit.

Acknowledgements. This study is partly supported by the RNF 01/0006 project of the Bulgarian Science Fund and SCOPES IZ73Z0-128089 and SNF 20021-127123/1 of the Swiss National Fund.

References

R. Vassileva, R. Atanassova, E. Stefanova, P. Marchev, I. Peytcheva, K. Kouzmanov. 2010 Minor and trace element content of sulphides from the Madan polymetallic deposits, Central Rhodopes: a LA-ICP-MS study. National Conference with international participation GEOSCIENCES 2010 52-53.

D. J. Vaughan (Editor). 2006. Sulfide Mineralogy and Geochemistry. Reviews in Mineralogy and Geochemistry, MSA, Chantilly, Virginia, 714 p.

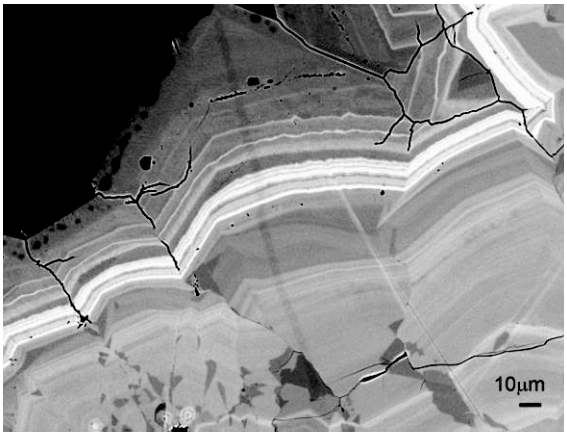

Figure 1: BSE image of oscillatory-zoned pyrite crystals and marcasite relics

P06-P11
Geochemistry of carbonate in Central Asia salt lakes

A. Darin[1], I. Kalugin[1], N. Maksimova[1], G. tretiakov[1]
[1]Institute of geology and mineralogy SB RAS, geology, Novosibirsk, Russian Federation

X-ray fluorescent microanalysis with syncrotronic radiation was used to study the spatial distribution of major and trace elements along the sediment cores with a spatial resolution of 50 - 100 microns. Were studied bottom sediments in two salt lakes of Central Asia: Shira (Khakassia, Russia), Telmen (Mongolia). The bottom sediments of these lakes contain the annual layers of thickness ~ 0.5 mm. Annual layer consists of carbonate and organic parts.

Sample preparation. Cores were cut in the laboratory. Were prepared slabs size 170x30x20 mm. Samples were dried in the freezer and impregnated with epoxy resin. For the analysis were prepared the plate thickness of 2 mm.

Analysis. Geochemical study was done using a scanning X-ray fluorescence analysis with synchrotron radiation in the Siberian Synchrotron Radiation Center at station X-ray microanalysis [Darin et all, 2005]. For scanning the excitation energy on 18 and 24 keV were used, scanning step 50, 100 and 200 microns. In each point was made analysis of the following elements: Cl, K, Ca, Ti, V, Cr, Mn, Fe, Ni, Cu, Zn, Ga, As, Se, Br, Rb, Sr, Y, Zr, Nb, Mo, Ba, Pb, Th, U. Elements concentration profilograms were combined with photographs of the samples (fig.1).

Main results. Variations of the contents of elements associated with changes in the mineral composition of sediments and reflect the region climate change.

A.V. Daryin, I.A. Kalugin, N.V.Maksimova, L.G. Smolyaninova, K.V. Zolotarev Use of a scanning XRF analysis on SR beams from VEPP-3 storage ring for research of a cores bottom sediments Teletskoe Lake with the purpose of high resolution quantitative reconstruction of last millennium paleoclimate // Nuclear Instruments and Methods in Physics Research A 543 (2005) 255-258.

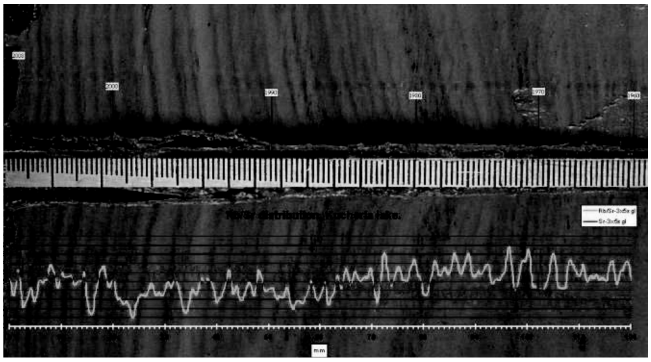

Figure 1

P07-P01
Structure and function of the B-repeat from *Listeria monocytogenes* InlB

W. Bleymueller[1], M. Ebbes[1], H. Niemann[1]
[1]Bielefeld University, Biochemie IV, Bielefeld, Germany

Internalin B (InlB) is a surface protein of the pathogenic bacterium *Listeria monocytogenes*. This protein binds the extracellular domain of the human receptor tyrosine kinase Met to induce uptake of the bacteria by phagocytosis into non-phagocytic cells. InlB consists of different domains, only one of which is involved in the binding of Met. We are working on the B-repeat, a domain in the middle of InlB, to which no function is allotted at the moment. We obtained a native data set with a resolution of 1.3Å. No obvious homologs exist, so we had to solve the phase problem experimentally. To this end, we used SeMet-crystals. From these crystals we measured a four-wavelength MAD data set at DESY, X12. The structure was solved with ShelxD. The crystals contain four molecules per asymmetric with one internal and the N-terminal Se-Met per molecule. ShelxD located five out of these eight Se atoms. Solvent flattening in ShelxE including the native data produced an excellent experimental electron density in which we built the model.

The B-repeat has an ubiquitin-like beta-grasp fold but also shares structural similarity with repeat domains of bacterial mucin-binding and adhesion proteins. From these results we gathered that the B-repeat has a potential binding function. Further we tested different constructs of InlB in cell scattering assays and via surface plasmon resonance experiments. The presence of the B-repeat was required to stimulate scattering of MDCK cells. Contrarily, the surface plasmon resonance experiments showed that an InlB construct containing the B-repeat and a construct without the B-repeat had a similar binding affinity towards the Met receptor and that the B-repeat did not bind to Met at all. From this we conclude that the B-repeat binds a yet unidentified host cell receptor that functions as co-receptor in Met activation. Taken together our results suggest that other members of the B-repeat domain family may function as spacer or receptor binding domain in bacterial extracellular multi-domain proteins.

P07-P02
Crystal structure of the yeast peroxisomal α/β-hydrolase Lpx1

S. Thoms[1], J. Gärtner[1], H. Niemann[2]
[1]Georg-August-Universität Göttingen, Universitätsklinikum, Göttingen, Germany
[2]Universität Bielefeld, Fakultät für Chemie, Bielefeld, Germany

Yeast peroxisomes show an aberrant vacuolated morphology in the absence of Lpx1, a protein that localizes to peroxisomes and belongs to the α/β-hydrolase superfamily. The natural substrate of Lpx1 and the reaction that it catalyzes are so far unknown. Here, we present the 1.8 Å crystal structure of Lpx1. The structure reveals an unusual location of the acid residue from the catalytic triad after strand β6 of the canonical α/β-hydrolase fold. The active site is covered by a four-helix cap domain. The potential substrate binding site is located at the interface between the α/β-hydrolase core and the cap domain. The active site is accessible from the protein surface by at least two routes. A tunnel leads from the active site further into the protein interior and widens into a cavity. Lpx1 forms homodimers, in which the dimerization interface is formed by the α/β-hydrolase core folds of the two protomers. A non-canonical C-terminal helix of one protomer embraces the cap domain of the other, thereby contributing a further dimerization contact. This unusual C-terminal helix sticks out from the core fold to which it is connected by an extended flexible loop. We analysed the requirement of this helix for dimerization and piggy-back import into peroxisomes using a microscopy-based interaction assay in mammalian cells and biochemical assays *in vitro*. Surprisingly, the C-terminal helix is dispensable for piggy-back import and dimerization. The unusually robust self-interaction suggests that Lpx1 is imported into peroxisomes as a dimer.

P07-P03
p { margin-bottom: 0.08in; } Kinase domain of Ethylene Receptor activated CTR1 from *A. thaliana* is regulated through activation loop phosphorylation and dimerization

H. Mayerhofer[1], S. Panneerselvam[1], J. Müller-Dieckmann[1]
[1]EMBL Hamburg, EMBL Hamburg, Hamburg, Germany

p { margin-bottom: 0.08in; }
Signalling of the phytohormone ethylene is initiated by disulfide linked membrane bound receptor dimers with similarity to bacterial two-component systems (TCS). In *A. thaliana* the TCS-like ethylene receptors interact with the cytosolic serine/threonine kinase CTR1, a proposed mitogen activated protein kinase kinase kinase (MAPKKK), and manipulate its activity subject to ethylene binding. The three-dimensional structures of the active, tri-phosphorylated and the unphosphorylated, inactive kinase domain of CTR1 in complex with staurosporine illustrate the conformational rearrangements that form the basis of activity regulation. The active kinase domain forms dimers in solution, while the unphosphorylated kinase is a monomer. This strongly suggests another layer of activity regulation of CTR1 *in vivo*.
Steric restraints further indicate regulation of kinase activity across dimers, which points to CTR1 mediated ethylene receptor crosstalk.

Figure 1

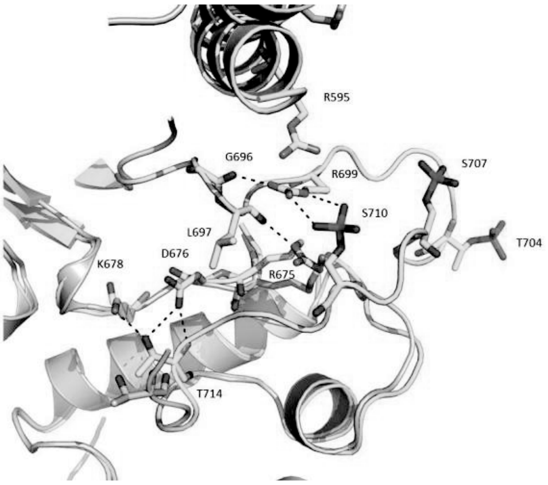

Figure 2

P08-P01
Mineralogy of Mg-bearing industrial minerals (Brucite-hydromagnesite) in polygenetic marble, Yazd, Iran

B. Taghipour[1,2]
[1]Shiarz Uinersity, Earth sciences, Shiraz, Iran, Islamic Republic of
[2]Shiraz University, earth science, Shiraz, Iran, Islamic Republic of

The study area is located in 40 km southwest of Yazd in eastern Shir-kuh range. Intrusive bodies occur as dyke and small stock. Chemical composition of intrusive bodies is in the range of granodiorite, diorite, and gabbro. The nature of magmatism is clac-alkaline, which is generated in orogenic setting. Cretaceous carbonate rocks in vicinity of those intrusions are transformed into various marbles and skarns. The following mineral assemblages are characteristic: Forsterite + serpentine + talc+brucite + hydromagnesite + calcite + dolomite
Brucite porphyroblasts are only the most widespread mineral in marbles. The peak of metamorphism is begun with periclase and forsterite (>700 ºC) occurrences. Then low temperature paragenesis like carbonate and hydrous minerals took place in 25 ºC. There are several stages in the marble evolution which imply the polygenic genesis of the marbles.

P08-P02
Production of cordierite and spinel based ceramics using bauxite, kaoline, serpentinite and dunite

E. Thomaidis[1], G. Kostakis[1]
[1]Technical University of Crete, Mineral Resources Engineearing, Chania, Greece

Ceramic bodies, mainly constituted of cordierite or spinel, were produced using Greek raw materials. For this purpose samples of bauxite, from the feedstock of the alumina plant at Ag. Nikolaos (Boiotia), samples of two different kaolines of Milos and one from Drama district (East Macedonia), as well as samples of serpentinite and dunite from the Vourinos area (Kozani district, West Macedonia), were used.

The bauxite was constituted mainly of diaspore, relatively high content of boehmite and hematite, and minor amounts or traces of goethite, calcite, chlorite, anatase and rutile. The kaolines of Milos contained high amounts of opal, cristobalite and low amounts of tridymite, quartz and alunite, while the kaoline of Drama contained high amounts of quartz, and muscovite, and traces of potassium feldspar. The serpentinite was mainly composed of chrysotile, considerable amounts of lizardite and antigorite and low content of calcite. The dunite was mainly composed of forsterite and chrysotile, low amounts of lizardite and amorphous and traces of calcite.

From the raw materials above, samples of various mixtures, after milling and pressing in cylinder shaped tablets were heated at temperatures between 1250 - 1350 ^{o}C for 1 to 8 h, to obtain ceramic bodies. Their mineralogical composition, the shrinkage at burning, the open porosity, the density and the compressive strength of these ceramic products were determined.

From the mixtures of bauxite with the kaoline of Drama and the serpentinite and dunite, respectively, resulted ceramic bodies resistant to heating up to 1300 ^{o}C. The crystalline phases present in these ceramic bodies were cordierite in high percent, mullite in considerable amount and quartz, hercynite and spinel in low amounts. Their open porosity, after heating at 1300 ^{o}C for one hour was 0.7 and 1.1 % respectively, their density 2.55 and 2.59 g/cm^3, respectively, their shrinkage 3.71 and 3.85 %, respectively, and their compressive strength 2.0 kN/cm^2.

The ceramic bodies resulted from the mixtures of bauxite with the kaolines of Milos and the dunite were constituted mainly of cordierite and low amounts of enstatite, hercynite, mullite, and spinel. Their open porosity, after heating at 1300 ^{o}C for one hour was 17.5 and 18.6 % respectively, their density 1.99 and 1.97 g/cm^3, respectively, their shrinkage 0.40 and 1.73 %, respectively, and their compressive strength 3.0 kN/cm^2.

From the mixtures of bauxite with the serpentinite and the dunite resulted ceramic bodies resistant to heating up to 1350 ^{o}C. The crystalline phases present in these ceramic bodies were spinel, mullite and hercynite. Their open porosity, after heating at 1350 ^{o}C for one hour was 1.0 % (mixture with serpentine) and 2.0 % (mixture with dunite), their density 2.95 and 2.85 g/cm^3, respectively, their shrinkage 7.5 and 7.3 %, respectively, and their compressive strength 4.3 kN/cm^2.

P08-P03
Microstructural analyses of natural and synthesized NaCl

C. Tommaseo[1]
[1]Technical University, Mineralogy, Berlin, Germany

Texture formation of rocksalt from Portugal and Iran have been studied by electron backscattered diffraction. The texture is compared with synthesized salt samples annealed at different temperatures with different additives to understand their origin. It is supposed that the grain orientations in correlation with their next-nearest neighbours' orientations in the material in dependence of the external conditions (temperature, pressure, deformation, additives) give information about their origin. Specific oriented grains are surrounded by typical grain orientations which might help to get information about the process taking place during texture development.

Goal of the study is to find an explanation (approach of the problem) for different (relevant or less relevant) processes taking place in for example recrystallization, corrosion etc., focussing mainly on grain orientation in dependence of the mentioned environmental conditions, which is indirectly connected with grain boundaries, influencing properties such a creep resistance (Thompson, 1990) and susceptibility to intergranular corrosion (Atkinson, 1988). In fact, it is found that the corrosion process initiates and proceeds in channels along dislocations in grain boundaries, which are concerned in the case of high energy boundaries. An idea to promote corrosion resistance would be to create low energy boundaries by adding an amorphous phase, which is thermodynamically more stable than the currently most studied nanomaterials. This assures that the NaCl sample can be manipulated in a wide temperature and pressure range without any additional phase transformations, which would complicate the work. An additional influencing factor is the increase of temperature over the recrystallization temperature, which is still a point of debate. Higher temperature exerts grain growth enhancing the proportion of the low angle boundaries to the high angle boundaries.

A.W. Thompson, W.A. Backofen (1971) The effect of grain size on fatigue. Metall. Trans., Vol.2, pp. 2004-06.
H.V. Atkinson (1988) Theories of normal grain growth in pure single phase systems. Acta Metall., 36, 469-491.

P08-P04
Oxygen ion Diffusion in La$_{2-x}$Sr$_x$CuO$_{4\pm\delta}$Investigated with Oxygen Isotope Back Exchange and Diffraction Methods

R. Sura[1], M. Ceretti[2], C. Prestipino[2], W. Paulus[2,3], J. Schefer[1], L. Keller[1], K. Conder[3], E. Pomjakushina[3]
[1]Paul Scherrer Institute, Laboratory for Neutron Scattering, Villigen PSI, Switzerland
[2]University of Rennes, Sciences Chimiques de Rennes, Rennes, France
[3]ICG Montpellier, Chimie et cristallochimie des matériaux (C2M), Montpellier, France

The understanding of oxygen ion conduction in solids at moderate temperatures is a key issue for the development of oxygen membranes in solid oxide fuel cells (SOFCs) [1, 2, 3]. The oxygen diffusion in La$_{2-x}$Sr$_x$CuO$_{4-\delta}$ can be decreased by Sr doping as reported by Opila [2]. Sr doping can therefore be used to investigate deeper how diffusion and structure correlate. For this we need to examine high quality single crystal to avoid porosity and grain boundaries present in polycrystalline samples and influencing therefore the equilibrium. We have succeeded to grow La$_{2-x}$Sr$_x$CuO$_{4\pm\delta}$ single grain crystals by using a mirror furnace and tested them with X-ray Laue (Fig. 1a, 1b) and neutron diffraction (Fig. 1c, 1d).

We did Oxygen Isotope Back Exchange (OIBE) experiments (Fig 2) between 40 ^{0}C to 1000 ^{0}C we proved that free oxygen mobility can be realized for x = 0, 0.05 already below 500 ^{0}C but is depressed for x = 0.1 and 0.15. This gives evidence that low temperature oxygen mobility relies on Sr doping in La$_2$CuO$_4$. In order to correlate structure and oxygen diffusion as a function of temperature we will perform neutron measurements on grain free 0.05 and 0.15 single crystals. Later this data will be combined with SIMS (yields the diffusion constant and anisotropy on a macroscopic scale by observing the ^{18}O diffusion on oriented single crystals). The goal of my thesis is to clarify how the presence of Strontium modifies the structure and subsequently the lattice dynamics of $La_{2-x}Sr_xCuO_{4\pm\delta}$ to suppress the oxygen diffusion.

[1] Y. Tsujimoto *et al., Nature* **450**, 1062-1066 (2007)
[2] A.Villesuzanne *et al., J. Solid State Electrochem*. **15**, 357-366 (2011)
[3] L. Le Dréau, Thesis, submitted June, 2011 (University of Rennes)
[4] E.J. Opila, *J. Am. Ceram. Soc.* **6**, 2363(1995) Figure 2.

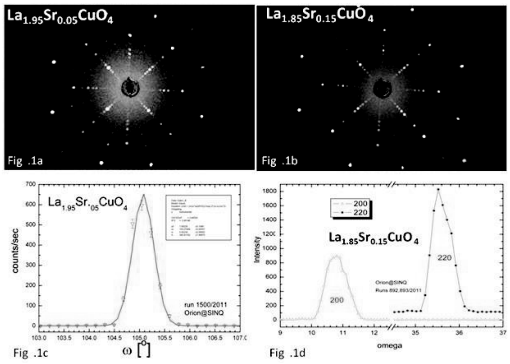

Figure 1: **1a, 1b:** Back scattering Laue pictures of as grown single crystals. Data collected at LDM@PSI.
1c, 1d: ω scan for (002) basic reflection measured on a high quality single crystal of $La_{1.95}Sr_{0.05}CuO_4$ and (200), (220) reflections measured on $La_{1.85}Sr_{0.15}CuO_4$ Data collected at ORION@SINQ.

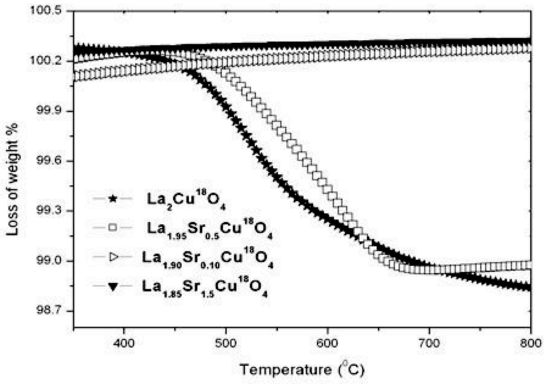

Figure 2: Oxygen Isotope Back Exchange (OIBE) in La2-xSrxCuO4 showing the suppression of oxygen diffusion for high Sr doping (x).

P08-P05
The dynamic three-dimensional A^3B^5 models on the example of GaAs

K. Iskakova[1], R. Akhmaltdinov[1]
[1]KazNPU, Physics and Mathematics, Almaty, Kazakhstan

The dynamic three-dimensional modeling compounds A^3B^5 is considered. During the initial structure is taken compound GaAs. This crystal structure consists of two FCC lattices, which are shifted relative to each other by ¼ the space diagonal. In the center of origin is As atom with four nearest neighbors of Ga at the vertices of a tetrahedron. Each ion crystal is surrounded by four nearest-neighbor ions of opposite sign. At a distance of ¼ diagonal are four ions with Q_iQ_j = -1, at a distance radius of coverage 2 - 19 pairs of ions of opposite signs $Q_iQ_j = \pm 1$. Linking system creates a procedure for GaAs nuclei tetrahedral combinations, similar to the case of reach 1 in all 38 cores as the centerpiece. Further increase the radius of coverage (3, 4, 5, 6) shows the trend growth of tetrahedral combinations according to the number of cores (110, 282, 498, 918).

On the basis of the direct lattice can construct the reciprocal lattice and define the properties of the Fermi surface. A radius of coverage one can take arbitrary (millions of skeletons). The highspeed computations provides for the dynamic simulation of the properties of real crystals of GaAs.

It was also found that crystals of this type is the uneven buildup of atoms from the central atom in a uniform increase in the radius of coverage. This should affect the uneven growth and the occurrence of violations in the structure at various treatments, such as pressure. This feature distinguishes the GaAs crystal from a crystal with FCC-lattice [1, 2].

These conclusions will be valid for other similar structures (Si, sphalerite and diamond).

Reference:

[1] Iskakova K.A. Computer modeling of the potential energy of the crystal structures of solids. // Tez. Proceedings. 6-th International Conference on Radiation heterogeneous processes. - Kemerovo, Russia: p. 174, (1995).
[2] Iskakova K.A., Starostenkov M.D., Kuketaev T.A. Computer simulation and calculation of the structure of GaAs Materials 7-th International School-Seminar. Barnaul - Ust-Kamenogorsk, Altai State University, Russia, p. 76-77. (2003).

P09-P01
X-ray Diffraction and Surface Acoustic wave analysis of $Ba_{0,65}Sr_{0,35}TiO_3$ thin films

A. Njeh[1], S. Msedi[2], H. Fuess[3], M.H. Ben Ghozlen[2]
[1]Faculté des sciences de Gafsa, Physique Informatique et mathématiques, Gafsa, Tunisia
[2]Faculté des Sciences de Sfax, Physique des Matériaux, Sfax, Tunisia
[3]University of Technology, Materials Science, Darmstadt, Germany

Bulk Acoustic Wave (BAW) resonators using Barium Strontium Titanate (BST) oxide thin films have an attractive attention for GHz applications [1]. The surface acoustic waves (SAWs) technique is becoming an attractive tool for accurately and nondestructively characterizing the elastic property of thin film. This acoustic wave mode is very sensitive to surface modification also in the depth of nanometers [2]. Barium strontium titanate (BST) bulk ceramics was used as target for dc-magnetron sputtering thin film deposition. Thin films of stoichiometric BST were deposited on $TiO_2/Pt/SiO_2/Si$ substrate with a thickness of 300 and 400 nm. The microstructural properties of the films were characterized by x-ray diffraction. The BST films present a cubic perovskite structure with a dense and smooth surface. The dispersion features of SAWs propagating on different directions of $BST/TiO_2/Pt/SiO_2/Si$ films are investigated to instruct an accurate and facile fitting process for determining Young's modulus and Poisson ratios of the films [3]. The elastic modulus of BST films is distinctly influenced by the distance between the BST bulk ceramic target and the substrate during the deposition process.

[1] Volatier A., Defay A., Aid M., N'hari A., Ancey B., Dubus B., *Appl. Phys. Letters*, 2008, 92, 032906.
[2] Leonhardt M., Schneider D., Kaspar J., Schenk S., *Surface & Coatings Technology*, 2004, 185, 292.
[3] Schneider D., Schwarz T., *Surface & Coatings Technology*, 1997, 91, 136.

P09-P02
Structural investigations of lead-free piezoceramics

H. Fuess[1], L.A. Schmitt[1], J. Kling[1], M. Hinterstein[1], W. Jo[1], S. Hayn[1], M. Gröting[1], H.-J. Kleebe[1], J. Rödel[1], K. Albe[1]
[1]TU Darmstadt, Materials Science, Darmstadt, Germany

In this study we focus on the influence of micro- and nanostructure evolution of lead-free piezoceramics with emphasis on the quasi-binary $Bi_{1/2}Na_{1/2}TiO_3$-$BaTiO_3$ (BNT-BT) and quasi-ternary $Bi_{1/2}Na_{1/2}TiO_3$-$BaTiO_3$-$K_{0.5}Na_{0.5}NbO_3$ (BNT-BT-KNN) system. The materials crystallize in a perovskite related structure. Samples were investigated by combining transmission electron microscopy, X-ray and neutron diffraction as a function of composition, and electric field [1].
For specific compositions a core-shell structure, composed of a rhombohedral *R*3*c* phase with domain-like morphology embedded in a weakly polar *P*4*bm* matrix phase was observed [2, 3].
An electric field-induced phase transformation in the quasi ternary system BNT-BT-KNN from tetragonal *P*4*bm* to rhombohedral *R*3*c* phase was verified by *in situ* electron microscopy [4] and neutron diffraction experiments [5].
Moreover high resolution transmission electron microscopy (HRTEM) studies (imaging and HRTEM simulation) and density functional theory (DFT) calculations on BNT-BT 94-06 revealed a homogeneous A-site occupation, without any specific chemical ordering. Different contrast of the HRTEM images could be attributed to slightly tilted nanometer sized regions [6].

[1] L. A. Schmitt, J. Kling, M. Hinterstein, M. Hoelzel, W. Jo, H.-J. Kleebe, H. Fuess *J. Mater. Sci.* **46**, 4368-4376 (2011)
[2] L. A. Schmitt, H.-J. Kleebe, *Functional Materials Letters*, Topical issue on lead-free ferroelectrics **3** (1), 55-58 (2010)
[3] L. A. Schmitt, M. Hinterstein, H.-J. Kleebe, H. Fuess, *J. Appl Crytallogr.* **43** (4), 805-810 (2010)
[4] J. Kling, X. Tan, W. Jo, H.-J. Kleebe, H. Fuess, J. Rödel, *J. Am. Ceram. Soc.* **93** (9), 2452- 2455 (2010)
[5] M. Hinterstein, M. Knapp, M. Hölzel, W. Jo, A. Cervellino, H. Ehrenberg, H. Fuess, *J. Appl. Crystallogr.* **43**, 1314 - 1321 (2010)
[6] J. Kling, S. Hayn, L. A. Schmitt, M. Gröting, H.-J. Kleebe, K. Albe, *J. Appl. Phys.* **107**, 114113 (2010).

Keywords: diffraction, ferroelectrics, piezoelectric ceramics, transmission electron microscopy

P09-P03
Hydrogen peroxide - a new promising solvent for the synthesis of eulytite ($Bi_4(SiO_4)_3$) crystals

E. Marina[1], A. Marin[1], V. Balitsky[1], T. Bublikova[1]
[1]Institute of Exprimental Mineralogy RAS, Laboratory of the Minerals Synthesis and Modifications, Chernogolovka, Russian Federation

Crystals of bismuth orthosilicate (eulytine) are uses for scintillator in the high-energy physics, computer tomography, dosimetry. The monocrystalline bismuth orthogermanate with eulytine structure is one of most perspective materials for these purposes. However, the bismuth orthosilicate have better scintillation characteristics in comparison with bismuth orthogermanate (for example, the highlighting time (0.1 m.s.) is better in three times). On the other hand, the producing of eulytite from highly viscosity melt is still hard task.
It's known that in contemporary science and manufacture an explicit tendency can be observed towards replacement of monocrystalline materials with ceramics of equal or improved functional characteristics. In comparison with technology of monocrystals growth the optical ceramic's technologies have a more advantages. First of all, it is rather simple and inexpensive manufacturing of ceramics, possibility of high level of alloying at uniform distribution of luminophors. Also that is especially important, possibility to making of larger-sized products, including given shape. Progress in manufacturing techniques of oxidation ceramics has been reached only in last decade owing to use of powders of initial oxidation components.
Our main purpose was to find a reliable and reproducible method of fine-crystalline bismuth orthosilicate production for creating scintillation ceramics on its basis, and, in addition, to estimate the size and morphology of the fractions obtained. We had been grown up for the first time eulytine crystals in the hydrothermal solutions of hydrogen peroxide. Since the system is missing elements that are not included in the composition of eutyline, this automatically settles the problem of solvent's impurities in the obtained crystals. It is of great importance for the growth of small crystals, because technologically it is as very complicated process of nano- or micro- particles segregation from the source solvent and from the foreign solid phases, created in the process of growth; therefore, it is desirable, that all the components of the solution are involved in the crystallization.
Hydrothermal synthesis of the fine crystalline bismuth orthosilicate was produced from hydrogen peroxide solutions at temperature 260 C and pressure about 500 bar. Starting material was stoichiometric mix of Bi2O3 и SiO2. The solvent was aqueous solution of hydrogen peroxide with concentrations from 1 to 5 wt %. The fine crystalline eulytite got in experiments with duration from 7 to 12 days. Autoclaves with Teflon lining have volume of 100 ml. The best results have been received at growth of crystals in solutions H2O2 with concentration from 3 to 5 wt %. X-ray patterns show the presence of eulytine eumorphic crystals virtually without admixtures of other minerals.
We had been received powders of bismuth orthosilicate with the sizes of crystals from first tens micron to the tenth shares of millimeter.

P09-P04
Phasenneubildungen und Quantifizierung von gebrannten Kalksteinen mit unterschiedlichen Calcitgehalten

R. Martin[1], E. Thorsten[1], P. Herbert[1], W. Thomas[1]
[1]Martin-Luther-Universität, Mineralogy and Geochemistry, Halle, Germany

Durch Brennen von Kalkstein (hauptsächlich bestehend aus Calcit, $CaCO_3$) kalziniert dieser und es entsteht CaO (Branntkalk), dieser wiederum reagiert mit Wasser exotherm zu Portlandit ($Ca(OH)_2$, Löschkalk). Hauptsächlich in der Bau-, Chemie- und der Stahlindustrie finden Produkte aus allen Verarbeitungsstufen Verwendung(Oates 1998).
Beim Brennen von Kalksteinen mit deutlichen Gehalten von Dolomit, Quarz, Glimmer oder Tonmineralen entstehen beim Brennprozess neben CaO auch Si-, Al- und Mg-Phasen (z.B. C_2S, $C_2(A,F)$, C_3A, MgO). Zudem kann es im Hochofenprozess zur Bildung von Sinterhäuten um Branntkalkstücken kommen, die ein

Zusammenbacken bewirken und sich zu Agglomeraten (sog. „Schlackebären“) verbinden. Diese sind nach Austritt aus dem Ofen bis zu 40 cm groß und können sowohl den Brennprozess als auch den nachfolgenden Löschprozess empfindlich stören.
In einem von der Arbeitsgemeinschaft industrieller Forschungsvereinigungen (AiF) geförderten Projekt werden Kalkstein- und Branntkalkproben sowie die „Schlackebären“ untersucht.
Für das Entstehen der Phasen, die im Branntkalk neben CaO vorkommen, sind oftmals komplexe Reaktionen erforderlich. Es wird bei ca. 1050°C gebrannt, das Vorhandensein der Phase

Hatrurit (C_3S) in den „Schlackebären“ deutet auf lokale Maximaltemperaturen von über 1200°C hin (Philips et al. 1959).
Für die Entstehung der Sinterhäute muss man die Entwicklung der silikatischen Beimengungen des Kalksteins im System K_2O-Al_2O_3-SiO_2 betrachten, so ist die Bildung einer eutektischen Schmelze ab Temperaturen von knapp 1000°C möglich, im System Tridymit-Kalifeldspat-Mullit liegt das Eutektikum bei 985°C (Rankin et al. 1915, Schairer 1957).
Zur Untersuchung der Phasenbeziehungen vor und nach dem Brand und der Reaktionsmechanismen werden in erster Linie röntgenographische Methoden (RFA und XRD) angewendet. Die Phasen werden zusätzlich mit der Rietveldmethode quantifiziert und ein Reaktionsmodell erstellt.
Literatur

J.A.H. Oates (1998) Lime and limestone; WILEY-VCH Verlag GmbH
B. Phillips, A. Muan (1959) Phase equilibria in the system CaO-Iron Oxides-SiO2 in air; J. Am. Ceram. Soc. 42, 413-423
G.A. Rankin, F.E. Wright (1915) The ternary system CaO-Al2O3-SiO2; Am. J. Sci. 39, 1-79
J.F. Schairer (1957) Melting relations of the common rock-forming oxides; J. Am. Ceram. Soc. 40, 215-235

P09-P05
Microstructure Development of Magnesia Cement during Hydration

K. Schollbach[1], H. Pöllmann[1]
[1]Martin-Luther-University Halle-Wittenberg, Institute of Geosciences and Geography, Halle (Saale), Germany

Magnesia cement is an acid-base cement that was discovered in 1867 by Sorel and Dumas. It is produced by the reaction of magnesium oxide with a concentrated magnesium chloride solution to form the 3-1-8 ($3Mg(OH)_2xMgCl_2x8H_2O$) and the 5-1-8 phase ($5Mg(OH)_2xMgCl_2x8H_2O$). Magnesia cement is a fast setting, high early strength cement that is resistant to saline solutions and has a high E-modulus. Due to these properties it is used in deep geological repositories in salt domes.

The reaction mechanism of magnesia cement is little understood. Setting occurs through gelation, before crystalline phases are detectable. According to Deng and Zhang (1999) polynuclear aquahydroxo complexes of uncertain composition are probably formed during this reaction, that lead to the crystallization of either the 3-1-8 or 5-1-8 phase.

To study the phase formation and the micro structural development during this process cryotransfer-SEM was used. The samples were prepared with the stoichiometric starting composition of the pure 3-1-8 and 5-1-8 phase. A third sample had the starting composition to form the 5-1-8 phase and $Mg(OH)_2$. All samples were prepared with reactive MgO, calcined at 800°C. Duration of the hydration reaction and its different stages were investigated using heat flow calorimetry (Figure 1) and the reaction products were characterized using XRD. The samples were frozen in liquid nitrogen at different stages during the hydration and characterized using cryotransfer-SEM and EDX-analysis.

XRD analysis shows that the reaction products for both stoichiometric samples were the 5-1-8 phase, with an amorphous content between 20 and 25wt%. The third sample contained about 57wt% 5-1-8 phase, 18wt% $Mg(OH)_2$ and 16wt% amorphous phase.

Using cryo-SEM to investigate the microstructure after the first 5min, MgO dissolving in $MgCl_2$ solution is visible. An amorphous phase is formed (Figure 2a), that appears in all samples after 4 to 6h. It has a higher chloride concentration than the surrounding areas according to EDX analysis. The 5-1-8 phase appears to be crystallizing from this phase and forms a homogeneous dense matrix consisting of needles (Figure 2b). Several pores are visible in the matrix, that are probably due to air inclusion during mixing. The microstructural development appears to be similar in all samples.

References:

Sorel, S. & Dumas, M. (1867), On a new Magnesium Cement, Compt. Rend. Hebd. Des Sciences, 65, 102
Deng, D.H. & Zhang, C.M. (1999), The Formation Mechanism of the hydrate phases in magnesium oxychloride cement, Cem. Concr. Res., 29, 1365

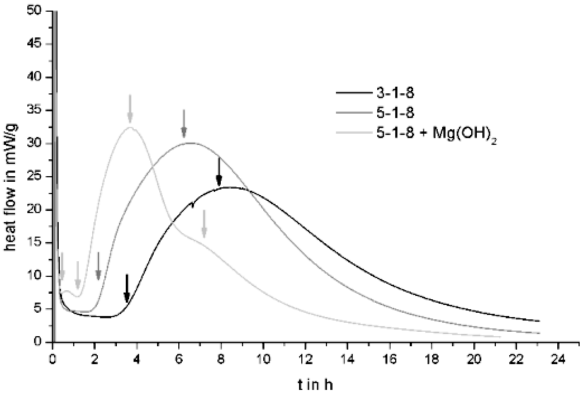

Figure 1) Heat flow during hydration of all three magnesia cement samples. Arrows mark points during which hydration was stopped and microstructure investigated using cryo-SEM.

Figure 1

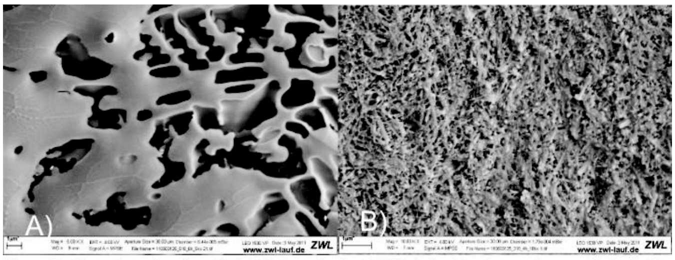

Figure 2) a) Amorphous phase found in the 5-1-8 sample after 6h b) Typical matrix of magnesia cement in the 3-1-8 sample after 6h

Figure 2

P09-P06
Growth Evolution of Nanosized $Bi_5Ti_3FeO_{15}$ by Hydrothermal Method Along with the Reaction Time

Z. Hong[1], T. Zhang[1], Y. Zhang[1], J. Yang[1,2]
[1]Zhejiang University, Department of Materials Science & Engineering, Zhejiang, Austria
[2]Vienna University of Technology, Institute of Materials Chemistry, Vienna, Austria

Semiconductor photocatalysts with high photocatalytic activity have received more and more attention because of their important role on environmental applications such as air purify, water disinfection, hazardous waste remediation and water purification. In general, there are two main categories for semiconductor photocatalysts: one is the titania dioxide(TiO_2) and its modification by doping method, and the other is the novel narrow bandgap semiconductor materials, such as $Bi_5Ti_3FeO_{15}$. The latter, narrow bandgap semiconductor materials with characters of absorbing the visible light, can degrade the organic pollutants and split the water under visible light, thus became the focus in the research in recent years[1; 2].

$Bi_5Ti_3FeO_{15}$, belonging to aurivillius phase compounds, is a kind of very attracting semiconductors due to a lot of advantages. $Bi_5Ti_3FeO_{15}$ not only processes excellent photocatalytic activities due to their narrow bandgap, but also has ferromagnetism properties caused by their unique layered structure[3]. Thus, $Bi_5Ti_3FeO_{15}$ becomes to a new research focus and a lot of methods were used to synthesize it, such as solid-state reaction method, sol-gel processing, chemical coprecipitation, etc. Nevertheless, fewer papers were reported to prepare $Bi_5Ti_3FeO_{15}$ by hydrothermal method, and there are still a lot of unknown areas.

In this work, hydrothermal method was adopted to prepare $Bi_5Ti_3FeO_{15}$. Bi(NO3)3·5H2O, Fe(NO3)3·9H2O and P25(TiO_2) were used as staring materials, and NaOH and Na_2CO_3 were used as aided mineralizer. The research focused on the growth of Bi5Ti3FeO15 under different reaction time (from 1h to 48h) by hydrothermal method, while the ratio of raw materials and reaction temperature were fixed. The evolution of Bi5Ti3FeO15 crystalline phases and morphologies were studied, and pure phase of the Bi5Ti3FeO15 could be obtained through 48h reaction, as shown in Fig.1.

[1]J.S. Jang, S.S. Yoon, P.H. Borse, K.T. Lim, T.E. Hong, E.D. Jeong, O.S. Jung, Y.B. Shim, H.G. Kim, Synthesis and characterization of aurivillius phase Bi5Ti3FeO15 layered perovskite for visible light photocatalysis. Journal of the Ceramic Society of Japan 117 (2009) 1268-1272.

[2]J.S. Jang, P.H. Borse, J.S. Lee, K.T. Lim, C.R. Cho, E.D. Jeong, M.G. Ha, M.S. Won, H.G. Kim, Photocatalytic Performance of Nanocrystalline Bi5Ti3FeO15 Layered Perovskite Under Visible Light. Journal of Nanoscience and Nanotechnology 10 (2010) 5008-5014.

[3]C.H. Hervoches, A. Snedden, R. Riggs, S.H. Kilcoyne, P. Manuel, P. Lightfoot, Structural behavior of the four-layer aurivillius-phase ferroelectrics SrBi4Ti4O15 and Bi5Ti3FeOl5. Journal of Solid State Chemistry 164 (2002) 280-291.

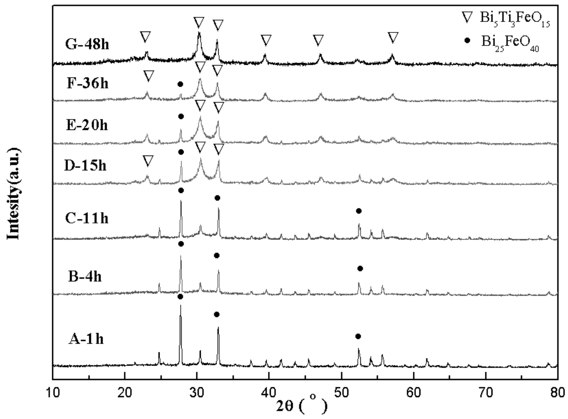

Figure 1: The prepared Bi5Ti3FeO15 material exhibited visible-light photocatalysitic ability and weak ferromagnetism.
XRD patterns for Bi5Ti3FeO15 samples prepared under different hydrothermal times.

P09-P07

Hierarchical Growth of $CdSe/Fe_3O_4$ Nanocomposites by Solvothermal Method and Their Growth Mechanism

J. Yang[1,2], F. Li[1], L. Zhou[1], Z. Hong[1]
[1]Zhejiang University, Department of Materials Science & Engineering, Zhejiang, China
[2]Vienna University of Technology, Institute of Materials Chemistry, Vienna, Austria

CdSe quantum dots (QDs) have attracted extensive attentions in fundamental studies and technical applications such as optoelectronic devices, biophotonic imaging, and fluorescence labels. Fe_3O_4 nanomagnetic particles also have important application in magnetic resonance imaging and drug carrier. However, either of them can only afford people with only singe function. A combination of optical and magnetic properties in a single material would extend the application of both quantum dots and magnetic particles. Therefore, fluorescent-magnetic nanocomposites would have great application prospects. A combination of optical and magnetic properties in a single material would extend the application of both quantum dots and magnetic particles. Therefore, fluorescent (CdSe)-magnetic (Fe_3O_4) nanocomposites would have great application prospects [1; 2; 3].

In the present study, Fe3O4/CdSe nanocomposites were prepared via high-temperature decomposition of organometallic precursors. The research focused on the growth of Fe3O4/CdSe nanocomposites along with the solvothermal time and their fluorescence properties. High crystallinity and monodispersed Fe3O4 nanoparticles with average size about 6-8nm served as core, and CdSe shell grew on the surface of Fe3O4 nanoparticles under different reaction times (from 2min to 15min). As the reaction time increased, the absorbance and luminescence peaks of Fe3O4/CdSe nanocomposites had red-shifts (Fig.1). And when the reaction time over 15min, a hierarchical growth phenomenon was detected when the sample dispersed in CH_2Cl_2 solvent, as shown in Fig.2. The prepared $CdSe/Fe_3O_4$ nanocomposites were systemically characterized by lots of methods, such as UV-Vis spectra, photoluminescence spectra (PL), X-ray diffraction(XRD), transmission electron microscopy (TEM, HRTEM) and physicians practice management systems (PPMS), etc. Based on the characterization, a mechanism for hierarchical growth was proposed.

Fig.1 Fig.2

[1]Y. Zhang, S.N. Wang, S. Ma, J.J. Guan, D. Li, X.D. Zhang, Z.D. Zhang, Self-assembly multifunctional nanocomposites with Fe3O4 magnetic core and CdSe/ZnS quantum dots shell. Journal of Biomedical Materials Research Part A 85A (2008) 840-846.

[2]G.H. Du, Z.L. Liu, D. Wang, X. Xia, L.H. Jia, K.L. Yao, Q. Chu, S.M. Zhang, Characterization of Magnetic Fluorescence Fe3O4/CdSe Nanocomposites. Journal of Nanoscience and Nanotechnology 9 (2009) 1304-1307.

[3]G.H. Du, Z.L. Liu, Q.H. Lu, X. Xia, L.H. Jia, K.L. Yao, Q. Chu, S.M. Zhang, Fe3O4/CdSe/ZnS magnetic fluorescent bifunctional nanocomposites. Nanotechnology 17 (2006) 2850-2854.

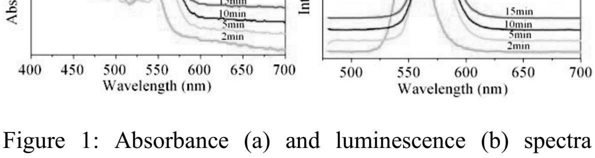

Figure 1: Absorbance (a) and luminescence (b) spectra for Fe3O4/CdSe nanocomposites prepared under different reaction times, other parameters were fixed.

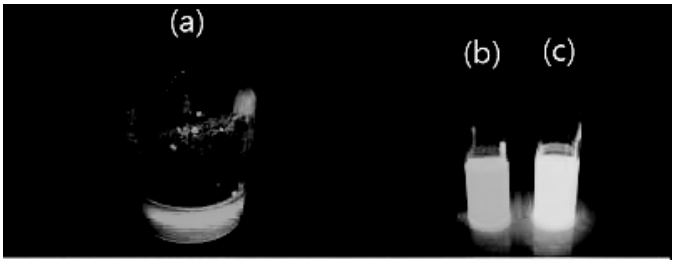

Figure 2: UV-photoluminescence of Fe3O4/CdSe anocomposites prepared under 15min, (a) is photoluminescence of the samples dispersed in CH_2Cl_2 solvent, (b) and (c) is the UV-photoluminescence of the upper and lower layers respectively.

P09-P08
New views on Australian opal and opalized objects

M. Liesegang[1], R. Milke[1]
[1]Freie Universität Berlin, Institute for Geological Sciences, Berlin, Germany

Several approaches have been made to resolve the factors leading to the formation of precious opal, much less to the far more frequently occuring common opal, or their interrelations.

We investigated silicified materials from the opal fields of Andamooka (South Australia) and Yowah (Queensland) by petrographic microscopy, XRD, SEM and EMPA. The opaline silica replaced several substances such as trigonal crystals, clasts in a silicified breccia, wood, clay, ooids and rhombic, elongated minerals of uncertain origin.

SEM investigations reveal the abundant presence of Opal-A, commonly consisting of submicron-sized spheres composed of up to three shells. Stacking faults in the otherwise regular array are frequently observed. Extensive cementation of the particles avoids a play-of-color. Agglomerates of tiny spheres form precursors of spheres >2 µm with a shell structure. Lepispheres and rosettes in the range of 2 - 25 µm consist of Opal-CT. Astonishingly, all Opal-A and Opal-CT structures occur together with micro- and megaquartz on the mm to cm scale. Occasionally, Opal-CT also occurs as a fibrous margin around chalcedony-filled pores.

The types of opal vary with the replaced materials. Wood preserved delicate cellular features, two different types of cracks, and a mixture of opal, anatase and kaolinite. A strongly silicified breccia is made up of ooid structures, that consist of Opal-A, co-existing in a single clast with orthoclase, (Ba, Ce)-gorceixite-florencite, alunite, barite and possibly goyazite.

X-ray powder diffractograms after heating experiments show decreasing Opal-A, increasing size of coherent scattering regions and shifting of characteristic peaks towards more ordered phases. The FWHM decreased markedly. Opal-A samples initially possess varying degrees of crystallinity.

The mean water content of Opal-A is in the range of 4 - 7 wt% with a positive correlation between the water content and the FWHM. Opal-CT contains up to 9.5 wt% water, owing to adsorbed water in the pore space between the individual platelets. Impurities of all Opal-A samples are Al, Fe, Ca and Na, all but Al appearing only in traces (< 1000 ppm). The size of Opal-A spherules correlates positively with the sodium content, lending support to an assumption by Stewart et al. (2010) that points to the role of the most abundant salts for opal shell precipitation.

In some limonite nodules round structures (ca. 1 µm in diameter) were found with marked enrichment in P_2O_5-, SO_3- and MnO. They might attest to the role of microorganisms during opal formation. Similar enrichment was also found in pseudomorphs after rhombic crystals.

The dissolution-reprecipitation processes leading to the formation of opal are a complex interplay of factors such as pH, chemistry of involved solutions, composition of the host material, temperature, pressure and time. The key to its understanding is on the chemical and structural micro- and nanoscale.

References

Stewart, A. M., Chadderton, L.T., Senior, B.R., 2010. Self-assembly in the growth of precious opal. *Journal of Crystal Growth*, 312(3), pp. 391-396.

P09-P09
Search for new compositions using new crystallographic data bases

B. Kodess[1], P. Kodess[2]
[1]ICS@E-VNIIMS, Metrology of Crystals, Moscow, Russian Federation
[2]ICS&E, Materials Science, Aurora, CO, United States

Some of the features of making new materials which have better performance characteristics are considered. Previously, there has been already developed various methods of investigating and developing various compositions, such as factor analysis, which helped reduce the number of testing combinations. The successful implementation of the results of the factor analysis largely depends on the suggested initial hypothesis, on the amount of dispersion subject to be explained, on clearly defined main factors and therefore properly defining the notions of these factors. Many factors can be in different directions and thus influence the final requirement for the composition and structure.

The crystallographic data bases (DB) storing highly reliable data represent an additional reserve for better search of characteristics when identifying relations like composition-structure-dispersivity-properties. The DB have been used especially in connection with the extensive use of nano-fragmentary materials operating in aggressive environment and wing to DB we are developing a better technology of search based on a system-information approach. The system analysis serves as a basis for multi-criteria optimization process during selection of material compositions for assembling blocks. Therefore, the use of the system approach together with an expert evaluation provides building a flexible management system and making necessary decisions in fuzzy conditions.

These new approaches for optimization of composition and heat treatment conditions are being considered here for the purpose of obtaining materials with high strength and durable properties. Examples are given of the use of these new properties in valves for vehicle engines, for bearings and gears and other parts, having large loads. The changing of additive content in the suggested alloys is accompanied with the maintaining of the required level of safety and robust concerning assemblies.

P09-P10
Phase Relations and Thermodynamic Properties of 1.13 nm Tobermorite and Xonotlite

K.T. Fehr[1], R. Hochleitner[2], A. Günther[1]
[1]Ludwig-Maximilians Universität, Geo-& Umweltwissenschaften, München, Germany
[2]Mineralogische Staatssammlung, München, Germany

The physico-mechanical properties of steam cured building materials are determined by the type and the structure of the CSH phases. These binders are formed during the hydrothermal curing at elevated temperatures under saturated steam pressure.

Depending on the type of material and hardening temperature 1.13 nm tobermorite ($C_5S_6H_5$) or xonotlite ($C_6S_6H_6$) are the predominant phases with semicrystalline CSH-phases as minor components. Thermodynamic as well as kinetic studies [1] show, that 1.13 nm tobermorite in association with quartz is metastable and reacts to xonotlite and/or gyrolite ($C_4S_6H_5$).

It is the aim of industrial research to be able to predict the properties of steam cured building materials that are related to the amount and type of CSH phases formed. Unfortunately, accurate and reliable thermodynamic data for many of these phases are still missing. Furthermore, the phase associations in steam cured materials vary widely from experimentally obtained phase relations in the CSH system that have been surveyed by means of synthesis experiments [2,3,4]. CSH phases can be synthesised high above there field of stability as shown for xonotlite [5].

A Schreinemaker's analysis along the tie-line $CaSiO_3$-SiO_2-H_2O yield to 4 invariate points in the pressure region < 0.35 GPa. The field of stability for 1.13 nm tobermorite is limited by the reactions (1) 1.13 nm tobermorite = xonotlite + gyrolite + H_2O, (2) 1.13 nm tobermorite = xonotlite + truscottite + H_2O, (3) 1.13 nm tobermorite = xonotlite + quartz + H_2O.

The reaction (1) and (3) were determined in the pressure region 0.05 up to 0.35 GPa. Both reactions proceed in the field of stability of xonotlite with temperatures < 240°C [6].

Thermodynamic properties for enthalpy and entropy of xonotlite were calculated of the univariant reaction xonotlite = wollastonite + H_2O (4) and for 1.13 nm tobermorite of reaction (3). Heat capacities were obtained by use of low temperature DSC measurements.

[1] Zürn S.G. & Fehr K.T. (1996), Europ. J. Mineral., Vol. 8, Suppl. 1, 328.
[2] Buckner, D.A., Roy, D.M. & Roy, R. (1960), Amer.J.Sci., 258, 132-148.
[3] Harker, R.I. (1964), J.Amer.Ceram.Soc.;47, 521.
[4] Roy, D.M. & Roy, R. (1962), in 4th ISSC, Vol.1, 307.
[5] Gustafson, W.I. (1974), J.Petrol., 15, 455-496.
[6] Aghmaghani, A (1984), Diss. University of Hannover, p. 74.

P09-P11

Stability relations of xonotlite-polytypes within and beyond the stability field of xonotlite

A. Günther[1], K.T. Fehr[1], R. Hochleitner[2]
[1]University, Department of Earth & Environmental Sciences, Munich, Germany
[2]Museum, Mineralogical State Collection, Munich, Germany

The physico-mechanical properties of steam cured building materials are determined by the type and the structure of the Calcium-Silicates-Hydrates or CSH phases. These binders are formed during hydrothermal curing at elevated temperatures under saturated steam pressures. Depending on the type of material and hardening temperature 1.13 nm tobermorite or xonotlite are the predominant phases in addition with semi crystalline CSH-phases as minor components. The crystal chemistry of xonotlite ($Ca_6Si_6O_{17}(OH)_2$) is mainly controlled by its four different polytypes. For xonotlite four ordered monoclinic polytypes are known (M2a2b2c, M2a2bc, Ma2b2c, Ma2bc). In nature xonotlite mainly occur as intergrowths of two or more polytypes up to four polytypes as determined by x-ray powder diffraction (Bernstein et al., 2009). The thermal stability of xonotlite is represented by the univariant reaction xonotlite = 6 wollastonite + H_2O. Within the stability field xonotlites synthesized from wollastonite glass under hydrothermal conditions consist as intergrowth of up to four polytypes like natural samples. In all samples the M2a2b2c polytype was found but the predominance of the polytypes varies with temperature. Not only within its stability field but also far beyond xonotlite-crystals are consisting as intergrowths of varies polytypes and in addition, can be crystallized metastably at temperatures and pressures up to 400°C and 0.45 GPa, respectively.

Ref.: Bernstein, S.; Fehr, K.T. & Hochleitner, R. (2009): Crystal chemistry of Xonotlite $Ca_6Si_6O_{17}(OH)_2$. Part I: Determination of polytypes using X-Ray Powder Diffraction (XRPD). N. Jb. Min. 186, 153-162

P10-P01

Crystal Structure and Thermochemical Classification of Ba_2In

M. Bischoff[1], R. Niewa[1]
[1]Universität Stuttgart, Institut für Anorganische Chemie, Stuttgart, Germany

In 1966 Bruzzone studied the systems Sr-In and Ba-In [1]. In the system Ba-In only the In-rich phases have been studied in detail [2]. According to the phase diagram of Bruzzone, several Ba-rich phases exist, but are not characterized at all, including a low-temperature and a high-temperature phase of Ba_2In. In 2010 $Ba_9[In]_4$ and $Ba_9[In]_4[H]$ [3, 4] with nearly identical unit cell and positional parameters of the metal atoms were presented. $Ba_9[In]_4$ was discussed to replace both polymorphs of Ba_2In in the phase diagram [3].

Recently, we have obtained single phase samples and crystals with the composition Ba_2In. Ba_2In crystallizes in the orthorhombic space group *Pnma* (No. 62) with the unit cell parameters a = 809.73(3) pm, b = 591.34(2) pm, c = 1093.90(4) pm (Co_2Si structure type). The crystal structure can be rationalized with an indium substructure realizing a slightly distorted hexagonal closed packing. Barium atoms are localized in all trigonal bipyramidal and octahedral holes. Both barium and indium atoms are slightly displaced from the ideal positions. $BaIn_6$ octahedra form a 3D-framework via edge- and face-sharing, leading to shortest Ba-Ba distances which are slightly shorter than in elemental barium. The trigonal bipyramids $BaIn_5$ form a three-dimensional framework via corner- and edge-sharing. The indium atoms are coordinated by 11 barium atoms. Ten of those form a polyhedron, which may be regarded as a trigonal prism of barium, whose two rectangular faces are single capped and the third one twice. Additionally, one edge is single capped.

Synthesis experiments at various temperatures and cooling rates exclusively resulted in the described modification of Ba_2In. Furthermore, differential thermal analysis was employed to check the presence of a second modification. On heating the as-cast sample one endothermal signal at 547 °C can be observed. This signal was assigned to the melting of the sample. During cooling as well as in every further heating cycle two signals appear. The second signal may lead to the conclusion that there should be a high-temperature modification, but we are unable to present any further indication for a solid-solid phase transition. In contrast, we assign the two signals to a peritectic reaction and a liquidus with comparably low slope. There was no sign of a significant homogeneity range within the atomic Ba:In-ratio from the structure refinements. Chemical analysis and ^1H NMR spectroscopy revealed the presence of minor hydrogen impurities in the range of 3 atom-%.

[1] G. Bruzzone, J. Less-Common Met. **11** (1966) 249-258.
[2] M. Wendorff, C. Röhr, Z. Anorg. Allg. Chem. **631** (2005) 338-349.
[3] V. Smetana, A. Simon, Z. Naturforsch. **65b** (2010) 643-645.
[4] M. Wendorff, H. Scherer, Z. Anorg. Allg. Chem. **636** (2010) 1038-1044.

Indium substructure (small grey spheres) stuffed with barium atoms (large dark-grey spheres). Coordination polyhedron surrounding In. Distances are given in pm.

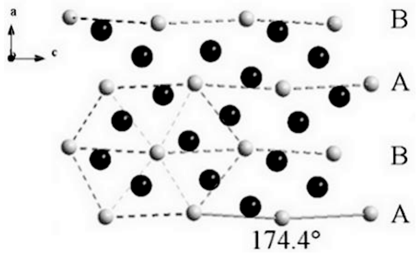

Figure 1

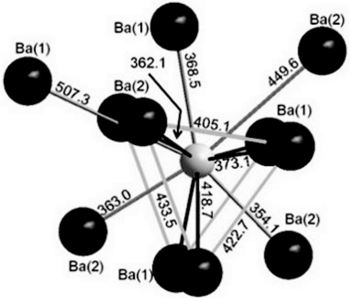

Figure 2

P10-P02
Luminescence of divalent europium in alkaline earth metal hydrides

N. Kunkel[1], H. Kohlmann[1]
[1]Universität des Saarlandes, Anorganische Festkörperchemie, Saarbrücken, Germany

Luminescence energies of divalent lanthanides including Eu(II) depend strongly on the chemical environment. Due to this dependence and the high intensity of the $4f^65d^1 \rightarrow 4f^7$ transitions, which are parity allowed and mostly involved in the emission process, the Eu^{2+}-ion shows remarkable luminescence properties[1]. The strong dependence of the emission energies on the coordination sphere makes the design of phosphors emitting different colors of radiation imaginable. However, studies on the constitution of the host lattice have focused mostly only oxides, halides, borates and nitrides. Although properties of several europium hydrides have been studied before [2], to the best of our knowledge, luminescence of divalent europium in a hydridic matrix, especially in alkaline earth metal hydrides, has never been studied before. For the pseudo-binary system $Eu_xSr_{1-x}H_2$ a complete solid solution series was found (a = 637.6(1) pm - 12.1(3)*x pm, b = 387.0(1) pm - 6.5(2)*x pm, c = 732.2(2) pm - 10.1(4)*x pm). Europium doped alkaline earth metal hydrides $Eu_xM_{1-x}H_2$ (M = Ca, Sr, Ba) with a small europium concentration (x = 0.005) were found to exhibit luminescence with a maximum emission wavelength of 764 nm (M = Ca), 728 nm (M = Sr) and 750 nm (M = Ba). The emission energy shows an extremely large redshift compared to for instance $SrF_2:Eu^{2+}$ 416 nm or $SrO:Eu^{2+}$ 625 nm [1], which may be due to the softness of the hydride ligand and its strong ligand field. Theoretical calculations (Wien2k [3], LDA+U) confirm a decrease in band gaps with an increase in the europium content of the solid solution. Considering the hydride fluoride analogy [4], it should be possible to substitute hydride by fluoride and vice versa in order to design a continuously variable radiation of almost any desired colour.

References
[1] P. Dorenbos, *J. Lum.*, **2003**, *104*, 239.
[2] H. Kohlmann, *Eur. J. Inorg. Chem.*, **2010**, 2582.
[3] P. Blaha, K. Schwarz, P. Sorantin, *Comput. Phys. Commun.*, **1990**, *59*, 399.
[4] C. E. J. Messer, *J. Solid State Chem.*, **1970**, *2*, 144.

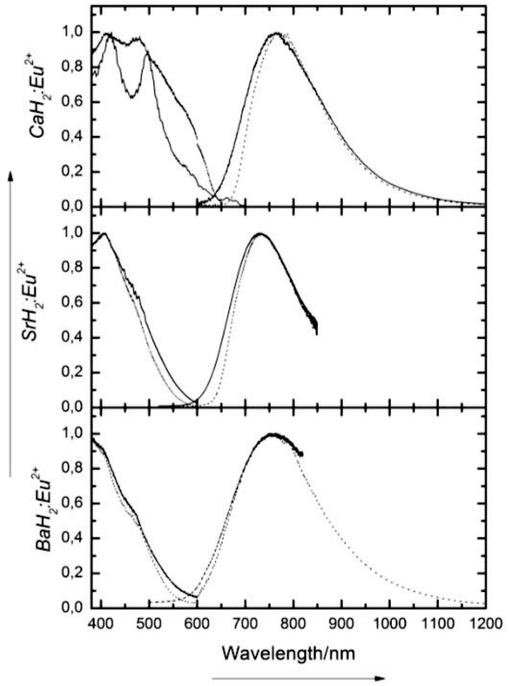

Figure 1: Luminescence spectra of $MH_2:Eu^{2+}$ (M = Ca, Sr, Ba; 0.5 Mol% Eu2+). Solid lines correspond to spectra measured at room temperature, dotted lines at 10 K. Band below 600 nm originates from excitation, emission band above 600 nm. Intensity is in arbitrary units.

P10-P03
Gemischte Thiooxowolframate $A^I_2[W^{VI}S_xO_{4-x}]$

A. Lehner[1], M. Braitsch[1], R. Caroline[1]
[1]Univ. Freiburg, Anorg. Chemie, Freiburg, Germany

Gemischte Thiooxoorthowolframate(VI) $[WS_xO_{4-x}]^{2-}$ wurden erstmals im 19. Jahrhundert dargestellt [1,2]. Die spektroskopischen Eigenschaften dieser Ionen wurden intensiv untersucht [3], während kaum detaillierte Studien der Kristallstrukturen ihrer Salze vorliegen [4]. Wir präsentieren hier die erste systematische Untersuchung der Kristallchemie von Alkalimetall- und Ammoniumthiooxowolframaten anhand von Röntgendiffrakto-metrie und Bandstrukturrechnungen. Die Strukturchemie und Bindungssituation wird dabei im Vergleich mit den Ergebnissen unserer Untersuchung analoger Thiooxomolybdate [5,6] vorgestellt. Die Synthesen der Salze $A_2[WS_xO_{4-x}]$ (A = NH_4: x = 2; A = K, Rb: x = 1,2,3; A =Cs: x = 2,3) erfolgte durch Einleiten von H_2S-Gas in alkalische Lösungen der Oxowolframate. Aus den gelben Thiooxowolframatlösungen ließen sich die Salze phasenrein und einkristallin erhalten. Die Verbindungen weisen weit mehr polymorphe Formen auf als bisher erwartet wurde: zusätzlich zu drei bekannten A_2BX_4-Typen wurden vier neue Strukturtypen erhalten. Die Monothiowolframate von K^+ und Rb^+ kristallisieren als Hydrate. Während alle Verbindungen mit $[WS_2O_2]^{2-}$-Anionen isotype monokline Strukturen

($(NH_4)_2[WS_2O_2]$-Typ, $C2/c$, z.B. $K_2[WS_2O_2]$: a = 1126.5(4), b = 708.2(2), c = 971.5(4) pm, β = 121.86(3)°) bilden, sind die K^+- und Cs^+-Salze dimorph und kristallisieren zusätzlich in den bisher unbekannten Strukturtypen ($P2_1/c$ bzw. $Pbcn$). Die Trithiowol-framate von Rb+ und Cs+ kristallisieren im orthorhomischen β-$K_2[SO_4]$-Typ ($Pnma$), der auch von den Tetrathiowolframaten gebildet wird. Am Beispiel der Cs-Dithiooxowolframate wurde der thermisch induzierte Phasenübergang (bei ca. 100 °C) von der orthorhombischen

Struktur (*Pbcn*, $V_{Formeleinheit}$ = 805 10^6 pm^3) in die monokline Form ($(NH_4)_2[WS_2O_2]$-Typ, *C*2/*c*, $V_{Formeleinheit}$ = 797 10^6 pm^3) thermoanalytisch untersucht. Bei ca. 260 °C tritt unter Volumenzunahme eine Umwandlung in eine neue Phase im β-$K_2[SO_4]$-Typ (*Pnma*) ein. In den wasserfreien Salzen sind die $[WS_xO_{4-x}]^{2-}$-Anionen so gepackt, dass die Oxo-Liganden vier- bis fünffach durch Kationen koordiniert sind, während die Thio-Liganden Koordinationszahlen von 6 bis 7 aufweisen. Die Anordnung der Wolframattetraederanionen lässt sich auf einfache Metallpackungen zurückführen. Die Strukturen der Salzhydrate und Ammoniumsalze werden hinsichtlich ihrer Wasserstoffbrückenstruktur diskutiert.

Die Bindungssituation wird anhand der Zustandsdichten aus FP-LAPW-Bandstrukturrechnungen auf Basis der experimentellen W-S-/W-O- Abstände analysiert.

[1] E. Corleis, Liebigs Ann. Chem. 1886, 232, 244-270. [2] G. Krüss, Liebigs Ann. Chem. 1884, 225, 1. [3] K. H. Schmidt, A. Müller, Coord. Chem. Rev. 1974, 14, 115. [4] A. Müller, W. Sievert, Z. Anorg. Allg. Chem. 1974, 403,251. [5] A. Lehner, K. Kraut, C. Röhr, Acta Crystallogr. 2010, A66, 186. [6] A. Lehner, C. Röhr, Z. Anorg. Allg. Chem. (in Vorbereitung).

Kation	Anion		
	$[WSO_3]^{2-}$	$[WS_2O_2]^{2-}$	$[WS_3O]^{2-}$
$(NH_4)^+$		◆	
K^+	△, ◊	◆,●	
Rb^+	▼	◆	■
Cs^+		◆, □	■

Symbol	Strukturtyp	Raumgruppe
◊	$K_2[MoO_4]$-Typ	$C2/m$
△	eigener Typ, $K_2[WSO_3]\cdot 1.5\ H_2O$	$C2/c$
▼	eigener Typ, $Rb_2[MoSO_3]\cdot H_2O$	$R\bar{3}m$
◆	$(NH_4)_2[WS_2O_2]$-Typ	$C2/c$
●	eigener Typ, $K_2[MoS_2O_2]$	$P2_1/c$
□	eigener Typ, $Cs_2[MoS_2O_2]$	$Pbcn$
■	β-$K_2[SO_4]$-Typ	$Pnma$

Figure 1

P10-P04

Zn-Indide der Alkalimetalle mit der Anionenstruktur des ß-rhomboedrischen Bors

V. Mihajlov[1], C. Röhr[1]
[1]Universität Freiburg, Anorg. und Analyt. Chemie, Freiburg, Germany

ß-rhomboedrisches Bor, ß-B_{105} (trig., *R*-3*m*, Z = 3), ist eine der allotropen Modifikationen des elementaren Bors. Die Kristallstruktur besteht aus zwei kristallographisch unterschiedlichen B_{12}-Ikosaedern im Verhältnis 1:3 und zwei verbrückten kondensierten Dreifachikosaedern B_{28}, die über exo-Bindungen miteinander verknüpft sind (Abb. 1). Sie stellt eine hierarchische Variante von $MgCu_2$ dar, bei der die Ikosaeder die Cu- und die Dreifachikosaeder die Mg-Plätze einnehmen ($(B[B_{28}]_2B_{12}(B_{12})_3)$). Einkristallstrukturanalysen zeigen, dass entsprechend der Wade-Regeln nicht alle Borlagen der B_{28}-Einheit voll besetzt sind [1].

Analoge Gallide und Indide existieren aus sterischen Gründen nur mit A^+ in den Lücken , z.B. $Na_{26}K_8Ga_{99.1}$ [2] oder $K_{14}Na_{20}In_{96.3}$ [3]. Die Elektronenbilanz wird entsprechend durch stärker ausgedehnte Defekte im Anionenteilgitter wiederhergestellt [4].

Ein Ausgleich des durch die zusätzlichen *A*-Atome eingebrachten Elektronenüberschusses kann durch den Einbau von elektronenärmeren Elementen der späten Übergangsmetallreihe erreicht werden, z.B. in $K_{34}Zn_{18.8}In_{86.2}$ [5]. Ausgehend von dieser defektfreien Phase wurde der sterische Einfluss der Kationengröße auf die Struktur systematisch durch Austausch der Alkalimetalle röntgenographisch anhand von Einkristalldaten untersucht. Das Zn/In-Verhältnis bleibt dabei annähernd gleich, die Valenzelektronenkonzentration (vec) pro *M* beträgt 3.16 und liegt damit im engen Bereich zwischen 3.10 und 3.38, in dem alle Verbindungen mit diesem Strukturtyp auftreten. Berechnungen der elektronischen Strukturen mittels FP-LAPW-DFT-Methoden zeigen in Übereinstimmung hiermit ein deutlich ausgeprägtes Minimum in der totalen Zustandsdichte am Ferminiveau.

Drei der sechs Kationenpositionen *A*(1, 2, 3) (Σ 14 Atome) weisen eine kleinere Koordinationssphäre mit der Koordinationszahl (CN) 12 (gekappte Tetraeder) und die Positionen *A*(4, 5, 6) (Σ 20 Atome) eine größere mit einer CN von 15 bzw. 16 auf.

Ausgehend von $K_{34}Zn_{18.8}In_{86.3}$ führte der sukzessive Austausch von K^+ durch das kleinere Kation Na^+ zu der Grenzzusammensetzung $K_{14}Na_{20}Zn_{16.7}In_{88.3}$ (a = 1771.44(5), c = 3890.7(2) pm), bei der alle *A*(1, 2, 3)-Lagen mit Na^+ und *A*(4, 5, 6)-Lagen mit K^+ besetzt sind. Umgekehrt erfolgte der Austausch von K^+ auf den Lagen *A*(4, 5, 6) durch größere Kationen ebenfalls nahezu vollständig, so dass $Rb_{13.3}K_{20.7}Zn_{18.9}In_{86.1}$ und $Cs_{12.3}K_{21.7}Zn_{19.2}In_{85.8}$ (a = 1838.30(5)/1846.27(9), c = 4017.97(2)/4039.7(2) pm) die Randverbindungen darstellen.

Als Bildungsvoraussetzung für den vorgestellten Strukturtyp können somit zum einen der bereits erwähnte enge vec-Bereich und zum anderen ein Kationen/Anionen-Radienverhältnis von r_A/r_M = 0.97 - 1.14 für die Lagen *A*(1) bis *A*(3) bzw. r_A/r_M = 1.14 - 1.31 für *A*(4) bis *A*(6) genannt werden.

[1] G. A. Slack, C. I. Hejna, M. F. Garbauskas, J. S. Kasper, *J. Solid State Chem.*, **76**, 52 (1988).
[2] C. Belin, M. Charbonnel, *J. Solid State Chem.*, **64**, 57 (1986).
[3] B. Li, J. D. Corbett, *JACS*, **127**, 926 (2005).
[4] C. Belin, M. Charbonnel, *Coord. Chem. Rev.*, **178-180**, 529 (1998).
[5] B. Li, J. D. Corbett, *Inorg. Chem.*, **45**, 8958 (2006).

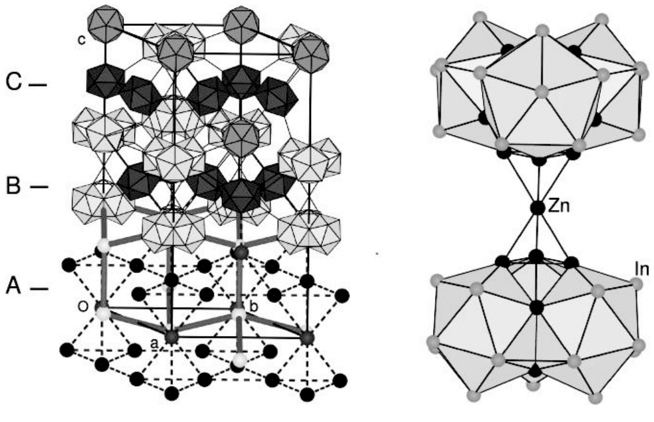

Figure 1

P10-P05

Zwischen Zintl, Hume-Rothery und Laves: *M*-reiche intermetallische Phasen A^2-M^{12}-M^{12} (A^2 = Ca, Sr, Ba / M^{12} = Zn, Cd, Hg)

M. Schwarz[1], C. Röhr[1]
[1]Albert-Ludwigs-Universität , Institut f. Anorg. u. Anal. Chemie, Freiburg, Germany

Intermetallische Phasen der Erdalkalimetalle (A^2) mit Elementen der Gruppe 12 (M^{12}) weisen eine vielfältige Strukturchemie auf, die geprägt ist vom Ladungsübertrag von A^2 auf M^{12} (Größe: ΔEN_{A-M}), der Valenzelektronenkonzentration (v.e.c.) und geometrischen Einflüssen(r_A/r_M) . Als binäre *M*-reiche Phasen sind der $NaZn_{13}$-Typ, der $BaCd_{11}$-Typ und mit gleicher Zusammensetzung der $BaHg_{11}$-Typ bekannt. Um Erkenntnis über die strukturbestimmenden Faktoren zu gewinnen, wurden die M^{12}-Atome, die sich bezüglich ihrer EN und Radien unterscheiden, gegeneinander ersetzt. Die Synthesen der ternären Verbindungen erfolgte aus den Elementen bei 750°C. Die Strukturaufklärung erfolgte mittels Röntgenbeugung an Einkristallen.

Ausgehend von den binären Randverbindungen A^2Zn_{13} [1] (A^2 = Ca, Sr, Ba; $NaZn_{13}$-Typ, kubisch, $Fm3c$, CsCl-analoge Anordnung von Snubcubes und Ikosaedern, Abb. a) konnte Zn durch Hg/Cd zu 4/0 % für das Ca-, zu 22/5 % für das Sr- und zu 35/0 % für das Ba-Zinkid ersetzt werden. Allen ternären, wie auch den bereits bekannten binären Verbindungen ist gemein, dass das Ikosaederzentrum statistisch unterbesetzt ist, so dass das Ferminiveau mit dem Minimum der Pseudobandlücke (berechnet mit FP-LAPW) zusammen fällt.

Für Verbindungen mit $BaCd_{11}$-Typ (binäre Randphasen: $CaZn_{11}$ [2], $SrCd_{11}$, HP/HT-$SrZn_{11}$ [3] und $BaCd_{11}$ [4], tetragonal, $I4_1/amd$, Abb. b) wurde dieselbe Tendenz zur Vergrößerung der Phasenbreiten von Ca zu Ba beobachtet. Für das Ca-Zinkid wurde Zn durch Hg/Cd zu 2/9 %, für das Sr-Cadmid wurde Cd durch Hg zu 18 % und für das Ba-Cadmid wurde Cd durch Hg/Zn zu 54/13 % ersetzt. Die sich durch ihre deutlich größere Koordinationssphäre von den anderen *M*-Atomlagen unterscheidende Lage *M*(1) in den Kanälen wird dabei bevorzugt vom größeren *M* besetzt [5], was sich vor allem bei den Ca-Zinkiden bemerkbar macht, bei denen Cd bzw. Hg ausschließlich auf dieser Lage eingebaut wird.

Ausgehend vom Mercurid $SrHg_{11}$ ($BaHg_{11}$-Typ, kubisch, $Pm3m$, Abb. c) wurde Hg bis zu einem Gehalt von 45 % durch das ähnlich große aber weniger elektronegative Cd ersetzt, was den Existenzbereich dieses Typs bezüglich ΔEN_{A-M} hin zu kleineren Werten erheblich erweitert.

Zusätzlich konnte die in einem neuen Strukturtyp kristallisierende Verbindung $Ba_3Hg_{9.9}Zn_{1.1}$ ($Pmmn$, a = 701.2(3), b = 1706.9(8) und c = 627.3(3) pm, Abb. d) erhalten und charakterisiert werden. Die Struktur besteht aus Zick-Zack-Ketten aus alternierend orientierten Pyramidenschichten ähnlich denen in $BaAl_4$, die Kanäle an den Abknickstellen der Schichten ähneln mit der darin enthaltenen *M*-Lage *M*(5) denen in $BaCd_{11}$.

[1] M. Wendorff, C. Röhr. *J. Alloys Compds.* **421**, 24 (2006).
[2] M. Wendorff, C. Röhr. *Z. Naturforsch.* **62b**, 1549 (2007).
[3] S. Kal, E. Stoyanov, Th. L. Groy, U. Haussermann. *Acta Crystallogr.* **C63**, i96 (2007).
[4] G. Bruzzone, *Gazz. Chim. Ital.* **102**, 234 (1972).
[5] V. Mihajlov, C. Röhr, *Z. Anorg. Allg. Chem.* **636**, 1792 (2010).

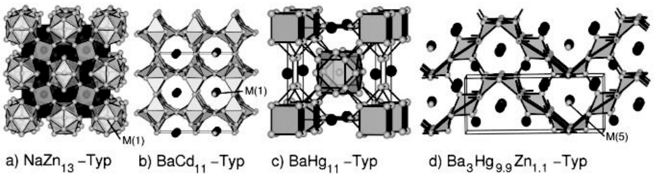

a) $NaZn_{13}$-Typ b) $BaCd_{11}$-Typ c) $BaHg_{11}$-Typ d) $Ba_3Hg_{9.9}Zn_{1.1}$-Typ

Figure 1

P10-P06

Anomalous compression behaviour of quartz and SiO_2-glass - a high pressure study up to 1,5 GPa

P. Mirwald[1], T. Loerting[2]
[1]Univ. Innsbruck, Institute Mineralogy & Petrography, Innsbruck, Austria
[2]Univ. Innsbruck, Institute Chemical Physics, Innsbruck, Austria

The PVT-behaviour of homogeneous phase is assumed to be characterized by continuous properties, only terminated by phase transitions. However, an increasing number of observations indicate that solids may exhibit PVT anomalies. Among the silicates anomalous compression behaviour was found for zeolites and cordierite [1-3], both representing oxidic frame work structures characterized by cages which tend to incorporate H_2O in considerable amounts.

A frame work silicate without that property is quartz. Based on previous compression work [4-6] we re-examined the isothermal compression behaviour of quartz and SiO_2-glass up to 1.5 GPa at room temperature using a piston cylinder apparatus which allows a resolution of the piston displacement (Pd) in the order of 10^{-4} and a pressure monitoring in 0.33 MPa intervals. Pb and NaCl being characterized by continuous and high compressibility were used as reference materials.

Fig. 1 shows as an example the behaviour of quartz, of the piston-displacement ($\Delta Pd/\Delta P$; ΔP=10 MPa) vs. pressure which has been derived from the compression loop (inset). In accordance with previous work [4, 5] a broad anomaly is observed which sets in at 0.35 and ends at 0.85 GPa appearing as a hump in the $\Delta Pd/\Delta P$-track of the compression (P_{up}) and decompression stroke (P_{down}). A strikingly similar anomalous behaviour was observed for SiO_2 glass with a similar hump in the $\Delta Pd/\Delta P$-track between 0.35 and 0.85 GPa .

While the general compressional volume decrease of the two SiO_2 materials is mainly to be related to a gradual diminution of the spaces between the SiO_4 groups by Si-O-Si angle bending, tetrahedral distortion and very slight Si-O bond compression, e.g. [7], this anomaly displayed at strikingly similar pressure by both materials, rather insinuates a specific change in the interaction of oxygen over the pressure interval.

[1]Hazen, R.M. (1983): Science, 219, 1065.
[2]Belitzky, I. A. et al. (1992): Phys. Chem. Min., 18, 497.
[3]Mirwald, P.W. et al. (1984): Phys. Chem. Min., 11, 140.
[4]Bridgman, P.W. (1925): Am. J. Sci., 10, 359.
[5]Bridgman, P.W. (1928): Am. J. Sci., 15, 287.
[6]Adams, L.H. & Gibson, R.E. (1931): J. Wash. Acad. Sci., 21, 381.
[7]Thompson, R.M. & Downs, R.T., (2010): Am. Min., 95, 104.

Fig.1: Compression behaviour of quartz up to 1.5 GPa at 23°C. Plot of piston displacement differences (ΔPd)/10 MPa vs. pressure derived from the compression loop displayed in the inset.´

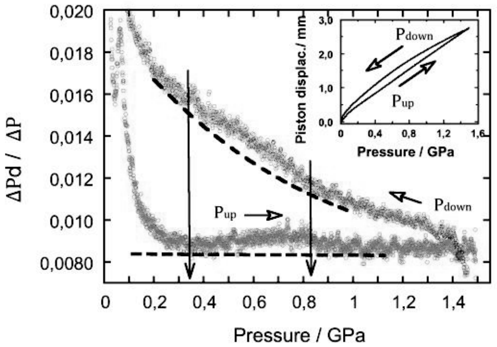

Figure 1

P10-P07

Crystal Structure Analysis of Layered Compounds Cr_xTiS_2

K.-I. Ohshima[1], S. Ikeda[1], T. Kawasaki[1], M. Takahashi[1]
[1]University of Tsukuba, Institute of Materials Science, Tsukuba, Japan

A single-crystal X-ray structure analysis of Cr_xTiS_2 (x=0.22, 0.31, and 0.72) at room temperature has been performed to investigate both the ordered atomic arrangements of intercalated Co atoms and their site occupancies, as well as the nature of the chemical bond from the electron density distribution (EDD) obtained by the maximum entropy method. The superstructures of the Co atoms are observed to be 2ax2ax2c unit cells for x=0.22 , and $\sqrt{3}$ax$\sqrt{3}$ax2c unit cells for x=0.31 and 0.72 The overlapping of EDDs between Cr and S atoms and Ti and S atoms corresponds to the covalent bonding in the van der Waals gap layer and TiS_2 layer. It is found that the nature of the covalent bonding between Cr and S atoms causes a decrease in the interatomic distance.

P10-P08

Investigation of structural phase transitions in Letovicite (NH4)3H(SO4)2 at low

Y.J. Sohn[1], K. Sparta[1], S. Prinz[1], M. Meven[2], G. Roth[1], G. Heger[1]
[1]Institut für Kristallographie, RWTH Aachen University, Aachen, Germany
[2]FRM II, TU München, Garching, Germany

Letovicite $(NH_4)_3H(SO_4)_2$ (TAHS) undergoes five successive phase transitions at atmospheric pressure [1]. The rhombohedral (*R-3m*) high-temperature phase I of TAHS is known for its superprotonic conductivity [2] and a detailed crystal structure analysis was done with single-crystal neutron diffraction [3]. Most characteristics of monoclinic (*C2/c*) TAHS-II at room temperature are the H-disorder in a $(SO_4)H(SO_4)$ dimer and the reorientational behaviour of the ammonium groups [4] . Since the H-disorder plays a significant role in structural phase transitions of Letovicite, single-crystal neutron diffraction was necessary. Our previous X-ray studies with an image plate detector (STOE-IPDS II) showed some additional superstructure reflections. This was interpreted as a doubling of the monoclinic unit cell in **b** direction. With this knowledge, a complete dataset of Bragg reflection intensities was collected at the four-circle diffractometer HEiDi at FRM II using a single-crystal of TAHS (3x3x3 mm^3) up to $\sin\theta/\lambda = 0.7$ Å-1 ($\lambda = 0.87$ Å) at 138.5 K. The III/IV-phase transition has a second-order character and the crystal structure of TAHS-IV was refined using JANA2006 [5]. Due to the large number of required parameters, certain constraints had to be made in the refinement process. The crystal structure analysis of TAHS-IV indicated a slight rotation of SO_4 tetrahedra and of NH_4 groups along the **b** axis. This reorientation may result from the stronger N-H···O hydrogen bond networking between the NH_4 and the SO_4 tetrahedral groups in TAHS-IV. The IV/V-phase transition of TAHS has a first-order character and shows a clear hysteresis. According to the observation of a twinning in phase V no further neutron diffraction measurements could be performed, since the separate collection of those twinned reflections (up to four times) was impossible. However, the much smaller crystal used for X-ray diffraction seemed to have survived the IV/V-phase transition and no distinct evidence of a possible twinning was detected. The crystal structure analysis of TAHS-V indicated the triclinic space group symmetry (*P-1*) with lattice parameters very well corresponding to the literature values [6] as well as those obtained from our own X-ray powder diffraction experiments. Further crystal structure studies of TAHS-V have been carried out using SIR2002 [7] and SHELXL97 [8].

References
[1] K. Gesi, *Phys. Status Solidi.* **33** (1976) 479.
[2] L. Schwalowsky V. Vinnichenko, A. Baranov, U. Bismayer, B. Merinov & G. Eckold, *J. Phys. Condens. Matter*, **10** (1998) 3019.
[3] Y. J. Sohn, K. M. Sparta, M. Meven & G. Heger, *Acta Cryst.* B**67** (2011) 116.
[4] Y. J. Sohn, A. Loose, M. Merz, K. Sparta, H. Klapper & G. Heger, *Acta Cryst.* B**65** (2009) 36.
[5] V. Petricek, M. Dusek & L. Palatinus, JANA2006, *The crystallographic computing system.* Institute of Physics, Praha, Czech Republic (2006).
[6] P. M. Dominiak, J. Herold, W. Kolodziejski & K. Wozniak, *Inorg. Chem.* **42** (2003) 1590.
[7] M.C. Burla, M. Camalli, B. Carrozzini, G. L. Cascarano, C. Giacovazzo, G. Polidori & R. Spagna, *J. Appl. Cryst.* **36** (2003) 1103
[8] G. M. Sheldrick, *Acta Cryst.* A**64** (2008) 112.

P10-P09

Dimorphic $Ce_4N_2Se_3$ with Orthorhombic $Ce_4N_2Te_3$- and Monoclinic $Nd_4N_2Se_3$-Type Structure

F. Lissner[1], T. Schleid[1]
[1]Institut fuer Anorganische Chemie, Universitaet Stuttgart, Stuttgart, Germany

In the last 15 years, nitride chalcogenides of the lanthanides (and their halide derivatives) have been demonstrated to possess an extremely rich chemistry of formula and structure types [1], which are dominated by N^{3-} anions in tetrahedral neighbourhood of M^{3+} cations (M = La - Nd, Sm, Tb - Dy). For ternary nitride chalcogenides with the composition $M_4N_2Ch_3$ (Ch = S, Se, Te) five different types of crystal structures are known up to now.

The oxidation of cerium powder with selenium and sodium azide (NaN_3) yields the nitride selenide $Ce_4N_2Se_3$. Additional sodium chloride (NaCl) as flux secures fast reactions (7 d) at 900 °C in evacuated silica tubes as well as the formation of almost black single crystals. Dependent on the actual conditions of this reaction (using cerium trichloride or iodine) $Ce_4N_2Se_3$ can appear in two different crystal structures.

Three crystallographically independent Ce^{3+} cations, one N^{3-} and two Se^{2-} anions build up the orthorhombic $Ce_4N_2Te_3$-type structure [2] of $Ce_4N_2Se_3$ (A-type: *Pnma*, Z = 4; a = 702.78(2), b = 1141.27(5), c = 1088.10(5) pm). The cations reside in *sixfold* (2x) and *sevenfold* (1x) coordination of the anions forming (capped) trigonal prisms. The linkage of the $[NCe_4]^{9+}$ tetrahedra via *trans*-oriented edges induces corrugated strands $[NCe_{4/2}^{e}]^{3+}$ explainable by the alternating edges (Ce3···Ce3: containing a centre of symmetry, Ce1···Ce2: without any symmetry, Fig. 1). The strands get bundled along [010] like a hexagonal rod packing and are held together by the Se^{2-} anions.

In the monoclinic structure of $Ce_4N_2Se_3$ with $Nd_4N_2Se_3$-type setting [3] (B-type: *C2/c*, Z = 4; a = 1315.67(5), b = 1020.28(5), c = 651.32(2) pm, β = 90.083(2)°) only two different Ce^{3+}, one N^{3-} and two Se^{2-} ions occur. In this compound, the $[NCe_4]^{9+}$ units are first edge-linked (Ce1···Ce1) to bitetrahedra $[N_2Ce_6]^{12+}$, which then become cross-connected to $[N(Ce1)_{2/2}^{e}(Ce2)_{2/2}^{v}]^{3+}$ layers via their remaining four vertices (Ce2) (Fig. 2). The coordination numbers of the Ce^{3+} cations once again are *six* and *seven* relative to the anions (N^{3-} and Se^{2-}).

More details about the crystal structure parameters can be obtained from the Fachinformationszentrum (FIZ) Karlsruhe on quoting the depository number CSD-423104 (A-Type $Ce_4N_2Se_3$) and CSD-423105 (B-type $Ce_4N_2Se_3$).

[1] Th. Schleid, F. Lissner, *J. Alloys Compds.* **2008**, *451*, 610.
[2] F. Lissner, Th. Schleid, *Z. Anorg. Allg. Chem.* **2005**, *631*, 1119.

[3] F. Lissner, Th. Schleid, *Z. Anorg. Allg. Chem.* **2003**, *629*, 1027; *Z. Anorg. Allg. Chem.* **2005**, *631*, 427.

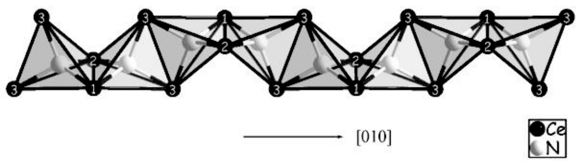

Figure 1: Linkage of *trans*-oriented edges of the $[NCe_4]^{9+}$ tetrahedra induces corrugated strands $[NCe_{4/2}^{e}]^{3+}$ in the $Ce_4N_2Te_3$-type structure.

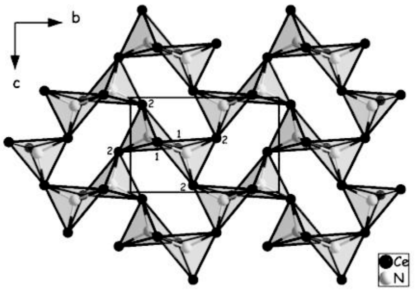

Figure 2: Bitetrahedra $[N_2Ce_6]^{12+}$ of edge-linked $[NCe_4]^{9+}$ units become cross-connected to $[N(Ce1)_{2/2}^{e}(Ce2)_{2/2}^{v}]^{3+}$ layers via their remaining four vertices in the $Nd_4N_2Se_3$-type structure.

P10-P10

Synthesis and characterisation of nano- and micro-sized NaB(OH)4-sodalites

A. Schulz[1], C. Rüscher[1], J.-C. Buhl[1]
[1]Leibniz Universität Hannover, Mineralogie, Hannover, Germany

A new synthesis route obtaining nano sized NaB(OH)4-sodalite has been developed. A characterisation could be achieved in comparison with the dehydration behaviour of micro crystalline NaB(OH)4-sodalite [1-3].

Teflon cups for the creation of autogeneous water pressure were filled with appropriate amounts of sodiummetasilicate, sodiumaluminate, Boracid and sodium hydroxide. The autoclaves were typically heated at 60°C using reaction times between 4 and 24 hours, which generates NaB(OH)4 sodalite with average crystal sizes between 35 and 100 nm. Follwing the procedure described earlier [1] where a solution of kaolinite, Boracid and sodium hydroxide is used together with heating at 200°C for 48 h typically microcrystalline samples are obtained. Samples were then systematically heated up to 200, 250, 300, 350, 400 and 450°C under He dry conditions in an TG/DTA apparatus (Setaram Setsys Evolution) recording the appropriate signals. The samples were further characterized by infrared absorption spectroscopy (KBr-method, Bruker Vertex 80v), and XRD (Bruker D4).

Enlarged part of the typical sodalite type XRD pattern of nano and micro sized NaB(OH)4 sodalites are compared in Fig. 1. The peak halfwidth of the nano-material proofs to be significantly larger compared to the micro crystalline sample, indicating the much smaller crystal size. Moreover there is a broad additional X-ray scattering indicating a significant non-crystalline contribution in the nanocrystalline sample. This can be related to some hydrosodalite type phase containing larger amount of water as shown in the IR absorption spectra (Fig. 2). Two steps of dehydration for samples heated at 200°C and 400°C are observed, namely BO(OH)2- and BO2-sodalite respectively, which was also observed for the microcrystalline sample. It could be shown that both forms nearly completely rehydrates for the nanocrystalline samples (Fig. 2 upper spectra) as well as for the microcrystalline samples even within the KBr pellet. This observation could be important concerning a better understanding and the optimisation of hydrogen reinsertion in (BHx-(OH)y-Oz)-zoned sodalite crystal systems [4]. Rehydration of outer zones of BO2-containing sodalites obtained in IR absorption spectra during heating experiments of micro and nano NaBH4-sodalites has been suggested, too [5].

[1] H.-H. E. Pietsch, M. Fechtelkord, J.-Chr. Buhl, J. Alloys Comp. 257 (1997) 168-174.
[2] C. H. Rüscher, J.-Chr. Buhl, Z. Krist. Suppl. 15 (1998) 113.
[3] C. H. Rüscher, Microp. Mesop. Mat. 86 (2005) 58-68.
[4] L. Schomborg, C. H. Rüscher, J.-Chr. Buhl. this issue.
[5] J.-Chr. Buhl, L. Schomborg, C. H. Rüscher, Microp. Mesop. Mat. 132 (2010) 210-218.

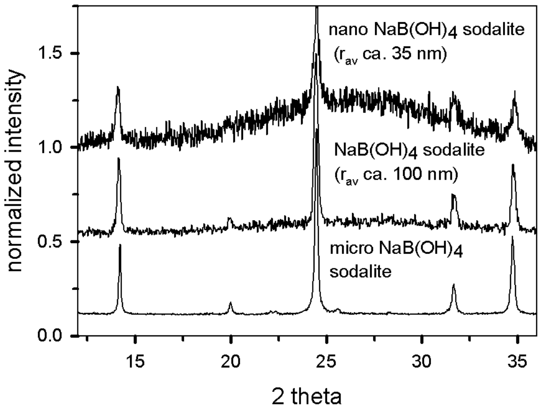

Fig. 1 Selected range XRD pattern of micro and nano-sized Na(BOH)4-sodalite, average crystal size as denoted.

Figure 1

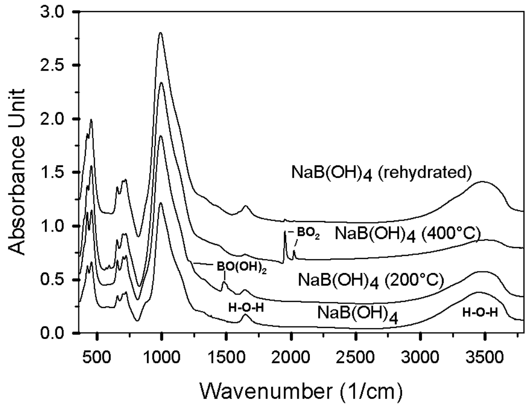

Fig. 2 IR- absorption of nano-sized Na(BOH)4-sodalite, heated at 200°C, 400°C and rehydrated.

Figure 2

P10-P11

Synthesis of Sodium Zincophosphate Sodalite influenced by Sodium-Polyacrylate and Triethanolamine

L. Robben[1,2], J.-C. Buhl[2], T.M. Gesing[1]
[1]Uni Bremen, Chemische Kristallographie fester Stoffe, Bremen, Germany
[2]Leibniz Universität Hannover, Institut für Mineralogie, Hannover, Germany

Sodium zincophospate sodalite synthesis was first described by Gier and Stucky [1]. Due to the quick and easy synthesis, resulting in highly crystalline material, this system is an ideal model system to study different aspects of the synthesis of sodalites. Here we describe the influence of two additives (sodium polyacrylate - PA; triethanolamine - TEA) on the synthesis products. PA is known to influence the morphology of $BaSO_4$ mesocrystals forming in an aqueous solution by its concentration [2]. TEA as an additive during synthesis of sodium alumosilicate chloride sodalite is able to lead to nano-crystalline products at low temperatures [3].

The synthesis (modified from Gier and Stucky [1]) was conducted by mixing 24 mmol $ZnCl_2$ and 30 mmol H_3PO_4 in 30 ml H_2O. Adding 84 mmol NaOH as a 2M solution a slurry is formed by shaking the reaction vessel. After 24 hours a microcrystalline product of sodium zincophosphate sodalite is formed, which is purified by filtration, washing and drying. The additives were given into the synthesis solution before adding NaOH. Using PA as additive, the added amount was varied (0.01 g, 0.1 g and 1 g). The product was filtered after 24 h and dried at 333 K. In the experiments with TEA the synthesis time was varied (0 h, 24 h) adding a constant amount of 0.1 ml TEA. The samples were examined by scanning electron microscopy and X-ray powder diffractometry. Rietveld refinements have been conducted on the XRD data to obtain lattice parameters, average crystallite sizes and the micro-strain.

The reference sample synthesized without additives shows large cuboids up to 10-15 µm along with smaller crystals and nano-crystalline sodalite particles. SEM pictures show that the addition of PA leads to a reduction of the crystal size and an increase of the material uniformity with increasing PA amount. Overall no cuboids with the distinct habit of sodalites but agglomerates of small particles appearing as small stacked plates can be observed. The Rietveld refinements show that the average crystallite sizes and the micro-strains of the samples vary in an opposite manner with respect to the amount of added PA (Fig. 1). Whereas the average crystal size decreases with increasing PA concentration, a strong increase of the micro-strain within the sodalite is observed. The addition of TEA leads to small crystals with equally strong developed {100}, {110} and {111} faces. The reason for this behavior is the influence of the additives on the crystal growth velocity in different directions [4].

References
[1] Gier, T E, Stucky, G D, Nature. 349 (1991) 508-510.
[2] Yu, S-H, Antonietti, M, Cölfen, H, Hartmann, J, Nano Lett. 3(2003) 379-382.
[3] Buhl, J C, Schuster, K, Robben, L, Micro. Meso. Mater. 142 (2011) 666-671.
[4] Holden, M A, Cubillas, P, Anderson, M W, Chem. Commun. 46 (2010) 1047-1049.

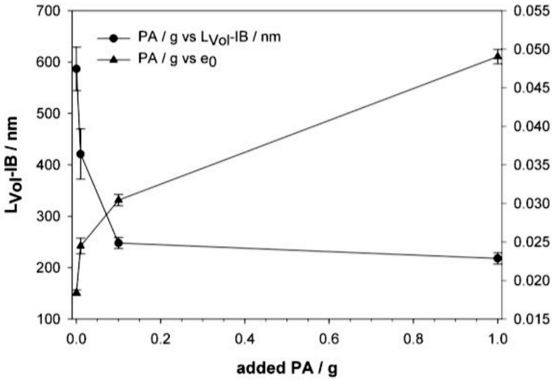

Figure 1: Development of average crystal sizes and micro-strain for the experiments using different PA concentration.

P10-P12

Order-disorder transitions in GeTe-rich germanium antimony tellurides elucidated by *in situ* Laue microdiffraction

P. Urban[1], M. Schneider[1], T. Schröder[1], X. Biquard[2], O. Oeckler[1]
[1]LMU Munich, Department of Chemistry, Munich, Germany
[2]ESRF, Grenoble, France

Metastable germanium antimony tellurides (GST) have received much attention as they dominate the field of phase-change materials (PCMs) for data storage, e.g. non-volatile RAM devices, and in addition exhibit interesting thermoelectric properties.[1] Whereas stable high-temperature phases (above ~ 500 °C), which exist for compositions $(GeTe)_{>3}Sb_2Te_3$, are characterized by a random distribution of Ge, Sb and voids on the cation positions of a rocksalt-type average structure, the vacancies order in 2D extended defect layers upon slow cooling. This finally leads to the stable ambient-temperature modifications with long-periodically ordered layered structures. Metastable single crystals of different compositions, which can be obtained by quenching the high temperature phases (grown by chemical vapor transport), exhibit twinned rhombohedral structures with pseudocubic metrics.[2] Short-range ordering in such metastable crystals leads to nanostructures characterized by the formation of twin domains and finite intersecting vacancy layers. *In situ* temperature dependent Laue microdiffraction experiments were performed at BM32 (ESRF) to elucidate diffusion mechanisms related to the order-disorder transitions from metastable to stable modifications. For multiply twinned (rhombohedral) crystals $(GeTe)_{\sim 16}Sb_2Te_3$, which do not show pronounced short-range order, cubic and rhombohedral domains with randomly distributed cation defects coexist during the heating process before a single-crystalline rocksalt-type phase is obtained at elevated temperatures. This indicates the discontinuous character of the phase transition. Depending on the defect concentration given by the nominal composition, different diffusion mechanisms can be identified as shown in detail for $(GeTe)_{\sim 12}Sb_2Te_3$ and $(GeTe)_{\sim 6}Sb_2Te_3$. For the latter, a long-periodically ordered structure with parallel defect layers (distorted to form van der Waals gaps) is observed upon heating before the high-temperature modification is formed. For $(GeTe)_{\sim 12}Sb_2Te_3$, however, an intermediate rhombohedral phase with no or little short-range order occurs as indicated by the absence of diffuse scattering, probably driven by both entropic and kinetic effects - long-range ordering would require extremely long diffusion pathways. The defect ordering processes strongly influence the thermoelectric characteristics of the materials and explain their hysteresis effects.

[1] M. N. Schneider, T. Rosenthal, C. Stiewe, O. Oeckler, *Z. Kristallogr.* **2010**, *225*, 463.
[2] M. N. Schneider, P. Urban, A. Leineweber, M. Döblinger, O. Oeckler, *Phys. Rev. B* **2010**, *81*, 184102.

P10-P13

$PbCa_2Al_8O_{15}$ - a structure with a novel aluminate anion made up of AlO_4 tetrahedra and AlO_5 trigonal bipyramids

M. Weil[1], C. Artner[1]
[1]TU Wien, Strukturchemie, Wien, Austria

During attempts to grow crystals in the system CaO-PbO-TeO_3 from a lead oxide flux, the title compound crystallized accidentally under atmospheric conditions in a corundum crucible at temperatures below 950 °C. A few colourless block-shaped single crystals were isolated from a polycrystalline red matrix that consisted mainly of minium.

The title compound crystallizes in a novel structure type in the space group *Pnma* with four formula units and lattice parameters of a = 5.3702(1), b = 27.9903(4), c = 8.8811(1) Å, V = 1334.95(3) Å^3, $R[F^2 > 2s(F^2)] = 0.024$, $wR2 = 0.059$, 5600 structure factors, 122 parameter.

The asymmetric unit contains one Pb, one Ca, four Al and eight O atoms. Except the Pb and one O atom situated on mirror planes, all other atoms are in general positions. Three Al atoms exhibit a slightly distorted tetrahedral coordination with a mean Al─O bond length of 1.759 Å, and one Al atom is in a considerably distorted trigonal-bipyramidal coordination with a mean Al─O bond length of 1.885 Å. The presence of both AlO_4 and AlO_5 groups has been observed in $Ca_4Al_6O_{13}$ [1].

One AlO_4 tetrahedron forms infinite chains parallel to [100] *via* corner-sharing. These chains are linked by parallel chains of edge-sharing AlO_5 trigonal bipyramids into layers *A* of six-membered double rings extending parallel to (010). The second layer *B* is made up of the remaining two AlO_4 tetrahedra. These tetrahedra share corners resulting in likewise six-membered double rings. The parallel layers *A* and *B* are finally linked into a three-dimensional framework by common corners.

Charge compensation is achieved by the Pb^{2+} and Ca^{2+} cations, which are situated in the voids of the anionic framework, and are surrounded by 7 and 6 oxygen atoms, respectively, both within distorted coordination polyhedra.

References

[1] Kahlenberg, V., Fischer, R. X., Shaw, C. S. J., *Am. Mineral.* **85**, 1492-1496 (2000).

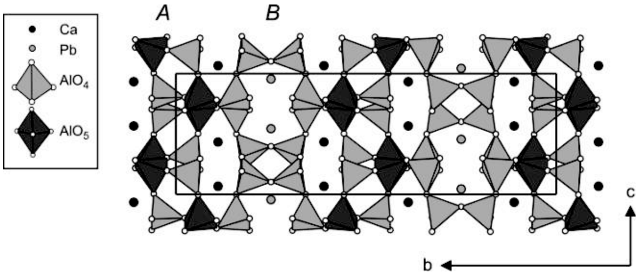

Figure 1: The crystal structure of PbCa2Al8O15 in a projection along [100]

P10-P14

Structure Elucidation of $[Co(NH_3)_6][Co(CO_3)_3]$

F. Hinrichs[1], N.-P. Pook[1], A. Adam[1]
[1]Institut für Anorganische und Analytische Chemie, TU Clausthal, Clausthal-Zellerfeld, Germany

A green solution of tricarbonatocobaltate(III) reacts with hexaammincobalt(III)-chloride to hexamminecobalt(III) tricarbonatocobaltate(III) [1]. Compounds with the $[Co(CO_3)_3]$-anion are often used as an analytical titrant and as an oxidant in organic chemistry [2]. Nevertheless, no x-ray single crystal data of the title compound are published, except [3].

The preparation of $[Co(NH_3)_6][Co(CO_3)_3]$ succeeded in different ways [1,4]. The structure solution of this compound can only be obtained in the monoclinic space group $P2_1/c$ (No. 14) with the cell parameters a = 17.826(1), b = 10.551(1), c = 13,748(1) Å, β = 104.56(1) °, V_{EZ} = 2502.7(3) Å^3 and Z = 8.

The structure involves four crystallographically different cobalt atoms. Two of them are located in the complex cation $[Co(NH_3)_6]^{3+}$ where each is coordinated by six ammonia molecules. The other two built up the complex $[Co(CO_3)_3]^{3-}$ anion, where the metal centre is chelated by three carbonato ligands. All cobalt atoms show an octahedral coordination sphere. In Fig. 1 the asymmetric unit is briefly shown.

The compound is investigated by x-ray single crystal diffraction, infrared and Raman spectroscopy.

References

[1] G. Wangila, R. B. Jordan, *Inorganica Chimica Acta*, **2003**, *343*, 347.
[2] a) J. A. Baur, C. E. Bricker, *Analytical Chemistry*, **1965**, *37 (12)*, 1461.
b) M. Vasatova, J. Zyka, *Microchemical Journal*, **1977**, *22*, 34.
c) M. F. M. El Ghandour, A. Abd El Razek, *Microchemical Journal*, **1984**, *30*, 201.
[3] S. Taghipourian, A. Adam, *Z. Kristallogr. Suppl. Issue*, **2003**, *20*, 155:
[4] T. P. McCutcheon, W. J. Schuele, *J. Amer. Chem. Soc.*, **1953**, *75*, 1845.

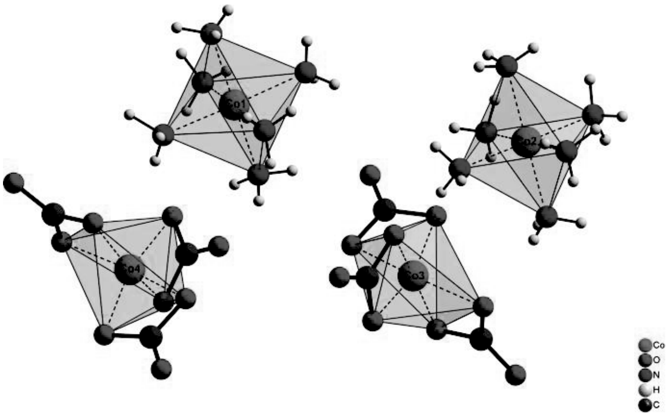

Figure 1: Asymmetric unit of [Co(NH3)6][Co(CO3)3]

P10-P15

Synthesis, Crystal Structure and Vibrational Spectrum of Di-μ-aqua-bis[(nitrato)(phenanthroline)(pyridinium-4-carboxylato)-copper(II)]nitrate, $[\{Cu(NO_3)(INAH)(phen)\}_2(\mu\text{-}H_2O)_2]NO_3$

N.-P. Pook[1], A. Adam[1]
[1]Institut für Anorganische und Analytische Chemie, Niedersachsen, Clausthal-Zellerfeld, Germany

Some structures of copper complexes are known, where the copper atoms are bridged by heterocyclic aromatic molecules like isonicotinate or nicotinate and additionally coordinated with chelating ligands such as phenanthroline or bipyridine [1-3].

The crystals of the title compound could be obtained from a water-methanol solution. Its crystal structure has been determined by single-crystal X-ray diffraction. The compound crystallizes in the monoclinic space group $P2_1/c$ with a = 10.353(1), b = 9.254(1), c = 20.383(2) Å, β = 96.27(1)°, Z = 2 (refer to the "dimeric building blocks") and V_{EZ} = 1941.1(3) Å^3. Copper shows a distorted octahedral coordination sphere with phenanthroline, pyridinium-4-carboxylate, nitrate and two water molecules acting as bridging ligands. Two edge-sharing CuN_2O_3 polyhedra form the "dimeric building blocks" (Figure 1). π-π-Interactions between phenanthroline as π-donor and pyridinium-4-carboxylate as π-acceptor connect these "dimeric building blocks" and stack them in a 1D-chain-like manner along the *c*-axis. Furthermore an extended hydrogen network stabilizes this structure. For further characterization IR and Raman spectroscopy and also elemental analysis were carried out.

[1] D. Xu, A. Xie, Y. Xu, C. Zhang, W. Chen, J. Coord. Chem. **1996**, *39*, 273. [2] D. Xu, A. Xie, Y. Xu, K. Nishikawa, N. Yasuoka, J. Coord. Chem. **1998**, *43*, 115. [3] D. Xu, A. Xie, Y. Xu, K. Nishikawa, N. Yasuoka, J. Coord. Chem. **1998**, *43*, 237.

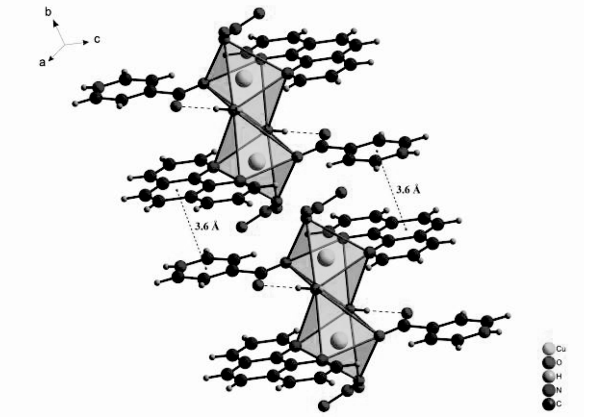

Figure 1: Edge-sharing CuN2O3-polyhedra and π-π connected "dimeric building blocks"

P10-P16

Dimensional reduction in uranyl oxysalts with general formula $A_n(UO_2)_p(TO_4)_q(H_2O)_r$ (A = monovalent cation, T = S, Se, Cr, Mo)

V. Kovrugin[1], V. Gurzhiy[1,2], S. Krivovichev[1], I. Tananaev[3]
[1]St. Petersburg State University, Crystallography Department, St. Petersburg, Russian Federation
[2]St. Petersburg State University, Chemical Faculty, St. Petersburg,
Russian Federation
[3]Frumkin Institute of Physical Chemistry and Electrochemistry RAS, Moscow, Russian Federation

Inorganic oxysalts are remarkable by the large diversity of structures and chemical compositions. Long et al. [1] proposed the principle of dimensional reduction for the description of decreasing dimensionality of chalcogenide structural units in Re sulphides and selenides. This principle was applied to various materials, including organic-inorganic composites [2], and certain inorganic oxysalts systems [3]. The principle of dimensional reduction indicates that incorporation of an ionic reagent and water into parent highly-condensed results in formation of derivative compou dimensionality of the structural unit. I principle of dimensional reduction to uranyl oxysalts with general formula $A_n(UO_2)_p(TO_4)_q(H_2O)_r$, where A^+ = monovalent cation, and T^{6+} = S, Se, Cr, Mo [4].

Inorganic Structures

The relationship between structure and composition for the compounds with general formula $A_n(UO_2)_p(TO_4)_q(H_2O)_r$ may be visualized using the UO_2TO_4 - A_2TO_4 - H_2O compositional diagram (Figure 1). Though the borders between different fields are not clearly defined, some relationships are noteworthy. The compounds with the general formula $A_2(UO_2)(TO_4)_2(H_2O)_2$ are known to crystallize in two orthorhombic modifications, 1D [5] and 2D [3]. Thus, the point **11** in Figure 1 is located on the border between the fields of dimensionality 1 and 2.

For demonstration of the principle of dimensional reduction in the system, one may consider the line in the diagram originating from its left corner and ending at the top corner of the diagram. The line describes compounds with the $A_n(UO_2)_p(TO_4)_q$ composition [3, 6-8]. The points **23**, **29**, **27**, and **35** correspond to the structures with the dimensionality of the structural units 3, 2, 1, and 0, respectively. The points **16** and **8** are located on the borders between 2D-and-3D, 1D-and-2D fields, respectively. Thus, the dimensionality of the structural unit is decreasing from the points **23** to **35**, and it is in agreement with the principle of dimensional reduction.

This work was supported by Federal Target Program „Scientific and Scientific-Pedagogical Personnel of the Innovative Russia" (contract 02.740.11.0326) and the grant from the budget of Saint-Petersburg State University (code 3.37.84.2011).

(1) Long, J. R.; McCarty, L. S.; Holm, R. H. *J. Am. Chem. Soc.* **1996**, *118*, 4603-4616.
(2) Haddad, S.; Awwadi, F.; Willet, R. D. *Cryst. Growth Des.* **2003**, *3*, 501-505.
(3) Krivovichev, S. V. *Structural Crystallography of Inorganic Oxysalts*; Oxford University Press: Oxford, 2009.
(4) Kovrugin, V. M.; Gurzhiy, V. V.; Krivovichev, S. V.; Tananaev, I. G. *Inorg. Chem.* **2011**, in publishing.
(5) Ling, J.; Sigmon, G. E.; Ward, M.; Roback, N.; Burns, P. C. *Z. Kristallogr.* **2010**, *225*, 230-239.
(6) Krivovichev, S. V.; Cahill, C. L.; Burns, P. C. *Inorg. Chem.* **2002**, *41*, 34-39.
(7) Krivovichev, S. V.; Burns, P. C. *Solid State Sci.* **2003**, *5*, 481-489.
(8) Krivovichev, S. V.; Burns, P. C. *Can. Mineral.* **2005**, *43*, 713-720.

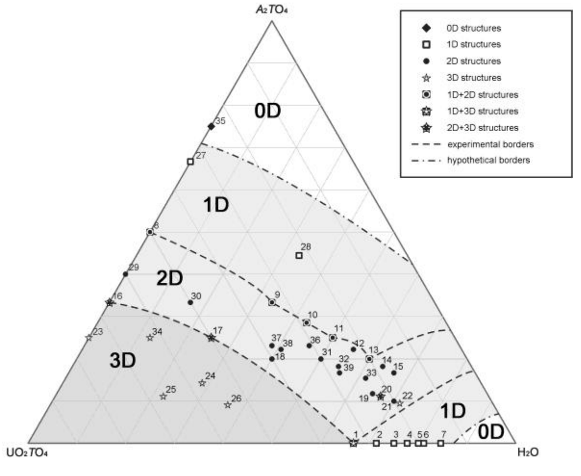

Figure 1. Dimensional fields on the compositional diagram of the UO_2TO_4 - A_2TO_4 - H_2O system.

P10-P17
Isomorphous transition metal substitution in $PbAlBO_4$

M.M. Murshed[1], A. Rusen[2], R. Fischer[2], T.M. Gesing[1]
[1]Universität Bremen, Chemische Kristallographie fester Stoffe-FB2, Bremen, Germany
[2]Universität Bremen, Kristallographie, FB5, Bremen, Germany

Metal borates are of continuing research interest because of their useful nonlinear optical properties. As a possible candidate $PbGaBO_4$ was first reported by Park et al. [1] followed by some isostructural $PbMBO_4$ compounds for M = Cr, Mn, Fe [2] and Al [3]. The mullite-type crystal structure of $PbMBO_4$ is built of infinite chains of edge-sharing MO_6 octahedra parallel to the *b*-axis, which are bridged by trigonal planar BO_3 groups. The Pb^{2+} cation occupies the interstitial position in the channels, and locates at the apex of a PbO_4 square pyramid. Isomorphous substitution of aluminum with trivalent transition metals would provide a range of miscibility in the $PbAl_{1-x}M_xBO_4$ system, which would help to tune the crystal chemistry and related physical properties. Here, we report on the synthesis, crystal structure and spectroscopic investigations of a series of $PbAl_{1-x}Fe_xBO_4$ compounds for x = 0 - 1.0. Both two end members $PbAlBO_4$ and $PbFeBO_4$ were produced by conventional solid state reactions, and other members ($0 < x < 1$) by glycerin method [4]. To describe the X-ray diffraction profiles, the fundamental parameter approach was applied in the Rietveld refinements. With increasing compositional x-value in the $PbAl_{1-x}Fe_xBO_4$ system, (i) the cell volume expanded almost linearly, (ii) cell parameter *b* increased linearly and, *a* and *c* non-linearly, (iii) B—O bond lengths remained close to the mean value of 137.8(4) pm, and (iv) average M—O bond lengths increased. The stereoactivity of the $6s^2$ lone electron pair (E) of the Pb^{2+} cation was monitored in terms of PbO_4 distortion with respect to the Al/Fe ratio in the system. The bond-valence sums around the Pb^{2+} cations of the two end members are close to empirical value, which showed a curved trend with a maximum value of ~16% over-bonded behavior at the mid-range of x-values. The maximum MO_6 octahedral distortion was observed for the end members, while the minimum value lies at x ~ 0.5. The Fourier transform infrared (FTIR) powder spectra have been described in three distinct band groups: BO_3, MO_6 and PbO_4E. Deconvolution of the absorption feature between 1200 cm^{-1} and 1400 cm^{-1} requires four fitted bands, which were assigned to B—O stretching vibrations of the trigonal planar BO_3 group. With increasing Fe^{3+} incorporation into $PbAl_xFe_{1-x}BO_4$ the shift of the MO_6 octahedral band group toward lower wavenumbers can be explained by the decrease of the vibrational force constants of M—O. Absorptions caused by the vibrations of the heavy atom lead were seen in the far-IR region.

Reference

[1] H. Park, J. Barbier: *Acta Crystallogr.* E57 (2001) i82. [2] H. Park, et al.: *Chem. Mater.* 15 (2003) 1703. [3] H. Park et al. *Solid State Sci.* 5 (2003 565. [4] Th. M. Gesing et al.: *J. Eur. Ceram. Soc.* (2011) doi:10.1016/j.jeurceramsoc.2011.04.004.

P10-P18
Boron Mullites

H. Lührs[1], R.X. Fischer[1], H. Schneider[1]
[1]University of Bremen, Geosciences, Bremen, Germany

The crystal structure of mullite can incorporate a large variety of ions [1]. A solid-solution series between mullite and $Al_{18}B_4O_{33}$ was proposed by [2]. In contrast, [3] showed that only up to 20 mole % B_2O_3 can be incorporated. However, their syntheses did not correspond to a 1:1 isomorphous substitution of silicon by boron and thus does not represent the desired solid solution. Our approach is to use starting compositions where boron replaces silicon in equal amounts. Powdered samples were prepared at 1200°C, following the synthesis route of [3]. X-ray powder diffraction (XRD) techniques and Rietveld refinements were applied and the behavior at high temperature was studied by XRD and simultaneous thermal analyses (STA). The initial Si/Al ratio was verified using X-ray fluorescence spectroscopy. All given B_2O_3 contents correspond to the initial weights of the gel.

STA of the precursor material revealed a linear decrease of the mullite formation temperature with the boron content, indicating formation of phases with different compositions. Below ~ 10 mole % B_2O_3 mullite is the only phase, with increasing boron content more and more alumina is present as an impurity. Crystallinity can be improved by further heat treatment at 1300 and 1400°C and results in a transformation of the alumina phase to θ- and α-alumina. After long time heat treatment (90h at 1400°C) α-alumina was observed in all samples containing more than 3 mole % B_2O_3. The amount of alumina increases with the boron content whereas mullite decreases. Thus meaning that boron-mullite decomposes at 1400°C.

Rietveld refinements in space group *Pbam* resulted in good fits using only the metrical parameters of the mullite unit cell. A variation of lattice parameters with increasing boron content and increasing syntheses temperature was observed (Fig. 1). The changes are most distinct for lattice parameter *c*, where a significant decrease with increasing boron content is observed. After 90h heat treatment at 1400°C, *c* becomes as large as for boron free mullite again. For *b* and especially for *c,* the observed parameters fall outside the range observed for boron-free mullites [4]; for *a*, changes are within this range as shown in Fig. 1.

Different formation temperatures, phase composition, changes of lattice parameters and diffracted intensities indicate that a high amount of boron can be incorporated into the mullite structure but boron mullites decompose at 1400°C. The alumina impurities indicate that there is no complete solid solution between mullite and aluminum borate.

^{11}B MAS NMR spectroscopy measurements of single phase boron mullite samples indicate the presence of threefold coordinated boron.

References

[1] H. Schneider & S. Komarneni (2005), Mullite, Wiley-VCH Verlag, Weinheim.

[2] A. Dietzel, & H. Scholze, Glastechn. Ber. **28**, pp.47-51 (1955).

[3] K.J. Griesser et al. (2008), Mineralogy and Petrology **92** (3-4) pp. 309-320 (2008).

[4] R.X Fischer et al., J. Eur. Ceram. Soc. **16**(2) pp. 109-113 (1996)

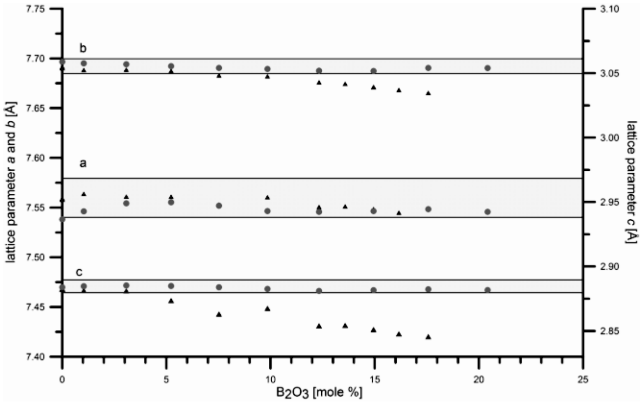

Figure 1: Lattice parameters vs. initial boron content. Triangles: 1200°C syntheses, circles: after 90h at 1400°C, grey: variation of a, b and c observed in mullites with varying Al_2O_3 content [4].

P10-P19

Synthese und Kristallstruktur des Nickel(II)-Dodekahydroxo-*closo*-Dodekaborat-Hydrats $[Ni(H_2O)_6][B_{12}(OH)_{12}]$

L.W. Zimmermann[1], T. Schleid[1]
[1]Universität Stuttgart, Institut für Anorganische Chemie,
Stuttgart, Germany

Seit der ersten Synthese des Dodekahydroxo-*closo*-Dodekaborat-Anions im Jahre 1999 [1] sind nur Salze der Alkalimetalle sowie weiterer einwertiger Kationen bekannt und strukturell untersucht [2]. Nun gelang die Synthese des ersten Dodekahydroxo-*closo*-Dodekaborats mit einem divalenten Übergangsmetall-Kation sowie dessen strukturelle Charakterisierung mit Hilfe der Röntgen-strukturanalyse. Die Darstellung von $[Ni(H_2O)_6][B_{12}(OH)_{12}]$ erfolgte aus einer warmen, wässrigen Lösung von $Cs_2[B_{12}(OH)_{12}] \cdot 2\ H_2O$ [1], in die eine konzentrierte $NiCl_2$-Lösung getropft wurde. Der ausgefallene Feststoff wurde 5 Stunden in Wasser gekocht und danach abfiltriert. Die aus dieser Synthese erhaltenen $[Ni(H_2O)_6][B_{12}(OH)_{12}]$-Einkristalle waren von minderer Qualität und konnten trigonal (a = 1027,81(6), c = 1408,85(9) pm) indiziert werden, das erhaltene Pulverdiffraktogramm ließ jedoch auf eine niedrigere Symmetrie schließen. Um bessere Kristalle dieser Verbindung zu erhalten, wurden 0,5 g Agar mit 2,6 g $Ni[SO_4] \cdot 6\ H_2O$ in 20 ml heißem Wasser gelöst. Nach dem Abkühlen wird eine Lösung aus 0,25 g $Cs_2[B_{12}(OH)_{12}] \cdot 2\ H_2O$ in 20 ml Wasser auf das entstandene Gel aufgebracht. Innerhalb weniger Tage entstanden dabei grüne Einkristalle von rautenförmiger Gestalt. $[Ni(H_2O)_6][B_{12}(OH)_{12}]$ kristallisiert im triklinen Kristallsystem in der Raumgruppe P-1 (a = 728,35(3), b = 739,92(3), c = 795,83(3) pm, α = 88,741(2), β = 88,739(2), γ = 85,448(2)°, Z = 1). Das Nickel(II)-Kation wird von sechs Wassermolekülen oktaedrisch koordiniert (d(Ni-O) = 203 - 206 pm). Die Hydratwasserhülle des $[Ni(H_2O)_6]^{2+}$-Kations bildet mit den Hydroxidgruppen des $[B_{12}(OH)_{12}]^{2-}$-Anions ein Netzwerk von Wasserstoffbrücken aus. Dabei sind sowohl Wasserstoffbrücken von Hydratwasserstoffatomen zu den an den *quasi*-ikosaedrischen B_{12}-Cluster gebundenen Sauerstoffatomen zu beobachten als auch von den Hydroxidwasserstoffatomen letzterer zu den Hydratwassersauerstoffatomen. Die Erstgenannten fallen mit interatomaren Abständen von Wasserstoff zu Sauerstoff von 175 bis 209 pm wesentlich stärker aus als die Zweitgenannten, die mit Abständen oberhalb 229 pm einen geringeren Anteil zur Bindung zwischen der Hydrathülle des Ni^{2+}-Kations und den OH-Gruppen des Clusteranions beisteuern. Das $[B_{12}(OH)_{12}]^{2-}$-Anion selbst liegt gegenüber der idealen Ikosaedersymmetrie nur leicht verzerrt vor, die interatomaren Abstände zwischen den benachbarten Boratomen betragen 178 bis 182 pm, die zwischen Bor- und Sauerstoffatomen liegen zwischen 143 und 145 pm und damit in einem für diesen Verbindungstyp wohlbekannten Bereich [2]. In der Gesamtstruktur ist ein Anion von acht $[Ni(H_2O)_6]^{2+}$-Kationen umgeben und ein Kation von acht Clusteranionen, so dass die Packung Analogien zur CsCl-Struktur aufweist.

Literatur

[1] T. Peymann, A. Herzog, C. B. Knobler, M. F. Hawthorne, *Angew. Chem. Int. Ed.* 38, **1999**, 1062-1064.

[2] T. Peymann, C. B. Knobler, S. I. Kahn, M. F. Hawthorne, *J. Am. Chem. Soc.* 123, **2001**, 2182-2185.

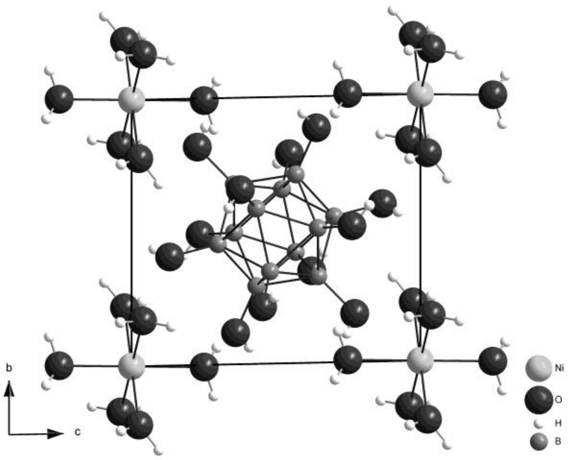

Figure 1: Kristallstruktur von $[Ni(H_2O)_6][B_{12}(OH)_{12}]$

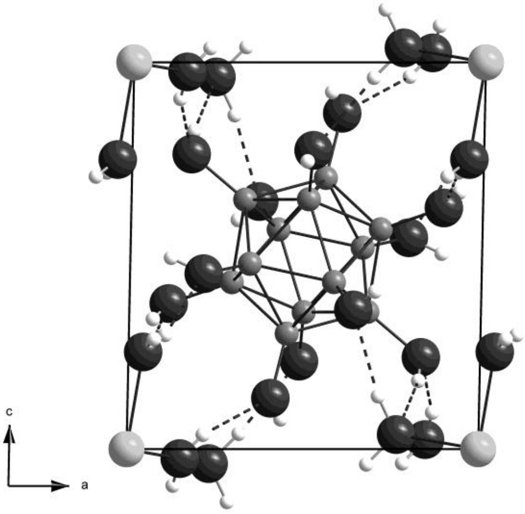

Figure 2: Wasserstoffbrückenbindungen in $[Ni(H_2O)_6][B_{12}(OH)_{12}]$

P10-P20

Ein Lithium-Natrium-Aluminium-Oxophosphat der Zusammensetzung $Li_8NaAl_3[PO_4]_2[P_2O_7]_3$ mit Na^+-leitenden Kanälen

S.J. Metzger[1], T. Schleid[1]
[1]Universität Stuttgart, Institut für Anorganische Chemie,
Stuttgart, Germany

Als Li^+-Kationen leitende Oxophosphate wurden schon vor mehr als 10 Jahren die Verbindungen der formalen Zusammensetzung $(Li1)_1(Li2)_2(Li3)_6M_3[(P1)_2O_7]_3[(P2)O_4]_2$ (M = Al, Ga, Cr, Fe) beschrieben [1]. Isotyp zu dieser Verbindungsklasse konnte nun der neue Vertreter $Na(Li2)_2(Li3)_6Al_3[(P1)O_4]_2[(P2)_2O_7]_3$ synthetisiert werden, bei dem die ionenleitenden Kanäle durch Na^+-Kationen besetzt sind. Farblose, plättchenförmige Einkristalle von $Li_8NaAl_3[PO_4]_2[P_2O_7]_3$ lassen sich durch Erhitzen von $Na[H_2PO_4]$ und $Li[H_2PO_4]$ unter Stickstoffatmosphäre in einem Korundschiff innerhalb von 10 Tagen bei 750 °C gewinnen und kristallisieren in der trigonalen Raumgruppe P-3c1 (Nr. 156) mit den Gitterparametern a = 961,03(6), c = 1357,44(9) pm und Z = 2. Der Aufbau der Kristallstruktur lässt sich als eine Abfolge von anionischen Schichten vom Typ $\{Al[PO_4]_2[P_2O_7]_3\}^{9-}$ beschreiben, die parallel zur (001)-Ebene verlaufen und durch die Li^+- und Na^+-Kationen getrennt werden (Abb. 1). Die sich auf der speziellen *Wyckoff*-Lage 2b befindlichen, kristallographisch einzigartigen Na^+-

Kationen, welche oktaedrisch von sechs O^{2-}-Anionen (d(Na-O) = 243 pm, 6x) umgeben sind, liegen in der Kristallstruktur in Kanälen in Richtung [001] vor, längs der die Ionenleitung stattfindet. Die beiden kristallographisch unterschiedlichen Li^+-Kationen kommen analog zu der prototypischen Verbindung $(Li1)_1(Li2)_2(Li3)_6Al_3[(P1)_2O_7]_3[(P2)O_4]_2$ (a = 955,3(1), c = 1349,2(2) pm) auf den *Wyckoff*-Lagen 4*d* (Li2) und 12*g* (Li3) zu liegen. Dabei werden diese von jeweils 4 O^{2-}-Anionen mit Abständen von 189 - 213 pm tetraedrisch umgeben, wobei das Tetraeder um $(Li3)^+$ stark verzerrt ist. Das oktaedrisch von Sauerstoff koordinierte, kristallographisch singuläre Al^{3+}-Kation (d(Al-O) = 189 - 192 pm) bildet mit den isoliert vorkommenden *Ortho*- und *Pyro*-Phosphat-Einheiten die anionische Schichtstruktur. Dabei verbinden die isoliert vorliegenden $[PO_4]^{3-}$-Tetraeder (d(P1)-O) = 151 - 154 pm) drei der $[AlO_6]^{9-}$-Oktaeder über gemeinsame Ecken. Die $[P_2O_7]^{4-}$-Einheiten (d(P2)-O) = 150 - 159 pm, ∢(P2-O-P2) = 135°) verbinden drei der $[AlO_6]^{9-}$-Oktaeder, wobei zwei der Oktaeder nur ein Sauerstoffatom mit der *Pyro*-Phosphat-Einheit gemein haben und das dritte Oktaeder chelatisierend von zwei O^{2-}-Anionen der $[P_2O_7]^{4-}$-Einheit angegriffen wird. Somit ist jedes Al^{3+}-Kation von zwei *Ortho*- und drei *Pyro*-Phosphat-Anionen umgeben. Die Schichten vom Typ $\{Al[PO_4]_2[P_2O_7]_3\}^{9-}$ werden von den dazwischen liegenden Li^+-Kationen zur Zusammensetzung $\{Li_8Al_3[PO_4]_2[P_2O_7]_3\}^-$ abgesättigt und ergeben ein wabenförmiges Muster, welches senkrecht dazu von den ionenleitenden Kanälen für die Na^+-Kationen durchbrochen wird (Abb. 2).

[1] S. Piosson, F. d'Yvoire, Ng.-H.-Dung, E. Bretey, P. Berthet, *J. Solid State Chem.* **138**, 32-40 (1998).

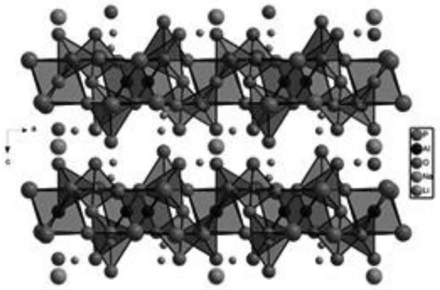

Figure 1: Schichten der Zusammensetzung $\{Al[PO_4]_2[P_2O_7]_3\}^{9-}$

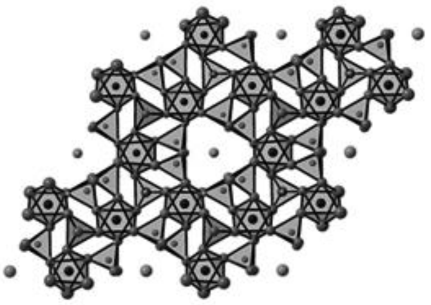

Figure 2: Blick auf die Kristallstruktur von $Li_8NaAl_3[PO_4]_2[P_2O_7]_3$ in Richtung [001]

P10-P21

Single Crystals of BaY_2Se_4 with $CaFe_2O_4$-Type Structure

C.M. Schurz[1], C.F. Kuhn[1], T. Schleid[1]
[1]Universität Stuttgart, Institut für Anorganische Chemie, Stuttgart, Germany

Historically the crystal structure of calcium ferrite $CaFe_2O_4$ was first refined in 1957 (Decker and Kasper, 1957). Since this time many compounds with the general composition $M^{II}M^{III}Ch_4$ (M^{II}: divalent cation, M^{III}: trivalent cation, Ch: chalcogenide anion) crystallizing in this structure type were characterized. For the best of our knowledge, the recently published lutetium salts $BaLu_2Ch_4$ (Schurz and Schleid, 2011) were the latest examples dealing with this topic. Dark red, needle shaped single crystals of BaY_2Se_4 were obtained after heating a mixture of Y, YCl_3, Se and BaN_3Cl along with $BaCl_2$ as flux at 920 °C for 10 days designed to produce Y_3NSe_3. The crystal structure of the title compound (orthorhombic, *Pnma*, a = 1271.16(8), b = 417.65(3), c = 1508.23(9) pm, Z = 4, further information is gathered in Table 1 and available on quoting CSD-422980 at FIZ Karlsruhe: crysdata@fiz-karlsruhe.de) crystallizes isotypically with $CaFe_2O_4$ as well as the other known barium yttrium salts of BaY_2Ch_4 (Ch = O, S, Te) (Costa et al., 1989; Lowe-Ma et al., 1995; Narducci et al., 2000) and thus represents the last missing piece of this short series. The expansion of the lattice parameters of these ternary chalcogenides BaY_2Ch_4 (a: from 1039 pm for Ch = O to 1365 pm for Ch = Te; b: from 345 pm for Ch = O to 444 pm for Ch = Te; c: from 1211 pm for Ch = O to 1614 pm for Ch = Te) is coherent with the increasing radii of the chalcogenide anions (from 138 pm for Ch = O to 221 pm for Ch = Te) (Shannon, 1976). Each of the two crystallographically different trivalent Y^{3+} cations is part of chains of edge- and corner-connected $[(Y1)(Se2)(Se3)_3(Se4)_2]^{9-}$ and $[(Y2)(Se1)_3(Se2)_2(Se4)]^{9-}$ octahedra running along [010]. These chains are fused to a three-dimensional framework $\{[Y_2Se_4]^{2-}\}$ with channels occupied by Ba^{2+} cations (Figure 1). As consequence those are surrounded by eight Se^{2-} anions forming bicapped trigonal prisms. The three selenide anions $(Se1)^{2-}$, $(Se2)^{2-}$ and $(Se3)^{2-}$ are coordinated by five cations, each with the shape of a distorted square pyramid, while for $(Se4)^{2-}$ the five contacts to the two different kinds of cations define a highly distorted trigonal bipyramid.

Costa, G.A. et al. (1989): Powder Diffr., 4, 24-25.
Decker, B.F., Kasper, J.S. (1957): Acta Crystallogr., 10, 332-337.
Lowe-Ma, C.K. et al. (1995): J. Solid State Chem., 117, 363-372.
Narducci. A.A. et al. (2000): J. Alloys Compds., 303, 432-439.
Schurz, C.M., Schleid, Th. (2011): Crystals 1, to be published.
Shannon, R.D. (1976): Acta Crystallogr., A 32, 751-767.

	x/a	z/c	U_{eq} [a)]	$d(Ba^{2+}–Se^{2-})$	$d(Y1^{3+}–Se^{2-})$	$d(Y2^{3+}–Se^{2-})$
Ba	0.24085(4)	0.66439(3)	97(1)	Se3: 329.9 (2×)	Se4: 282.4 (2×)	Se1: 281.7
Y1	0.07966(6)	0.40014(5)	83(2)	Se1: 331.0 (2×)	Se3: 285.4	Se4: 286.2
Y2	0.56466(6)	0.60875(5)	84(2)	Se2: 336.0 (2×)	Se3′: 287.6 (2×)	Se1′: 287.0 (2×)
Se1	0.08561(6)	0.07719(5)	82(2)	Se4: 345.7	Se2: 288.5	Se2: 287.9 (2×)
Se2	0.29366(6)	0.33648(5)	93(2)	Se4′: 348.7		
Se3	0.37337(6)	0.02512(5)	82(2)			
Se4	0.47612(6)	0.78322(5)	95(2)	$CN(Ba^{2+}) = 8$	$CN(Y1^{3+}) = 6$	$CN(Y2^{3+}) = 6$

a) $U_{eq} = {}^1/_3\,(U_{11} + U_{22} + U_{33})$.

Figure 1: Atomic parameters, U_{eq} values (in pm^2), interatomic distances (in pm) and coordination numbers (CN) of the cations for BaY_2Se_4; *Wyckoff*-position 4*c* with $y/b = {}^1/_4$ for all atoms.

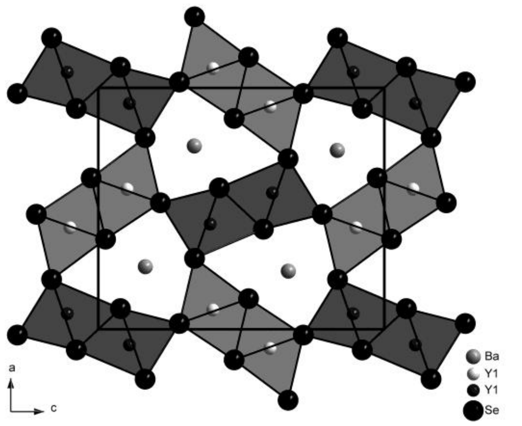

Figure 2: View at the CaFe2O4-type crystal structure of BaY2Se4 along [010].

P10-P22

New orthomolybdates in the Cs-Fe(II,III)-Mo-O system: $Cs_4Fe(MoO_4)_3$, $Cs_2Fe_2(MoO_4)_3$ and $CsFe_5(MoO_4)_7$

A. Sarapulova[1], T. Namsaraeva[1,2], D. Mikhailova[1,3],
N. Kuratieva[1,4], A. Senyshyn[5], H. Ehrenberg[1,6], B. Bazarov[2]
[1]IFW Dresden, Institute for Complex Materials, Dresden, Germany
[2]Russian Academy of Sciences, Baikal Institute of Nature Management, Ulan-Ude, Russian Federation
[3]Max Planck Institute for Chemical Physics of Solids, Dresden, Germany
[4]Russian Academy of Sciences, Nikolaev Institute of Inorganic Chemistry, Novosibirsk, Russian Federation
[5]Technische Universität München, Forschungsneutronenquelle Heinz Maier-Leibnitz FRM-II, München, Germany
[6]Karlsruhe Institute of Technology, Institute for Applied Materials Karlsruhe, Germany

Three new complex molybdenum oxides $Cs_2Fe_2(MoO_4)_3$, $Cs_4Fe(MoO_4)_3$ and $CsFe_5(MoO_4)_7$ with the average oxidation states of Fe +2 and +2.6 were obtained during a study of phase formation in the system Cs-Fe(II,III)-Mo-O and investigated by X-ray single crystal analysis at room temperature and 100K [1].

The polycrystalline $CsFe_5(MoO_4)_7$ was obtained by synthesis in dynamic vacuum with a step-like temperature increase up to a final temperature of 973 K during 20 h. Single crystals of $Cs_2Fe_2(MoO_4)_3$, $Cs_4Fe(MoO_4)_3$ and $CsFe_5(MoO_4)_7$ were grown from the stoichiometric mixtures of Cs_2MoO_4, Fe_2O_3, FeO and MoO_3 by the flux method in sealed silica tube.

All diffraction patterns were analyzed by full-profile Rietveld refinements, using the software package WinPLOTR. Magnetic properties have been studied with a superconducting quantum interference device (SQUID) from Quantum Design. Elastic coherent neutron scattering experiments were performed on the high-resolution powder diffractometer SPODI at the research reactor FRM-II (Garching, Germany) with monochromatic neutrons of 1.5481(1) Å wavelength.

The structure of cubic $Cs_2Fe_2(MoO_4)_3$ (*P*2$_1$3, a = 10.9161(2) Å, Z = 4) is very similar to the one of pseudocubic $Cs_2Co_2(MoO_4)_3$ [2] with a weak orthorhombic distortion. Hexagonal $Cs_4Fe(MoO_4)_3$ (*P-62c*, a = 6.2922(16) Å, c = 23.937(13) Å, Z = 2) is isostructural to the high-temperature modification of $Rb_4Mn(MoO_4)_3$ [3]. $CsFe_5(MoO_4)_7$ crystallizes in monoclinic symmetry (*P*2$_1$*/m,* a = 6.9239(6) Å, b = 21.4477(19) Å, c = 8.6374(8) Å, β= 101.667(2)°, Z = 2) and represents a new structure type. This structure contains three crystalographically independent Fe-sites and consists of isolated FeO_6-octahedra and Fe_4O_{18}-units of edge-sharing FeO_6-octahedra, which are connected with MoO_4-tetrahedra via corners, forming a three-dimensional framework. $CsFe_5(MoO_4)_7$ orders magnetically with a ferromagnetic component at T_C=10 K, proposed as a canted antiferromagnet. Its antiferromagnetic structure at 0 T was described by combination of two propagation vectors **k**=(1/2, 0, 0) and **k**=(0, 0, 0) with magnetic moments of 2.6 μ_B, 1.6 μ_B and 3.5 μ_B for three independent Fe-sites. Two magnetic-field induced transitions are observed at 0.25 T and 1.9 T at 2 K.

[1] DOI: 10.1002/ejic.201100061 [2] S. F. Solodovnikov, R. F. Klevtsova, V. G. Kim, P. V. Klevtsov, *Zh. Strukt. Khim.* 27 (1986) 928-933. [3] S.F. Solodovnikov, R.F. Klevtsova, L.A. Glinskaya, P.V. Klevtsov, *Kristallografiya* 33 (1988) 1380- 1386

P10-P23

A novel crystal structure type shown by a flux-grown tetragonal Ba-Y-silicate and its isotypic Ho-analogue

M. Wierzbicka-Wieczorek[1], U. Kolitsch[2,3], E. Tillmanns[2]
[1]Fridrich-Schiller University, Institute for Geosciences Mineralogy Dept., Jena, Germany
[2]University of Vienna, Institute of Mineralogy and Crystallography, Vienna, Austria
[3]Natural History Museum, Department of Mineralogy and Petrography, Vienna, Austria

As part of a completed project (FWF P17623-N10), which was focused on the synthesis of new microporous mixed-framework silicates containing octahedrally coordinated M^{3+} cations, we present two new silicates with a novel structure type: $Ba_5Y_{13}Si_8O_{41}$ and isotypic $Ba_5Ho_{13}Si_8O_{41}$ [1]. These silicates crystallized as small, colorless, prismatic crystals from a high-temperature flux (MoO_3-based flux mixtures in Pt crucibles in air; T_{max} = 1150°C, cooling rate 2 K/h, T_{min} = 900°C). The crystal structures have been determined from single-crystal X-ray intensity data. The two new compounds crystallize in the tetragonal space group *I*-42*m* (no. 121), with *a* = 18.934(3) / 18.927(3), *c* = 5.358(1) / 5.358(1) Å, *V* = 1920.8(6) / 1919.4(6) Å^3, *R*(*F*) = 2.49 / 1.76 %, respectively (Y/Ho). The structure refinements showed that both isotypic silicates are racemically twinned, with twin ratios closely approaching a 50:50 ratio.

Final unrestrained occupancy refinements result in the following chemical formulae: $Ba_{5.20}Y_{13}Si_8O_{41}$ and $Ba_{5.20}Ho_{13}Si_8O_{41}$. These formulae are nearly charge-balanced (81.4 positive vs. 82 negative charges). Low electron densities (< 1.8 e/Å^3) next to the Ba1 and Ba2B sites may represent additional Ba^{2+} cations representing the missing positive charges. Alternatively, a small portion of the Ba sites may be occupied by very minor amounts of Y/Ho^{3+} cations in a statistical way.

The asymmetric unit of $Ba_{5.20}Y/Ho_{13}Si_8O_{41}$ contains three Ba sites (two of which are partially occupied), three Y/Ho atoms (one of which is split), two non-equivalent Si and seven O atoms. Most of the atoms are located on special positions. Atoms Y1/Ho1 and Y2/Ho2 are both [7]-coordinated with average Y/Ho-O bond distances of 2.37/2.37 and 2.34/2.34 Å, respectively. In contrast, Y3/Ho3 is bonded only to five oxygen atoms, which results in a shorter mean Y/Ho-O distance of 2.22/2.18 Å. However, the Y3/Ho3 site is in fact split, with Y3-Y3' and Ho3-Ho3' distances of 0.528(5) and 0.796(2) Å. The Y1/Ho1O$_7$ and Y1/Ho2O$_7$ polyhedra are connected to each other via two or three edges to form dense (110) slabs that are linked to neighbouring, symmetry-equivalent slabs via common edges (Fig. 1). The slabs are further bonded to SiO_4 tetrahedra to form a three-dimensional framework. The Si2O$_4$ tetrahedron shares two edges with Y2/Ho2-O polyhedra, while the Si1O$_4$ tetrahedron only shares one edge. Large tetragonal channels are occupied by the Y3/Ho3-O polyhedra, which are corner-linked along [001] to form infinite chains. The Ba1 site occupies the remaining space in these large channels between the slabs and the chains. The Ba2 site occupies voids in a smaller tetragonal channel running parallel to [001] at *x* = 0.5. The Ba2 site is split, an additional adjacent Ba2B site has a occupancy of 0.045(5) Å for the Y/Ho compound.

Reference:
[1] Wierzbicka-Wieczorek (2007): Ph.D. Thesis, University of Vienna, 186 pp.

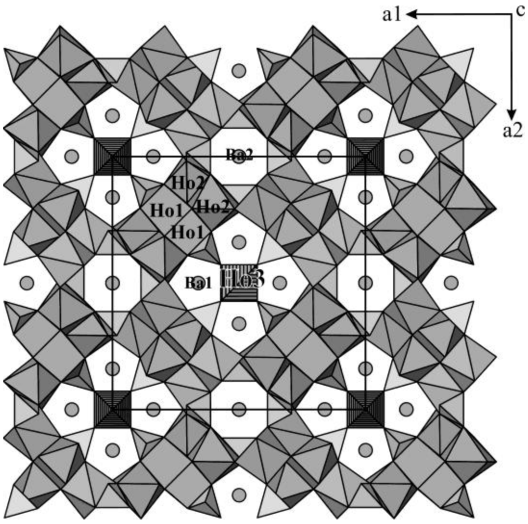

Figure 1: View of Ba5.2Ho13Si8O41 along [001]

P10-P24

Synthesis and Crystal structure of $Li_2H_2P_2O_6 \cdot 2\ H_2O$

P. Wu[1], M. Gjikaj[1]
[1]Institut für anorganische und analytische Chemie, TU Clausthal, Clausthal-Zellerfeld, Germany

The first reaction leading to hypophosphoric acid was reported by Schiel [1] and the salt was characterized by Salzer [2]. Since 1960 few studies were performed on hypodiphosphate [3-5]. LeBret *et al*. reported the crystal structure of $Ni_2P_2O_6 \cdot 12\ H_2O$ [6]. In this work we report the synthesis and the single-crystal structure of lithium dihydrogen hypodiphosphate dihydrate, $Li_2H_2P_2O_6 \cdot 2\ H_2O$.

The title compound crystallizes in the monoclinic space group $P\ {}_1/n$ with a = 6.144(1), b = 5.155(1), c = 12.106(3) Å, β = 104.03(2)°, V = 372.0(1) $Å^3$ and Z = 2.The crystal structure of $Li_2H_2P_2O_6 \cdot 2\ H_2O$ is characterized by discrete $[H_2P_2O_6]^{2-}$ anions in staggered conformation, tetrahedral $[LiO_4]$ and water molecules, held together by hydrogen bonds (Fig. 1). The P-P distance amounts to 2.182 Å and the P-O bond lengths range from 1.502 to 1.546 Å, similar to those reported previously [3-7]. The hydrogen-bond lengths between O atoms of water molecules and O atoms of $[H_2P_2O_6]^{2-}$ anions range from 2.848 to 3.148 Å, the O-H···O angles from 157.8 to 158.4°.

[1] J. Schiel, *Ann.Chem. Pharm*. **109** (1859) 317.
[2] T. Salzer, *Ann. Chem*. **187** (1877) 322.
[3] A. Wilson, H. McD. McGeachin, *Acta Cryst*. **17** (1964) 1352.
[4] R. L. Collin, M. Willis, *Acta Cryst.* **B27** (1971) 291.
[5] S. Hagen, M. Jansen, *Z. Anorg. Allg. Chem.* **621** (1995) 149.
[6] J. M. Haag, G. C. LeBret, D. A. Cleary, B. Twamley, *J. Solid State Chem*. **178** (2005) 1308.
[7] E. Leininger, T. Chulski, *Inorg. Synth.* **4** (1953) 68.

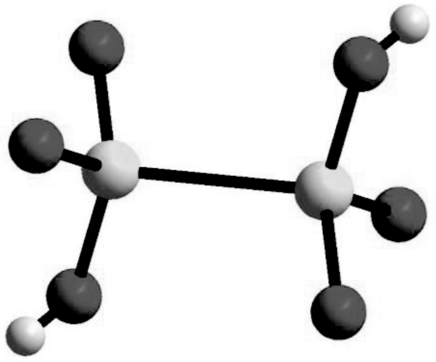

Figure 1: Crystal structure of $Li_2H_2P_2O_6 \cdot 2\ H_2O$ along [100]

P10-P25

Synthesis, Crystal structure and Vibrational Spectrum of $SrH_2P_2O_6 \cdot 2\ H_2O$

Y. Liao[1], M. Gjikaj[1]
[1]Institut für Anorganische und Analytische Chemie, TU Clausthal, Clausthal-Zellerfeld, Germany

Alkaline earth hypothiodiphosphates were first reported by Klingen *et al.* [1]. Since then, compounds with the hypothiodiphosphate anion $[P_2S_6]^{4-}$ have enjoyed considerable attention, because of their interesting magnetic, optical and structural properties [2-4]. The corresponding alkaline earth hypodiphosphates, $M_2P_2O_6$ are unknown.

$SrH_2P_2O_6 \cdot 2\ H_2O$ crystallizes in the monoclinic space group $C\ 2/c$ with a = 10.830(4), b = 6.268(1), c = 10.615(3) Å, β = 106.93(3)°, V = 689.3(2) $Å^3$ and Z = 4. The crystal structure is characterized by discrete $[H_2P_2O_6]^{2-}$ anions in staggered conformation with tetravalent phosphorus, $[SrO_8]$ and water molecules, which are involved in a hydrogen-bond network. The main characteristic of the $SrH_2P_2O_6 \cdot 2\ H_2O$ is the dihydrogen hypothiodiphosphate anion (Fig. 1). The $[H_2P_2O_6]^{2-}$ anions are located at a center of inversion with P - P distances of 2.168 Å and P - O bond lengths ranging from 1.511 to 1.590 Å. These values agree very well with those reported previously e.g. for $Co_2P_2O_6 \cdot 12\ H_2O$ [6] and $Ni_2P_2O_6 \cdot 12\ H_2O$ [7].

[1] W. Klingen, W. Krause, *Z. Anorg. Allg. Chem*. **396** (1973) 271.
[2] H. Falius, W. Krause, *Z. Anorg. Allg. Chem*. **477** (1981) 21.
[3] P. J. S. Foot, N. G. Shaker, *Mater. Res. Bull*. **18** (1983) 173.
[4] R. Clement, O. Garnier, J. Jegoudez, *Inorg. Chem*. **25** (1986) 1404.
[5] E. Leininger, T. Chulski, *Inorg. Synth*. **4** (1953) 68.
[6] S. Hagen, M. Jansen, *Z. Anorg. Allg. Chem*. **621** (1995) 149.
[7] J. M. Haag, G. C. LeBret, D. A. Cleary, B. Twamley, *J. Solid State Chem*. **178** (2005) 1308.

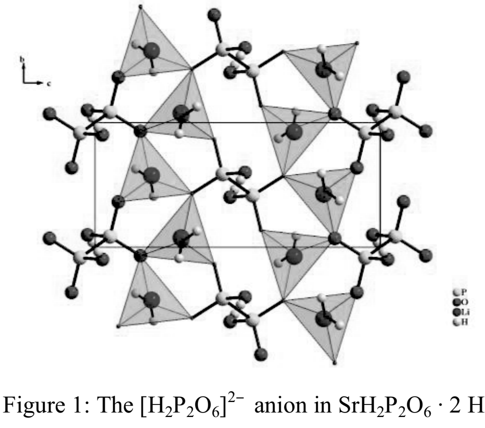

Figure 1: The $[H_2P_2O_6]^{2-}$ anion in $SrH_2P_2O_6 \cdot 2\ H_2O$.

P10-P26

$Ho_4Te_{11}O_{29}$: The First Mixed-Valent Rare-Earth Metal(III) Oxotellurate(IV,VI)

P. Höss[1,2], T. Schleid[2]
[1]Karlsruher Institut für Technologie, Institut für Nukleare Entsorgung, Eggenstein-Leopoldshafen, Germany
[2]Universität Stuttgart, Institut für Anorganische Chemie, Stuttgart, Germany

Mixed-valent oxotellurates(IV,VI) are a rather small class of ternary compounds with less than 20 known and structurally characterized representatives, containing mostly mono- or divalent cations. The bismuth(III) oxotellurate(IV,VI) $BiTeO_4$ (≡ $Bi_2Te_2O_8$; Te^{IV}:Te^{VI} = 1:1) [1] is the only example including a trivalent metal so far. The title compound $Ho_4Te_{11}O_{29}$ could now be obtained as the first mixed-valent rare-earth metal(III) oxotellurate(IV,VI) and exhibits an unusually high Te^{IV}:Te^{VI} ratio of 10:1. $Ho_4Te_{11}O_{29}$ crystallizes triclinically in space group $P{-}1$ ($a = 679.18(4)$ pm, $b = 1371.65(8)$ pm, $c = 1524.26(9)$ pm, $\alpha = 67.423(3)°$, $\beta = 87.592(3)°$, $\gamma = 83.514(3)°$, $Z = 2$) [2]. The crystal structure contains four crystallographically different Ho^{3+} cations in eight- and sevenfold oxygen coordination. By sharing common edges these holmium-oxygen polyhedra construct double chains with the composition ${}_{\infty}^{1}\{[Ho_4O_{20}]^{28-}\}$ running along the [010] direction. The oxotellurate partial structure comprises two types of discrete oxopolytellurate(IV,VI) anions, namely oxoenneatellurate(IV,VI) $[(Te1)^{VI}Te^{IV}{}_8O_{24}]^{10-}$ and oxotridecatellurate(IV,VI) $[(Te2)^{VI}Te^{IV}{}_{12}O_{34}]^{14-}$. Both of their centers consist of $[Te^{VI}O_6]^{6-}$ octahedra with chain fragments of oxotellurate(IV) units attached in accordance with their inversion symmetry. The linkage of all oxotellurate building blocks within both oxopolytellurate(IV,VI) anions results from covalently bonded oxygen atoms. Fused by common oxygen atoms the oxopolytellurate(IV,VI) units and the ${}_{\infty}^{1}\{[Ho_4O_{20}]^{28-}\}$ double chains form layers parallel to the (100) plane. Along [100] these are exclusively linked through strong secondary $Te^{IV}\cdots O^{2-}$ interactions, which are also well known in ternary rare-earth metal(III) oxotellurates(IV) with $M_2Te_3O_9$, $M_2Te_4O_{11}$ and $M_2Te_5O_{13}$ as general compositions, and without those a three-dimensional structure could not be achieved at all.

[1] P. Thomas, B. Jeansannetas, J. C. Champarnaud-Mesjard, B. Frit, *Eur. J. Solid State Inorg. Chem.* **1996**, *33*, 637.
[2] P. Höss, *Dissertation*, Univ. Stuttgart, **2009**.

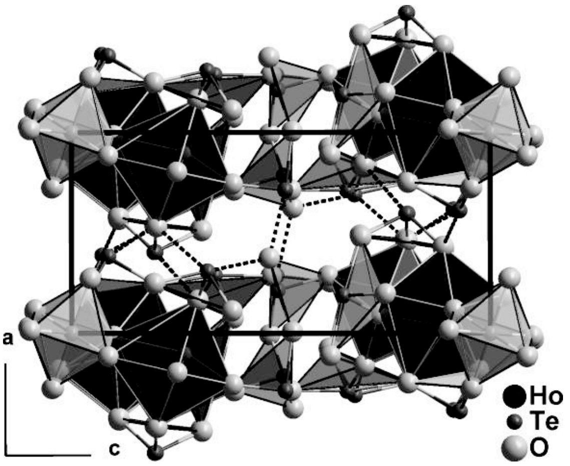

Figure 1: Crystal structure of $Ho_4Te_{11}O_{29}$ viewed along [010]

P10-P27

Crystal structure and polytypism of a new REE-orthosilicate

T. Malcherek[1], J. Schlüter[1], M. Cooper[2], T. Husdal[3]
[1]Universität Hamburg, Geowissenschaften, Hamburg, Germany
[2]University of Manitoba, Dept. of Geological Sciences, Winnipeg, Canada
[3]private, Bodø, Norway

A yet undescribed rare earth calcium aluminium fluorosilicate mineral found in the granite pegmatites Øvre Lapplægeret and Stetind in Norway is reported. The idealized composition, determined by electron microprobe analysis is $(Y,Ln)_6CaAl_2Si_4O_{18}(F,OH)_6$, where the lanthanoides, Ln, are dominated by Dy, Er, Gd and Yb. The Ln/Y ratio is close to 1/3. The amount of hydroxyl-anions substituting for F may be low to absent, but clear evidence for OH-stretching modes was found by infrared spectroscopy in one crystal. X-ray single crystal diffraction reveals two types of crystals of the new mineral species. The first type shows orthorhombic symmetry, space group Pban, with average lattice parameters of a=15.99(2)Å, b=5.53(1)Å, c=9.65(1)Å. These crystals exhibit diffuse scattering streaks along [001]. The intensity of these nearly continuous streaks varies between individual crystals. The crystal structure is characterised by chains of edge sharing AlO_6-octahedra along [010] and by (001) layers of rare earth elements and Ca-atoms, each eightfold coordinated by F and O. Isolated Si-tetrahedra and additional eightfold coordinated REE-sites link the AlO_6-chains and the layers. Disorder of Si across two sites related by symmetry occurs for one type of Si-tetrahedra. The second type of crystals show distinct diffraction maxima superimposed on the streaks observed in the first type. One crystal from the Stetind locality shows no diffuse streaks, but sharp reflections from a monoclinic lattice with lattice parameters a′=11.05Å, b′=5.524Å, c′=14.399Å, ß=103.32° instead, with an additional monoclinic twin lattice related by a diad along [101]′. Superposition of the three crystal lattices gives rise to an orthorhombic superlattice with A=a, B=b and C=3c. The order-disorder (OD)-character of the new mineral and its ordered polytype structures emerging from these observations will be discussed.

P10-P28

Structural characterization of $[Cu_3Cl_6(C_5H_5N)_2]$ from powder data

L. Fink[1], T. Bernert[1], Y. Krysiak[1], E. Alig[1], M.U. Schmidt[1]
[1]Anorg. Analyt. Chemie, Universität Frankfurt, Frankfurt, Germany

The copper-pyridine complex [Cu3Cl6(C5H5N)2] (I), was prepared by thermal decomposition at 190 °C in air, starting from [CuCl2(C5H5N)2].

The crystal structure was determined from laboratory X-ray powder data [1] with direct methods and Patterson methods using EXPO2009 [3], and refined subsequently with the Rietveld method using TOPAS [4]. The compound crystallizes in space group P1¯. The structure consists of edge sharing Jahn-Teller-distorted octahedra around the copper atoms. Three of these octahedra are linked together. The central copper atom (located on a centre of inversion) is coordinated by six chlorine atoms, while the other copper atom (on general position) is coordinated by five chlorine atoms and one nitrogen atom of the pyridine ring. Further connection of these groups by edge sharing with the neighboring units builds up polymeric chains parallel [001], see Figure 1.

[1] Yasar Krysiak, Thomas Bernert, Lothar Fink, Edith Alig, Martin U. Schmidt, in preparation.

[2] McConnell, A. A., Nuttall, R. H., J. Mol. Struct., 1978, 49.
[3] Altomare, A., Camallt, M., Cuocci, C., Giacovazzo, C. Moliterni, C. Rizzi, R., J. Appl. Cryst., 2009, 42.
[4] Coelho, A. A.: TOPAS Academic 4.1, 2007, Coelho Software, Brisbane, Australia.
[5] Diamond Vers. 3.2g, Crystal Impact GbR, Bonn, Germany.

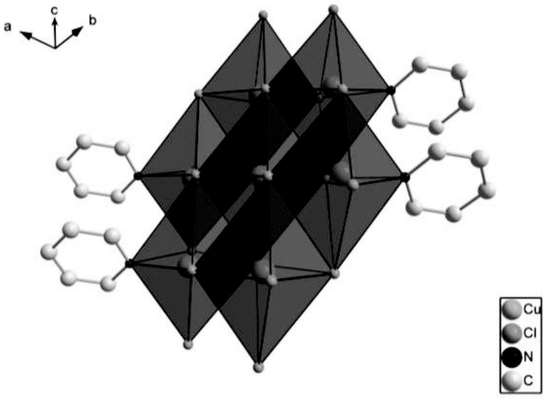

Figure 1: Part of the crystal structure of [Cu3Cl6(C5H5N)2], showing the coordination of the copper atoms (picture created with Diamond [5])

P10-P29

Synthesis, crystal structure and high temperature behavior of gallogermanate tetrahydroborate sodalite $Na_8[GaGeO_4]_6(BH_4)_2$

I. Poltz[1,2], L. Robben[1], J.-C. Buhl[2], T.M. Gesing[1]
[1]Universität Bremen, Chemische Kristallographie fester Stoffe, Bremen, Germany
[2]Leibniz Universität Hannover, Institut für Mineralogie, Hannover, Germany

Sodalites are proposed for applications in future key technologies like hydrogen storage [1]. Especially the enclathration of hydride salts into sodalite cages provides an interesting model system to study principles of hydrogen storage in zeolite cavities. An incorporation of hydrogen species in the form of hydride salt $NaBH_4$ was already obtained from mild hydrothermal syntheses for sodalites with aluminosilicate, aluminogermanate and gallosilicate frameworks [2, 3]. With regard to the fine-tuning and controlled change of β-cage properties in zeolites the complete substitution of aluminosilicate framework atoms by gallium and germanium is of special interest. Here we describe the first results of the temperature dependent studies on tetrahydroborate sodalite to get more insight on the interaction between the guest anions and the framework. This will help to clarify the structure-property relationship for possible future applications.

The hydrothermal synthesis was carried out in a Teflon coated steel autoclave. 1 g of the beryllonite analogous phase $NaGaGeO_4$ [4] as Ga- and Ge-source, and $NaBH_4$-granulate were each briefly stirred in 1 ml 2 M NaOH solution at 338 K. Then, both suspensions were combined and 1 ml 2 M NaOH solution was additionally added. After a hydrothermal treatment for 4 h at 423 K the sample was washed with deionized water and dried at 383 K for 1 h. The product was characterized by XRD and IR-spectroscopy. The XRD pattern of the synthesis product shows sodalite as the main phase along with a small amount (<5 wt%) of the starting material $NaGaGeO_4$. The crystal structure was refined by the Rietveld method providing a lattice parameter of 913.6(1) pm (P-43n). The presence of the BH_4^--group is additionally confirmed by the observation of its tetrahedral vibrational modes in the IR-spectrum. The temperature dependent (TD) development of the sodalite lattice parameter was evaluated (Fig. 1). It shows an initial linear increase with a kink at 528 K, followed by a rapid decrease above 648 K. The TD Raman spectra indicate the oxidation of the BH_4^--anions in this temperature range (523-548 K) in combination with a shift of the tetrahedral framework vibrations. Caused by the oxidation of the cage filling molecule the thermal expansion of the sodalite is slowed down. The drastic decrease above 648 K is caused by the beginning destruction of the sodalite framework.

[1] Weitkamp, J., Fritz, M., Ernst, S., Int. J. Hydrogen Energ. **20** (1995), 967-970.
[2] Buhl, J.-Ch., Gesing, Th.M., Rüscher, C.H., Micro. Meso. Mater. **80** (2005), 57-63.
[3] Buhl, J.-Ch., Gesing, Th.M., Höfs, T., Rüscher, C.H., J. Solid State Chem. **179**
(2006), 3877-3882.
[4] Robben, L., Poltz, I., Buhl, J.-Ch., Z. Kristallogr. NCS **225** (2010), 421-422.

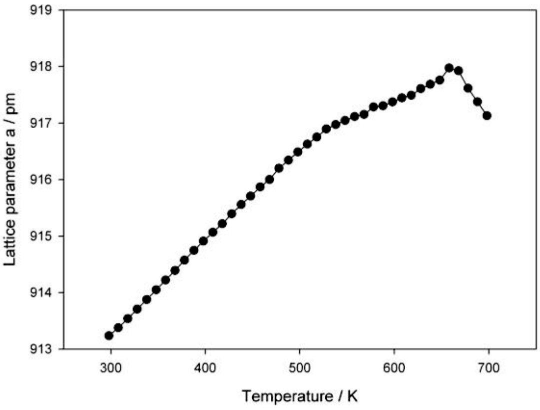

Figure 1: Development of the lattice parameter *a* of the gallogermanate tetrahydroborate sodalite.

P10-P30

Structure solution, solid state kinetics and PDF analysis of pyridine complexes from powder data

L. Fink[1], T. Bernert[1], E. Alig[1], N. Külcü[1], M.U. Schmidt[1]
[1]Anorg. Analyt. Chemie, Universität Frankfurt, Frankfurt, Germany

[NiCl2(C5H5N)] was prepared from [NiCl2(C5H5N)4] by thermal decomposition via [NiCl2(C5H5N)2] [1].

The crystal structure of [NiCl2(C5H5N)] was solved from powder data [2] using Patterson-function and direct methods included in EXPO2009 [3]. In [NiCl2(C5H5N)], the nickel atoms are octahedrally coordinated by five chlorine atoms and one nitrogen atom of the pyridine ring. Due to the edge sharing of the octahedra, one-dimensional polymeric chains pack parallel to the [010] direction.

With the knowledge of both crystal structures, [NiCl2(C5H5N)2] [4], as well as [NiCl2(C5H5N)], the solid state kinetics of the thermal decomposition could be determined. The time- and temperature-resolved powder diffraction patterns were evaluated with quantitative Rietveld refinement using TOPAS [5]. The analogous copper phases are well known, except [CuCl2(C5H5N)]. The powder pattern of this compound could not be indexed. To get more information, pair distribution function (PDF) analysis was performed [6] using laboratory powder data. The PDF analysis leads to the local structure, which for copper is given by a typical Jahn-Teller-distorted octahedron.

[1] Liptay, G., Wadsten, T., Borbely-Kuszmann, A., J. Thermal Anal., 1986, 31.

[2] Bernert, T., Fink, L., Alig, E., Hammer, S. M., Schmidt, M. U., Külcü, N., in preperation.
[3] Altomare, A., Camallt, M., Cuocci, C., Giacovazzo, C. Moliterni, C. Rizzi, R., J. Appl. Cryst., 2009, 42.
[4] Alig, E., Bernert, T., Fink, L. Külcü, N., Yesilkaynak, T., Acta Cryst., 2010, E66.
[5] Coelho, A. A.: TOPAS Academic 4.1, 2007, Coelho Software, Brisbane, Australia.
[6] Qui, X., Thompson, J. W., Billinge, S. J. L., J. Appl. Cryst., 2004, 37.

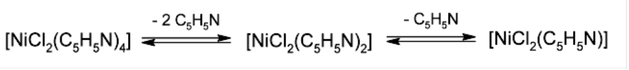

$$[NiCl_2(C_5H_5N)_4] \xrightleftharpoons{-\,2\,C_5H_5N} [NiCl_2(C_5H_5N)_2] \xrightleftharpoons{-\,C_5H_5N} [NiCl_2(C_5H_5N)]$$

Figure 1: The thermal decomposition of [NiCl2(C5H5N)4]

P10-P31

Structural units with edge-sharing between actinyl polyhedra and TO_4 (T = Cr, S, Si, As, P, V) tetrahedra: synthesis and crystal structure of novel $[(CH_3)_3CNH_3]_4[(UO_2)_2(CrO_4)_4]$ *tert*-butylamine uranyl chromate

O. Siidra[1], S. Krivovichev[1], E. Nazarchuk[1]
[1]Saint-Petersburg State University, Crystallography, Saint-Petersburg, Russian Federation

Dark yellow perfectly shaped transparent single crystals of $[(CH_3)_3CNH_3]_4[(UO_2)_2(CrO_4)_4]$ (**1**) up to 1.5 mm long were obtained by hydrothermal methods. A suitable crystal of **1** was mounted on a Bruker three-circle Smart APEX II X-ray diffractometer operated at 50 kV and 40 mA. The structure of **1** (*Pbca*, *a* = 10.327(3), *b* = 18.257(5), *c* = 35.285(10)Å, *V* = 6653(3)Å^3, R_1 = 0.033) contains two symmetrically independent U^{6+} cations, which are bonded to two O atoms each, forming $(UO_2)^{2+}$ uranyl ions. Uranyl ion is coordinated by five O atoms arranged at the equatorial vertices of UO_7 pentagonal bipyramids. The structure contains four symmetrically independent Cr sites each coordinated by four oxygen atoms. $U(2)O_7$ bipyramids share common equatorial edges to form U_2O_{12} dimers. The scheme of linkage for $Cr(1)O_4$ and $Cr(4)O_4$ tetrahedra with U_2O_{12} dimers and isolated UO_7 bipyramids is usual. These units are interconnected via common corners. But $Cr(2)O_4$ and $Cr(3)O_4$ tetrahedra share common edges with U_2O_{12} and UO_7 units in unique way for uranyl chromates. Thus both monodentate and bidentate linkage of CrO4 tetrahedra and U_2O_{12}, UO_7 units provide the formation of [UO2)2(CrO4)4] sheets (Fig. 1). The interlayer space between the layers is filled by $(CH_3)_3CNH_3$ protonated amine molecules (Fig. 1). Edge sharing between hexavalent actinyl polyhedra and tetrahedral oxoanions has been frequently observed in uranyl sulfates, but never in chromates. Thus, the studied compound is the first example of bidentate linkage of UO_7 pentagonal bipyramids (*PBP)* and CrO_4 tetrahedral oxoanion.

Geometrical parameters of bidentate coordination of uranyl ions by tetrahedral oxoanions have been studied using data available for uranyl phosphates, arsenates, vanadates, silicates, sulfates and chromates (only structures with uranyl ions in *PBP* coordination were taken into account). Data indicate that, whereas bidentate coordination has a strong influence upon the $U\text{-}O_{br}$ bond length (it appears to be essentially longer than the average $U\text{-}O_{eq}$ bond length in the *PBP* coordination, the bond-length distortions within the TO_4 tetrahedra are much less sensitive to the bonding interactions with uranyl ions. The latter observation can, however, be somewhat deteriorated by the participation of the tetrahedra in bonding to other types of cations in the structure.

This work was financially supported by St. Petersburg State University internal budget grant (3.37.84.2011) and DFG-RFBR collaboration grant (#11-05-91330)

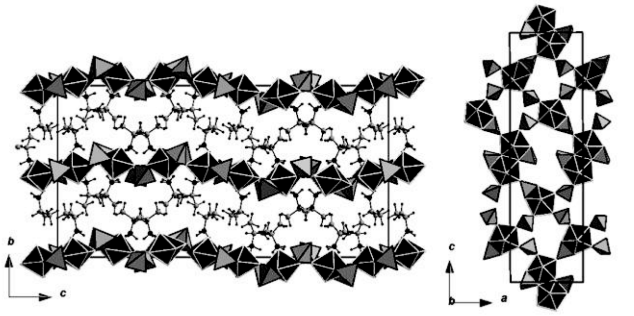

Figure 1: General projection of the crystal structure of $[(CH_3)_3CNH_3]_4[(UO_2)_2(CrO_4)_4]$ (designations: UO_7 polyhedra = black, CrO_4 tetrahedra = grey) (left) and projection of $[UO_2)_2(CrO_4)_4]$ layer along the *b* axis (right).

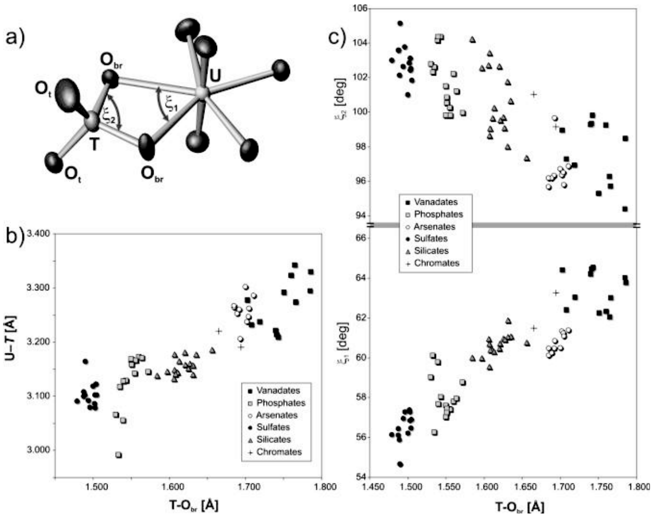

Figure 2: (a) Scheme of bidentate linkage of UO_7 *PBP* and TO_4 tetrahedral oxoanion; (b) the U···T distance versus $T\text{-}O_{br}$ bond lengths; (c) the ξ_1 and ξ_2 valence angles versus $T\text{-}O_{br}$ bond lengths.

P10-P32

Synthetic analogues of naturally occurring Pt_2HgSe_3 and Pd_2HgSe_3 phases: Crystal structure study

F. Laufek[1], A. Vymazalova[1], M. Drabek[1], J. Drahokoupil[2]
[1]Czech Geological Survey, Laboratory of X-ray diffraction, Praha 5, Czech Republic
[2]Institute of Physics, Prague, Czech Republic

Two naturally occurring phases Pt_2HgSe_3 and Pd_2HgSe_3 were synthesised and structurally characterized. Recently, Pt_2HgSe_3 unknown phase was discovered in hematite-rich auriferous veins, known as jacutinga, from Cauê iron-ore deposit (Itabira district, Minas Gerais, Brazil). This Pt-Hg selenide was observed in one polished section as a grain with size of 50 μm and occurs on an aggregate of atheneite, potarite and hematite [1]. Analogical Pd-bearing phase Pd_2HgSe_3 was observed in gold-bearing carbonate veins at Hope’s Nose, Torquay, Devon, England [2].

Because of extremely low amount of natural samples and difficulties connected with their isolation, the above-mentioned phases were synthesized from elements by conventional solid-state reactions. Stoichiometric amounts of individual elements were sealed in silica glass tubes and resultant mixtures were heated at selected temperatures. Samples with Pt_2HgSe_3 and Pd_2HgSe_3 were heated at 400°C. After long-term annealing, the samples were quenched in a cold-water bath. All attempts to prepare single crystals suitable for single-crystal examinations failed; hence the crystal structures of Pt_2HgSe_3, and Pd_2HgSe_3 were determined from powder X-ray diffraction data. The programs EXPO2004 and SuperFlip were used for structure determinations; subsequent refinements were performed width FullProf program.

Pt_2HgSe_3 and Pd_2HgSe_3 are isostructural compounds. Phases crystallize in space group *P-3m*1, (*a* = 7.34 Å, *c* = 5.29 Å, *V* = 247 Å^3 for Pt_2HgSe_3) and Z = 2. Their crystal structures are composed of layers of [Pt(Pd)Se_6] octahedra and [Pt(Pd)Se_4] squares running parallel to (001)planes. The Se atoms are arranged in layers perpendicular to the **c**-axis forming the *Kagomé*-nets. These nets show AB stacking sequence along the **c**-axis. The Hg atoms are positioned in anti-cubooctahedral voids (defined by Se atoms) between these layers. The crystal structures of Pt_2HgSe_3 and Pd_2HgSe_3 are isostructural with $Pt_4Tl_2X_6$ (X = S, Se, or Te) phases [3] and can be easily derived from that of the mineral sudovikovite ($PtSe_2$, *P-3m*1). Pt_2HgSe_3 phase was recently described as a new mineral jacutingaite [4].

[1] A. R. Cabral, H. F. Galbiatti, R. Kwitko-Riberio, B. Lehmann, *Terra Nova,* 20, 32-37 (2008).

[2] W. H. Paar, A. C. Roberts, A. J. Criddle, D. Topa, *Mineral. Mag*., 62, 257 - 264 (1998).

[3] W. Bronger, B. Bonsmann, *Z. Anorg. Chem*., 621, 2083-2088 (1995).

[4] A. Vymazalová, F. Laufek, M. Drábek, A. R. Cabral, J. Haloda, T. Sidorinová, B. Lehmann, H. F., Galbiatti, J. Drahokoupil, *Can. Mineral*. (submitted).

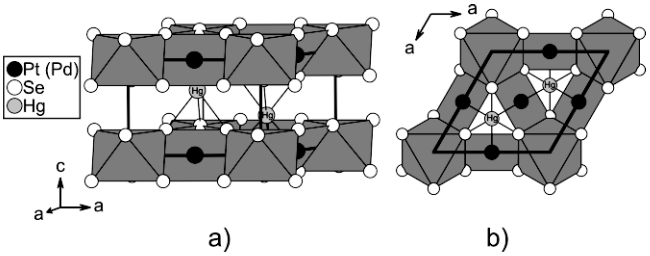

Figure 1: Polyhedral representation of Pt_2HgSe_3 and Pd_2HgSe_3 phases showing [Pd(Pt)Se_6] octahedra and [Pt(Pd)Se_4] squares. (a) Perspective view, (b) view along the **c**-axis.

P10-P33

Structural Parameters in the System (Sr-Ba)TiO_3

B. Kodess[1], P. Kodess[2], V. Smatrakov[1]
[1]ICS@E-VNIIMS, Metrology of Crystals, Moscow, Russian Federation
[2]ICS&E, Materials Science, Aurora, CO, United States

At present the attention of researchers working in materials science and solid state physics is increasingly focused on disordered systems - solid solutions, doped materials, etc. An effect of atom substitution in crystal originates from both dimension factors and features of the electron configuration of substituting atoms that, as a rule, essentially modifies material properties. Disorder in crystal lattice in itself can significantly and, sometimes, dramatically influence on the electron structure and related properties. Recently experimental methods of study of the electron density distribution and its numerical characteristics in partially disordered compounds using full X-ray measurement data were well developed. Based on high precision experimental data determination of structural parameters and thermal atom movement characteristics allows mapping the deformation and valence electron density in real space unit sell.

We investigate disorder ABO3 oxide perovskite family on base $SrTiO_3$. Variations of composition can noticeably influence also on their dielectric properties. The Ba concentration variation from x=0.0 to x=0.4 causes a slight monotone increase in dielectric constant. Further increasing x leads to a sharp enhancement of this tendency.

A modified method of growth from melt Sr(1-x)Ba(x)TiO3 crystals presented. Melt of KF - KVO was used. The crystal composition was varied by changes of SrO:BaO relation in the charge. The crystal composition was analyzed by an X - Ray microprobe and was established that the crystal composition inhomogeneity is no more than 0.2 - 0.4 % . Precision X-Ray diffraction studies of crystals were carried out. Ba substitution of Sr led to increasing of lattice parameters and to a small decrease of thermal parameters of Ba and Sr atoms. Changes of properties at partial substitution of Sr atoms by Ba ones are discussed.

P10-P34

Single Crystal Growth and Structure Determination of Synthetic Hydroromarchite, $Sn_6O_4(OH)_4$

H. Reuter[1], D. Schröder[1]
[1]Universität Osnabrück, Institut für Chemie, Osnabrück, Germany

Aqueous solutions of tin(II) salts contain a lot of different mono- and polynuclear, cationic or anionic, oxo-hydroxo species depending on its salt and proton concentrations. From neutral solutions, colourless tin(II) monoxide, SnO, separates in form of a bad defined, voluminous, water insoluble precipitate, containing different amounts of water. Only on certain conditions one can prepare a stoichiometric exact hydrate having the composition, SnO · 1/3H_2O. Some older structure investigations [1],[2] revealed that this compound is a polynuclear molecular oxide hydroxide with formula $Sn_6O_4(OH)_4$.

This compound is also known to be a so-called anthropogenic mineral because it was found from archaeologists on many tin artefacts which were covered for long periods by water. In mineralogy this compound is named hydroromarchite.

In contrast to the importance of this compound in chemistry and mineralogy the structural data are of limited precision, obviously because it is difficult to growth appreciate single crystals.

By chance we found single crystals of the title compound which were of high quality and large enough for X-ray diffraction experiments, in a more than ten years old sample of ^{n}BuSnH_3 in toluene.

$Sn_6O_8H_4$: tetragonal, *P*-4$2_1$*c* (no. 114), a = 7.8809(2) Å, c = 9.0595(4) Å, V = 562.67(3) Å^3, Z = 2, d_{cal} = 4.983 g/cm^3, μ(MoKa) = 13.124 mm^{-1}, F_{000} = 736, 2q_{max} = 70°, 24673 reflection collected, 1243 unique reflections, R_{int} = 0.0298, multi-scan absorption correction, T_{min} = 0.3161, T_{max} = 0.3718, completeness 100%, 35 parameters refined, absolute structure parameter = 0.04(5), R_1 [I > 2s(I)] = 0.0149, R_1 [all data = 0.0297], wR_2 [I > 2s(I)] = 0.0158, wR_2 [all data = 0.0299], De_{max} = 0.775 eÅ^{-3}, De_{min} = -0.763 eÅ^{-3}.

The poster will describe the experimental conditions of crystal growth as well as the molecular (Fig. 1) and crystal structure and its determination in more detail.

References:

[1] Howie, R. A.; Moser, W. *Nature* **1968**, *219*, 372-373.

[2] Abrahams, I.; Grimes, S. M.; Johnston, S. R.; Knowles, J. C. *Acta Crystallogr.* **1996**, *C52*, 286-288.

Figure legend: Ball-and-stick model of the $Sn_6O_4(OH)_4$-molecules with bond lengths in Å; with exception of the hydrogen atoms all other atoms are shown as 35% thermal displacement ellipsoids.

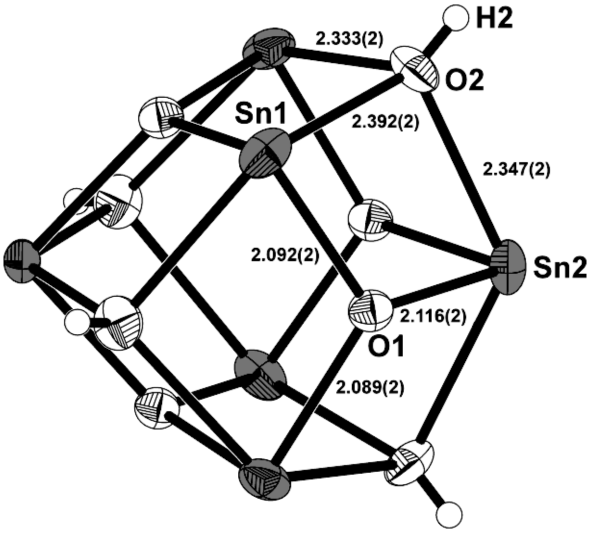

Figure 1

P11-P01
Neutron powder diffraction investigation and thermal stability of $(Bi_{1-x}Sr_x)_2(Al/Ga)_4O_{9-x}$

T.M. Gesing[1], G. Nénert[2], H. Schneider[3], R.X. Fischer[3]
[1]Chemische Kristallographie fester Stoffe, Institut für Anorganische Chemie, Bremen, Germany
[2]Institut Laue-Langevin, Grenoble, France
[3]Universität Bremen, Kristallographie, FB Geowissenschaften, Bremen, Germany

$Bi_2M_4O_9$ compounds (M = Al, Ga, Fe) are described to have potential as electrolytes in solid oxide fuel cells (SOFC) [1]. It has been suggested that the electrical conductivity results from an increase of oxygen vacancies due to the requirement of charge neutrality with the substitution of Bi^{3+} by Sr^{2+} [2].

The samples were synthesized using the glycerine nitrate as well as EDTA/citric acid methods [3], and washed with nitric acid to remove impurity phases. Whereas small amounts of Bi_2O_3 and strontium metallates were always found in the as synthesized samples no indication for these impurities were detected after washing. Thermal expansion and thermal stability were investigated using high-temperature powder X-ray measurements using a HTK1200N heating chamber evaluated by Rietveld refinements. The crystal structure of $(Bi_{1-x}Sr_x)_2Al_4O_{9-x}$ has been investigated by neutron powder diffraction data collected using the high resolution powder diffractometer D2B at the ILL. Powder neutron data were collected at room conditions and at high temperature. While the thermal expansions of non-doped bismuth-metallate mullite-type compounds do not show any discontinuities [4], a clear discontinuity is observed in the investigated strontium-doped materials between 1050 K and 1150 K. This discontinuity leads to smaller lattice parameters and unit-cell volume in the case of the aluminate phase. Replacing half of the aluminum atoms by gallium, a stronger decrease of the corresponding lattice parameters is observed with respect to the pure strontium doped aluminate. In the corresponding gallate compound the final *a* lattice parameter was found larger than it was before the heating cycle. A second heating cycle did not show any deviation for the lattice parameters before and after the heating, which means that the lattice parameter change corresponds to an exsolution of strontium. Because divalent strontium replaces trivalent bismuth, an oxygen deficiency is introduced into the structure which leads to a mullite typical tri-cluster formation. In the Rietveld refinements of the crystal structure of $(Bi_{1-x}Sr_x)_2Al_4O_{9-x}$ based on neutron powder diffraction data a tri-cluster of Al_3O could be refined without applying any constraints together with the Bi/Sr and O3 occupancies as dependent parameters. These results indicate that 6(1) atom-% strontium out of initially 20 atom-% used for the synthesis were incorporated into the structure.

[1] J.B. Goodenough: *Ann. Rev. Mater. Res.* 33 (2003) 91. [2] S. Zha et al.: *Solid State Ionics* 156 (2003) 197. [3] Th. M. Gesing et al.: *J. Eur. Ceram. Soc.* (2011)
doi:10.1016/j.jeurceramsoc.2011.04.004. [4] R. X. Fischer et al.: *Acta Crystallogr.* A65 (2009) s232.

P11-P02
New Li-Na-ionic conductor materials: $(Li, Na)_{2x}[Zn_{2-x}SiO_4]$

S. PARK[1], C.J. Pietsch[1], L. Garcia B. Lara[1]
[1]Kristallographie/LMU, Geo- & Umweltwissenschaften, München, Germany

In exploring material systems environmentally and economically reasonable for all-solid-state Li-ionic batteries, the willemite (α-Zn_2SiO_4)-topology has given attention to us for its extremely wide intrinsic chemical and thermal stability. As a consequence, a new synthetic willemite-type compound, $(Na, Li)_{0,46}[ZnSiO_4]$ could be obtained. This structure containing Li- and Na cations in its six membered-ring (6MR) channel is confirmed by neutron powder diffraction (SPODI, FRMII) [1]. The presence of non-framework alkali metal cations within 6MR-channels of the willemite-topology is new to its numerous variants reported so far [2-4; references therein]. In addition, our temperature-variable neutron powder diffraction study [5] could resolve long-range dynamic disorder at these new sites for Li and Na, as shown in **Figure**. Very recently, single crystals of $(Li, Na)_{2x}[Zn_{2-x}SiO_4]$ compounds have been synthesized successfully using molten NaCl at 1173 K (diameter of single crystal: up to 50 microns). Single crystal X-ray diffraction with one of those compounds agree with $(Na, Li)_{0,15}[Zn_{1,93}SiO_4]$. Further new willemite-type structures with varying their (Li, Na)-contents are presented at this joint meeting DGK-DMG-ÖMG at Salzburg 2011.

References

1. C.J. Pietsch, *Herstellung von Li-Na-Ionenleitermaterialien,* Bachelor Thesis, Geo- und Umweltwissenschaften, Ludwig-Maximilians-Universität München, 2009.
2. G.T. Chandrappa, S. Ghosh, K.C. Patil, J. Mater. Synth. Proc. **7**(1999), 273-279.
3. J. Sato, H. Kobayashi, K. Ikarashi, N. Saito, H. Nishiyama, Y. Inoue, J. Phys. Chem. B **108** (2004), 4369-4375.
4. E. Ozel, H. Yurdakul, S. Turan, M. Ardit, G. Cruciani, M. Dondi, J. Eur. Ceram. Soc. **30** (2010), 3319-3329.
5. L. García Benítez Lara, *Li-ion Battery Materials Li/Na Willemite-type,* Master Thesis, Geo- und Umweltwissenschaften, Ludwig-Maximilians-Universität München, 2010.

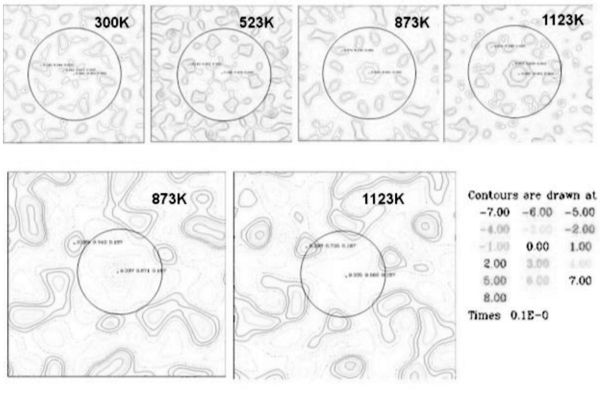

Figure 1: Difference Fourier maps evaluated from neutron powder diffraction data (SPODI_FRMII) of Na/Li-willemite show positive densities of neutron scattering lengths (nsl) at

(0,0,0), i.e. the center of 6MR-channel for missing Na, and negative nsl at (1/3, 2/3, 0,187) for missing Li. The changes in nsl-densities at these positions at elevated temperatures clearly point to dynamic motions of Na (top) and Li (below) in channels of Na/Li-willemite.

P11-P03

(Li,Cr)$FePO_4$: New structure model, neutron powder dataand transition to superionic phases

J. Schneider[1], M. Hölzel[2], E. Schmidbauer[1]
[1]Ludwig-Maximilioans-Universität München, Dept. für Geo- und Umweltforschung, München, Germany
[2]TU-Darmstadt, Strukturforschung, Darmstadt, Germany

Due to the rapid development of portable electronic devices the search for better and cheaper positive electrode materials led among others to the series $LiMPO_4$ [1] with M=Fe, Co, Mn, Ni and olivine type structure (space group Pnma). $LiFePO_4$ was particularly well investigated [2] in view of increasing the electronic conductivity by solid-solution doping with metals supervalent to Li^+.

Prelimary analysis of room temperature neutron powder data [3] obtained at FRMII and recent structure simulations [4] showed that relaxation of structure symmetry, for instance to space group $P2_12_12_1$, leads to noticeable amelioration of fits. The straight chain of Li ions in b-direction is then replaced by a more realistic zig-zag chain together with the corresponding Li probability density functions.

Transitions to superionic high temperature phases have been found in several Li ion conductors [5]. Analysis of high temperature neutron powder data [3] obtained at FRMII show a distinct change of slope of the Li atom displacement parameters as a function of temperature indicating similar transitions to a superionic high temperature phase. Cation doping with Cr ions, meant to increase the electronic conductivity of $LiFePO_4$, remarkably lowers this transition temperature by about 200K.

[1] Padhi et al., J. Electrochem. Soc. **144** (1997) 1188-1194
[2] Chung S. et al., Nature Materials **1** (2002) 123-128
[3] Schneider J., EPDIC XII, Geneva 2006
[4] ENDEAVOUR, Crystal Impact GbR, Bonn
[5] Buehrer W., Altdorfer F., Mesot J., Bill H., Carron P. and Smith H.G. J. Phys.: Condens. Matter 3 (1991) 1055-1064

P12-P01

Garnet-Chloritoid-Kyanite schists from the Eclogite Zone, Tauern Window, Austria

G. Hoschek[1]
[1]Institute Mineralogy Petrology, University Innsbruck, Innsbruck, Austria

Garnet-Chloritoid-Kyanite schists from the Eclogite Zone, Tauern Window, Austria
Gert Hoschek
Institute of Mineralogy-Petrography, University of Innsbruck, Innrain 52, 6020 Innsbruck, Austria

Metamorphic PT-conditions of the assemblage garnet-chloritoid-kyanite from pelitic samples of the Eclogite Zone are determined recently in good agreement by Smye et al. (2010, 2011) and Hoschek et al. (2010). Work in progress for three samples is based on microprobe analyses and Thermocalc average PT-calculations combined with pseudosections in the K2O-Na2O-CaO-FeO-MgO-MnO-Al2O3-SiO2-TiO2-H2O system. Stability of this assemblage (+phengite, paragonite, rutile, quartz, H2O) for the XRF composition of sample A is restricted to a narrow region at c. 15 kbar/595°C - 25 kbar/565°C. For samples B and C smaller PT-regions resulted at c. 22.5-24.5 kbar, 575°C and 24.5kbar, 570°C (+ jadeite).

Observed garnet zonations are compared with calculated results for prograde PT-paths and fractional resp. equilibrium garnet crystallization. Calculations with an asymmetric phengite solution model resulted in c. 2.5 kbar higher pressure compared with the symmetric model. However average PT-conditions for garnet-chloritoid-kyanite assemblages partly in the coesite-quatz transition region are questionable in view of Tauern rocks lacking coesite relicts.

Different Mg/(Mg+Fe) values are measured in chloritoid from matrix resp. inclusions in garnet and secondary overgrowth of kyanite by chloritoidt is frequently observed. A clockwise PT-path is therefore suggested within or more likely overstepping the garnet-chloritoid-kyanite stability field and reentering the chloritoid growth region upon exhumation from peak conditions (e.g. Dachs et al. 2005). Definition of equilibrium assemblages is hampered by retrograde overprint due to a later heating event at lower PT-conditions.

References:

Dachs E., Kurz, W. & Proyer, A. (2005): Mitt. Österr. Miner. Ges. 150, 199-226.
Hoschek G., Konzett, J. & Tessadri, R. (2010): Eur. J. Mineral. 22, 721-732.
Smye, A.J., Greenwood, L.V. & Holland, T.J.B. (2010): J. metamorphic Geol. 28, 753-768.
Smye, A.J., Bickle, M.J., Holland, T.J.B., Parrish, R.R., Condon, D.J. (2011): Earth Planet. Sci. Lett.
doi:10.1016/j.epsl.2011.03.037.

P12-P02

Petrographic characteristics and electron microprobe investigations on major lithotypes of the Rosh Pinah Formation, Southern Namibia

S. Rode[1]
[1]Institut für Mineralogie, Lagerstättenlehre und Petrologie, Freiberg, Germany

The Rosh Pinah Formation constitutes a part of the Port Nolloth Zone (Gariep Belt) and is widely known for the occurrence of stratabound Pb-Zn deposits. In order to understand the metamorphic history of the ore-bearing volcanosedimentary lithologies of the Rosh Pinah Formation, a careful petrological and mineral chemical study of common lithotypes, including two different mica schists and one metapsammite has been carried out.

The amphibole mica schist is characterised by green amphiboles crosscutting the foliation defined by biotite and chlorite. The lithotype contains zoned garnet crystals, which overgrow the main foliation. Amphiboles are ferro-hornblende or ferro-edenite. The biotite-muscovite mica schist consists of rotated biotite and garnet blasts arranged within a matrix of foliated muscovite and opaque minerals (mostly ilmenite and titanite). Garnet is partially chloritised or replaced by biotite. The metapsammite is arranged in Bouma Cycles and is predominantly composed of angular quartz and microcline grains. Minor types of metapsammites are biotite- and garnet-rich without visible foliation.

All analysed garnets representing different lithotypes show similar chemical evolution with a rimward decrease of spessartine in favor of almandine and almost unzoned grossular and pyrope. The garnet chemistry suggests a prograde metamorphic evolution with slightly increasing temperatures and high pressures for all three samples. The schists have been affected by upper greenschist-facies metamorphism and strong polyphase deformation. The first stage of the Gariepian orogeny is characterised by biotite and garnet at c. 545 Ma. During the late-tectonic stage, amphiboles grow at c. 630 °C / 6.5 kbar (after Zenk & Schulz 2004) and crosscut the main foliation. Chlorites indicate the last stage of metamorphism with a range of crystallisation temperature of 260 - 340 °C (after Cathelineau 1988, modified by Xie et al. 1997). The metapsammite was also affected by upper greenschist-facies metamorphism, while biotite, garnet and muscovite crystallised during the late stage of prograde metamorphism.

References

Cathelineau, M. (1988): Cation site occupancy in chlorites and illites as a function of temperature. Clay Miner. **23**. 471-485.

Xie, X., Byerly, G.G. & Ferell, R.E.Jr. (1997): IIb-trioctahedral chlorite from the Barberton greenstone belt: crystal structure and rock composition constrains with implications on geothermometry. Contr. Min. Pet. **126**. 275-291.

Zenk, M. & Schulz, B. (2004): Zoned Ca-amphiboles and related P-T evolution in metabasites from the Barrovian metamorphic zones in Scotland. Miner. Mag. **68**. 769-786.

P12-P03

Geochemical constraints on the two-mica granites classification of the South Bohemian Batholith (Bohemian Massif)

M. René[1]

[1]Institute of Rok Structure and Mechanics, Academy of Sciences of the Czech Republic, Geochemistry, Prague 8, Czech Republic

The South Bohemian Batholith (SBB) is the largest granitoid complex (6000 km^2) within the Bohemian Massif. It intruded high-grade metamorphic rocks (predominantly various types of paragneisses and migmatites) of the Moldanubian Zone. Two-mica granites represent the most significant rock type of this magmatic body. Three main geochemical two-mica granite types can be distinguished in the SBB: the low-Th Deštná granite, the intermediate-Th Eisgarn granite and the high-Th Lipnice and Steinberg granites. All these granites are peraluminous (A/CNK = 1.02-1.34) with low CaO concentrations. Th concentrations and REE element patterns are quite distinct class marks for the above mentioned three geochemical types of two-mica granites. The highest bulk content of REE is significant for the Lipnice and Steinberg granites, whereas the lowest bulk of REE was observed in the Deštná granites.

The Deštná granites are leucocratic biotite-muscovite granites with predominance of muscovite. They contain very common schlieren or small nodular aggregates of restitic biotite. Their accessory minerals assemblage usually included in K-feldspar consists of monazite, zircon, apatite, and a significant occurrence of xenotime. These granites are characterized by very low contents of Th and Zr and by the absence of a negative Eu anomaly. The Eisgarn granites are texturally highly variable granites (porphyritic and/or equigranular, fine- to medium-grained), with a variable ratio of muscovite and biotite. The accessory minerals assemblage is formed by apatite, zircon and monazite. These granites are characterized by higher ratio LREE/HREE (La_N/Yb_N = 32-40) and particularly remarkable negative Eu anomaly. The Lipnice granite is a fine- to medium-grained monzogranite usually containing high amounts of restite enclaves. The Steinberg granite is a hiatalporphyritic, medium-grained monzogranite with a strong dimensional fabric of K-feldspar phenocrysts. The accessory minerals assemblage of apatite, monazite and zircon is significant for both granite types. Both granite types are characterized by high content of Zr and Hf and by LREE/HREE high ratio (La_N/Yb_N = 34-42).

This study was supported by the Ministry of Education, Youth and Sports of the Czech Republic (project No. ME10083).

P12-P04

Accessory minerals in contact metamorphism II: crystal chemistry and Raman spectroscopy of Ba-rich white micas from the innermost contact aureole of the Lienz/Edenwald tonalite

M. Tribus[1], P. Tropper[1], U. Haefeker[1]

[1]University of Innsbruck, Institute of Mineralogy and Petrography, Innsbruck, Austria

Ba-micas can occur in a variety of geological environments, but mostly they occur in contact metamorphic rocks. In the vicinities of plutons the formation of Ba-micas is a product of metasomatic processes. The ideal composition of the dioctahedral Ba-rich white mica ganterite $[Ba_{0.5}(K+Na)_{0.5}]Al_2(Si_{2.5}Al_{1.5})(OH)_2$, represents a 1:1 mixture along the solid solution between muscovite/paragonite (true micas) and the Ba-brittle mica.

The micas of this study occur in the Lienz contact aureole adjacent to the Edenwald tonalite in the surrounding quartzphyllitic Austroalpine basement. Geothermometry using Ti-in-biotite thermometry yielded temperatures of 680 ± 33°C for the innermost part of the aureole. Electron microprobe analyses of the white micas showed that the Ba content reaches up to 13.38 wt.% BaO, even though Ba is not the dominant interlayer cation. The formula of a typical Ba-rich white mica is $Ba_{0.3}K_{0.41}Na_{0.22})_{\Sigma 1.00}(Al_{1.93}Mg_{0.02}Fe_{0.03}Ti_{0.02})_{\Sigma 2.00}$ $[Si_{2.66}Al_{1.34}O_{10}]$ $(OH)_2$. Increasing Ba concentrations correlate with an increase in Na and a decrease in K. The octahedral position is mostly filled by Al, whereas only traces of Ti, Fe^{2+} and Mg are present. The Ba-rich micas are characterized by higher concentrations of Al[T] and lower K contents than in normal Na-K micas. The composition of the Ba-rich white micas can be described by various exchange vectors: 1.) the simple interlayer $[Na]=[K]_{-1}$ exchange and 2.) the $[Al][T]=[Si][T]_{-1}$ substitution which occurs over the complete range of Ba contents. The substitution on the tetrahedral site is balanced by a $[Ba]=[K]_{-1}$ exchange in the interlayer position. The often-cited Ba-substitution including elements on the octahedral site $[Ba][Fe, Mg]=[K]_{-1}[^{VI}Al]_{-1}$ is not well developed and only a slightly negative correlation between Ba^{2+} and Mg^{2+} and a positive correlation between Ba^{2+} and Ti^{4+} can be observed. Therefore, the composition of the Ba-rich with micas in the contact aureole of the Lienz tonalite can be described with a combination of the coupled substitution namely $[Ba][Al^{IV}]=[K]_{-1}[Si]_{-1}$ and the simple $[Na]=[K]_{-1}$ exchange vector. Complete solid solutions between muscovite and Ba-rich white micas were observed since Ba contents range from 0.07 wt.% up to 13.38 wt.% BaO. The micro-Raman spectra of the Ba-rich white micas corresponds well with the standard muscovite pattern. The comparison between micas with lower (0.07- 0.26 apfu) and higher (0.29-0.37 apfu) Ba contents yielded that the peaks at 265 cm^{-1} and 396 cm^{-1} show a distinct shift as a function of the Ba content of the micas.

P12-P05

Accessory mineral in contact metamorphism I: major, minor and trace element variations of apatite and tourmaline as a function of metamorphic grade in the contact aureole of the Lienz tonalite

M. Tribus[1], P. Tropper[1]

[1]University of Innsbruck, Institute of Mineralogy and Petrography, Innsbruck, Austria

The distribution of major and trace elements in accessory minerals can provide important information on the metamorphic evolution of rocks. The aim of this investigation is to evaluate the influence of increasing temperature on the chemical composition of apatite and tourmaline using samples along a well-defined profile within the contact aureole of the Lienz/Edenwald tonalite. Minor element variations in apatites do not seem to vary systematically, but a distinct increase towards the contact was observed in Mn, Cl and ΣREE+Y. The increasing incorporation of REE+Y can be described by the coupled substitution $(REE+Y)^{3+}+Na^{+1}=Ca^{2+}_{-2}$. The major anion constituents, F and OH, show a systematic variation with respect to the metamorphic grade. On the other hand Cl does not vary consistently, although an overall increase towards the contact was observed. The elevated Cl contents in the innermost part of the aureole closest to the pluton probably results from the circulation of hydrothermal fluids associated with the intrusion process.

In contrast to apatites, tourmalines from this contact aureole are characterized by complex textural zoning, which is also reflected in strong chemical zoning. This zoning pattern displays at least two main growth events, where the inner rim shows higher Al[T], Ca and Ti contents and lower Si, Mg[Y] Al[Y] contents compared to the composition of the core and outer rim. With increasing metamorphic grade the tschermak-substitution becomes more significant (Henry & Dutrow, 1996), which results in higher amounts of Al and lower Si and Mg contents. The chemical zoning of the investigated tourmalines can thus be interpreted as a prograde growth sequence from the core (Variscan?, Eo-Alpine?) to the inner rim and growth during decreasing metamorphic grades from thev inner rim to the outer rim. This chemical trend are can be observed in all contact metamorphic samples throughout the contact aureole.

This study shows that accessory minerals do provide important information concerning 1.) the extent of a thermal overprint, 2.) the polymetamorphic nature (tourmaline) of rock samples as well as 3.) evidence of episodes of localized fluid/rock interactions (apatite).

Henry, D.J. & Guidotti, C.V. (1985): Tourmaline as petrogenetic indicator mineral: an example from the staurolite-grade metapelites of NW Maine. American Mineralogist, **70**, 1-15.

P12-P06

Petrologie und Geothermometrie des Pseudofulgurits von Kaltenbach (Gemeinde Vitis, Niederösterreich)

P. Tropper[1], D. Braunhofer[1]
[1]University of Innsbruck, Institute of Mineralogy and Petrography, Innsbruck, Austria

Im Juli 2007 wurde in Kaltenbach nördlich von Zwettl, NÖ, im Ackerboden eine glasartige Substanz gefunden. Das Aggregat befand sich wenige Meter entfernt von einem Strommast unmittelbar unterhalb einer 20 kV Freilandstromleitung. Die Tatsachen, dass die Glasmasse direkt unter der Freilandleitung aufgefunden wurde und zusätzlich unmittelbar über der Fundstelle ein frisch reparierter Bruch an einem Leiterseil festzustellen war, legten die Vermutung nahe, dass ein Blitzereignis in ursächlichem Zusammenhang mit der Entstehung des glasigen Gebildes stehen könnte (Brandstätter et al., 2008). Die Proben des Pseudofulgurits von Kaltenbach zeigen einen z.T. exotischen Mineralbestand, der durch den extremen Temperaturanstieg erklärbar ist. Durch die rasche Abkühlung ist die Schmelze in eine mehr oder weniger homogene Glasmatrix im Zentralbereich und einen kristallisierten Bereich am Rand umgewandelt worden. Der Mineralbestand der Proben besteht neben den Mineralen Quarz, Feldspat und reliktischem Kyanit auch noch aus Mullit, Cr-Spinell, Spinell, Osumilith, Amphibol, Zirkon, Baddeleyit, Rutil, Fe-P-, Fe-P-Ni- und Fe-P-Si-Globuli. Auffallend sind die vielen Fe-P Globuli. Bei sehr großer Vergrößerung kann man in den Globuli eine Zonierung feststellen. Die Fe-P und Fe-P-Ni „Kugeln“ bestehen aus P-reichen und P-armen Bereichen bzw. Fe-armen und Fe-reichen Bereichen und die Fe-P-Si „Kugeln“ weisen schwankende Si-Gehalte auf.

Die mehr oder weniger homogene Glasmatrix ist ein erster Hinweis auf die hohe Bildungs- bzw. Umwandlungstemperaturen. Nach Essene und Fischer (1986) kann man mithilfe des Si-Gehalts in den Fe-Si Globuli eine Temperatureingrenzung vornehmen. In einer Probe (KS_3) wurde ein Fe-Si Globuli mit einem Si-Gehalt von $X_{Si} = 0.3$ [X_{Si} = Si/(Si+Fe)] gefunden. Weiters tritt die Umwandlung von Zirkon ($ZrSiO_4$) ab einer Temperatur oberhalb von 1950 K (1677°C) zu Zirkonoxid (ZrO_2) und Siliziumoxid (SiO_2) auf. Da auch Quarz aufgeschmolzen wurde kann man von Temperaturen von mindestens 1950-2000K bei extrem reduzierenden Bedingungen von 10^{-12}-$10^{-12,75}$ log$f$ [O_2] ausgehen. Im Zuge der Abkühlung bildeten sich Osumilith, Spinell und Mullit.

Das Auftreten von Fe-P Globuli weist wahrscheinlich auf die Anwesenheit von Düngemitteln im Boden hin (Pasek & Block, 2009), weil es handelt sich hier um einen gedüngten Ackerboden in dem dieser Pseudofulgurit gefunden wurde.

Brandstätter F., et al. (2008). Annalen des Naturhistorischen Museums Wien, 110A, 1-16.
Essene E.J., Fisher D.C. (1986). Science, Vol. 234, 189-193.
Pasek M., Block K. (2009). Nature Geosciences, 2, 553-556.

P12-P07

Experimental investigations on the gabbro-eclogite transformation using natural starting materials: the role of fO_2

P. Tropper[1], K. Richard[2]
[1]University of Innsbruck, Institut für Archäologien, Innsbruck, Austria
[2]University of Innsbruck, Institute of Mineralogy and Petrography, Innsbruck, Austria

The aim of this study is to provide experimental constraints on the gabbro-eclogite transition and compare the results to the locality Bärofen in the Koralpe (Styria, Austria) where a well-described gabbro-eclogite transformation has been observed. Miller & Thöni (1995) obtained Permian ages for the magmatic protoliths and an Eo-Alpine age for the eclogite-facies metamorphic overprint of these rocks. Textural and petrographic investigations showed that the primary magmatic assemblage plagioklase (An_{60-76}) + clinopyroxene$_1$ + orthopyroxene (X_{Mg} = 71-76) reacts in microdomains to form spinel, clinopyroxene$_2$, garnet, kyanite, hornblende and corundum. Fluid influx lead to the progression of reactions involving plagioclase such as An = Gr + Ky + Qtz and An + H_2O = Zo + Ky + Qtz, which lead to the formation of Ca-rich garnets (X_{Ca} = 53-91) as well as zoisite and kyanite. Reactions along the plagioclase/orthopyroxene interface such as An + En/Fs = Di/Hed + Ky lead to the formation of clinopyroxene$_2$ and kyanite. Within this domain, Mg-rich garnet (X_{Mg} = 33-35) forms via the model reaction An + En/Fs = Py/Alm + Di/Hed + Qtz. Model reactions involving the An-component lead to an increase in the Ab-component in the remaining plagioclase, which eventually breaks down via the reaction Ab = Jd + Qtz. Thermobarometry of fully equilibrated metagabbros yields P-T conditions of 670 - 700°C and 1.7 - 2.1 GPa for the Eo-Alpine eclogite-facies overprint.

The experimental investigations were aimed at reconstructing the observed mineral assemblages not only as a function of P and T but also as a function of fO_2 using drilled cores of fine-grained gabbros from the Odenwald. In all experiments H_2O was present and buffered (NNO, HM) as well as unbuffered experiments with regard to fO_2 were conducted Experimental conditions in the piston-cylinder were 700°C and 2 GPa. Buffered (HM, NNO) and unbuffered experiments with $a(H_2O)$=1 resulted in the mineral assemblage omphacite/jadeite + zoisite + paragonite ± garnet ± hornblende. In the HM experiments, garnet as well as hornblende were absent, but garnet + hornblende occur in the NNO experiments, which represent fO_2 conditions much closer to the natural observations. The lack of kyanite and the occurrence of paragonite is consistent with the investigations of Tropper & Manning (2004) under these conditions. Therefore, lack of paragonite in the natural samples is most likely due to a suppression of $a(H_2O)$ (e.g. brines) during eclogite-facies metamorphism.

Miller , C. & Thöni, M. 1995 Origin of eclogites from the Austroalpine Ötztal basement (Tyrol, Austria): geochemistry and Sm-Nd vs. Rb-Sr isotope systematics. Chemical Geology 122, 199-225.

Tropper, P. & Manning, C.E. 2004 Paragonite stability at 700°C in the presence of H_2O-NaCl brines. Contributions to Mineralogy and Petrology 147, 740-749.

P12-P08

Fluid (melt) rock-interactions constrained by spinel composition in peridotite xenoliths

C. WAGNER[1], M.-L. Pascal[1]
[1]UPMC, ISTeP, Magmas-Minéraux-Matériaux, Paris, France

Chromian spinel is widely recognized as an important petrogenetic marker in basic and ultrabasic systems in the upper mantle and lower crust. In peridotites, Cr-spinel is one of the best indicators of partial melting, as an increase in its Cr/(Cr+Al) atomic ratio (cr*) reflects increasing degree of partial melting. Furthermore, its compositional variations in Cr-Al, Mg-Fe^{2+} and ferric/ferrous ratio can be used to constrain P, T and fO_2 conditions of the mantle, as well as to trace fluid (melt)-rock interactions, through the development of thermodynamic and empirical models based on experimental studies (crystallization of Cr-spinel in basaltic melts, mostly at atmospheric pressure, and peridotite melting).

We present here a detailed investigation of Cr-Al spinels from a suite of anhydrous and hydrous peridotite xenoliths from three outcrops of the Devès volcanic province (French Massif Central). The nodules are fresh, encased in a thin basaltic rim in sharp contact with the peridotite, and devoid of any invasion of the host basaltic melt along fractures. All samples are olivine-rich lherzolites (60-72 vol%) with variable orthopyroxene (7-26 vol%), clinopyroxene (1-18 vol%) and spinel (1-5 vol%) [1]. Most of the xenoliths record mantle metasomatism which has developed amphibole (2-20 vol%) and minor mica. The amphibole (+/- mica) forms selvages as well as veins or disseminated crystals, commonly associated with relict spinel.

The spinels show compositional variations as a function of increasing distance from the amphibole selvage: cr* decreases from 0.6 to <0.1, whereas mg* (Mg/Mg+Fe^{2+}) increases from 0.2 to 0.8; Fe^{3+} and Ti decrease. However, the slope of these trends varies depending on the xenoliths. The spinel composition far from the selvage matches that of spinel from anhydrous xenoliths. Relict spinel embayed in mica is richer in Cr, Fe and contains less Al than spinel in amphibole; their Fe^{3+} content varies between different xenoliths. Some xenoliths thus record the ongoing progressive metasomatic imprint along percolation paths (metasomatic sequences), while other metasomatized xenoliths, with rare small relict spinels, are completely re-equilibrated. The compositional trends of spinel are used to constrain the profiles of chemical potentials across these metasomatic sequences.

[1] Wagner and Deloule, 2007, Geochim. Cosmochim. Acta, 71, 4279-4296

P12-P09

The Virorceo Layered Intrusion, Argentina

G. Ferracutti[1], E. Bjerg[1], A. Mogessie[2]
[1]Universidad Nacional del Sur -CONICET, Geology-INGEOSUR, Bahia Blanca, Argentina, Argentina
[2]Institut fur Erdwissenschaten, Karl-Franzens Universität, Bereich Mineralogie und Petrologie, Graz, Austria

Virorco is a layered mafic-ultramafic (M-UM) intrusion located in the Sierras de San Luis, Argentina (Fig. 1). This intrusion is part of a M-UM belt that extends over 100 km from NE to SW. The rocks constituting this belt carry a sulfide mineralization consisting of pyrrhotite, pentlandite and chalcopyrite, in veins and as disseminated to massive ore. Disseminated spinels are frequently associated with the sulfide minerals as well as platinum group minerals (PGM).

Ferracutti et al. (2011) defined three types of layering in the Virorco body based on the petrology, geochemistry and textural features: a) colloform layering corresponding to gabbroidic rocks of the chilled magin (Fig. 2A), b) Compositional layering, which consist of mesoscale layering of pyroxenitic and hornblenditic alternating layers (Fig. 2B), and c) macroscale layering, which comprise pyroxenitic layers (Fig. 2C). All these layering show distinctive geochemical characteristics, with the more depleted rocks constituting the compositional layering and the more evolved the chilled margin, and three REE/Chodrite profile (Fig.2D, Sun & McDonough, 1989).

The UM rocks of the belt, show a very clear relationship between the presence of spinels and the levels with mineralization of base metals (BM), PGM and content of PGE (Ferracutti et al, 2005). These features and the Cu/Pd vs. Pd and Cu/Pt vs. Ni/Pd relationships, allow the distinction of two groups of rocks, one with ratios that are typical of mantle rocks and the other depleted in PGE. The last one is interpreted as the result of an earlier sulphide segregation which removed Pt and Pd from the magma chamber. The parental magma of the M-UM rocks was a Mg-rich mafic magma with tholeiitic affinity. This conclusion is based on the evaluation of the whole rock chemistry, PGE and BM contents, textural evidences and comparisons with deposits from the world.

The Virorco layered M-UM body and the remaining bodies in the area bear similar characteristics to well known stratified complexes developed in extensive tectonic regimes. Although more work is required, the available evidences suggest that BMS and PGM mineralization are very probably associated with deeper stratigraphic levels where ultramafic rocks are dominant.

References

Ferracutti G., Mogessie A. & Bjerg E. (2005). Chemical and mineralogical profile of the Las Águilas mafic-ultramafic drill core, San Luis Province, Argentina. Mit Öst Min Ges 151: 40.

Ferracutti G., Bjerg E. & Mogessie A. (2011) Caracterización del bandeado ígneo en el cuerpo máfico-ultramáfico de Virorco, San Luis. In: XVIII Cong Geo Arg (Eds. Leanza, Franchini, Impiccini, Pettinari, Sigismondi, Pons & Tunik), Simp Dep miner en Arg: modelos y técnicas de exploración, 1092-1093.

Sun, S. & McDonough, W. (1989). Chemical and isotopic systematic of oceanic basalts: implications for mantle composition and processes. In:, Magmatism in ocean basin (Eds.: Saunders A. D. & Norry M. J.). Geo Soc Lon, Spec Pub 42: 313-345.

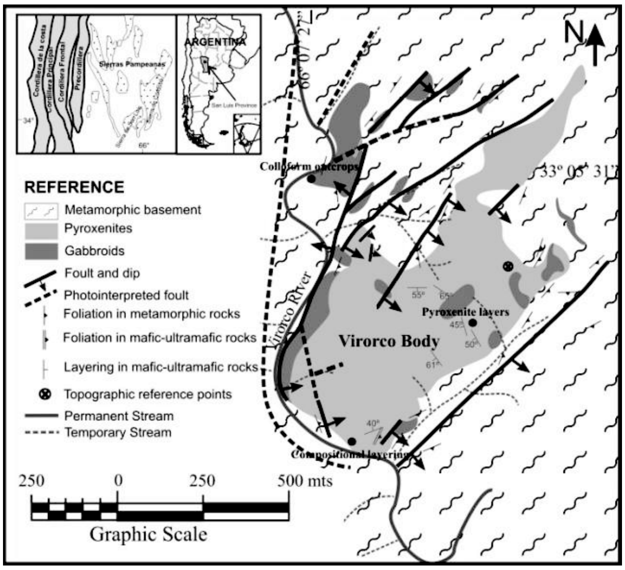

Figure 1

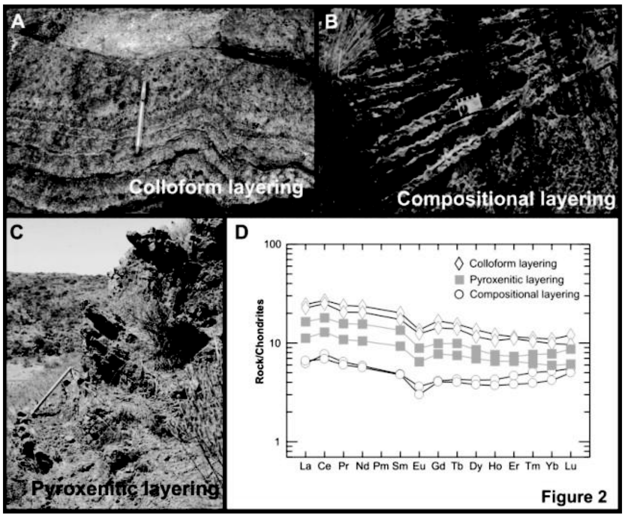

Figure 2

P12-P10
Occurrence of high grade metamorphic rocks within the low grade Three Pagodas strike-slip shear zone, Kanchanaburi Province, western Thailand: Petrology and Geochronology

P. Nantasin[1], C.A. Hauzenberger[1], X. Liu[2], K. Krenn[1],
P. Wathanakul[3], Y. Dong[2], M. Thöni[4]
[1],, Austria
[2],, China
[3],, Thailand
[4],, Austria

Four well defined large scale strike-slip shear zones exposed in western Thailand are the result of the India-Asia collision and are named from north to south, Mae Ping shear zone, Three Pagodas shear zone, Ranong shear zone and Khlong Marui shear zone. Within the Three Pagodas shear zone, a narrow lenticular basement slice of high grade metamorphic rocks, called Thabsila gneiss, is exposed within the NW-SE trending shear zone. The Thabsila gneiss is juxtaposed by fault contacts to the very low to unmetamorphic rocks of the shear zone. The high grade basement slice can be subdivided into 4 units based on lithology: 1) Unit A is composed of marble, mica schist and quartzite, 2) unit B comprises mylonites, 3) unit C is composed of only calcsilicate, and 4) unit D comprises various varieties of gneisses. Classic geothermobarometry and pseudosection calculations were employed in order to estimate the P-T conditions of these high grade metamorphic units. Age of metamorphism and exhumation were constrained from LA-ICP-MS U-Pb zircon age and Rb-Sr biotite isochron age. Geothermobarometry reveals a P-T variation among the 4 units. Unit A experienced medium amphibolite facies conditions of 560-650 °C and 4-7 kbar while units B, C and D experienced upper amphibolite facies metamorphism, around 640-720 °C and 7.5-9 kbar. Metamorphic zircon rims yield a metamorphic age of ~50-60 Ma, while Rb-Sr biotite cooling ages are ~ 32-36 Ma. These P-T-t data suggest that the Thabsila gneiss experienced peak amphibolite facies /lower granulite metamorphism during the early collision between India and Asia. Subsequently, whilst lateral southeastward extrusion of the Indochina terrane during Oligocene, it was exhumed due to strike-slip faulting along the Three Pagodas shear zone. Final cooling of the basement rocks down to a temperature of ~350 - 300 °C is indicated by the biotite Rb-Sr ages.

P12-P11
Petrological and geochemical investigation of basaltic trachyandesites from Weitendorf

K.E. Kuerbisch[1], A. Mogessie[1]
[1]Universität Graz, Erdwissenschaften, Graz, Austria

The studied area Weitendorf is located in the Styrian Basin (Fig.1). In this Basin two magmatic main phases occurred, an intermediate high - K volcanism in the Miocene and an alkaline volcanism in the Plio- and Pleistocene. In the Ottnangien volcanic activity concentrated in Bad Gleichenberg, Mitterlabill & St. Nikolai. In the lower Badenien it moved to the northern edge of Bad Gleichenberg resulting in the formation of the Weitendorf and Walkersdorf volcanics (EBENER & SACHSENHOFER, 1991). In this study petrographic and geochemical investigations have been conducted on representative samples from the volcanic outcrop of Weitendorf in order to understand its origin and paleotectonic position.

The mineral phases identified in the representative samples are Olivine with $Fo_{73.9}$ to $Fo_{87.6}$, Plagioclase (Labradorit with $An_{66.1}$ to An_{69} and Andesin with $An_{48.3}$ to $An_{49.5}$), Alkalifeldspar (Na - Sanidin with $Or_{38.5}$ to $Or_{61.6}$) as well as Clinopyroxene (Augite, Diopside) $En_{46.2}$ $Fs_{6.5}$ $Wo_{0.362}$ to $En_{50.8}$ $Fs_{8.4}$ $Wo_{41.8}$ and Orthopyroxene $En_{60.2}$ $Fs_{13.9}$ to $En_{77.4}$ $Fs_{35.4}$.

Major and trace element analyses of the representative samples from Weitendorf have been plotted in different chemical diagrams (e.g. oxide-oxide Harker diagrams or the Total Alkali-Silica plot). On the K2O-SiO2 diagram the data plot in a cluster around the intersection K2O = 2.9% and SiO2 = 52.5 Gew%, indicating a calc - alkaline composition and the basalts are classified as shoshonites. In addition, the major element compositions of samples from Weitendorf were compared with samples from Mitterlabill, Walkersdorf, Paldau, St. Nikolai, Wiersdorf and Bad Gleichenberg (SLAPANSKY et al.1999) in order to find out whether there is any similarity in origin or magma source. The results showed that the Miocene volcanics of the Styrian Basin can be distinguished in two geochemically different groups, which also show different geographical position and age. High- K latites and dacites from Mitterlabill, St. Nikolai and Wiersdorf are of Karpatian age, while shoshonite series from Weitendorf, Paldau, Bad Gleichenberg and Walkersdorf exhibit a range of age mostly from Karpatian to lower Badenian time. The geochemistry of the investigated volcanic rocks from Weitendorf show strong relation to subduction, but the actual magma generation seems to have occurred long after the end of active subduction in an extensional tectonic regime (Fig.2).

References :

EBENER, F. & SACHSENHOFER, R. F. (1991): Mitt.Abt. Geol. Und Paläon. Landesmuseum Joanneum; Graz. 1-96

HIDEN, STINGL (1988): Geol. Paläont. Mitt. Innsbruck; Band 23

SLAPANSKY, P., BELOCKY, R., FRÖSCHL, H., HRADECKY, P., SPINDLER, P..(1999): Abhandlung der Geol. Bundesanstalt, Band 56/1. 419-434

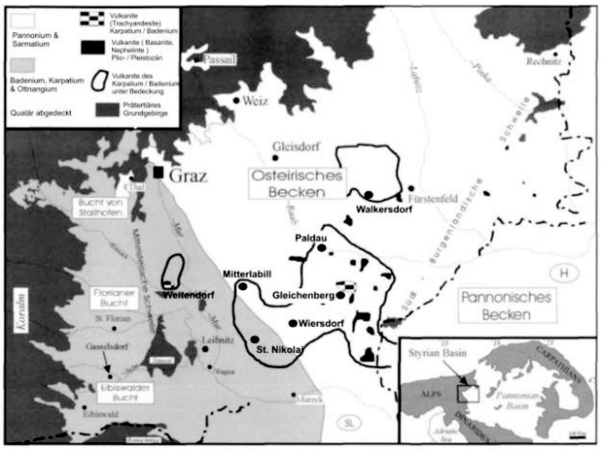

Figure 1: *Geological map of the styrian basin; (Graphic Hiden & Stingl,1988)*

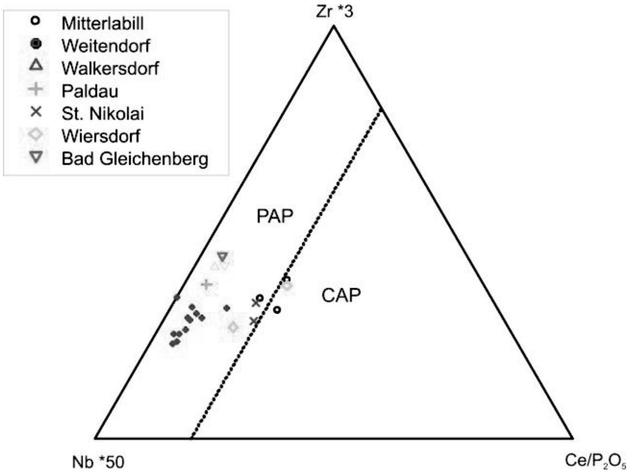

Figure 2: Geotectonic classification after Müller et.al., 1992; CAP: „continental arc position; PAP: „Postcollisional arc Position

P12-P12
Zur Mineralogie des goethitischen Eisenerzvorkommens von Drakona, West-Kreta, Griechenland

G. Alevizos[1], E. Steiakakis[1], A. Stratakis[1]
[1]Technical University of Crete, Mineral Resources Engineering, Chania, Greece

Eisenerzvorkommen sind auf West-Kreta weit verbreitet. Einige dieser Vorkommen wurden in früheren Zeiten bergmännisch genützt. Sie treten innerhalb der Phyllit-Quarzit-Serie (PQS) auf, die als eine der tektonischen Einheiten der Hochdruck/Tieftemperatur metamorphen Phyllit-Decke Kretas und des Peloponnes interpretiert wird. Die PQS setzt sich meist aus Phylliten und Quarziten zusammen, sowie aus Metakonglomeraten, Marmoren, Kalkphylliten und Metabasalten [1]. Die Thermochronologie der Hochdruck/Tieftemperatur metamorphen Gesteinen der PQS kann das Alter der Mineralisierung in der Abscherungszone Kretas begrenzen. Sauerstoffisotopendaten von Goethiten, die aus Eisenerzvorkommen West-Kretas stammen, weisen auf niedrige Bildungstemperaturen, zwischen 31^{o} und 40^{o} C und eine Tiefe von ca. 1 bis 1.5 km, hin [2].

Das untersuchte Vorkommen liegt 20 km südlich von Chania in der Nähe des Ortes Drakona. Das Eisenerz tritt in Form von Lagergang innerhalb der Phyllite und Quarzite der PQS auf und wird von den Karbonatgesteinen der Tripolis-Einheit überlagert. Die mineralogischen Bestandteile der Eisenerze sind meistens Goethit und Quarz. Untergeordnet treten Kryptomelan, Muskovit und seltener Talk auf. Die Phyllite und Quarzite sind innerhalb der Kontaktzone stark zerrüttet und brecciiert. Sie sind durch eisenreiche Lösungen intensiv imprägniert, die in Form von Goethit ausgefällt wurden. Der Goethit bildet oft kollomorphe Massen, die rhythmisch aufgebaut sind. Die Eisenvererzung wird gelegentlich von einer Manganmineralisation in Form von Kryptomelan begleitet. Der Kryptomelan bildet meistens feinfilzige Massen, die oft einen konzentrisch-schaligen Aufbau z. T. in Wechsellagerung mit Goethit entwickeln. Bei gleichzeitiger Abscheidung von Mangan- und Eisen-Hydroxiden aus Verwitterungslösungen, die oft zu einer scharfen Trennung von Mangan und Eisen führt, tritt eine Foam-Textur auf.

Anhand der erzmikroskopischen Untersuchung des Eisenerzvorkommens von Drakona geht hervor, daß die massive Vereisenung der Wirtgesteine (Phyllite und Quarzite) durch eisenreiche Lösungen epigenetischen Ursprungs hervorgerufen wurde. Die Eisenerzvorkommen West-Kretas werden mit Eisensulfidmineralisationen geringen Ausmaßes, die an mehreren Stellen der weiteren Region auftreten, genetisch verknüpft. Dies gibt Anlaß zur Annahme, daß die Zersetzung der Eisensulfide zu einer sekundären Eisenmobilisation geführt hat und folglich zur Bildung der Eisenerze.

Literatur

[1]Dornsiepen, U. F. & Manutsoglu, E. (1994). Zur Gliederung der Phyllit-Decke Kretas und des Peloponnes. Z. dt. geol. Ges. 145, S.286-304.

[2]Seidel, M., Pack, A., Sharp, Z. & Seidel, E. (2005). The Kakopetros and Ravdoucha Iron-Oxide Deposits, Western Crete, Greece: Fluid Transport and Mineralization within a Detachment Zone. Soc. of Econ. Geologists, Inc. Econ. Geology, v.100, pp.165-174.

P12-P13
Geochemical and Sr-Pb-Nd Isotopic Study of the Shakhtama Porphyry Mo-Cu System (Russia): Implications for Magma Sources

A. Berzina[1], A. Berzina[1], V. Gimon[1], R. Krymsky[2], P. Serov[3]
[1]Institute of Geology and Mineralogy, Novosibirsk, Russian Federation
[2]Russian Geological Research Institute (VSEGEI), Saint Petersburg, Russian Federation
[3]Geological Institute of the Kola Science Centre RAS, Apatity, Russian Federation

This paper presents geochemistry and Sr-Nd-Pb isotope compositions of the porphyritic intrusions associated with Mo-Cu mineralization and barren precursor granitoid plutonic rocks. Porphyry-type Mo-rich (Cu) Shakhtama deposit is located in the Eastern Transbaikalia (Russia) within the Shakhtama granitic pluton, bordering the southern margin of Mongol-Okhotsk orogenic belt. The mineralization is genetically related to the emplacement of post-collisional J_3 shallow level porphyritic intrusions dominated by granite- and granodiorite porphyries. Porphyry stocks and dikes are hosted in precursor collisional multiphase pluton (J_2-J_3) of dioritic to granitic composition.

Major, trace and REE element data indicate that the plutonic and porphyry rocks share much in common. They show variable SiO_2 contents (53-75 wt%) and are characterized by high K_2O (1.8-6 wt%), high Sr (360-950 ppm), low Y (9-20 ppm) and Yb (0.8-1.8 ppm), their A/CNK values are <1.1. The rocks belong to I-type high-K calc-alkaline and shoshonitic series and are characterized by enrichment in LREE and depletion in HREE. They show negative Nb, Ta, and Ti anomalies. Both plutonic and porphyry series include two distinct groups of granitoids: 1) rocks with geochemical characteristics of K-adakites and 2) ordinary calc-alkaline granitoids. Similar coeval adakitic and ordinary, high-K, I-type, calc-alkaline postcollisional granitoids of Late Triassic age were first described at the eastern margin of the Tibetan Plateau (Xiao et al., 2007). Relatively high Sr/Y and La/Yb ratios and negative Nb and Ti anomalies of the adakitic group of rocks suggest the presence of residual garnet and amphibole in the source, implying that the crustal thickness exceeded 40 km.
Sr and Pb isotopic signatures for the ore-bearing porphyries and plutonic rocks show close values and narrow ranges, suggesting that they could have been generated from similar or the same source rocks. Isotopic compositions have relatively high Sr and Pb ratios with crustal characteristics ($^{87}Sr/^{86}Sr = 0.7071 - 0.7078$; $^{206}Pb/^{204}Pb = 15.51 - 15.74$, $^{207}Pb/^{204}Pb = 15.57 - 15.61$, $^{208}Pb/^{204}Pb = 38.27 - 38.50$). The values of $\varepsilon_{Nd}(t)$ in Shakhtama plutonic and porphyry rocks range from -0.7 to +2.1 and Nd model age (T_{DM}) ranges from 800 to 1200 Ma. Based on isotopic and geochemical characteristics, we propose a lower crustal magma source (probably Precambrian metaigneous crustal rocks). Shakhtama rocks show relatively high concentrations of Ni, Cr, V (up to 270, 779, 150 ppm, respectively), as well as high #Mg (0.5-0.7). This may suggest that primary melts have interacted with mantle material and that Shakhtama adakitic rocks were derived by the melting of thickened delaminated lower crust within the litospheric mantle. Parent melts for ordinary higk-K calc-alkaline rocks were probably generated at higher crustal levels.
References:

Xiao L., Zhang H.F., Clemens J.D., et al. Late Triassic granitoids of the eastern margin of the Tibetan Plateau: Geochronology, petrogenesis and implications for tectonic evolution. Lithos. 2007. v. 96. pp. 436-452.

P12-P14
Petrological investigation of the metamorphic rocks of the Oswaldgraben

S. Raic[1], M. Aberra[1]
[1]University of Graz, Dept. of Mineralogy/Petrology, Graz, Austria

The investigated area "Oswaldgraben" lies in the region of Voitsberg NE of Kainach *(*Fig.1*)*. Representative samples were collected for detailed petrographic and petrological study in order to find out if the rocks from this area belong to the Rappold Complex which is polymetamorphic or to the Wölz Complex that has been affected only by one metamorphic event. Both complexes belong to the Austroalpine unit and differ in their metamorphic histories, which becomes noticeable in the polymetamorphic mineral assemblages and polymetamorphic garnet generations of the Rappold Complex. Detailed petrographic study and electronmicroprobe analyses of the phases identified in the different rock types indicate certain characteristics. The garnets have a composition ranging from Alm_{57-74}, Grs_{9-21}, Sps_{1-6}, Prp_{6-14}. Garnets from Metabasites (garnet-amphibolites) have a composition Alm_{60-73}, Py_{12-23}, Grs_{5-20}, Sps_{1-4}.
Amphiboles in the garnet-amphibolites are calcic-amphiboles and correspond mainly to tschermakitic hornblendes and tschermakites with $X_{Mg} = 0.52-0.681$, $(Na+K)_A = 0.34-0.48$ and $(Ca+Na)_B = 1.76-1.89$. Ca_B lies between 1.41 an 1.62 and Na_B between 0.23 and 0.42Al(IV) varies in tschermaktic hornblendes between 1.632 and 1.75 and in tschermakites between 1.751 and 1.875. All analysed feldspars (in garnet-micashists, garnet-amphibolites) have a composition ranging from Oligoclase (An_{12-27}) - Andesine (An_{31-33}) to minor Albite (An_{10}), with an exception of the feldspars in the marbles that are mainly orthoclase. Based on the plot Mg - (Fe^{2+}+Mn) - R^{3+} ($R^{3+} = Al^{VI} + Ti^{4+} + Cr^{3+}$) the biotites can be calssifed as phlogopite, meroxen and lepidomelane. The FeO content in chlorites varies between 17 and 32 wt. %, depending on the minerals they are coexisting with, and plot in the clinochlor field.
Applying the garnet-biotite thermometer (Holdaway, 2000) and the garnet-amphibole-plagioclase barometer (Dale et al., 1998) on garnet-amphibolites the results gave pressure- and temperature conditions of 9.1 kbar and 653°C. Based on the petrographic study, mineral composition of the different phases as well as composition profiles along large garnet porphyroblasts and P-T calculations, it is suggested that the samples from the Oswaldgraben represent a monometamorphic mineral assemblage and therefore belong to the Wölz Complex.
References:

Dale J., Holland T., Powell R., 2000. Hornblende-garnet-plagioclase thermobarometry: a natural assemblage calibration of the thermodynamics of hornblende. Contrib. Miner. Petrol., 140, pp.353-362
Holdaway, J., 2000. Application of new experimental and garnet Magules data to the garnet-biotite geothermometer. American Mineralogist, vol.85, no.7-8, pp.881-892.
Schmid, S. M., Fügenschuh, B., Kissling, E. & Schuster, R., 2004. Tectonic map and overall architecture of the Alpine orogen. Eclogae Geologicae Helvetiae, 97, pp. 93-117.

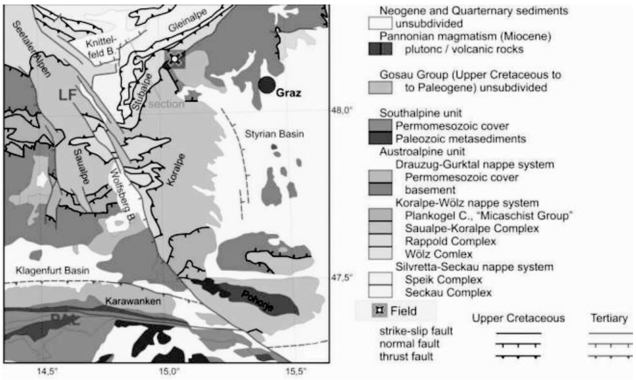

Figure 1: Tektonic map of the Austroalpine-Units in the Koralpe-,Saualpe-,Stubalpe- and Gleinalpe area (Schmid et al., 2004)

P12-P15
Fluid-mobile elements in subduction zones: an experimental approach

A. Mutter[1], A. Holzheid[1], M. Wilke[2]
[1]Institute of Geosciences, Mineralogy, Kiel, Germany
[2]GFZ, Chemie und Physik der Geomaterialien , Potsdam, Germany

The aim of this project is to experimentally elucidate the role and evolution of fluids released during subduction. Especially the knowledge of solid-fluid partitioning behavior of trace elements as well as volatiles within the subducting slab is essential to quantify the flux of volatiles and fluids in the entire subduction zone (Zack and John, 2007, Spandler et al. 2007, Kessel et al. 2005).

Thus, as the chemical signatures of subduction zone magmas are mixing results (Poli and Schmidt, 2002), we will experimentally investigated different lithological bulk components, as potential sources of LILE, REE and HSFE at sub-arc conditions. Instead of conducting single point analysis at a given P/T (e.g. Kessel et al., 2005) or single crystal analyses, to derive partitioning data, we track a more dynamic approach. Our goal is to investigate the evolution, and thus the change in the composition of basalts, gabbros and their respective fluids, as we steadily move down along the subduction path.

As solid starting materials three natural samples, two basalts and a gabbro, as well as a synthetic silicate glass were used. The natural samples are from ODP Leg 206 and Site 1256D (IODP expeditions 309 and 312), see Teagle et al. (2006) for more details. The synthetic glass is of gabbroic composition. Pure water was used as leaching agent. Powdered solid starting materials (200 mg) were placed together with the water (1 g) in Au capsules (width/length: 46 / 100 - both in mm). The temperature and pressure was held at 400°C / 4 kbar, corresponding to a depth of ~12 km (CSPV experiments, Kiel) and at 500°C / 7 kbar, corresponding to a depth of ~21 km (IHPV experiments, Potsdam). Both, the fluid and the residual silicate phases, were recovered after terminating the experiments. The fluid phases were analysed with ICP-MS and ICP-OES techniques (inorganic geochemistry lab, University Kiel and Institute of Geosciences, University of Bremen). The residual silicate phases are powders. Small glass spheres (fusion whole-rock glasses) were manufactured from the solid residue using the technique described by Fedorowich et al. (1993). The major and minor element contents of these glass spheres were than analysed by electron microprobe and the trace element concentrations were measured by LA-HR-ICP mass spectrometry (, University Münster and University of Bremen). Comparison of the bulk composition of the individual silicate starting materials (natural and synthetic samples) and their corresponding post-run silicate charges as well as the post-run fluid chemistries reflect only a minor mobility of trace elements at pressure and temperature conditions comparable to the upper part of the subduction slab.

Reference:

Zack T. & John T. (2007) Chemical Geology 239, 199.

Spandler C., Mavrogenes J., Hermann J. (2007) Chemical Geology 239, 228.

Kessel R., Ulmer P., Pettke T. (2005) Nature 437, 724.

Poli S. & Schmidt MW (2002Annual Review of Earth and Planetary Science 30, 207.

Teagle et al. Proc. IODP 309/312, 1.

Fedorowich, J.S, Richards, J.P, JAIN, J.C, Kerrich, R., Fan, J. (1993), Chemical Geology 106, 229.

P12-P16

Decompression experiments on dacitic magma: Insights from residual glass compositions and plagioclase CSDs

N. Blum-Oeste[1], B. Schmidt[1]

[1]Geowissenschaftliches Zentrum Göttingen, Experimentelle und angewandte Mineralogie, Göttingen, Germany

Kinetic processes during magma ascent may have a strong influence on the eruption style. In water bearing dacitic magmas decompression induced exsolution of water and accompanying crystallisation of plagioclase are the main processes which drive the system towards a new equilibrium state. We present new data on the evolution of residual glass composition and crystal size distributions of plagioclase from decompression experiments.

Experiments have been conducted in CSPVs at 850°C. After an initial equilibration at 2 kbar decompression rates between 6.3 and 450 bar/h were applied to final pressures between 50 and 1550 bar where samples were rapidly quenched. Complementary equilibrium experiments were done at corresponding pressures. The glass composition evolves from the initial state towards the equilibrium at the final pressure. The completeness of this re-equilibration depends on run duration and reaction rates. We introduce the "re-equilibration index" (REI), a fraction between 0 (initial state) and 1 (final state) which allows comparison of chemical components in terms of re-equilibration at different decompression rates. REI divided by the decompression duration gives the "re-equilibration speed" (RES).

The REI varies among oxides and it decreases with increasing decompression rate. The highest REIs of ~0.9 have been found for MgO, K_2O and Al_2O_3 at 6.3 bar/h whereas Na_2O shows the lowest with 0.25 at this decompression rate. Towards faster decompression all REIs tend to decrease, which shows a decreasing completeness of re-equilibration. At 450 bar/h the highest REIs are ~0.25.

RESs increase from below ~0.005/h at 6.3 bar/h up to almost 0.08/h for Al_2O_3 at 450 bar/h. The variability of RESs of different oxides also increases with decompression rates. At 450 bar/h the RESs reach from <0.005/h up to 0.08/h. Although RESs increase that much from low to high decompression rates this does not compensate for the decreasing duration available for re-equilibration as REIs clearly show.

The volume fraction of plagioclase decreases from ~21% at 6.3 bar/h to ~16% at 450 bar/h which fits the decrease in REIs. The population density of small crystals decreases whereas the population density of larger crystals increases from slow to fast decompression. This reflects a transition from nucleation controlled crystallisation at slow decompression to a growth dominated regime at fast decompression. As RESs show re-equilibration is faster in the growth dominated regime.

P12-P17

Corundum-kyanite-fuchsite rocks from the Kodagu District, Southern India

M.M. Raith[1], R. Schumacher[1]

[1]University of Bonn, Steinmann Institut, Bonn, Germany

Since about 2004, polished ruby corundum-fuchsite rocks with a blue and white corona texture are popular items available for purchase at the mineral shows around the world. The traded rocks from a small occurrence in the westernmost part of the Archaean Dharwar Craton (Kodagu District, Karnataka, India) represent the eye-catching members of a suite of highly aluminous rocks which comprises fuchsite-bearing corundum-kyanite, kyanite-corundum and pure kyanite rocks, and probably forms an enclave of Cr-enriched high-alumina metasediments within a prominent unit of Bt+Grt±St+Ky schists. Such Cr-enriched argillaceous metasediments are typical components of Sargur-type greenstone belts in the Dharwar Craton, and reflect a significant contribution from ultramafic sources. Chemical attributes and the fine-grained nature of the corundum-fuchsite rocks suggest they formed through potassic infiltration metasomatism from the kyanite-corundum members of the suite. During the early Proterozoic the area experienced HP-amphibolite facies metamorphism (~650 °C, 8-10 kbar; this contribution).

The rocks exhibit a conspicuous porphyroblastic texture defined by tabular pink corundum crystals up to 1 cm in diameter, set in a fine-grained fuchsite matrix. Bluish-green kyanite commonly rims the euhedral ruby accentuating its outline. In some cases a fine aggregate of fuchsite replaces the kyanite. The kyanite/fuchsite rim is separated from the fuchsite matrix by a white shell of coarser-grained muscovite and quartz. Accessory rutile occurs in all domains. The high Cr contents of the rocks (1300-2900 ppm) are reflected in elevated Cr-contents of all phases (Crn 0.30-0.65, Ky 0.30-0.74, Ms 0.25-0.12, Rt 0.9 wt% Cr_2O_3). Depending on its textural setting, white mica shows subtle compositional variation: Ms-coats on Crn ($Ms_{77}Ce_{14}Pg_{18}$; 0.35 wt% TiO_2; 0.25 wt% Cr_2O_3); Ms+Qz-shell ($Ms_{77}Ce_7Pg_{15}$;

0.12 wt% TiO_2; 0.02 wt% Cr_2O_3); Ms-matrix ($Ms_{75}Ce_9Pg_{14}$; 0.98 wt% TiO_2; 0.12 wt% Cr_2O_3).

The proximity of corundum with quartz in the muscovite shell asks for explanation, as both minerals do not coexist at any crustal metamorphic conditions. The extension of the Ms+Qz-shells along the planar fabric of the rock suggests they represent strain shadows developed around the rigid corundum grains during low-temperature deformation. In such a case, dilation-controlled infiltration of aqueous fluids into the extensional gashes offers a straightforward explanation of the coronal texture and mineral chemical features: (1) development of a closed kyanite rim through an interface-controlled dissolution-precipitation reaction of corundum with dissolved silica (SiO_2^{aq}), (2) simultaneous precipitation of almost Cr-free muscovite from the fluid with coarsening of the adjacent fuchsite matrix, (3) replacement of the kyanite rim by fuchsite through reaction with K^+ and SiO_2^{aq}.

P12-P18

Na-K-Interdiffusion in Alkali Feldspars

A.-K. Schaeffer[1], G. Neusser[2], R. Abart[1], E. Petrishcheva[1]
[1]University of Vienna, Department of Lithospheric Research, Vienna, Austria
[2]Free University Berlin, Institute of Geological Sciences, Berlin, Germany

During exchange experiments between Sanidine (X_{Or} 0.85) with K-rich KCl/NaCl-melt unexpected geometries of concentration profiles were observed that deviate from what would have been expected for linear diffusion. Exchange fronts with inflection point propagate through the crystal. The front sharpness depends on the composition difference between the exchanged and unexchanged domains of the grain. These fronts initially propagate with $t_{1/2}$, the propagation rate deviates from this relation towards slower diffusion in experiments with runtimes exceeding 16 days. While the propagation of the fronts is equal in all crystallographic directions, their width differs significantly, the greatest difference being observed between the directions normal to (010) and (001).

A first hypothesis to explain the front geometry is that this might be due to a composition dependence of the diffusion coefficient. Such a composition dependence has first been found by Christoffersen et al. (1983). They report that diffusion is faster for K-rich than for Na-rich compositions. To explain the shape of the diffusion front very specific conditions have to be met, as both the difference between the lowest and highest value of D and the composition where D changes fastest with composition, influence the shape, width and propagation of the diffusion front.

Another controlling factor might be the coherency strain occurring across the diffusion front due to lattice mismatch caused by the exchange of different-sized ions. At the beginning the strain is mostly concentrated in the thin exchanged rim and may function as an additional driving force for the diffusion. As the exchange front propagates further into the feldspar and widens the strain is distributed over a bigger volume and is thus reduced. This might both explain the unexpected geometry of the front and the finding that the propagation of the front deviates from the $t_{1/2}$ relation with time.

References

Christoffersen et al. (1983): Inter-diffusion of K and Na in alkali feldspars: diffusion couple experiments. -American Mineralogist, Vol. 68, pp. 1126-1133.

P12-P19

Chemistry and paragenesis of barium feldspar and Ba-Cr mica from the Mesoarchaean volcano-sedimentary belt of Ghattihosahalli, South India

M.M. Raith[1], T.C. Devaraju[2], B. Spiering[1]
[1]University of Bonn, Steinmann Institut, Bonn, Germany
[2]'Rajamangala' Saptapur, Dharwad, India

The volcano-sedimentary Ghattihosahalli belt has been re-examined with a special focus on the chemistry and paragenesis of barium feldspar and associated Ba-Cr mica. Barium feldspars occur in a narrow argillaceous transition zone separating upper barite-bearing quartzite strata from lower mafic (amphibolite) - ultramafic (spinifex-textured serpentinite and tremolite-chlorite and talc-carbonate schists) strata (Devaraju et al., 1999). The belt bears evidence of deposition in a sabkha-like environment and has experienced amphibolite facies metamorphism (5 kbar and 540 °C).

The layer-scale paragenetic variation recorded in the barian-chromian metasedimentary sequence of the belt comprising of (1) Ky+Mic+Qz, (2) Ba-Kfs+Pl+Mic+Qz, (3) Brt+Mic+Qz, (4) Brt+Hy+Mic+Qz, (5) Brt+Cls+Mic+Qz, (6) Brt+Cls/Hy+Qz, (7) Brt+Qz, (8) Qz mimics bulk compositional variations in the original sediments and indicates limited metamorphic element migration. Barium feldspar forms untwinned porphyroblastic and xenoblastic grains in a finely banded matrix of barite, quartz and minor Ba-Cr mica. Porphyroblastic grains are either celsian ($Cls_{98-76}Or_{2-20}Ab_{1-8}$) or hyalophane ($Cls_{45-35}Or_{45-59}Ab_{8-17}$) showing delicate oscillatory zonations, repeated resorptional truncations, and occasional euhedral growth patterns. These may also comprise of celsian cores with anhedral hyalophane ($Cls_{45-35}Or_{45-62}Ab_{5-14}$) rims/overgrowths. Xenoblastic grains are largely hyalophane with cores ($Cls_{45-35}Or_{45-59}Ab_{8-17}$) that are resorbed and overgrown by somewhat more barian 'mantles' ($Cls_{45-40}Or_{45-50}Ab_{12-16}$), and pervaded by delicate networks of barian micro-veins. Thin K-feldspar rims ($Cls_{7-2}Or_{92-97}Ab_{1-2}$) on celsian and barian rims ($Cls_{70-58}Or_{26-38}Ab_{4-8}$) of hyalophane at Brt+Qz resorption domains have formed during late-stage fluid infiltration. Micas are solid solutions of muscovite, celadonite, paragonite and ganterite [$(K_{0.5}Ba_{0.5})Al_2[Al_{1.5}Si_{2.5}O_{10}](OH)_2$], with up to 0.5 $Cr^{[6]}$ substitution for $Al^{[6]}$. Micas in assemblage (1) remain close to Ms, but approach ganterite composition in assemblages (3)-(5). Zoned grains show cores enriched in Ba (Cr).

Textural criteria indicate growth of xenoblastic hyalophane during amphibolite facies metamorphism with involvement of mica, barite and quartz as reactant phases. Porphyroblastic barium feldspars, however, formed prior to development of the pervasive foliation and are inferred to have derived from harmotome-like gel via cymrite through dehydration. Such a transformation under increasing P-T conditions coupled with fluctuating pore fluid composition is thought to facilitate partial dissolution and redeposition to produce the complex oscillatory growth zonation.

Devaraju, T.C., Raith, M.M. & Spiering, B. (1999). Mineralogy of the Archaean barite deposit of Ghattihosahalli, Karnataka, India. Canadian Mineralogist, 37, 603-617.

P12-P20

Crystallographic preferred orientation of rutile needles in high-grade garnet: precipitates or the result of epitactic overgrowth?

A. Proyer[1], G. Habler[2], R. Abart[2]
[1]Freie Universität Berlin, Institut für Geowissenschaften, Berlin, Germany
[2]Universität Wien, Department für Lithosphärenforschung, Wien, Austria

The compositions of solid solution minerals at very high temperatures and pressures are commonly not well preserved during subsequent stages of metamorphism but altered by processes such as diffusion and precipitation. Reconstruction of original compositions includes the necessity to evaluate the genetic nature of inclusions. Even though inclusions showing a crystallographic orientation relation with the host phase are generally considered to be precipitates, some instances are known, where overgrowth also resulted in an oriented inclusion relationship (e.g. sagenitic rutile in garnet). Rutile needles, strictly oriented in three dimensions in the Grt-direction of the host are a rather common feature observed at high grades, particularly in ultrahigh-pressure rocks. In a detailed TEM-investigation of inclusion-host relationships between such Grt-parallel rutile needles and their garnet host from a UHP-eclogite, Hwang et al. (2007) found only very limited crystallographic relationship between the rutile and garnet lattices. Based on that and on the fact that a rutile precipitation process in garnet cannot be formulated isochemically, they concluded that these Rt-needles are not precipitates but must have formed by some alternative mechanism.
We have measured the crystallographic orientation of more than 200 rutile needles in the outer rim of a garnet from a microdiamond-bearing garnet kyanite micaschist from the Greek Rhodope using Electron Backscatter Diffraction (EBSD) and found clear but complex relationships between the rutile and garnet lattices: Only very few rutile needles correspond to a simple Rt // Grt relation. The majority of Rt needles showsRt oriented along a cone at an angle of 26-29° with respect to Grt , thus forming small circles around Gt in the stereographic projection. Although 12 positions along the small circle are occupied by Rt, three double maxima were observed, which are at an angle of about 6° off the Grt{101} mirror plane. Therefore a special orientation of the Rt lattice is preferred which is repeated by the {101} mirror plane and by the Grt three fold axis. Less than 5 % of the measured rutile orientations do not pertain to either one of these topotactic relations.This evidence supports the precipitate nature of the rutile needles and corroborates the proposition made earlier by Proyer et al. (2009, 2010) that precipitates such as rutile in garnet can form by non-isochemical reactions, i.e. by a partial openness of the host mineral and exchange with the rock matrix with regard to rapidly diffusing species with or without particular channelways or a fluid-induced reaction front moving through the crystal ("open system precipitation").

References:

Hwang S.L., Yui T.F., Chu H.T., Shen P., Schertl H.P., Zhang R.Y. & Liou J.G. (2007),J. metamorphic Geology 25: 349-362
Proyer A., Krenn K. & Hoinkes G. (2009), J. metamorphic Geology 27: 639-654
Proyer A., Krenn K. & Hoinkes G. (2010),Acta Mineralogica Petrographica, Abstract Series Vol 6, p. 211

P12-P21

Formation of carbonates in volcanic rocks by interaction with magmatic and hydrothermal fluids

A. Simonyan[1], K. Voges[1], H. Behrens[1], S. Dultz[1], J. Fiebig[2]
[1]Institute for Mineralogy, Leibniz University of Hannover, Hannover, Germany
[2]Institute of Geosciences, J.W. Goethe University of Frankfurt, Frankfurt am Main, Germany

The first attempt to drill into an active volcano was made by the Unzen scientific drilling project (USDP) in the years from 1999 to 2004. The USDP hole was drilled about 2 km into the side of Mount Unzen trying to reach the conduit of the 1990-95 eruption. The project yielded a couple of unexpected results, i.e. the temperature in the borehole was much lower than expected, and the drilling cores were highly altered with large amounts of secondary minerals such as carbonates, chlorite and pyrite, supposed to be products of reactions of discharged volcanic fluids with the host rocks. These surprising findings inspired us to use the drilling cores in combination with experimental work to identify the mechanisms of fluid-rock interaction, in particular the carbonation and decarbonation of rocks which is important for understanding the magma degassing processes, and main processes for storage of CO_2 in cavities or in porous/brecciated volcanic rocks.
We started a series of experiments to have a closer look on the influence and mechanisms of the interaction between rock and fluids, using unaltered volcanic lavas from Mt. Unzen that are interpreted to be the precursor of the altered rocks from the drilling core. Our focus was on the carbonation and decarbonation of rocks and minerals (especially hornblende), triggered by CO_2-bearing fluids.
A series of hydrothermal fluid /rock interaction experiments in different systems (56 in total), i.e., dacite or pure amphibole, amphibole + plagioclase, $CaCO_3$ and fluid bilding phase $H_2O+H_2C_2O_4 \cdot 2H_2O$, $H_2C_2O_4 \cdot 2H_2O$, $Ag_2C_2O_4$ in different proportions were conducted in the cold seal pressure vessels (CSPV)at temperatures from 300 to 700°C and at pressures from 100 to 500 MPa, respectively. Applicability of this tecnique was confirmed by a reproduction of experiments with olivines after Dufaud et al. (2009).
The run duration was varied from one to eight weeks, whereas the fluid/rock ratio was varied between 0.2 and 9.5. The first analyses of the experimental products show that amphiboles participate in exchange reactions with the formation of new mineral phases. However the size of produced phases was too small for proper identification and new phases can not be polished for quantitative analysis. The formation of calcite was observed only at 300 MPa and 400 °C in the system equilibrated with CO_2-dominated fluid (water-poor). Individual calcite crystals were identified at the surface of amphibole minerals by Raman spectroscopy. The comparison of the Raman spectra show that our experimentally-produced calcite phases are identical to those from the drilled conduit rocks of Unzen volcano. Further experiments are required to reproduce natural mineral assemblages and to bracket typical conditions for carbonate formation in the Unzen conduit.

References

Dufaud et al., 2009, Chem. Geol., 265, 79-87.

P12-P22

Dolomite decomposition at ultrahigh pressures: textural evidence from two impure marbles from the Dabie-Sulu UHP belt, China

A. Proyer[1], F. Rolfo[2], Y.-F. Zhu[3], D. Castelli[2], R. Compagnoni[2]
[1]Freie Universität Berlin, Institut für Geowissenschaften, Berlin, Germany
[2]University of Torino, Torino, Italy
[3]Peking University, Peking, China

The reaction histories of two marbles that possibly experienced peak metamorphic pressures above the dolomite breakdown reaction to magnesite + aragonite were investigated. A dolomitic marble (sample D) from Xinyan village in eastern Dabie Shan, consists mainly of dolomite, omphacite and Na-bearing tremolite, with some additional calcite, phengite, Ce-rich epidote, rutile and zircon. Quartz occurs only as inclusions in tremolite, and magnesite as inclusions in dolomite; tiny relics of talc are included both in omphacite and tremolite. Magnesite relics usually sit in the cores of dolomite grains and are either fresh or partly to completely replaced by calcite ± subordinate poorly crystallized "talc". Matrix calcite is spotted by dolomite exsolutions, while rare calcite inclusions in omphacite or dolomite have no such exsolutions. Another dolomitic marble (sample S) was taken directly from the contact with an eclogite layer in a quarry NW of Sanqingge village in the Sulu terrane. It is composed of dolomite, calcite, Na-bearing tremolite, talc and some chlorite. The matrix calcite has a strange and complex polycrystalline and porous texture and quite commonly contains corroded magnesite in the central parts. It also contains fine grained, Fe-hydroxides with minor silica content, which according to Raman analyses is are most likely goethite with some amorphous silica. Concentrations of this BSE-bright material particularly outline former grain boundaries of magnesite which apparently got replaced by calcite. Tremolite contains inclusions of omphacite and quartz as well as of magnesite and calcite. Dolomite also contains inclusions of omphacite and fresh magnesite.

In spite of their different geologic location, both rocks have seemingly had a very similar reaction history: starting with the peak assemblage magnesite + aragonite + omphacite + talc + rutile ± phengite, during decompression, the reactions 1) mst + arag = dol, 2) omp + tlc = amph ± qtz and 3) arag = cc were passed subsequently. In sample D magnesite (except inclusions) and talc were fully consumed during reactions (1) and (2) respectively, while in sample S, aragonite and omphacite were consumed. The remaining magnesite in both samples was later corroded by a reaction with a strong kinetic control, as otherwise it would be replaced by dolomite, not calcite. Fe from magnesite was much less mobile than Mg and remained in the form of goethite in (S). The P-T conditions of magnesite replacement are controversial: The reaction could be a result of omphacite (from adjacent eclogite) continuing to react with magnesite to produce amphibole + Ca2+, but the poor crystalline nature of calcite, Fe-hydroxide and silica found at the magnesite site could also reflect a late low-temperature event. From textural observations, a UHP-assemblage of magnesite + aragonite is rather certain for (D), but at this point questionable for (S).

P12-P23

Localized reactions forming prograde and retrograde coronas in a high-pressure calcite marble from Dabieshan

A. Proyer[1], F. Rolfo[2], D. Castelli[2], R. Compagnoni[2]
[1]Freie Universität Berlin, Institut für Geowissenschaften, Berlin, Germany
[2]University of Torino, Torino, Italy

The overall metamorphic reaction in an impure calcite marble from Changpu, eastern Dabie Shan, China, an area belonging to the Wuhe–Pailou Unit for which peak metamorphic conditions of 3.3 GPa and 720°C were inferred by Rolfo et al (2004), is partitioned into local reaction domains defined by isolated grains of omphacite, garnet, epidote, quartz and ilmenite in the calcite matrix. Chemically homogenous omphacite in some instances gets partial or complete rims of quartz. More commonly, it has partial or complete rims of chemically variable amphibole. At a distinctly later stage, the omphacite core can be replaced by an albite-diopside-amphibole symplectite. Garnet in most cases develops a thick corona of epidote plus some quartz and calcite or is completely pseudomorphed. In other cases, this corona consists partly or entirely of amphibole. Primary epidote, as well as all corona epidote, develops compositional zoning with enrichment of mainly Ce3+ at the grain margins. Large grains of matrix quartz are partly transformed into albite, which is very porous and often contains tiny specks of Ce-rich epidote. Epidote near albitized quartz develops albite coronas. Large ilmenite grains in the matrix develop thick overgrowths of titanite, but in several instances an intermediate step of rutile formation is preserved.

Rare relics of talc in epidote indicate that the first breakdown reaction during exhumation was talc + omphacite ± garnet = amphibole ± epidote ±quartz (still within the eclogite facies). The second reaction was the common breakdown of omphacite + quartz to symplectite + albitized quartz. The distance between reaction partners controls what type of rim or corona develops around garnet (epidote remote from omphacite and amphibole near omphacite) and even quartz is only albitized when an Al-bearing mineral is found nearby. Epidote adjacent to quartz decomposes into albite + minute grains of Ce-rich epidote (allanite).

Omphacite crystals with thick quartz coronas are encrusted by fine-grained pargasitic amphibole along the quartz-omphacite grain boundary. The quartz coronas are considered to be older than omphacite breakdown to amphibole, most likely even prograde (replacement of a plagioclase precursor by omphacite with increasing pressure). The coronae around and pseudomorphs after garnet often contain omphacite – interpreted as relic inclusions of the garnet. This omphacite is not altered into amphibole, indicating either that garnet breakdown precedes that of omphacite or that the chemical potentials at the garnet site are not suitable to promote omphacite breakdown.

Additional accessory phases are zircon, apatite, pyrite, pyrrhotite, chalcopyrite and barite.

References:

Rolfo, F., Compagnoni, R., Wu W. & Xu, S. 2004. A coherent lithostratigraphic unit in the coesite eclogite complex of Dabie Shan, China: geologic and petrologic evidence. Lithos, 73, 71-94.

P12-P24

MANTLE XENOLITHES FROM SOUTHERN AFRICA AND STYRIA: A COMPARISON

L. Konrad[1], C.A. Hauzenberger[1], J. Konzett[2]
[1]University of Graz, Deptartment of Earth Sciences, Graz, Austria
[2]University of Innsbruck, Deptartment of Mineralogy and Petrography, Innsbruck, Austria

Mantle rocks can be brought to the surface by various volcanic processes. Kimberlitic pipes sample commonly deep seated asthenospheric mantle rocks from old cratons, while alkali basalts include samples from shallower depths (lithospheric mantle). Different mantle xenoliths from a kimberlitic source (South Africa, Kimberley Area and Lesotho, Letseng-la-Terae) and from an alkali basalt source (Styrian Vulkanic Arc, Beistein and Waxenegg) were chosen to investigate major, trace and rare earth element distributions in single minerals such as garnet, clinopyroxene, orthopyroxene and olivine. PT estimates from the individual mantle xenoliths allow to constrain the depth of the mantle source. The samples found at Kimberley are mainly garnet lherzolites and phlogopite-garnet lherzolites. The application of various geothermobarometers involving major- and trace element exchange between the primary lherzolite phases yields P-T conditions of ~1100-1200°C and ~4-5 GPa for most samples. Garnet and clinopyroxene trace and rare earth element patterns clearly indicate mantle metasomatism by a probably carbonatitic melt phase. Samples from the Letseng-la-Terae kimberlite contains a suite of xenoliths, mainly peridotites and pyroxenites, some of which show evidence for metasomatism. The suite of xenoliths include: 1) fine grained (Grt-) lherzolites, 2) coarse grained (Grt-) lherzolites, 3) harzburgites, 4) foliated (deformed) (Grt-) lherzolites, and 5) phlogopite-rich lherzolites. Metasomatic overprint by a melt phase is more evident than in samples from Kimberley. Secondary clinopyroxene grows at the expense of olivine and orthopyroxene or occurs as recrystallized rim around larger clinopyroxene crystals. Various geothermobarometers involving major- and trace element exchange between the primary lherzolite phases yields P-T conditions of ~1350°C and ~6.5 GPa. The recrystallized and/or newly grown mineral phases observed in the deformed areas yield significantly lower PT conditions, which are ~1230°C and ~4.5 GPa. The samples found at Kapfenstein are amphibole bearing wherlites where olivine consists of 85 mol.% Fo, Cr-Diopside has a X_{Mg} of 0.86 and 0.63-0.83 wt. % Cr_2O_3. Amphiboles can be classified as pargasites. The financial support by the Austrian Acadamy of Science is gratefully acknowledged. This study is a contribution to IGCP 557.

P12-P25

Metamorphic evolution of kyanite eclogites from Pohorje, Slovenia: An approach through secondary replacement textures

H. Taferner[1], C.A. Hauzenberger[1]
[1]University of Graz, Dept. of Mineralogy/Petrology, Graz, Austria

The Pohorje Mountains of Slovenia contain the southeasternmost HP and UHP rocks known from the Austroalpine Basement Units (Jának et al., 2004). They are built up of three main tectonic units that were emplaced during the Cretaceous (Fodor et al., 2003) and a pluton of granodioritic to tonalitic composition in the central part of the massif. The investigated kyanite eclogites are products of metamorphosed (eclogite facies with subsequent amphibolite facies retrogression) gabbros and gabbroic cumulates. To refine previous P-T results proposed in the literature, thermodynamic P-T pseudosections were constructed using the Perplex software package of Connolly (1990). Additionally, conventional geothermobarometric calculations were performed. Following reations, applicable for the equilibrium between garnet, clinopyroxene, phengite, kyanite and quartz/coesite, were used for P-T estimations: (1) Prp + 2 Grs + 3 Cel = 3 Ms + 6 Di, (2) 3 Di + 2 Ky = Prp + Grs + 2 Qtz/Coe and (3) 3 Cel + 4 Ky = Prp + 3 Ms + 4 Qtz/Coe. The calibra-tion of Krogh Ravna and Terry (2004) yields peak metamorphic conditions of 2.7 GPa and 820°C, calculations using activity corrected endmembers in Perplex, including the internally consistent data set of Holland and Powell (1990), result in peak metamorphic conditions of 2.2 GPa and 820°C. The retrograde evolution is indicated in the formation of secondary replacement textures such as (1) coronae of amphibole around garnet, (2) pseudomorphs of biotite and plagioclase after phengite, (3) cpx-plag-amph symplectite textures replacing omphacite and (4) symplectites of spin-cor-plag after kyanite that generated under disequilibrium conditions. These are interpreted to be textures caused by decompression indicating the rapid exhumation history of the eclogites. Coronae of amphibole around garnet are of pargasitic to magnesiohornb-lendic composition and a product of the reation between garnet and omphacite. Omphacite in a first step breaks down to a symplectite mainly consisting of low Na-clinopyroxene and plagioclase and in a second step to Na-Ca-amphibole and plagioclase. Kyanite is partially or totally replaced by a symplectite, typically concentrically arranged, consisting of plagioclase, spinel and corundum. Fig. 1 and Fig. 2: Symplectite of an-cor-sp-plag after kyanite within omphacite (left) and garnet (right). Connolly, J. A. D., (1990). Multivariable phase diagrams; an algorithm based on generalized thermodynamics. American Journal of Science, 290, 666-718. Fodor, L., Balogh, K., Dunkl, I. et al., 2003. Structural evolution and exhumation of the Pohorje-Kozjak Mts., Slovenia. Annales Univ. Sc. Budapest., Sectio Geol., 35, 118-119. Janák, M., Froitzheim, N., Lupták, B., Vrabec, M., Krogh Ravna, E. J., 2004. First Evidence for ultrahigh-pressure metamorphism of eclogites in Pohorje, Slovenia: Tracing deep continental subduction in the Eastern Alps. Tectonics, 23, TC5014. Krogh Ravna, E. J. & Terry, P., 2004. Geothermobarometry of UHP and HP eclogites and schists- an evaluation of equilibria among garnet-clinopyroxene-kyanite-phengite-coesite/quartz. J. of M. Geol., 22, 579-592.

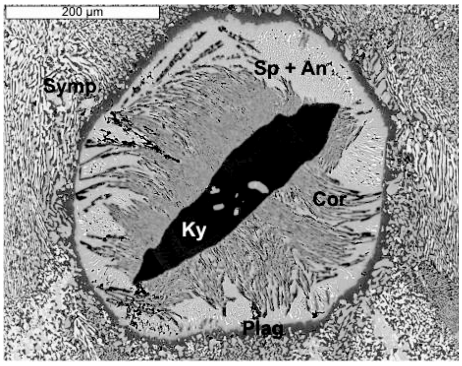

Figure 1

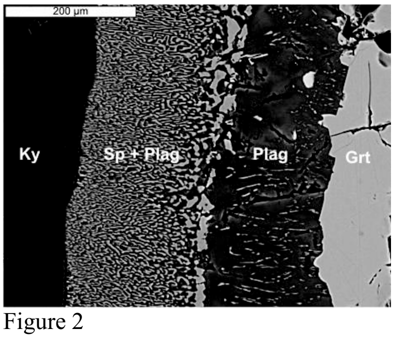

Figure 2

P12-P26

Geochemical Characteristics of Garnets from Tanzanian Kimberlites (Mwadui, Nyangwale, and Galamba kimberlites)

M. Mandl[1], C.A. Hauzenberger[1], J. Konzett[2], R. Jumanne[3], J.M. Gobba[4]
[1]University of Graz, Department of Earth Sciences, Graz, Austria
[2]University of Innsbruck, Institute of Mineralogy and Petrography, Innsbruck, Austria
[3]Williamson Diamond Mine, Petra Diamonds Ltd., Tanzania, Tanzania, United Republic of
[4]Gobbex Ltd., Tanzania, Tanzania, United Republic of

More than 350 kimberlite pipes and clusters have been found in Tanzania up to date. Many of the occurrences are found in and around Shinyanga, northern Tanzania. They are characterised by the presence of crater deposits, suggesting that minimal erosion has taken place in this region since Neogene times (~50 Ma) when the kimberlites were emplaced. The kimberlites are typically found in Archean granitic basement and meta-sediments. The most prominent kimberlite pipe, the Mwadui kimberlite, which is mined for diamonds, is one of the word largest and measures ~146 ha at surface.

Since only weathered crater deposits are exposed, no mantle xenoliths were found in the four visited / sampled kimberlite pipes: 1) Singida kimberlite, 2) Nyangwale kimberlite, 3) Mwadui kimberlite, 4) Galamba kimberlite. However, garnets could be sampled either in heavy mineral separates or as garnet megacrysts.

This is one of the first reports on the geochemical characteristics of garnets recovered from Tanzanian kimberlites. These garnets have been studied using major, trace and rare earth element compositions in order to obtain information on the underlying upper mantle.

Garnets from the Williamson diamond mine are cm sized megacrysts. Garnets do not show any chemical zoning, are pyrope rich with low contents of spessartine, grossular, and knorringite components. TiO_2 values are high with 0.9-1.2 wt.%, and P_2O_5 and Na_2O typically below 0.1 wt.%.

From the Nyangwale kimberlite only few garnet samples from heavy mineral concentrates were obtained. The chemical composition is slightly different from the Mwadui kimberlite. The Cr_2O_3 values are significantly higher with 3.7-4.8 wt.%, FeO ranges from 4-5 wt.%, and the TiO content is ~0.5 wt.%.

The Galamba kimberlite is situated to the east of the Mwadui kimberlite. The chemical composition of the garnet is slightly different from the garnet megacrysts from the Mwadui kimberlite. The garnets from the Galamba kimberlite are higher in Cr_2O_3 (0.9-2.5 wt.%) while TiO_2 content is lower (0.3-0.9 wt.%).

This is a contribution to IGCP 557. The financial support from the Austrian Academy of Science is gratefully acknowledged.

References

STIEFENHOFER, J. & FARROW, D.J. (2004): Geology of the Mwadui kimberlite, Shinyanga district, Tanzania, Lithos 76, 139-160.

DAWSON J.B. & STEPHENS W.E. (1975): Statistical classification of garnets from kimberlite and associated xenoliths, Journal of Geology 83, 589-607.

P12-P27

Occurrence of chromian kyanite in eclogites from Pohorje, Slovenia

H. Taferner[1], C.A. Hauzenberger[1]

[1]University of Graz, Dept. of Mineralogy/Petrology, Graz, Austria

The Pohorje Mountains of Slovenia are part of the Austroalpine Basement Units (Eastern Alps) and underwent an eo-Alpine eclogite facies overprint in the Turonian (93-90 Ma) with subsequent amphibolite facies retrogression (Thöni, 2006). The investigated kyanite-eclogites comprise the peak metamorphic mineral assemblage omphacite + garnet + amphibole + kyanite ± phengite ± corundum ± zoisite ± quart. A retrograde overprint caused by decompression is seen in secondary replacement textures such as diopside and albite symplectites around omphacite and corundum, spinel and plagioclase symplectites around kyanite. These kyanite eclogites are geochemically characterized by noticeable amounts of chromium (up to 4900 ppm) in bulk composition. High concentrations of MgO (up to 15%), Al_2O_3 (up to 23%) and Ni (up to 460 ppm) and low ones in SiO2 (43%) are typical for these rocks. In addition CaO and Al_2O_3 increase with decreasing MgO. These facts suggest an olivine, plagioclase and spinel bearing gabbroic cumulate as protolith. Some kyanite eclogites of this region show rare chromium-bearing turquoise coloured kyanites and pink chromium bearing corundum. Textural observations show that the Cr-kyanites formed in two different ways. A first type is characterized by tiny Cr-spinel inclusions within a larger turquoise coloured kyanite. Highest Cr contents and most intense turquoise colour are seen close to the Cr-spinel. A second type is formed around larger chromite crystals reacting with omphacite and garnet forming chromian kyanite and Cr-bearing corundum. A pargasitic amphibole corona is developed around the chromite - chromian kyanite - Cr-bearing corundum. This texture can be described by the kyanite forming endmember reaction parg + ky = spin + py + di + jd and parg + ky = sp + py + jd + grs. The formation of corundum is given by the reaction parg + cor = sp + ky + jd + grs. Again, highest Cr values are found close to the chromite and is decreasing with increasing distance to the chromite. The shown Cr distribution images illustrate these observations. Cr_2O_3 in kyanite reaches up to 14 wt% in the immediate vicinity to the spinel while corundum crystals contain up to 7 wt% Cr_2O_3. Surrounding pyroxenes and amphiboles are also showing elevated Cr_2O_3 contents close to Cr-spinel in an analogous manner.

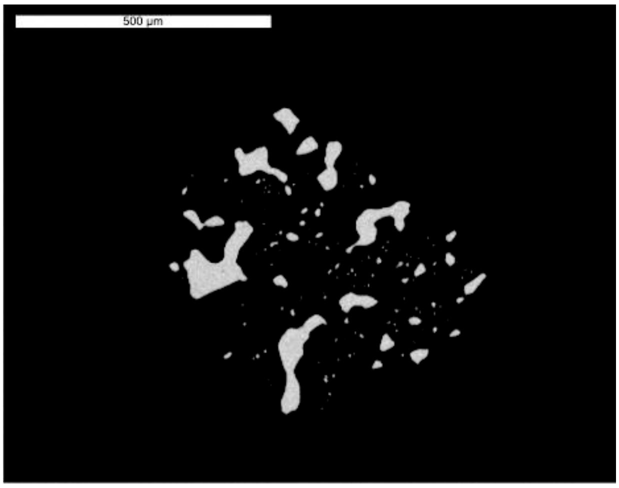

Figure 1

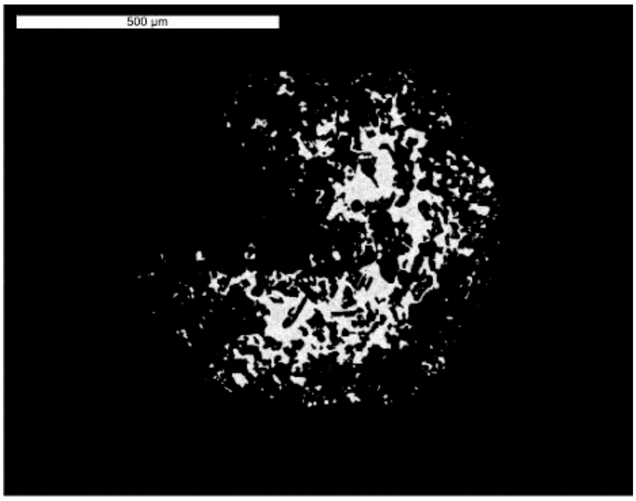

Figure 2

Figure 1 and Figure 2.: Cr-distribution maps of samples PM22 (left) and PM26 (right) illustrating the features mentioned above.

THÖNI, M., 2006. Dating eclogite facies metamorphism in the Eastern Alps-approaches, results, interpretations: a review. Mineralogy and Petrology, 88, 123-148.

P12-P28

Petrology and geochemistry of marbles of the Austroalpine Koralpe-Wölz nappe system (Eastern Alps)

B. Puhr[1], G. Hoinkes[1], R. Schuster[2]
[1]Universität Graz, Institut für Erdwissenschaften, Graz, Austria
[2]Geologische Bundesanstalt, Wien, Austria

Siliceous dolomitic marbles were investigated regarding their petrological and geochemical characteristics in order to reconstruct the metamorphic evolution of this rock type during pre-Alpine and Alpine Events.

The investigation area was set within the Koralpe-Wölz nappe pile which represents an eo-Alpine high pressure metamorphic part of the Austroalpine Basement. The Koralpe-Wölz nappe stack can be subdivided into several lithostratigraphic complexes [from bottom to top: the Wölz and Greim Complexes (greenschist to greenschist-amphibolite transitional zone), the Rappold Complex (amphibolite facies), the Koralpe-Saualpe, Millstatt and Sieggraben Complexes (ecolgite facies) and the Plankogel and Radenthein Complexes (greenschist-amphibolite transitional zone)] which altogether indicate an eo-Alpine inverted metamorphic gradient for the tectonic lower and an normal metamorphic gradient for the tectonic upper part of the nappe pile.

Within the investigation area east of the Tauern Window an increasing eo-Alpine metamorphic subduction type field gradient from North to South is clearly documented in metabasites and metapelites and is confirmed by metacarbonates of the siliceous dolomitic system (CMSCH). Cc-Dol-Qu-Phl - assemblages are characteristic for the northernmost Wölz Complex and represent Cc-Dol-solvus temperatures of 437-463°C. The first occurrence of Tre occurs further south in the Greim complex at temperatures of 540-562°C. Further southward Tre is followed by Di which is the dominant index mineral in the Rappold- (660-691°C) and the Millstatt-, Koralpe-Saualpe- (680-740°C) and Pohorje Complexes. Fo (partly coexisting with Ti-Chu) occurs occasionally within the stability field of Di in the southern Koralpe-Saualpe Complex and is probably stabilized by high P_{H_2O}. Fo accompanied by Spl representing the highest metamorphic temperatures of ca. 760°C occurs in the Sieggraben Complex at the Eastern end of the Alps. Apart from (Permian?) Di-inclusions in Alpine Tre of the Millstatt and Rappold Complexes there is no evidence of polymetamorphism neither by pre-Alpine relics nor mineral chemical zoning.

Sr-isotope ratios of pure marbles imply a Lower Paleozoic (Silur/Devon) age of their sedimentation. Based on Sr, O and C-isotope investigations all complexes can be devided into two groups: The Rappold, Plankogel and Koralpe-Saualpe Complexes show ^{87}Sr/^{86}Sr-values less than 0,70847 and strongly scattering δ^{18}O (19,3 to 31) and δ^{13}C-data (-1 to 4,8). The second group (Wölz, Pohorje, Millstatt and Radenthein Complexes) is characterized by Sr-values above 0,70855 and a narrow range of δ^{18}O and δ^{13}C-values (17,7 to 25,8 and -0,1 to 2,9, respectively). Despite significant overlaps isotope ratios may help to correlate tectonic complexes of common tectonometamorphic history.

P12-P29

Geology and Petrography of the Tershin Mafic-Ultramafic intrusive Rocks of Sero Area, NW Iran

M. Asadpour[1,2], S. Heuss-Aßbichler[1], S.M. Pourmoafi[2]
[1]LM-University, Earth and Environmental Sciences, Munchen, Germany
[2]Shahid Beheshti, Geology, Tehran, Iran, Islamic Republic of

The Zagros orogenic system is part of the Tethyan orogenic collage, which was formed by the NW-ward subduction of Neo-Tethyan oceanic lithosphere and the subsequent continental collision between Gondwana and Eurasia from Mesozoic to Tertiary time. The Tershin complex is located in the Sero region at the NW-ward corner of the Zagros orogenic system , near border of Turkey. It is suggested to be of Precambrian to post Upper Cambrian age. Mafic rocks like Gabbro , Olivine gabbro and Hornbland gabbro are widespread in this region. Field work, however, revealed that main part of the complex comprises Ultramafic rocks . The fact that various Ophiolite complexes occur in this region , like Khoy in the northern part and the Coloured Melange Sero in the southern part of this region , suggests that this Complex may be also part of the Tethyan Ophiolites. This would be a link between the Middle Eastern and other Asian Ophiolites. In this study we will present preliminary results about the geology and petrography of the Mafic - Ultramafic rocks from Tershin Complex.

This Mafic-Ultramafic intrusive coplex occurs as a roughly elliptical shape body (3-7Km in diameter) , withen non-metamorph series of Paleozoic limestone . It caused an thermal aureole with Marble and Skarn . The Ultramafic rocks are classified as Wehrlite , Harzbrgite , Pyroxenite and Hornblendite . Main mineral phases are Olivin , Orthopyroxene , Clinopyroxene , Hornblende , Biotite and Opaque minerals . They show typical cumulate textures and Corona structure around Olivin . In Gabbro , Pricokilin textures of Plagioclase was observed too . Exsolution of Clinopyroxene in Orthopyroxene is a typical feature . All rocks in Sero region are metamorphosed and show the typical paragenesis of Greenshist facies and intresting mylonitized . The Gabbro of deformationin Tershin complex , however , is weak mylonites are indications for tectonic events .

The different Ultramafic rocks can be explained as accumulates in magma chamber as the result of both differentiation and crystallization . The intrusion at relatively shallow crustal levels corresponds to the Alaskan type . Same type of rocks were observed in Turkey.

Key words: Mafic-Ultramafic complex, Petrography, Tectonic, Zagros orogenic system, NW Iran

P12-P30

Zincian Clinopyroxene a Sophisticated Petrogenetic Indicator for Zinc-Rich Metamorphic Rocks

A. Huber[1], S. Heuss-Aßbichler[1]
[1]Ludwig-Maximilians-Universität, für Geo- und Umweltwissenschaften, München, Germany

Detailed geochemical studies were performed to derive the systematics of zinc content in clinopyroxenes and various skarn types (Nakano, 1998; Nakano et al 1991, 1994). However up to now, no correlation between zinc concentration in clinopyroxene and petrogenetic terms could be deduced. The purpose of this study is to present the observed correlation between natural clinopyroxen from several metamorphic zinc-rich terrains with regard to the known prevailing pressure-, temperature- and fluid conditions in terms of fugacity ratio fS_2/fO_2.

Electron microprobe analysis were performed to determine Zn as trace element. Various clinopyroxenes from several skarn deposits were analysed, e.g. El Hammam/Morocco, Dartmoor/Great Britain, Breitenbrunn (Erzgebirge)/Germany, Långban and Åmmeberg/Sweden, King Island/Australia and Arendal/Norway. In addition various metamorphic rocks were analyzed, like calc-silicate (Monzoni/Italy), peridotite (San Carlos-Arizona/U.S.A.) and granulite (Franklin-New Jersey/USA). All clinopyroxenes are members of the hedenbergite-diopside solid solution series. Additionally some pyroxenes exhibit a fassaite $[Ca(Mg,Al)(Si,Al)_2O_6]$ or an aegirine $[NaFe^{3+}Si_2O_6]$ component. Minor components are johannsenite $[CaMn^{2+}Si_2O_6]$ and jadeite $[NaAlSi_2O_6]$. The average zinc content in clinopyroxene varies between 50 ppm and 4980 ppm. Highest zinc contents up to 8800 ppm were analyzed in pyroxene in contact with sphalerite (Zn,Fe)S from Åmmeberg/Sweden skarn deposit. A clinopyroxene from Franklin-New Jersey/USA shows up to 7980 ppm Zn.

The majority of the clinopyroxenes were formed at low-pressure terrains. They display low average zinc concentrations (< 850 ppm), which is in good agreement with Nakano et al. (1991, 1994) and Nakano (1998). According to Nakano (1998) characteristic thresholds of zinc concentration in skarn clinopyroxene correlate with different skarn types. Incorporating our data, the Nakano classification can be extended. At Cornwall Evans (1993) observed a zonal sequence of Fe, Pb-Zn, Cu, Sn skarn ore mineralization with decreasing distance of the intrusive body. Accordingly, reflecting this sequence, an increasing zinc concentration in clinopyroxene correlates with increasing metamorphic temperatures.

However some clinopyroxenes stand out due to their extraordinary high zinc contents. Highest values (up to 5000 ppm in average) were detected in clinopyroxene from Pb-Zn skarn deposits (Bergslagen/Sweden). Remarkably high zinc concentrations (up to 4300 ppm) were detected in clinopyroxene from Franklin-New Jersey/U.S.A.. The clinopyroxenes of both areas were affected by equivalent metamorphic peak conditions of > ~0.4 GPa / > ~600°C . This is in good agreement with the high-pressure stability of petedunnite ($CaZnSi_2O_6$). The endmember of zinc clinopyroxene solid solutions is stable at high pressures (> 0.8GPa) (Huber et al. 2011). Accordingly, significant zinc enrichment in natural clinopyroxenes is associated with elevated pressures during mineralization processes.

Totally different mechanisms of zinc enrichment in clinopyroxene occur along the contact with zinc-ore. There is obviously a negative correlation between petedunnite component in clinopyroxene and fugacity ratio of f_{S2}/f_{O2} during formation.

P13-P01

Relation between hydrous strain and the cationic exchange properties for the Na rich-montmorillonite exchanged with Cd (II), Co (II), Zn (II) and Ni (II) cation: An XRD profile modeling approach

W. OUESLATI[1], R. CHALGHAF[1], H. BEN RHAIEM[1], A. BEN HAJ AMARA[1]
[1]Faculté des sciences de bizerte-laboratoire de physique des matériaux lamellaires et nanomatériaux hybrides, physics, Zarzouna-Bizerte, Tunisia

This work aims to examine, by quantitative XRD analysis, the effect of an applied hydrous strain on the cationic exchange process of a dioctahedral smectite (Na-rich montmorillonite SWy-2). The hydrous constraint was created by a continuous, in situ, hydration-dehydration cycles using variation of %RH rate [1] (i.e. under controlled atmosphere, variable %RH). The starting and final samples was deposit in contact with saturated Cd(II), Co(II), Zn(II) and Ni(II) chloride solutions respectively in order to examine retained materials stress who affects the CEC(i.e. Cationic Exchange Capacity)of the host materials. An XRD profile modeling approach is adopted to describe all structural changes induced by the environmental evolution of the %RH rate. The quantitative analysis of XRD patterns is achieved using an indirect method based on the comparison of experimental XRD patterns with calculated ones. This investigation allowed us to determine several structural parameters related to the nature, abundance, size, position and organization of exchangeable cation and water molecule in the interlamellar space along the c* axis [2]. Qualitative obtained results show an evolution of the hydration behavior, versus the number of hydration -dehydration cycle, from homogeneous (i.e. two water sheet in the interlamellar space “2W”) to heterogeneous hydration state (i.e. intermediate one and two water sheet “1W-2W”) ascribed by an interstratified phases due probably to a heterogeneous saturation of the exchangeable site of the host materials or to a new organization and species distribution in the interlamellar space. These results were quantitatively explained in the proposed model layer structure MLS by coexistence of more than one “crystallite” specie saturated by more than one exchangeable cations in the interlamellar space and thereafter partial saturation of exchangeable site. Using optimum structural parameter values, deduced from the best agreement between experimental and theoretical XRD profile, some equations who described respectively the evolution of CEC, interlamellar water rate, kinetic exchange process versus the applied hydrous strain were derived.

[1] W. Oueslati, M.S. Karmous, H. Ben Rhaiem, B. Lanson, A. Ben Haj Amara, Z. Kristallogr. Suppl. 26, 417 (2007).
[2] W. Oueslati, H. Ben Rhaiem , A. Ben Haj Amara, Desalination 271, 139 (2011).

P13-P02

On the Localization of Plastic Flow under Compression of NaCl, KCl and LiF Crystals

S. Barannikova[1], L. Zuev[1]
[1]Institute of Strength Physics & Materials Science, Russian Academy of Sciences, Tomsk, Russian Federation

In recent years, investigations of the localization of plastic flow in metals and alloys have revealed that the plastic flow over the entire flow curve from the yield point to failure of the specimen is localized and the forms of macrolocalization are determined by the deformation hardening laws acting at the corresponding stages of the process [1]. In earlier works, the problem of macroscopic localization of the plastic strain was studied predominantly for face centered cubic metal single crystals under tension. However, it is important to obtain information on the localization of macrostrain in alkali halide crystals that have been traditionally used for investigating the mechanisms of plastic flow.

In this respect, the possibility of using the polarization optical method for analyzing stresses (the photoelasticity method) with the aim of investigating deformation processes in alkali halide crystals is pression along the [001] axis on an Instron testing machine. The recording of the compression curve from the beginning of loading to a complete failure of the specimen was accompanied by the sequential recording of the displacement vector fields **r**(x, y) for points on the (010) face of the test specimens by the double exposure speckle photography technique [1]. The longitudinal, transverse, shear, and rotational components of the plastic distortion tensor at all points of the observed surface were calculated using the numerical differentiation of the fields **r**(x, y) with respect to the coordinates x and y.

The plastic flow localization patterns for alkali halide crystals under compression are investigated. The main spatiotemporal regularities of the strain localization at the stages of deformation hardening in these single crystals are established. The relation is traced between the orientation of localized strain zones and the crystallography of slip systems of the test specimens at the initial stages of plastic deformation (fig.1). The velocity of motion of localized strain zones under compression is determined.

[1] L. B. Zuev, Ann. Phys. **16**, 286 (2007

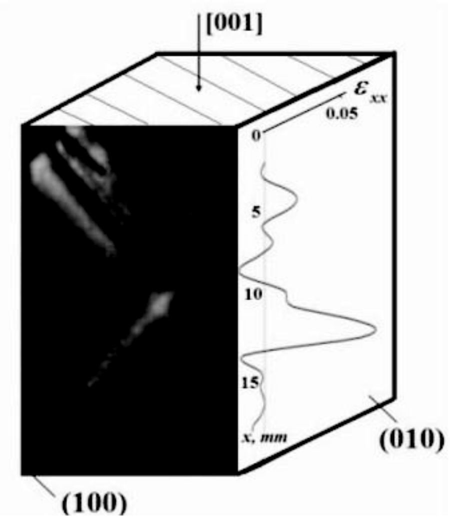

Figure 1

P13-P03

Effect of an applied strain caused by alkaline perturbation on the cationic exchange capacity and hydration properties of dioctahedral smectite saturated with Co^{2+} cation: quantitative XRD investigation.

R. Chalghaf[1], W. Oueslati[1], M. Ammar[1], H. Ben Rhaiem[1],
A. Ben Haj Amara[1]
[1]Faculté des sciences de bizerte-laboratoire de physique des matériaux lamellaires et nanomatériaux hybrides, physics, Zarzouna-Bizerte, Tunisia

This work aims to determine the strain effect caused by an alkaline perturbation, obtained by varying pH solution value, on the cationic exchange process in the case of Na rich-montmorillonite (Swy-2) in contact with saturated Co^{2+} solutions.This goal was accomplished in two steps. First, the host material (Na rich-montmorillonite) was deposit in contact with solution saturated by Co^{2+} cation with variable pH values (i.e. from pH=4 to pH=9) in order to determine the relation between the applied strain and the CEC of the starting materials. In the second step, strained materials (saturated Co^{2+} specimen) was considered like starting sample and used to verify the effect of the "materials history" on the selective exchange process studied by [1]. An XRD profile modeling approach is adopted to describe all structural changes induced by the environmental evolution of the pH rate. The quantitative analysis of XRD patterns is achieved using an indirect method based on the comparison of experimental XRD patterns with calculated ones. This investigation allowed us to determine several structural parameters related to the nature, abundance, size, position and organization of exchangeable cation and water molecule in the interlamellar space along the c* axis.

Obtained results showed:

-An evolution of the hydration behavior (from 1W to 2W [2]) of the sample saturated Co^{2+} versus the pH rate.

-An interstratified hydration character for the low and high pH rate.

-The CEC values, obtained from theoretical model, fluctuate versus the pH rate and the maximum value was marked at $pH \approx 7$.

-Major change in the organistaion of the exchangeable cation and water molecule in the interlmellar space.

-The applied strain "delete" the "materials history" and the new starting Na-rich montmorillonite was characterized by d_{001}=12.6Å.

-Using strained material for the selective exchange process a discordance with the results obtained by [1] was showed in the in the case of bi-ionic solutions (saturated by Pb^{2+}, Cu^{2+}).

[1] W. Oueslati, M.Meftah, H. Ben Rhaiem, and A. Ben Haj Amara Advances in Materials Science and Engineering, 2009, ID 385673.
[2] W. Oueslati, H. Ben Rhaiem , A. Ben Haj Amara, Desalination 271, 139 (2011).

P13-P04

Examination of Magnetic and Adsorption Properties of Magnetically Modified Zeolite and Clay

Z. Dikmen[1]
[1]Anadolu University, Physics, Eskisehir, Turkey

In this study deals with gaining magnetic properties to natural zeolite and clays. In this process, we add iron oxide particles to zeolite and clay substences, as a result of that substences gain some magnetic and adsorption properties. Finally we compare the magnetic and adsorption properties of zeolite and clays. Firstly, instrumental characterization of the natural clay and natural zeolite sample were performed by various techniques such as XRD, XRF, TG/DTA, SEM and then magnetically modified clay and magnetically modified zeolite samples are prepared. The fractions of clay and zeolite samples that have dimensions smaller than 63μm have been separated by sieving. They were mixed and intensively ground with powder forms of magnetite in a mortar. The resulting powder mixture was slowly heated up to 950°C at 1°C/min and maintained at this temperature for 6 hours. The solid sample was cooled and washed with de-ionized water until no Cl^- ions were detected in the eluted water, and then dried at 80°C during 16 hours. Adsorption and magnetic properties of the magnetically modified samples are examined. As a result of adsorption experiments, it is observed that, magnetically modified clays have larger specific surface area and average pore diameter compared to magnetically modified zeolites (Table 1).

However the result of magnetic measurements, show that, saturated magnetization and remnant magnetization values of magnetically modified zeolites larger when compared to values taken from magnetically modified clays (Table 2).

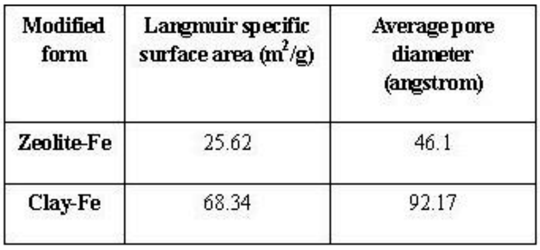

Modified form	Langmuir specific surface area (m^2/g)	Average pore diameter (angstrom)
Zeolite-Fe	25.62	46.1
Clay-Fe	68.34	92.17

Figure 1

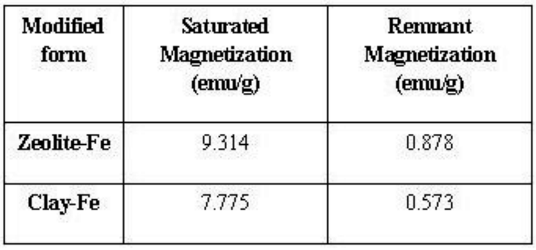

Modified form	Saturated Magnetization (emu/g)	Remnant Magnetization (emu/g)
Zeolite-Fe	9.314	0.878
Clay-Fe	7.775	0.573

Figure 2

P14-P01

Nb-Ta-Ti oxides fractionation in topaz-bearing granites of the Krušné Hory/Erzgebirge area

M. René[1]
[1]Institute of Rok Structure and Mechanics, Academy of Sciences of the Czech Republic, Geochemistry, Prague 8, Czech Republic

Niobium- and tantalum-bearing oxide minerals are common in topaz granites and related rocks. The most common Nb-Ta-bearing minerals in these parageneses are Nb-Ta-bearing rutile and columbite-group minerals (CGM). These minerals were detailed studied in Krásno-Horní Slavkov, Geyer, and Ehrenfriedersdorf ore districts. Topaz-bearing granites form two distinct magmatic suites in the Krušné Hory/Erzgebirge area. The first suite is formed by high-P (>0.4 wt% P_2O_5), highly evolved S-type granites (Horní Slavkov-Krásno, Geyer and Ehrenfriedersdorf ore districts). The second topaz granite suite is formed by low-P (<0.4 wt% P_2O_5), aluminous A-type granites (Altenberg and Zinnwald/Cínovec). These topaz-bearing granites show highly variable Ta/Nb ratio with the lowest values of this ratio in low-P granites from the Cínovec granite cupola (0.16-0.41). The Ta/Nb ratios in high-P topaz granites vary from 0.17 to 0.55 in topaz granites of the Sauberg granite stock (Ehrenfriedersdorf ore district) to 0.34-0.64 in topaz granites of the Krásno-Horní Slavkov ore district and to 0.74-1.12 in topaz granites of the Geyer granite stock.

In all these topaz-bearing granites, Nb and Ta are predominantly hosted in rutile and to a lesser extent, in CGM. Rutile contains significant levels of Ta (up to 37 wt.% Ta_2O_5) and Nb (up to 24 wt.% Nb_2O_5), with Ta/(Ta + Nb) ratio ranging from 0.04 to 0.61. Columbite-group minerals are represented mostly by columbite-(Fe) and rarely by columbite-(Mn), with Mn/(Mn + Fe) ratio ranging from 0.16 to 0.94. The increase of Mn/(Mn + Fe) ratio in CGM is typically attributed to fractional crystallization in rare-metal enriched granites. The exceptionally rare Fe-rich, W-bearing ixiolite occurs as inclusions in Nb-Ta-bearing rutile from quartz-free alkali-feldspar syenites in the Horní Slavkov-Krásno ore district (Vysoký Kámen stock) and/or as small grains in topaz-bearing granite from the Ehrenfriedersdorf ore district. Wodginite was found only in the topaz-albite microgranite of gneissic breccia matrix that occurs in the upper most part of the Hub topaz-albite granite stock of the Horní Slavkov-Krásno ore district. In wodginite, the Mn/(Mn + Fe) ratio is 0.42-0.51, whereas the coexisting tapiolite-(Fe) has a distinctly lower Mn/(Mn + Fe) ratio close to 0.06. This study was supported by the Czech Science Foundation (project No. 205/09/0540).

P14-P02

Visible gold and freibergite from Variscan, late-orogenic, vein-type sulphidic lead-zinc mineralizations of the Siegerland-Wied district, Rhenish Massif

A. Hellmann[1], F.M. Meyer[1]
[1]RWTH-Aachen University, Institute of Mineralogy and Economic Geology, Aachen, Germany

Metasediment-hosted, late-orogenic lead-zinc deposits are widespread in the Rhenish Massif and occure in the Siegerland-Wied-; Bad Ems-;Bensberg -;Hunsrück- and the Ramsbeck districts. Common to all districts is the spatial and temporal association of the mineralized Pb-Zn veins with synorogenic structures, the common assemblage sphalerite + galena ± chalcopyrite ± fahlore, their origin from low saline fluids (Erlinghagen, 1989; Hein, 1993) and relative uniform Pb-isotopic values (Krahn, 1988).

Here we present some new petrological data on late-orogenic Pb-Zn mineralizations in the Siegerland-Wied district of the Rhenish fold and thrust belt, with emphasize on associated gold mineralization. Native gold is previously reported in paragenesis with millerite + hauchecornite from decomposed ullmannite crystals and in association with fahlore (Fenchel et al., 1985).

Complex Pb-Zn-Cu-Co-Fe-ore from the abandoned Aurora Cu-Co mine near Siegen shows an assemblage of euhedral pyrite-, siderite-, and quartz crystals, cataclastically sheared along micro-shear zones. Alloclasite and cobaltite partly replace pyrite, are fractured, and embedded in an assemblage of sphalerite, chalcopyrite and galena. Visible gold is found within pyrite and is located in the vicinity of cracks filled by chalcopyrite. This suggests a contemporaneous formation of gold and Cu-, Zn-, Pb-sulfides.

Nickel ore collected from an old heap of Professor Ullmann´s Co and Ni bearing mine Aufgeklärtes Glück, near Siegen, where ullmannite was detected first by Ullmann himself in 1804, shows an assemblage of euhedral siderite, quartz, pyrite and ullmannite crystals ($(\mathrm{Ni}_{0.94}\mathrm{Co}_{0.01\text{-}0.02})(\mathrm{Sb}_{0.78\text{-}0.84},\mathrm{As}_{0.02\text{-}0.25})\mathrm{S}_{1.01}$). The assemblage is cataclastically sheared and the fractures are healed with chalcopyrite, galena, sphalerite and subordinate tetrahedrite, freibergite and native gold. Ullmannite is hydrothermally altered involving a coupled substitution of the type CoAs - NiSb, showing Ni + Sb slightly enriched. Ullmannite is investigated for invisible gold in a survey by laser ablation ICP-MS, but concentrations are b.d.l.

Freibergite, with the composition of $\mathrm{Cu}_{7.03\text{-}7.06}\,\mathrm{Ag}_{2.89\text{-}2.96}\,\mathrm{Fe}_{0.32\text{-}0.34}\,\mathrm{Zn}_{1.83\text{-}1.84}\,\mathrm{As}_{0.05\text{-}0.06}\,\mathrm{Sb}_{3.77\text{-}3.78}\,\mathrm{S}_{12.37\text{-}12.50}$, is reported for the first time from the Siegerland-Wied district. It is previously reported from Pb-Zn mineralizations of the Hunsrück district and gives evidence that the mineralization is of variscan age (Krahn, 1988).

Native gold from both localities is rich in Ag, with a fineness of 890 and 840, respectively, suggesting its contemporaneous formation with Pb-Zn-mineralization.

References

Erlinghagen, K.P. (1989). N. Jb. Mineral. Mh., p. 557 - 567.
Fenchel et al.(1985). Die Sideriterzgänge im Siegerland-Wied-Distrikt.-Geol. Jb., D 77, 517 pp., 128 Abb., 38 Tab., 31 Taf., Hannover.
Hein, U.F. (1993). Mineral. Mag. 57, p. 451-467.
Krahn, L. (1988). Dissertation RWTH-Aachen, IV + 199 S., 72 Abb., 24 Tab.; Aachen.

P14-P03

Invisible gold in Co-Fe-Ni-sulpharsenides measured by Laser-Ablation ICP-MS and new crystal -chemical data in the system FeAsS-CoAsS-NiAsS from ores of hydrothermal cobalt -copper-gold (-nickel) mineralizations of the Siegerland-Wied district, Rhenish Massif

A. Hellmann[1], F.M. Meyer[1], A.I. Metzmacher[1]
[1]RWTH-Aachen University, Institute of Mineralogy and Economic Geology, Aachen, Germany

We present first time LA-ICP-MS data for Au in cobalt-sulpharsenides and new crystal-chemical data on Co-Fe-(Ni)-sulpharsenides of hydrothermal cobalt ores from the Siegerland-Wied district in the Rhenish Massif. The sulpharsenides occure in hydrothermal quartz veins related to synorogenic steep-dipping reverse faults of the Variscan fault and thrust belt.

We investigated 13 different cobalt occurrences of the Siegerland-Wied siderite district in terms of mineralogy and mineral chemistry by EPMA. In addition, XRPD was carried out to obtain structural information on cobalt-minerals.

The Co-Fe-(Ni)-sulpharsenides are commonly fine grained (< 50 µm) unzoned crystals. The sulpharsenides form disseminations, clusters and bands of euhedral crystals in older siderite and quartz veins or replace older pyrite and marcasite grains.

Co-Fe-(Ni)-sulpharsenides are mostly alloclasite and not glaucodote as previously reported in the literature (Gies, 1970). Cobaltite is second in abundance followed by arsenopyrite and cobalt-bearing arsenopyrite. Glaucodote is rather uncommon. Where the arsenopyrite endmember is present, it is slightly earlier than-, and replaced by the cobalt-bearing members of the series. Ni-concentrations for some of the cobaltites are relative high and represent cobaltite-gersdorffite s.s. with an i.s.s. observed at the maximum of 0.5 apfu Ni.

Au was measured in situ on polished sections with LA-ICP-Quadrupol-MS using an ArF-Excimer Laser (193 nm) and He as carrier gas. The spot size was 35 mm, energy density = 0.56 - 0.59 GW/cm^2 and f = 4 Hz. A synthetical pyrrhotite standard Po 726 B2-SRM doped with 46.1 ppm Au and PGE´s was used as reference material (Sylvester et. al., 2005). The detection limit for Au in alloclasite is about 1 ppm.

The background was measured for 100 sec. and the signal for 200 sec. on both standard and sample. The standard measurement was repeated twice after every 6 samples. Sulphur concentrations measured by EPMA were used as internal standard.

Two types of signals were obtained from the samples. Continuous signals are interpreted as an indicator of invisible gold distributed homogeneously within the crystal lattice, whereas spikes are interpreted to originate from inclusions of sub-micrometer sized gold particles.

The measured concentration of homogeneous distributed Au varies from b.d.l. to 500 ppm for alloclasite. The median for all values is about 22 ppm Au. The substitution mechanism for gold in alloclasite and cobaltite is the matter of further investigations and is possibly related to As deficiency and excess S in the phases under investigation.

References

Gies, H. (1970). N. Jhb Min., Abh. 112(3), p-279 - 301.

Sylvester P.J. et al. (2005). Synthesis and evaluation of a fused pyrrhotite standard reference material for platinum group element and gold analysis by laser ablation ICP-MS. 10th International Pt Symposium Oulu, 8-11 August.

P15-P01

Triacetone Triperoxide Hapten Structure for the Development of Antibodies

W. Kraus[1], M.A. Walter[1], F. Emmerling[1], R.J. Schneider[1], M.G. Weller[1], U. Panne[1]
[1]BAM, Berlin, Germany

Triacetone triperoxide (TATP) is an improvised explosive that, due to its properties, is a potential security threat. The simple, inexpensive synthesis and the lack of direct detection methods make TATP the foremost amateur explosive. Because of its atypical structure (i.e., the absence of any nitro groups and its low density), the identification within a short time frame has been hitherto troublesome using conventional methods.

An antibody-based sensing system could be a reliable and advantageous method given that the antibody will specifically distinguish the structure of TATP from that of innocuous substances.

TATP can be easily synthesized from acetone and hydrogen peroxide. The product does not contain nitrogen, but it forms a nonagonal ring without distinctive side chains and/or electron rich substituents, which are usually required for excellent immunological recognition.

As an additional complication, different conformations have to be considered. There are two stable (and separable) TATP conformers[1,2] at room temperature. One forms the regular and more stable twisted boat-chair (D_3) conformation, and the other forms the twisted chair-chair conformation (C_2) (ΔE = 1.85 kcal/mol = 7.75 kJ/mol). The objective of this work was to synthesize a conjugate, which should be almost identical to the 3D structure of TATP, in order to obtain highly selective and high-affinity monoclonal or polyclonal anti-TATP antibodies. The structure should be confirmed through X-ray diffraction analysis.[3]

The X-ray structure of the cyclic TATP molecule has been described previously.[4,5,6] In the crystal structure, the nonagonal ring adopts a twisted boat-chair conformation with a local symmetry close toD_3. As a result of the centrosymmetry of space group $P2_1/c$, both conformers (the right-handed (Δ) and left-handed (Λ)) are present in the crystal structure.[7]

TATP hapten crystallizes in the triclinic space group P-1 with one molecule in the asymmetric unit. The molecules form dimers via hydrogen bonds.

A comparison of the molecular conformation of the nonagonal ring of both structures reveals that the bond lengths and angles do not differ significantly and are nearly the same. This study underlines the importance of a thorough structural characterization of both, the target compound and the hapten mimic.

(1) Denekamp, C.; Gottlieb, L.; Tamiri, T.; Tsoglin, A.; Shilav, R.; Kapon, M. Org. Lett. 2005, 7, 2461.

(2) Widmer, L.; Watson, S.; Schlatter, K.; Crowson, A. Analyst 2002, 127, 1627.

(3) Walter, M. A.; Pfeifer, D.; Kraus, W.; Emmerling, F.; Schneider, R. J.; Panne, U.; Weller, M. G., Langmuir 26, 15418-15423.

(4) Dubnikova, F.; Kosloff, R.; Almog, J.; Zeiri, Y.; Boese, R.; Itzhaky, H.;Alt, A.; Keinan, E. J. Am. Chem. Soc. 2005, 127, 1146.

(5) Groth, P. Acta Chem. Scand. 1969, 23, 1311.

(6) Jensen, L.; Mortensen, P. M.; Trane, R.; Harris, P.; Berg, R. W. Appl. Spectrosc. 2009, 63, 92.

(7) Reany, O.; Kapon, M.; Botoshansky, M.; Keinan, E. Cryst. Growth Des. 2009, 9, 3661.

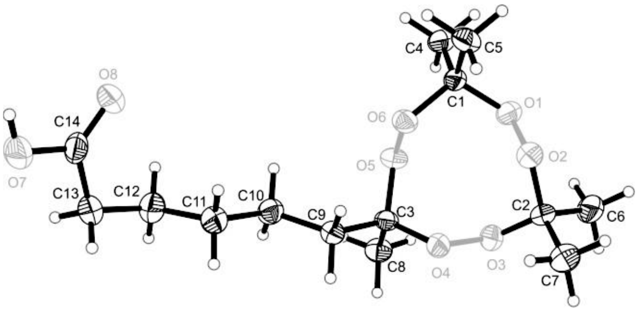

Figure 1

P15-P02
Barbituric Acid: Crystal Structure of The Enol Tautomer

J. Glinnemann[1], J. Brüning[1], M.U. Schmidt[1], M.R. Chierotti[2]
[1]Goethe-Universität, Inst. f. Anorganische u. Analytische Chemie, Frankfurt/Main, Germany
[2]University, Dipartimento di Chimica I. F. M., Torino, Italy

Barbituric acid had been known until recently solely in the keto tautomeric form **1** (Fig. 1) in the gas phase, in solution, and in the solid state. In contrast, the recently discovered tautomeric polymorph [1], thermodynamically stable at ambient, is composed of molecules in the enol form **2** [2]. This polymorph is obtained by grinding or milling from the commercial form with the keto tautomer. All attempts to obtain single crystals of the new phase by recrystallisation failed.

Since the grinding/milling processes yield powders of poor crystallinity, as judged from in-house X-ray powder diffraction, high-resolution X-ray synchrotron and neutron powder diffraction were performed [3]. The crystal structure was solved and refined from the X-ray synchrotron data and additionally refined from the neutron data, to obtain reliable interatomic distances and angles involving hydrogen atoms.

In the crystal structure planar molecules form zigzag chains *via* two N−H···O hydrogen bonds. Interconnection of the chains is performed by O−H···O hydrogen bonds, leading to a three-dimensional hydrogen-bond framework (Fig. 2).

The crystal structure of the new polymorph of barbituric acid does not compare to any of the hitherto known structures of this compound. The latter consist of the keto tautomeric, *i. e.* trioxy tautomeric, molecules and are layer structures. They exhibit mutually different hydrogen-bonding systems. In the crystal structure of the new polymorph a molecule performs the largest number of hydrogen bonds of all polymorphs known.

Crystal data

Monoclinic, space-group type $P2_1/n$ (no. 14), $Z = 4$.

a = 11.87614(6) Å, b = 0 8.91533(4) Å, c = 4.83457(3) Å, β = 95.0854(4)°,

V = 509.868(5) Å^3.

References

[1] Chierotti, M. R., Gobetto, R., Pellegrino, L., Milone, L., Venturello, P.: *Cryst. Growth Des.* **2008**, *8*, 1454−1457.

[2] Schmidt, M. U., Brüning, J., Glinnemann, J., Hützler, M. W., Mörschel, Ph., Ivashevskaya, S. N., van de Streek, J., Braga, D., Maini, L., Chierotti, M. R.: *Angew. Chem. Int. Ed.* 2011, in print.

[3] Proposal 20080185: *Crystal and molecular structure of a new tautomeric polymorph of barbituric acid*. http://www.psi.ch/.

Figure captions

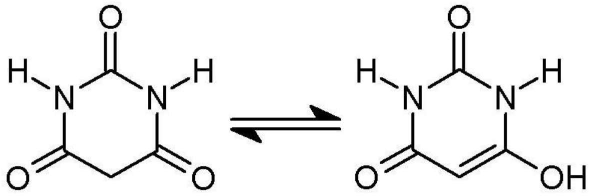

1 **2**

Figure 1: Barbituric acid in the keto (**1**) and enol (**2**) tautomers.

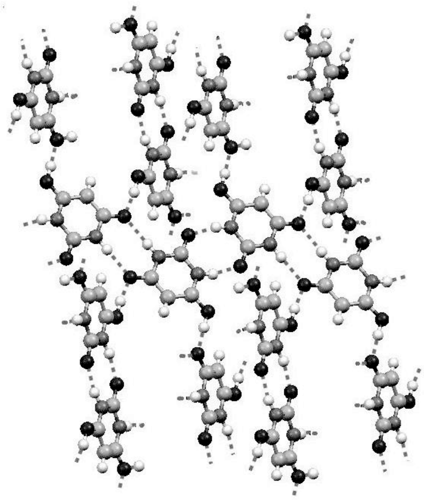

Figure 2: Hydrogen-bond framework with molecules in the enol tautomeric form.

P15-P03
Kristallstrukturbestimmung von 2-Methyl-3-buten-2-ol aus Röntgenpulverdaten

S.M. Hammer[1], E. Alig[1], J. van de Streek[2], M.U. Schmidt[1]
[1]Goethe-Universität, Institut fuer Anorganische und Analytische Chemie, Frankfurt am Main, Germany
[2]Avant-garde Materials Simulation Deutschland GmbH, Freiburg, Germany

2-Methyl-3-buten-2-ol ($C_5H_{10}O$, MBO) liegt bei Raumtemperatur als leichtflüchtige, brennbare Flüssigkeit vor (Schmelzpunkt −39 °C, Siedepunkt 97 °C[1]). MBO ist ein Abbauprodukt von verschiedenen Vertretern aus der Gruppe der Terpene; es wird überwiegend in Pflanzen gebildet, z. B. in Kiefern. Die Pflanzen geben MBO an die Atmosphäre ab, dort wird es weiter abgebaut und gilt als mögliche Quelle von sekundären organischen Aerosolpartikeln[2].

Die Kristallstrukturbestimmung von MBO erfolgte mittels Röntgenpulverdiffraktometrie. Die Messung wurde mit Cu-Kα_1-Strahlung in Transmission auf einem STOE-Stadi-P-Diffraktometer mit einem Ge(111)-Monochromator und einem linearen PSD (position-sensitive detector) durchgeführt. Das flüssige MBO wurde bei Raumtemperatur in eine Glaskapillare (0,7 mm Durchmesser) eingefüllt, die anschließend verschlossen wurde. Die Lösung kristallisierte direkt im Stickstoffstrom auf dem Diffraktometer aus (Kühlung von Oxford Cryosystems).

Das gemessene Röntgenpulverdiagramm konnte widerspruchsfrei mit dem Programm *DICVOL*91[3] indiziert werden. Die Indizierung ergab eine monokline Zelle mit a = 15,3 Å, b = 18,8 Å, c = 6,5 Å, β = 102.5° (Z = 12) in $P2_1/n$ mit drei unabhängigen Molekülen in der asymmetrischen Einheit.

Die Struktur wurde mit Realraummethoden mittels Simulated Annealing unter Verwendung des Programms *DASH*[4] gelöst. Es waren sowohl die Positionen und die Orientierungen der

Moleküle als auch die Torsionen freigegeben (21 Parameter). Anschließend erfolgte eine Rietveld-Verfeinerung mit dem Programm *TOPAS*[5]. Für alle Bindungslängen und -winkel wurden Restraints definiert. Eine Optimierung der endgültigen Kristallstruktur erfolgte mit dispersionskorrigierten DFT Rechnungen mit dem Programm *GRACE*[6].

Referenzen

[1] K. N. Campbell, L. T. Eby, *J. Am. Chem. Soc.* **1941**, *63*, 2683-2685.

[2] H. C. Chang, J. C. Jiang, S. H. Lin, N. H. Weng, M. C. Chao, *J. Chem. Phys.* **2001**, *115*, 3215-3218.

[3] A. Boultif, D. Louër, *J. Appl. Cryst.* **1991**, *24*, 987−993.

[4] W. I. F. David, K. Shankland, J. van de Streek, E. Pidcock, W. D. S. Motherwell, J. C. Cole, *J. Appl. Cryst.* **2006**, *39*, 910−915.

[5] A. A. Coelho, *TOPAS Academic 4.1*, **2007**, http://www.topas-academic.net.

[6] J. van de Streek, M. A. Neumann, *Acta Crystallogr. B* **2010**, *66*, 544-558.

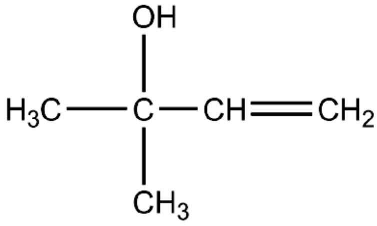

$H_3C-C(OH)(CH_3)-CH=CH_2$

2-Methyl-3-buten-2-ol

Figure 1

P15-P04
New Dinuclear Copper and Manganese Clusters with Penta- and Hexadentate Hydrazone Schiff Base Derivatives

A. Ellern[1], D. Dragancea[2], S. Baca[2,3], P. Koegerler[3]
[1]Iowa State University, Chemistry, Ames, IA, United States
[2]Academy of Science of Moldova, Institute of Chemistry, Chisinau, Moldova, Republic of
[3]RTWH Aachen University, Institut fuer Anorganische Chemie, Aachen, Germany

Molecular species containing more than one metal ion have received significant attention due to the possibility of cooperative behavior between the metal ions, which lead to interesting new magnetic phenomena. The synthetic challenge involves finding simple and efficient approaches to incorporate multiple metal ions in a small, single molecular entity. Owing to the presence of different kinds of potential donor sites, carbohydrazone derivatives of substituted salicylic aldehyde have been selected as building blocks in the self-assembly of polynuclear coordination compounds. Two new Cu(II) and Mn(II) complexes with Schiff bases, namely $[Cu_2(L^1)(DMF)(NO_3)(H_2O)_{1.75}]$ (DMF) (**1**) and $[Mn_2(H_2L^2)_2]$ (**2**) (where H_2L^1 and H_4L^2 are derived from the condensation of 3,5-di-*t*butylsalicylaldehyde and carbohydrazide) have been synthesized and characterized (Figure).

The X-ray structure determination of metal clusters with organic polydentate ligands is always dealing with necessity of treating the terminal groups with constraints and restraints which definitely improves final molecular geometry. This is more or less relevant for the above-mentioned small clusters. How far you can go with artificial crystal modeling? Similar cases with large and giant clusters will be presented.

Acknowledgements: This study was supported by Alexander von Humboldt Foundation, the German Federal Ministry of Education and Research (Grant MDA 08/022) and the Academy of Sciences of Moldova (Grant No. 09.820.05.10GF).

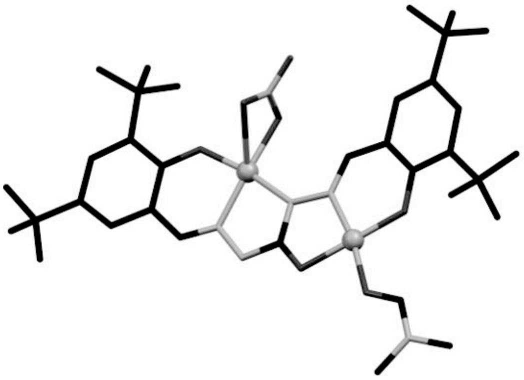

Figure 1

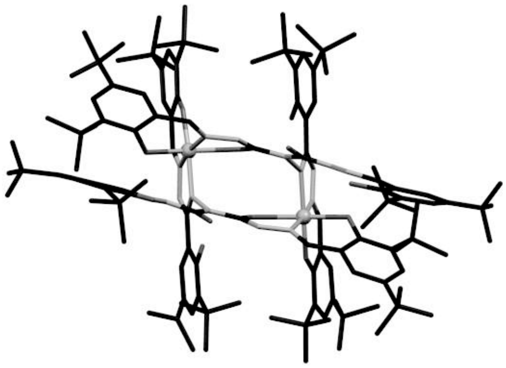

Figure 2

P15-P05
Hydrogen-Bonding Patterns in a PABA Proton Transfer Compound

A. DIREM[1], W. FALEK[1], N. Benali-Cherif[1]
[1]LASPI2A, Institut des sciences et techniques, Khenchela, Algeria

Hydrogen bonding is undoubtedly the most widespread of the specific interactions linking molecules with suitable functional groups together in the solid state. Knowledge of the patterns of hydrogen-bonds will be useful in the recognition and development of synthons to design desired materials possessing interesting structures and properties for crystal engineering [1,2].

The crystal structure of the compound, p-carboxyanilinium bisulphate [3], displays a variety of strong and weak intermolecular hydrogen bonds in which all potential donors and acceptors are involved. Bisulfate anions and p-carboxyanilinium cations are interconnected with bifurcated and three-centre O-H...O, N-H...O and C-H...O hydrogen bonds.

Bifurcated and threefurcated interactions in p-carboxyanilinium bisulphate.

[1] Desiraju, G. R. (2002). Acc. Chem. Res. 35, 565.

[2] Desiraju, G. R. (2003). Crystal Design: Structure and Function Perspectives in Supramolecular Chemistry vol. 7

[3] Benali-Cherif, N., Direm, A., Allouche, F., Boukli-H-Benmenni, L. & Soudani, S. (2007). Acta Cryst. E63, 2054-2056.

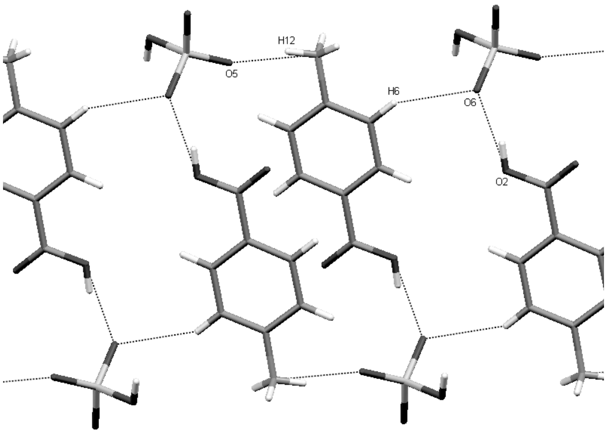

Figure 1

P15-P06

Crystal structure determination of 5’-deoxy-5-fluorouridine from laboratory X-ray powder diffraction data

S. Bekö[1], D. Urmann[1], M.U. Schmidt[1]
[1]Goethe-University, Institute for Inorganic and Analytical Chemistry, Frankfurt am Main, Germany

The title compound, $C_9H_{11}FN_2O_5$, is a prodrug of 5-fluorouracil actually market by F. Hoffmann-La Roche AG under the registered trade name Furtulon® and is used as cytostatic drug especially in course of chemotherapy to cure breast and colorectal cancer [1].
Its crystal structure was solved from laboratory X-ray powder diffraction data by means of real-space methods using the program *DASH 3.1* [2] and refined by the Rietveld method with *TOPAS 4.1* [3].
For indexing and structure solution the powder pattern was truncated to a real-space resolution of approximately 3.4 Å, background-subtracted with a Bayesian high-pass filter [4] and indexed with the program *DICVOL91*, resulting in a triclinic cell with space group *P*1, Z = 2, with two independent molecules per asymmetric unit [5]. Subsequently a Pawley refinement [6] was carried out to extract integrated intensities and their correlations. The crystal structure was solved in direct space with simulated annealing (SA). The molecule has one flexible torsion angle, which was left free during the SA. In 50 SA runs, the crystal structure was found 18 times. Subsequently the structure was refined. Suitable chemical restraints from *Mogul* [7] were added for bond lengths, angles, and for the planarity of the fluorouracil group, including all C, N, O, F and the H atoms. A common isotropic displacement parameter for the C and N atoms was refined. For the F and O atoms individual isotropic displacement parameter were assigned. The refinement yielded acceptable *R* values (R_{exp} = 1.375%, R'_{exp} = 4.054%, R_p = 1.872%, R'_p = 5.603%, R_{wp} = 2.549%, R'_{wp} = 7.514%). The hydrogen-atom positions were finally adjusted using the DREIDING/X6 force field [8] within the program package Cerius^2 [9].
The compound crystallises in the triclinic space group *P*1, Z = 2 with a = 4.805083(86) Å, b = 9.25018(16) Å, c = 11.67807(22) Å, α = 79.41500(70) °, β = 78.32967(70) °, γ = 88.78080(72) ° and V = 499.618(16) Å^3. Both independent molecules differ in their hydrogen-bond patterns, the conformations of the furanosyl rings and the torsion angles between the two ring systems [10].

[1] Cook, A. F., US Patent No. 4 071 680, 1978. Cook, A. F., Holman, M. J., Kramer, M. J. & Trown, P. W., *J. Med. Chem.*, 1979, **22**, 1330-1335. [2] David, W. I. F., Shankland, K., van de Streek, J., Pidcock, E., Motherwell, W. D. S., Cole, J. C, *J. Appl. Cryst.*, 2006, **39**, 910-915. [3] Coelho, A. A., TOPAS Academic version 4.1 (Computer Software), Brisbane 2007. [4] David, W. I. F. & Sivia, D. S. (2001). *J. Appl. Cryst.* **34**, 318-324. [5] Boultif, A. & Louër, D. (1991). *J. Appl. Cryst.* **24**, 987-993. [6] Pawley, G. S. (1981). *J. Appl. Cryst.* **14**, 357-361. [7] Bruno, I. J., Cole, J. C., Kessler, M., Luo, J., Motherwell, W. D. S., Purkis, L. H., Smith, B. R., Taylor, R., Cooper, R. I., Harris, S. E. & Orpen, A. G. (2004). *J. Chem. Inf. Comput. Sci.* **44**, 2133-2144. [8] Mayo, S. L., Olafson, B. D. & Goddard III, W. A. (1990). *J. Phys. Chem.* **94**, 8897-8909. [9] Accelrys (2003). *Cerius*2, Version 4.9. Accelrys Ltd., Cambridge, England. [10] Bekö, S. L., Urmann, D. and Schmidt, M. U., *in preparation*.

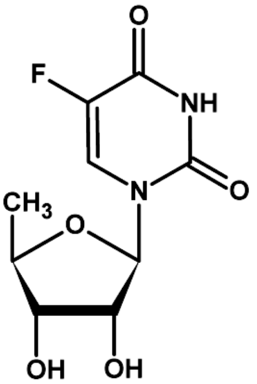

Figure 1

P15-P07

Cytosinium-hydrogen maleate-cytosine

W. FALEK[1], A. DIREM[1], N. Benali-Cherif[1]
[1]LASPI2A, Institut des sciences et techniques, Khenchela, Algeria

The Cytosine may be found in very small quantities as a post-modified form, 5-methylcytosine, in certain nucleic acids such as in tuberculinic acid. More recently, 5-fluoro-cytosine (5-FC) has been used as a prodrug in suicide gene therapy of cancer with the crystal structure of bacterial cytosine deaminase (bCD).
The crystal structures of cytosine [1] and cytosine monohydrate were determined many years ago. Many inorganic cytosinium salts have been previously synthesized: chloride [2], nitrate [3] and dihydrogenphosphate [4,5].
Cytosinium salts of organic acids are also common, the structures of a number of these including trichloroacetate, Cytosinium 3,5-dinitrosalicylate [6] and hydrogen maleate [7] have been recently reported.

[1] Barker, D. L. & Marsh, R. E. (1964). *Acta Cryst.* 17, 1581-1587.
[2] Mandel, N. S. (1977). *Acta Cryst.* B33, 1079-1082.
[3] Cherouana, A., Bouchouit, K., Bendjeddou, L. & Benali-Cherif, N. (2003). *Acta Cryst.* E59, o983-o985.
[4] Jasko ´ lski, M. (1989). *Acta Cryst.* C45, 85-89.
[5] Bagieu-Beucher, M. (1990). *Acta Cryst.* C46, 238-240.
[6] Smith, G., Wermuth, U. D. & Healy, P. C. (2005). *Acta Cryst.* E61, o746-o748.
[7] Balasubramanian, T., Muthiah, P. T. & Robinson, W. T. (1996). *Bull. Chem.Soc. Jpn*, 69, 2919-2922

P15-P08

Charge density analylsis of bis(phenolato) metal complexes

T.S. Dols[1], C.W. Lehmann[2], J. Okuda[1], T.P. Spaniol[1]
[1]RWTH Aachen University, Department of Inorganic Chemistry, Aachen, Germany
[2]Max-Planck Institut f. Kohlenforschung, Chemische Kristallographie, Mülheim an der Ruhr, Germany

Transition metal complexes with bridged bis(phenolato) ligands are used in olefin polymerization. To improve the product properties, structural changes of homogeneous catalysts and their precatalysts are correlated with their impact on polymerization. The molecular structure of the ligand has a strong influence on the stereochemistry of the resulting polymer [1]. The bis(phenolate) ligands have been tuned by different substituents on the aromatic rings as well as by modifying the bridging unit. Sulfur atoms as part of the bridge can improve the catalytic activity, obviously as a result of hemilabile interactions between the soft donor atom and the hard metal center [2]. In several S-C-C-S bridged bis(phenolato)titanium complexes, the M…S interactions lead to a stereorigid O,S,S,O-tetradentate coordination in solution [3]. Such a system has made it possible to polymerize styrene in homogeneous phase to isotactic polystyrene [1]. The results prove the high conformational stability of the metal complexes under the conditions of polymerization.

Focus of our investigations is on metal complexes where, according to the HSAB principle [4], the hard metal centers are interacting with the soft donor atom of the bisphenolato ligand. It is known that this additional interaction can enhance the polymerization activity [3]. The link between the metal center and the neutral donor atom influences the coordination geometry. According to the HSAB principle the interaction between the soft donor atom in the ligand and the Lewis acidic/electrophilic metal center is unbalanced. Besides the structural analysis of the sulfur-bridged bis(phenolato) metal complexes [5] we are interested in the electronic effect of different types of donor atoms in the ligand backbone, e.g. nitrogen or oxygen. Comparing the topology of the charge density based on multipole refinements [6,7] of high resolution X-ray diffraction data will help to clarify the significance of the mismatched interactions in the investigated bis(phenolato) titanium complexes.

[1] Beckerle, K., Manivannan, R., Lian, B., Meppelder, G.-J.M., Raabe, G., Spaniol, T.P., Ebeling, H., Pelascini, F., Mülhaupt, R., Okuda, J. Angew. Chem. 2007, 119, 4874-4877. [2] Froese, R.D.J., Musaev, D.G., Morokuma, K.,Organometallics, 1999, 18, 373. [3] Capacchione, C., Manivannan, R., Barone, M., Beckerle, K., Centore, R. Oliva, L., Proto, A., Tuzi, A. Spaniol, T.P., Okuda, J. Organometallics, 2005, 24, 2971. [4]. R.G. Pearson, J. Am. Chem. Soc. 1963, 85, 3533-3539. [5] Dols, T.S., Spaniol, T.P., Okuda, J. Acta Cryst. C, 2009, m443-m446. [6] Volkov A., Macchi, P., Farrugia L. J., Gatti C., Mallison P.R., Richter T., Koritsanszky T. XD2006. University of New York, Buffalo, USA 2006. [7] Hansen N.K., Coppens P. Acta Cryst. A, 1978, 34, 909.

This work was supported by DFG, priority program 1178: Experimental Charge Density as the Key to Understand Chemical Interactions.

P15-P09

Modes of Coordination in Zinc-Allyl Compounds. A Combined Experimental X-Ray and Quantum-Chemical *ab initio* Study

C. Lichtenberg[1], J. Engel[2], T.P. Spaniol[1], J. Okuda[1], G. Raabe[2]
[1]RWTH Aachen University, Anorganische Chemie, Aachen, Germany
[2]RWTH Aachen University, Organische Chemie, Aachen, Germany

The coordination mode of bis(allyl)zinc has been studied experimentally in the solid state and the results are compared to structures obtained from quantum-chemical *ab initio* calculations on various levels of theory starting from six different initial geometries. In the solid state the allyl ligands were found to bind to the tetrahedrally coordinated metal atom via pure σ bonds without significant π contributions in a bridging μ^2-η^1:η^1 coordination mode (Figure 1). Our quantum-chemical calculations revealed that also for isolated molecules in the gas phase σ bonding is energetically favoured over η^2 and η^3 π bonding.

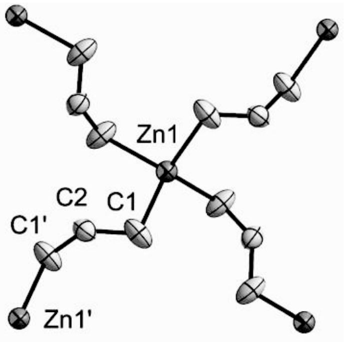

Figure 1: Coordination of the metal atom in the crystal structure of bis(allyl)zinc.

P15-P10

Vibrational (FT-IR and Raman) Spectroscopy, Thermal analysis and Scanning Electron Microscopy of New Polymeric Complex: [Cd(*N*-Meim)$_2$Ni(*m*-CN)$_4$]$_n$

G.S. Kurkcuoglu[1], T. Unaldi[1,2]
[1]Eskisehir Osmangazi University, Physics, Eskisehir, Turkey
[2],, Turkey

The cyano-bridged heterometallic complex, *trans*-[Cd(*N*-Meim)$_2$Ni(m-CN)$_4$]$_n$ (*N*-Meim=N-methylimidazole), has been synthesized and characterized by vibrational (FT-IR and Raman) spectroscopy, single crystal X-ray diffraction, thermal analyses, elemental analyses and scanning electron microscopy (SEM) techniques. The crystallographic analyses reveal that the complex has polymeric 2D networks. The molecular structure of complex is shown in Fig. 1. The complex crystallizes in monoclinic crystal system and C*2m* space group. In this complex, four cyanide groups of [Ni(CN)$_4$]$^{2-}$ coordinated to the adjacent Cd(II) ions and distorted octahedral geometry of the complex is completed by two nitrogen atoms of *trans* *N*-Meim ligands. The morphological properties of the complex were studied by SEM. SEM images of freshly prepared sample of the complex studied are shown in Figure 2. Scanning electron microscopy studies indicate the complex is monoclinic with space group and supports the layered structure.

Acknowledgement This work was supported by the Research Fund of Eskisehir Osmangazi University. Project number: 201019024.

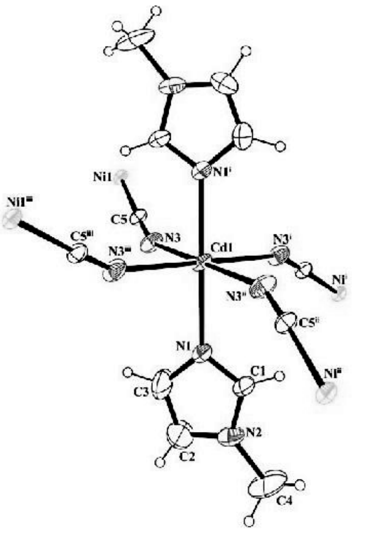

Fig. 1 An ORTEP-3 drawing of the complex

Figure 1

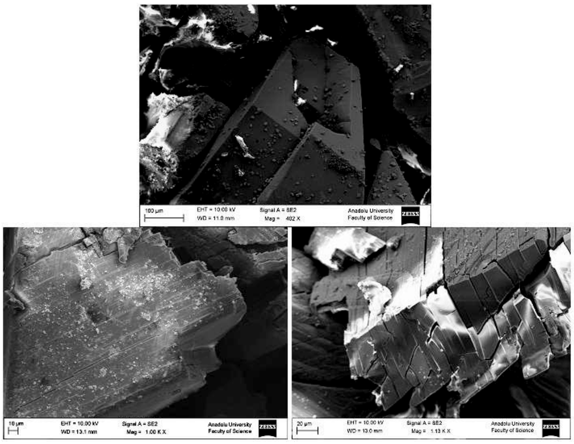

Fig. 2 SEM images of the complex.

Figure 2

P15-P11

Empirical bond valence of metal arene π-bonding in cationic bismuth(III) arene complexes

B. Bredenhagen[1], W. Frank[1]
[1]Heinrich Heine Universität, Institut für Anorganische und Strukturchemie II, Düsseldorf, Germany

The bond valence method [1] was very rarely used for evaluation and rationalization of bonding in metalorganic compounds (*e. g.* for estimating the bond strength of metal arene π-bonds in arene complexes [2]).

Extending former investigations [3] of compounds containing π-arene-complexed $BiCl_2^+$ units we recently synthesized the new π-complexes $[(1,2,4,5\text{-}(CH_3)_4C_6H_2)BiCl_2][AlCl_4]$ (**1**) and $[((CH_3)_5C_6H)BiCl_2][AlCl_4]$ (**2**) and further characterized the known [4] compound $[(C_6H_6)BiCl_2][AlCl_4]$(**3**). X-ray studies of these compounds allow a detailed view into the bonding situation of cationic bismuth arene π-complexes.

To quantify the strength of the metal arene π-bonding we make use of the bond valence method [1]. In our approach the valence of the metal arene interaction is indirectly calculated as the difference of the total metal valence and the valence sum of bismuth chlorine interactions.

Figure 1 shows the results as well as the bismuth ring-centroid distance for **1** to **3** and selected further examples documenting the wide range of bond strengths related to bismuth carbon π-bonding.

References:

[1] I. D. Brown, *Chem. Rev.* **2009**, *109*, 6858.
[2] W. Frank, *Z. Anorg. Allg. Chem.* **1990**, *585*, 121.
[3] W. Frank, J. Weber, E. Fuchs, *Angew. Chem. Int. Ed.* **1987**, *26*, 74.
[4] T. Auel, E. L. Amma, *J. Am. Chem. Soc.* **1968**, *90*, 5941.
[5] W. Frank, J. Schneider, S. Müller-Becker, *J. Chem. Soc., Chem. Commun.* **1993**, 799.
[6] W. Frank, *J. Organomet. Chem.* **1990**, *386*, 177.
[7] J. Sanderson, C. A. Bayse, *Tetrahedron* **2008**, *64*, 7685.

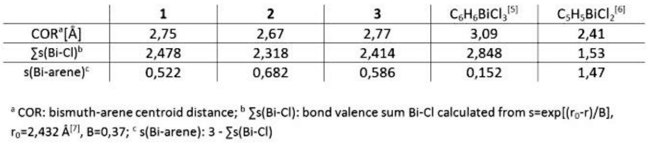

	1	**2**	**3**	$C_6H_6BiCl_3$[5]	$C_5H_5BiCl_2$[6]
COR[a][Å]	2,75	2,67	2,77	3,09	2,41
∑s(Bi-Cl)[b]	2,478	2,318	2,414	2,848	1,53
s(Bi-arene)[c]	0,522	0,682	0,586	0,152	1,47

[a] COR: bismuth-arene centroid distance; [b] ∑s(Bi-Cl): bond valence sum Bi-Cl calculated from $s=\exp[(r_0-r)/B]$, $r_0=2{,}432$ Å[7], B=0,37; [c] s(Bi-arene): 3 - ∑s(Bi-Cl)

Figure 1

P15-P12

Empirical bond valence of metal arene π - bonding in cationic mercury(I) arene complexes

M. Seidemann[1], W. Frank[1]
[1]Heinrich Heine Universität Düsseldorf, Institut f. Anorganische und Strukturchemie II, Düsseldorf, Germany

The bond valence method [1] was very rarely used for evaluation and rationalization of bonding in metalorganic compounds (*e. g.* for estimating the bond strength of metal arene π-bonds in arene complexes [2]).

Extending former investigations [3] we synthesized new mercury(I)-arene complexes ($[(CH_3C_6H_5)_2Hg_2][AlCl_4]_2$ (**1**) and $[(arene)_2Hg_2][Al_4O_2Cl_{10}]$ (arene = 1,2,4 - $(CH_3)_3C_6H_3$ (**2**), $(CH_3)_5C_6H$ (**3**))) and reinvestigated the structure of $[((CH_3)_6C_6)_2Hg_2][AlCl_4]_2 \cdot CH_3C_6H_5$ (**4**) [3]. X-ray studies of these compounds allow a detailed view on the bonding situation of mercury(I) arene complexes. The main focus lies on the strength of the cation π - interaction between the central Hg_2^{2+} unit and the respective arene.

As it has been postulated before [4] there are in principal two different modes of coordination of the arene to the Hg_2^{2+} cation. The Hg_2^{2+} dumbbell can be enclosed by the two arene molecules in a sandwich-like arrangement (model 1) or the aromatic ligands coordinate in the direction of the Hg-Hg bond vector (preferred bonding direction; model 2). The coordinating chlorine atoms of the anions occupy the other position, respectively. Which model is preferred, seems to depend on the basicity of the arene. Compound **1** shows a coordination according to model 1, while compounds **2** to **4** prefer model 2.

To get a quantitative estimation of the strength of the π - bonds we make use of the bond valence method [1]. To transfer this concept that usually deals with inorganic solids to metalorganic complexes in an easy way, the valence sum of the metal arene π - interaction is calculated indirectly as the difference of the total metal valence and the valence sum of metal chlorine interaction. Figure 1 shows the results for **1** - **4**, documenting the strength of the metal arene π -interaction.

References:

[1] I. D. Brown, *Chem. Rev.* **2009**, *109*, 6858.
[2] W. Frank, G. Korrell, G. J. Reiss, *J. Organomet. Chem.* **1996**, *506*, 293.
[3] W. Frank, B. Dincher, *Z. Naturforsch., Teil B* **1987**, *42*, 828.

[4] R. W. Turner, E. L. Amma, *J. Inorg. Nucl. Chem.* **1966**, *28*, 2411.

[5] N. E. Brese, M. O´Keeffe, *Acta Crystallogr., Sect. B* **1991**, *B47*, 192.

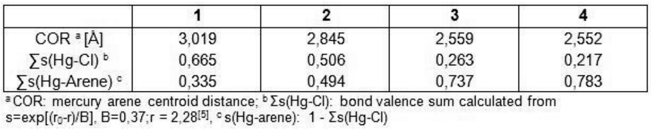

	1	2	3	4
COR [a] [Å]	3,019	2,845	2,559	2,552
∑s(Hg-Cl) [b]	0,665	0,506	0,263	0,217
∑s(Hg-Arene) [c]	0,335	0,494	0,737	0,783

[a] COR: mercury arene centroid distance; [b] Σs(Hg-Cl): bond valence sum calculated from $s=\exp[(r_0-r)/B]$, B=0,37;r = 2,28[5], [c] s(Hg-arene): 1 - Σs(Hg-Cl)

Figure 1

P15-P13

Structural study of amino acid salts consisting nitrate anions

B.-C. Rim[1,2], B.-C. Nourredine[1,3]
[1]Centre Universitaire Abbes LAGHROUR-Khenchela, Institut des Sciences et technology, Khenchela, Algeria
[2]UNIVERSITY, Khenchela-Algeria, Algeria
[3]University, Khenchela-Algeria, Algeria

Amino acids salts are interesting for NLO applications. Their importance is due to the fact that all the amino acids have chiral symmetry and several compounds crystallize in noncentro-symmetric space groups [1]. Thus, salts of amino acids with different organic/inorganic acids have been explored.

Several new complexes incorporating natural amino acids and nitrate anions have been recently crystallized [2] and their structural, optical [3], thermal properties and structural phase transitions [4] have been investigated.

In this present work, which is part of project of searching for potential new hybrid compounds obtained by the addition of amino acids with nitric acid, we will discuss crystalline structures of new salts based on nitrate anions, amino acids published by our research team during the last ten years.

All materials of this type are characterized by the presence of strong N-H...O and O-H...O hydrogen bonds connecting anionic and cationic entities together which participate in the stability and the cohesion of crystal structures.

In these compounds Intramolecular bond lengths in nitrate anions depend closely to 3D intermolecular interactions.

[1] Bhat M.N., Dharmaprakash S.M., *J. Cryst. Growth*, 2002, 236, 376-380. [2] N. Benali-Cherif, H. Boussekine, Z. Boutobba & N. Dadda Acta Cryst. (2009). E65, o2744.[3] Bouchouit K., Sofiani Z., Derkowska B., Abed S., Benali-cherif N., Bakasse M., Sahraoui B., *Opt. Commun.*, 2007, 278, 180-186. Perpétue G. J., Janczak J., *Acta Cryst*, 2004, C60, 768. [4] Baran J., Drozd M., Głowiak T., S'ledz' M., Ratajczak H., *J. Mol. Struct*. 372, 131. Mylrajan, M. Srinivasan T.K.K., *J. Raman Spectrosc*., 1985, 16, 412. [5] Benali-Cherif N., Boussekine H., Boutobba Z., Kateb A., *Acta Cryst*, 2007, E63, o3287.

Keywords: amino acids, hydrogen bonds, hybrid compounds, x-ray diffraction

P15-P14

Fluconazole and its cocrystals with carboxylic acids

N. Lah[1], J. Kastelic[2], I. Leban[1], D. Kikelj[3]
[1]University of Ljubljana, Faculty of Chemistry and Chem. Technology, 1001 Ljubljana, Slovenia
[2]Krka d.d., 8501 Novo mesto, Slovenia
[3]University of Ljubljana, Faculty of Pharmacy, 1001 Ljubljana, Slovenia

Fluconazole is a wide spectrum triazole antifungal agent used in the treatment of localized candidiasis and systemic therapy of candidial infections, dermatophytic fungal infections and cryptococcal meningitis. It is used as accompanying therapy for immunodeficient patients, i.e. patients with AIDS or cancer, and patients taking immunodepressive agents.

To influence the physico-chemical properties (for example solubility) of the active ingredient we have prepared several cocrystals of fluconazole with dicarboxylic acids[1] and have recently expanded our work to the preparation of cocrystals with monocarboxylic and aromatic carboxylic acids. Along these lines, the crystal structure of 1:1 cocrystal of fluconazole and salicylic acid will be presented and compared with the structures of related fluconazole cocrystals.

[1] J. Kastelic, Z. Hodnik, P. Sket, J. Plavec, N. Lah, I. Leban, M. Pajk, O. Planinsek and D. Kikelj, *Cryst. Growth Des.*, **2010**, *10*, 4943-4953.

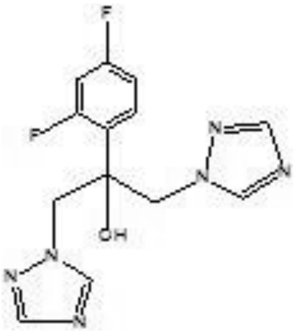

Figure 1

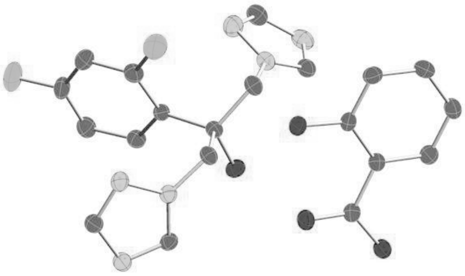

Figure 2

P16-P01

Structural and biochemical investigation of the APP-DR6-interaction

S. Kemmerzehl[1], M. Kuester[1], S.O. Dahms[1], D. Roeser[1], M.E. Than[1]
[1]Leibniz Institute for Age Research - Fritz-Lipmann-Institute, Than Laboratory - Protein crystallography, Jena, Germany

Death receptors such as the death receptor 6 (DR6) belong to the tumor necrosis factor receptor superfamily (TNFR) and are characterized owing to their intracellular existing death domain. TNFRs are associated with a broad assortment of cellular responses ranging from apoptotic to proinflammatory signaling. Intracellular signaling occurs due to recruitment of interaction partners via specialized intracellular domains such as the death domain after ligand induced accumulation of receptor molecules. This finally results in a caspase cascade and hence proapoptotic signaling. In general TNFRs recognize their ligands by their extracellularly exposed cystein-rich domains (CRDs). In most cases a trimerized ligand interacts with three distinct receptor molecules that bind to its interprotomer grooves[1]. Actually only for the p75NTR an overal similar but dimeric binding mode is shown[2]. DR6 itself has long been an orphan receptor until recently Nikolaev *et al.* 2009 could identify APP as its possible ligand. Hence DR6 was associated with Alzheimer's disease[4].

Here we present the crystal structure of the extracellular ligand binding domain of the DR6 consisting of its four CRDs refined to a resolution of 2.2 Å. Based on this data and the above mentioned general ligand binding modes of TNFRs we analyzed the structural features of the proposed APP-DR6-complex[5]. This analysis is supported by in vitro binding studies using distinct APP and DR6 constructs. Interestingly, there is currently no indication for a trimerized APP while on the other side self as well as heparin induced dimerization of APP were shown[6]. Due to the fact that we could figure out the heparin induced DR6 dimerization we additionally tested the influence of heparin on the APP-DR6-interaction.

[1] Ashkenazi A., Nat Rev Cancer.(2002), Jun;**2(6):**420-30.
[2] Gong, Y. *et al.*, Nature (2008), 454, 789-793.
[4] Nikolaev A. *et al.*, Nature (2009), 4**57**, 981
[5] Kuester M. *et al.*, *J. Mol. Biol.* (2011) **409**, 181-201
[6] Dahms SO. *et al.*, PNAS (2010) **107**(12) 5381-5386

P16-P02
Crystal structure of metarhodopsin II

M. Szczepek[1], H.-W. Choe[1], Y.J. Kim[1], J.H. Park[1], E. Pai[2], N. Krauss[3], O. Ernst[2], K.P. Hofmann[1], P. Scheerer[1]
[1]Charité - University Medicine Berlin, Institute of Medical Physics and Biophysics, Berlin, Germany
[2]University of Toronto, Department of Biochemistry, Toronto, Canada
[3]Queen Mary University of London, School of Biological and Chemical Sciences, London, United Kingdom

G-protein-coupled receptors (GPCRs) are seven transmembrane helix (TM) proteins that transduce signals into living cells by binding extracellular ligands and coupling to intracellular heterotrimeric Gproteins (Gαβγ) [1]. The photoreceptor rhodopsin couples to transducin and bears its ligand 11-cis-retinal covalently bound via a protonated Schiff base to the opsin apoprotein [2]. Absorption of a photon causes retinal cis/trans isomerization and generates the agonist all-trans-retinal in situ. After early photoproducts, the active G-protein-binding intermediate metarhodopsin II (Meta II) is formed, in which the retinal Schiff base is still intact but deprotonated. Dissociation of the proton from the Schiff base breaks a major constraint in the protein and enables further activating steps, including an outward tilt of TM6 and formation of a large cytoplasmic crevice for uptake of the interacting C terminus of the Gα subunit [2]. Owing to Schiff base hydrolysis, Meta II is short-lived and notoriously difficult to crystallize. We therefore soaked opsin crystals with all-trans-retinal to form Meta II, presuming that the crystal's high concentration of opsin in an active conformation (Ops*) [3,4] may facilitate all-trans-retinal uptake and Schiff base formation. Here we present the 3.0Å and 2.85Å crystal structures [5], respectively, of Meta II alone or in complex with an 11-amino-acid C-terminal fragment derived from Gα (GαCT2). GαCT2 binds in a large crevice at the cytoplasmic side, akin to the binding of a similar Gα-derived peptide to Ops* [4]. In the Meta II structures, the electron density from the retinal ligand seamlessly continues into the Lys 296 side chain, reflecting proper formation of the Schiff base linkage. The retinal is in a relaxed conformation and almost undistorted compared with pure crystalline all-trans-retinal. By comparison with early photoproducts we propose how retinal translocation and rotation induce the gross conformational changes characteristic for Meta II. Furthermore, we compare new crystallographic and spectroscopic results of the native light-induced rhodopsin crystals with our soaked opsin crystals [5] and discuss the recently published constitutively active rhodopsin mutant structure [6].

Figure 1 | Structures of inactive rhodopsin, active Meta II and Meta II in complex with a Gα fragment.

[1] Rosenbaum DM, Rasmussen SG & Kobilka BK, Nature 459, 356-363 (2009).
[2] Hofmann KP, Scheerer P, Hildebrand PW, Choe HW, Park JH, Heck M, Ernst OP, TIBS 34, 540-552 (2009).
[3] Park JH, Scheerer P, Hofmann KP, Choe HW, Ernst OP, Nature 454, 183-187 (2008).
[4] Scheerer P, Park JH, Hildebrand PW, Kim YJ, Krauss N, Choe HW, Hofmann KP, Ernst OP, Nature 455, 497-502 (2008).
[5] Choe HW, Kim YJ, Park JH, Morizumi T, Pai EF, Krauss N, Hofmann KP, Scheerer P, Ernst OP, Nature 471, 651-55 (2011).
[6] Standfuss J, Edwards PC, D Antona A, Fransen M, Xie G, Oprian DD, Schertler GF, Nature 471, 656-60 (2011).

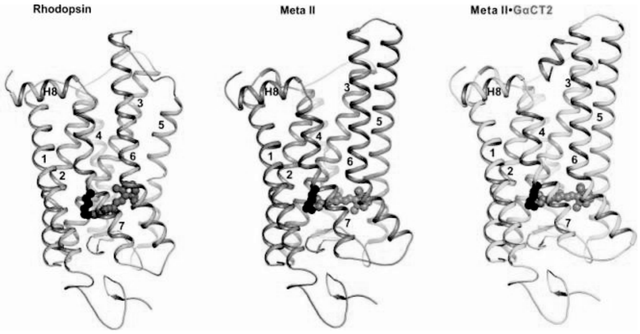

Figure 1

P17-P01
Controls on the industrial regrind milling process of coarse-grained ores by SEM-based image analysis

D. Sandmann[1], B. Schulz[1], J. Gutzmer[1], A. Eickhoff[2]
[1]Institut für Mineralogie, Lagerstättenlehre und Petrologie, Freiberg/Sachsen, Germany
[2]LANXESS Deutschland GmbH, Operations Consulting, Leverkusen, Germany

Combined SEM-based BSE image aquisition and EDX elemental analysis is a modern tool in the investigation of ores and processed ores. This tool is especially valuable when trying to monitor the efficiency of mineral processing through the numerous steps of a processing plant. However, despite the obvious advantages of quantifying mineralogical composition and relevant fabric attributes there are numerous pitfalls that need to be considered when applying this analytical tool.

In the particular case study the performance of a regrind mill in processing chromite ores was monitored using a Mineral Liberation Analyzer (MLA) Quanta 600 FEG by FEI Company. Samples were taken in time intervals from feed and product lines of the regrind mill. Prepared as particle mounts they were found to be a source of uncertainty as chromite (4.8 g/cm^3), gangue minerals (2.7-3.5 g/cm^3) and epoxy raisin (1.15 g/cm^3) have very different densities. Large grain size of chromite (<1 mm) favoured gravity separation during the hardening of the epoxy mount. Effects on particle distribution density, grain size distribution and mineral abundance are documented by comparison of results obtained for horizontal and vertical sections through the grain mounts.

For example, the abundance of chromite in the feed material varies from 90 - 70 wt% in the horizontal sections of the samples. The abundance of chromite was found to be systematically lower

(80 - 60 wt%) in the samples from the product of the regrind mill. When vertical mount sections are considered, the same effects are observed but at somewhat lower absolute abundance, 80 - 60 wt% and 70 - 50 wt% , respectively, in the feed and product lines. The shapes of the curves for cumulative passing of chromite grains are systematically shifted of about 150 µm toward lower grain sizes at P50. In the grain size distribution curves of feeder chromite and gangue minerals, normal distributions with a maximum at 250 µm diameter are observed. In the grain size distribution curves for the product a reduction of the most abundant particle size fraction is accompanied by the shift towards lower grain sizes.

It was difficult to assess, if the regrind mill led to a significant increase of the degree of liberation of chromite as the feed chromite was found to be already highly liberated (>80 % fully liberated). This degree of liberation was not found to increase markedly in the product. Similar is true for parameters such as chromite mineral recovery, chromite mineral liberation by particle composition and chromite mineral liberation by free grain surface. Comparison of samples with different chromite modes but along the time line appears as inappropriate for the evaluation if liberation parameters are changed by the milling process. It is therefore recommended to (1) compare feed and product samples with similar modes of the target mineral and (2) to compare the liberation parameters coupled not to mode but to grain sizes.

P17-P02

Petrographische und geochemische Untersuchungen an Sphaleriten aus den Pb-Zn-Lagerstätten des Drauzugs (Österreich/Slowenien) als Grundlage für die Entwicklung eines Vererzungsmodells

E. Henjes-Kunst[1], J. Raith[1], F. Melcher[2]
[1]Montanuniversitaet Leoben, Resource Mineralogy, Leoben, Austria
[2]Bundesanstalt für Geowissenschaften und Rohstoffe, Hannover, Germany

Im Drauzug (Österreich/Slowenien) sind etwa 200 Pb-Zn-Vererzungen an bestimmte Horizonte triassischer Karbonate gebunden (Cerny, 1989). Obwohl einige dieser Lagerstätten (z.B. Bleiberg, Mezica) insbesonders während der 70er und 80er Jahre des vergangenen Jahrhunderts bereits intensiv untersucht wurden, konnte die Entstehung dieser Vererzungen im Drauzug bisher nicht zweifelsfrei geklärt werden. Einige der offenen Fragen betreffen etwa die Herkunft der Metalle, die PTX-Bedingungen der erzbildenden Fluide aber auch das Alter der Vererzung. Zwei kontrastierende genetischen Modelle die i.w.S. dem SEDEX-Modell und dem MVT-Modell entsprechen wurden für die Entstehung der Lagerstätten diskutiert (vgl. Schroll, 2008 cum.lit.): (1) Syngenese: Vererzung zeitgleich mit der Sedimentation des Nebengesteins vor etwa 220 Ma (Schulz, 1968). (2)Epigenese: Vererzung erst nach Abschluss der Sedimentation der Nebengesteine während ihrer Diagenese vor etwa 200 Ma (Leach *et al.*, 2003). Die Frage nach der Genese wurde kürzlich auf Grund des Nachweises fossiler sulfatreduzierender Bakterienfilamente und ZnS Nanostrukturen in Sphaleriten aus der Lagerstätte Bleiberg (Kucha *et al.*, 2010) wieder aktuell.

In Rahmen einer laufenden Doktorarbeit soll über einen multidisziplinären methodischen Ansatz ein erneuter Versuch gemacht werden die Genese dieser Lagerstätten zu klären. Dazu sollen in-situ Isotopenmessungen (S, Pb) und Altesdatierungen (Rb-Sr) an petrographisch und chemisch genau charakterisierten Sphaleriten gemacht werden. In diesem Beitrag werden die Ergebnisse der petrographischen und geochemischen Untersuchungen an Sphaleriten aus unterschiedlichen Lagerstätten präsentiert.

Die Proben wurden hinsichtlich ihrer Textur und ihrer Spurenelementzusammensetzung verglichen und charakterisiert. Dafür wurden Sphalerite aus verschiedenen Lagerstätten, und aus verschiedenen stratigraphischen Erzhorizonten bezüglich ihrer Petrographie (Textur, Paragenese), ihres Kathodolumineszenzverhaltens (KL) und mittels der Elektronenstrahlmikrosonde (EMS) auf ihre Spurenelementsignatur (Fe, Cd, Ge, Pb, As, Au, Ni, Tl) untersucht. Diese Untersuchungen dienen dazu herauszufinden, ob bei den Sphaleriten aus unterschiedlichen Lagerstätten und/oder stratigraphischen Horizonten eine für den gesamten Drauzug konsistente Untergliederung von Sphalerittypen/-generationen möglich ist. Die bisherigen Untersuchungen haben gezeigt, dass es in einzelnen Lagerstätten Sphalerite unterschiedlicher Textur und Zusammensetzung gibt. Bestimmte Texturen und Spurenelementgehalte sind aber nicht immer auf eine Lagerstätte und/oder Horizont beschränkt, sondern sind in verschiedenen Lagerstätten/Horizonten zu finden. In Bleiberg und Mezica kommen z.B. Cd-reiche Sphalerite mit auffällig blauer Lumineszenz in mehreren Erzhorizonten vor. Andererseits gibt es auch Sphalerite, die bisher entweder nur in einem Horizont oder in nur einer Lagerstätte nachgewiesen werden konnten, wie z.B. die Sphalerite in der Lagerstätte Topla.

References

Cerny, I. (1989). Die karbonatgebundenen Blei-Zink-Lagersta etten des alpinen und ausser-alpinen Mesozoikums; Die Bed eut-ung ihrer Geologie, Stratigraphie und Faziesgebundenheit für Prospektion und Bewertung. Carbonate-bound lead-zinc deposits of the Alpine and extra-Alpine Mesozoic; implications for prospecting and evaluation of their stratigrap hy and facies relationships. Archiv für Lagerstätten-forschung der Geologischen Bundesanstalt 11, 5-125.
Kucha, H., Schroll, E., Raith, J. G. & Halas, S. (2010). Mi crobial sphalerite formation in carbonate-hosted Zn-Pb ores, Bleiberg, Austria; micro- to nanotextural and sulfur isotope evidence. Economic Geology and the Bulletin of the Society of Economic Geologists 105, 1005-1023.
Leach, D. L., Bechstadt, T., Boni, M. & Zeeh, S. (2003). T riassichosted MVT ZnPb ores of Poland, Austria, Slovenia and Italy. Dublin: IAEG.
Schroll, E. (2008). Die Blei-Zink Lagerstätte Bleiberg die Geschichte ihrer Erforschung. Klagenfurt: Naturwiss. Verein für Kärnten.
Schulz, O. (1968). Die synsedimentaere Mineralparagenese i moberen Wettersteinkalk der Pb-Zn-Lagerstaette Bleiberg-Kre uth (Kaernten). The syngenetic mineral paragenesis in the u pper Wetterstein limestone of the Bleiberg-Kreuth lead-zinc deposit,Carinthia.
TMPM. Tschermaks Mineralogische und Petrographische Mit teilungen 12, 230-289.

P17-P03

A novel pilot program for homogeneity testing of natural analogs of synthetic mineral reference materials

P. Michalak[1], A. Renno[1], M. Wiedenbeck[2], S. Merchel[3], F. Munnik[3]
[1]Institut für Mineralogie TU Bergakademie Freiberg, Freiberg, Germany
[2]Helmholtz-Zentrum Potsdam Deutsches GeoForschungsZentrum, Potsdam, Germany
[3]Helmholtz-Zentrum Dresden-Rossendorf, Dresden, Germany

The growing demand for elements (PGE, REE and refractory metals) desired by the high-tech industry stresses the need for searching for them in non-conventional raw materials. Natural variability of distribution of such elements within the matrices of mineral carriers, frequently, at the micro- and submicrometer level requires employing hi-resolution spatial microanalytical techniques as an essential step in quantitative measurements as well as quality assurance procedures. The necessity for providing reliable, traceable and comparable results for such measurements at the picogram sampling scale makes the use of certified reference materials to be of critical importance. The database of certified reference materials in the form of solutions, powders, pellets, glass beads etc. has been developed by several research groups as well as governmental agencies with certifying capabilities. Unfortunately, among such materials natural and synthetic minerals are scarce (Jochum 2010).

Such a lack of mineral reference materials was an incentive for creating a consortium of several German scientific and federal institutions with a common goal of providing a sufficient quantity of synthetic mineral reference materials with concentrations of economically important elements certified at the submicrometer level useful for in-situ analyses with a number of microanalytical methods.

Due to various geological processes natural minerals may develop heterogeneous elemental distribution as well as many structural features that seriously limit their suitability as reference materials. A logical assumption on superiority of synthetic minerals over natural minerals can be made as far as one is able to control chemical and structural homogeneity of the grown crystal. This can be assured by inventing robust homogeneity testing procedure employing both absolute and matrix-corrected methods.

In this study we introduce a systematic approach to homogeneity testing of reference materials using their natural analogs. Microanalytical techniques were selected and introduced on a step-by-step basis in a sequence, depending on their sensitivity and spatial resolution: light and electron microscopy, EPMA, SIMS, PIXE-PIGE, LA-ICPMS, µ-SXRF. The pilot program was launched using three minerals, each representing a different group of minerals of a specific interest to the industry: pyrite, columbite-tantalite and sanidine. All specimens were tested with reflected-light microscopy and scanning electron microscopy (BSE images) and showed no inhomogeneities apart from cracks and some minor inclusions. The results of the chemical homogeneity test will be presented in detail.

The research was supported by the Free State of Saxony, European Union and Helmholtz Association.

References:

K.P. Jochum, 2010, Goldschmidt Conference Abstracts 2010, A470.

P18-P01

Raman spectra of Synthetic Orthophosphates used for Nuclear Waste Management

H. Schlenz[1], J. Heuser[1], S. Schmitz[1], C. Babelot[1]

[1]Forschungszentrum Juelich, Nukleare Entsorgung und Reaktorsicherheit, Juelich, Germany

One of the central tasks in nuclear waste management is the safe conditioning of actinides like e.g. U, Th or Pu resulting from the re-processing of nuclear fuel. Besides borosilicate glasses promising candidates to accomplish that task safely are ceramic orthophosphates that own the crystal structure and properties of the mineral monazite. Monazite is monoclinic (SG $P2_1/n$) and exhibits an extraordinary chemical durability and radiation resistance [1,2,3]. For the development of new conditioning matrices orthophosphates with compositions $LnPO_4$ (Ln = La, Ce, Nd, Sm, Eu) were synthesized as first simulation phases without incorporated actinides. These phases were partly radiated by the bombardment with heavy Kr-ions in order to simulate radiation damage caused by α- emitters (α-recoil effect).

The quality of all phases (radiated and non-radiated) was first characterized by powder x-ray diffraction. The short range order and medium range order was investigated by raman spectroscopy. Using this technique structural changes due to radiation damage can be detected quite easily [4,5,6]. Resulting raman spectra show a high resolution and allow the discrimination of up to 30 different raman frequencies.

As a first result significant correlations between chemical composition, crystal structure, radiation damage and thermodynamic properties of the investigated ceramics can be detected and will be demonstrated in detail.

The findings of our investigation will be the basis for the further development and evaluation of *real* monazite-type conditioning ceramics containing larger amounts of the actinides U, Th, Pu, Am, Cm and Np.

[1] .A. Boatner, B.C. Sales, In: W. Lutze, R.C. Ewing (Eds.): *Radioactive waste forms for the future*, Amsterdam, North-Holland (1988).

[2] G.R. Lumpkin, *Elements* **2** (2006) 365.

[3] W.J. Weber, A. Navrotsky, S. Stefanovsky, E.R. Vance, E. Vernaz, *MRS Bulletin* **34** (2009) 46.

[4] G.M. Begun, G.W. Beall, L.A. Boatner, W.J. Gregor, *J. of Raman Spectroscopy* **11** (1981) 273.

[5] E.N. Silva, A.P. Ayala, I. Guedes, C.W.A. Paschoal, R.L. Moreira, C.-K. Loong, L.A. Boatner, *Optical Materials* **29** (2006) 224.

[6] L. Nasdala, R. Grötzschel, S. Probst, B. Bleisteiner, *Canadian Mineralogist* **48** (2010) 351.

P18-P02

Structure analysis of monazite-type ceramics used for nuclear waste management

S. Schmitz[1], H. Schlenz[1], D. Bosbach[1]

[1]Forschungszentrum Juelich GmbH, Institute for Energy- and Climate Research, Department of Nuclear Waste Management and Reactor Safety, Jülich, Germany

The further development of the conditioning and disposal of nuclear waste poses a major challenge in the near future. In this context, monazite ceramics ($LnPO_4$, Ln = La, Ce, Nd, Sm, Eu, Gd) appear to be promising alternative matrices to borosilicate glasses for the immobilization of actinides like U, Th and Pu.

Monazite is a natural thorium ore, chemically variable and highly radiation resistant [1]. The eldest known monazites including thorium are determined up to 3.2 Ma in age [2]. The high melting temperatures of about 2000 °C are a disadvantage of monazite phases and at a first glance this seems to be a drawback.

However, our initial phase is $NdPO_4$ with a melting temperature of 1975±20 °C [3]. Our intention is to reduce the melting and sintering temperature of this particular monazite phase, but maintaining the positive properties of monazite simultaneously (high chemical durability and high radiation resistance).

In order to include tetravalent actinides (e.g. Th, U, Pu), a second phase is used for charge balance. We used cheralite ($CaTh(PO_4)_2$) and huttonite ($ThSiO_4$) as solid solution end member. Both phases are isostructural to monazite [4, 5, 6]. Two solid solution series $NdPO_4$-$CaTh(PO_4)_2$ and $NdPO_4$-$ThSiO_4$ were synthesized by solid state reactions at T=1400 °C and atmospheric pressure for several hours.

The sample properties were analyzed chemically by EDX, structurally by XRD and Raman spectroscopy and thermally by TG-DSC. The analysis by SEM e.g. shows compact conglomerates of crystallites with diameters of 1-4 µm.

As a first result a complete solid solution along the $NdPO_4$-$CaTh(PO_4)_2$ join and along the $NdPO_4$-$ThSiO_4$ join does actually exist, respectively. Furthermore cell parameters show a significant shift as a function of chemical composition. Results of detailed rietveld refinements will be presented.

[1] L.A. Boatner, B.C. Sales, In: W. Lutze, R.C. Ewing (Eds.): *Radioactive waste forms for the future*, Amsterdam, North-Holland **1988** [2] B. Rassmussen, I.R. Fletcher, J.R. Muhling, *Geochim. Cosmochim Acta* **2007,** 71, 670-690 [3] Y. Hikichi, T. Nomura, *J. Am. Ceram. Soc.* **1987,** 70, C-252-C-253 [4] P.E. Raison, R. Jardin, D. Bouëxère, R.J.M. Konings, T. Geisler, C.C. Pavel, J. Rebizant, K. Popa, *Phys Chem Minerals* **2008,** 35, 603-609 [5] H.-J. Förster, *American Mineralogist*, **1998,** 83, 259-272 [6] L. Cartz, F. G. Karioris, K. A. Gowda, *Radiation Effects* **1981**, 67, 83-85

P18-P03

Characterization of synthetic $Sm_{1-x}Ce_xPO_4$ Ceramics used for Nuclear Waste Management

J. Heuser[1], H. Schlenz[1], D. Bosbach[1]
[1]Forschungszentrum Jülich GmbH, Nuclear Waste Management and Reactor Safety, Jülich, Germany

The conditioning of nuclear waste from nuclear power plants is an important issue according to science and society. Therefore the research on an appropriate matrix for the immobilization of e. g. actinides is of great interest.

Beyond the widely used borosilicate glasses, ceramics are promising materials for the conditioning of actinides like U, Th and Pu.

Monazite-type ceramics with compositions $Sm_{1-x}Ce_xPO_4$ ($0 \leq x \leq 1$) represent an important material in this field. To obtain a suitable host matrix for radionuclides, the characterization of monazites of different chemical composition and their thermal and structural behaviour is essential. Monazite was chosen because of its outstanding properties according to radiation resistance and chemical durability [1,2,3].

Our aim is to find a composition with a minimum melting point or an eutectic mixture in order to improve the production design for future industrial synthesis. Therefore we synthesized Samarium-Cerium-monazites as mentioned above, that can be used as simulation phases for radionuclide-doped matrices. Thirteen different compositions of the aforementioned solid solution were prepared by hydrothermal synthesis at $T = 220$ °C, $p \approx 25$ bar following [4].

The sample properties were analysed chemically by electron microscopy (EDX), structurally by powder x-ray diffraction (XRD) and Raman spectroscopy and thermally by TG-DSC. By means of our characterizations we could show that the solid solution with endmembers $SmPO_4$ and $CePO_4$ doesn`t show ideal behaviour. Accordingly we assume a minimum of melting point in the compositional range around $Sm_{0.6}Ce_{0.4}PO_4$. First results particularly related to crystal structure analysis of the investigated ceramics will be presented.

[1] G. R. Lumpkin, *Elements* **2006**, *2*, 365-372. [2] A. Meldrum, L.A. Boatner, R. C. Ewing, *Physical Review B* **1997**, *56*, 13805-13814. [3] E. H. Oelker, F. Poitrasson, *Chemical Geology* **2002**, *191*, 73-87. [4] H. Meyssamy, K. Riwotzki, A. Kornowski, S. Naused, M. Haase, *Advanced Materials* **1999**, *11*, 840-844

P18-P04

Characterization of turquoise and its imitations

H. Pristacz[1], G. Giester[1], C. Lengauer[1], E. Libowitzky[1]
[1]Universität Wien, Institut für Mineralogie und Kristallographie, Wien, Austria

A variety of gemologically improved turquoises as well as imitations are currently on the gem market, which usually cannot be distinguished by simple optical methods. The aim of the present investigation is an evaluation of non-destructive techniques, which allow a fast and unambiguous identification of turquoise and its replications. A series of relevant samples with blue or bluish-green color, raw material as well as cabochons, have been studied by means of X-ray powder diffraction (PXRD), infrared (IR) and Raman spectroscopy, handheld X-ray fluorescence spectrometry (XRF), and thermogravimetric analysis (TGA).

The PXRD **(I)** patterns recorded on a Nonius KappaCCD diffractometer show that dyed magnesite, calcite and dolomite are often used as turquoise imitations. We further identified minerals of the alunite group. In the PXRD patterns of specimens labeled reconstructed turquoise, we observed solely calcite and gibbsite. Diffraction lines of stabilized turquoise as described by Lind et al. (1983), which were assigned to berlinite, could not be confirmed.

IR spectra **(II)** were recorded on a Bruker Tensor 27 spectrometer using the attenuated total reflectance (ATR) technique. In addition to the characteristic absorption bands of turquoise some infrared spectra revealed absorption bands at 1725 cm^{-1} and 1450 cm^{-1}. These bands also occur in the absorption spectrum of a polymer-impregnated turquoise reported by Banerjee (1972).

Raman spectroscopy **(III)** can be useful for the identification of natural and polymer-impregnated turquoise. The disadvantage of this method, however, is the interference of the Raman signal by strong luminescence phenomena of natural and treated turquoise.

For the investigation of the chemical composition of the samples a Bruker Tracer III-V^+ XRF analyzer **(IV)** was used. Analyses of blue dyed carbonates exhibit high contents of Fe, Cu and Ni.

TGA studies **(V)** were done with a Mettler SDTA851e, up to 1100°C under N_2 atmosphere. The data reveal four different weight loss properties. Turquoise from Arizona indicates approximately 20% weight loss above an onset at 220°C. A treated turquoise from Mexico shows three weight loss events above an onset at 130°C, with a total weight loss of 23%. Two additional polymer-impregnated turquoises consequently exhibit weight losses of 36%. The ideal H_2O/OH content of turquoise is 17.7wt%. The PXRD data of the TGA-heated samples indicate the presence of $Al_{0.67}Fe_{0.33}PO_4$, $AlPO_4$, $CuAlO_2$ and corundum.

Summarizing the measurement efficiency of the above mentioned techniques **I, II, III** and **IV** with measuring times of less than one minute each, are valuable and powerful tools for the characterization of gemological turquoise-type material.

LIND, T., SCHMETZER, K., BANK, H. (1983): The Identification of turquoise by infrared spectroscopy and X-ray powder diffraction. Gems & Gemology, 19, 164-168.

BANERJEE, A. (1972): Ein Beitrag zum Thema Türkis. Zeitschrift der Deutschen Gemmologischen Gesellschaft, 21, 86-102.

P18-P05
Defects in natural gem-quality triphylite

E. Libowitzky[1], A. Beran[1], A. Wieczorek[2], R. Wirth[3]
[1]Universiät Wien, Institut für Mineralogie und Kristallographie, Wien, Austria
[2]Friedrich-Schiller-Universität Jena, Institut für Geowissenschaften, Jena, Germany
[3]Deutsches GeoForschungsZentrum GFZ Potsdam, Potsdam, Germany

While triphylite, olivine-type $LiFe[PO_4]$, occurs in Li- and P-rich pegmatites, its synthetic analogue is currently used as a storage cathode in rechargeable Li (LFP) batteries. For the chemo-physical properties of the latter, defects play an important role. Thus, for comparison, a natural gem-quality single-crystal of triphylite was studied by optical and electron microscopy, energy-dispersive X-ray spectrometry (EDS), as well as infrared (IR) and Raman spectroscopy.

EDS analyses indicated an intermediate composition of the sample within the triphylite-lithiophilite solid-solution series, i.e. $Li(Fe_{0.57}Mn_{0.43})[PO_4]$. While the sample appeared clear and transparent with the unaided eye and at low optical microscope magnification, numerous µm-sized, platy inclusions oriented parallel to (100) were revealed by inspection with > 40x objectives. These lamellar features were confirmed in a transmission electron microscopy (TEM) investigation of a focused ion beam (FIB)-prepared sample section. EDS analyses showed a composition enriched in Fe and depleted in P, i.e. roughly $Fe_2Mn[PO_4]_2$. Using micro-Raman spectroscopy the lamellar defects could be identified as sarcopside, $\Diamond(Fe,Mn)_3[PO_4]_2$, which is a triphylite-related olivine-type mineral with 25% vacancies at the metal sites.

Polarized IR spectra of oriented polished sample sections indicated also the presence of hydrous defects. Three characteristic O-H stretching bands are present with their maximum absorption parallel to [001], i.e. at 3475, 3444 (strongest), and 3418 cm^{-1}. According to their intensity the water concentration of the sample is ca. 5 wt-ppm. The bands can be assigned to hydrous defects in the structure of triphylite itself (under the assumption of vacancies, comparable to structural OH defects in olivine), or to hydrous mineral inclusions within the host phase. Two hydrous phosphate minerals, well known as alteration products of triphylite, are proper candidates for the latter. Phosphoferrite, $(Fe,Mn)_3[PO_4]_2 \cdot 3H_2O$, and reddingite, $(Mn,Fe)_3[PO_4]_2 \cdot 3H_2O$, both endmembers of a complete solid-solution series, are characterized by an intense Raman O-H stretching band at 3443 cm^{-1} with a shoulder at its low-energy side. However, due to the extremely low concentration of hydrous phase, this compelling assignment cannot be confirmed by any other method.

P18-P06
Mg-rich ludlamite and Mg-rich whiteite-(CaFeMg) from the phosphate pegmatite boulder at Laggerhof, Carinthia

U. Kolitsch[1,2], G. Giester[2], F. Brandstätter[1]
[1]Naturhistorisches Museum, Mineralogisch-Petrographische Abteilung, Wien, Austria
[2]Universität Wien, Institut für Mineralogie und Kristallographie, Wien, Austria

Over the last three decades, a singular phosphate pegmatite boulder at Laggerhof, Carinthia, a locality which is part of an area hosting phosphate-bearing and Al- and Mg-enriched pegmatites, has provided a suite of rare phosphate species, including augelite, burangaite, gormanite, perhamite, whiteite-(CaFeMg) and zanazziite (Walter, 1998; Niedermayr & Brandstätter, 2005).

One sample recently collected from this boulder by Mr. Christian Auer was found to contain unusual, Mg-rich varieties of ludlamite (new for the locality) and whiteite-(CaFeMg). Their crystallography was studied in detail by structure refinements using single-crystal X-ray diffraction data, and showed distinct differences by comparison to the available literature data.

Mg-rich ludlamite forms reddish brown to yellow-brown, blocky, cloudy crystals and weakly translucent grains in a matrix of altered siderite and minor muscovite. SEM-EDS analyses showed, in some crystal fragments, very minor Ca and Mn as additional foreign elements.

The crystal structure of Mg-rich ludlamite, space group $P2_1/a$, a = 10.526(2), b = 4.550(1), c = 8.994(2) Å, ß = 104.01(3)°, V = 417.94(15) Å^3, Z = 2, was refined to $R1(F)$ = 3.84 %. The unit cell is distinctly smaller than that reported in earlier studies for nominally pure ludlamite, $Fe_3(PO_4)_2 \cdot 4H_2O$: a = 10.541(5), b = 4.646(4), c = 9.324(5) Å, ß = 100.43(2)°, V = 449.08 Å^3 (Abrahams & Bernstein, 1966; see also Ito & Mori, 1951). Specifically, the cell volume has decreased by 7%, and the b angle has increased by 3.58°. The refinement demonstrates that one of the two Fe positions, Fe(1), has 33(1)% of its Fe substituted by Mg. The other position, Fe(2) shows a substution of 12(1)%. The refined bulk formula is $(Fe_{2.43}Mg_{0.57})(PO_4)_2 \cdot 4H_2O$. The considerable Mg-for-Fe substitution results in strong changes of the geometry of the FeO_6 octahedra and the hydrogen-bonding scheme. It appears possible that a Mg-dominant analogue of ludlamite may exist in nature.

Mg-rich whiteite-(CaFeMg) was found as a single, pink-brown, glassy, transparent grain in matrix, in direct contact with the Mg-rich ludlamite. The crystal structure was refined in space group $P2/a$ (a = 14.850(2), b = 6.956(1), c = 9.943(2) Å, b = 110.18(3)°, V = 964.0(3) Å^3, Z = 2) to $R1(F)$ = 4.6 %. No twinning was observed. The unit-cell parameters are distinctly smaller than those reported for type whiteite-(CaFeMg), a = 14.90(4), b = 6.98(2), c =10.13(2) Å, ß = 113.07(10)°, V = 969.3 Å^3 (Moore & Ito, 1978), but similar to those determined very recently for whiteite-(CaFeMg) from Canada, a = 14.8700(15), b = 6.9785(5), c = 9.9268(10) Å, ß = 110.110(1)°, V = 967.31(15) Å^3 (Capitelli et al., 2011). SEM-EDS analyses showed Fe, Mn (Fe:Mn ~ 2:1), Mg, Al, Ca and P. No Na was detectable (EPM analyses are planned). The refined formula is $(Ca_{0.54}Mg_{0.46})(Fe_{0.85}Mg_{0.15})(Mg_{1.96}Fe_{0.04})Al_2(PO_4)_4(OH)_2 \cdot 8H_2O$ (Fe includes all Mn). Crystal-chemical details will be discussed.

References

Abrahams, S.C. and Bernstein, J.L. (1966): Crystal structure of paramagnetic ludlamite, $Fe_3(PO_4)_2 \cdot 4H_2O$, at 298°K. Journal of Chemical Physics, 44, 2223-2229.

Capitelli, F., Chita, G., Cavallo, A., Bellatreccia, F. and Della Ventura, G. (2011): Crystal structure of whiteite-(CaFeMg) from Crosscut Creek, Canada. Z. Kristallogr. 226 (in press).

Ito, T. & Mori, H. (1951): The crystal structure of ludlamite. Acta Crystallographica 4, 412-416.

Moore, P. B. & Ito, J. (1978): I. Whiteite, a new species, and a proposed nomenclature for the jahnsite-whiteite complex series. II. New data on xanthoxenite. III. Salmonsite discredited. Mineralogical Magazine 42, 309-323.

Niedermayr, G. & Brandstätter, F. (2005): Neue Mineralfunde aus Österreich LIV. Perhamit und Rockbridgeit, zwei neue Phosphate vom Laggerhof am Millstätter See, Kärnten. Pp. 283-284 in: Niedermayr, G., C. Auer, F. Bernhard, H.-P. Bojar, F. Brandstätter, A. Ertl, K. Ettinger, V. M. F. Hammer, B. Leikauf, W. Postl, M. Sabor, R. Schuster, R. Seemann & F. Walter (2005): Neue Mineralfunde aus Österreich LIV. Carinthia II, 195./115., 277-315.

Walter, F. (1998): Exkursion E4 am 27.9.1998 - MinPet 98 (Pörtschach am Wörthersee/Kärnten) - Die Pegmatite des Millstätter See-Rückens. Mitt. Österr. Mineral. Ges., 143, 437-450.

P18-P07

Crystal structure and hydrogen bonding in vauxite, $FeAl_2(PO_4)_2(OH)_2{\cdot}6H_2O$ from Vitlovac locality, Bosnia and Herzegovina

T. Djordjevic[1], J. Stojanovic[2], U. Kolitsch[3]
[1]Universität Wien, Institut für Mineralogie und Kristallographie, Wien, Austria
[2]Institute for Technology of Nuclear and Other Mineral Raw Materials, Applied Mineralogy Unit, Belgrade, Serbia
[3]Naturhistorisches Museum, Wien, Austria

Light blue prismatic crystals of Fe^{3+}-bearing vauxite from Vitlovac near the lead-zinc mine Srebrenica in Bosnia and Herzegovina, associated with quartz, sphalerite, galena, pyrite, chalcopyrite, and calcite, were investigated by wet chemical analysis, single-crystal structure refinements at 293, 200 and 100 K (CCD area detector data, Mo*K*a radiation, 2q_{max} = 65°), powder infrared and single-crystal Raman spectroscopy.

The chemical analysis yielded (wt. %): FeO 15.25, Fe_2O_3 9.81, Al_2O_3 10.94, P_2O_5 34.64 and H_2O 22.09, sum 99.70.

The crystal structure of vauxite was refined using single-crystal X-ray diffraction data. Vauxite is triclinic, space group *P*-1, with *a* = 6.1635(1)/6.1612(1)/6.1602(1), *b* = 9.1417(2)/9.1177(2)/9.1038(2), *c* = 11.5997(2)/11.5901(2)/11.5830(2) Å, *a* = 108.1538(12)/108.2063(13)/108.2315(13), *b* = 98.2860(12)/98.3058(13)/98.3002(13), *γ* = 92.0140(13)/92.1187(13)/92.1922(13)°, *V* = 612.3(2)/610.0(2)/608.1(2) Å^3, at 293/200/100 K, respectively (*Z* = 2). The refinement yielded *R*1(*F*) = 0.0243/0.0288/0.0272 for 3137/3702/3716 ‘observed reflections’ with F_o^2 ³ 4σ(F_o^2) for 293/200/100 K, respectively.

Baur et al. (1968) originally solved the crystal structure of vauxite and determined the positions of the non-H atoms. The present contribution reports, for the first time, also the positions of the H atoms and their role in the hydrogen-bonding scheme. The crystal structure of vauxite is characterized by infinite chains of alternating and edge-connected Fe2$O_4(OH)_2$ and Al2$O_4(OH)_2$ octahedra. Parallel to this chain, and flanking it on two opposite sides, are vertex-linked chains of P2O_4 tetrahedra alternating with Al1O_4(OH)(H_2O) octahedra. The mixed tetrahedral-octahedral chains are linked through vertices from H_2O molecules to the octahedral chain. This triple chain is further interlinked by the P1O_4 tetrahedron, which shares vertices with the octahedra around Al1, Al2 and Fe2. This infinite triple chain unit is connected to neighboring units of the same kind via vertex-linked Al3-centered octahedra in direction [010], and via Fe1-centered octahedra in direction [100]. Two free water molecules are located in the channels extended parallel to [100] and are hydrogen-bonded to the framework structure. Unrestrained refinements of the O-H bond lengths in the room-temperature model resulted in values ranging between 0.65(3) and 1.07(4) Å. The hydrogen-bonding scheme undergoes no changes with decreasing temperature.

Unpolarized single-crystal Raman and powder FT-infrared spectra confirm the presence of PO_4 and OH groups, H_2O molecules and lattice vibrations involving Al-O and Fe-O bonds. The band positions of the OH stretching vibrations in the range between ca. 3700-3000 cm^{-1} indicate medium-strong to weak hydrogen bonds, in agreement with the refined O···O distances.

References:

Baur, W.H. & Rama Rao, B. (1968): The crystal structure and the chemical composition of vauxite. Am. Mineral., 53, 125-1028.

P18-P08

Gd-enriched xenotime from zircon breakdown reaction in metamorphosed phosphatic sandstone (Serra da Vereda Formation, Espinhaço fold belt, Brazil)

G. Morteani[1], G. Franz[2], D. Rhede[3], A. Gerdes[4]
[1]Hydroisotop GmbH, Isen, Germany
[2]Technische Universität Berlin, Berlin, Germany
[3]Geoforschungszentrum, Potsdam, Germany
[4]Universität Frankfurt, Frankfurt/M, Grenada

Detrital zircon crystals in a phosphatic sandstone, metamorphosed under amphibolite facies conditions, show unusual textures sugesting a simplified breakdown reaction of the zircon (detrital) + fluid = zircon (metamorphic) + xenotime. The phosphatic sandstone is part of the Serra de Vereda Fm in the Espinhaco fold belt, Brazil, a prominent lithologic unit, which extends over approximately 1000 km N-S from the southern border of the state Piaui into the state of Minas Gerais. Next to quartz and white mica the rock contains the characteristic minerals lazulite and dumortierite, which are responsible for the blue colour, minerals of the svanbergite-crandallite group, hematite, rutile, kyanite and others. Zircon textures vary from detrital grains to skeletal grains filled with abundant inclusions, replaced in patches, along zones or in rim areas by metamorphic zircon. The metamorphic zircon is clearly visible in high-resolution back scattered electron images due to its lower contrast in comparison to detrital zircon. Detrital grains yield concordant but variable LA-ICP-MS U-Th-Pb ages of the provenance area, whereas metamorphic grains yield strongly reset ages. Due to the large number of inclusions no metamorphic age could be obtained until now. Metamorphic zircon differs in composition mainly in Y, U, Th, Hf content. A typical mineral, which replaces detrital zircon and occurs together with metamorphic zircon, is xenotime. In some crystals it is volumetrically abundand, but crystals larger than about 10µm are rare. Xenotime crystals are strongly enriched in Gd (up to 12 wt% Gd2O3), Dy and Tb, which produce a typical chondrite-normalized REE pattern with a hump in the middle REE. The xenotime cystals are very heterogeneous, even in small crystals of less than 10 µm in size. In some crystals Gd-rich and Gd-poor zones occur close together in direct contact. We speculate that the fluid present during metamorphism was strongly enriched in P and was therefore responsible for the formation of the Y-REE phosphate during breakdown reactions.

P18-P09

Raman spectroscopic investigations in the join Plumbojarosite - Corkite - Kintoreite

M. Kaliwoda[1], A. Guenther[2], R. Hochleitner[1], A.M. Gigler[2], C. Rewitzer[2], K.-T. Fehr[2]
[1]Mineralogical State Collection, LMU, Munich, Germany
[2]Ludwig-Maximilians University, Department of Geo- and Environmental Science, Munich, Germany

The three minerals plumbojarosite, corkite and kintoreite belong to the alunite $KAl_3(SO_4)_2(OH)_6$ supergroup (1). All of them are secondary formed minerals, in which potassium is substituted by lead and aluminium by iron three plus. Furthermore plumbojarosite is a sulphate and kintoreite is a phosphate. Whereat, corkite is the mixed anion member with SO_4/PO_4 in the amount of 1:1.

Giuseppetti & Tadini (2) recommended the a-centric space group *R*3*m* with lower symmetry for corkite, whereas Sato et al. (3) suggested, for a SO_4-rich corkite, R-3m as well as Kolitsch (unpubl., cited after (1)) for a corkite from Dernbach, Germany.

Accepting this space group, the existence of a discrete mineral corkite would be questionable.

During our study corkite minerals from a new locality in Portugal have been investigated by Raman and IR spectroscopy. The spectra of corkites with different composition (4) have been compared to spectra of plumbojarosite (Figure 1) and kintoreite. Kintoreite from the type locality *Kintore open cut* (Broken Hill, New South Wales, Australia) is relatively sulphate- and zinc-rich (5). Spectra of a nearly sulphate-free and zinc-free end-member kintoreite are presented for the first time.

(1) Bayliss, P., Kolitsch, U., Nickel, E.H. and Pring, A. (2010): Alunite supergroup: recommended nomenclature. Min. Mag. 74, pp. 919-927.
(2) Giuseppetti, G. and Tadini C. (1987): Corkite, its structure and ordered arrangement of the tetrahedral cations. N. Jb. Min. Mh. P 71-81.
(3) Sato,E., Nakai, I., Miyawaki, R. and Matsubara, S.(2009): Crystal structures of alunite family minerals. N. Jb. Miner. Abh. 185/3, p 313.-322.
(4) Hochleitner et al. (2011): Crystallochemical investigations in the join Plumbojarosite - Corkite - Kintoreite. Joint Meeting of the DGK, DMG and ÖMG Salzburg. Same session.
(5) Pring, A., Birch, W.D., Dawe, J., Taylor, M., Deliens, M. and Walenta, K. (1995): Kintoreite, a new mineral of the jarosite-alunite family. Min Mag., 59, p. 143-148.

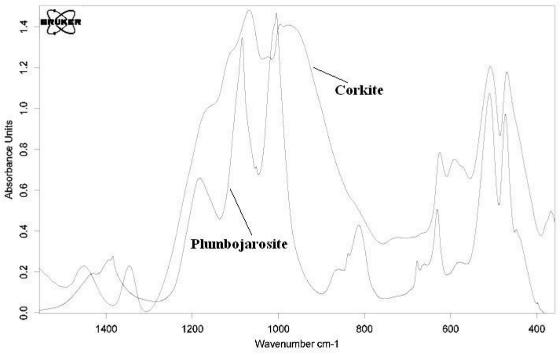

Figure 1: FTIR spectra of corkite and plumbojarosite

P19-P01
Mineralinos - Mineralogy for Children: A Project for Children from 8 to 12

A. Greif[1], M. Bayer[1], C. Seifert[2], A. Dziwetzki[2]
[1]TU Bergakademie Freiberg, Institut für Mineralogie, Freiberg, Germany
[2]TU Bergakademie Freiberg, terra mineralia, Freiberg, Germany

Since October 2008 the exhibition “terra mineralia” at the Freudenstein Castle in Freiberg/ Saxony more than 3.500 mineral specimens, gem stones and meteorites from all over the world are shown. This worldwide greatest private mineral collection is since 2004 a permanent loan of the foundation „Pohl-Ströher-Mineralienstiftung“ at TU Bergakademie Freiberg with a total of circa 20.000 specimens. It contains excellent specimens from minerals deposits in Europe, Asia, Africa, and America to be viewed on a journey through these continents.

A major concern of the exhibition concept is aside the pleasure for the senses the integration of knowledge modules on characteristic and utilization of the minerals shown, and the introduction of children and young persons to scientific work. Dedicated to this is a special area, the „Expedition“ to arouse pupil's and students' enthusiasm for natural sciences. Besides the necessary equipment as microscopes, scales of hardness, crystal models and a density balance, many mineral and rock samples are available to young researchers to become more familiar, touch and investigate. These materials are also used by the „mineralinos“, a series of events founded in April 2010 where children from 8 to 12 with interest in minerals and collecting meet. Once a month they can gain first experience with scientific investigation methods.

The focus of the series of events is on the introduction to the world of minerals including recognition and determination of the main mechanical and optical properties of minerals. For each mineral got to know a profile is made to be introduced to the systematic of minerals. Wooden models illustrate the crystal forms and train the spatial imagination. Furthermore the „mineralinos“ get useful tips to build up an own minerals collection. They learn what to pay attention to in collecting minerals specimens and why the location of a mineral is of great importance. With guidance they can determine their first minerals finds.

This year aside many fascinating themes like „Salt - White gold“ or „Meteorites - Visitors from outer space“ a course in stone cutting and polishing and an excursion on the topic „Mining in the Erzgebirge mountains“ is offered.

Information: http://www.terra-mineralia.de

P20-P01
Structure solution of decagonal ZnMgDy quasicrystal

T. Örs[1], W. Steurer[1]
[1]ETH Zurich, Dept. of Materials, Lab. of Cryst., Zürich, Switzerland

Here we report the first structure solution of decagonal ZnMgDy quasicrystal (d-ZnMgDy) based on single crystal X-ray diffraction data. Samples with the composition ($Zn_{57.6}Mg_{40.8}Dy_{1.6}$) were prepared by induction melting followed by annealing at 375°C for 10 months. The alloys were then quenched to room temperature. The resulting samples consist mainly of a hexagonal phase with the d-ZnMgDy existing as the secondary phase. The morphology of the decagonal phase is typically needle-like. These grains are of 50 µm in length and approximately 15 µm in other dimensions. X-ray diffraction experiments were carried out both in-house (Oxford Xcalibur PX diffractometer, CCD detector, Mo Kα radiation) and at the Synchrotron facility in Swiss-Norwegian beam line, ESRF, Grenoble (λ=0.6980 Å).

The Laue group was specified to be 10/mmm with a periodicity of 5.22 Å along the periodic direction. No systematic extinctions were observed. SUPERFLIP program package [1] (based on charge flipping and low density elimination algorithms) was used for structure solution.

[1] L. Palatinus, G. Chapuis, Journal of Applied Crystallography 2007 40, 786-790.

Keywords: quasicrystal, decagonal

P20-P02
Decagonal phases in Al-Ni-Rh system

D. Logvinovich[1], W. Steurer[1]
[1]ETH Zurich, Department of Materials, Zurich, Switzerland

The interest in the Al-Ni-Rh decagonal phase structure is triggered by the fact that it is formed at the Al and Ni concentration where also the extensively studied Al-Ni-Co decagonal phase [1] is stable. Due to the similar number of electrons in Ni (28) and Co (27), X-ray diffraction does not allow distinguishing between these elements and thus solve the latter structure unambiguously. Instead of Co, the new decagonal phase contains Rh (45). The latter also has a larger atomic radius than Co. This will allow studying the important Ni/Rh order in the average structure.

The discovery of decagonal quasicrystals in Al-Ni-Rh system has been recently reported in literature [2]. The structural studies available up to now are limited to high-resolution transmission electron microscopy (HRTEM) and electron diffraction (ED) [2-4]. According to them the reported decagonal phase has a period of 4 Å along the 10-fold axis. No refined structural model of that phase is available up to date.

Recently we have succeeded in growing single crystals of the 4Å-decagonal phase of Al-Ni-Rh system large enough for single crystal diffraction experiments. The crystal structure of that phase has been solved in 5D-space (space group: $P10_5/mmc$) by charge-flipping algorithm. The solution reveals that Rh-atoms preferentially occupy centers of the transition metal atom occupation domains. The diffraction experiments reveal weak diffuse scattering within Bragg layers.

In course of our investigations two other phases were obtained: a new decagonal phase and an approximant with 16Å periodicity along 10- and pseudo-10-fold axes respectively.

[1] A. Cervellino, T. Haibach, W. Steurer, *Acta Crystallogr. Sect. B: Struct. Sci.* **2002**, *58*, 8. [2] K. Tsuda, *Philos. Mag. Lett.* **1996,** *73*, 271. [3] B. Grushko, S. Mi, *Z. Kristallogr.* **2003,** *218*, 389. [4] B. Przepiorzynski, S. Mi, B. Grushko, M. Surowiec, *Intermetallics* **2007,** *15*, 918.

Keywords: decagonal quasicrystal, approximant, x-ray diffraction

P20-P03

Ab-initio calculations on the stability of heptagonal ordering in Gallium

H. Orsini-Rosenberg[1], S. Deloudi[1], W. Steurer[1]
[1]ETH Zurich, Lab. of Crystallography, Department of Materials, Zurich, Switzerland

Sevenfold symmetry is the lowest rotational symmetry not yet observed in quasicrystals. However, there are several strong hints that indicate the existence of heptagonal quasicrystals (QCs) [1]. In a previous *ab-initio* study [2] it was shown that theoretical sevenfold approximants, designed from promising known boride and borocarbide structure types by using a supertile approach, were acceptably stable within the range of error. Due to the fact that these structures and their associated tilings are ternary, the weak matching rules automatically imposed on the edges of the tiles only allow for a limited number of possible structural arrangements. The configurational degrees of freedom can be increased by investigating the monatomic structure of γ-Ga, a metastable low temperature phase that forms when undercooling liquid Ga to below -35.6 °C. Its structure consists of regular sevenfold antiprisms centered by a single Ga atom. Additionally it can be described as a periodic arrangement of one of the three heptagonal rhombic unit tiles, namely the fat tile with an ideal acute angle of 3π/7 (= 77.12°, in the structure 76.15°).

For the missing two unit tiles (with acute angles π/7 and 2π/7), decorations were be designed by using similar atomic arrangements as for the fat tile (*i.e.* γ-Ga). As only periodic structures can be accessed by means of *ab-initio* total energy calculations, the unit tiles were subsequently used to decorate approximants. Therefore various theoretical structure types were generated, either by periodic arrangement of single tiles or hexagon supertiles of the rhomb tiles, or by creating rational heptagonal approximants using the cut-and-project method.

The first-principles DFT calculations were performed with the VASP code [3], using a plane-wave basis set, the GGA algorithm and PAW-PBE pseudopotentials. Total energies were calculated for all theoretical Ga structure types, as well as the electron localization function (ELF), and the atom relaxation movements were investigated. The possibility of stabilizing the designed structures by dopant atoms was also explored: the rational approximant structures mentioned above exhibit a small number of voids or holes too large for Ga atoms, which were filled with other atoms from the boron group (In and Tl) by 3 to 5 at.%. The binary convex hulls for these systems were also calculated.

From our results we compare the mechanical and energetical stability of different types of theoretical heptagonal approximants, in relation to the stable modifications of Gallium. From the structure types decomposing during relaxation we could draw conclusions about the mechanisms of heptagonal ordering in Gallium. We were also able to estimate the influence of doping on the stability of our approximants.

[1] W. Steurer, Phil. Mag. **87** (2007) 2707. [2] H. Orsini-Rosenberg, W. Steurer, Phil. Mag. **91** (2011) 2567. [3] Vienna Ab-initio Simulation Package; G. Kresse, J. Furthmüller, Phys. Rev. **B 54** (1996) 11169.

P21-P01

Electron Microprobe Study of Aluminosilicate Garnet

C.A. Geiger[1], J. Fournelle[2]
[1]Universität Salzburg, Materialforschung & Physik, Salzburg, Austria
[2]University of Wisconsin, Department of Geoscience, Madison, WI, United States

The aluminosilicate garnets comprise an important rock-forming mineral group. The most common end-members are given by the ideal formula $\mathbf{E}_3Al_2Si_3O_{12}$, where **E** = Fe^{2+} (almandine), Mn^{2+} (spessartine), Mg (pyrope), and Ca (grossular). Synthetic garnet can, depending on the species, contain minor Fe^{3+}, Mn^{3+}, and OH^-. Slight atomic disorder over the three different cation sites may also occur. Natural crystals are considerably more complex.

Electron probe microanalysis (EPMA) provides the standard method to determine garnet composition. However accurate determinations are not always a simple matter and uncertainties exist. We have started a study on synthetic aluminosilicate crystals in order to i) determine more exactly their compositions and stoichiometries and ii) better understand some possible complications in the electron microprobe method and data analysis.

Synthetic almandine, spessartine, pyrope, and grossular samples are being studied. Pyrope has been investigated with simple oxide/silicate standards. Previously observed problems were reproduced: low stoichiometry for Al and high for Si and Mg. Fournelle (2007) noted chemical peak shifts for Al and Mg Ka in garnets, however this effect was eliminated here by proper peaking. Earlier suggestions concerning the issue of mass absorption coefficients were not seen, and the Probe for EPMA software utilized demonstrated that there was not much difference between the most recent FFAST values vs. older Heinrich values. Similarly, a matrix correction based on CITZAF was compared with that form PAP, with little difference in Al (both low) and Mg values (both high), though PAP had higher Si values and CITZAF had lower ones.

One assumption in traditional EPMA is that the intensity of a single peak channel is representative of the integral of all X-ray counts under the total peak, which is the true measure of composition. It is known that this is not true for “light elements” (Be to F) and bonding effects skew the relationship. We performed detailed wavescans of the complete integral peaks of Si, Al and Mg Ka for both standards and pyrope. Mg and Si peak scans showed little or no difference between pyrope and standard, but the Al scans gave reproducible differences of 3% between the Al_2O_3 standard and unknown, with possible differences in the Al K satellite region. This yielded an “area peak factor” correction of 1.03, which brings the Al closer to the theoretical value, but not all the way, to a stoichiometry of 2, Si to almost 3, and Mg closer to 3 but still too high. One possibility, which has to be evaluated further, is whether there may be solid solution between pyrope ($Mg_3Al_2Si_3O_{12}$) and a minor majorite ($Mg_3(Mg,Si)Si_3O_{12}$) component involving the coupled substitution 2Al = Mg,Si at the octahedral site.

P21-P02

Temperature-dependent Raman characterization of Stibnite (Sb_2S_3)

P. Sereni[1], M. Musso[1], C. Oberauer[1], P. Knoll[2]
[1]University of Salzburg, Department of Materials Engineering and Physics, Salzburg, Austria
[2]University of Graz, Department of Experimental Physics, Graz, Austria

We are presently extending our investigations focused on the polarization-dependent Raman characterization of Stibnite (Sb_2S_3) [1] by exploring the temperature dependence in the range from 290 K to 77 K. The results obtained using a FT-Raman spectrometer set to high-resolution (1 cm^{-1}) and with polarized laser excitation at 1064 nm will be presented and compared to those mentioned in Ref. [1].

[1]] P. Sereni et al., AIP Conference Proceedings **1267**, 1131-1132 (2010)

P21-P03

Recrystallisation of Metamict Allanite

U. Bismayer[1], T. Beirau[1], C. Paulmann[1]
[1]Universität Hamburg, Mineralogie, Hamburg, Germany

Allanite is a common accessory mineral in igneous rocks. Through the incorporation of radiogenic elements and the resulting alpha-decay, in nature it becomes metamict on the geological time scale. As a consequence the periodic ordered crystal structure of the mineral is partially destroyed and becomes locally disordered. This study is focused on the recrystallisation behaviour on annealing of highly metamict allanite from Altai Mountains, Russia. The chemical composition was measured by electron microprobe analysis (EMA) and x-ray fluorescence analysis (XRF). The structural recovery upon annealing was followed by X-ray powder diffraction (XRD), single-crystal synchrotron diffraction and infrared spectroscopy (FTIR). A basic kinetic analysis is presented that shows that the recrystallisation process of the metamict material consists of at least two different kinetic mechanisms.

P21-P04

Application of Raman spectroscopy to quantitative analysis of carbonates

B. Schmidt[1], N. Pukallus[1,2], J. Sauthoff[1]
[1]University Göttingen, GZG, Mineralogy, Göttingen, Germany
[2]University Göttingen, GZG, Crystallography, Göttingen, Germany

Synthetic carbonates of the binary solid solution series calcite-magnesite (Cal-Mgs), calcite-siderite (Cal-Sd) and magnesite-siderite (Mgs-Sd) were prepared in piston cylinder or hydrothermal experiments. Solid solution crystals were obtained in the Cal-Mgs system in the range Cal100 to Cal52Mgs47, in the Cal-Sd system from Cal100 to Cal65Sd35 and in the Mgs-Sd system over the entire range. The crystals were measured by Raman spectroscopy and their chemical composition was determined by electron microprobe analysis.

Linear correlations between Raman shift and chemical composition were obtained for the T, L, ν1 and ν4 bands of the Cal-Mgs series, for the T and ν4 bands of the Cal-Sd series and for the T and L bands of the Mgs-Sd series. Using these correlations the chemical composition in the binary solid solution series can be determined with an error of 3 to 8 mol%. The application of the obtained calibrations to natural samples was successfully tested by measuring a number of natural carbonate specimens.

The linear correlations of the T and L modes in all three binary solid solution series were used to construct a ternary diagram, which enables the determination of ternary carbonates in the system Cal-Mgs-Sd. Its application was tested by a number of natural carbonates. In particular specimens from the dolomite-ankerite (Dol-Ank) solid solution show some larger deviation from the model, resulting in an error of about 15 mol%. Further work is in progress to study the effect of Mn on Raman band positions of carbonates.

P21-P05

Orientation-dependent REE photoluminescence of zircon, xenotime and monazite

C. Lenz[1], D. Talla[1], L. Nasdala[1]
[1]Institut für Mineralogie & Kristallographie, Universität Wien, Wien, Austria

Introduction

In Earth sciences, the Rare Earth Elements (REE) distribution in different minerals is used to trace geochemical signatures of formation processes and their genetic implications. One challenging task in REE spectroscopy of the last decades was the detection of different REE in different mineral hosts by luminescence methods [1]. It has become commonplace to interpret REE luminescence by evaluating the Stark level splitting caused by the crystal field interaction [2]. The presence of REE ions at more than one non-equivalent structural positions and semi-quantitative suggestion on rare-earth content is supposed [3-6], however, without regarding the orientation-dependence of REE emissions [7], which is often neglected and insufficiently investigated on synthetic analogue.

Methods & Samples

We have studied REE mono-doped single-crystals of zircon ($ZrSiO_4$), xenotime (YPO_4) and monazite ($CePO_4$) synthesized with flux technique. Common REE in minerals are chosen as dopants (Dy^{3+}, Sm^{3+}, Ho^{3+}, Tb^{3+}, Eu^{3+}, Er^{3+}). Steady-state photoluminescence (PL) and Raman spectra were obtained in quasi back-scattering geometry using a Renishaw RM1000 system with the 488 nm Ar^+ emission line. Oriented measurements of polished sections parallel to the crystallographic *c*-axis were made.

Results & Discussion

The luminescence of REEs is characterized by specific transitions between different spin-orbit coupled spectral levels which are well studied [8]. In crystalline materials, these spectroscopic states further split into Stark sublevels because of the crystal field interaction. The luminescence of REEs is dependent on both the type of REE incorporated and the symmetry of the REE-substituted crystallographic cation-site. Our results show that the crystal orientation has a strong influence on the REE photoluminescence with respect to the polarization of the laser (due to symmetry selection rules of specific transitions). Generally, the luminescence intensity strongly increases with polarization direction of the laser parallel to the optical axis (crystallographic *c*-axis within tetragonal structures of zircon and xenotime). In various cases intensity ratios between bands change drastically, peak positions moved, or whole sets of bands disappear as is exemplary shown for transitions of Eu^{3+}, Ho^{3+} and Dy^{3+} in xenotime (Fig. 1).

References

1 Gaft, M. et al. (2005) *Luminescence spectroscopy of minerals and materials,* Springer.

2 Reisfeld, R. et al. (2004) MOL PHYS *102*(11): p. 1319-1330.

3 Dexpert-Ghys, J. et al. (1996) J Lumin *69*(4): p. 203-215.

4 Czaja, M. et al. (2009) Phys Chem Miner *7*: p. 1-9.

5 Barbin, V. et al. (1996) Chem Geol *130*(1-2): p. 77-86.

6 Friis, H. et al. (2009) Phys Chem Miner *37*(6): p. 333-342.

7 Owen, J.J. (1998) JOSA B, 1998. *15*(2): p. 684-693.

8 Dieke, G.H. (1968) *Spectra Energy Levels of Rare Earth Ions in Crystals,* Wiley Interscience.

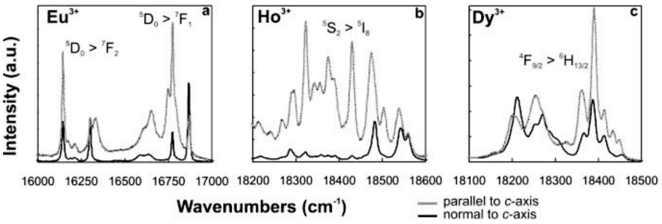

Figure 1: PL spectra of xenotime single-crystals doped with Eu^{3+} (a) Ho^{3+} (b) and Dy^{3+} (c). Samples were measured with the electric field vector of the incident beam of light oriented parallel or normal to the crystallographic c-axis.

P21-P06

Semi-quantitative detemermination of the Fe-Mg ratio in synthetic cordierite using Raman spectroscopy

U. Haefeker[1], R. Kaindl[2], P. Tropper[1]
[1]Universität Innsbruck, Mineralogie und Petrographie, Innsbruck, Austria
[2]Joanneum Research Forschungs mbH, Materials - Inst. f. Oberflächentechnologien und Photonik, Niklasdorf, Austria

Natural Cordierite with the idealized composition $(Mg,Fe)_2[Al_4Si_5O_{18}]*x(H_2O,CO_2)$ occurs mostly as the orthorhombic polymorph with an ordered Al/Si-distribution on the tetrahedral sites. The structure contains six-membered rings of $(Si,Al)O_4$, which are stacked along the direction of the c-axis. The rings are linked laterally and vertically by additional (Al,Si) tetrahedrons and thus different tetrahedrally coordinated sites and channel sites have to be distinguished in the structure: $(M)_2(T_11)_2(T_26)_2(T_23)_2(T_21)_2(T_16)O_{18}(Ch0,Ch1/4)$ (e.g. Bertoldi et al., 2004). Mg and Fe in varying fractions are located in the octahedrally coordinated M-sites. The incorporation of Fe leads to multiple structural changes. A linear expansion of the mean M-O-distances within the octahedra leads to an elongation of the unit cell in a and b. The distance of T_11-O decreases slightly, leading to a contraction in the direction of the c-axis (e.g. BOBERSKI & SCHREYER, 1990; GEIGER & GRAMS, 2003). The variations in bond lengths cause detectable changes of the vibration energies of certain vibrational modes and thus can be determined with Raman spectroscopy, which was the aim of this investigation. For this purpose, H_2O-bearing, well ordered orthorhombic cordierites with Mg-Fe^{2+} ratios of 0, 0.25, 0.5, 0.75 and 1 were synthesized in a hydrothermal apparatus at 700°C and 0.3 GPa. For the Fe-bearing samples CCO-buffered capsules were used. To investigate the effects of the Fe-Mg-exchange on the positions of the Raman peaks, unpolarized spectra were recorded in the region from 100 to 1250 cm^{-1}. The results show that most of the peaks shift towards lower wave numbers with increasing X_{Fe}.

Although the determination of the exact mode energy is difficult for several peaks due to overlaps, accurate data can be obtained for the peaks in the region of 260, 425 and 1010 cm^{-1} and linear least squares estimation of the data yields:

$X_{Fe} = -0.206 * P_{260} + 53.864$; $R^2 = 0.993$
$X_{Fe} = -0.085 * P_{425} + 36.652$; $R^2 = 0.997$
$X_{Fe} = -0.185 * P_{1010} + 187.81$; $R^2 = 0.9927$

Either one of these equations can then be used for the determination of the Mg-Fe ratio in cordierites.

References

BERTOLDI, C. et al. (2004): Lithos, 78, 389-409.

BOBERSKI, C. & SCHREYER, W. (1990): Eur. J. Mineral., 2, 565-584.

GEIGER, C.A. & GRAMS, M. (2003): Contrib. Mineral. Petrol., 145, 752-764.

P21-P07

Cu-Sn sulfides: synthetic approaches and multianalytical characterisation of old materials for new technologic substrates for energy devices

F. Di Benedetto[1], I. Bencistà[1], G. Fornaciai[1], M. Innocenti[1], A. Lavacchi[2], G. Montegrossi[3], W. Oberhauser[2], L. Pardi[4], M. Romanelli[1]
[1]Università di Firenze, Dipartimento di Chimica, Sesto Fiorentino, Italy
[2]CNR, ICCOM, Sesto Fiorentino, Italy
[3]CNR, IGG, Firenze, Italy
[4]CNR, IPCF, Pisa, Italy

Global environmental concerns and increasing demand for energy are opening new opportunities for using renewable energy resources. The kesterite-like quaternary chalcogenides attracted a relevant interest from worldwide researchers, due to their good performances (up to 10 % conversion efficiency) and to the lack of relevant environmental concerns associated with their production.

A reconsideration of the whole Cu-Fe-Zn-Sn-S has been undertaken, to reach two main goals: 1) set up a way to synthesise (promising) binary and ternary phases for applicative purposes, and 2) re-examine the most studied quaternary mineral phases, i.e. stannite, kesterite and kuramite.

Electrochemical Atomic Layer Epitaxy (ECALE) method has been used to obtain Cu_xS and Sn_xS_y on Ag(111). The amount of the elements deposited in the first layers was determined by the oxidative stripping of cations, followed by the reductive stripping of anions. Valence state and effective metal-to-anion ratios of the obtained thin films were studied through X-ray Photoelectron Spectroscopy (XPS). Cu_xS film reveals Cu in his formally monovalent state and the ratio Cu/S as ~ 1:1. Thus, a attribution to the structure of covellite, CuS, is proposed. XPS characterisation of Sn_xS_y indicates that layers are self-arranged towards the layered crystal structure of berndtite, SnS_2.

Synthetic kuramite nanoparticles, obtained by a solvothermal approach, were investigated by X-ray Absorption Spectroscopy (XAS) at Cu K-edge to verify: a) the possible occurrence of Cu(II) as a formal discrete state, and b) the synthesis-dependent random metal distribution in the structural sites. The XANES spectrum is fully comparable with those of the most common sulphide minerals containing tetrahedral Cu. The EXAFS region was fitted starting from the structural model of kuramite, where the first shell coordination for Cu resulted at 2.28(2) Å. This value agrees with the shortest Cu(II)-S bond distances in sulfide minerals (e.g. natural kuramite, 2.31 Å, covellite, 2.30 Å, tetrahedrite, 2.25 Å). The pre-edge region exhibits a very weak peak, which is observed in several Cu(II) standards (e.g. malachite and CuO). This suggest that Cu(II) can be considered in part as a discrete state in the sample (as required by charge balance). Finally, one has to mention that the fitting of successive coordination shells suggests the occurrence of random metal distribution (traced by the scattering of the heavy Sn ions).

P21-P08
Thermoelastic properties of single crystal sanidines

P. Schröer[1], F. Wiethoff[1], P. Sondergeld[1], J. Schreuer[1]
[1]Ruhr-Universität Bochum, Institut für Geologie, Mineralogie und Geophysik, Bochum, Germany

The elastic properties of natural feldspars have been extensively studied at room temperature by Russian groups between about 1960 and 1975 (see [1] for a review). Unfortunately, their samples suffered from imperfections like cracks, pores and inclusions, from twinning and poorly characterized states of Al/Si-order and of exsolution. It is therefore not surprising that the elastic constants obtained recently on K-rich sanidine [2] and albite [3] differ significantly from the previously reported ones. Our work focuses on the study of the elastic properties of monoclinic alkali feldspar single crystals as functions of composition, temperature and structure. To this end we employ the innovative method of resonant ultrasound spectroscopy (RUS). This technique offers the unique possibility to determine all independent elastic stiffnesses coefficients of a crystal species on a single sample within one experimental run with highest internal consistency.

Our samples were cut from large single crystals of gem quality showing no hint on twinning or exsolution phenomena. The composition $K_{1-x}Na_xAlSi_3O_8$ ranges from $x \approx 0.05$ to $x \approx 0.27$ with minor amounts of Ba^{2+} and Fe^{3+} and almost no Ca^{2+}. As determined by X-ray diffraction methods all samples are high- or low-sanidines. The individual elastic constants c_{ij} depend clearly on the chemical composition of the sanidines, in particular on the K/Na ratio. Most sensitive, however, is the shear resistance c_{44} which is closely related to the structural instability that drives the ferroelastic phase transition in alkali feldspars. With increasing albite component the transition temperature increases leading to a softening of c_{44} at room temperature and an increase of $\partial c_{44}/\partial T$ (Fig. 1).

At temperatures above about 1000 K distinct ultrasound dissipation effects develop in the sanidines. The effect is most pronounced in Eifel sanidines and probably related to the rapid change of their optical axis angle $2V$ reported in literature [4].

[1] Aleksandrov, K.S., Prodaivoda, G.T., Crystallogr. Rep. 38 (1993), 698-709.
[2] Haussühl, S., Z. Kristallogr. 204 (1993), 67-76.
[3] Brown, J.M., Abramson, E.H., Angel, R.J., Phys. Chem. Min. 33 (2006) 256-265.
[4] Zeipert, C., Wondratschek, H., N. Jb. Mineral. 9 (1981), 407-415.

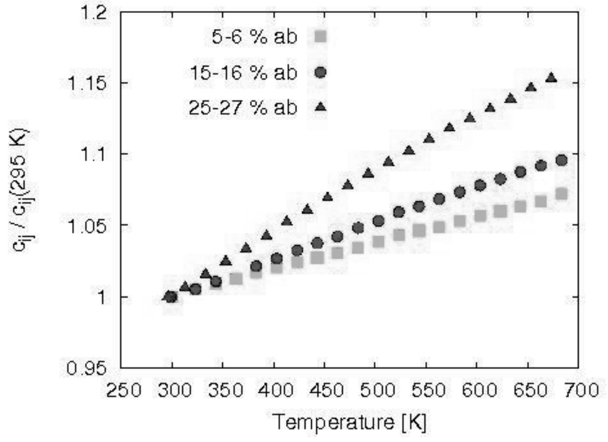

Figure 1: Temperature evolution of c_{44} of three sanidine samples with different Na content.

P21-P09
Incorporation of hydrous species in periclase

B. Joachim[1], E. Gardés[2], A. Wohlers[3], N. Norberg[3], R. Abart[1,3], W. Heinrich[3]
[1]University of Vienna, Department for Lithospheric Research, Vienna, Austria
[2]CIMAP, CEA-CNRS-ENSICAEN-Université de Caen Basse Normandie, Caen Cedex, France
[3]German Research Centre for Geosciences (GFZ), 3.3., Potsdam, Germany

Single, synthetic crystals of periclase were sealed in a platinum capsule with excess amounts of pure H_2O. Experiments were performed in a vertical Harwood type Internally Heated Pressure Vessel (IHPV) at 0.5 GPa and 1200°C for 20 h. Reaction products were analyzed with Infrared- and Raman-spectroscopy, and by Transmission Electron Microscopy.

IR-spectra of dry synthetic periclase show no bands in the spectral interval 3000-4000 cm^{-1}, confirming the absence of hydrous species. Spectra of water-doped crystals show bands at 3297, 3302 and 3312 cm^{-1}. At least two of these bands (3297 and 3312 cm^{-1}) may unambiguously be ascribed to OH-defects in the MgO structure. Following Freund and Wengeler (1982) they are interpreted as OH stretching vibrations. The calibration method according to Libowitzky and Rossmann (1997) was used to quantify the hydrogen concentration expressed as H_2O-equivalent and gives 7 ppm H_2O.

Identical peak positions were observed in Raman-spectra measured on a polished OH-doped periclase. An H_2O-bearing SiO_2-glass with a known concentration of 332 ppm was measured as a reference. The water concentration was calculated to an average value of about 10 ppm using the Comparator technique developed by Thomas et al. (2008).

In contrast to measurements recorded in the center of the periclase crystals, IR-spectra measured at the edge of the crystals show an additional band at 3697 cm^{-1}, which is interpreted as OH stretching vibration in $Mg(OH)_2$ (Freund and Wengeler, 1982). This is confirmed by TEM-measurements on ion-thinned foils, extracted from the edge of water-doped periclase crystals that show brucite precipitates of approximately rectangular shape with a side length of about 100 nm. We interpret this feature as being due to diffusion of molecular water into periclase during water-doping, which reacts with MgO, stemming from the periclase, to brucite during cooling.

References:

Freund F, Wengeler H (1982). The infrared spectrum of OH-compensated defect sites in C-doped MgO and CaO single crystals. Journal of Physics and Chemistry of Solids, vol. 43, pp. 129-145.

Libowitzky E, Rossmann GR (1997). An IR absorption calibration for water in minerals. American Mineralogist, vol. 82, pp. 1111-1115.

Thomas SM, Thomas R, Davidson P, Reichart P, Koch-Müller M, Dollinger G (2008). Application of Raman spectroscopy to quantify trace water concentrations in glasses and garnets. American Mineralogist, vol. 93, pp. 1550-1557.

P21-P10

Optical spectroscopy of varicoloured kyanites from Loliondo, Tanzania

M. Wildner[1], A. Beran[1], F. Koller[2]
[1]Universität Wien, Institut für Mineralogie und Kristallographie, Wien, Austria
[2]Universität Wien, Department für Lithosphärenforschung, Wien, Austria

Isolated single-crystals of gem-quality kyanites from Loliondo, Arusha region, Tanzania, occurring in dark blue, light green, ochre and orange colour varieties, were available for spectroscopic investigations. According to EMP data, the orange kyanite is characterised by MnO contents of 0.23 wt%, the FeO content amounts to 1.02 wt%. The ochre kyanite shows the highest FeO content with 1.31 wt% and reveals slightly but significantly enhanced MnO values of 0.06 wt%. The FeO content of the light green kyanite corresponds to that of the orange sample, but contains no other minor elements with concentration levels essentially above the microprobe detection limit. The dark blue sample shows a 'usual' FeO value of 0.39 wt%, while the Cr_2O_3 content of this kyanite is 0.28 wt%.

Polarised optical absorption spectra were measured along the extinction directions on (100) crystal plates ($n_{\beta'}$, $n_{\gamma'}$). Spectra of the orange kyanite are dominated by a strong broad band centred at 21300 cm^{-1} and a weaker one with components around 10700 and 9200 cm^{-1}. These bands are assigned to Mn^{3+} ions replacing six-fold coordinated Al. The relatively high Fe content is evidenced by several minor, spin-forbidden bands of octahedrally coordinated Fe^{3+}. In the ochre coloured sample, these bands are prominent at 26300, 27000, 23100 and around 22400 cm^{-1}, in addition to weaker Mn^{3+} absorption features. The colour of the light green kyanite is caused by the above mentioned bands due to Fe^{3+} and a broad weak IVCT band around 16000 cm^{-1}. Spectra of the dark blue kyanite are dominated by two broad bands at 24200 and around 16600 cm^{-1} due to Cr^{3+}, whereas the Fe^{3+} bands are only weakly developed.

Polarised OH absorption spectra measured on (100) plates show maximum absorption parallel to the $n_{\beta'}$ extinction direction. No essential absorption component can be observed parallel to the $n_{\gamma'}$ direction. The spectrum consists of a band triplet with bands at 3386, 3410 and 3440 cm^{-1}, dominated by the 3386 cm^{-1} band, and a band doublet with maxima at 3275 and 3260 cm^{-1}. A relatively strong OH band at 3340 cm^{-1} characterises the OH pattern of the ochre sample. The position of the OH bands and their pleochroic scheme is in complete agreement with the results obtained for light to dark blue kyanites from different localities of high-grade metamorphic rocks (Bell et al. 2004; Wieczorek et al. 2004). The (semi-) quantitative water content, derived from the IR absorbances amounts to 17 wt.ppm H_2O for the dark blue kyanite and 14 wt.ppm for the light green sample. The orange kyanite has the lowest OH defect concentration (3 wt.ppm) and the ochre sample shows an intermediate value of 7 wt.ppm H_2O. The obtained values suggest different water activities prevalent within the geological environment.

Bell D.R., Rossman G.R., Maldener J., Endisch D., Rauch F. (2004) Amer. Mineral. 89, 998

Wieczorek A., Libowitzky E., Beran A. (2004) Schweizer. Mineral. Petrogr. Mitt. 84, 333

P21-P11

Al/Si-ordering phenomena in sanidine megacrystals from the Eifel as investigated by NMR- and IR-spectroscopy

K. Demtröder[1], J. Schreuer[1]
[1]Ruhr-Universität Bochum, Institut für Geologie, Mineralogie und Geophysik, Bochum, Germany

Sanidine megacrystals from Volkesfeld (Riedener Kessel, East Eifel volcanic field) with up to about 10 kg in weight are characterized by very low concentrations of dislocations indicating near hydrothermal growth conditions. Most remarkably are their unique optical properties [1]. Fast irreversible changes of their optical axes angle $2V$ start already at moderately high annealing temperatures of about 1025 K. These effects have been interpreted by rapid changes of the Al/Si-distribution. However, the underlying atomistic processes are not yet understood. Therefore, we investigated Al/Si-ordering phenomena on sanidine megacrystals from four different eruptive centers (Essinger Maar, Kerpener Maar, Rockeskyll volcanic complex and Rieden caldera) of the quaternary volcanic fields of the Eifel employing ^{29}Si-NMR and IR-spectroscopy in combination with single crystal and powder X-ray diffraction. Orthoclase from Madagascar and adularia from Switzerland served as references.

All investigated Eifel sanidines ($K_{1-x}Na_xAlSi_3O_8$ with $0.15 < x < 0.3$) show irreversible optical anomalies at temperatures above 1073 K. According to [2] this corresponds to a decrease in the Al/Si order from $2t_1 \approx 0.70$ to 0.58. However, analyses of the tetrahedral bond distances as determined by X-ray diffraction according to [3] yield only slight changes of $2t_1$ from about 0.58 before to about 0.56 after annealing (100 h at 1375 K). Similar results are derived from lattice parameters b and c^* using the procedure described in [4]. Further, NMR- and IR-spectra also show no significant changes after annealing. The ^{29}Si-NMR-spectra of the megacrystals consist of eight different peaks in the range from -85 ppm to -104 ppm which characterize different environments of the two independent tetrahedral positions T_1 and T_2. The changes in peak positions and areas induced by annealing are smaller than 5%.

Our contradictory results suggest that the optical axes angle of potassium feldspars is not only influenced by the state of Si/Al-ordering but may also be sensitive to other parameters like the content of volatiles.

[1] C. Zeipert, H. Wondratschek: Ein üngewöhnliches Temperverhalten bei Sanidinen von Volkesfeld/Eifel. N. Jb. Mineral, Mh. **9** (1981) 407-415

[2] S.-C. Su, P. H. Ribbe, F. D. Bloss: Alkali feldspars: Structural state determination from composition and optic axial angle 2V. Am. Min. **71** (1986) 1285-1296

[3] P. H. Ribbe, G. V. Gibbs: Statistical analysis and discussion of mean Al/Si-O bond distances and the aluminium content of tetrahedra in feldspars. Am. Min. **54** (1969) 85-94

[4] H. Kroll, P. H. Ribbe: Determination (Al,Si) distribution and strain in alkali feldspars using lattice parameters and diffraction-peak position: A review. Am. Min. **72** (1987) 491-506

P21-P12

Optical and spectral artifacts in polished ore mineral sections

E. Libowitzky[1], A. Bechtold[1], P. Friesl[1], L. Oberwandling[1], M. Wildner[1]
[1]Universität Wien, Institut für Mineralogie und Kristallographie, Wien, Austria

Anomalous optical phenomena in polished sections of cubic ore minerals have been known for a long time and tentatively attributed to tectonic strain, trace element impurities, etc. (Klemm, 1962). For pyrite, magnetite and chromite, as well as cuprite Libowitzky (1994a,b,c) showed that these artifacts in the form of anomalous optical anisotropy colors resulted from surface defects introduced by classical mechanical (diamond) polishing. In the present bachelor work, the list of investigated ore minerals was extended, and Raman spectra from polished sections were compared to those from untreated samples. In addition to the above mentioned minerals, the sample set contained gersdorffite, cobaltite (pseudo-cubic), nickel-skutterudite, pentlandite, fahlore, sphalerite, and for comparison the FeS_2 polymorph marcasite and related löllingite and arsenopyrite.

Reflected light microscopy of the cubic phases revealed anomalous optical anisotropy in sphalerite sections, thus making the common twins well visible. However, bright internal reflections in Fe-poor samples and observation with high-magnification objectives corrupt the visibility of these weak effects. Even weaker effects were observed also in nickel-skutterudite and cobaltite. The polished sections of gersdorffite, pentlandite, and fahlore appeared optically isotropic in all cases.

Micro-Raman spectra were acquired both from the polished sample surface and from untreated spots, i.e. holes in the surface or raw bulk samples. A 20 mW Ar^+ (blue, 488 nm) and a HeNe (red, 633 nm) laser were applied for excitation. Whereas spectra of untreated samples, e.g. pyrite, revealed sharp bands with FWHMs close to the spectral resolution, spectra of mechanically polished surfaces showed considerably broadened and shifted bands. For example, bands of pyrite were shifted up to 11 cm^{-1} and broadened by a factor > 2. The effect was stronger on (100) than on (111) faces. Blue laser excitation caused more severe artifacts, which is in agreement with an only shallow penetration depth of the shorter wavelengths in strongly absorbing matter (limited to the very surface layers). Therefore, the described effects are negligible in only weak absorbers, such as spinels, cuprite and sphalerite.

Due to absorption phenomena, bad artifacts with completely altered spectra may result also from burning of the sample by a too strong laser focused on a very small spot.

Klemm DD (1962) N Jb Miner Abh 97, 337-356.
Libowitzky E (1994a) Phys Chem Minerals 21, 97 - 103.
Libowitzky E (1994b) Eur J Mineral 6, 187-194.
Libowitzky E (1994c) Can Mineral 32, 353-358.

P21-P13

Martite in Banded Iron Formations: a mineralogical characterization and its implication for analyses of ironoxides on the Martian surface

B. Orberger[1], C. Wagner[2], A. Tudryn[1], J.-M. Greneche[3],
R. Pichon[1], J. Fabris[4]
[1]Université Paris Sud XI, Sciences de la Terre, Orsay, France
[2]UPMC, Magmas-Minéraux-Matériaux, Paris, France
[3]Université le Mans, Lab. Physique de l'état condensé, Le Mans, France
[4]UFMG, Chimie, Belo horizonte, Brazil

Martitisation is a pseudomorphic replacement of magnetite by hematite due to redox-reactions and can be explained via maghemite by oxygen diffusion and cation transfer in the solid state (Davies et al., 1968), expressed by the reaction: $4\ Fe_3O_4 + O_2 = 6(g)\ Fe_2O_3$ (Lepp, 1957), or in acid and neutral to alkaline environments, respectively ($FeFe_2O_3 + 2H^+ = Fe^{++} + Fe_2O_3+H_2O$; Holser and Schneer, 1961; $2Fe_3O_4+H_2O = 3Fe_2O_3+2H^++2e^-$; Garrels and Christ, 1965). The mechanisms of transformation are still poorly understood. Martite from a mesoarchean banded iron formation (BIF) in Southern India and from paleoproterozoic BIFs from the Minas Gerais area were studied by optical microscopy, SEM, Raman-and Mössbauer spectrometry, Curie Balance, the hysteresis cycle, DRX and electronmicroprobe. The Indian martite forms massive iron-oxide bands composed of cubic and octahedral crystals showing the characteristic dissolution along well-defined cleavage planes. Magnetite forms rarely a few micron large patches within the hematite. Scarce goethite particles are present. The octahedral martite crystals from Brazil are composed of hematite along cleavage planes, magnetite remains still finely intergrown. Chemically hematite and magnetite of both martite occurrences (India and Brazil) show homogenously distributed traces of Al_2O_3, MgO, MnO and ZnO, but heterogeneously distributed SiO_2, CaO, Cr_2O_3, TiO_2 and V_2O_5. Mössbauer spectrometry at 300K) shows only the presence of hematite while Raman spectrometry analyzed hematite, magnetite and goethite. These results were confirmed by XRD, where magnetite was however only visible during long-term measurement at key intervals. Curie Balance analyses indicate the presence of magnetite and hematite. The origin of the Indian martite may be a result of hydrothermal alteration of magnetite around 2.5 Ga, while goethite was formed during modern weathering (Orberger et al. 2009). Our study provides important tools for a better evaluation of the mineralogical data which will be obtained from the Martian surface by the Mars Science Laboratory by DRX (launch date programmed for November 2011) and which were already obtained by Mössbauer spectrometry (Mimo II) being part of the Spirit and Opportunity Rovers.

References

Davis, B.L., Rapp, G., Walawender, M.J. (1968). Fabric and structural characteristics of the martitisation process. American Journal of Science, V. 266, 482-496.
Lepp, H. (1957). Stages in the oxidation of magnetite. American Mineralogist, 42, 679-681.
Garrels, R.M., Christ, C.L. (1965). Solutions, minerals and euilibria. New York, Harper and Row, 450p.
Holser, W.T., Schneer, C.J. (1961). Hydrothermal magnetite. Geol. Soc. America Bull., 72, 369-386.
Orberger, B., Wagner, C., Wirth, R., Noret, A., Gallien, JP, Jayananda, M., Rouchon, V., Quricio, E., Montagnac, G., Massault, M. : Origin of Fe-oxide sphérules in banded iron formation of the 2.9. Ga old Bababudan group, Southern India. Precambriran World, Mars 2009, Fukuoka, Japan.

P21-P14

K-edge XANES Spectroscopy on sulfur and phosphor in silicates

J. Goettlicher[1], R. Steininger[1]
[1]Karlsruhe Institute of technology, Institute for Synchrotron Radiation, Eggenstein-Leopoldshafen, Germany

Although recently investigations on sulfur speciation in silicate glasses using X-ray near edge structure (XANES) spectroscopy at the S K-edge have been published or submitted [e.g. 1-10] the nature of S in silicate structures is only partly understood. Here, the idea is to see if features from S K-edge XANES spectra of crystalline S-containing silicates where crystal structure data (e.g. from X-ray diffraction) include sulfur coordination can be assigned to S structural units. The spectral features of such silicates may then be used to identify S valence and coordination in silicate structures where access to structural information via X-ray diffraction is not possible. Up to now only few data exist about S speciation in crystalline silicates [e.g. 11-13]. Hence, a study has been performed to systematically record S K-edge XANES spectra for different types of silicates. Measurements were performed at the SUL-X beamline of the synchrotron radiation source ANKA. The spectra of the nesosilicates jasmundite, ternesite and ellestadite, of the sorosilicate phosphoinnelite, and the phyllosilicates delhayelite and tuscanite exhibit a wide variety of shapes. Delhayelite and phosphoinnelite where sulfur is given as SO_4^{2-} show additionally a complex pattern of resonances at energies below the sulfate resonance which means reduced S species are present. In the spectrum of jasmundite the broad resonance at about 2474.5 eV has been assigned to $[SCa_8]$ according to crystal structure data from X-ray diffraction [14]. S coordination in Ca and Si rich blast furnace slags should be close to $[SCa_8]$ units because their XANES spectra show similar features as for jasmundite. In ternesite, ellestadite and tuscanite S^{6+} has been confirmed. Of course, S speciation does not primary depend on the type of silicate but should be a result of redox conditions during mineral formation, e.g. the shift of S K_a fluorescence emission lines in sodalite group minerals have been used as a redox proxy [15]. S K-edge XANES spectroscopy of the tectosilicates of sodalite type gave reduced sulfur species for lazurite, hackmanite (sodalite variety), in helvines and in ultramarine color pigments. Phosphoinnelite, delhayelite, hackmanite and ultramarine spectra show pre-edges below 2470 eV. Their interpretation in terms of electron transitions is not yet understood. Under intense photon beam an increase of the pre-edge in the hackmanite spectrum and the occurrence of additional pre-edge peaks have been observed. Because some of the investigated silicates minerals contain also phosphorus the study has been extended to P containing silicates, and first results will be presented.

References:
[1] Metrich N., Clocchiatti R. (1996) GCA, 60, 4151-4160;
[2] Paris E., et al. (2001) Can. Mineral., 39, 331-339;
[3] Metrich N., et al. (2002) Geophys. Res. Lett., 29, 33-1-33-4.;
[4] Backnaes L., et al. (2008) J. Amer. Ceram. Soc., 91, 721-727;
[5] Wilke M., et al. (2008) Amer. Mineral., 93: 235-24;
[6] Evans K.A., et al. (2009) GCA, 73, 6847-6867;
[7] Jugo PJ. et al. (2010) GCA, 74, 5926-5938;
[8] Stelling, J., et al. (2011, accepted) GCA;
[9] Klimm K., et al. (2011, submitted);
[10] Wilke M., et al. (2011, submitted);
[11] Fleet ME., et al. (2005) Can. Mineral. 43, 1589-1603;
[12] Goettlicher J., et al. (2010) SNI 2010, 24.-26.02., FU Berlin;
[13] Goettlicher J. (2010) IMA, 21.-27.08., Budapest, HU;
[14] Glasser LSD, Lee CK (1981) Acta Cryst, 37, 803-806; Hettman K. et al. (2010) DMG-Abstracts, p98

P21-P15
The Electric Field Gradient In Natural Chrysoberyl And Sinhalite

W. Lottermoser[1], S.-U. Weber[2], M. Grodzicki[1], G. Redhammer[1], G. Tippelt[1], F. Litterst[3], S. Dlugosz[2], K.-D. Becker[2], H. Bank[4], G. Amthauer[1]
[1]Paris-Lodron-University, Dep. of Materials Engineering and Physics, Salzburg, Austria
[2]Univ. of Technology , Inst. of Physical and Theoretical Chemistry, Braunschweig, Germany
[3]Univ. of Technology, Inst. of Condensed Matter Physics, Braunschweig, Germany
[4]Gebrüder Bank OHG, Idar-Oberstein, Germany

This work reports on the evaluation of the electric field gradient EFG in two olivine-type minerals with low iron content, viz. a natural chrysoberyl (ideal formula Al_2BeO_4:Fe, 0.03 Fe ions pfu, space group Pnma, a = 9.4203(9)Å, b = 5.4871(5)Å, c = 4.4331(4)Å, Z=4) and sinhalite (ideal formula $MgAlBO_4$:Fe, 0.04 Fe ions pfu, space group Pnma a = 9.906(1)Å, b = 5.691(1)Å, c = 4.337(1)Å, Z=4). Iron in the olivine structure may be located on the two non-equivalent crystallographic sites M1 (point symmetry -1) and M2 (point symmetry m), respectively. Unlike in the isostructural alexandrite (Weber et al. 2007), there is no indication for Fe^{2+} in the chrysoberyl lattice, but the temperature-dependent Mössbauer spectra can all be reproduced by three subspectra with hyperfine parameters typical for Fe^{3+} located. In accordance with the results on alexandrite powder samples (Weber et al. 2007), Fe^{3+} in chrysoberyl has strong preference for the M2 site with a minor tendency to occupy M1. Whereas the angle parameters can unequivocally be assigned to Fe^{3+} on M1, on M2 they cannot due to the large linewidth. However, the calculated angles are not contradictory to ascribing this subspectrum to M2. In addition, the calculated quadrupole splittings and asymmetry parameters are in quantitative agreement with the experimental values. Experiments for explaining the large linewidth mentioned above are on course.

In the Mössbauer spectra of sinhalite the doublets exhibit distinct asymmetries with regard to the direction of the incident g-rays. Nevertheless, the spectra have been fitted with a single doublet without any restrictions using starting parameters for the quadrupole splitting and the angles between the EFG and the crystallographic axes as obtained by the electronic structure calculations for Fe^{2+} at the M2 position. Unlike in our earlier investigations (Weber et al. 2009) there is no indication for a second doublet associated with Fe^{2+} on the M1 position. The detected asymmetry in the powder spectrum has therefore to be attributed to texture. This conclusion is confirmed by the single crystal Mössbauer spectrum recorded under magic angle that yields a completely symmetric doublet. Hence, the whole iron content of sinhalite is divalent and can be located on the M2 position exclusively. This is in accordance with other experimental results, as well as the electronic structure calculations. Summarizing, even small amounts of Fe in minerals can be used as nanoprobe in order to derive reasonable EFG tensors leading to distinct site attributions.

Acknowledgements: Financial support of the Austrian Fund for Scientific Research (FWF) under the grant number P18329-N20 is gratefully acknowledged.

Reference:
Weber S.U., Grodzicki M., Lottermoser W., Redhammer G.J., Tippelt G., Ponahlo J., Amthauer G. (2007), ^{57}Fe Mössbauer spectroscopy, X-ray single-crystal diffractometry, and electronic structure calculations on natural alexandrite, Phys Chem Minerals, 34, 507-515
Weber S.U., Grodzicki M., Lottermoser W., Redhammer G.J., Topa D., Tippelt G., Amthauer G. (2009), ^{57}Fe Mössbauer spectroscopy, X-ray single-crystal diffractometry, and electronic structure calculations on natural sinhalites , Phys Chem Minerals, 36, 259-269

P21-P16
The Electric Field Gradient In Synthetic Fayalite (A Supplement)

W. Lottermoser[1], S.-U. Weber[2], A. Kirfel[3]
[1]Paris-Lodron-University, Dep. of Materials Engineering and Physics, Salzburg, Germany
[2]Univ. of Technology, Inst. of Physical and Theoretical Chemistry, Braunschweig, Germany
[3]University of Bonn, Steinmann Inst. of Geology, Mineralogy and Paleontology, Bonn, Germany

The electric field gradient (EFG) tensor is a central quantity when studying the relationship between structural and chemical properties in solids because it provides a most sensitive measure for the size and shape of the electric charge distribution around a given nucleus on a certain crystallographic site. Especially in case of low site symmetries the evaluation of this tensor with regard to its direction and magnitude is non-trivial but strongly correlated with other physical properties. Experimentally, the EFG is determined by Mössbauer spectroscopy yielding the quadrupole splitting D. Additionally, from single crystal spectra the asymmetry parameter $h = (V_{XX}-V_{YY})/V_{ZZ}$, representing the rhombic distortion of the EFG-ellipsoid, can be obtained, as well as the orientation of the EFG-tensor with respect to the crystallographic axes from the intensity distribution of the Mössbauer peaks with two angle parameters b and a (see, e.g., Gonser 1975). Theoretically, the EFG-tensor is derived from electronic structure calculations in the local density approximation (Grodzicki 1980). This is commonly regarded as the state-of-the-art treatment of large systems, i.e. with about 100 atoms per unit cell. A third method to derive the EFG tensor has been developed in our group (semi-quantitative approach). It uses the deformation electron densities (DED) r as derived from X-ray or synchrotron diffraction data and produces four-dimensional hyperareas dependent on their cartesian coordinates x,y,z as floating in space with the functional value of r being shown as transparency of the chosen colour (opacity). In this program system, it is possible to click on the relevant density hyperareas and to integrate them over their volume in space. Using a point charge formalism the EFG resulting from these integrated hyperareas is automatically calculated with resulting eigenvectors and eigenvalues together with a screen plot for control purposes.

The methods mentioned above had been applied to several compounds in the past, in particular synthetic fayalite a-Fe_2SiO_4 (Lottermoser et al. 2002). There, the evaluation of the EFG was quite successful yielding cluster sizes of up to 97 atoms around the two crystallographically non-equivalent iron sites with the exception of the semi-quantitative approach where in particular the azimuthal components of the EFG were not well met. Using the very accurate synchrotron structure data by A. Kirfel with a R-value of 0.6% and a sophisticated version of our DED program, however, it was now possible to achieve an overall agreement between calculated and experimental EFG orientations of a few percent.

Acknowledgements: Financial support of the Austrian Fund for Scientific Research (FWF) under the grant number P18329-N20 is gratefully acknowledged.

Reference:

Gonser U. (1975) From a strange effect to Mössbauer spectroscopy In: U. Gonser (Ed.), Topics in Applied Physics, vol. 5, Mössbauer Spectroscopy. Springer, Berlin-Heidelberg-New York, 1-51

Grodzicki M. (1980), A self-consistent-charge Xa method ,J Phys, B13, 2683-2692

Lottermoser W., Steiner K., Grodzicki M., Jiang K., Scharfetter G., Bats J.W.,

Redhammer G.J., Treutmann W., Hosoya S., Amthauer G. (2002), The electric field gradient in synthetic fayalite a-Fe_2SiO_4 at moderate temperatures, Phys Chem Minerals, 29, 112-121

P22-P01
Magnetic and nuclear phase transitions in $LiCrGe_2O_6$: a neutron diffraction study between 0.3 K and 1473 K

G. Redhammer[1], A. Senyshyn[2], G. Tippelt[1], G. Roth[3]
[1]University of Salzburg, FB Materialwissenschaften & Physik, Salzburg, Austria
[2]Forschungsneutronenquelle FRM-II, Garching, Germany
[3]RWTH Aachen, Institut für Kristallographie, Aachen, Germany

Pyroxene-type compounds have a rich magneto- and crystal chemistry. Especially the Li-bearing silicates $Li(M^{3+})Si_2O_6$ with M = Fe, Ga, Sc, V show crystallographic phase transitions from a low temperature *P*2$P2_1/c$ to a high temperature *C*2/*c* structure between 230 and 340 K [1]. In an actual study this $P2_1/c \leftrightarrow C2/c$ phase transition was also found in $LiFe^{3+}Ge_2O_6$ but shifted to higher temperatures [2]. In this presentation we have investigated the pyroxene type material $LiCr^{3+}Ge_2O_6$ using neutron diffraction over a wide temperature range between 0.3 K and 1473 K using a polycrystalline sample. The 298 K structure of $LiCrGe_2O_6$ was determined previously on a synthetic single crystal using XRD methods [3]. In-situ low and high temperature XRD experiments were also done to determine the lattice parameter variation and the thermal expansion tensor.

Similar to $LiFeGe_2O_6$ a $P2_1/c \leftrightarrow C2/c$ phase transition was found between 1130 K and 1170 K. Neutron diffraction experiments yield identical results to XRD experiments, however, exact variation of bond lengths and bond angles with temperature also could be extracted and the nuclear structure of the *C*2/*c* high temperature phase was determined in analogy to $LiFeGe_2O_6$. The phase transition is accompanied by a large volume increase of 1.9 % and several alterations in the structural geometries; in the *C*2/*c* modification, the tetrahedral bridging angle is 170.8(2)° at 1473 K, while at room temperature, the two independent chains in $P2_1/c$ have kinking angles of 150.2(1)° and 137.2(2)° respectively. Distinct non-linear variations with temperature are observed especially for the Li-O3 bond lengths and several large alterations in bond lengths at the phase transition could be detected.

Magnetic ordering is observed below 5 K. The magnetic structure is characterized by a pure antiferromagnetic arrangement of spins, both within and between the M1 chains; spins are within the *a*-*c* plane with a neglecting component along the *b*-axis (Figure 1).

[1] Redhammer & Roth, 2004, Z. Kristogr. 219, 585-605
[2] Redhammer et al. 2010 Phys. Chem. Mineral. 37, 685 - 704
[3] Redhammer et al. 2008 Acta Crystallogr. C64. i97 - i102

Figure 1: Diagram of the magnetic structure of $LiCrGe_2O_6$ at 0.5 K in a projection onto the a-c plane.

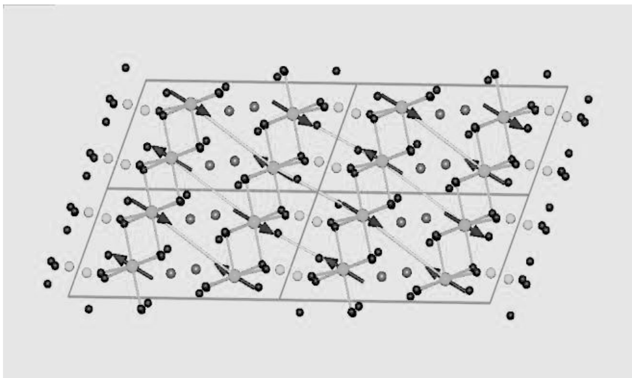

Figure 1: Diagram of the magnetic structure of $LiCrGe_2O_6$ at 0.5 K in a projection onto the a-c plane.

P22-P02
Characterizing Co-Re-based high temperature alloys with synchrotron

D. Mukherji[1], J. Wehrs[1], H. Ekerlebe[2], A. Stark[2], P. Staron[2], R. Gilles[3], J. Rösler[1]
[1]Technische Universität Braunschweig, Institut für werkstoffe, Braunschweig, Germany
[2]Helmholtz-Zentrum Geesthacht, Geesthacht, Germany
[3]Technische Universität München, Forschungsneutronenquelle Heinz Maier-Leibnitz (FRM II), Munich, Germany

There is a primary need to develop alloys with very high melting point as the Ni-base superalloys (presently the dominant material in the hot section of gas turbines) are now reaching limits posed by their melting temperatures. Single crystal Ni-superalloys operate close to their melting temperature and component cooling and thermal barrier coating prevents the base metal in the turbine blades from melting. It is becoming apparent that Ni-base superalloys must be supplemented with new materials to allow significant increase in the gas entry temperatures in future gas turbines [1]. High melting Co-Re-Cr based alloys introduced by the TU Braunschweig in 2007 [2] show promise as a new material class for high temperature application. The Co-Re alloys have a very complex microstructure with many phases in different morphologies. The phases include Cr- and Ta- carbides and Cr_2Re_3-type sigma phase. Further, the Co-solid-solution matrix undergoes an allotropic modification from hcp to fcc at high temperatures (above 1200°C) [3]. Microstructural stability in the service temperature range of 1000° - 1200°C is of concern for alloy development. In-situ synchrotron measurement with Small-angle X-ray Scattering (SAXS) and diffraction (XRD) in combination with a dilatometer was carried out recently at the HARWI beamline (DESY, Hamburg) to investigate microstructural evolution at these temperatures. The set up allows to perform very fast measurements at defined temperatures for the observation of kinetic changes.

References:
[1] J. H. Perepezko, Science, 326 (2009) 1068-1069.
[2] J. Rösler, D. Mukherji, T. Baranski: *Adv. Eng. Mater.* 9 (2007) 876-881.
[3] D. Mukherji, P. Strunz, R. Gilles, M. Hofmann, F. Schmitz, J. Rösler: *Materials Letters* 64 (2010) 2608-2611.

P22-P03
The Chemical Crystallography Beamline at Petra III.14: Current Status and Developments

C. Paulmann[1], A. Berghäuser[1], D. Novikov[2], U. Bismayer[1], D.C. Meyer[3], S. Park[4], W. Schmahl[4], D. Ropers[1], C. Lehmann[5], S. van Smaalen[6], S. Techert[7]
[1]Mineralogisch-Petrographisches Institut, Fachbereich Geowissenschaften, Universität Hamburg, Hamburg, Germany
[2]Hasylab/DESY, Hamburg, Germany
[3]Institut für Experimentelle Physik, TU Freiberg, Freiberg, Germany
[4]Dept. für Geo- und Umweltwissenschaften, Sektion Kristallographie, LMU München, München, Germany
[5]MPI für Kohlenforschung, Mülheim, Germany
[6]Laboratory of Crystallography, Universität Bayreuth, Bayreuth, Germany
[7]MPI für biophysikalische Chemie, Göttingen, Germany

Most undulator beamlines at the new PETRA III are already in user operation and others are in their final construction phase. Once all new beamlines are operating in full user mode, it is planned to shut down DORIS III by the end of 2012. This shutdown will discontinue a number of very successful beamlines and instruments which serve techniques not currently implemented at PETRA III. In order to carry on these activities in the future and to provide competitive beamlines and instrumentation for techniques not requiring ultimate brilliance, additional beamlines are planned to be build in two additional halls (PETRA III.14) and shall be available for full user operation in summer 2014.

One of these beamlines will focus on activities currently being performed at experimental stations like D3, F1 and BW1. The research areas of the user community range from chemical crystallography over materials and earth science till life sciences. Typical applications cover diffuse scattering studies, charge density analysis, phase transitions, also under external fields, disordered and modulated structures all at ambient and non-ambient conditions (low/high temperature, high pressure). An increasing number of novel compounds only form extremely small crystals unsuitable even for the most intense rotating anode X-ray generators equipped with focussing optics. In addition, compounds containing heavier elements require synchrotron radiation energies beyond common available laboratory X-ray radiation sources.

As a result of several user workshops, a joint research BMBF project (coordination: University Hamburg) has been granted in June 2010 to build up a new beamline at PETRA III.14 dedicated for a large range of crystallographic research fields. With the beginning of 2011 the detailed planning of experimental halls, beamline layout (optics and instrumentation) gained up in speed. The Chemical Crystallography beamline will be located in the eastern hall with a short undulator (N < 20) as source, delivering photon energies in the range of 10 to 35 keV (25 - 35 keV: 5th harmonic) using a CEMO-type double-crystal monochromator (Si111 and Si311). Within an experimental hutch of currently 9 m x 4 m size the beamline will offer two independent diffractometers. First, a completely new Kappa-diffractometer equipped with two independent detector circles, a high-resolution polarising digital microscopes and a xyz-stage able to carry sample loads of up to 10 kg. For loads up to 5 kg the circles will provide a sphere of confusion below 25 µm. In addition, a refurbished eulerian-type diffractometer (D3 or BW1) possibly with an optional horizontal scattering plane will be installed as option for heavier sample loads.

P22-P04
Shocked quartz in Sahara fulgurite

M. Ende[1], S. Schorr[2], G. Kloess[1], A. Franz[1], M. Tovar[3]
[1]Universität Leipzig, IMKM, Leipzig, Germany
[2]Helmholtz Zentrum Berlin, Kristallographie, Berlin, Germany
[3]Helmholtz Zentrum Berlin, Institut Komplexe Magnetische Materialien , Berlin, Germany

Comparative strain analyses were performed on quartz crystals in a Sahara fulgurite and two rock crystals. For the strain analyses neutron diffraction experiments with subsequent Rietveld refinement were performed, which also gave the possibility to determine the lattice parameters of the quartz.The shock induced stress cannot be measured directly by neutron or X-ray diffraction, because it is an extrinsic property. Yet, there is a relationship between the stress and the measurable strain, which is known as stress-strain curve and unique for each material. The study is carried out by applying the Williamson-Hall method based on an integral breadth analysis of the obtained Bragg peaks in the neutron diffraction pattern. Taking into account the results obtained by Langenhorst *et al.* (1994) the quartz crystals in the fulgurite could be ranged in a stage of deformation, where the causal shock pressure reaches about 25 GPa. The analysis of the lattice parameters only gives the uniform macro strain, so the results may differ from those of the integral breadth method. Compared with the results of Skála and Hörz (2001), which report about no measurable change in the unit cell volume until a shock pressure of 22 GPa, the obtained unit cell volume of the quartz crystals in the Sahara fulgurite reveals a shock pressure between 22 GPa and ~ 30 GPa. XRCT (X-ray computed tomography) studies of the fulgurite are performed additionally in order to get an impression about the fusion behaviour, the expansion of the fulgurite and the distribution of the stressed quartz crystals. The phase contrast showed that the shocked quartz crystals are concentrated at the outer shell of the Sahara fulgurite. Comparing the average density of the fulgurite with the average bulk density of quartz based sand, it can be concluded that the fulgurite expands more than 35 % during its formation.

Langenhorst, F. (1994): Shock experiments on pre-heated α- and β-quartz: II. X-ray and TEM investigations. *Earth and Planetary Science Letters*, **128**, 683-698.
Skála R., Hörz F. (2001): Unit-cell dimensions of experimentally shock-loaded quartz revisited. *Meteoritics & Planetary Science*, **36**, 192-193.

Figure 1: 2D longitudinal section of the examined Sahara fulgurite (edge length of voxels: 5 µm). The inner surface is widely smooth, whereas the outer surface shows a "streusel cake-like" roughness.

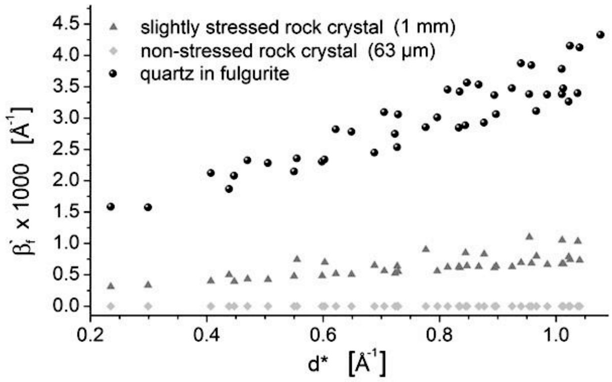

Figure 2: 2D longitudinal section of the examined Sahara fulgurite (edge length of voxels: 5 µm). The inner surface is widely smooth, whereas the outer surface shows a "streusel cake-like" roughness.

P22-P05
Better Instrument Design for Better Data

M. Adam[1], D. Bahr[2], G. Bryant[2], J. Kaercher[2], B. Michell[2], C. Ollinger[2], M. Ruf[2]
[1]Bruker AXS GmbH, Marketing, Karlsruhe, Germany
[2]Bruker AXS Inc., Madison, United States

Traditionally normal- or fine focus sealed Mo tubes with flat monochromators and pinhole collimators were the primary beam components of choice for structure determination of small molecules. Driven by the need for exceptional flux and flux density for structural biology, multilayer X-ray mirrors for Cu radiation were developed that provide small, focused X-ray beams with unprecedented intensity and beam quality. Improved deposition methods now also allow the manufacture of high intensity Mo and Ag multilayer optics. Multilayer optics are ideally suited to be coupled with microfocus sources and are now a premier choice in small molecule crystallography. Microfocus source mirror combinations provide very stable, high intensity X-ray beams with beam sizes between 80 and 120 micrometers. These small beams ideally match with today's smaller and smaller crystals to be investigated, depart from the traditional beam sizes of 500 to 800 micrometers and provide a new challenge for instrument design. Mechanical stability of primary beam components has to be brought to a new level and goniometer accuracy and reproducibility are more important than ever. Smallest spheres of confusion and better spatial detector resolution are all parameters that improve data quality. This presentation will discuss aspects of instrument design that are important to provide best crystallographic data possible.

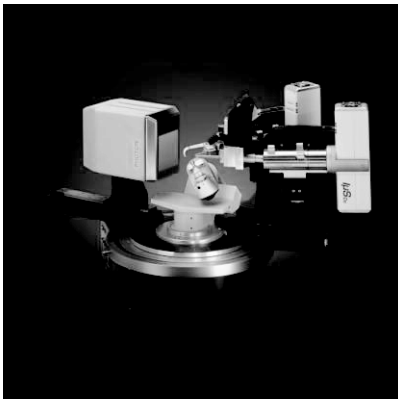

Figure 1

P22-P06
Neutron studies on bentonite bonded moulding sands

C. Eulenkamp[1], G. Jordan[1], W.W. Schmahl[1], M. Hoelzel[2],
E. Calzada[2], B. Schillinger[2]
[1]LMU München, Geo- und Umweltwíssenschaften, München, Germany
[2]TU München, Forschungsneutronenquelle Heinz Maier-Leibnitz (FRM II), Garching, Germany

Bentonites are used in numerous industrial applications. In the casting industry, ~8 wt.% are applied to quartz sand to plasticize and stabilize sand moulds. Smectites as the main component of bentonite provide cohesive strength to these non-permanent sand moulds. One important reason for this sand mould property is the ability of the clay minerals to reversibly adsorb and desorb water between their silicate layers. As a consequence, the interlayer lattice spacing expands or contracts, respectively.

During the casting process, the moulding sand is shock heated and water is expelled from the sand. The dehydration comprises pore and interlayer water. Water and vapour move along the temperature gradient in the sand towards cooler areas (Schillinger et al. 2011). With increasing temperature the smectites dehydrate progressively. In the industrial production lines the moulding material is processed and reused. A complete rehydration of the smectites and efficient reconditioning of the sand is important for a low rate of casting defects. Hydration states of smectites can be determined with powder diffraction methods by measuring the (001) reflection. We used the thermal high resolution neutron powder diffractometer SPODI, Forschungsneutronenquelle Heinz Maier-Leibnitz (FRM II) to obtain structural information on the smectite lattice spacing.

In order to produce industrially equivalent moulding sand samples, we experimentally simulated the casting process (Schillinger et al. 2011). Moulding sands with 12 wt.% of bentonite have been dehydrated and rehydrated in several cycles. SPODI samples have been taken prior to the experiment, after dehydration, and after rehydration. Neutron powder diffraction patterns of the same moulding sand at different conditions were taken. The raw sands showed smectite $d_{(001)}$ values of ~ 19 Å. The basal spacings of dehydrated smectites were ~12.6 Å. Swelling to 19 Å by rehydration was observed in even less than 150 minutes. This shows that on the basis of neutron diffraction the recycling flux of moulding sand in the industrial application may be optimized.

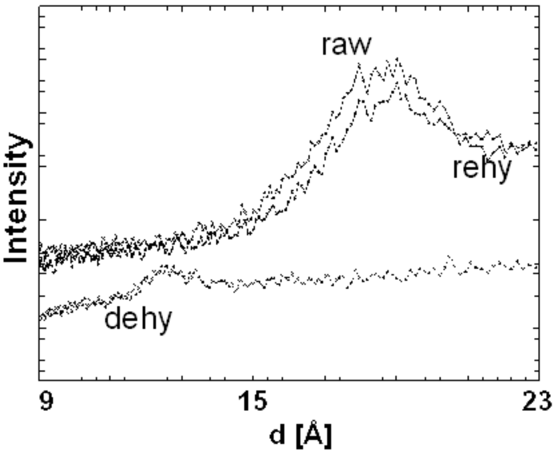

Figure 1: Neutron powder diffraction profiles of smectite (001) obtained at SPODI (FRM II)

P22-P07
Microcracks, Dislocations and Slip Bands in Silicon

T. Jauss[1], J. Wittge[1], C. Ehlers[1], C. Kiefl[1], A.N. Danilewsky[1], A. Cröll[1], D. Allen[2], P. McNally[2], J. Garagorri[3], M.R. Elizalde[3], B.K. Tanner[4]
[1]Universität Freiburg, Kristallographie, Freiburg, Germany
[2]Dublin City University, The RINCE Institute, Dublin, Ireland
[3]University of Navarra, CEIT and Tecnun, San Sebastián, Spain
[4]Durham University, Department of Physics, Durham, United Kingdom

Microcracks, dislocations and slip bands are generated in originally defect free silicon wafers during the wafer handling and heat treatments during device production. Such defects reduce the yield and performance of semiconductor devices. Typical mineralogical methods like polarizing light microscopy, scanning electron microscopy and X-ray diffraction are applied to understand the cleavage behaviour and dislocation formation in silicon as a result of mechanical defects and thermal strain. For the actual study Silicon samples were artificially damaged with a well defined load using a nanoindenter with a Vickers tip. The size and orientation of the microcracks originating at the corners of such an indent are characterised by light and scanning electron microscopy. X-ray diffraction imaging (topography) is capable of depicting the dislocations, slip bands and microcracks around the indents with a very high strain sensitivity. The strain distribution around the microcracks becomes visible with polarizing infrared light microscopy and is compared to the high resolution X-ray topography. Finally spatially resolved high resolution X-ray diffractometry shows a variation in the full width at half maximum of the rocking curves around the microcracks. From lattice constant measurements by the method of Bond and reciprocal space maps the residual strain is calculated.

Series of rocking curves which are taken from undisturbed to damaged areas show a clearly anisotropic distribution of the diffracted intensity. The bending of the lattice planes around an indent can be measured up to 380 µm distance for 5 N indentation load. This corresponds well with the approx. 310 µm contrast size measured from diffraction imaging. The reciprocal space maps show, that the lattice planes around an indent are both tilted and strained. The residual stress of 1.65 MPa is calculated around the indent.

The 5 N indents with microcracks of about 20 µm length are well visible in the polarised infrared microscopy too but with a smaller sized strain field contrast. Such defects act as sources for dislocation loops and slip bands during the heat treatments. The influence of absolute temperature, heating time above the brittle-tensile transition as well as the direction of temperature gradients on distribution, speed and size of slip bands becomes obvious during *in-situ* topography experiments [1]. In addition local temperature gradients along the wafer influence the formation and multiplication of dislocations. From the analysis of the type of dislocations, their speed and direction of glide we propose a three-dimensional model which predicts in a wafer the regions of high dislocation density as well as completely dislocation free volumes as a function of the initial strain field and the heat treatment [2].

[1] Danilewsky, A. N.,et al. (2011) *J. Crystal Growth,* **318,** 1157-1163.
[2] Wittge, J.,et al. (2010) *J. Appl. Cryst.,* **43,** 1036-1039.

P23-P01
XRD analysis of the corrosion products of research reactor fuel elements

A. Neumann[1], M. Klinkenberg[1], H. Curtius[1], D. Bosbach[1]
[1]Research Center Juelich, IEK-6, Juelich, Germany

Corrosion experiments of unirradiated UAl$_x$-Al and U$_3$Si$_2$-Al research reactor fuel elements were carried out under repository relevant conditions in order to identify and quantify the secondary phases formed by reactions with formation waters being expected in final repositories due to an accidental influx from the enclosing salt formations. This analysis is important for safety assessment issues as such phases quantitatively may act as a barrier against the migration of the released radioactive inventory. In detail the anaerobic experiments were carried out in glass autoclaves at 90°C in repository relevant solutions of defined composition [1].

After termination of the corrosion period WAXS measurements and Rietveld analysis were the major methods being applied for the identification and quantification of the crystalline and amorphous corrosion products which have been subdivided into different grain size fractions previously. The corrosion products, i. e. the secondary phases of the research reactor fuel elements were identified via “Search/Match” database retrieving. The identified phases were LDH structures, lesukite (aluminium chlorohydrate), elemental iron, residues of uncorroded nuclear fuel, and different iron containing phases like akaganeite, goethite, and lepidocrocite. The quantitative analysis showed that LDH compounds and lesukite are the major crystalline phases which are observed. Rietveld analysis also revealed the content of amorphous phases. To account for an accurate determination of the phase quantities, i.e. for the application of the Brindley [2] correction the average particle diameter has previously determined by REM and image analysis.

For safety assessments the potential for retention of radionuclides has to be focused on the sorption capacities of the major phases as these may additionally applied as a backfilled barrier in order to prevent the migration of radionuclides out of the final repository in deep geological formations.

[1] H. Curtius, G. Kaiser, Z. Paparigas, B. Hansen, A. Neumann, M. Klinkenberg, E. Müller, H. Brücher, D. Bosbach, Reports of the Research Center Jülich, 2010, Jülich-4333
[2] G. W. Brindley, Phyl. Mag., 1945, 36, 347-369

P23-P02

Kristallstrukturbestimmung aus Röntgenpulverdaten: Das Anti-Diarrhoetikum Loperamid-Hydrochlorid

D. Podgorski[1], J. Brüning[2], E. Alig[1], J.W. Bats[3], M.U. Schmidt[1]
[1]University Frankfurt, Inorganic Chemistry, Frankfurt am Main, Germany
[2]Merck KGaA, Darmstadt, Germany
[3]University Frankfurt, Organic Chemistry, Frankfurt, Germany

Die Verbindung Loperamid-Hydrochlorid ($C_{29}H_{34}Cl_2N_2O_2$) [1], bekannt unter dem Handelsnamen Imodium®, wird in der Therapie gegen Diarrhö eingesetzt. Es gehört zur Substanzklasse der Opioide, zeigt aber nicht deren typische Nebenwirkungen. Loperamid wirkt hauptsächlich im Darm, indem es die Darmaktivität reduziert. [2]

Bisher sind nur die Kristallstrukturen von Loperamid-Hydrat [3] (freie Base) und Loperamid-Hydrochlorid-Tetrahydrat [4] bekannt. Die kommerzielle Form ist jedoch Loperamid-Hydrochlorid-Anhydrat. Zur Klärung der Kristallstruktur wurde eine Polymorphensuche durchgeführt; dabei konnten dünne verwachsene Plättchen des Anhydrats erhalten werden. Die Kristallqualität reichte nicht für eine Strukturbestimmung aus Einkristallen aus. Daher wurde die Kristallstruktur aus guten Röntgenpulverdaten bestimmt. Die Rietveldverfeinerung wurde mit dem Programm *TOPAS* [5] durchgeführt. Die Verfeinerung konvergierte mit $R_p = 0.0251$, $R_{wp} = 0.0827$, $\chi^2 = 1.598$. Loperamid-Hydrochlorid kristallisiert in $P2_1/c$ mit $Z = 4$ und $a = 16.7077(6)$, $b = 12.3780(3)$, $c = 13.2164(3)$ Å, $b = 101.639(2)°$. Die Moleküle sind über Wasserstoffbrücken $\mathrm{N-H\cdots Cl}$ und $\mathrm{O-H\cdots Cl}$ zu Ketten verbunden. Die Ketten ordnen sich durch ionische Wechselwirkungen zu Schichten an. Die Schichten sind nur durch Van-der-Waals-Wechselwirkungen miteinander verbunden, was eine Begründung dafür sein könnte, dass die Verbindung in dünnen Plättchen kristallisiert.

[1] R. A. Stokbroekx, J. Vandenberk, A. H. M. T. Van Heertum, G. M. L. W. Van Laar, M. J. M. C. Van der Aa, W. F. M. Van Bever, P. A. J. Janssen (1973). *J. Med. Chem.* **16**, 782-786.

[2] J. van Rompay, J. E. Carter (1990). *Anal. Profil Drug Subst.* **19**, 341-365.

[3] G. Germain, J. P. Declerq, M. van Meerssche, M. H. J. Koch (1977). *Acta Cryst.* B**33**, 942-944.

[4] Caira, M. R., Gerber, J. J. & Lötter, A. P. (1994). *Supramolecular Chemistry* **5**, 225-230.

[5] A. A. Coelho (2007). *TOPAS* Academic, version 4.1.

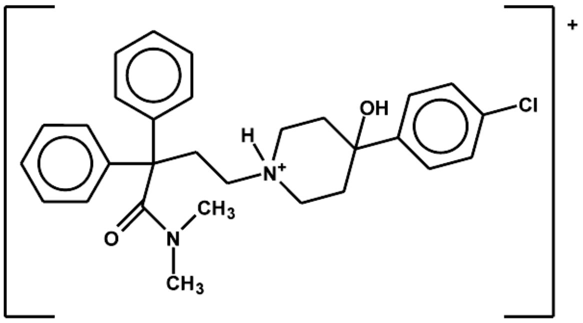

Figure 1

P23-P03

Indexing powder diffraction patterns. A renewal of the Runge-de Wolff indexing method

R. Heinemann[1], D. Stöckelmann[1], H. Kroll[1], W. Hoffmann[1]
[1]Universität Münster, Institut für Mineralogie, Münster, Germany

Motivation

Current indexing programs taking advantage of increasing computing capabilities use Monte-Carlo methods in parameter space to solve unknown powder patterns. Thereby, they ignore information inherent in metrically invariant relations between Q values (vector squares) in the reciprocal lattice. Originally, these relations have been introduced into indexing techniques by Runge (1917) and de Wolff (1957, 1963). The relations were not developed further, however, and because of their special character they were of minor usefulness in the design of indexing programs.

Approach

In the Runge-deWolff method, indexing is attempted by the search of a parallelogram configuration among reciprocal lattice vectors H_i. Their Q values fulfil the relation...., where $\omega_i = 2, 2, -1, -1$. This special parallelogram equation has been generalized by Stöckelmann et al. (2010) so that now any four reciprocal lattice vectors that define a reciprocal plane can be identified as such rather than reciprocal lattice vectors that are arranged in the special parallelogram configuration. In a reciprocal lattice plane with mesh size 4 there exist 8648 different configurations each with four lattice vectors, all being characterized by a specific set of ω_i values. The high density of these metrically invariant relations provides an extension of the indexing capability of the Runge-de Wolff method that is unequalled so far.

Results

The general parallelogram equation provides the central equation of a new indexing program LATIN (*lat*tice *in*variants) currently in progress. In practical tests we find that due to the completeness of the approach a large number of false configurations are found apart from the correct combinations. The false results must be recognized as such and then sorted. For that purpose we have developed a number of criteria.

Prospect

After identifying several reciprocal planes LATIN will combine those which comprise the largest number of lattice points in order to span the reciprocal space. For that purpose the various invariant spatial combinations developed by Stöckelmann et al. (2010) will come into play.

References

Runge, C. (1917) Die Bestimmung eines Kristallsystems durch Röntgenstrahlen. Phys. Zeitschr. **18**, 291-301.

Stöckelmann, D., Kroll, H., Hoffmann, W. and Heinemann, R. (2010), A system of metrically invariant relations between the moduli squares of reciprocal-lattice vectors in one-, two- and three-dimensional space. Journal of Applied Crystallogr., **43**, 269-275.

Wolff, P.M. de (1958) Detection of simultaneous zone relations among powder diffraction lines. Acta Crystallogr. **11**, 664-665.

Wolff, P.M. de (1963) Indexing of powder diffraction patterns. Advances in X-Ray Analysis **6**, 1-17.

P23-P04

The occurrence and identification of calcium-rich dolomite in the lower Muschelkalk of Saxony-Anhalt

E. Thorsten[1], R. Martin[1], K. Ronny[1], P. Herbert[1], W. Thomas[1]
[1]Martin-Luther-Universität, Mineralogy and Geochemistry, Halle, Germany

In the system calcite-magnesite-siderite a solid solution series between dolomite ($CaMg(CO_3)_2$) and ankerite ($Ca(Fe_xMg_{1-x})(CO_3)_2$, with $x \leq 0.7$) exists. Beside this, magnesite and siderite form a complete solid solution series. In the crystal structure of dolomite two non-uniform metal sites are occupied by either Ca or Mg, ideally. A substitution of the Mg site by Fe is possible up to about 70 mol% leading to a solid solution series with the end-member ankerite. Moreover, in sedimentary carbonates dolomites with Ca-excess ($Ca(Ca,Mg)(CO_3)_2$) are frequently observed (Blake et al. 1982; Drits et al. 2005; Reeder and Dollase 1989).

Both, the substitution of iron as well as the Ca-excess in dolomites ($Ca(Ca,Mg,Fe)(CO_3)_2$) effect an increase of the lattice parameters. Consequently, in x-ray diffraction pattern the reflection positions 2q are similarly shifted to lower values and, moreover, the intensities are increased. For phase identification and for quantification using the Rietveld-method both facts lead to substantial uncertainties especially when the atomic ratio Ca/Mg > 1.

In a joint project supported by the AiF carbonates from the lower Muschelkalk of Saxony-Anhalt have been analysed and quantified combining optical and electron microscopy, XRD and XRF. In a thin layer of ca. 20 cm within the Oolite horizon of the provenience in Stassfurt the principal phase is a dolomite with distinct Ca-excess. Chemical analysis of individual grains done by SEM-EDX and calibrated electron microprobe revealed an average stoichiometry of $Ca_{1.10(5)}Mg_{0.85(5)}Fe_{0.05(2)}(CO_3)_2$. This Ca-excess lies within the limits reported by Blake et al. 1982 and Drits et al. 2005.

Comparing calcite (cc), magnesite (mg), siderite (sd), dolomite (Ca-excess) and ankerite the lattice parameters taken from literature and determined by our studies are directly correlated to the specimen stoichiometry. Taking into account the strongest reflection 104 which is free from coincidences with reflections of additional phases the dependence is expressed by eq. 1 (n is the percentage of the phase):

$d= (n_{cc}*d_{cc} + n_{mg}*d_{mg} + n_{sd}*d_{sd}) / (n_{cc} + n_{mg} + n_{sd})$

Thus, depending on the composition the lattice parameters of Fe-rich ankerites and Ca-enriched dolomites can be identical and therefore the determination of the stoichiometry is essential for exact Rietveld-quantification.

References:

Blake DF, Peacor DR, Wilkinson BH (1982) The sequence and mechanism of low-temperature dolomite formation: Calcian dolomites in a Pennsylvanian Echinoderm. J. Sed. Petrol. 52(1):59-70

Chai L, Navrotsky A, Reeder RJ (1995) Energetics of calcium-rich dolomite. Geochim. Cosmochim. Acta 59(5):939-944

Drits VA, McCarty DK, Sakharov B, Milliken KL (2005) New insights into structural and compositional variability in some ancient excess-Ca dolomite. The Can. Mineral. 43:1255-1290

Reeder R, Dollase W (1989) Dolomite structural variation in the dolomite-ankerite solid-solution series. Am. Mineral. 74:1159-1167

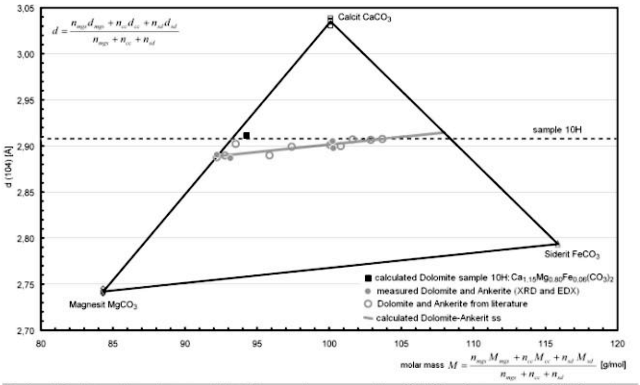

Fig: Correlation between the molar mass and the lattice parameters, expressed by d(104). The reflex position or d(104) of sample 10H implies Ankerite, but EDX data show insufficient Fe-content. According to Drits et al. (2005) it can be recalculated to a Ca-excessed Dolomite.

Figure 1

P23-P05

NEW X-RAY DATA OF THE SKARN MINERALIZATION FROM MRACONIA PERIMETER, ROMANIA

M.A. Anason[1], E. Bilal[1], S. Marincea[1], D.G. Dumitras[1]
[1]Universiti of Bucharest, Geology, Bucharest, Romania

This paper aims to provide new X-ray powder data on the main minerals from the skarn in the upper basin of Mraconia Valley, Almăj Mountains, as well as on the associated mineralization.

Methods

X-ray diffractometry is the method most used to identify the mineral species. This method presents a number of advantages, namely: ensure full decipher reticular structure of minerals, gives indications on employment through structural cation positions (if clay minerals) is non-destructive.

Results

The X-ray power data recorded for the representative sample of the andradite where used for the least-squares refinement of the unit-cell parameters. The obtained values reported by Marincea (1992) i.e. a =11.984(3) Å - 12.041(3) Å, being indicative for andradite.

Scheelite is the mean exponent of the high-temperature hydrothermal phase, occurring as isolated crystals or clusters of crystals, generally included in the andradite mass. As observed by Marincea (1992) the UV response colour is characteristic for two different generations of scheelite, as follows: (1) a first generation, with yellow fluorescence, characteristic for a Mo-bearing scheelite, associates only with andradite, and (2) a second generation, that fluoresces in blue-violet tints, The cell parameters obtained as mean of those obtained for scheelite samples, as refined by least-squares analysis of the X-ray powder data, are: a = 5.242(3) Å, c = 11.370(7) Å and V = 312.5(4) $Å^3$.

Molybdenite is widespread in the associations from Mraconia. The unit-cell parameters, obtained by least-sqares refinement of the X-ray power datasets obtained for eight representative samples are a = 3.151(6) Å, c = 12.292(9) Å and V = 105.7(2) $Å^3$.

Muscovite occurs sporadically like lamellar agregate, with characteristic habitus. This mineral indicate the existence of some hydrothermal processes with the contribution of substance (K, Al). The cell parameters obtained as mean of those obtained for quartz samples, as refined by least-squares analysis of the X-ray powder data, are: a = 5.168(2) Å, c = 9.017(4) Å, c = 20.033(5), β =95.03° and V = 931.24(1) $Å^3$.

Calcite is widespread in the skarn area, where this mineral forms the fillings of a system of fractures affecting the skarn mass. The average values are a = 4.983(6), c = 17.026 (3) Å, and V = 367.3(1) A^3, slightly smaller than those given by Effenberger et al. (1981) for the stoichiometric calcite [a = 4.9896(2) Å and c =

17.0610(11) Å] and suggesting very limited Mg-for-Ca substitutions.

Conclusions

By applying difractometry X-ray were analyzed minerals crystallized: scheelite,quartz, calcite, muscovite, andradite, molybdenite, pyrite from the skarne.

References:

Marincea, Ş. (1992): Metasomatite occurrences in the upper basin of the Mraconia Valley (Almăj Mts.) and the superposed mineralization. *Rom. J. Mineral Deposits*, **75**, 45-53.

P23-P06

More reliable intensity extraction from powders using texture

J. Gräßlin[1], L.B. McCusker[1], C. Bärlocher[1], F. Gozzo[2],
B. Schmitt[2], L. Lutterotti[3]
[1]ETH Zürich, Material Science, Zürich, Switzerland
[2]Swiss Light Source, PSI, Villigen, Switzerland
[3]University of Trento, Department of Materials Engineering and Industrial Technology, Trento, Switzerland

The intensity variation in the XRD pattern obtained from a textured sample as a function of sample orientation (tilt and rotation) can be applied to resolve the relative intensities of overlapping reflections [1]. With the new Si-microstrip detector (Mythen II) [2] on the MS Beamline at SLS and the new features in the program *Maud* [3], both the experimental and the data analysis procedures could be redesigned. Thereby, a significant improvement in the quality of the extracted reflection intensities was achieved.

To test this modified method, two samples of a Zr-phosphate with a known crystal structure [4] were measured: a textured sample using the revised experimental setup and data collection strategy, and an untextured sample in a 0.5mm capillary. Both datasets were collected at the SLS using the Mythen detector. For the analysis, reflections up to $d_{\min} = 1.0$ Å were considered, and a reflection separation factor of 0.5*FWHM was used to define the overlap groups.

Comparison of the structure factors extracted from conventionally measured powder diffraction data with those derived from a textured sample indeed shows a significant improvement. The agreement between the amplitudes obtained with a LeBail extraction using *Maud* for the untextured data and those calculated from the refined crystal structure can be expressed as an *R* value of 0.547 for overlapping reflections. Amplitudes derived in a joint extraction using 16 powder patterns (different orientations) collected on a textured sample yielded an *R* value of 0.334 for overlapping reflections. The quality of the extraction could be further improved by combining the amplitudes derived from the textured sample with those derived from the untextured one. This combination results in an *R* value of 0.310.

The texture method proved to be a way to significantly improve the reliability of extracted reflection amplitudes for the structure solution process. This should allow crystal structures to be solved that are not easily accessible using conventional powder diffraction data. An attempt to determine the structure of the Niobium silicate AM-11 [5] by applying this method is in progress.

[1] C. BAERLOCHER et al., Z. Kristallogr. 219 (2004), 803-812. [2] A. BERGAMASCHI et al., J. Synchrotron Rad. 17 (2010), 653-668. [3] L. LUTTEROTTI, Nucl. Inst. Meth. B 268 (2010), 334-340. [4] J. DONG et al., Microporous Mesoporous Mater. 104 (2007), 185. [5] J. ROCHA et al., Chem. Commun. (1998), 2687-2688.

P23-P07

Powder diffraction optics for High-resolution X-ray Diffractometer

G. Schuck[1], A. Iwata[1], Y. Ueji[2]
[1]Rigaku Europe SE, XRD, Berlin, Germany
[2]Rigaku Corporation, Japan, Japan

The multipurpose, fully-automated horizontal X-ray diffractometer SmartLab can install a parabolic multilayer mirror for parallel-beam optics (CBO), an ellipsoidal multilayer mirror for convergent-beam optics (CBO-E) or a Johansson type crystal for monochromatization of the incident X-rays to the $K\alpha_1$ ($K\alpha_1$ system) in order to perform high-resolution powder diffraction measurements.[1]

The $K\alpha_1$ system is designed as the position of the focal point of the Johansson type crystal is corresponding to the conventional X-ray source. Therefore, the CBO system can be used in the same way as the conventional $K\alpha$ system. Consequently, the $K\alpha$ system and the $K\alpha_1$ system can be easily switched. The advantage which can carry out all measurements with horizontal sample mounting and the advantage only in the simple exchange of the slit switched to the Bragg-Brentano optics, the convergent-beam optics, the parallel-beam optics have been inherited even in the $K\alpha_1$ system.

Since the diffracted X-rays is not obstructed in the $K\alpha_2$, the separation of the diffracted X-rays becomes easy in the $K\alpha_1$ system. Therefore, the indexing becomes easy, and it can conjugate for the measurement for the unknown structure analysis.

It is possible to use the $K\alpha_1$ monochromatized X-rays by the Bragg-Brentano optics and the convergent-beam optics in which the diffracted X-rays focus on the detector plane. Therefore, the high-speed and high-intensity measurement is possible using the high-speed one-dimensional position sensitive X-ray detector D/teX Ultra.

[1] *The Rigaku Journal (English version),* 26(2) (2010) 29-30

P23-P08

Interpretation of non-isothermal oxidation kinetics of Nitrides from YbScSZ

N. Martinez M[1], F.A. Cordero Peña[2], E. Schweda[3]
[1]Simon Bolivar University, Materials of Science, Baruta. Edo Miranda, Venezuela
[2]Simón Bolivar University, Earth Science, Baruta. Edo Miranda, Venezuela
[3]Tuebingen university, Inorganic Chemistry, Tuebingen, Germany

Introduction: Compound of Nitride were an important high temperatur structural and engineering material. An understanding of oxidation behavior of YbScSZ is crucial to its use as a high temperatur materials. This study, describes the oxidation kinetics of this compound at relatively low temperatur with non-isothermal data.

Methods:TG/DTA experiment were performed using a Netzch STA 449F3 thermoanalyser (Exton, PA). Scans were measured in an atmosphere of air at a different heating rate. The different powder-phase composition was identified by X-Ray diffraction (XRD; Model D500 θ/2θ and θ/θ, Bruker company Germany) using CuKα (λ = 154.18 pm) over scan range 10-110°

Results: Non-Isothermal methods were aplicated in the kinetics analysis. The method of Coats and Redfern (1964) was used to calculated the kinetics parameters A and E assuming very kinetics model expresións. The kissinger equation (Bamford and Tipper 1980) permited the calculation of E assumming the peak temperatur of the corresponding DTA reaction peak.

The oxidation behavior were divided in three steps. An initial periods with linear oxidation. This phase ist the induction periods bevore the reaction. The second period identifited with the reaction janders, This phase can be described by one diffusion cotrolled reaction. so after step two, was found that oxidation up to 80% degree is describe by the phase boundary-controlled reaction.

Conclusions: The thermal oxidation on Nitride in air flowing gas presents tree steps. Two linear oxidation step I, one diffusions controlled steps (II) and one phase Boundary-Controlled ration (III). In the phase Boundary-controlled reaction were two exothermic peaks and must be due to the Cystallization of Fluorit structure and diffusion of the cations in the structur (unstable structur)

References

1. N. J. Martinez Meta, E. Schweda, J.Solid State Chem., 179(2006 1486-1489

2. A. F. Gualtieri, M. Gemmi and M. Dapiaggi, American Mineralogist, Volumen 88, pages 1560-1574.2003

3. Shiro Shimada adn M. Inagaki. Solid State Ionics 63-65 (1993) 312-317

4. N. J. Martinez Meta, E. Schweda, J. Lira. X Congreso Venezolano de Quimica.

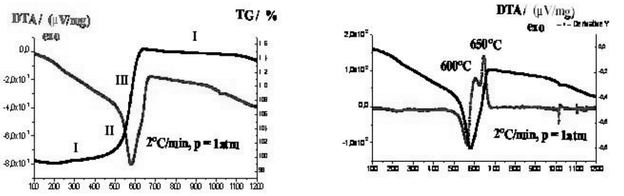

Oxidatiion Reaction from ScYb SZN

Curve DDTA / DTA from ScYbSZN

Figure 1

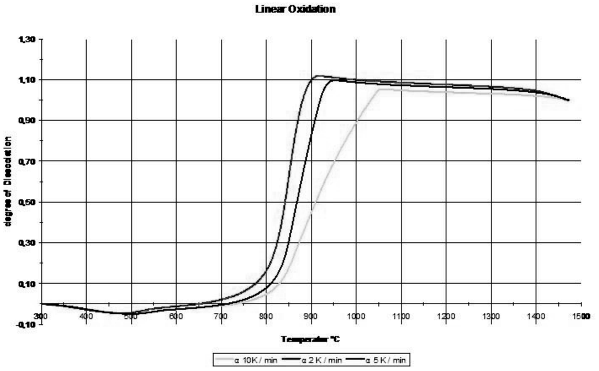

Figure 2

P23-P09
High temperature XRD study of nano-sized WO_3 grown by flame spray pyrolysis

J. Birkenstock[1], S. Pokhrel[2], L. Mädler[2]
[1]University of Bremen, FB5-Geosciences-Kristallographie, Bremen, Germany
[2]University of Bremen, Foundation Institute of Materials Science (IWT), Department of Production Engineering, Bremen, Germany

A powder of nanosized WO_3 particles, that were produced by FSP (flame spray pyrolysis [1]), were studied by in-situ high-temperature x-ray powder diffraction. The sample was measured at various constant temperatures while it was heated between these measurements at a rate of 20 K/min to set the next measurement temperature. All diagrams were fitted using the Rietveld-software package BRASS 2.0 [2].

Initially, at room temperature the calculated crystallite size was about 7 nm which was consistent with that measured by high resolution TEM. Accordingly very broad peaks were displayed, yet could still be fitted nicely using the structure model of the stable monoclinic structure [3], ICSD entry 80056 (P 2_1/n). Initially due to the strong peak broadening it was not possible to assign either the monoclinic or the orthorhombic phase to the observed pattern, yet the monoclinic model gave a significantly better fit in the end. At 550 °C the stable orthorhombic structure was identified. Applying entry 50730 [4] (P b c n) again yielded a reasonable fit, still with rather small crystallite sizes of about 15 nm.

At 800 °C much smaller peak widths were observed. The fit of the tetragonal model (P 4/n c c) corresponding to ICSD entry 50732 [4] was again reasonable and yielded an average crystallite size of about 90 nm.

On cooling the above phase transformation succession was reversed, i.e. again the succession of the stable phases of WO_3 was observed. The crystallite sizes remained much larger than the initial ones, yet decreased slightly from 90 nm (tetragonal high temperature phase) over about 75 nm (orthorhombic intermediate phase) to about 50 nm (monoclinic room temperature phase).

The lattice parameters for the initial nanocrystals turned out to be significantly different from those of the final product which were in good agreement with the reference values. The unit cell volume, though, was practically the same as that of the latter.

In general it was shown that WO_3 samples produced by FSP yield non oxygen-deficient stable WO_3 and not one of the oxygen-deficient or meta-stable phases. The material shows the temperature-dependent behavior as expected for stable non deficient WO_3 while it is recrystallizing to bigger crystals on phase transformations. At temperatures above 700 °C a needle-shaped crystal growth was observed by HR-TEM.

[1] Pokhrel, S., Birkenstock, J., Schowalter, M., Rosenauer, A., Mädler, L. (2009). Crystal Growth & Design, 10, 632-639.
[2] Birkenstock, J., Fischer, R. X., Messner, T. (2010). The Bremen Rietveld Analysis and Structure Suite.
[3] Woodward, P.M., Sleight, A.W., Vogt, T. (1995). Journal of Physics and Chemistry of Solids, 56(56), 1305-1315.
[4] Vogt, T., Woodward, P.M., Hunter, B.A. (1999) Journal of Solid State Chemistry, 144, 209-215.

Index